

**GEORGIA DOT RESEARCH PROJECT 22-17**

**Final Report**

**NONDESTRUCTIVE/NONCONTACT  
INSPECTION PROTOCOLS AND  
TECHNOLOGIES FOR AGING  
MECHANICALLY STABILIZED EARTH  
AND MODULAR BLOCK RETAINING  
WALLS**

**VOLUME II**



**Office of Performance-based Management and Research**  
600 West Peachtree Street NW | Atlanta, GA 30308

**October 2025**

## TECHNICAL REPORT DOCUMENTATION PAGE

1. Report No.: FHWA-GA-25-2217	2. Government Accession No.: N/A	3. Recipient's Catalog No.: N/A	
4. Title and Subtitle: Nondestructive/Noncontact Inspection Protocols and Technologies for Aging Mechanically Stabilized Earth and Modular Block Retaining Walls, Volume II		5. Report Date: October 2025	
		6. Performing Organization Code: N/A	
7. Author(s): Marcel Maghiar, Ph.D. Gustavo O. Maldonado, Ph.D. PE Soonkie Nam, Ph.D. Shakil Ahmed Md. Mehrab Hossain & Charles Lawal		8. Performing Organization Report No.: 22-17	
9. Performing Organization Name and Address: Georgia Southern University Department of Civil Engineering & Construction 201 COBA Drive, BLDG 232, Statesboro, GA 30458 Phone: 912-478-1894 Email: mmaghiar@georgiasouthern.edu		10. Work Unit No.: N/A	
		11. Contract or Grant No.: PI#0019323	
12. Sponsoring Agency Name and Address: Georgia Department of Transportation (SPR) Office of Performance-based Management and Research 600 West Peachtree St. NW Atlanta, GA 30308		13. Type of Report and Period Covered: Final; April 2023 – October 2025	
		14. Sponsoring Agency Code: N/A	
15. Supplementary Notes: Prepared in cooperation with the U.S. Department of Transportation, Federal Highway Administration.			
16. Abstract: This volume is the second in a series. The other volume in the series is FHWA-GA-25-2217 Volume I. As Mechanically Stabilized Earth and Modular Block retaining walls age within Georgia's highway infrastructure, their stability and safety are critical concerns. Currently, unlike bridges, these retaining walls lack standardized inspection protocols, and studies show that, nationwide, a significant number of them exhibit signs of distress such as cracking or bulging. GDOT's Research Project RP 22-17 addresses this by exploring nondestructive, noncontact inspection using advanced sensing technologies. The project specifically evaluates terrestrial LiDAR, Close-Range Photogrammetry (CRP), and Infrared Thermography (IRT), using a robotic total station (RTS) for reference. Key findings indicate that terrestrial LiDAR, particularly Target-Based LiDAR, with field-acquired targets at high-resolution, is soundly effective in detecting small, near-centimeter displacements. Visual-Alignment LiDAR also showed comparable accuracy with less field work, but requiring highly overlapped scans and more post-processing. The goal is to proactively detect issues like structural movement and deterioration, which can extend the service life of those walls, enhance safety, and reduce costly repairs. The research aims to equip GDOT with a data-informed strategy for monitoring critical displacements in these essential infrastructure components.			
17. Keywords: MSE and MB walls, Inspection Protocol, Terrestrial LiDAR, Close-Range Photogrammetry, Infrared Thermography		18. Distribution Statement: No Restriction	
19. Security Classification (of this report): Unclassified	20. Security Classification (of this page): Unclassified	21. No. of Pages: 399	22. Price: Free

GDOT Research Project 22-17

Final Report

NONDESTRUCTIVE/NONCONTACT INSPECTION PROTOCOLS AND  
TECHNOLOGIES FOR AGING MECHANICALLY STABILIZED EARTH AND  
MODULAR BLOCK RETAINING

VOLUME II

By

Marcel Maghiar

Professor, Department of Civil Engineering & Construction

Gustavo O. Maldonado

Professor, Department of Civil Engineering & Construction

Soonkie Nam

Associate Professor, Department of Civil Engineering & Construction

Shakil Ahmed,

Mehrab Hossain and Charles Lawal

Graduate Research Assistants, Department of Civil Engineering & Construction

Georgia Southern University Research and Services Foundation

Contract with

Georgia Department of Transportation

In cooperation with

U.S. Department of Transportation,  
Federal Highway Administration

October 2025

The contents of this report reflect the views of the authors, who are responsible for the facts and accuracy of the data presented herein. The contents do not necessarily reflect the official views or policies of the Georgia Department of Transportation or the Federal Highway Administration. This report does not constitute a standard, specification, or regulation.

SI* (MODERN METRIC) CONVERSION FACTORS				
APPROXIMATE CONVERSIONS TO SI UNITS				
Symbol	When You Know	Multiply By	To Find	Symbol
<b>LENGTH</b>				
in	inches	25.4	millimeters	mm
ft	feet	0.305	meters	m
yd	yards	0.914	meters	m
mi	miles	1.61	kilometers	km
<b>AREA</b>				
in <sup>2</sup>	square inches	645.2	square millimeters	mm <sup>2</sup>
ft <sup>2</sup>	square feet	0.093	square meters	m <sup>2</sup>
yd <sup>2</sup>	square yard	0.836	square meters	m <sup>2</sup>
ac	acres	0.405	hectares	ha
mi <sup>2</sup>	square miles	2.59	square kilometers	km <sup>2</sup>
<b>VOLUME</b>				
fl oz	fluid ounces	29.57	milliliters	mL
gal	gallons	3.785	liters	L
ft <sup>3</sup>	cubic feet	0.028	cubic meters	m <sup>3</sup>
yd <sup>3</sup>	cubic yards	0.765	cubic meters	m <sup>3</sup>
NOTE: volumes greater than 1000 L shall be shown in m <sup>3</sup>				
<b>MASS</b>				
oz	ounces	28.35	grams	g
lb	pounds	0.454	kilograms	kg
T	short tons (2000 lb)	0.907	megagrams (or "metric ton")	Mg (or "t")
<b>TEMPERATURE (exact degrees)</b>				
°F	Fahrenheit	5 (F-32)/9 or (F-32)/1.8	Celsius	°C
<b>ILLUMINATION</b>				
fc	foot-candles	10.76	lux	lx
fl	foot-Lamberts	3.426	candela/m <sup>2</sup>	cd/m <sup>2</sup>
<b>FORCE and PRESSURE or STRESS</b>				
lbf	poundforce	4.45	newtons	N
lbf/in <sup>2</sup>	poundforce per square inch	6.89	kilopascals	kPa
APPROXIMATE CONVERSIONS FROM SI UNITS				
Symbol	When You Know	Multiply By	To Find	Symbol
<b>LENGTH</b>				
mm	millimeters	0.039	inches	in
m	meters	3.28	feet	ft
m	meters	1.09	yards	yd
km	kilometers	0.621	miles	mi
<b>AREA</b>				
mm <sup>2</sup>	square millimeters	0.0016	square inches	in <sup>2</sup>
m <sup>2</sup>	square meters	10.764	square feet	ft <sup>2</sup>
m <sup>2</sup>	square meters	1.195	square yards	yd <sup>2</sup>
ha	hectares	2.47	acres	ac
km <sup>2</sup>	square kilometers	0.386	square miles	mi <sup>2</sup>
<b>VOLUME</b>				
mL	milliliters	0.034	fluid ounces	fl oz
L	liters	0.264	gallons	gal
m <sup>3</sup>	cubic meters	35.314	cubic feet	ft <sup>3</sup>
m <sup>3</sup>	cubic meters	1.307	cubic yards	yd <sup>3</sup>
<b>MASS</b>				
g	grams	0.035	ounces	oz
kg	kilograms	2.202	pounds	lb
Mg (or "t")	megagrams (or "metric ton")	1.103	short tons (2000 lb)	T
<b>TEMPERATURE (exact degrees)</b>				
°C	Celsius	1.8C+32	Fahrenheit	°F
<b>ILLUMINATION</b>				
lx	lux	0.0929	foot-candles	fc
cd/m <sup>2</sup>	candela/m <sup>2</sup>	0.2919	foot-Lamberts	fl
<b>FORCE and PRESSURE or STRESS</b>				
N	newtons	0.225	poundforce	lbf
kPa	kilopascals	0.145	poundforce per square inch	lbf/in <sup>2</sup>

\* SI is the symbol for the International System of Units. Appropriate rounding should be made to comply with Section 4 of ASTM E380.  
(Revised March 2003)



## TABLE OF CONTENTS

EXECUTIVE SUMMARY.....	351
CHAPTER 11. INFRARED THERMOGRAPHY ANALYSIS.....	357
INTRODUCTION .....	357
RESEARCH METHODOLOGY .....	358
Area of Study.....	358
Method and Material.....	359
Flow Chart for IRT Methodology .....	360
RESULTS AND DISCUSSION - CROSSGATE RD .....	362
West to East MSE Wall – Crossgate .....	362
<i>Polygon Analysis on Panels</i> .....	363
<i>Isotherm Analysis:</i> .....	365
East to West MSE Wall – Crossgate: .....	367
<i>Polygon Analysis on Panels</i> .....	369
Conclusion For Crossgate .....	371
RESULTS AND DISCUSSION - OLD RIVER ROAD .....	372
West to East Wall - Old River Road .....	373
<i>Polygon Analysis on Panels</i> .....	374
<i>Isotherm Analysis:</i> .....	375
East to West Wall - Old River Road .....	377
<i>Polygon Analysis on Panels</i> .....	379
<i>Isotherm Analysis</i> .....	380
Conclusion on Old River Road .....	382
RESULTS AND DISCUSSION - KING GEORGE BOULEVARD .....	382
West to East Wall - King George.....	384
<i>Polygon Analysis (Panel-Specific Areas)</i> .....	385
<i>Conclusion for West to East</i> .....	387
East to West Wall - King George.....	387
<i>Polygon Analysis (Panel-Specific Areas)</i> .....	389
<i>Conclusion for East to West</i> .....	390
THERMAL PERFORMANCE ANALYSIS OF MSE WALLS OF SELECTED SITES.....	391
Crossgate MSE Wall (Least Reliable).....	391

Old River Road MSE Wall (Moderate Reliability) .....	391
King George Boulevard MSE Wall (Superior Reliability) .....	392
Comparison with Previous Studies.....	394
Distinguishing Defects from Joints & Visual Validation.....	395
Conclusion .....	395
Recommendations for the Walls and for Further Studies .....	396
<b>CHAPTER 12. CONCLUSIONS AND RECOMMENDATIONS.....</b>	<b>398</b>
<b>DESCRIPTION OF THE ANALYZED MEASURING/MODELING TECHNIQUES.....</b>	<b>398</b>
Measuring/Modeling Techniques Studied at the CW .....	399
Measuring/Modeling Techniques Studied at the B1-Crossgate .....	401
Measuring/Modeling Techniques Studied at B2-Old River.....	403
Measuring/Modeling Techniques Studied at B3-Sandersville.....	404
Measuring/Modeling Techniques Studied at B4-King George.....	405
<b>CONCLUSIONS INFERRED FROM WORK AT THE CW SITE.....</b>	<b>406</b>
Inferences regarding the ability to capture small displacements at CW .....	406
Inferences regarding the relative accuracy of measurements at the CW.....	410
Inferences on the noise level inherent to different techniques at the CW site.....	413
<b>CONCLUSIONS INFERRED FROM WORK AT THE B1-CROSSGATE SITE .....</b>	<b>415</b>
Inferences regarding the relative accuracy of measurements at B1-Crossgate .....	415
<b>CONCLUSIONS INFERRED FROM WORK AT THE B2-OLD RIVER SITE .....</b>	<b>418</b>
Inferences Regarding Repeatability of Measurements at B2-Old River .....	418
Inferences Regarding the Relative Accuracy of Measurements at B2-Old River ..	420
Inferences Regarding the Noise Associated with RTS, TB, & VA at B2-Old River:.....	422
<b>CONCLUSIONS INFERRED FROM WORK AT THE B3-SANDERSVILLE SITE...423</b>	
Inferences Regarding the Relative Accuracy of Measurements at B3-Sandersville.....	423
Inferences comparison of Photogrammetry vs TB LiDAR at B3-Sandersville.....	425
<b>CONCLUSIONS INFERRED FROM WORK AT THE B4-KING GEORGE SITE.....426</b>	
Inferences regarding the relative accuracy of measurements at B4-King George .	426

OVERALL CONCLUSIONS .....	429
FINAL REMARKS FUTURE STUDIES AND RECOMMENDATIONS .....	434
ADVICE ON WORKFORCE DEVELOPMENT .....	436
FUTURE RESEARCH.....	437
CHAPTER 13. NARRATED INSPECTION PROTOCOL: PROPOSED FRAMEWORK.....	441
PART A: CLOSED TRAVERSE – LOCAL SYSTEM OF REFERENCE .....	446
PART B: LASER SCANNING .....	450
Scanner, Strong Tripod, and Software .....	450
Planning the Scanning Work .....	454
Scanning at each station .....	455
PART C: ACQUISITION OF IMAGES FOR SUPPLEMENTARY ANALYSIS.....	456
PART D: LiDAR POSTPROCESSING .....	458
Noise Removal .....	459
Recommended alternative registration approaches .....	460
Georeferencing .....	462
PART E: OPTIONAL PHOTOGRAMMETRY POSTPROCESSING.....	463
PART F: LiDAR COMPARISON AMONG EPOCHS VIA CLOUDCOMPARE .....	464
PART G: MAINTENANCE AND REHABILITATION DECISIONS .....	466
CHAPTER 14. GDOT TECHNOLOGIES, RATING SYSTEM, AND GAM .....	468
CURRENT GDOT RESOURCES, GAPS, AND RECOMMENDATIONS .....	468
Assessment and Potential Leverage of Existing GDOT Equipment and Software.....	468
Identified Gaps in Data Workflow .....	472
Recommended Specifications for a Collection Program at GDOT .....	473
CONDITION RATING SYSTEM .....	475
GAM APPLICATION AND DATABASE MODEL .....	478
Recommendations for GAM Application and Database Model Updates .....	478

Data Model Expansion for New Data Types .....	478
Application Tools for Data Visualization and Analysis.....	479
Data-Driven Condition Assessment.....	480
APPENDIX A. TRAVERSE CALCULATION DETAILS DATA .....	481
APPENDIX B. SUPPLIMENTARY DATA OF THERMOGRAPHY ANALYSIS.....	492
APPENDIX C1. LEICA SCANSTATION OPERATING PROTOCOL .....	528
APPENDIX C2. NOISE REMOVAL PROTOCOLS IN CYCLONE CORE .....	548
APPENDIX C3. VISUAL-ALIGNMENT REGISTRATION ON CYCLONE CORE .....	557
APPENDIX C4. TARGET-BASED REGISTRATION IN CYCLONE CORE.....	577
APPENDIX C5. GEOREFERENCING IN CYCLONE CORE.....	580
APPENDIX C6. ACQUIRE TARGETS FROM SOFTWARE (CYCLONE CORE).....	601
APPENDIX C7. METASHAPE PROTOCOL .....	604
APPENDIX C8. CLOUDCOMPARE PROTOCOL.....	626
APPENDIX C9. PIX4D MAPPER PROTOCOL .....	645
APPENDIX C10. DRONEDEPLOY PROTOCOL.....	682
APPENDIX C11. FLIR RESEARCH STUDIO SOFTWARE PROTOCOL .....	709
APPENDIX D. MSE WALL INSPECTION FORMS.....	716
ACKNOWLEDGMENT .....	737
REFERENCES.....	739

## LIST OF FIGURES

Figure 136. Flowchart. IRT systematic flowchart for methodology .....	360
Figure 137. Photo. Thermographic and Digital Image of the West to East MSE Wall – Crossgate.....	362
Figure 138. Graph. Images temperature plot – West to East – Crossgate .....	364
Figure 139. Graph. Standard deviation plot of images – West to East – Crossgate .....	365
Figure 140. Graph. Isotherm 1 temperature plot – West to East Crossgate.....	366
Figure 141. Graph. Isotherm 2 temperature plot – West to East Crossgate.....	367
Figure 142. Graph. Thermographic and Digital Image of the East to West Wall – Crossgate .....	367
Figure 143. Graph. Images temperature plot – East to West Crossgate .....	369
Figure 144. Graph. Standard deviation plot of images – East to West Crossgate .....	370
Figure 145. Graph. Isotherm 1 temperature plot – East to West Crossgate.....	370
Figure 146. Graph. Isotherm 2 temperature plot – East to West Crossgate.....	371
Figure 147. Graph. Standard deviation of Isotherms 1 and 2 – East to West Crossgate .....	371
Figure 148. Photo. Thermographic and Digital Image of the West to East Wall – Old River Road .....	372
Figure 149. Graph. Images temperature plot – West to East Old River Road.....	374
Figure 150. Graph. Standard deviation plot of images – West to East Old River Road.....	375
Figure 151. Graph. Isotherm 1 temperature plot – West to East Old River Road.....	376
Figure 152. Graph. Isotherm 2 temperature plot – West to East Old River Road.....	376
Figure 153. Graph. Standard deviation of Isotherms 1 and 2 – West to East Old River Road .....	377
Figure 154. Photo. Thermographic and Digital Image of the East to West Wall – Old River .....	377
Figure 155. Graph. Images temperature plot – East to West Old River Road.....	379
Figure 156. Graph. Standard deviation plot of images – East to West Old River Road.....	380
Figure 157. Graph. Isotherm 1 temperature plot –East to West Old River Road .....	380
Figure 158. Graph. Isotherm 2 temperature plot – East to West Old River Road .....	381
Figure 159. Graph. Standard deviation of Isotherms 1 and 2 – Old River Road.....	381
Figure 160. Photo. Thermographic and Digital Image of the West to East Wall – King George .....	383
Figure 161. Graph. Images temperature plot – West to East King Goerge .....	385
Figure 162. Graph. Standard deviation plot of images – West to East King Goerge .....	385
Figure 163. Graph. Polygon 1 temperature plot – West to East King George .....	386
Figure 164. Graph. Standard deviation of Polygon 1 – West to East Crossgate .....	386
Figure 165. Photo. Thermographic and Digital Image of the East to West Wall – King George.....	387
Figure 166. Graph. Images temperature plot – East to West King George .....	389
Figure 167. Graph. Standard deviation of Polygon 1 – East to West Crossgate .....	389
Figure 168. Graph. Polygon 1 temperature plot – East to West King George .....	390
Figure 169. Graph. Standard deviation of Polygon 1 – East to West King George .....	390
Figure 170. Photos. Typical targets and pole.....	452
Figure 171. Photo. Eight scanning stations (scans) completed at a bridge near Sandersville, GA .....	454

## LIST OF TABLES

Table 54. West to East MSE Wall – Crossgate (APPENDIX B) .....	364
Table 55. East to West MSE Wall – Crossgate (APPENDIX B) .....	368
Table 56. West to East MSE Wall – Old River Road (APPENDIX B).....	373
Table 57. East to West MSE Wall – Old River Road (APPENDIX B).....	378
Table 58. West to East MSE Wall – King George (APPENDIX B) .....	383
Table 59. East to West MSE Wall – King George (APPENDIX B) .....	387
Table 60. Defects and Anomalies in Crossgate .....	392
Table 61. Defects and Anomalies in Old River .....	393
Table 62. Defects and Anomalies in King George .....	394
Table 63. Recommended IRT inspection intervals for the MSE walls.....	396
Table 64. Final Estimated Noise Levels .....	433
Table 65. Summary of Narrated Protocol for Inspection of MSE/MB Walls.....	443
Table 66. National Overview of Retaining Wall Inspection Frequencies and Condition Rating Systems .....	476
Table 67. Proposed GDOT MSE/MBW Condition Rating Categories (Based on Terrestrial LiDAR – TB & VA Methods) .....	477

## EXECUTIVE SUMMARY

Mechanically Stabilized Earth (MSE) and Modular Block (MB) retaining walls are becoming ubiquitous and significant components of Georgia’s highway infrastructure. As these structures age, ensuring their continued stability and safety becomes increasingly critical. Unlike bridges, however, retaining walls currently lack broadly adopted standardized inspection protocols. Across the U.S., over 160 million square feet of retaining walls are constructed annually, yet studies show a concerning number of walls exhibit signs of distress—such as cracking, bulging, leaning, settling, spalling, growth of vegetation or roots, loss of backfill, etc. In response to this growing concern, GDOT is pursuing a practical, data-informed strategy for monitoring and maintaining these structures. To support this effort, GDOT launched Research Project RP 22-17 to develop a nondestructive, noncontact inspection framework using advanced sensing technologies. This study evaluated the capabilities of terrestrial LiDAR, Close-Range Photogrammetry (CRP), and Infrared Thermography (IRT), with an accurate robotic total station (RTS) serving as the reference instrument. These tools were assessed for their effectiveness in detecting structural movement and early signs of deterioration, enabling a more proactive approach to wall maintenance. Timely identification of these issues can help extend the service life of the walls, enhance safety, and reduce the risk of costly repairs.

### **Key Findings:**

- **Terrestrial LiDAR Accuracy and Reliability:** Terrestrial LiDAR techniques particularly Target-Based (TB) LiDAR—consistently outperformed Close-Range Photogrammetry (CRP) in detecting small displacements. At the Control Wall (CW) site, TB LiDAR, using high-

resolution field-acquired targets, detected displacements as small as 3 mm. Visual-Alignment (VA) LiDAR delivered comparable accuracy with less field effort, though it required more extensive postprocessing. Nonetheless, VA LiDAR requires highly overlapped scans registered in a close-neighboring pattern, preferably closing a registration loop. An alternative TB LiDAR method, which involved scanning targets in the field but acquiring them via software, offered slightly lower accuracy than the other two approaches but struck a balance by reducing both fieldwork and postprocessing demands.

- **CRP Performance:** Among CRP methods, models created using Agisoft Metashape and DroneDeploy (in this case with auxiliary elevated control points), at the Control Wall, presented estimated noise levels of ~18.5 mm, while the noise for TB and VA LiDAR models was ~7 mm. Nevertheless, multi-epoch comparisons of full CRP models may reveal artifacts—such as surface warping and false displacements, making CRP less reliable for high-precision displacement tracking.
- **Determination of Noise Levels from Multiple Estimations:** Noise thresholds were estimated through point-position and distance-based comparisons (using the accurate RTS instrument) and through full point-cloud comparisons (using the CloudCompare software via its C2C and M3C2 schemes). Measurements completed at the CW and B2-Old River sites resulted in the following estimation of the associated noise levels. TB LiDAR (9.1 mm), VA LiDAR (11.4 mm), and the 1-second Robotic Total Station (9.8 mm) exhibited lower noise levels compared to CRP models, which reached up to 18.4 mm.



These results indicate that LiDAR methods can confidently detect displacements greater than ½ inch (12.5 mm).

- **Control Wall Testing:** Simulated displacements of 3–34 mm at the CW site demonstrated that LiDAR techniques along with CloudCompare could reliably capture fine-scale changes across entire wall surfaces. TB and VA LiDAR showed minimal error spread, whereas photogrammetric models presented larger errors and misidentified static regions as displaced.
- **Infrared Thermography:** IRT was used as a nondestructive method to assess thermal behavior and detect near-surface anomalies in MSE retaining walls. Inspections at Crossgate, Old River Road, and King George Blvd. sites revealed no significant defects affecting structural integrity.
- **Integration of Photographic Data in Wall Inspections:** This study highlights the value of combining photographic imagery with terrestrial LiDAR for retaining wall inspections. LiDAR provides precise spatial data, while photographs capture surface conditions such as cracks, spalling, efflorescence, erosion, and vegetation. Together, they enable more reliable assessments. Though photogrammetric modeling is not essential when LiDAR is used, overlapping images with reference markers can be processed in Agisoft Metashape if needed. Photographs should be collected during each LiDAR epoch via UAVs or handheld cameras to maintain consistency across inspections.

## Recommendations:

- **Preferred Modeling Techniques:** For monitoring near-centimeter-level wall displacements, TB LiDAR (with field-acquired targets) is recommended, followed by VA LiDAR (with highly overlapped scans registered in a close-neighboring pattern, preferably closing a loop) and TB LiDAR (with software-acquired targets). All mentioned methods support effective displacement detection via cloud comparison using the CloudCompare software. CRP is suitable for visual documentation but should not be solely relied upon for structural displacement monitoring.
- Photographic imagery should be routinely integrated into retaining wall inspections to capture surface-level indicators such as cracking, efflorescence, and vegetation intrusion that may not be fully visible in LiDAR data.
- **Protocol Development:** To ensure reliable displacement monitoring, it is recommended that GDOT establish and adopt standardized protocols centered on the generation and comparison of multi-epoch LiDAR models, georeferenced to common GCPs, established through well-balanced closed traverses. A summarized, narrated protocol has been developed to guide this process, supported by detailed subprotocols (included in the report appendices) that provide step-by-step instructions for using the relevant instruments and software tools.
- **Workforce Needs:** Effective training is essential for equipping personnel with the skills required to carry out the proposed inspection activities. Key competencies include establishing accurate GCPs, conducting field scans, registering multiple scans into a unified

model, and georeferencing the final product within a consistent local coordinate system for multi-epoch comparison using CloudCompare. Georgia Southern University currently offers an *Introduction to Terrestrial LiDAR* course that covers many of these core topics. Adoption of these skills will improve data accuracy, reduce subjectivity in inspections, and support better infrastructure lifecycle management. As an optional enhancement, close-range photogrammetric modeling can be included in the training to broaden the technical capabilities of inspection personnel.

- **Future Research Directions:** Opportunities include:
  - Comprehensive long-term monitoring and documentation of wall displacements.
  - Integrating AI for automated anomaly detection
  - Real-time UAV monitoring systems
  - IoT sensor integration for surface and subsurface health
  - Evaluating cost-effectiveness vs traditional inspections
  - Adapting and adopting low-cost or open-source alternatives for wider use

## **Conclusion:**

This research confirms that advanced remote sensing technologies—particularly terrestrial LiDAR methods supported by accurate reference networks and cloud-based analysis tools—offer a reliable, nondestructive framework for monitoring MSE and MB retaining walls. By detecting subtle displacements and surface-level anomalies, these methods enable a shift from subjective visual inspections to objective, data-driven asset management. Among the evaluated techniques, Target-Based and Visual-Alignment LiDAR approaches demonstrated superior precision in displacement detection. Infrared Thermography, while less effective for identifying structural

defects, proved useful as a supplementary tool for detecting near-surface anomalies under favorable conditions. The integration of LiDAR data with photographic imagery further enhances inspection quality by capturing both geometric and visual indicators of deterioration. With standardized protocols and targeted workforce training, GDOT should be well-positioned to proactively manage wall infrastructure, extend service life, and potentially reduce maintenance costs. Continued research into long-term monitoring, AI-driven anomaly detection, and real-time UAV systems will further strengthen this inspection framework.

## **CHAPTER 11. INFRARED THERMOGRAPHY ANALYSIS**

### **INTRODUCTION**

The escalating deterioration of civil engineering structures, particularly reinforced concrete assets like bridges and MSE walls, poses significant economic, social, and environmental challenges. Traditional inspection methods often fall short in detecting critical subsurface defects such as delamination, voids, and cracks, which are prevalent in these vital infrastructure components. To overcome these limitations, IR (IRT) has emerged as a highly effective NDT technique. IRT operates on the principle that damaged or deteriorated areas exhibit distinct heat transfer characteristics, allowing thermal cameras to identify temperature variations indicative of subsurface anomalies (Hiasa et al., 2016; Maldague, 2001). Recent technological advancements, including the integration of machine learning and artificial intelligence, have further enhanced IRT's capabilities for automated and precise defect detection and analysis in complex environments (Ibrahim et al., 2024; Shrestha et al., 2025). This makes IRT an indispensable tool for the proactive assessment and long-term resilience of critical civil engineering assets.

IRT has been extensively applied across various structural inspection contexts, including concrete retaining walls, MSE walls, and bridge decks. For concrete retaining walls, studies by Zhao and Chen (2013) demonstrate IRT's ability to detect surface cracks, voids, and delamination, while Huang et al., (2019) developed predictive maintenance strategies for MSE walls using thermal imaging. On bridge decks, IRT is crucial for identifying delamination's and other defects (Sirca and Adeli, 2018; Titman, 2001), with recent advancements in integrating

neural networks for rapid and automated inspections (Debees & Catbas, 2025; Jin & Zou, 2021). Beyond specific structures, IRT proves effective for general concrete defect detection, capable of characterizing surface crack depth (Aggelis et al., 2011). The integration of IRT with advanced computational methods, such as deep learning models, significantly enhances its accuracy and efficiency for automated damage detection (Aljagoub & Cheng, 2025). Furthermore, combining IRT with other NDT techniques like Ground Penetrating Radar (GPR) and Terrestrial Laser Scanning TLS provides more comprehensive and reliable assessments of structural conditions (Garrido et al., 2018), solidifying IRT's role as a cornerstone of modern SHM.

## **RESEARCH METHODOLOGY**

### **Area of Study**

This research applied IR(IRT) to inspect MSE and Modular Block (MB) retaining walls supporting bridge infrastructure in Georgia. Three distinct bridge locations were selected as case studies: Crossgate (Chatham County), Old River Road (Interstate-16, Jim Gillis Historic Savannah Parkway), and King George Boulevard (Georgetown, Chatham County). These sites were chosen to represent diverse characteristics in MSE wall construction, age, traffic volume, and environmental exposure, enabling a comprehensive comparative analysis. The Crossgate retaining wall, constructed in 2015, supports the Jimmy Deloach Bridge, handling significant daily traffic. Rated in good condition by the NBI, it undergoes biennial inspections. The Old River Road Bridge on I-16, with its MSE walls built between 2018 and 2021, is a critical freight corridor. The King George Boulevard Bridge, constructed in 2016, serves a growing

metropolitan area and provided a geometrically uniform MSE wall for analysis. This multi-site approach ensured robust and generalizable research findings.

## **Method and Material**

A detailed field investigation collected thermal images of MSE walls under natural conditions, capturing both daytime heating and nighttime cooling cycles. Surveys followed strict environmental criteria: at least a 10 °C surface temperature difference during the survey, a 5 °C difference over the previous 24 hours, and stable air temperatures within  $\pm 3$  °C during and  $\pm 10$  °C before the survey. Direct sunlight and precipitation were avoided. Image metadata—dates, times, temperature, humidity, wind speed, and camera distance (20–22 ft for Crossgate/Old River and 43–65 ft for King George)—were recorded. Emissivity values were set at 0.94 for rough and 0.95 for smooth concrete. The FLIR T420Bx thermal camera was used, featuring an 80×60 FPA detector, 100 mK thermal sensitivity, fixed focus, 7.5–14  $\mu\text{m}$  LWIR spectral range, and 9 Hz refresh rate. Its dual-sensor capability captured thermal and optical images simultaneously, aiding data correlation. Thermal data were processed in FLIR Research Studio (v2024.03.01) for analysis Image Upload and Palette Selection: Enhancing visual contrast.

- Color Palette Enhancement: Fine-tuning for anomaly visibility.
- Plot Tool: Generating horizontal/vertical temperature profiles (Min, Max, Mean).
- Region of Interest (RoI) Analysis: Defining specific areas (e.g., using polygons) to mask irrelevant features and focus on concrete panels. Statistical parameters (Max, Min, Mean, Standard Deviation) within RoIs quantified thermal uniformity.
- Image Export: Saving images and raw temperature data for further analysis.

- Isotherm Operation: Segmenting images into distinct temperature ranges (Isotherm 1 for hotter, Isotherm 2 for cooler) to identify thermal bridging or localized heat accumulation/dissipation.

The procedures for thermal imaging using the FLIR T420BX camera are detailed in APPENDIX C10, which outlines the image acquisition and processing workflow. Subsequent visualization and analysis of the thermal data using FLIR Research Studio are presented in APPENDIX C11.

### Flow Chart for IRT Methodology

The IRT methodology followed a systematic flowchart (showed in Figure 136):

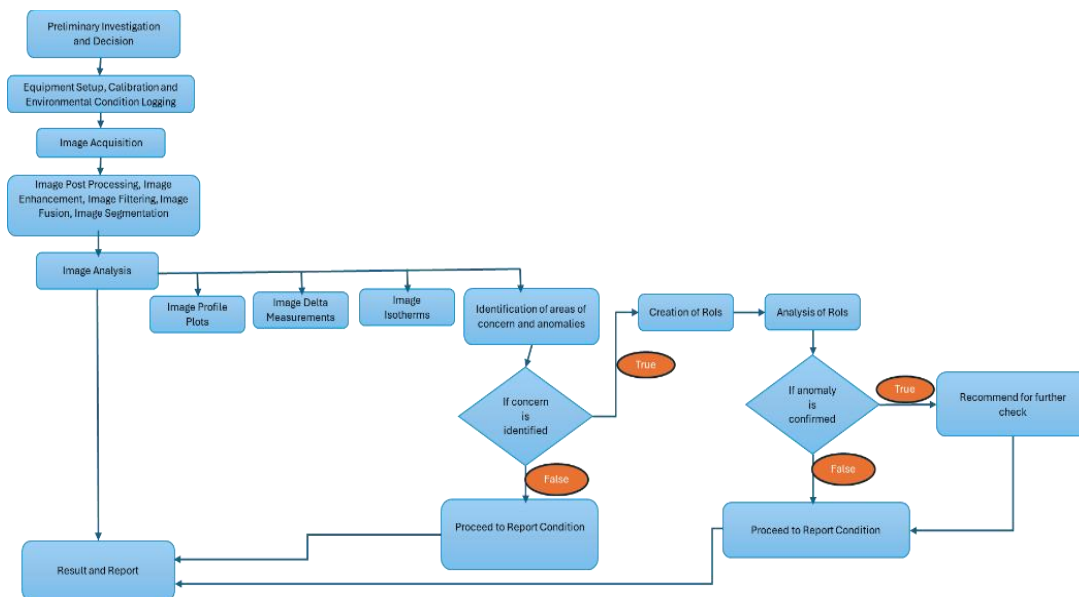


**Figure 136. Flowchart. IRT systematic flowchart for methodology**

The process commences with the Preliminary Investigation and Decision, where sites are evaluated for inspection based on visual assessments, structural importance, or historical performance data. This initial step ensures a targeted and justified application of thermal imaging techniques. Subsequently, the Equipment Setup, Calibration and Environmental Condition



Logging phase involves the preparation and calibration of thermal imaging devices, along with the documentation of critical environmental parameters such as ambient temperature, humidity, and wind speed. These factors are essential for maintaining consistency and reliability in thermal data acquisition across various field locations. The Image Acquisition stage follows, during which thermal images are captured under controlled conditions to reflect the in-situ behavior of the retaining walls. These images are then subjected to Image Post Processing, Image Enhancement, Image Filtering, Image Fusion, Image Segmentation, a comprehensive step encompassing multiple digital processing techniques aimed at improving image clarity, isolating relevant thermal features, and integrating multiple datasets to enhance interpretability. Within the Image Analysis phase, advanced diagnostic tools are utilized, including Image Profile Plots, Image Delta Measurements, and Image Isotherms. These tools facilitate the extraction of thermal gradients, temperature differentials, and contour patterns that are critical for identifying irregularities in heat distribution. The subsequent step, Identification of Areas of Concern and Anomalies, involves the delineation of zones exhibiting abnormal thermal behavior, potentially indicating structural distress or material inconsistencies. If no concern is identified, the workflow advances to Proceed to Report Condition. However, in instances where anomalies are suspected, Creation of RoIs enables focused analysis on specific segments of the structure. These regions are then scrutinized in the Analysis of RoIs step to determine the validity and significance of the detected anomalies. Should the anomalies be confirmed, the process recommends Recommend for Further Check; otherwise, it continues to Proceed to Report Condition. The methodology culminates in the Result and Report phase, where all findings are compiled into a comprehensive technical report. This structured approach ensures a thorough, repeatable, and scientifically

grounded methodology for utilizing IRT in the condition assessment of aging MSE retaining walls, facilitating data-driven decisions regarding their maintenance and rehabilitation.

## RESULTS AND DISCUSSION - CROSSGATE RD

The first site discussed in the results section is the Crossgate MSE Wall. The analysis of this wall is presented in two parts: "West to East MSE Wall – Crossgate" (Figure 137) and "East to West MSE Wall – Crossgate" (Figure 148). The Crossgate MSE wall, characterized by its trapezoidal geometry, showed considerable temperature variations, particularly at its ends. These variations were primarily influenced by environmental factors such as vegetation and atmospheric conditions.

### West to East MSE Wall – Crossgate

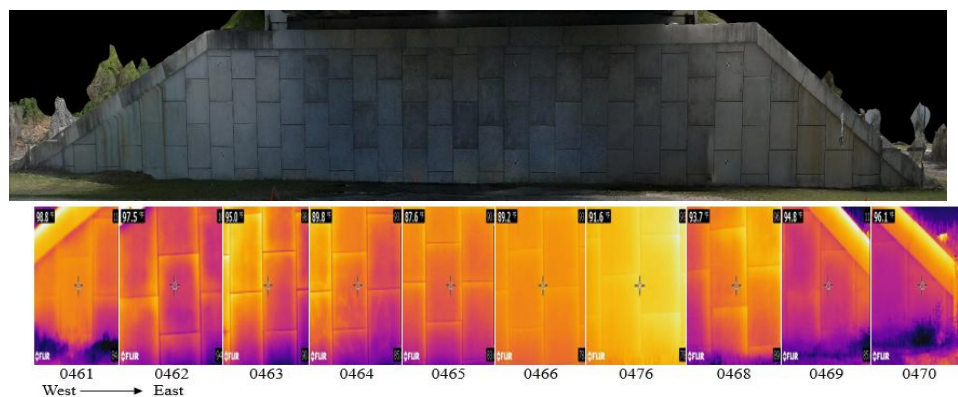


**Figure 137. Photo. Thermographic and Digital Image of the West to East MSE Wall – Crossgate**

Ends of the Wall (Images 0461, 0470): The thermal analysis revealed significant temperature extremes. Table 54 indicated the western end (Image 0461) had a maximum of 115.33°F and a minimum of 83.25°F, a difference of 32.08°F. The eastern end (Image 0470) showed even wider

variations, with a maximum of 122.38°F and a minimum of 83.77°F, a difference of 38.61°F. These extremes were attributed to localized environmental influences.

### ***Polygon Analysis on Panels***

Despite the extreme temperatures at the end, a focused analysis using polygon segmentation on the concrete panel areas revealed no significant anomalies. The maximum temperatures in these specific zones were 100.23°F (Image 0461) and 97.03°F (Image 0470), with minimums around 83.25°F and 85.26°F. Standard deviations (Figure 139) ranged from 1.14 to 3.71, which was deemed reasonable given the presence of vegetation in the lower portions of the wall. The temperature differences in these panel-specific regions (12-18°F) were influenced by vegetation but did not indicate serious defects.

**Table 54. West to East MSE Wall – Crossgate (APPENDIX B)**

West to East Wall - Crossgate												
Images					Isotherm 1				Isotherm 2			
Images	Max [F]	Min [F]	Mean [F]	St. Dv.	Max [F]	Min [F]	Mean [F]	St.Dv .Iso1	Max [F]	Min [F]	Mean [F]	St.Dv. Iso2
Img 0461	115.33	83.25	97.42	4.59								
Img 0462	104.11	93.18	97.78	0.90	104.11	97.00	97.99	0.71	97.00	93.18	96.28	0.65
Img 0463	98.09	90.60	94.87	1.31	98.07	94.00	95.43	0.87	93.99	90.60	93.08	0.73
Img 0464	92.49	85.87	89.78	1.06	92.49	88.91	90.19	0.72	88.90	85.87	88.17	0.53
Img 0465	89.64	84.49	87.68	0.81	89.64	87.00	88.00	0.49	86.99	84.49	86.34	0.46
Img 0466	89.64	84.49	87.68	0.81	89.64	87.00	88.00	0.49	86.99	84.49	86.34	0.46
Img 0467	93.57	87.32	90.90	1.00	93.52	90.00	91.19	0.79	90.00	87.32	89.44	0.52
Img 0468	96.20	88.41	93.64	1.06	96.17	93.01	94.08	0.65	93.00	88.41	92.07	0.74
Img 0469	112.28	83.95	94.77	4.18	98.16	94.00	94.96	0.61	93.99	83.95	90.74	2.16
Img 0470	122.38	83.77	95.82	5.41								

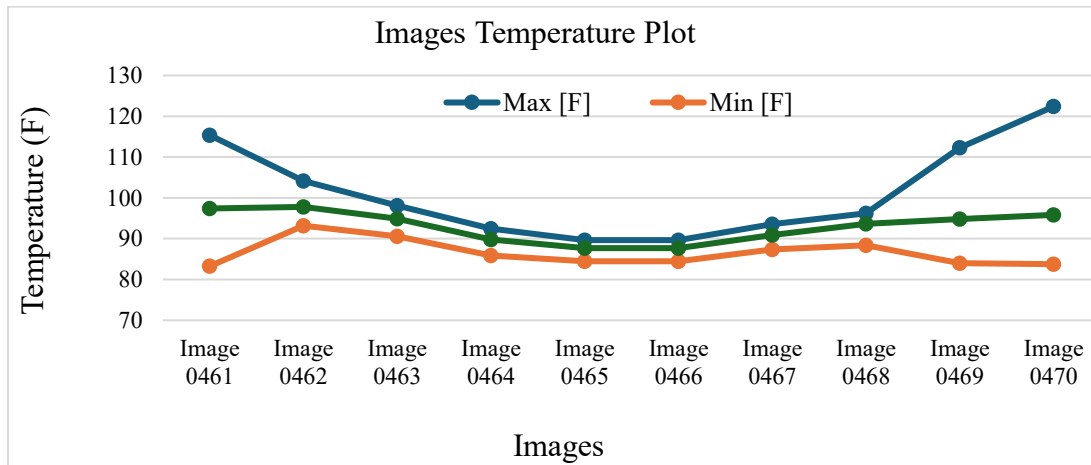


**Figure 138. Graph. Images temperature plot – West to East – Crossgate**

Central Sections: Figure 138 showed the central segments of the wall (e.g., Images 0465, 0466) exhibited remarkable thermal stability. Maximum temperatures were around 89.64°F and minimums around 84.49°F, resulting in narrow ranges of approximately 5°F. The mean

temperatures were consistently around 87.68°F, with low standard deviations (around 0.81), indicating uniform heat distribution and minimal thermal stress on the concrete panels.

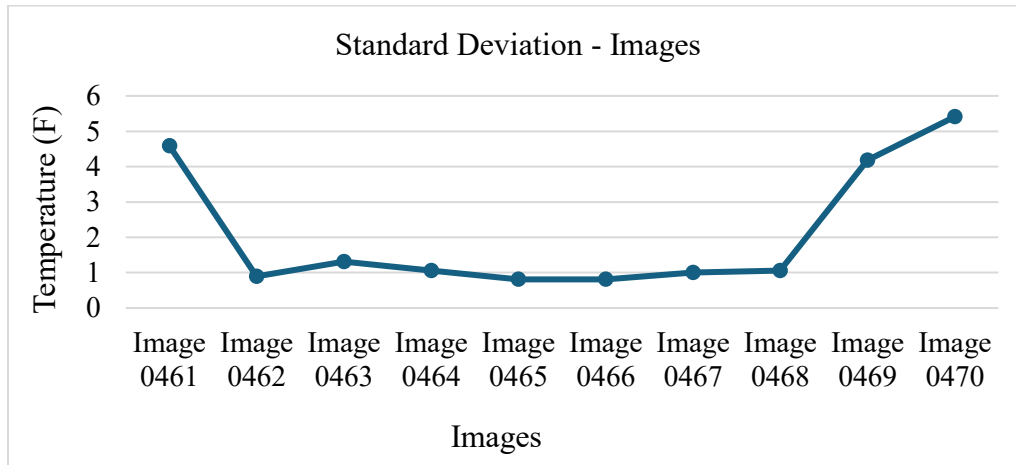


**Figure 139. Graph. Standard deviation plot of images – West to East – Crossgate**

### ***Isotherm Analysis:***

Isotherm 1 (Hotter Upper Regions): Figure 140 showed consistent temperature distributions, with maximums like 104.11°F (Image 0462) and 98.16°F (Image 0469) at the ends of the wall. Temperature differences in these regions were mostly low (2-4°F) except for Image 0462 (7°F) due to coping elements and proximity to the irregular end. Standard deviations were generally low (0.49-0.87), indicating consistent thermal variation.

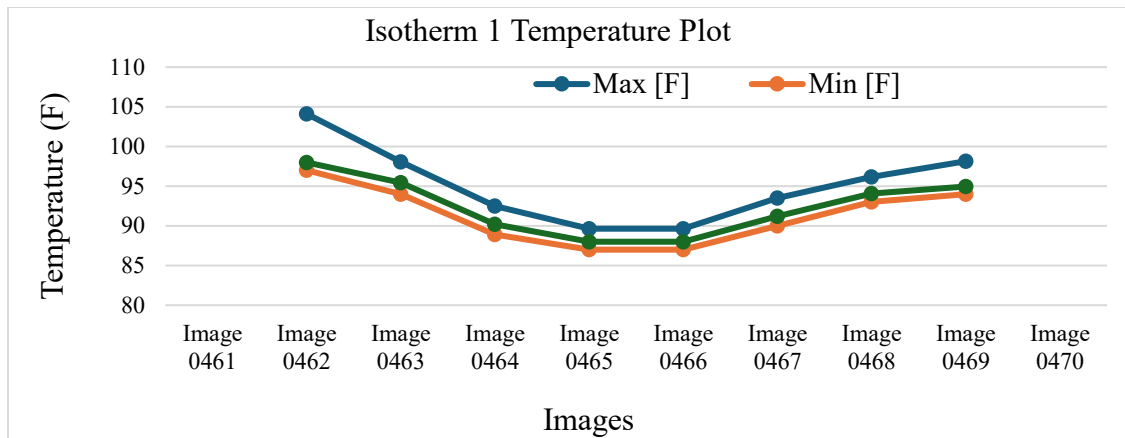


**Figure 140. Graph. Isotherm 1 temperature plot – West to East Crossgate**

Isotherm 2 (Cooler Lower Regions): Figure 141 Displayed stable temperature ranges, with maximums like 97°F (Image 0462) and 94°F (Images 0469, 0463). Temperature differences were small (2-5°F) in central images, but Image 0469 showed a 10°F difference due to vegetation influence at the irregular end. Standard deviations were mostly low (0.46-0.874), with Image 0469 having a higher deviation (2.16) also due to vegetation. These variations were considered minor localized influences rather than significant concerns.

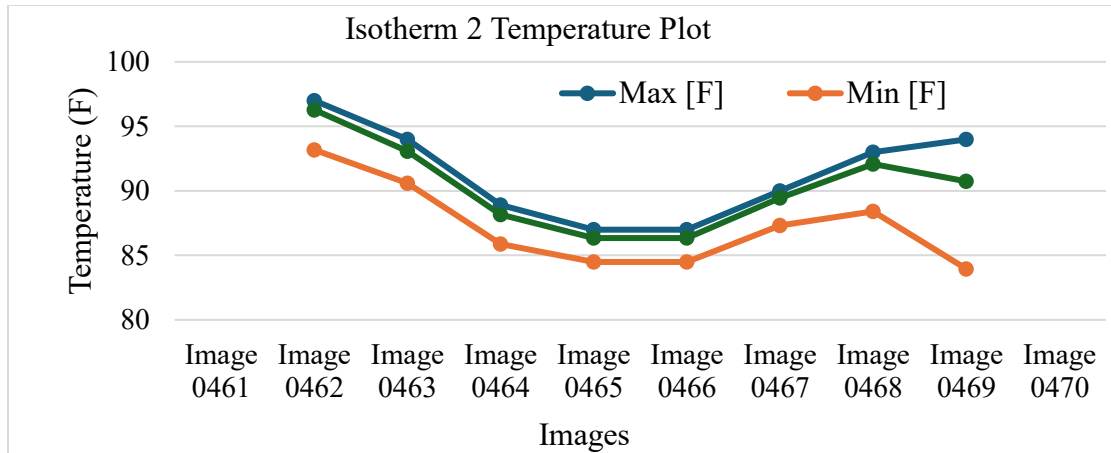


**Figure 141. Graph. Isotherm 2 temperature plot – West to East Crossgate**

**East to West MSE Wall – Crossgate:**



**Figure 142. Graph. Thermographic and Digital Image of the East to West Wall – Crossgate**

**Table 55. East to West MSE Wall – Crossgate (APPENDIX B)**

East to West Wall - Crossgate												
Images					Isotherm 1				Isotherm 2			
Images	Max [F]	Min [F]	Mean [F]	St.Dv. Img	Max [F]	Min [F]	Mean [F]	St.Dv Iso 1	Max[F ]	Min[F ]	Mean[F ]	St.Dv.Iso 2
Img0471	114.00	84.05	97.56	3.67								
Img0472	97.29	90.12	93.64	1.18	97.29	92.81	94.12	0.80	92.80	90.12	91.96	0.66
Img0473	98.42	89.40	93.46	1.40	98.42	93.50	94.51	0.70	93.49	89.40	92.28	1.00
Img0474	93.13	88.73	91.17	0.76	93.13	90.50	91.44	0.54	90.49	88.73	90.02	0.36
Img0475	91.60	86.99	89.58	0.81	91.60	88.96	89.92	0.51	88.95	86.99	88.37	0.43
Img0476	90.57	86.32	88.67	0.70	90.57	88.10	88.95	0.43	88.10	86.32	87.56	0.36
Img0477	91.81	84.80	89.36	1.06	91.81	88.01	89.63	0.74	88.00	84.80	87.19	0.65
Img0478	96.09	87.62	92.58	1.17	96.09	91.01	92.85	0.91	91.00	87.62	90.35	0.55
Img0479	99.03	89.40	95.31	1.47	99.03	94.01	95.85	1.01	94.00	89.40	93.02	0.77
Img0480	98.73	90.26	94.82	1.99								

Ends of the Wall (Images 0471, 0480): This side also showed in Table 55, significant thermal variations. Image 0471 had a maximum of 114°F and a minimum of 84.05°F (29.95°F difference). Image 0480 showed a maximum of 98.73°F and a minimum of 90.26°F (8.47°F difference). Higher standard deviations (3.67 for 0471, 1.99 for 0480) corroborated greater variability at the ends, again linked to geometry and local environmental exposure.



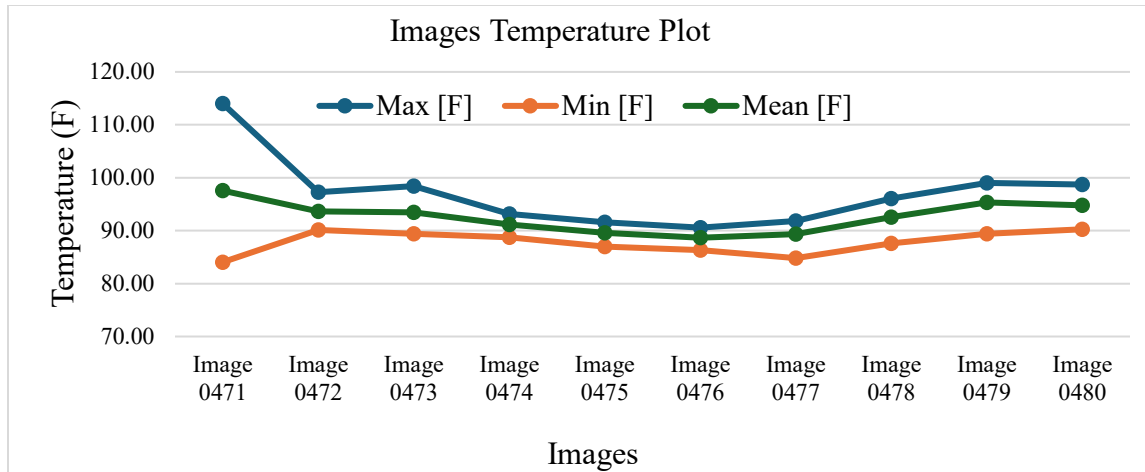


**Figure 143. Graph. Images temperature plot – East to West Crossgate**

### *Polygon Analysis on Panels*

Similar to the West-to-East side, detailed polygon analysis on the concrete panels revealed no defects. From Figure 143 maximum temperatures in these areas were 104.18°F (0471) and 98.72°F (0480), with minimums of 90.48°F and 90.30°F. Temperature differences ranged from 8°F to 14°F, slightly elevated due to vegetation at the lower wall, but standard deviations (1.17-1.49) indicated stable conditions.

Central Sections: The central sections showed consistent thermal behavior with narrow temperature ranges (e.g., Image 0474: 4.4°F difference, 0.76 std dev; Image 0476: 4.25°F difference, 0.7 std dev). The overall standard deviation from Figure 144, in this area (0.7-1.47) indicated consistency, suggesting no major concerns.

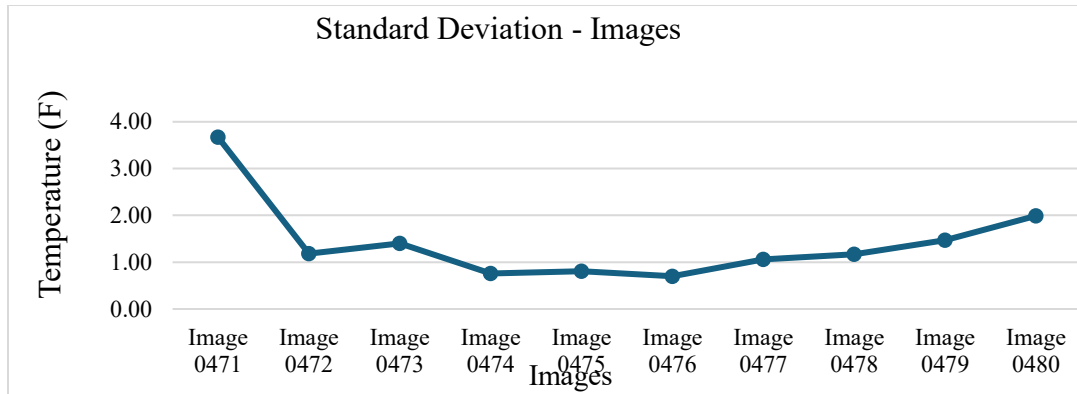


**Figure 144. Graph. Standard deviation plot of images – East to West Crossgate**

Figure 144, (hotter upper regions) and Isotherm 2, from Figure 146, (cooler lower regions) charts demonstrated a reliable thermal profile for the East-to-West wall. Temperature differences were generally narrow (e.g., 2.47-5.02°F for Isotherm 1, 1.76-4.6°F for Isotherm 2). Standard deviations from Figure 147 were consistently low (0.43-1.01 for Isotherm 1, 0.36-0.77 for Isotherm 2), suggesting thermal stability despite minor localized environmental influences.

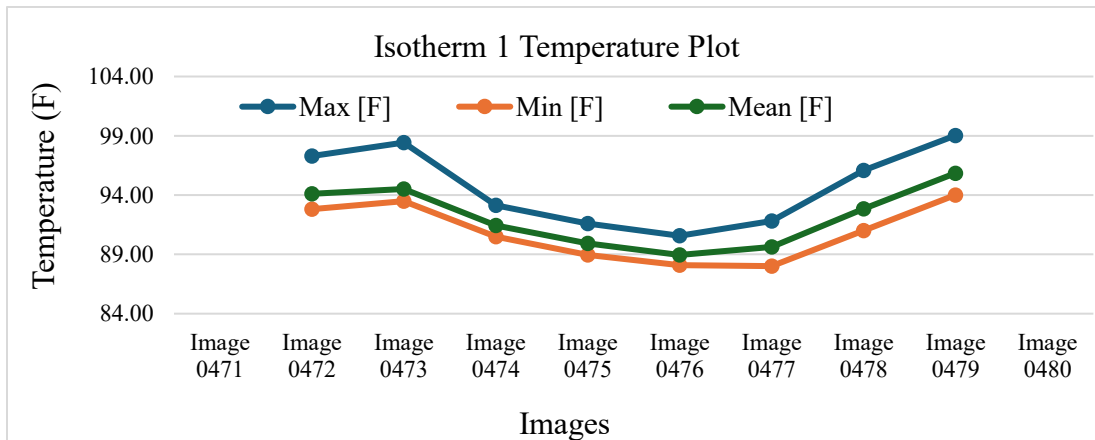


**Figure 145. Graph. Isotherm 1 temperature plot – East to West Crossgate**

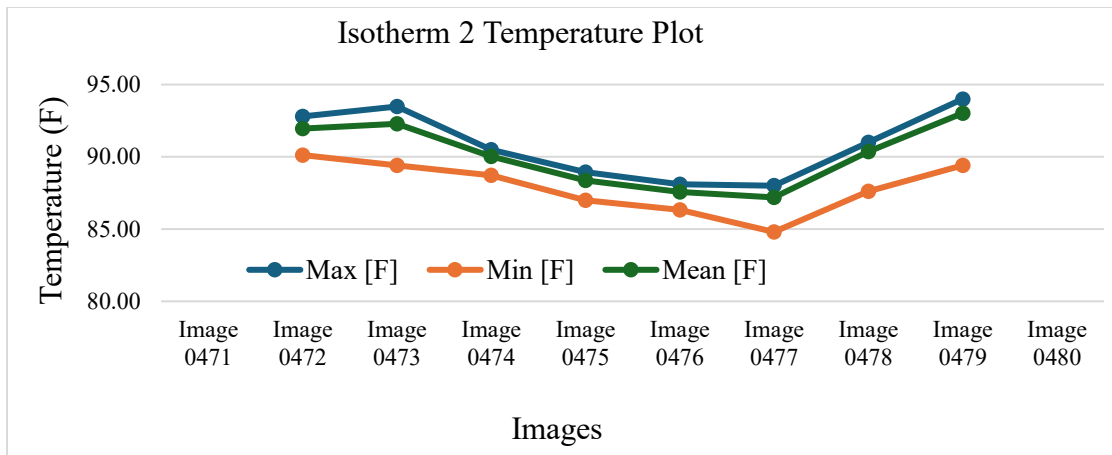


**Figure 146. Graph. Isotherm 2 temperature plot – East to West Crossgate**

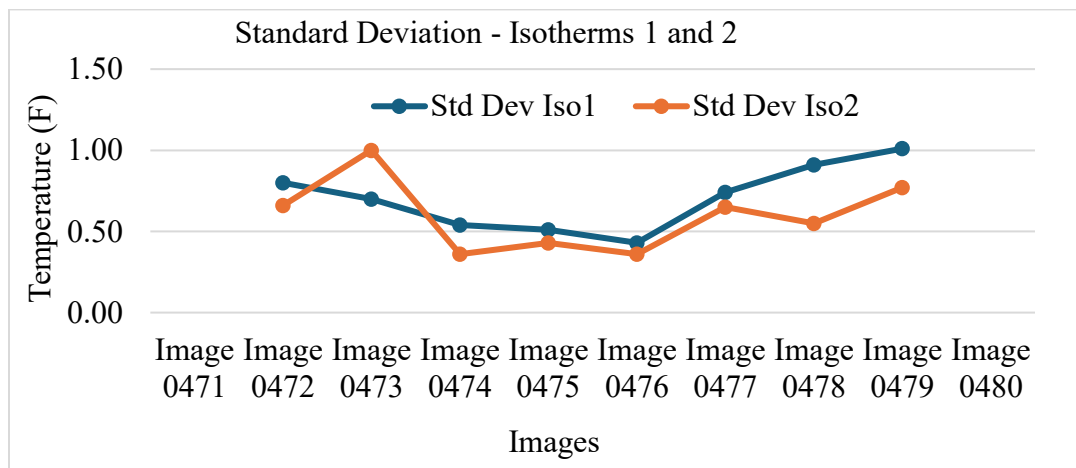


**Figure 147. Graph. Standard deviation of Isotherms 1 and 2 – East to West Crossgate**

### Conclusion For Crossgate

Overall, the Crossgate MSE wall exhibited robust thermal stability in its central sections. While localized temperature variations were observed at the ends due to their trapezoidal geometry and environmental factors (like vegetation), these variations, after detailed polygon and isotherm analysis, were not indicative of any significant subsurface defects or anomalies that would compromise the wall's integrity. The study concluded that the thermal patterns were consistent with the external conditions and did not signal any structural concerns

## RESULTS AND DISCUSSION - OLD RIVER ROAD

The second site analyzed in the results section is the Old River Road MSE Wall. The analysis of this wall is presented in two parts: "West to East Wall - Old River Road" in Figure 151 and "East to West Wall - Old River Road" in Figure 154. The Old River Road MSE wall, also trapezoidal in shape, exhibited temperature variations influenced by its geometry and environmental factors like vegetation and atmospheric conditions, particularly at its ends. However, the concrete panels themselves showed overall thermal stability.

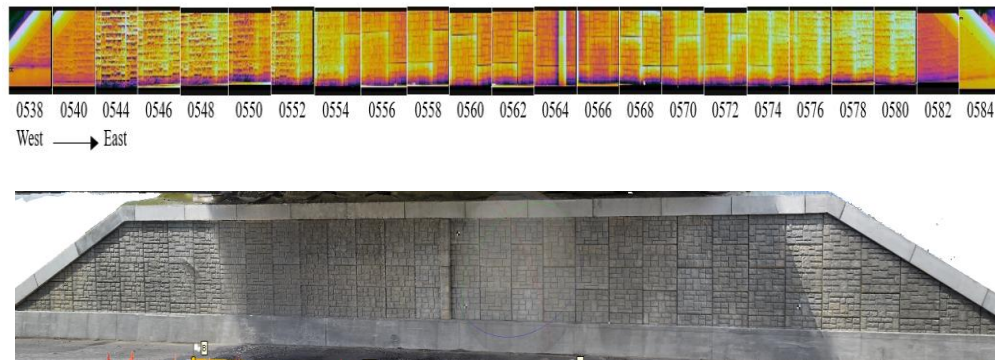


**Figure 148. Photo. Thermographic and Digital Image of the West to East Wall – Old River Road**

**Table 56. West to East MSE Wall – Old River Road (APPENDIX B)**

West to East Wall - Old River Road												
Images					Isotherm 1				Isotherm 2			
Images	Max [F]	Min [F]	Mean [F]	St.Dev Img	Max [F]	Min [F]	Mean [F]	St.Dv. Iso1	Max [F]	Min [F]	Mean [F]	St Dv Iso2
Img0538	86.46	60.26	80.17	3.35								
Img 0540	86.23	52.49	80.40	2.39								
Img 0544	81.93	77.08	80.18	0.70	81.93	79.40	80.40	0.48	79.40	77.08	78.95	0.38
Img 0546	81.64	76.80	80.02	0.66	81.64	78.70	80.10	0.55	78.70	76.80	78.31	0.33
Img 0548	81.41	76.47	79.82	0.64	81.41	78.49	79.90	0.53	78.49	76.47	78.12	0.32
Img 0550	81.87	77.33	80.09	0.53	81.87	79.00	80.17	0.43	79.00	77.33	78.68	0.27
Img 0552	81.31	77.11	80.04	0.45	81.31	79.00	80.09	0.37	79.00	77.11	78.71	0.24
Img 0554	81.12	77.43	79.85	0.45	81.12	79.00	79.92	0.34	79.00	77.43	78.59	0.33
Img 0556	81.07	76.27	79.27	0.49	81.07	78.49	79.36	0.36	78.49	76.27	78.02	0.39
Img 0558	80.50	76.08	78.93	0.51	80.50	78.00	79.01	0.38	78.00	76.08	77.53	0.38
Img 0560	80.14	75.70	78.56	0.48	80.14	77.69	78.63	0.38	77.69	75.70	77.29	0.35
Img 0562	82.60	74.81	78.29	0.56	82.60	77.49	78.41	0.38	77.49	74.81	76.94	0.46
Img 0564	80.76	74.01	78.02	0.94	80.76	77.00	78.23	0.76	77.00	74.01	76.38	0.50
Img 0566	80.50	73.28	77.69	0.77	80.50	76.50	77.83	0.59	76.50	73.28	75.83	0.52
Img 0568	79.72	73.86	78.09	0.65	79.72	77.00	78.21	0.44	77.00	73.86	76.36	0.53
Img 0570	79.85	73.71	78.03	0.67	79.85	76.70	78.13	0.50	76.70	73.71	76.07	0.48
Img 0572	80.17	73.76	78.13	0.74	80.17	77.00	78.29	0.47	77.00	73.76	76.21	0.62
Img 0574	80.05	73.36	78.13	0.79	80.05	76.50	78.27	0.53	76.50	73.36	75.69	0.58
Img 0576	80.48	73.56	78.50	0.84	80.48	76.50	78.61	0.64	76.50	73.56	75.72	0.63
Img 0578	80.53	73.14	78.58	1.00	80.53	76.59	78.73	0.74	76.59	73.14	75.60	0.79
Img 0580	81.33	73.45	79.04	1.06	81.33	76.80	79.19	0.80	76.80	73.45	75.75	0.81
Img 0582	89.50	55.33	80.48	2.97								
Img 0584	91.09	55.24	79.84	5.95								

**West to East Wall - Old River Road**

Ends of the Wall: The thermal analysis showed in Table 56 temperature extremes at the wall's ends. For instance, Image 0584 recorded a maximum of 91.09°F and Image 0540 a minimum of 42.49°F. These variations were attributed to localized factors such as atmospheric exposure and surrounding vegetation.

### ***Polygon Analysis on Panels***

Despite the extremes at the ends, a focused polygon analysis on the concrete panel areas revealed no critical abnormalities. From Figure 149, maximum temperatures in these specific zones were around 81.77°F (Image 0538) and minimums around 74.18°F (Image 0582). The standard deviations ranged between 0.79 and 1.18, and temperature differences were between 6.3°F and 8.07°F, indicating thermal stability within the panels and no major concerns.

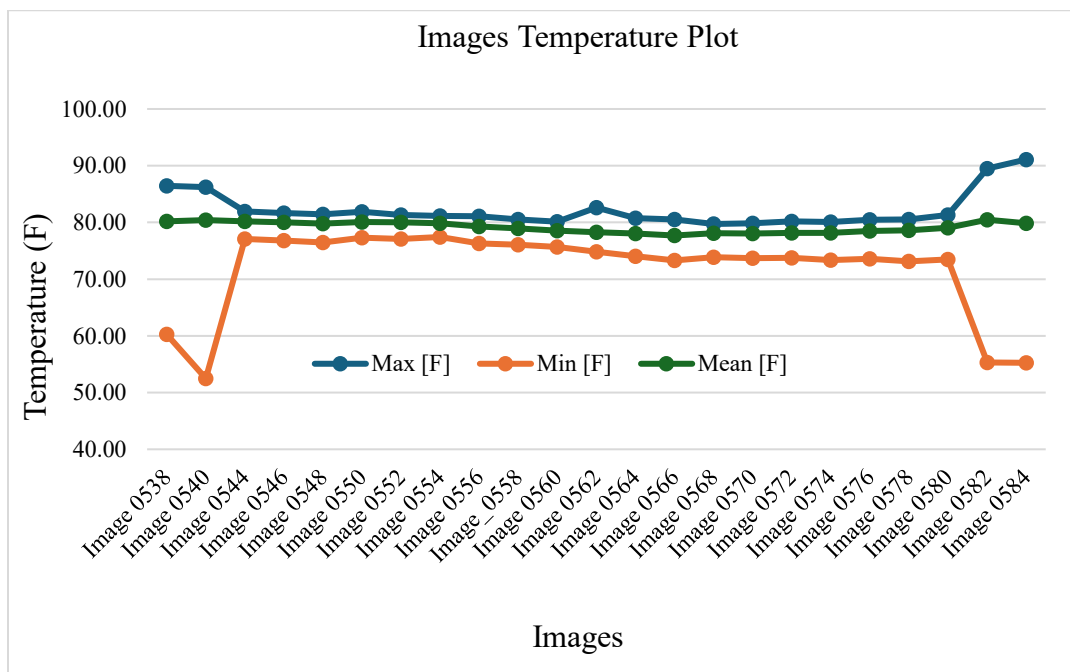


**Figure 149. Graph. Images temperature plot – West to East Old River Road**

Central Sections: The middle sections of the wall demonstrated consistent thermal profiles. Mean temperatures were stable (e.g., 80.04°F in Image 0552), with small differences (less than 4°F) between maximum and minimum readings. From Figure 150, Low standard deviation values (e.g., 0.45 in Images 0552 and 0554) underscored this stability. Slight deviations were noted in Images

0562 and 0564 (temperatures ranging from 74°F to 83°F), associated with adjacent column elements, but these were localized and did not signify major defects.

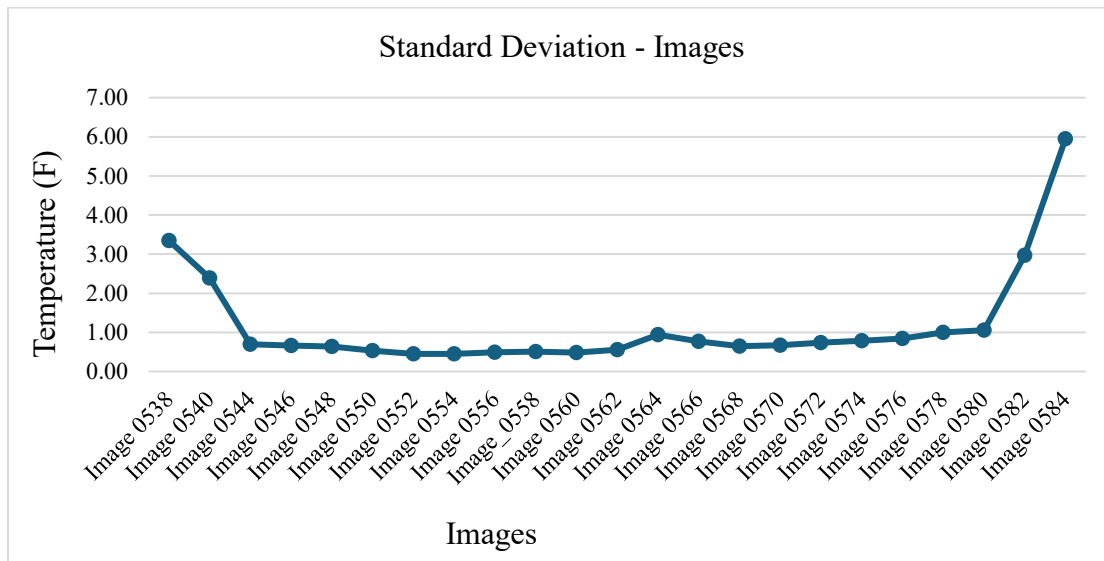


**Figure 150. Graph. Standard deviation plot of images – West to East Old River Road**

### ***Isotherm Analysis:***

Isotherm 1 (Hotter Regions): Figure 151 Showed hotter regions concentrated towards the upper sections, with a maximum of 82.60°F (Image 0562) and a minimum of 76.50°F (Images 0576, 0578), yielding an overall temperature variation of 6.1°F. Low standard deviations (e.g., 0.34 in Image 0554) reaffirmed stability.

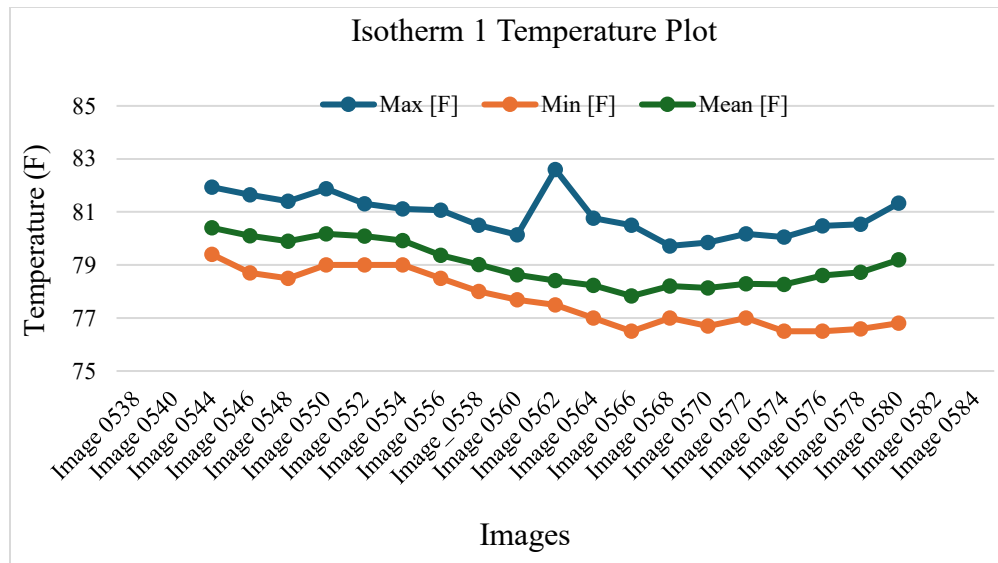


**Figure 151. Graph. Isotherm 1 temperature plot – West to East Old River Road**

Isotherm 2 (Cooler Regions): Reinforced the delineation of hotter regions in Figure 152, at the top and cooler clusters at the base. Maximum temperatures reached 79.40°F (Image 0544) and minimums 73.14°F (Image 0578), with a 6°F difference across the region. Standard deviations from Figure 153, remained low (e.g., 0.24 in Image 0552), indicating overall thermal uniformity.

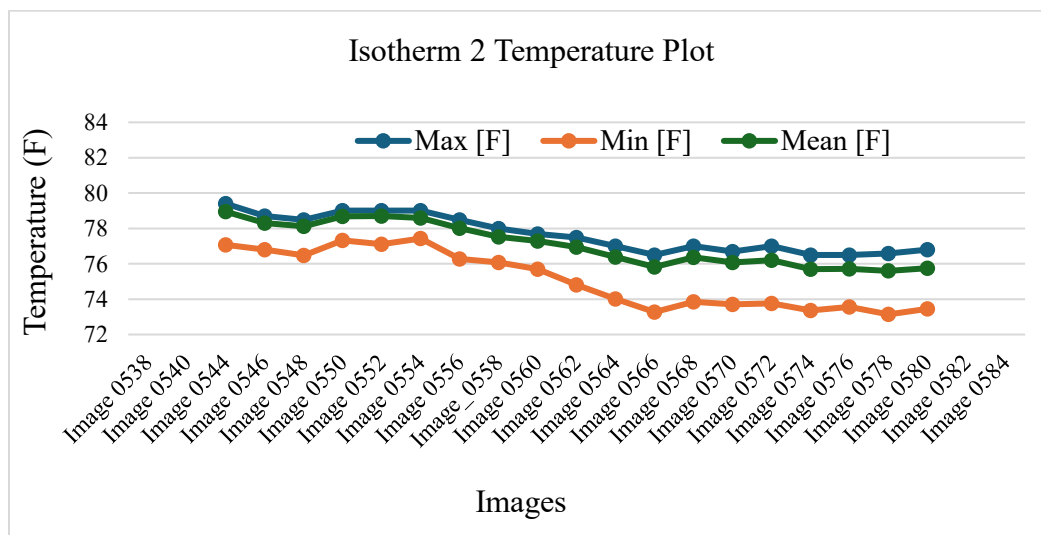


**Figure 152. Graph. Isotherm 2 temperature plot – West to East Old River Road**



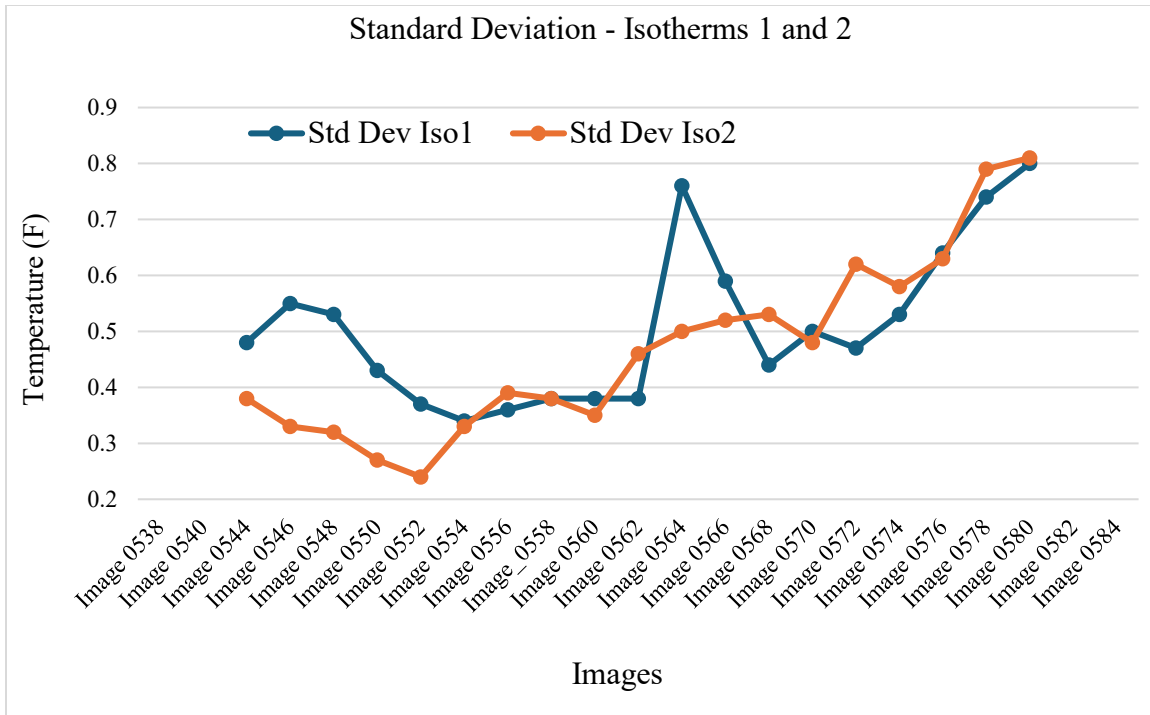


**Figure 153. Graph. Standard deviation of Isotherms 1 and 2 – West to East Old River Road**

#### East to West Wall - Old River Road

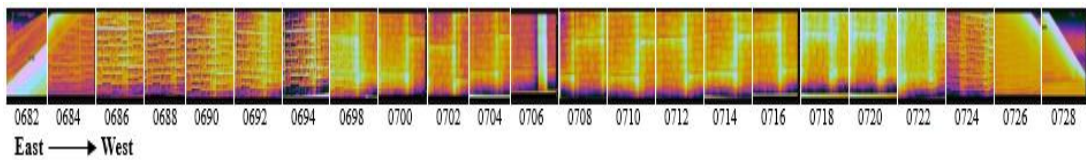


**Figure 154. Photo. Thermographic and Digital Image of the East to West Wall – Old River**

**Table 57. East to West MSE Wall – Old River Road (APPENDIX B)**

East to West Wall - Old River Road												
Images					Isotherm 1				Isotherm 2			
Images	Max [F]	Min [F]	Mean [F]	St.Dv. Img	Max [F]	Min [F]	Mean [F]	St.Dv. Iso1	Max [F]	Min [F]	Mean [F]	St.Dv. Iso2
Img 0682	83.57	47.83	71.79	8.58								
Img 0684	84.30	50.22	78.43	1.83								
Img 0686	79.96	74.28	77.98	0.68	79.96	77.00	78.10	0.55	76.99	74.28	76.61	0.36
Img 0688	80.18	74.91	77.97	0.67	80.18	77.00	78.09	0.55	76.99	74.91	76.64	0.32
Img 0690	79.77	75.54	78.25	0.54	79.77	77.31	78.33	0.45	77.30	75.54	77.02	0.26
Img 0692	79.51	76.53	78.47	0.37	79.51	78.01	78.57	0.27	78.00	76.53	77.75	0.21
Img 0694	80.36	76.50	78.49	0.43	80.36	77.90	78.57	0.35	77.89	76.50	77.69	0.19
Img 0696	78.99	75.78	77.95	0.34	78.99	77.11	77.97	0.30	77.10	75.78	76.83	0.24
Img 0698	78.84	75.26	77.62	0.34	78.84	77.00	77.66	0.28	76.99	75.26	76.70	0.26
Img 0700	78.35	75.72	77.19	0.27	78.35	76.61	77.20	0.25	76.60	75.72	76.40	0.18
Img 0702	78.60	74.99	77.07	0.41	78.60	76.30	77.14	0.31	76.29	74.99	75.94	0.26
Img 0704	77.96	75.05	76.86	0.31	77.96	76.11	76.88	0.28	76.10	75.05	75.87	0.20
Img 0706	78.99	73.92	76.78	0.80	78.99	76.11	76.95	0.69	76.10	73.92	75.61	0.39
Img 0708	77.80	74.04	76.61	0.48	77.80	75.81	76.71	0.33	75.80	74.04	75.35	0.32
Img 0710	78.03	73.77	76.60	0.46	78.03	75.50	76.66	0.35	75.49	73.77	75.13	0.28
Img 0712	77.90	73.82	76.60	0.47	77.90	75.50	76.66	0.35	75.49	73.82	75.11	0.28
Img 0714	77.67	73.99	76.43	0.49	77.66	75.31	76.49	0.38	75.30	73.99	74.91	0.27
Img 0716	77.89	73.47	76.33	0.52	77.89	75.01	76.40	0.41	75.00	73.47	74.64	0.27
Img 0718	77.31	73.08	76.07	0.60	77.31	74.91	76.19	0.39	74.90	73.08	74.40	0.35
Img 0720	77.56	73.02	76.09	0.63	77.56	74.71	76.20	0.43	74.70	73.02	74.21	0.35
Img 0722	77.97	73.26	76.10	0.60	77.97	74.80	76.18	0.47	74.79	73.26	74.37	0.30
Img 0724	79.17	73.44	76.52	0.72	79.17	75.31	76.62	0.59	75.30	73.44	74.81	0.36
Img 0726	86.19	47.16	77.10	0.93								
Img 0728	86.71	53.85	74.81	7.83								

Ends of the Wall: From Table 57, Similar to the West-to-East side, the ends of this wall (Images 0682, 0684, 0726, 0728) exhibited significant temperature differences (e.g., 86.71°F in Image 0728 to 47.16°F in Image 0726). These large thermal differences were linked to environmental factors like vegetation and atmospheric conditions.

### *Polygon Analysis on Panels*

Despite the extreme thermal variations at the ends, further analysis using the polygon tool on the concrete panels confirmed no significant concerns or anomalies. From Figure 155, Maximum temperatures in these panel-specific areas were around 79.96°F to 80.96°F, with minimums around 73.35°F to 75.12°F. Standard deviations ranged from 0.74 to 1.17, and temperature differences from 4.8°F to 7.5°F, indicating that the panels themselves were thermally sound.

Central Sections: The central sections showed highly consistent temperature behavior. Standard deviations from Figure 156, were as low as 0.27 (Image 0700), with minimal differences (less than 3°F) between maximum and minimum temperatures. A localized variation was observed in Image 0706 (temperatures from 74°F to 79°F) due to an adjacent column, but this did not imply a major defect. The maximum standard deviation in the central area (excluding the column region) was 0.72 (Image 0724), with a 5.73°F difference, which was considered insignificant.

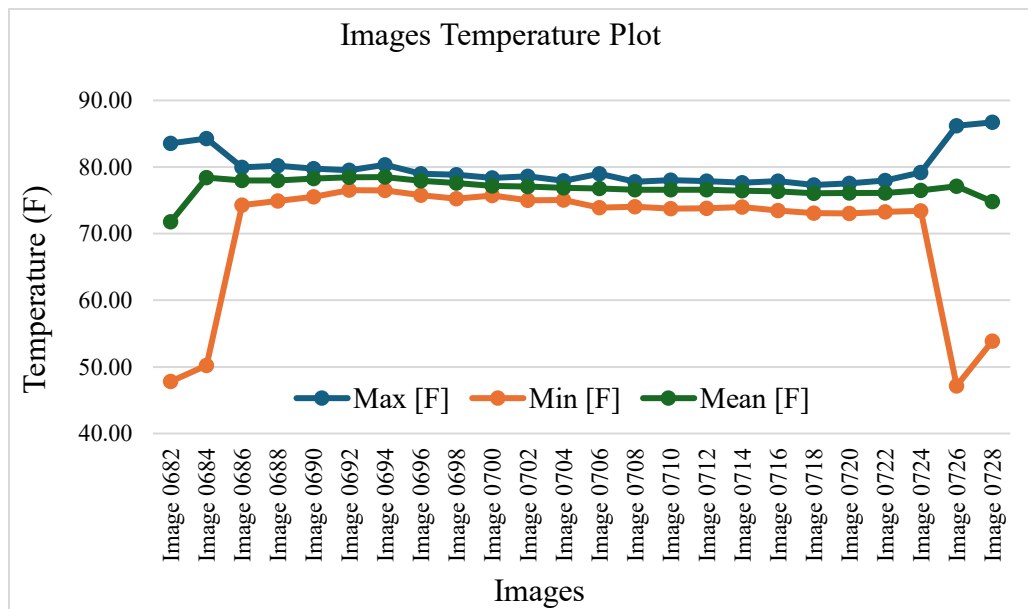


**Figure 155. Graph. Images temperature plot – East to West Old River Road**

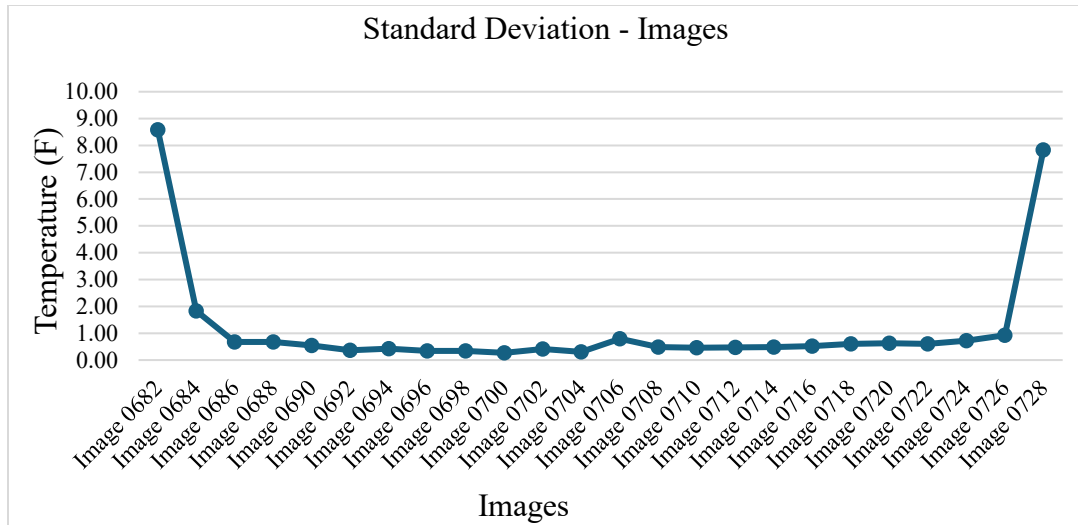


**Figure 156. Graph. Standard deviation plot of images – East to West Old River Road**

### *Isotherm Analysis*

Isotherm 1 (Hotter Regions): Figure 157 showed hotter areas predominantly in the upper sections, with minimal temperature variation (e.g., 80.36°F max in Image 0694, 74.71°F min in Image 0720, with a 5.7°F overall difference). Standard deviations were consistently low (e.g., 0.25 in Image 0700).

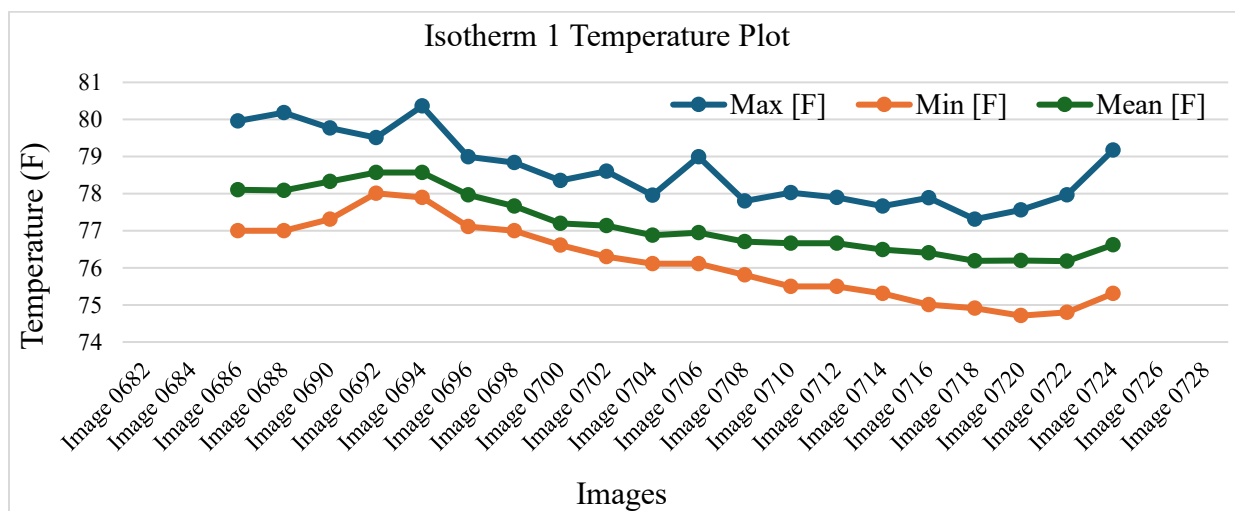


**Figure 157. Graph. Isotherm 1 temperature plot – East to West Old River Road**

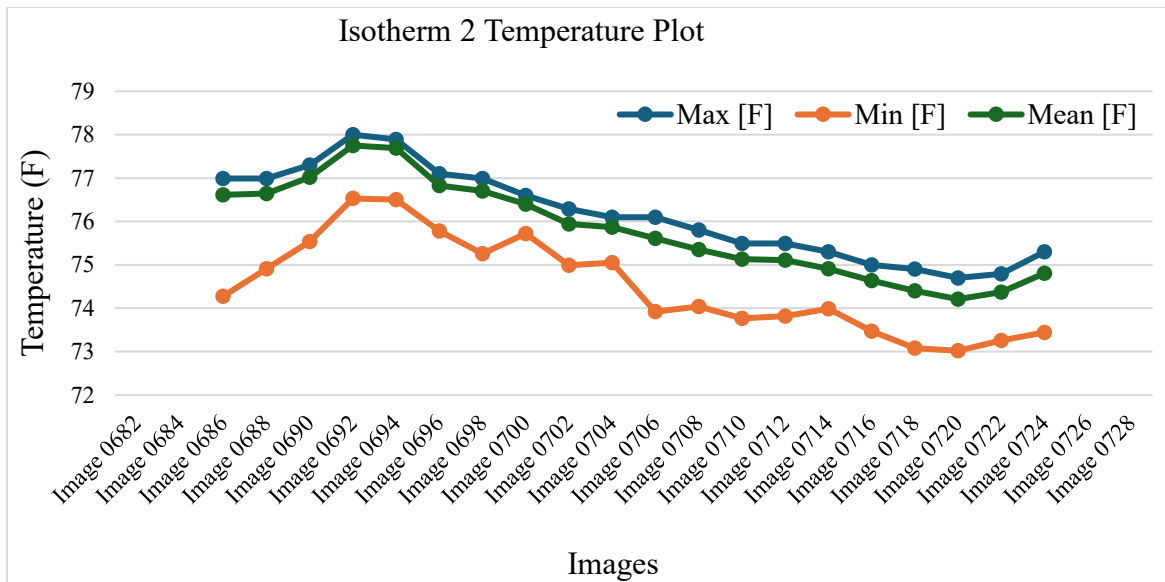


**Figure 158. Graph. Isotherm 2 temperature plot – East to West Old River Road**

Isotherm 2 (Cooler Regions): Figure 158 Reinforced the thermal patterns with hot regions at the top and cooler areas at the base. Maximum temperatures reached 78°F (Image 0692) and minimums 73°F (Image 0692), with a 5°F overall difference. Standard deviations from Figure 159 were low (e.g., 0.18 in Image 0700), emphasizing temperature consistency.

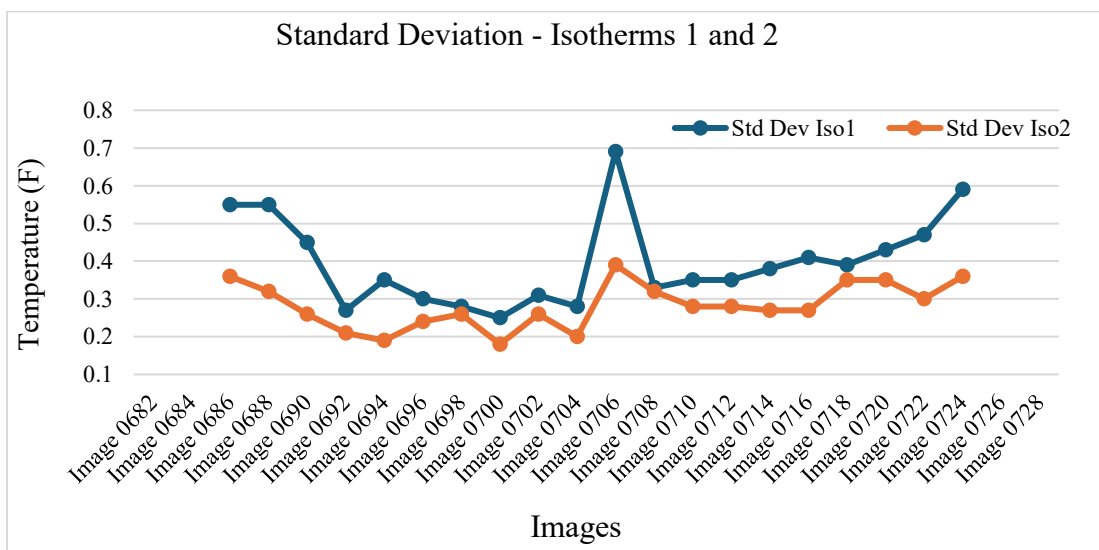


**Figure 159. Graph. Standard deviation of Isotherms 1 and 2 – Old River Road**

## **Conclusion on Old River Road**

In summary, the Old River Road MSE wall demonstrated overall thermal stability, particularly within its central concrete panel sections. While significant temperature fluctuations were observed at the trapezoidal ends and near structural elements like columns due to environmental and geometric influences, detailed analysis confirmed that these were localized variations and not indicative of any underlying structural defects or anomalies. The wall's thermal performance was found to be robust and reliable under the observed conditions.

## **RESULTS AND DISCUSSION - KING GEORGE BOULEVARD**

The third site analyzed in the results section is the King George Boulevard MSE Wall. The analysis of this wall is presented in two parts: "West to East Wall - King George" in Figure 160 (Section 4.6) and "East to West Wall - King George" (Section 4.7). The King George Boulevard MSE wall, characterized by its rectangular geometry, generally exhibited consistent thermal characteristics. While some temperature variations were observed, particularly at the ends and in areas influenced by external factors like light poles, the overall thermal performance of the concrete panels was stable and reliable.

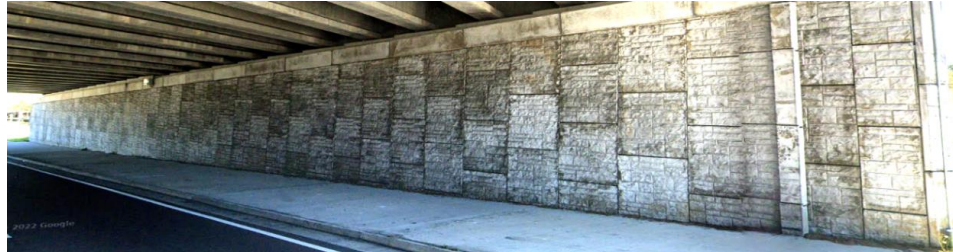
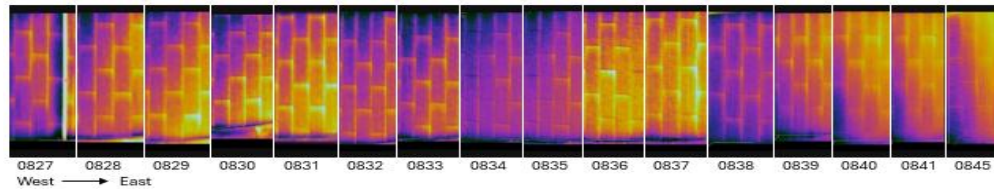


**Figure 160. Photo. Thermographic and Digital Image of the West to East Wall – King George**

**Table 58. West to East MSE Wall – King George (APPENDIX B)**

West to East Wall - King George								
Images					Polygon 1			
Images	Max [F]	Min [F]	Mean [F]	St.Dv. Img	Max [F]	Min [F]	Mean [F]	St.Dv. P1
Img 0827	74.72	64.57	67.87	1.33	74.72	64.57	67.88	1.32
Img 0828	69.99	64.18	66.94	0.75	69.99	64.18	66.93	0.72
Img 0829	68.14	63.21	65.71	0.70	67.91	63.21	65.71	0.69
Img 0830	67.09	63.55	65.27	0.56	67.09	63.57	65.30	0.55
Img 0831	65.96	62.60	64.57	0.45	65.96	62.91	64.60	0.42
Img 0832	66.43	62.22	64.23	0.51	66.03	62.22	64.21	0.43
Img 0833	71.31	62.17	63.78	0.55	65.15	62.17	63.74	0.42
Img 0834	67.33	61.14	63.38	0.54	64.63	61.48	63.35	0.39
Img 0835	66.85	61.43	63.42	0.51	64.72	61.43	63.40	0.42
Img 0836	64.95	61.52	63.21	0.35	64.35	61.69	63.24	0.31
Img 0837	64.61	61.18	63.16	0.38	64.42	61.31	63.20	0.34
Img 0838	66.26	61.55	63.39	0.55	64.55	61.84	63.31	0.32
Img 0839	65.20	60.17	62.53	0.57	64.04	60.30	62.56	0.49
Img 0840	64.97	58.82	62.18	0.81	64.12	59.27	62.18	0.72
Img 0841	65.39	58.58	62.34	0.83	64.23	58.58	62.30	0.74
Img 0845	65.06	52.48	60.19	1.49	63.23	54.15	60.14	1.34

## **West to East Wall - King George**

General Observations: The rectangular geometry of this wall minimized variability compared to the trapezoidal walls at other sites. However, from Table 58, the first (Image 0827) and last (Image 0845) images showed higher temperature variations due to increased environmental exposure.

Temperature Ranges and Standard Deviations: From Figure 161, Image 0827 (western end) recorded a maximum of 74.72°F and a minimum of 64.57°F, a difference of 10.15°F, with a standard deviation of 1.33. This was attributed to a nearby column and increased exposure. Image 0845 (eastern end) showed a maximum of 65.06°F and a minimum of 52.48°F, a difference of 12.58°F, with a standard deviation of 1.49, also due to greater exposure.

Central Sections: The central sections demonstrated significant thermal consistency. For example, Image 0830 had a maximum of 67.09°F and a minimum of 63.55°F, a difference of 3.54°F, with a standard deviation of 0.56. Image 0837 showed even greater uniformity with a 3.43°F difference and a standard deviation of 0.38 in Figure 162.



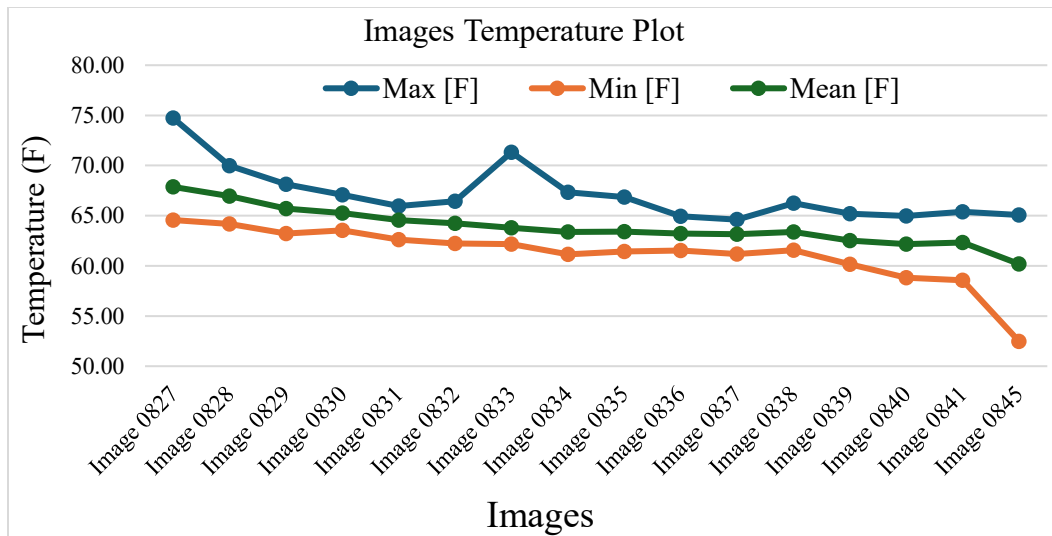


**Figure 161. Graph. Images temperature plot – West to East King Goerge**

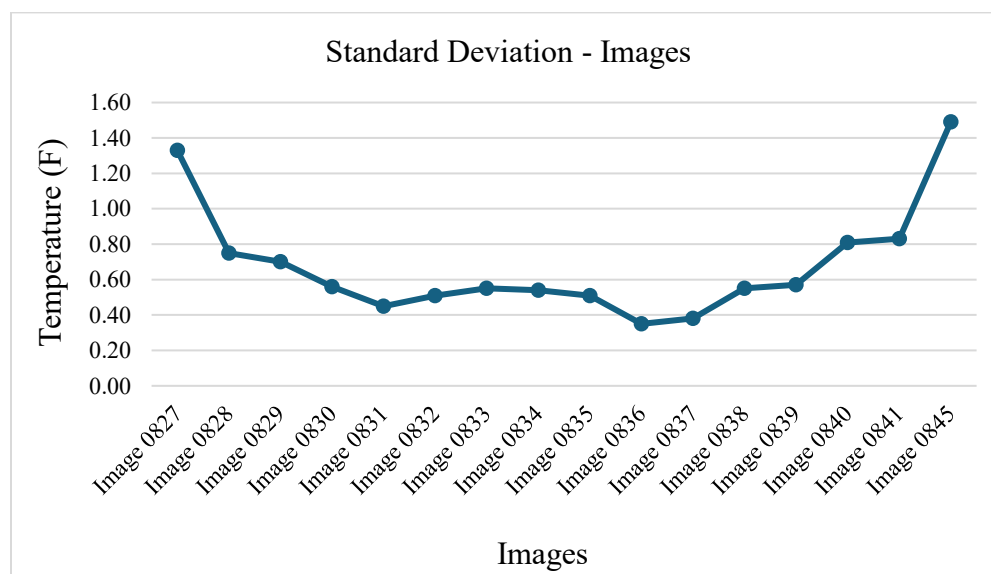


**Figure 162. Graph. Standard deviation plot of images – West to East King Goerge**

### ***Polygon Analysis (Panel-Specific Areas)***

This analysis in Figure 163, which excluded elements like beams and walkways, confirmed the thermal stability of the concrete panels. Image 0827 (panel area) had a 10.15°F difference and a standard deviation Figure 164 of 1.32. Image 0836 (central panel) showed a very low 2.66°F

difference and a standard deviation of 0.31, indicating high thermal consistency. Image 0845 (panel area) had a 9.08°F difference and a standard deviation of 1.34.

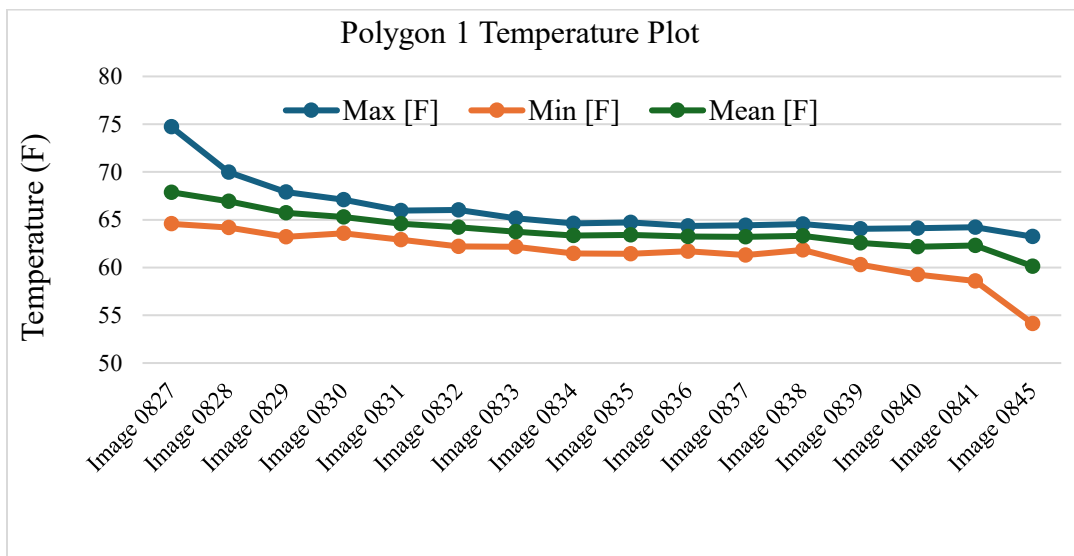


**Figure 163. Graph. Polygon 1 temperature plot – West to East King George**

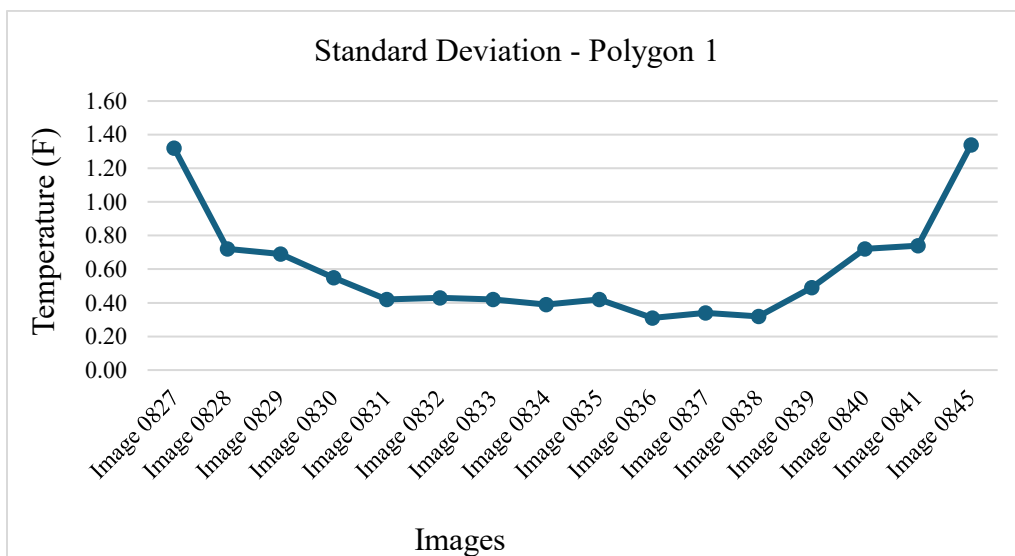


**Figure 164. Graph. Standard deviation of Polygon 1 – West to East Crossgate**

### *Conclusion for West to East*

Despite localized variations at the ends due to exposure and structural elements, the central sections of the West-to-East King George wall maintained stable thermal performance, with no significant defects or concerns identified.

### **East to West Wall - King George**

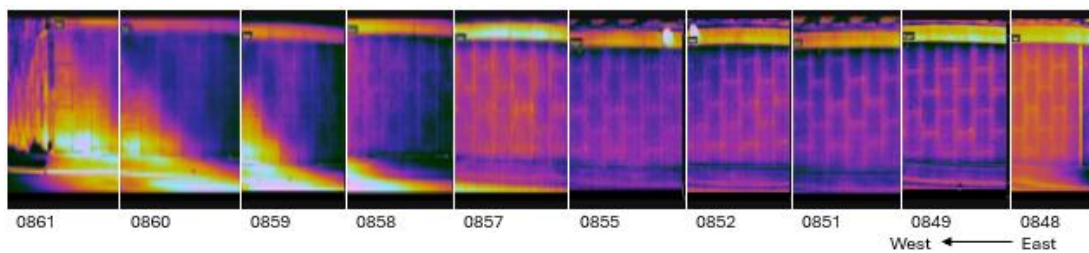


**Figure 165. Photo. Thermographic and Digital Image of the East to West Wall – King George**

**Table 59. East to West MSE Wall – King George (APPENDIX B)**

East to West Wall - King George								
Images					Polygon 1			
Images	Max [F]	Min [F]	Mean [F]	Std Dev Images	Max [F]	Min [F]	Mean [F]	Std Dev P1
Image 0848	67.08	59.17	62.95	0.86	65.24	60.25	62.79	0.55
Image 0849	66.32	61.64	63.24	0.53	63.86	61.82	63.09	0.25
Image 0851	66.48	61.62	63.24	0.50	63.93	61.62	63.12	0.26
Image 0852	116.61	61.81	63.46	1.76	64.15	62.11	63.26	0.27
Image 0855	125.42	59.15	63.38	1.95	63.83	61.76	63.16	0.24
Image 0857	65.36	61.46	63.44	0.47	64.13	62.16	63.35	0.20
Image 0858	69.94	61.45	64.16	1.06	65.52	61.45	63.81	0.38
Image 0859	71.96	62.18	65.67	1.91	71.06	62.18	65.18	1.31
Image 0860	72.25	61.08	66.35	2.09	71.23	61.08	65.59	1.47
Image 0861	72.97	56.29	66.38	2.15	71.44	63.98	66.81	1.72

General Observations: From Figure 165, This side of the wall experienced more interference from external elements like beam components, walkway structures, and environmental reflections (e.g., light poles), leading to increased variability compared to the West-to-East side.

Temperature Ranges and Standard Deviations: From Table 59 Image 0848 (eastern end) had a 7.91°F difference and a standard deviation of 0.86, influenced by a column and exposure. Image 0861 (western end) showed a higher 16.68°F difference and a standard deviation of 2.15, attributed to a nearby light pole.

Central Sections (Affected by Light Interference): From Figure 166, Images like 0852 and 0855 showed significant, but localized, temperature spikes (e.g., 54.8°F difference in Image 0852, 66.27°F difference in Image 0855) and high standard deviations in Figure 167, (1.76 and 1.95, respectively). These were identified as false positives caused by reflections from halogen lights and not indicative of material defects.

Central Sections (Unaffected): Other central images, such as 0849 and 0851, displayed consistent patterns with small differences (2.04°F and 2.31°F) and low standard deviations (0.25 and 0.26), confirming stable thermal distribution when external influences were minimized.

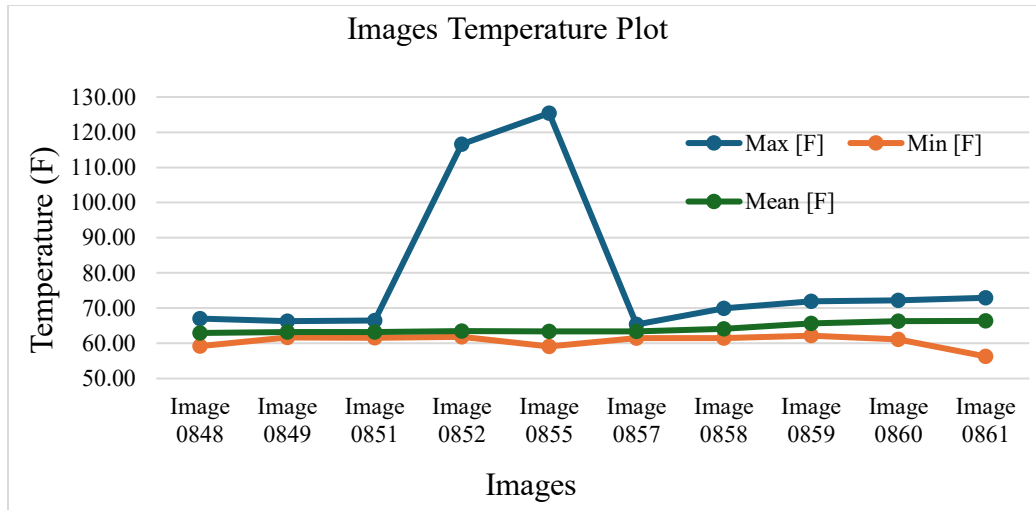


**Figure 166. Graph. Images temperature plot – East to West King George**

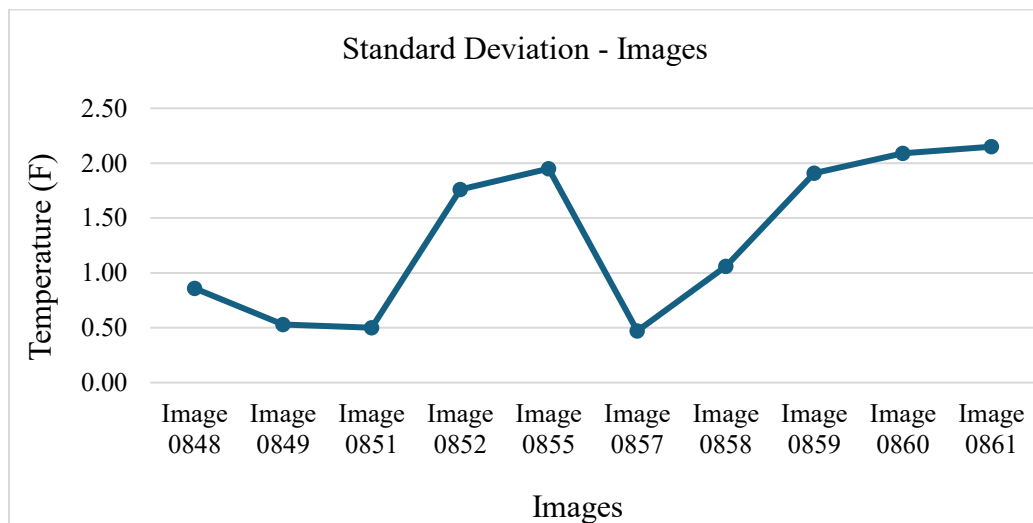


**Figure 167. Graph. Standard deviation of Polygon 1 – East to West Crossgate**

### ***Polygon Analysis (Panel-Specific Areas)***

This analysis helped to isolate the true thermal behavior of the panels in Figure 168. Image 0848 (panel area) had a 4.99°F difference and a standard deviation in Figure 169, of 0.55. Image 0857 (central panel) showed the lowest variability with a 1.97°F difference and a standard deviation of 0.20. The end images (e.g., Image 0861) still showed higher variability (7.46°F difference,

1.72 std dev) due to environmental influences, but these were not indicative of defects.

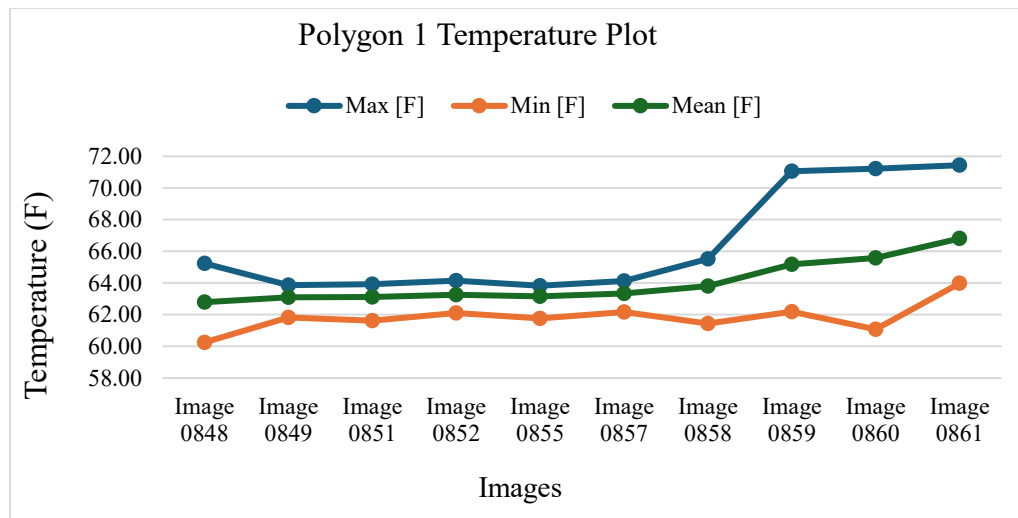


**Figure 168. Graph. Polygon 1 temperature plot – East to West King George**

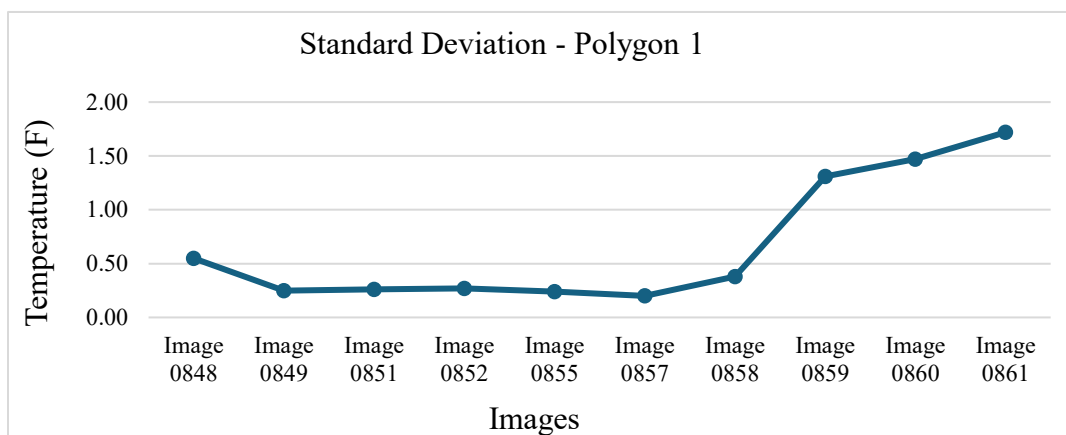


**Figure 169. Graph. Standard deviation of Polygon 1 – East to West King George**

### *Conclusion for East to West*

Despite the increased environmental and structural interferences, the polygon-focused analysis confirmed that the concrete panels of the East-to-West King George wall maintained reliable

thermal characteristics, with no major concerns or defects identified. The observed thermal patterns were consistent with the external conditions rather than underlying structural issues.

## **THERMAL PERFORMANCE ANALYSIS OF MSE WALLS OF SELECTED SITES**

Overall Approach: The analysis in Table 60. Defects and Anomalies in Crossgate focused on the central, more representative sections of the walls, excluding the irregularly shaped ends of Crossgate and Old River Road to ensure a consistent comparison. This was done because initial analyses confirmed no defects in those end sections, and their variability was primarily due to environmental factors. Table 61 shows the data for Old River and Table 62 shows for King George.

### **Crossgate MSE Wall (Least Reliable)**

- Showed the most significant thermal variability, particularly at its ends.
- Isotherm 1 and 2 analyses revealed temperature differences up to 10.04°F and higher standard deviations (e.g., 2.16 for Image 0469).
- While central sections were more stable, the overall pronounced variability at the ends made it the least reliable in terms of thermal performance, with variations attributed to localized environmental factors like vegetation and exposure.

### **Old River Road MSE Wall (Moderate Reliability)**

- Demonstrated better consistency than Crossgate but still had variability at its ends and near structural elements.
- Central sections showed reliable thermal behavior with narrow temperature differences (2.31°F to 2.87°F) and low standard deviations (below 0.5).

However, its extremities still exhibited thermal fluctuations (up to 5.11°F difference, 0.81 standard deviation), affecting its overall ranking compared to King George.

### **King George Boulevard MSE Wall (Superior Reliability)**

- Exhibited the most consistent and minimal thermal variability across all analyzed sections, largely due to its rectangular geometry.
- Polygon analysis showed consistently low temperature differences (as low as 1.97°F) and very low standard deviations (as low as 0.20).

Even areas with some external influences (like light poles) showed localized variability, but these were isolated and did not indicate defects, confirming the wall's high reliability.

**Table 60. Defects and Anomalies in Crossgate**

<b>Crossgate</b>								
<b>Images</b>	<b>Isotherm 1</b>				<b>Isotherm 2</b>			
	<b>Max [F]</b>	<b>Min [F]</b>	<b>ΔT [F]</b>	<b>Std Dev Iso1</b>	<b>Max [F]</b>	<b>Min [F]</b>	<b>ΔT [F]</b>	<b>Std Dev Iso2</b>
Image 0462	104.11	97.00	7.11	0.71	97.00	93.18	3.82	0.65
Image 0463	98.07	94.00	4.07	0.87	93.99	90.60	3.39	0.73
Image 0464	92.49	88.91	3.58	0.72	88.90	85.87	3.03	0.53
Image 0465	89.64	87.00	2.64	0.49	86.99	84.49	2.50	0.46
Image 0466	89.64	87.00	2.64	0.49	86.99	84.49	2.50	0.46
Image 0467	93.52	90.00	3.52	0.79	90.00	87.32	2.68	0.52
Image 0468	96.17	93.01	3.16	0.65	93.00	88.41	4.59	0.74
Image 0469	98.16	94.00	4.16	0.61	93.99	83.95	10.04	2.16
Image 0472	97.29	92.81	4.48	0.80	92.80	90.12	2.68	0.66
Image 0473	98.42	93.50	4.92	0.70	93.49	89.40	4.09	1.00
Image 0474	93.13	90.50	2.63	0.54	90.49	88.73	1.76	0.36
Image 0475	91.60	88.96	2.64	0.51	88.95	86.99	1.96	0.43
Image 0476	90.57	88.10	2.47	0.43	88.10	86.32	1.78	0.36
Image 0477	91.81	88.01	3.80	0.74	88.00	84.80	3.20	0.65
Image 0478	96.09	91.01	5.08	0.91	91.00	87.62	3.38	0.55
Image 0479	99.03	94.01	5.02	1.01	94.00	89.40	4.60	0.77



**Table 61. Defects and Anomalies in Old River**

Old River Road								
Images	Isotherm 1				Isotherm 2			
	Max [F]	Min [F]	$\Delta T$ [F]	Std Dev Iso1	Max [F]	Min [F]	$\Delta T$ [F]	Std Dev Iso2
Image 0544	81.93	79.40	2.53	0.48	79.40	77.08	2.32	0.38
Image 0546	81.64	78.70	2.94	0.55	78.70	76.80	1.90	0.33
Image 0548	81.41	78.49	2.92	0.53	78.49	76.47	2.02	0.32
Image 0550	81.87	79.00	2.87	0.43	79.00	77.33	1.67	0.27
Image 0552	81.31	79.00	2.31	0.37	79.00	77.11	1.89	0.24
Image 0554	81.12	79.00	2.12	0.34	79.00	77.43	1.57	0.33
Image 0556	81.07	78.49	2.58	0.36	78.49	76.27	2.22	0.39
Image 0558	80.50	78.00	2.50	0.38	78.00	76.08	1.92	0.38
Image 0560	80.14	77.69	2.45	0.38	77.69	75.70	1.99	0.35
Image 0562	82.60	77.49	5.11	0.38	77.49	74.81	2.68	0.46
Image 0564	80.76	77.00	3.76	0.76	77.00	74.01	2.99	0.50
Image 0566	80.50	76.50	4.00	0.59	76.50	73.28	3.22	0.52
Image 0568	79.72	77.00	2.72	0.44	77.00	73.86	3.14	0.53
Image 0570	79.85	76.70	3.15	0.50	76.70	73.71	2.99	0.48
Image 0572	80.17	77.00	3.17	0.47	77.00	73.76	3.24	0.62
Image 0574	80.05	76.50	3.55	0.53	76.50	73.36	3.14	0.58
Image 0576	80.48	76.50	3.98	0.64	76.50	73.56	2.94	0.63
Image 0578	80.53	76.59	3.94	0.74	76.59	73.14	3.45	0.79
Image 0580	81.33	76.80	4.53	0.80	76.80	73.45	3.35	0.81
Image 0686	79.96	77.00	2.96	0.55	76.99	74.28	2.71	0.36
Image 0688	80.18	77.00	3.18	0.55	76.99	74.91	2.08	0.32
Image 0690	79.77	77.31	2.46	0.45	77.30	75.54	1.76	0.26
Image 0692	79.51	78.01	1.50	0.27	78.00	76.53	1.47	0.21
Image 0694	80.36	77.90	2.46	0.35	77.89	76.50	1.39	0.19
Image 0696	78.99	77.11	1.88	0.30	77.10	75.78	1.32	0.24
Image 0698	78.84	77.00	1.84	0.28	76.99	75.26	1.73	0.26
Image 0700	78.35	76.61	1.74	0.25	76.60	75.72	0.88	0.18
Image 0702	78.60	76.30	2.30	0.31	76.29	74.99	1.30	0.26
Image 0704	77.96	76.11	1.85	0.28	76.10	75.05	1.05	0.20
Image 0706	78.99	76.11	2.88	0.69	76.10	73.92	2.18	0.39
Image 0708	77.80	75.81	1.99	0.33	75.80	74.04	1.76	0.32
Image 0710	78.03	75.50	2.53	0.35	75.49	73.77	1.72	0.28
Image 0712	77.90	75.50	2.40	0.35	75.49	73.82	1.67	0.28
Image 0714	77.66	75.31	2.35	0.38	75.30	73.99	1.31	0.27
Image 0716	77.89	75.01	2.88	0.41	75.00	73.47	1.53	0.27
Image 0718	77.31	74.91	2.40	0.39	74.90	73.08	1.82	0.35
Image 0720	77.56	74.71	2.85	0.43	74.70	73.02	1.68	0.35
Image 0722	77.97	74.80	3.17	0.47	74.79	73.26	1.53	0.30
Image 0724	79.17	75.31	3.86	0.59	75.30	73.44	1.86	0.36

**Table 62. Defects and Anomalies in King George**

King George				
Images	Polygon 1			
	Max [F]	Min [F]	$\Delta T$ [F]	Std Dev P1
Image 0827	74.72	64.57	10.15	1.32
Image 0828	69.99	64.18	5.81	0.72
Image 0829	67.91	63.21	4.70	0.69
Image 0830	67.09	63.57	3.52	0.55
Image 0831	65.96	62.91	3.05	0.42
Image 0832	66.03	62.22	3.81	0.43
Image 0833	65.15	62.17	2.98	0.42
Image 0834	64.63	61.48	3.15	0.39
Image 0835	64.72	61.43	3.29	0.42
Image 0836	64.35	61.69	2.66	0.31
Image 0837	64.42	61.31	3.11	0.34
Image 0838	64.55	61.84	2.71	0.32
Image 0839	64.04	60.30	3.74	0.49
Image 0840	64.12	59.27	4.85	0.72
Image 0841	64.23	58.58	5.65	0.74
Image 0845	63.23	54.15	9.08	1.34
Image 0848	65.24	60.25	4.99	0.55
Image 0849	63.86	61.82	2.04	0.25
Image 0851	63.93	61.62	2.31	0.26
Image 0852	64.15	62.11	2.04	0.27
Image 0855	63.83	61.76	2.07	0.24
Image 0857	64.13	62.16	1.97	0.20
Image 0858	65.52	61.45	4.07	0.38
Image 0859	71.06	62.18	8.88	1.31
Image 0860	71.23	61.08	10.15	1.47
Image 0861	71.44	63.98	7.46	1.72

### Comparison with Previous Studies

- The study compared its observed temperature differences ( $\Delta T$ ) with those reported in previous literature for known defects (e.g., cracks, delamination, voids).
- The  $\Delta T$  values observed across all three MSE walls (Crossgate, Old River Road, King George Boulevard) were significantly lower than the thresholds typically associated with structural defects in the referenced studies.

- This comparison strongly supports the conclusion that no significant cracks, voids, delamination, or other anomalies were detected in any of the MSE walls. The minor variations were consistently attributed to environmental factors or localized influences rather than structural integrity issues.

### **Distinguishing Defects from Joints & Visual Validation**

The section emphasizes the importance of careful temperature analysis to differentiate true structural cracks from normal modular panel joints, as they can exhibit similar thermal patterns. Abrupt fluctuations beyond expected joint behavior indicate a defect. Crucially, direct visual inspections were conducted at each site, and no observable cracks or structural defects were identified, further reinforcing the reliability of the thermal assessments.

### **Conclusion**

The study successfully demonstrated the effectiveness of IR(IRT) as a NDT method for evaluating thermal performance and identifying potential near surface or surficial anomalies in MSE retaining walls. The research, conducted on walls at Crossgate, Old River Road, and King George Boulevard, found no significant anomalies or defects that would compromise their structural integrity. Observed temperature variations were primarily attributed to external environmental factors (like vegetation, light poles, and atmospheric conditions) and structural geometry, rather than underlying defects. Trapezoidal walls (Crossgate and Old River Road) showed more variability at their ends, while the rectangular King George Boulevard wall exhibited more uniform thermal characteristics. The central sections of all walls consistently displayed thermal stability,

confirmed by narrow temperature ranges and low standard deviations. The analysis also concluded that the backfill material beneath the concrete panels did not significantly impact the observed surface temperatures due to the panel thickness. This research introduces a novel application of IRT to MSE walls, contributing to the field of NDT and offering a framework for optimizing infrastructure maintenance.

### **Recommendations for the Walls and for Further Studies**

Table 63 shows the recommendation for IRT inspection interval. Based on the findings, the following recommendations are made:

#### **IRT Inspection Intervals:**

The Crossgate Wall (10 years old) is recommended for annual IRT inspections because of its higher thermal variability, particularly at the ends, while the Old River Road (4 years old) and King George Boulevard (9 years old) walls are suitable for biennial inspections given their greater thermal stability in central sections. All inspections should be carried out under standardized conditions such as early mornings or late afternoons to ensure consistent and accurate results.

**Table 63. Recommended IRT inspection intervals for the MSE walls**

<b>Location</b>	<b>Year Constructed</b>	<b>Recommended IRT Inspection Routine</b>
Crossgate	2015	Annual
Old River Road	2021	Biennial
King George Boulevard	2016	Biennial

Focus Areas for Inspection: Greater attention should be given to wall ends, sections near vegetation, and areas exposed to light poles or other structural components, as these showed higher, though non-critical, variability.

Supplementary Techniques: To enhance reliability, supplementary NDT techniques like GPR could be used alongside IRT for validation in high-risk or complex regions.

Refining Protocols: Comparative analyses of IRT with other emerging Non-Destructive Evaluation (NDE) techniques are suggested to refine inspection protocols and establish industry standards.

Operator Training: Regular training programs for IRT inspectors are crucial to ensure consistency in data interpretation and accuracy.

### **Future Research:**

- Explore integrating advanced algorithms and artificial intelligence for automated detection and analysis of thermal anomalies to increase precision and efficiency.
- Investigate the long-term performance of MSE walls under varying climatic and environmental conditions to inform region-specific maintenance practices.

In essence, the study validates IRT as a reliable tool for MSE wall assessment and proposes a proactive, data-driven approach to infrastructure maintenance, emphasizing continuous improvement and technological integration.

## **CHAPTER 12. CONCLUSIONS AND RECOMMENDATIONS**

### **DESCRIPTION OF THE ANALYZED MEASURING/MODELING TECHNIQUES**

This study presents a compelling case for the adoption of advanced 3D remote-sensing technologies in infrastructure management, particularly for the monitoring of MSE/MB retaining walls at highway bridges, in Southeast Georgia. Several measuring/modeling techniques, including LiDAR CRP, and IRT, have been investigated and compared through rigorous field measurements, data collection, and data analyses, including comparison with measurements attained in the field with an accurate benchmarking instrument, a one-second robotic total-station device, referred to as RTS, from Leica Geosystems. This was accomplished at five different sites. Four of them were bridges located in Southeast Georgia, and one was a CW, at the Statesboro Campus of GSU. The four bridges were referred to as B1-Crossgate, B2-Old River, B3-Sandersville, and B4-King George. Each bridge site contained two MSE walls, although the CW consisted of just one wall, the façade of the Carruth Building. The research demonstrates that static, terrestrial LiDAR-based monitoring systems can achieve consistent, near-centimeter accuracy in detecting wall displacements/deformations anywhere on the full façades of the monitored walls. This represents a significant advancement over traditional visual inspection methods, providing engineers with quantitative data to make informed maintenance decisions.

The following subsections detail the methodologies and findings related to LiDAR and CRP. Conclusions pertaining to IRT are discussed separately in Chapter 11, within its dedicated Conclusions subsection.

## **Measuring/Modeling Techniques Studied at the CW**

At the CW site, several measuring/modeling techniques were investigated for a dual purpose, to compare their relative performance with respect to accurate benchmarking measurements, and to assess their ability to capture small, simulated displacements occurring between two times, Epoch 1 and Epoch 2. In this regard, the practical noise level associated with several of those techniques was estimated as well.

Two main LiDAR-based modeling techniques were employed. One of them is TB LiDAR, and uses targets acquired in the field, at high resolution, to stitch individual scans and generate full models, while registering them in a single system of reference. For that purpose, spherical targets were placed at all GCPs points and were acquired by each scan. These models, and/or the spatial data extracted from them, at Epochs 1 and 2, were referred to as LT1 and LT2, respectively. The other LiDAR-based technique was Visual-Alignment (VA) LiDAR which does not require targets to stitch/register individual scans. However, it requires properly and highly overlapped neighboring scans. These models and/or the spatial data extracted from them were designated as LV1 and LV2, for Epochs 1 and 2, respectively. Concerning georeferencing, both LiDAR approaches needed to acquire a minimum of three targets placed on the GCPs.

Regarding CRP, a total of 6 photo-based models were analyzed. Three were constructed using images captured with a handheld camera: (i) Model ML#, created in Agisoft's Metashape using a large set of photographs (ii) Model MM#, created in Agisoft's Metashape using a medium (or moderate) set of photographs, and (iii) Model MS#, created in Agisoft's Metashape using a small

set of photographs. The other three models were built from UAV-acquired imagery: (iv) Model MD#, generated in Agisoft Metashape, (v) Model DS#, generated in DroneDeploy using GCPs only, and (vi) Model DE#, generated in DroneDeploy using both GCPs and EACPs. When a given modeling technique was applied in both Epoch 1 and Epoch 2, the resulting models and associated data were labeled with the suffixes “1” and “2” in place of the # symbol to distinguish between them.

At Epochs 1 and 2, the 8 models generated of the CW, at Epochs 1 and 2, were, respectively, referred to as follows:

- (i) MS1 & MS2: Metashape software with a small # of pics from a hand-held camera.
- (ii) MM1 & MM2: Metashape software with a medium # of pics from a hand-held camera.
- (iii) ML1 & ML2: Metashape software with a large # of pics from a hand-held camera.
- (iv) MD1 & MD2: Metashape software with pics taken from a drone camera.
- (v) DS1 & DS2: DroneDeploy software with pics taken from a drone, using only GCPs.
- (vi) DE1 & DE2: DroneDeploy software with pics taken from a drone, Using GCPs & EACPs.
- (vii) LT1 & LT2: TB LiDAR.
- (viii) LV1 & LV2: Visual-Alignment LiDAR.

In this site, 6 CPs were marked on the CW for displacement monitoring purposes. Their locations, position coordinates, were measured with the RTS instrument, at Epochs 1 and 2, and the corresponding data is referred to as RTS1 and RTS2, respectively. In all cases, 6 PDs (position discrepancies) and 15 DDs among the 6 CPs were analyzed.



Additionally, CC software was employed to perform full-wall comparisons between two LiDAR datasets [LT1 vs. LT2] and two CRP datasets [MM1 vs. MM2]. To quantify the differences between the models, two distinct model-discrepancy approaches were applied: the 'absolute' distances derived from the C2C method, and the 'signed' distances obtained using the M3C2 technique. These comparisons were statistically robust, as they assessed spatial discrepancies across several million points, rather than a limited sample of just 6 CPs.

### **Measuring/Modeling Techniques Studied at the B1-Crossgate**

At the B1-Crossgate site, during the Summer 2023 academic term, a period designated as Epoch 1, two modeling techniques were investigated: Terrestrial LiDAR and CRP. Both were employed to model the two MSE walls at this site. Regarding LiDAR, two different registration approaches were implemented, TB LiDAR (TB LiDAR), and Visual-Alignment LiDAR (VA LiDAR). Concerning CRP, a model of the walls was generated using the online DroneDeploy software platform with pictures taken from an UAV, DJI's Matrice 30. In this case, EACPs were incorporated to improve the accuracy of the resulting model.

The initial research plan included remapping the walls one to two years later to evaluate the ability of the models to detect potential displacement over time. However, this plan had to be revised. In early Summer 2024, the original GCPs established in 2023 were unintentionally removed during shoulder and pavement work conducted by GDOT. This loss was discovered by the research team on June 7, 2024, and promptly reported to GDOT. Without the GCPs, no further spatial modeling or comparative analysis could be performed at that site. To mitigate this

setback, the research team introduced a CW site to the project. At the CW location, displacements of known small magnitudes (3, 5, 11, 17, 24, and 30 mm) were simulated to evaluate the precision and effectiveness of the Terrestrial LiDAR and Photogrammetry techniques in capturing subtle structural changes. This pivot ensured that the core objectives of the study remained intact and continued to yield meaningful data.

Nonetheless, the work completed at the B1-Crossgate site in Summer 2023 was still useful to compare the ability of the employed modeling techniques to generate accurate spatial representations, with respect to measurements completed with the accurate RTS instrument. For that purpose, 12 CPs were marked on the MSE walls, 6 per wall. The positional coordinates of these CPs were measured using the benchmarked RTS instrument, and they were referred to as RTS1. Additionally, the models and/or the set of coordinates extracted from them, were referred to as: TBL1, for the TB LiDAR method; VAL1 for the VA LiDAR technique, and DS1 for the CRP-based DroneDeploy model. For model evaluation, PDs were calculated by comparing the checkpoint data extracted from TBL1, VAL1, and DS1 against the reference RTS1 measurements.

## **Measuring/Modeling Techniques Studied at B2-Old River**

At the B2-Old River site, two LiDAR modeling techniques—TB and VA—were applied during two separate epochs (Fall 2023 and Fall 2024 academic terms) to evaluate measurement and modeling noise. TB LiDAR used spherical targets at GCPs for scan registration, while VA LiDAR relied on overlapping scans without physical targets. Both required three georeferencing targets, at least, to align models within the GCP-based coordinate system.

To assess displacements and model accuracy, 12 CPs were placed on the MSE walls and measured using an RTS instrument at both epochs, referred to as RTS1 and RTS2. The resulting models and data were labeled TBL1, TBL2 (for TB LiDAR) and VAL1, VAL2 (for VA LiDAR). Positional and DDs between CP coordinates and RTS measurements were analyzed across both epochs.

In addition, CC software was used to perform full-wall comparisons of the TBL1 and TBL2 models using two techniques: C2C for absolute distances, and M3C2 for signed distances. These comparisons involved analysis of millions of points, far beyond the 12 CPs.

Initially, at the B2-Old River site, two models of the same walls were generated one year apart, one in Epoch 1 and one in Epoch 2, to capture potential wall displacements occurring during that period. However, simultaneous accurate, reflectorless measurements, completed with the benchmarking RTS instrument, at those two times, led to infer that there were no measurable (above noise) wall displacements during that year. To reach that inference, the RMSV of positional discrepancies measured at 12 CPs, on the façades of those MSE walls, was considered.

At each epoch, those positions were measured twice in reflectorless mode with the accurate RTS instrument. The resulting RMSV was relatively low, 6.7 mm, which is very close to the *Reflectorless Floor Noise* of the RTS instrument (~6 mm). That floor noise was estimated earlier in this report in the section describing all employed instruments. Consequently, it was inferred that those walls did not displace from Epoch 1 to 2, and all measurements/models completed at those two different times were employed to estimate the noise associated with successive measurements, of the same static, undeformed structure, when employing twice the same measuring/modeling techniques.

### **Measuring/Modeling Techniques Studied at B3-Sandersville**

At the B3-Sandersville site, further studies included LiDAR-based modeling techniques. Investigations extended to analyze differences in TB LiDAR when employing field- or software-acquired targets, and differences in VA LiDAR when using close neighbors (highly overlapped) scans or randomly ordered (poorly overlapped) scans when visually aligning them. Additionally, a CRP modeling approach was studied at this site. It used the Agisoft Metashape software package with pictures taken from a hand-held DSLR, 24.1-MP (million pixel) camera. This model, and/or the measurements extracted from it, are referred to as MHP. Similarly, on this site, the measurements completed via the RTS instrument are simply referred to as RTS. Those extracted from the resulting TB LiDAR models are referred to as FTL (for TB LiDAR with field-acquired targets), STL (for TB LiDAR with software-acquired targets), and those from the resulting VA LiDAR models are referred to as LVL (for VA LiDAR using close-neighboring scans), and RVL (for VA LiDAR using randomly ordered scans). Furthermore, on this site, the

CC software was employed for full-wall comparisons of the FTL and MHP models. It used the previously referred two different schemes, C2C and M3C2, to determine positional discrepancies.

### **Measuring/Modeling Techniques Studied at B4-King George**

At the B4-King George site, during the Summer 2024 academic term, a period designated as Epoch 1, two modeling techniques were investigated: Terrestrial LiDAR and CRP. Both were employed to model the two MSE walls at this site. Regarding LiDAR, two different registration approaches were implemented TB LiDAR and VA LiDAR. For CRP, a photogrammetric model of the walls was generated using DSLR images captured with a hand-held camera, Nikon D5300, and processed in Agisoft's Metashape. A total of 2,449 photos were taken, and the model was scaled using a locally defined system of reference based on a closed traverse.

The work completed at this site proved valuable in comparing the relative accuracy of the employed modeling techniques with respect to field measurements obtained using the accurate RTS instrument. For this purpose, 16 CPs were marked on the MSE walls—8 on each wall. The positional coordinates of these CPs were measured using the benchmarking RTS instrument, and they were referred to as RTS1. Corresponding 3D coordinates were also extracted from the point-cloud models developed via LiDAR and photogrammetry. These models and/or their extracted coordinate sets were labeled as: TBL1 for the TB LiDAR method, VAL1 for the VA LiDAR method, and ML1 for the Metashape-generated CRP model. For model evaluation, PDs and DDs were calculated by comparing the CP data extracted from TBL1, VAL1, and MS1 against the RTS1 reference measurements.

## CONCLUSIONS INFERRED FROM WORK AT THE CW SITE

### Inferences regarding the ability to capture small displacements at CW

- The known magnitudes of the simulated displacements, at all 6 CPs, were 3, 5, 11, 17, 24, and 30 mm. Those displacements were also determined from the final models by vectorially subtracting the point positions in Epoch 1 (non-displaced configuration) from those in Epoch 2 (displaced configuration). For a given modeling technique, an overall measure of the magnitude of those errors is provided by its calculated RMSV. Using this error metric, the measuring/modeling techniques are ranked below from more to less accurate:

1. For [LT2 - LT1], the errors in displacements resulted in RMSV = 3.7 mm.
2. For [LV2 - LV1], the errors in displacements resulted in RMSV = 3.8 mm.
3. For [MD2 - MD1], the errors in displacements resulted in RMSV = 5.5 mm.
4. For [RTS2 - RTS1], the errors in displacements resulted in RMSV = 6.1 mm.
5. For [MM2 - MM1], the errors in displacements resulted in RMSV = 7.7 mm.
6. For [DE2 - DE1], the errors in displacements resulted in RMSV = 10.3 mm.
7. For [MS2 - MS1], the errors in displacements resulted in RMSV = 11.6 mm.
8. For [ML2 - ML1], the errors in displacements resulted in RMSV = 15.3 mm.
9. Model DS1 showed large inaccuracies. Therefore, DS2 was not generated.

The above ranking indicates that, for measuring small displacements (3-30 mm), the TB LiDAR approach achieved the highest performance, closely followed by the VA LiDAR

technique—with only a marginal difference between them. The third-best accurate result was obtained by the Metashape model generated using drone imagery, which relied solely on GCPs and did not incorporate EACPs. Surprisingly, the benchmarking measurements taken with the RTS instrument ranked fourth, though their associated RMSV value remained relatively low at 6.1 mm. Fifth place was occupied by the Metashape model created using a moderate number of images from a hand-held camera. All remaining models presented RMSVs exceeding 10 mm (1 cm). In addition, the standard deviation of the population  $\sigma$ , constitutes a good measure of dispersion of error when determining those displacements. In this regard, the following ranking was observed:

1. For [MD2 - MD1], the errors in displ. resulted in  $\sigma = \text{STD-P} = 2.6 \text{ mm}$ .
2. For [LT2 - LT1], the errors in displ. resulted in  $\sigma = \text{STD-P} = 3.9 \text{ mm}$ .
3. For [LV2 - LV1], the errors in displ. resulted in  $\sigma = \text{STD-P} = 4.0 \text{ mm}$ .
4. For [MM2 - MM1], the errors in displ. resulted in  $\sigma = \text{STD-P} = 4.9 \text{ mm}$ .
5. For [RTS2 - RTS1], the errors in displ. resulted in  $\sigma = \text{STD-P} = 5.8 \text{ mm}$ .
6. For [ML2 - ML1], the errors in displ. resulted in  $\sigma = \text{STD-P} = 6.1 \text{ mm}$ .
7. For [MS2 - MS1], the errors in displ. resulted in  $\sigma = \text{STD-P} = 7.5 \text{ mm}$ .
8. For [DE2 - DE1], the errors in displ. resulted in  $\sigma = \text{STD-P} = 8.7 \text{ mm}$ .
9. Model DS1 showed large inaccuracies. Therefore, DS2 was not generated.

The above standard-deviation values indicate that the Metashape model with UAV imagery (using GCPs, but no EACPs) obtained the least dispersion ( $\sigma = 2.6 \text{ mm}$ ) in

displacement errors, outperforming both LiDAR-based models. Nevertheless, the one-sigma dispersions attained by LT#, LV# and MM# were all  $\sigma \leq 5$  mm.

- The TB LiDAR approach—exhibiting the strongest modeling performance—was selected for an in-depth, full-wall analysis to assess its capability in detecting subtle wall displacements over time. This evaluation involved comparing complete models of the CW from Epochs 1 and 2 using CC software, leveraging both the C2C and M3C2 algorithms to measure model discrepancies via absolute and signed distances, respectively. Assuming a uniform determination of model-discrepancies (displacements) across the wall surface, cumulative probability values were interpreted as the proportion of wall area exhibiting displacements below predefined thresholds.

- (i) C2C Analysis: Approximately  $6.01 \times 10^6$  position discrepancies (absolute distances) were calculated between LT2 and LT1. The results showed that ~91.1% of the wall experienced displacements of  $\leq 3.0$  mm, closely matching the known static condition of ~96.5%. Only 3.5% of the wall—intentionally displaced using Styrofoam inserts—exhibited movement within the 3 mm to 34 mm range.
- (ii) M3C2 Analysis: Roughly  $4.94 \times 10^6$  signed position discrepancies were analyzed between LT2 and LT1. The data revealed that 95% of the wall surface fell within the displacement interval of  $[-3.8$  mm,  $+2.7$  mm], again consistent with the known condition of 96.5% static area.



Minor displacements detected in regions expected to remain static are attributed to the inherent, low-level noise of the TB LiDAR method. In summary, the TB LiDAR approach exhibited robust performance in accurately capturing all simulated wall displacements, including both static and intentionally altered regions. All this attained while determining ~6 and ~5 million points discrepancies (via the C2C and M3C2 schemes, respectively) between the compared clouds.

- Additionally, the CRP-based models MM1 and MM2, which were recognized, at this and at other sites, for their superior performance, were selected for a comprehensive, full-wall evaluation using CC comparison algorithms, C2C and M3C2. This model employed a moderate number of images from a handheld camera, Nikon 5300.

### **C2C Analysis:**

- a) The comparison between MM2 and MM1 involved approximately  $3.11 \times 10^6$  position discrepancies (absolute distances).
- b) Results indicated that 95% of the CW exhibited displacements  $\leq 27.7$  mm, which is unexpectedly high given the known conditions.
- c) Only about 30% of the wall showed displacements  $\leq 3$  mm, while roughly 90% displayed displacements below 34 mm.

These results imply that about 60% of the wall surface was detected as having moved, contradicting the actual condition in which only 3.5% was physically displaced using Styrofoam inserts.

### **M3C2 Analysis:**

- a) This comparison involved approximately  $0.16 \times 10^6$  signed position discrepancies between MM2 and MM1.
- b) It showed that 95% of the wall surface displaced within the range of  $[-34.5 \text{ mm}, +33.5 \text{ mm}]$ , again misaligning with the known condition that only around 3.6% of the wall experienced actual movement between 3 mm and 34 mm.

The apparent inaccuracies likely stem from photogrammetry modeling artifacts, such as wavy or rippled surfaces where none exist, floating textures, disconnected fragments, and nonexistent bulges, pits, or holes. These modeling anomalies introduced false displacement detections, which were evident in the MM2 vs MM1 visualization as widespread red regions, representing exaggerated or fictitious changes. Ultimately, both the C2C and M3C2 comparison schemes produced similarly inaccurate results in the MM2 vs MM1 analysis. These findings indicate the limitations of studied CRP-based photogrammetry model for detecting fine-scale displacements, especially when compared to more precise LiDAR methods.

### **Inferences regarding the relative accuracy of measurements at the CW**

- For each model analyzed, displacements at the 6 CPs were calculated vectorially by subtracting their RTS1 positions—measured using the RTS instrument at Epoch 1—from their modeled positions at Epoch 2. Given that the actual simulated displacements were

known (3, 5, 11, 17, 24, and 30 mm), the corresponding displacement errors could be quantified. Assuming these errors follow a Gaussian distribution, the 95% confidence interval was estimated as  $\{\mu - 1.96 \times \sigma, \mu + 1.96 \times \sigma\}$ . The maximum absolute value of either bound of this interval was taken as a representative measure of the noise associated with displacement estimation using this method. These noise estimates, ordered from smallest to largest, are as follows:

1. For [LT2-RTS1], the estimated noise level in displ. determination is: 12.8 mm.
2. For [MM2-RTS1], the estimated noise level in displ. determination is: 14.4 mm.
3. For [LV2-RTS1], the estimated noise level in displ. determination is: 15.5 mm.
4. For [MD2-RTS1], the estimated noise level in displ. determination is: 17.5 mm.
5. For [MS2-RTS1], the estimated noise level in displ. determination is: 17.7 mm.
6. For [ML2-RTS1], the estimated noise level in displ. determination is: 19.7 mm.
7. For [DE2-RTS1], the estimated noise level in displ. determination is: 22.2 mm.

This ranking indicates that the TB LiDAR model presented the smallest noise level, closely followed by the CRP-based MM# and VA LiDAR models. The above relative noise levels have been useful in ranking the models with respect to benchmarking measurements. However, they all involve the inherent error of the RTS instrument and cannot be considered as ground-truth noise of each model studied. Nevertheless, they still have been considered when determining the final estimated noise levels occurring when modeling the CW, as indicated later in this section.

- The distance-discrepancy study in this wall considered 15 non-repeated distances among the 6 CPs. Those distances were extracted from Epoch 1 models and compared against the corresponding distances RTS1, measured in the field, by the RTS instrument, also in Epoch 1. The corresponding RMSV is a statistical measure of the magnitudes of those DDs. Models ML1, MM1, MS1, MD1, LT1, and LV1 are ranked, from least to largest RMSV, as follows:

1. The [LV1 - RTS1] comparison resulted in DDs with RMSV = 1.7 mm.
2. The [LT1 - RTS1] comparison resulted in DDs with RMSV = 1.8 mm.
3. The [MS1 - RTS1] comparison resulted in DDs with RMSV = 6.6 mm.
4. The [MM1 - RTS1] comparison resulted in DDs with RMSV = 6.9 mm.
5. The [MM1 - RTS1] comparison resulted in DDs with RMSV = 7.4 mm.
6. The [MD1 - RTS1] comparison resulted in DDs with RMSV = 12.6 mm.

Additionally, assuming a Gaussian distribution of the discrepancies in distances, the 95% confidence interval was estimated as  $\{\mu - 1.96 \times \sigma, \mu + 1.96 \times \sigma\}$ . The maximum absolute value of either bound of this interval served as an indicator of the noise level associated with distance determination using these methods. These noise estimates, arranged from smallest to largest, are as follows:

1. For [LV1 - RTS1], the estimated noise level in distance determination is: 3.7 mm.
2. For [LT1 - RTS1], the estimated noise level in distance determination is: 3.8 mm.
3. For [MS1 - RTS1], the estimated noise level in distance determination is: 11.6 mm.
4. For [MM1 - RTS1], the estimated noise level in distance determination is: 13.5 mm.

5. For [ML1 - RTS1], the estimated noise level in distance determination is: 15.1 mm.
6. For [MD1 - RTS1], the estimated noise level in distance determination is: 31.9 mm.

The above rankings clearly indicate that both LiDAR models performed very well with only marginal differences. They clearly outperformed the CRP-based models. The relative RMSVs and associated noise levels presented above have been valuable for ranking the models in relation to benchmarking RTS measurement. However, these values inherently include error from the RTS instrument itself and, therefore, cannot be regarded as the true noise levels of the individual models. Despite this limitation, they were still factored into the process of estimating the final noise levels encountered when modeling the CW, as presented later in this section.

### **Inferences on the noise level inherent to different techniques at the CW site**

Practical noise level estimators were evaluated, compared, and integrated during the application of different remote-sensing and modeling techniques at the CW site. The most conservative estimates—derived from both direct measurements using the benchmarking RTS instrument and from final georeferenced data obtained from the following modeling measuring/modeling techniques—are as follows:

1. Conservative *Practical Noise Level* associated with LT#: 12.8 mm
2. Conservative *Practical Noise Level* associated with RTS: 13.5 mm
3. Conservative *Practical Noise Level* associated with LV#: 15.5 mm

4. Conservative *Practical Noise Level* associated with DE#: 22.6 mm
5. Conservative *Practical Noise Level* associated with MS#: 23.6 mm
6. Conservative *Practical Noise Level* associated with ML#: 26.0 mm
7. Conservative *Practical Noise Level* associated with MD#: 31.9 mm
8. Conservative *Practical Noise Level* associated with MM#: 34.5 mm

However, the values above may be overly conservative, particularly for the LiDAR-based models. The multi-million-point comparison, performed via the CC software, of the full CW, using TB LiDAR data revealed a 95% probability of displacement magnitudes being  $\leq 3.0$  mm using the C2C algorithm, and  $\leq 3.8$  mm using the M3C2 algorithm. This should be considered alongside the fact that 96.5% of the CW area exhibited no simulated displacement at all. Consequently, as indicated, the initially adopted noise thresholds were adjusted from the conservative estimates to the following moderately conservative values:

1. Adopted (at CW) *Practical Noise Level* associated with LT#: 6.3 mm
2. Adopted (at CW) *Practical Noise Level* associated with LV#: 8.4 mm
3. Adopted (at CW) *Practical Noise Level* associated with RTS: 9.9 mm
4. Adopted (at CW) *Practical Noise Level* associated with MM#: 18.4 mm
5. Adopted (at CW) *Practical Noise Level* associated with MS#: 18.4 mm
6. Adopted (at CW) *Practical Noise Level* associated with DE#: 18.7 mm
7. Adopted (at CW) *Practical Noise Level* associated with ML#: 20.9 mm
8. Adopted (at CW) *Practical Noise Level* associated with MD#: 21.1 mm

## CONCLUSIONS INFERRED FROM WORK AT THE B1-CROSSGATE SITE

The models considered at this site were 3 and they were completed at Epoch 1. They were designated as follows: TBL1 for TB LiDAR, VAL1 for visual-alignment LiDAR, and DS1 for the CRP via DronDeploy. This model employed pictures taken with the DJI's Matrice 30 drone. In this case, elevated, ACPs were incorporated to improve accuracy. The field measurements completed with the benchmarking RTS instrument were designated as RTS1.

### Inferences regarding the relative accuracy of measurements at B1-Crossgate

- The following values represent the magnitude of positional discrepancies (PDs) at 12 control points, calculated by subtracting field measurements (RTS1) from the corresponding positions derived from three generated models—TBL1, VAL1, and DS1—at Epoch 1:
  1. The [VAL1 - RTS1] comparison resulted in  $RMSV = 7.2$  mm.
  2. The [TBL1 - RTS1] comparison resulted in  $RMSV = 8.2$  mm.
  3. The [DS1 - RTS1] comparison resulted in  $RMSV = 28.6$  mm.

These results indicate that the VAL1 and TBL1 LiDAR-derived models exhibit similar relative discrepancies with respect to the RTS1 field measurements, with VAL1 performing slightly better. In contrast, the photogrammetric model DS1 shows significantly larger discrepancies, even after incorporating EACPs. Assuming those discrepancies follow a Gaussian distribution, approximately 95% of them are expected to

lie within the interval  $\{\mu \pm 1.96 \times \sigma\}$ . Based on this assumption, the estimated 95% confidence intervals for the models are:

1. For [TBL1-RTS1]:  $= \{7.6 - 1.96 \times 2.5, 7.6 + 1.96 \times 2.5\} = \{2.7 \text{ mm}, 12.5 \text{ mm}\}$
2. For [VAL1-RTS1]:  $= \{6.3 - 1.96 \times 3.6, 6.3 + 1.96 \times 3.6\} = \{-0.8 \text{ mm}, 13.4 \text{ mm}\}$
3. For [DS1-RTS1]:  $= \{26.6 - 1.96 \times 10.4, 26.6 + 1.96 \times 10.4\} = \{6.2 \text{ mm}, 47.0 \text{ mm}\}$

The maximum absolute value of each interval's bounds can be interpreted as an estimate of the noise level associated with each modeling technique: Those noise estimates are: 12.5 mm for TBL1; 13.4 mm for VAL1; and 47.0 mm for DS1. However, it is important to note that these estimates also include the noise measurement from RTS1. Therefore, they do not exclusively represent the intrinsic noise of the models themselves.

- The following values represent the magnitude of DDs calculated from 66 unique, non-repeated distances among the 12 CPs (control points). These discrepancies were obtained by subtracting precise RTS1 field measurements from the corresponding distances extracted from the models TBL1, VAL1, and DS1 at Epoch 1:
  - The [VAL1 - RTS1] comparison resulted in DDs with RMSV = 3.3 mm.
  - The [TBL1 - RTS1] comparison resulted in DDs with RMSV = 4.9 mm.
  - The [DS1 - RTS1] comparison resulted in DDs with RMSV = 23.3 mm



In this case, as with positional discrepancies, the VAL1 and TBL1 LiDAR-derived models significantly outperformed the photogrammetric model DS1 in terms of DDs with respect to RTS1 measurements. Among the LiDAR models, VAL1 exhibited slightly better agreement with the RTS1 reference measurements than TBL1. Notably, both LiDAR models achieved RMSVs less than 5 mm, indicating high agreement with RTS1 distance measurements. If those DDs follow a normal (Gaussian) distribution, approximately 95% of the values are expected to fall within the range of  $\{\mu \pm 1.96 \times \sigma\}$ . Based on this assumption, the estimated 95% confidence intervals for each model are as follows:

1. For [VAL1-RTS1]:  $= \{-0.7 - 1.96 \times 3.3, -0.7 + 1.96 \times 3.3\} = \{-7.1 \text{ mm}, 5.8 \text{ mm}\}$
2. For [TBL1-RTS1]:  $= \{-1.5 - 1.96 \times 4.7, -1.5 + 1.96 \times 4.7\} = \{-10.7 \text{ mm}, 7.7 \text{ mm}\}$
3. For [DS1-RTS1]:  $= \{5.6 - 1.96 \times 22.6, 5.6 + 1.96 \times 22.6\} = \{-38.7 \text{ mm}, 49.9 \text{ mm}\}$

The highest absolute value within each interval can be interpreted as an estimate of the total noise level associated with each modeling method: Those noise estimates are: 7.1 mm for VAL1; 10.7 mm for TBL1; and 49.9 mm for DS1. It should be emphasized, however, that these noise estimates also incorporate the uncertainty present in the RTS1 field measurements. As a result, they do not solely reflect the inherent noise of the models themselves.

## CONCLUSIONS INFERRED FROM WORK AT THE B2-OLD RIVER SITE

### Inferences Regarding Repeatability of Measurements at B2-Old River

- The magnitudes of PDs (position discrepancies) at 12 CPs were extracted from two TB LiDAR models—TBL1 and TBL2 (Epochs 1 and 2, respectively)—and two VA LiDAR models—VAL1 and VAL2—of the same walls. The results are as follows:
  1. The [TBL2 - TBL1] comparison resulted in PDs with RMSV = 7.0 mm.
  2. The [VAL2 - VAL1] comparison resulted in PDs with RMSV = 8.5 mm.

These results indicate that the TB LiDAR approach exhibits slightly lower noise and marginally better repeatability than the VA LiDAR method. However, as demonstrated in these VA LiDAR models, when scans have substantial overlap and are registered sequentially using a close-neighboring pattern—ideally forming a closed loop—the repeatability of the VA LiDAR technique approaches that of TB LiDAR. This holds true for full models that are relatively compact and involve a limited number of scans, as was the case for the models generated at B1–Old River. Notably, the RMSVs from both LiDAR methods are comparable to those obtained using the benchmarking RTS instrument, where the [RTS2 - RTS1] comparison resulted in an RMSV of 6.7 mm. As expected, the RTS device demonstrated the lowest noise and highest repeatability among the methods evaluated.

- The repeatability of the TB LiDAR modeling approach, recognized for its superior modeling performance, was further evaluated by comparing full 3D models of the same

walls, generated at Epochs 1 and 2. This analysis was conducted using CC software, applying both the C2C and M3C2 schemes. With 95% confidence, the following results were obtained for each wall:

North Wall, [N-TBL2 – N-TBL1] comparison:

- C2C “absolute” distance  $\leq 8.0$  mm, based on 14.11 million points.
- M3C2 “signed” distance range:  $-4.4$  mm to  $4.0$  mm, based on 4.25 million points.

South Wall, [S-TBL2 – S-TBL1] comparison:

- C2C “absolute” distance  $\leq 7.2$  mm, based on 13.47 million points.
- M3C2 “signed” distance range:  $-3.6$  mm to  $2.8$  mm, based on 4.57 million points.

These small positional discrepancies—captured with 95% probability by both C2C and M3C2 methods—highlight the strong repeatability of the TB LiDAR technique in producing consistent models of static wall structures.

- The magnitudes of DDs across 66 unique, non-repeated distances among 12 CPs were extracted from two TB LiDAR models (TBL1 and TBL2) and two VA LiDAR models (VAL1 and VAL2) of the same walls can be measured by their associated RMSVs:
  1. The [TBL2 - TBL1] comparison resulted in DDs with RMSV = 5.4 mm.
  2. The [VAL2 - VAL1] comparison resulted in DDs with RMSV = 7.5 mm.

These results indicate that the TB LiDAR method exhibits slightly lower noise and marginally better consistency than the VA LiDAR approach. For reference, the benchmarking instrument (RTS) produced an RMSV of 4.0 mm for the [RTS2 – RTS1] comparison—lower than both LiDAR-based results, as expected. Nevertheless, the repeatability achieved by both TB and VA LiDAR methods closely approaches that of the benchmarking RTS instrument.

### **Inferences Regarding the Relative Accuracy of Measurements at B2-Old River**

- The following values represent the magnitudes of PDs (position discrepancies) at 12 CPs, calculated by subtracting the accurate field measurements obtained with the benchmarking instrument (RTS1) from the corresponding positions extracted from the generated models—TBL1, TBL2, VAL1, and VAL2—at Epochs 1 and 2:
  - The [TBL1 - RTS1] comparison resulted in PDs with RMSV = 7.2 mm.
  - The [TBL2 - RTS1] comparison resulted in PDs with RMSV = 5.2 mm.
  - The [VAL1 - RTS1] comparison resulted in PDs with RMSV = 7.5 mm.
  - The [VAL2 - RTS1] comparison resulted in PDs with RMSV = 4.8 mm.

Based on the RMSV values, both TB and VA LiDAR models demonstrated comparable relative accuracy when evaluated against the RTS1 benchmark measurements. Notably, the second set of LiDAR models (TBL2 and VAL2) exhibited smaller discrepancies relative to RTS1 than their corresponding first sets (TBL1 and VAL1). This trend further supports the

assumption that no measurable wall displacements occurred between Epochs 1 and 2, indicating that the walls remained static during the observation period. Consequently, these results justify using the data to assess the repeatability of each modeling technique when applied twice to the same static structures.

- The following values represent the magnitudes of DDs across 66 unique, non-repeated distances among the 12 considered CPs. These were calculated by subtracting the accurate field measurements obtained with the benchmarking instrument (RTS1) from the corresponding distances extracted from the models TBL1, TBL2, VAL1, and VAL2, generated at Epochs 1 and 2:
  - The [TBL1 - RTS1] comparison resulted in DDs with  $RMSV = 6.7$  mm.
  - The [TBL2 - RTS1] comparison resulted in DDs with  $RMSV = 4.3$  mm.
  - The [VAL1 - RTS1] comparison resulted in DDs with  $RMSV = 7.7$  mm.
  - The [VAL2 - RTS1] comparison resulted in DDs with  $RMSV = 3.0$  mm.

In this case, both the TB and VA LiDAR models demonstrated comparable relative accuracy when evaluated against the RTS1 benchmark measurements. Once again, the second set of LiDAR models (TBL2 and VAL2) showed smaller discrepancies relative to RTS1 than the first set (TBL1 and VAL1). This further supports the use of these values to assess the repeatability of each modeling approach.

### **Inferences Regarding the Noise Associated with RTS, TB, & VA at B2-Old River:**

At the B2–Old River site, practical noise levels were estimated during the application of various measurement and modeling techniques used to capture the spatial geometry of the MSE walls at the bridge abutments. To achieve this, multiple estimators were considered, compared, and synthesized. Conservative estimates—based on actual measurements from the benchmarking RTS instrument and georeferenced outputs from the TB LiDAR and VA LiDAR models—are as follows:

Conservative (at B2-Old River) *Practical Noise Level* associated with RTS: 11.9 mm

Conservative (at B2-Old River) *Practical Noise Level* associated with TB LiDAR: 15.7 mm

Conservative (at B2-Old River) *Practical Noise Level* associated with VA LiDAR: 19.3 mm

However, these values may be overly conservative. CC analyses of the full point clouds from the TB LiDAR models indicated a 95% probability of achieving absolute positional discrepancies of  $\leq 8.0$  mm using the C2C method, and  $\leq 4.4$  mm using the M3C2 method. Based on this evidence, slightly lower—yet still cautious—noise levels were adopted and are referred to as *moderately conservative* estimates. They are:

Adopted (at B2-Old River) *Practical Noise Level* associated with RTS: 9.7 mm

Adopted (at B2-Old River) *Practical Noise Level* associated with TB LiDAR: 11.9 mm

Adopted (at B2-Old River) *Practical Noise Level* associated with VA LiDAR: 14.3 mm

## CONCLUSIONS INFERRED FROM WORK AT THE B3-SANDERSVILLE SITE

At this bridge site, the study of the modeling techniques generated the following inferences regarding the relative accuracy of their measurements:

### Inferences Regarding the Relative Accuracy of Measurements at B3-Sandersville

- The magnitudes of PDs (position discrepancies) at 12 CPs were evaluated by comparing the positions extracted from five different 3D models—MHP, STL, FTL, LVL, and RVL—against accurate field measurements obtained using the benchmarking RTS instrument. The RMSVs of the discrepancies are as follows:
  1. The [LVL - RTS] comparison resulted in PDs with RMSV = 9.4 mm.
  2. The [FTL - RTS] comparison resulted in PDs with RMSV = 10.2 mm.
  3. The [STL - RTS] comparison resulted in PDs with RMSV = 10.7 mm.
  4. The [RVL - RTS] comparison resulted in PDs with RMSV = 16.6 mm.
  5. The [MHP - RTS] comparison resulted in PDs with RMSV = 22.1 mm.

These results indicate that the LVL model, a visual-alignment LiDAR approach using a highly overlapped, close-neighboring stitching pattern, achieved the highest relative accuracy. The FTL model, a TB LiDAR method with field-acquired targets in high-resolution, performed similarly. The STL model, also TB but relying on software-acquired targets, ranked third. All three methods demonstrate comparable accuracy and

are suitable for reliably modeling the MSE walls at this bridge. In contrast, the RVL model—a visual-alignment LiDAR approach without a close-neighboring alignment strategy—exhibited significantly higher positional errors, approximately 60% greater than the top performers. The MHP model, based on CRP using a handheld DSLR camera, showed the largest discrepancies, with errors nearly doubling those of the top three methods.

- DDs were evaluated across 66 unique, non-repeated distances among the 12 CPs. These were calculated by comparing the distances extracted from the same five models MHP, STL, FTL, LVL, and RVL—against the RTS benchmark. The resulting RMSVs are ranked as follows:

1. The [FTL - RTS] comparison resulted in DDs with  $\text{RMSV} = 3.2 \text{ mm}$ .
2. The [LVL - RTS] comparison resulted in DDs with  $\text{RMSV} = 4.1 \text{ mm}$ .
3. The [MHP - RTS] comparison resulted in DDs with  $\text{RMSV} = 4.5 \text{ mm}$ .
4. The [STL - RTS] comparison resulted in DDs with  $\text{RMSV} = 4.9 \text{ mm}$ .
5. The [RVL - RTS] comparison resulted in DDs with  $\text{RMSV} = 15.3 \text{ mm}$ .

In this case, the FTL model achieved the least discrepancies (with respect to the RTS measurements), followed closely by LVL. Notably, the MHP model, which had the poorest performance in PD analysis, performed well in distance measurements, ranking third. Both MHP and STL showed discrepancies only slightly higher than the top two methods. The RVL model, however, again showed the least performance, with RMSVs three to four times higher than those of the other approaches. This reinforces the importance of using a



well-structured alignment strategy such as close-neighboring overlap when applying visual-alignment LiDAR techniques.

### **Inferences comparison of Photogrammetry vs TB LiDAR at B3-Sandersville**

- Given the strong root-mean-square performance of the MHP photogrammetry model, a more detailed evaluation was conducted by comparing its full point cloud to that of the FTL model, the most accurate TB LiDAR approach, using CC software. Both C2C and M3C2 schemes were applied to assess cloud discrepancies (PDs) with 95% confidence. The results for each wall are as follows:

#### North Wall, [N-FTL – N-MHP] comparison:

- C2C “absolute” distance  $\leq 42.2$  mm (based on 10.99 million points)
- M3C2 “signed” dist. range:  $-53.9$  mm to  $57.8$  mm (based on 18.98 million points)

#### South Wall, [S-FTL – S-MHP] comparison:

- C2C “absolute” distance  $\leq 39.3$  mm (based on 9.84 million points)
- M3C2 “signed” dist. range:  $-15.7$  mm to  $22.3$  mm (based on 28.65 million points)

These relatively large positional discrepancies—observed with 95% probability using both C2C and M3C2 methods—highlight the limitations of the photogrammetry approach when compared to TB LiDAR (with targets acquired in the field at high resolution). While MHP

(processed via Agisoft's Metashape using handheld DSLR imagery) performed reasonably in Root Mean Square (RMS)-based evaluations, it proved substantially less accurate than the FTL model in full-model comparisons. This underscores the superior spatial fidelity of TB LiDAR when precise geometric reconstruction is required.

## **CONCLUSIONS INFERRED FROM WORK AT THE B4-KING GEORGE SITE**

The models considered at this site were 3 and they were completed at Epoch 1. They were designated as follows: TBL1 for TB LiDAR, VAL1 for visual-alignment LiDAR, and ML1 for the CRP via Metashape. This model employed pictures taken with the NIKON D5300. In this case, elevated were incorporated to improve accuracy. The field measurements completed with the benchmarking RTS instrument were designated as RTS1.

### **Inferences regarding the relative accuracy of measurements at B4-King George**

- The following values represent the magnitude of positional discrepancies (PDs) at 12 control points, calculated by subtracting field measurements (RTS1) from the corresponding positions derived from three generated models—TBL1, VAL1, and ML1—at Epoch 1:
  1. The [VAL1 - RTS1] comparison resulted in  $RMSV = 6.2$  mm.
  2. The [TBL1 - RTS1] comparison resulted in  $RMSV = 5.3$  mm.
  3. The [DS1 - RTS1] comparison resulted in  $RMSV = 19.2$  mm.

These results indicate that the VAL1 and TBL1 LiDAR-derived models exhibit similar relative discrepancies with respect to the RTS1 field measurements, with VAL1 performing slightly better. In contrast, the photogrammetric model ML1 shows significantly larger discrepancies, even after incorporating EACPs. Assuming those discrepancies follow a Gaussian distribution, approximately 95% of them are expected to lie within the interval  $\{\mu \pm 1.96 \times \sigma\}$ . Based on this assumption, the estimated 95% confidence intervals for the models are:

- For [TBL1-RTS1]:  $= \{4.74 - 1.96 \times 1.96, 4.74 + 1.96 \times 1.96\} = \{0.90 \text{ mm}, 8.58 \text{ mm}\}$
- For [VAL1-RTS1]:  $= \{5.88 - 1.96 \times 1.90, 5.88 + 1.96 \times 1.90\} = \{2.16 \text{ mm}, 9.60 \text{ mm}\}$
- For [ML1-RTS1]:  $= \{18.2 - 1.96 \times 4.30, 18.2 + 1.96 \times 4.30\} = \{9.77 \text{ mm}, 26.63 \text{ mm}\}$

The maximum absolute value of each interval's bounds can be interpreted as an estimate of the noise level associated with each modeling technique: Those noise estimates are: 8.58 mm for TBL1; 9.60 mm for VAL1; and 26.63 mm for DS1. However, it is important to note that these estimates also include the measurement of noise from RTS1. Therefore, they do not exclusively represent the intrinsic noise of the models themselves.

- The following values represent the magnitude of DDs calculated from 66 unique, non-repeated distances among the 12 CPs (control points). These discrepancies were obtained by subtracting precise RTS1 field measurements from the corresponding distances extracted from the models TBL1, VAL1, and ML1 at Epoch 1:

1. The [VAL1 - RTS1] comparison resulted in DDs with RMSV = 3.8 mm.
2. The [TBL1 - RTS1] comparison resulted in DDs with RMSV = 3.8 mm.
3. The [ML1 - RTS1] comparison resulted in DDs with RMSV = 6.2 mm.

In this case, as with positional discrepancies, the VAL1 and TBL1 LiDAR-derived models significantly outperformed the photogrammetric model ML1 in terms of DD with respect to RTS1 measurements. Among the LiDAR models, VAL1 exhibited slightly better agreement with the RTS1 reference measurements than TBL1. Notably, both LiDAR models achieved RMSVs less than 5 mm, indicating high agreement with RTS1 distance measurements. Assuming that those DDs follow a normal (Gaussian) distribution, approximately 95% of the values are expected to fall within the range of  $\{\mu \pm 1.96 \times \sigma\}$ . Based on this assumption, the estimated 95% confidence intervals for each model are as follows:

- For [TBL1-RTS1]:  $= \{-1.1 - 1.96 \times 3.59, -1.1 + 1.96 \times 3.59\} = \{-8.14 \text{ mm}, 5.94 \text{ mm}\}$
- For [VAL1-RTS1]:  $= \{-0.9 - 1.96 \times 3.71, -0.9 + 1.96 \times 3.71\} = \{-8.17 \text{ mm}, 6.37 \text{ mm}\}$
- For [ML1-RTS1]:  $= \{1.0 - 1.96 \times 6.10, 1.0 + 1.96 \times 6.10\} = \{-10.95 \text{ mm}, 12.96 \text{ mm}\}$

The highest absolute value within each interval can be interpreted as an estimate of the total noise level associated with each modeling method: Those noise estimates are: 8.17 mm for VAL1; 8.14 mm for TBL1; and 12.96 mm for ML1. It should be emphasized, however, that these noise estimates also incorporate the uncertainty present in the RTS1 field measurements. As a result, they do not solely reflect the inherent noise of the models themselves.

## OVERALL CONCLUSIONS

- Floor noise of employed Robotic Total-Station instrument: Based on manufacturer specifications, the floor noise of Leica's one-second RTS instrument, used as an accurate benchmarking device, was estimated for a 40-meter range with 95% confidence. The corresponding floor noise values for two measurement types are as follows:

(i) Reflector-based floor noise: 2.1 mm

(ii) Reflector less floor noise: 5.6 mm

Reflector-based measurements were employed to obtain precise coordinates of GCPs, while reflector less measurements were used to determine the positions of CPs.

- Closed Polygonal Traverse: At each bridge site, an accurate, closed polygonal traverse is essential to properly establish the positions of at least four GCPs. These GCPs are critical for georeferencing any resulting models, whether derived from LiDAR or photogrammetry. In some cases, GCPs may need to be positioned near the monitored walls to support the spatial referencing of CPs. If such are to be used. This may require placing certain GCPs beneath the bridge deck, where GNSS signals may be unavailable or unreliable. Moreover, even when GNSS is accessible, RTK GNSS may not provide the positional accuracy necessary to detect small wall displacements. As an alternative, static GNSS—requiring a minimum of four hours of satellite data acquisition per station (point)—can achieve the needed precision, though it is time-intensive. For this reason, a

customized closed traverse is recommended, as it yields highly accurate GCP coordinates efficiently. It is also worth noting that CPs may not be necessary if comprehensive LiDAR or CRP models are generated for monitoring across multiple epochs.

- Performance of Considered CRP Methods: This study evaluated several CRP modeling approaches, with the most effective results achieved using Agisoft Metashape. Notably, model MD#, which utilized images captured by the onboard camera of DJI's Matrice 30 drone, and model MM#, based on a moderate number of images taken with a handheld Nikon D5300 DSLR camera, produced relatively accurate models—even in the absence of geotags and EACPs. While these models performed well in specific metrics, their overall accuracy remained below that of LiDAR-based models. In contrast, model DS1, developed using DroneDeploy without EACPs, exhibited significant inaccuracies. Although the inclusion of EACPs in subsequent modeling efforts led to noticeable improvements, the results still fell short of the accuracy achieved by LiDAR-based methods. Additionally, a model generated using the Pix4D Mapper platform also underperformed relative to LiDAR benchmarks. Unfortunately, several artifacts could be observed in the resulting CRP models, which can compromise both quality and accuracy. These artifacts typically stem from limitations in image acquisition, environmental conditions, or processing algorithms. Common issues include:

- (i) Noise and surface roughness (grainy or uneven surfaces).
- (ii) Ghosting or double surfaces due to movement during capture.
- (iii) Misalignment or warping from poor calibration or overlap.

- (iv) Holes or gaps in the mesh from occlusion or insufficient coverage.
- (v) Distorted geometry from inadequate georeferencing or sparse GCPs.

Mitigating these artifacts requires careful planning and execution, including:

- (i) Capturing well-overlapped images with high-resolution, calibrated cameras.
- (ii) Using abundant, well-distributed GCPs, and where possible, EACPs.
- (iii) Employing robust processing software with built-in quality control tools (e.g., Metashape).

Further analysis using CC revealed limitations in the point cloud generated by the MHP photogrammetry technique (with pictures taken with a hand-held Nikon D5300 camera). While suitable for visual documentation and general condition assessment, MHP exhibited greater discrepancies compared to LiDAR-based models. This underscores the value of integrating both technologies: photogrammetry excels in rapid, cost-effective visual assessments, whereas LiDAR provides the accuracy necessary for proper displacement monitoring.

- Performance of Considered Terrestrial LiDAR Methods: A key insight from most of the studied sites is the demonstrated repeatability and accuracy of static terrestrial laser approaches for detecting small displacements in retaining walls at bridge locations. The FTL technique (TB LiDAR with targets acquired in the field at high resolution) proved especially effective, offering exceptional accuracy. As a TB LiDAR method, FTL

involves acquiring targets in the field, but it requires more data collection and longer field time. Alternatively, the LVL technique—a VA LiDAR—aligns scans using a highly overlapped, close-neighbor pattern, ideally forming a closed loop. LVL produced models with accuracy comparable to FTL, and sometimes even slightly more accurate than FTL, while requiring less time in the field. However, it demands significantly more time for scan registration (stitching) in post-processing. Additionally, LVL still requires capturing at least three targets for georeferencing. An alternative to the highly accurate FTL and LVL methods is the STL technique, a TB LiDAR approach that uses field-placed targets, scanned at the same regular resolution used for all other objects in the site, but acquired via software. STL requires significantly less field time than FTL and less post-processing time than LVL, while still producing models with only slightly reduced accuracy.

- Recommended Modeling Techniques: Three of the LiDAR-based analyzed techniques, FTL, LVL, and STL, are suitable for modeling retaining (MSE/MB) walls at different time intervals to monitor potential displacements over time. Performing full model comparisons between epochs using CC software is strongly encouraged to detect and quantify changes accurately. The recommended selection of modeling techniques is ranked as follows:

**1<sup>st</sup> – FTL**: TB LiDAR with targets acquired in the field at high resolution for stitching (registration) and georeferencing purposes. It is very accurate but requires extra fieldwork. Nonetheless, it involves reduced postprocessing time.

**2<sup>nd</sup> – LVL**: Visual-Aligned LiDAR. This approach requires highly overlapped scans, following a successive close-neighbor pattern, ideally forming a closed loop. This technique still needs the acquisition of 3 field targets, at least for georeferencing



purposes. Its accuracy depends on appropriately overlapped scans. It involves less fieldwork than FTL, but it necessitates more extensive post processing time.

**3<sup>rd</sup> – STL:** A TB LiDAR approach in which targets are swiftly scanned in the field using the same medium resolution applied to the rest of the site, with target acquisition performed through software-based identification. It only slightly extends the amount of field work required by FTL and needs moderate postprocessing time, less than LVL. Accuracy wise, it is similar, but slightly less accurate than FTL.

- Noise Level for RTS and LiDAR: Based on the procedures outlined in this study, the expected noise levels for TB and Virtual-Alignment LiDAR techniques, at sites of similar scale to those analyzed, are summarized in the Table 64 below:

**Table 64. Final Estimated Noise Levels**

SITE	ESTIMATED NOISE LEVEL (mm)		
	RTS	TB LiDAR	VA LiDAR
CW	9.9	6.3	8.4
B2-Old River	9.7	11.9	14.3
Average	<b>9.8</b>	<b>9.1</b>	<b>11.4</b>

These results suggest that displacements greater than ½ inch (12.5 mm) should be reliably detected using both TB and VA LiDAR techniques. Furthermore, when using CC software, even smaller positional discrepancies between two epochs can be effectively identified, enhancing the precision of displacement monitoring.

- Integration of Photographic Imagery and Optional Photogrammetry

Photographic documentation is a valuable complement to terrestrial LiDAR in the inspection of MSE and MB retaining walls. High-resolution images help capture surface

features—such as cracks, efflorescence, erosion, and vegetation intrusion—that may not be fully represented in point-cloud data. These visuals enhance interpretation, support anomaly validation, and improve communication with stakeholders. Images should be captured during each LiDAR data collection epoch using UAV-mounted or hand-held cameras, depending on site conditions. Consistent viewpoints, metadata tagging, and alignment with LiDAR reference markers are recommended to ensure traceability and facilitate cross-validation. While photogrammetric modeling is not required, capturing images with sufficient overlapping and visible reference markers allows for optional 3D reconstruction using Agisoft Metashape. Postprocessing in Metashape offers a flexible workflow for generating georeferenced visual products, including orthophotos and dense point clouds—when further spatial analysis or visualization is needed. This approach supports both UAV and hand-held imagery and is particularly useful in areas where UAV access is limited. Standardized file naming and documentation practices are essential for maintaining consistency across datasets. Incorporating imagery into the inspection protocol strengthens structural assessments, supports future modeling efforts, and enables a more comprehensive understanding of wall conditions.

## **FINAL REMARKS FUTURE STUDIES AND RECOMMENDATIONS**

This work provides empirical evidence that current visual inspection practices could be significantly enhanced through integration of remote-sensing and quantitative 3D monitoring methods. The small displacement/deformation patterns captured at the CW site, and the almost no displacements captured at the B2-Old River site, offered valuable insights for establishing

science-based noise/performance thresholds. Moreover, the successful application of these methods in real-world bridge environments demonstrated their operational feasibility despite challenges like traffic and changing environmental conditions.

The practical implications of this research are significant for transportation agencies and infrastructure managers. The study provides empirical evidence that integrating LiDAR and RTS into routine inspection protocols can enhance the accuracy and efficiency of MSE wall monitoring. For instance, the ability to detect near-centimeter displacements allows for early intervention, reducing the risk of severe and disruptive failures while extending the lifespan of critical infrastructure. Additionally, the methodologies employed in these studies such as the use of GCPs for georeferencing and the application of CC analysis via its robust comparison schemes, C2C and M3C2, offer a scalable framework for adopting them in real-world settings. The successful deployment of these methods in diverse environments, including those affected by traffic and varying lighting conditions, further validates their operational feasibility.

From a broader perspective, this research contributes to the growing body of knowledge on infrastructure digital twins and smart monitoring systems. The methodologies developed and validated through these studies provide a framework for creating comprehensive digital records of retaining structures throughout their lifecycle. The multi-temporal point cloud analysis techniques employed in this study of MSE/MB walls could be extended to other critical infrastructure elements, potentially transforming how we monitor and maintain the built environment. The convergence of complementary results from the study of five (5) different sites provides strong validation of the proposed monitoring approaches. The consistent findings across

different sites, wall configurations, and scanner models significantly strengthen the case for adopting these technologies in routine inspection protocols. As transportation agencies seek to modernize their asset management practices, this research offers both technical justification and practical methodology for implementing more reliable, data-driven approaches to MSE/MB wall monitoring.

This study demonstrates that advanced remote-sensing technologies, especially the already accurate LiDAR-based methods, and the now continuously improving CRP techniques are not only effective, but essential for modern infrastructure monitoring. They can significantly enhance the inspection and monitoring of MSE and Modular Block walls. These methods offer high-resolution, quantitative insights that go far beyond what traditional visual inspections can achieve.

## **ADVICE ON WORKFORCE DEVELOPMENT**

To fully realize the potential of the analyzed and recommended modeling techniques, it is advised that GDOT invest in *workforce development* to build internal expertise in the application of LiDAR, photogrammetry, AI, and UAV-based systems for the monitoring of MSE/MB walls and/or other wide range of infrastructure assets. Noting especially those where the early detection of centimeter-level displacements/deformations could bring substantial benefits. That is, these technologies could enable early intervention, reduce the risk of failure, and extend infrastructure lifespan, generating long-term savings in maintenance, repair, and risk mitigation. Doing so may position Georgia as a national leader in smart infrastructure management.

The successful application of these methods, especially LiDAR, in real-world bridge environments, presents several advantages enhancing their operational feasibility: it involves minimum disruptions to traffic (shoulder protection should suffice); it does not require special lighting conditions; it does not need GNSS data availability/connection; it enhances safety, and reduces long-term costs. Their effective use requires specialized skills in:

- Georeferencing using GCPs
- 3D point cloud processing
- CC analysis (C2C and M3C2 schemes)
- UAV operations and Photogrammetric modeling
- Data interpretation and integration with asset management systems

Without a trained workforce, the adoption of these tools will remain limited, and their full potential will go unrealized.

## **FUTURE RESEARCH**

The findings of this study underscore the growing potential of advanced remote-sensing and non-contact technologies, particularly LiDAR (Light Detection and Ranging) and photogrammetry, for the inspection, assessment, and continuous monitoring of mechanically stabilized earth (MSE) and modular block (MB) retaining walls. These techniques represent a major shift from traditional, labor-intensive inspection practices toward more data-driven, high-precision, and

automated methods of infrastructure evaluation. However, despite the promising outcomes demonstrated in this research, there remain several areas where future studies can further expand and refine these approaches to enhance their accuracy, efficiency, and real-world applicability. One promising research direction involves the integration of machine learning (ML) and artificial intelligence (AI) algorithms with remote-sensing datasets to automate the detection, classification, and prediction of structural deformations. By developing and training intelligent models on large, diverse datasets derived from LiDAR point clouds and photogrammetric reconstructions, researchers can potentially identify subtle deformation patterns or early-stage damage indicators that may not be visible through conventional inspection methods. Such automated detection systems would enable proactive maintenance and more reliable early warning mechanisms, reducing the risk of costly structural failures and improving the overall resilience of critical transportation infrastructure.

Another area worth exploring is the implementation of real-time or near-real-time monitoring systems that leverage unmanned aerial vehicles (UAVs) equipped with LiDAR sensors or high-resolution cameras. These systems could perform periodic or continuous scans of wall surfaces, transmitting live data to centralized platforms for analysis and visualization. When combined with Internet of Things (IoT) sensor networks, such frameworks could capture not only surface-level displacements but also subsurface parameters such as temperature variations, soil moisture, or geotechnical strain. This level of integration would provide a comprehensive and multi-dimensional understanding of wall health, enabling transportation agencies to make informed, data-driven decisions and respond quickly to emerging problems.

Future studies should also consider conducting cost–benefit analyses to determine the economic feasibility of deploying LiDAR- and photogrammetry-based monitoring systems compared to traditional surveying and visual inspection methods. While the precision and comprehensiveness of these technologies are undeniable, their initial acquisition costs, specialized hardware (especially for LiDAR), and high computational requirements for processing dense datasets can limit accessibility. Evaluating long-term savings from reduced manual inspections, minimized downtime, and extended service life would help justify the investment. In parallel, exploring open-source or low-cost software alternatives could help democratize these technologies, making them feasible for smaller municipalities, developing agencies, or low-budget projects.

Expanding the research scope to include a broader range of wall designs, environmental conditions, and service ages would further strengthen the generalizability and robustness of future findings. The current study sites provide a strong baseline, but analyzing walls situated in different climatic zones—such as arid deserts, cold regions with freeze–thaw cycles, humid coastal environments, or saline areas prone to corrosion—could reveal how environmental stressors affect wall performance and the reliability of sensing data. Similarly, investigating MSE and MB walls in seismic regions or high-traffic corridors could highlight unique issues such as cyclic deformation, crack propagation, or settlement patterns induced by vibrations, which are often not apparent in stable settings.

Finally, future research should consider comparing walls with varying design typologies, reinforcement configurations, drainage systems, and foundation treatments to assess how these structural variables influence data acquisition and interpretation from different sensing methods. Such comparative analyses can identify method-specific limitations, optimize data fusion

strategies that combine LiDAR, photogrammetry, robotic total station (RTS), and infrared thermography (IRT), and lead to the creation of standardized inspection frameworks that can be adopted by transportation departments and engineering agencies worldwide. By systematically addressing these technical and contextual gaps, future work can enhance the integration, reliability, and scalability of remote-sensing technologies in infrastructure monitoring—ultimately promoting safer, more resilient, and cost-efficient management of MSE and MB wall assets.



## **CHAPTER 13. NARRATED INSPECTION PROTOCOL: PROPOSED FRAMEWORK**

This chapter presents the selected and proposed inspection activities designed to support the monitoring of MSE/MB walls. This protocol outlines a comprehensive methodology for the long-term inspection and structural health monitoring of Mechanically Stabilized Earth (MSE) and Modular Block (MB) retaining walls. Developed as part of a statewide initiative supported by the Georgia Department of Transportation (GDOT), the protocol aims to establish a standardized, non-destructive, and repeatable framework for documenting and assessing the performance of these critical infrastructure components over time.

Given the growing need for accurate condition assessments of aging retaining walls, this protocol integrates traditional surveying methods with advanced technology, terrestrial laser scanning (LiDAR), and rigorous postprocessing techniques. It provides step-by-step guidance on site preparation, data acquisition, model generation, scan registration, georeferencing, and multi-epoch analysis to identify displacements/deformations that may affect the structural behavior of MSE/MB walls.

The methodology is designed to support both initial baseline documentation and subsequent periodic inspections. It ensures spatial accuracy by employing a local closed traverse network defining needed Ground Control Points (GCPs), which serve as the foundation for georeferencing all 3D models at each site. The protocol further provides recommendations for scan planning, image acquisition, the use of spherical targets, accurate scan-registration

techniques, and appropriate georeferencing, all of which are crucial to achieving high-resolution, accurate and geometrically consistent datasets.

In addition to field procedures, the document details a full postprocessing workflow using Leica's Cyclone Core and CloudCompare software to produce and compare three dimensional representations of retaining walls across multiple epochs. This supports a data-driven approach to infrastructure maintenance, facilitating early detection of structural issues and enabling proactive interventions.

By combining precision instrumentation, reliable processing methods, and flexible data acquisition strategies, this protocol is intended to serve as an initial practical and scalable tool for DOT personnel, consultants, and infrastructure managers responsible for the inspection and preservation of MSE and MB retaining walls throughout Georgia.

To enhance clarity and support practical implementation, the following list presents a structured summary of the complete inspection protocol. This condensed version outlines the key tasks from initial site preparation through data postprocessing and multi-epoch analysis while preserving the logical sequence and essential content of the comprehensive narrative that follows. Each listed item corresponds to specific sections of the full protocol, providing clear reference points for further detail and context. Each step is designed to ensure consistency, accuracy, and repeatability across diverse site conditions and inspection campaigns. Table 65 shows the narrated protocol for the inspection of MSE/MB wall.

**Table 65. Summary of Narrated Protocol for Inspection of MSE/MB Walls**

<b>Step</b>	<b>Tasks at Each Site</b>	<b>References</b>
<b>1</b>	<b>Site Preparation and Traverse Establishment</b> <ul style="list-style-type: none"> <li>Visit each site to determine optimal vertex locations for a closed polygonal traverse near the MSE/MB wall. See examples in this report.</li> <li>If an on-site visit isn't feasible, use existing design and/or as-built plans to pre-select traverse points.</li> <li>The traverse establishes coordinates for Ground Control Points (GCPs), critical for georeferencing LiDAR models.</li> </ul>	<b>Narrative Part A</b>  APPENDIX A
<b>2</b>	<b>Ground Control Points (GCPs)</b> <ul style="list-style-type: none"> <li>Minimum required: 3 GCPs for LiDAR. However, more are recommended for redundancy.</li> <li>Typically, 5–8 GCPs are used per site. Nevertheless, the total number depends on the length of the walls to be monitored. See examples in this report.</li> <li>If supplementary close-range photogrammetry models were to be generated, the minimum number of GCPs for georeference purposes could be 4 (e.g., this is required by the DroneDeploy software). Additionally, GCPs should include EACPs (elevated auxiliary control points) to enhance accuracy.</li> </ul>	<b>Narrative Part A</b>  APPENDIX A
<b>3</b>	<b>Traverse Measurement and Adjustment (Balancing)</b> <ul style="list-style-type: none"> <li>Use a calibrated one-second total station.</li> <li>Perform angular balancing: Locally and Globally.</li> <li>Use the Bowditch Method to adjust distances and directions.</li> <li>Longitudinal precision should be better than 1:20,000, ideally 1:30,000 or 1:40,000, or even more as there is no limit in this regard. See examples in this report.</li> </ul>	<b>Narrative Part A</b>  APPENDIX C1
<b>4</b>	<b>Laser Scanning Planning (Epoch-Based)</b> <ul style="list-style-type: none"> <li>Multi-epoch scanning to monitor wall evolution over time.</li> <li>Pre-plan ST locations based on wall geometry and site layout.</li> <li>STs are typically placed 3–10 m from walls, spaced 8–30 m apart. See examples in this report.</li> <li>Scan sequence varies by wall length and complexity (e.g., 4–16 scans).</li> <li>In subsequent epochs, preferably use the same scanning planning, unless it needs improvement.</li> </ul>	<b>Narrative Part B</b>  APPENDIX C1

**Table 65. Summary of Narrated Protocol for Inspection of MSE/MB Walls (Continued)**

<b>Step</b>	<b>Tasks at Each Site</b>	<b>References</b>
<b>5</b>	<b>Targets and Setup (During Laser Scanning)</b> <ul style="list-style-type: none"> <li>• Use spherical white targets (e.g., 6" or 9") mounted on poles with known height.</li> <li>• Place targets over GCPs and stabilize them with bipods or tripods.</li> <li>• Record pole heights for accurate GCP position extraction.</li> <li>• When using targets to complete a TB registration approach, use a minimum of 3 common targets between each pair of neighboring scans that are to be registered together. However, more targets are preferred for redundancy and quality assurance.</li> <li>• When using targets for georeferencing purposes, use a minimum of 3 targets per project. However, more are preferred for redundancy and quality assurance.</li> </ul>	<b>Narrative Part B</b>  APPENDIX C1
<b>6</b>	<b>Execution of Laser Scanning</b> <ul style="list-style-type: none"> <li>• Use high-accuracy terrestrial scanners like Leica's P50.</li> <li>• Mount scanner on a sturdy tripod to prevent vibration artifacts.</li> <li>• At each station: Level the scanner.</li> <li>• Acquire needed targets (see previous point). They may be needed for TB registration and/or georeferencing purposes.</li> <li>• Acquire 360° horizontal and ~270° vertical coverage per ST.</li> </ul>	<b>Narrative Part B</b>  APPENDIX C1
<b>7</b>	<b>Acquisition of Photographic Images for Supplementary Analysis</b> <ul style="list-style-type: none"> <li>• <u>Purpose:</u> Incorporate images into the inspection workflow to complement 3D point-cloud LiDAR analysis with qualitative visual evidence of existing conditions.</li> <li>• Capture high-resolution photographs during each data collection epoch.</li> <li>• Could use UAV-mounted or hand-held cameras or both.</li> <li>• Focus on visual indicators: Efflorescence, cracking patterns, localized erosion, vegetation intrusion, rust stains, minor spalling, etc.</li> <li>• Align photographs with LiDAR epochs.</li> <li>• Use pictures for cross-validation with spatial data.</li> <li>• Photogrammetric models are not required when terrestrial LiDAR is used as the primary spatial data source. However, if they are desired, the previously captured photographs—provided they contain substantial overlap and include visible reference markers such as GCPs and EACPs—can be effectively used to generate them.</li> </ul>	<b>Narrative Part C</b>

**Table 65. Summary of Narrated Protocol for Inspection of MSE/MB Walls (Continued)**

<b>Step</b>	<b>Tasks at Each Site</b>	<b>References</b>
<b>8</b>	<b>LiDAR Postprocessing (Cyclone Core Software)</b> <ul style="list-style-type: none"> <li>• Export scans from scanner. Import scans to processing software (Cyclone Core).</li> <li>• Noise Removal if Necessary: Clean each scan to eliminate irrelevant elements that may be obstructing the models of the walls.</li> <li>• Register scans into a single point cloud using one of three suggested methods: TB (with targets acquired in the field), Visual-Alignment, or TB (with targets acquired via software).</li> <li>• Georeferencing: Align the unified scan cloud to GCPs using TB registration.</li> </ul>	<b>Narrative Part D</b>  APPENDIX C3, APPENDIX C4, APPENDIX C5, APPENDIX C6
<b>9</b>	<b>Optional Photogrammetric Postprocessing (Agisoft's Metashape Software).</b> <ul style="list-style-type: none"> <li>• Create a new Metashape model for each inspection epoch.</li> <li>• Import UAV and/or hand-held images of the MSE/MB wall.</li> <li>• Align photos.</li> <li>• Georeference by importing GCPs. Mark GCPs in images and update coordinate system.</li> <li>• Add scale bars between known points (e.g., GCPs)</li> <li>• Build dense cloud.</li> <li>• Export cloud for comparison purposes.</li> </ul>	<b>Narrative Part E</b>  APPENDIX C7
<b>10</b>	<b>Multi-Epoch LiDAR Comparison (CloudCompare Software)</b> <ul style="list-style-type: none"> <li>• <u>Purpose</u>: Detect wall displacement/deformation between epochs.</li> <li>• Clean, register, and georeference each epoch's LiDAR data in the same coordinate system.</li> <li>• Export in .las, .ply, or .e57 format and import into CloudCompare.</li> <li>• Use visual inspection for alignment.</li> <li>• Comparison methods: Cloud-to-Cloud (C2C) and Multiscale Model-to-Model Cloud Comparison (M3C2).</li> </ul>	<b>Narrative Part F</b>  APPENDIX C8
<b>11</b>	<b>Maintenance/Rehabilitation Decisions</b> <ul style="list-style-type: none"> <li>• <u>Purpose</u>: Support informed decision-making by analyzing structural changes across multiple inspection epochs using LiDAR and photographic data.</li> <li>• Use temporal comparisons of 3D models and photo images to detect displacements, deformations, and surface degradation.</li> <li>• Interpret anomalies in conjunction with field expertise and engineering judgment.</li> <li>• Evaluate the magnitude, location, and progression of changes to assess structural integrity.</li> <li>• Prioritize walls for maintenance or targeted repairs.</li> <li>• Recommend repairs and/or reconstruction when warranted by severity or risk.</li> </ul>	<b>Narrative Part G</b>

Once the sites containing these walls have been identified, the process of developing their initial and successive virtual 3D models essential for guiding subsequent inspections should be initiated. The following sections present the full narrated protocol, expanding upon the steps summarized above. This expanded account offers guidance on procedures, equipment, recommended practices, and methodological considerations necessary for accurate data acquisition and analysis. By elaborating on each phase from traverse setup and scanning strategies to postprocessing and temporal comparison this narrative serves as a practical reference for field personnel and analysts involved in the monitoring of MSE/MB retaining walls.

## **PART A: CLOSED TRAVERSE – LOCAL SYSTEM OF REFERENCE**

Before starting any modeling activities, it is advisable to visit the site to determine the optimal locations for the vertices of a closed polygonal traverse positioned near the MSE/MB retaining walls. This traverse is essential for accurately establishing the coordinates of GCPs (Ground Control Points), which are critical for the proper georeferencing of both LiDAR (Light Detection and Ranging) and CRP (Close-Range Photogrammetry) models. In situations where an on-site visit is not feasible, a careful examination of existing site documentation or as-built plans may be used to pre-select suitable traverse vertices. Examples of traverse calculations for all sites involved in this project are presented in Appendix A of this report.

A minimum of three (3) GCPs is required to geo-reference LiDAR-based models. However, CRP platforms such as DroneDeploy typically require at least four (4) GCPs to achieve stable

georeferencing within a consistent coordinate system. Additionally, CRP may even need substantially more GCPs, including EACPs (Elevated Auxiliary Control Points) to improve accuracy. Despite these minimum requirements, it is strongly recommended to include more than the bare minimum to ensure redundancy in case of accidental GCP loss. A practical approach is to add at least one additional point (e.g., 3+1 or 4+1), but even this may not provide sufficient redundancy in the event of accidental GCP loss. In this study, five (5) to seven (7) GCPs were used at each site to enhance the robustness and long-term reliability of the spatial referencing framework. Larger sites or more complex conditions may necessitate an even greater number of GCPs.

The traverse should be surveyed using a well-calibrated, high-precision instrument, preferably a one-second total-station device, to ensure optimal accuracy. Angular measurements should be rigorously verified through both local and global balancing procedures. Locally, each internal angle at a vertex should be measured twice and averaged. Similarly, the corresponding external angle should also be measured twice and averaged. These averaged values are then summed to determine the  $LA_{EC}$  with equation 22:

$$LA_{EC} = \text{Averaged Internal Angle} + \text{Averaged External Angle} - 360^{\circ} \quad (22)$$

Any deviation from  $360^{\circ}$  is corrected by equally distributing the  $LA_{EC}$  across both the internal and external angles at that vertex. After local balancing is completed for each vertex, global angular balancing is performed. This involves summing all locally balanced internal angles and

comparing their total to the theoretical sum for a closed traverse with ‘ $n$ ’ vertices, which is calculated by equation 23:

$$GA_{EC} = \left( \sum_{i=1}^n (\text{Locally Balanced Internal Angle})_i \right) - [(n - 2) \times 180^\circ] \quad (23)$$

This Global Angular Error of Closure ( $GA_{EC}$ ) is then corrected by uniformly adjusting all internal angles, thereby ensuring geometric consistency throughout the traverse. For the linear (distance) component, each traverse leg the distance between two consecutive vertices should be measured four times: twice from each endpoint. These values are average, with any outliers discarded and remeasured. After the angular balancing is finalized, the next step involves correcting the linear measurements using the Bowditch Method, also known as the Compass Rule. This technique assumes that linear measurement errors are proportional to the lengths of the traverse legs. By distributing the total longitudinal error of closure accordingly, the method refines both the distances and directions, ensuring the traverse closes geometrically and the endpoint coincides with the starting point. This adjustment is critical to minimizing accumulated errors and maximizing the reliability of the traverse. The resulting longitudinal precision is expressed as a ratio in equation 24:

$$\text{Longitudinal Precision} = 1 / \left( L_{EC} / P \right) \quad (24)$$

where  $L_{EC}$  is the Longitudinal Error of Closure, and  $P$  is the total perimeter of the traverse.



A longitudinal precision ratio of 1:20,000 is the minimum acceptable standard, with 1:30,000 or 1:40,000 preferred for high-accuracy applications. The following three cases illustrate typical values associated with these precision levels:

- For 1/20,000, a max error of 0.01 ft (3.05 mm) corresponds to a length of 200 ft (60.96 m).
- For 1/30,000, a max error of 0.01 ft (3.05 mm) corresponds to a length of 300 ft (91.44 m).
- For 1/60,000, a max error of 0.01 ft (3.05 mm) corresponds to a length of 400 ft (121.92 m).

For example, at a 1:20,000 precision, the vertices of a 40-meter traverse leg should have a relative positional error of  $\leq 2.0$  mm (i.e.,  $40/20,000 = 0.002$ ), which is smaller than the floor noise of the Leica TCRP 1201+ RTS instrument used in this study. According to its manufacturer, the floor noises of that device, at 40 m (95% confidence), are: 2.1 mm using a reflector, and 5.6 mm in reflectorless mode. These values represent theoretical limits. In practice, total measurement error will be higher due to factors such as position centering, instrument verticality, setup stability, targeting aiming, atmospheric conditions, etc. Achieving even finer traverse precisions of 1:30,000 or 1:40,000 would result in positional errors of 1.3 mm and 1.0 mm, respectively, for the referred 40-m leg—well below the RTS floor noise—thereby ensuring that the GCP network does not become a limiting factor in model accuracy.

## **PART B: LASER SCANNING**

At each location, comprehensive scanning and modeling of the entire wall structure(s) must be performed at multiple time intervals, referred to as epochs, to document its evolution over time. These intervals may span several months or years. For each epoch, multiple scans are acquired from various vantage points, near the wall(s), to ensure full spatial coverage and high-resolution detail. These individual scans must then be merged (registered) and georeferenced to produce a complete, coherent, and comparable model representing that specific epoch. It is essential that each finalized model be clearly labeled according to its corresponding epoch (e.g., Epoch 1, Epoch 2, etc.) to maintain temporal clarity and support comparative analysis.

### **Scanner, Strong Tripod, and Software**

A good accurate static, terrestrial, laser-scanning device should be used. Additionally, a sturdy, high-quality tripod is recommended for supporting the scanner. Since the instrument rotates at high speeds during operation, it can induce minor vibrations that may compromise stability if the tripod is not sufficiently rigid. Therefore, using a robust tripod is essential to provide a stable and vibration-resistant platform for accurate scanning.

An example of a good scanner is Leica's ScanStation P50. It is a high-performance, long-range terrestrial laser scanner designed for precise 3D data acquisition in complex and large-scale environments. It is particularly effective for applications involving infrastructure assessment, structural monitoring, and multi-epoch scanning campaigns. With a scanning range exceeding

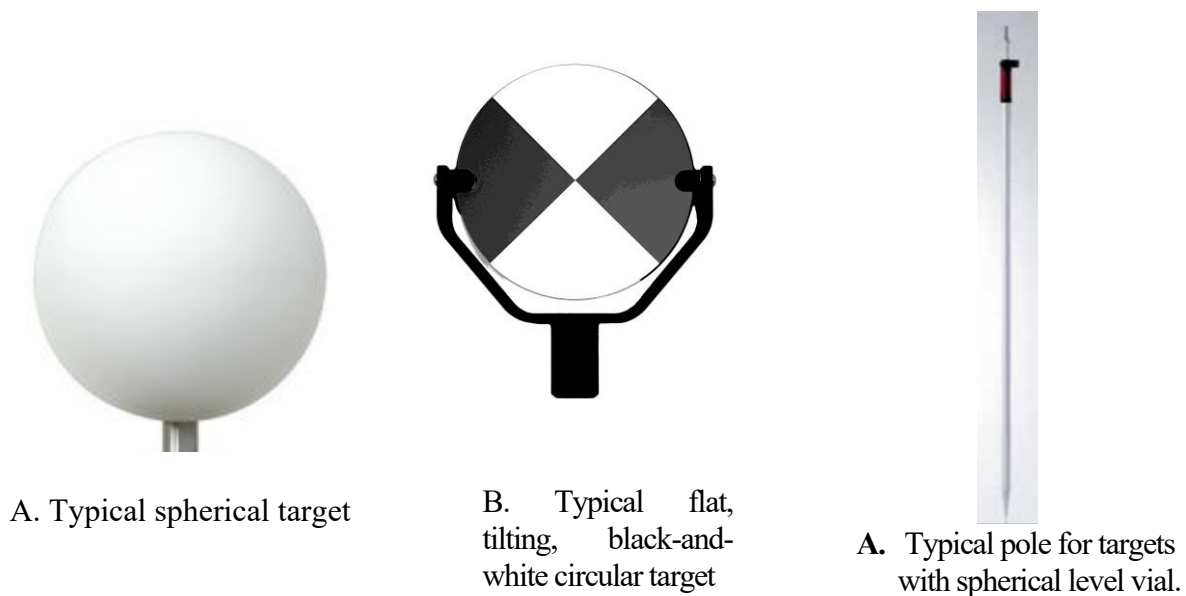
one kilometer, the P50 enables comprehensive data capture from various distances, making it ideal for inaccessible or hazardous locations. Data captured with the P50 is processed and managed using Leica's Cyclone Core software. It provides a robust platform for point cloud registration, editing, and analysis, supporting TB and visual-alignment registration workflows, enabling consistent alignment of scans across multiple epochs. The software also facilitates the integration of scan data into downstream modeling and visualization processes, ensuring continuity and accuracy throughout the project lifecycle. For detailed instructions on operating the P50, refer to APPENDIX C1.

### **Targets, Poles and Bipods/Tripods**

As indicated by Leica "Targets are the ideal accessory for registration and quality assurance. They allow for accurate georeferencing of scans to known control points, accurate registration of multiple scans to each other, and valuable quality assurance for individual scans". Before beginning the scanning process, ensure that all necessary targets are prepared and properly positioned. Regardless of the chosen registration method (see subsection below on those methods), at least three targets must be placed on three distinct GCPs to enable accurate georeferencing of the final point cloud models. However, using more than three targets is recommended, as this redundancy allows inspectors to discard any targets that may introduce larger registration errors. Each target should be positioned on a pole and its height, from bottom tip to center of the sphere should be recorded, as it will be needed in the data postprocessing stages.

If the targets are intended solely for georeferencing, it is not necessary for every scan to capture them. Instead, only the scans conducted in close proximity to each target need to acquire them. However, if the preferred TB registration method (see subsection below on those methods) is to be employed, a target should be placed on every GCP, and each target should be captured, at high resolution, from as many scan positions as possible. Ideally, when using this approach, all targets should be visible and captured from every scan, although achieving this level of coverage requires additional time in the field.

Spherical white targets are preferred over flat, black-and-white circular ones because they do not require reorientation toward each ST. This eliminates the need for manual adjustments, reducing the risk of introducing small errors while reorienting them.



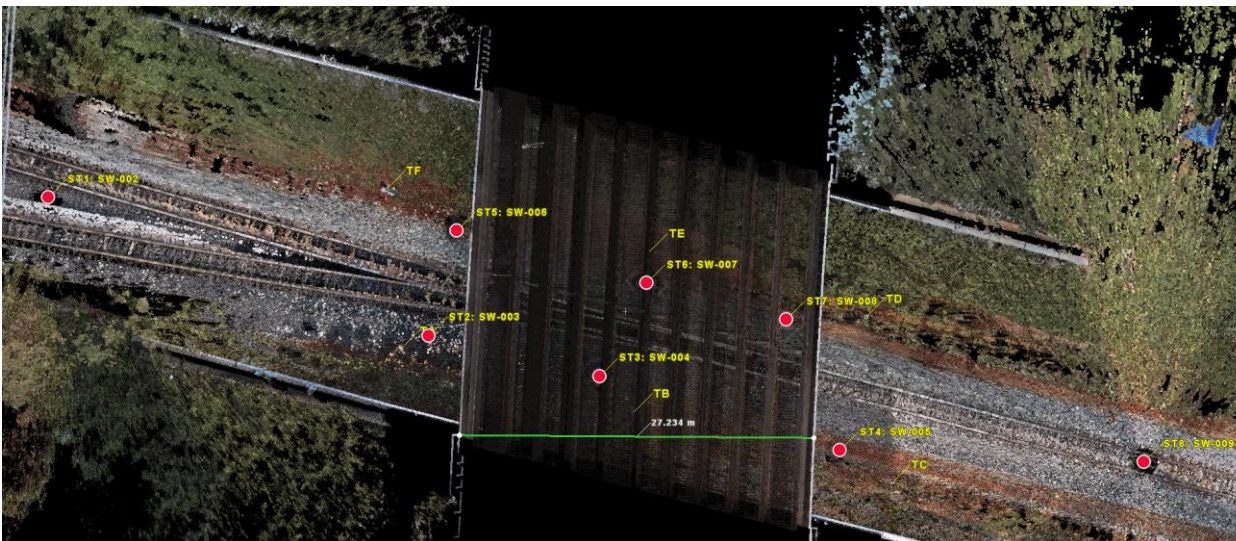
**Figure 170. Photos. Typical targets and pole.**

Figure 170 illustrates typical target types and a standard mounting pole. The pole should be equipped with a spherical level vial to ensure proper verticalization and should be stabilized using a telescopic bipod or preferably a tripod. The recommended diameters for these spherical targets are 6 or 9 inches. In most cases, a 6-inch diameter is sufficient; however, for targets placed at greater distances, the larger 9-inch targets are more suitable due to their improved visibility and detectability.

Each sphere must be mounted on a pole and positioned directly over a GCP, ensuring the pole is carefully aligned in a vertical orientation. For instance, in the project illustrated in Figure 171, 9-inch spheres were placed on the more distant GCPs, while 6-inch spheres were used for those closer to the scanner. It is essential to accurately measure the height of each pole—from its bottom tip to the center of the sphere—as this value is used to calculate the true location of the GCPs. Since the scanner records the center of each sphere, subtracting the measured pole height allows precise determination of the GCP position within the point cloud. In the example shown in Figure 171, six targets were used: TA (partially obscured by the dot representing ST1), TB, TC, TD, TE, and TF. Again, if a TB registration method is selected, it is recommended that all six targets be individually captured at high resolution by each scan. In this case, all six were acquired by each of the eight scans, enabling the option to apply TB registration during postprocessing.

## Planning the Scanning Work

Prior to the initial scanning and modeling of a site, a preliminary visit may be required to determine the optimal number and placement of scan positions. Alternatively, or additionally, existing site plans and documentation could be consulted to guide this planning process. For example, Figure 171 illustrates the locations of eight STs (red dots) used to model two MSE walls at a bridge near Sandersville, GA. In that figure, a reference distance of 27.234 m, marked in green to assist in estimating the approximate spacing between STs and their relative distances from the walls. Notably, stations ST1 and ST8 are positioned farther from the central cluster of stations (ST2 through ST7). This arrangement reflects the geometry of the MSE walls, which are tallest at their centers and taper in height toward the outer wings—necessitating less scanning coverage at the ends.



**Figure 171. Photo. Eight scanning stations (scans) completed at a bridge near Sandersville, GA**

The number of scanning stations required varies by site and should be determined based on the size, geometry, and complexity of the wall. For example, the research team employed 4 stations at the Control Wall (where the wall length was ~22 m), 6 stations at both B1–Crossgate and B2–Old River (where in both cases the length of each wall was ~52 m), 8 stations at B3–Sandersville, see Figure 171 (where the length of each wall was ~76 m), and 16 stations at B4–King George (where each wall length was ~68 m). However, in this latter case, 14 stations could have sufficed to only considering the wall surfaces facing King George Blvd. Scanning locations can be selected flexibly and do not require permanent markers. Typically, between 3 and 8 stations are positioned near each wall, approximately 3 to 10 meters from the structure and spaced roughly 8 to 30 meters apart. This configuration helps ensure high point density and complete surface coverage. Reduced spacing between stations increases overlaps, which can enhance alignment accuracy—particularly when using the visual-alignment registration approach. Additionally, close-spaced scans increase the point density of the resulting final models improving detail resolution.

### **Scanning at each station**

At each ST, begin by leveling the scanner to ensure proper vertical alignment. Once the scanner is correctly positioned, configure the scanning parameters and individually capture all visible spherical targets, preferably at high resolution. The number of targets captured per scan depends on the chosen registration method (refer to the subsection below for details). After acquiring the necessary targets, proceed with a full scan at medium resolution, covering a 360-degree horizontal field of view and approximately 270 degrees vertically. This excludes the conical area directly beneath the scanner, where the tripod obstructs visibility. APPENDIX C1 provides a

detailed scanning protocol specific to Leica's P50 scanner. All scans should be conducted at medium resolution to balance data quality with efficiency, as high-resolution scans significantly increase acquisition time. When using the Leica's C10, medium resolution yields a point spacing of approximately 10 millimeters at a 10-meter distance. The resolution of Leica's P50 scanner is recommended to achieve a denser spacing of about 6.3 millimeters at the same distance, resulting in slightly more detailed point clouds. This scanning process should be repeated consistently across all stations and epochs to ensure reliable temporal comparisons and accurate modeling of wall behavior over time.

## **PART C: ACQUISITION OF IMAGES FOR SUPPLEMENTARY ANALYSIS**

In structural inspections of MSE (Mechanically Stabilized Earth) and MB (Modular Block) retaining walls, photographic imagery plays a critical role in complementing 3D point-cloud LiDAR analysis. While LiDAR offers precise spatial data for detecting displacements and deformations, photographs provide indispensable qualitative evidence that enhances the interpretation of structural conditions and supports effective communication with stakeholders.

High-resolution images help document features not easily captured by LiDAR, such as efflorescence, cracks, erosion, vegetation intrusion, rust stains, and spalling—early indicators of wall degradation. These visuals help inspectors validate and contextualize LiDAR-derived anomalies. Photos should be taken during each data collection epoch using UAV-mounted or hand-held cameras. UAVs are ideal for broad coverage, though they may face limitations under bridges or in traffic-heavy areas. Hand-held cameras offer flexibility for close-up documentation,



especially when safe access is available along roadway shoulders. To ensure consistency, photographs must align with LiDAR epochs and reference markers. This alignment supports cross-validation between visual and spatial data. Images should also be taken from consistent viewpoints and cataloged using standardized naming and metadata, including date, location, and camera type.

Although photogrammetric modeling is not required when using terrestrial LiDAR, photographs can still be captured with sufficient overlap and reference markers to allow for optional model generation in Agisoft's Metashape. For this, images should be spatially coherent, well-documented, and taken with 60–80% forward and 40–60% side overlap. This overlap is essential for Metashape to accurately align photos and reconstruct spatial relationships. For vertical structures like MSE walls, capturing images from multiple angles—including oblique views—helps improve depth perception and surface detail. Camera settings should remain consistent throughout the session. Manual exposure and focus are recommended to avoid variations in lighting and sharpness. A low ISO setting helps reduce noise, and the same focal length should be maintained to ensure uniformity across the dataset. Reference markers such as Ground Control Points (GCPs) and Elevated Auxiliary Control Points (EACPs) should be clearly visible in multiple images. These markers are critical for georeferencing and scaling the model, even if photogrammetric reconstruction is not the primary goal. Their inclusion ensures flexibility for future modeling if needed. Lighting conditions also play a role in image quality. To avoid motion blur, especially with UAVs, a fast shutter speed should be used. Diffuse lighting—such as that found on overcast days or during early morning and late afternoon—helps minimize harsh shadows and overexposure. Photographers should maintain a consistent distance from the wall

surface and ensure full coverage of the area of interest. Particular attention should be given to structural features and defects, which may require close-up documentation. If you're manually placing Ground Control Points (GCPs) and scaling the model using known distances, you can work without GPS or other metadata.

Images should be organized using clear naming conventions that reflect the inspection date, wall ID, and camera type, making them easy to manage and trace throughout the processing workflow. By following these guidelines, field teams can produce high-quality imagery that integrates seamlessly into Metashape and supports both visual inspection and spatial analysis.

By incorporating photographic imagery into the inspection protocol, agencies like GDOT can enhance their ability to monitor wall conditions, verify structural changes, and communicate findings effectively. The synergy between visual and spatial data fosters a more comprehensive understanding of structural health and supports confident decision-making in maintenance and rehabilitation efforts.

## **PART D: LIDAR POSTPROCESSING**

After completing all scans in the field, postprocessing continues in an office or computer lab environment. The first step involves downloading the scan data from the scanner and importing it into a suitable software platform. For this project, the research team utilized Leica's Cyclone Core software.

The postprocessing workflow consists of three main steps. First, if necessary, individual scans may be cleaned to remove unwanted noise. Second, all scans are aligned into a unified point cloud within a common reference system, which may initially be arbitrary. Third, the consolidated point cloud is georeferenced to the coordinate system defined by the GCPs. These steps are described in detail in the subsections that follow.

## **Noise Removal**

The first step in postprocessing involves removing noise from the raw scan data to preserve only the relevant geometry of the wall and its surroundings. Common sources of noise include pedestrian and vehicular traffic, solar reflections (often appearing as beam-like artifacts), and background clutter. Leica's Cyclone Core software offers a suite of tools for manual and semi-automatic noise removal, allowing users to clean each scan—referred to as a ScanWorld—prior to registration. This early cleaning step helps prevent the propagation of unwanted data throughout the alignment and georeferencing processes. Each clean scan must be properly saved in both the Model and Control spaces (of the Cyclone Core software) to avoid repeating the cleaning in later stages. Detailed protocols for this process are provided in Appendix C2.

## Recommended alternative registration approaches

Three accurate methods are recommended for aligning and registering multiple scans. They are briefly described below in descending order of preference:

- (i) TB registration with high-resolution target acquisition in the field: This preferred method involves the use of physical targets—typically white spherical markers—that are scanned at high resolution directly in the field. Prior to performing the full scan at each station, these targets are individually captured to ensure their geometry is clearly defined within the resulting point cloud. For effective registration, each scan should include at least three targets that are also visible in adjacent scans, allowing for robust alignment across the dataset. When targets are evenly distributed and unobstructed, this approach yields highly accurate registration results. However, it does require additional time on site to capture each target at high resolution and demands careful planning to ensure proper placement, visibility, and coverage across all scan positions. Recommendation: Whenever possible, each scan should capture high-resolution images of targets located on all GCPs. However, if certain targets are not visible from a given scan position, it is acceptable to proceed without capturing them—provided that at least three (but preferably a minimum of 4) common targets are successfully acquired. These shared targets enable accurate alignment between the current scan and neighboring scans that also captured them, ensuring continuity in the registration process. APPENDIX C4, in this report, presents a detailed protocol for the TB registration process via Leica's Cyclone Core software.

(ii) Visual-Alignment registration: This is the second recommended method. It is fast because it does not rely on physical targets. Instead, the operator manually aligns overlapping scans based on recognizable features within the point clouds, such as corners, edges, or surface shapes. To improve the accuracy of this method, it is essential that close-neighbor scans have a high degree of overlap. The stitching process should proceed by successively registering close-neighboring highly overlapped scans, ideally following a closed-loop pattern. This approach helps minimize cumulative alignment errors and enhances the overall consistency of the registered dataset. When properly performed, this technique may attain similar accuracy as the TB approach. Nevertheless, this approach still requires acquiring a minimum of three targets, in the whole site, for georeferencing purposes. APPENDIX C3, in this report, presents a detailed protocol for the visual-alignment registration process via Leica's Cyclone Core software.

(iii) TB registration with target acquisition via software (in Cyclone Core): This is the third recommended method. It relies on physical targets placed in the field; however, unlike the high-resolution, field acquisition approach, the targets are not individually scanned prior to the full scan. Instead, they are captured passively as part of the general scanning process, without any special attention during data collection. The identification and acquisition of these targets are performed later within Cyclone Core, during post-processing. APPENDIX C6, in this report, presents a detailed protocol for acquiring scanned targets via Leica's Cyclone Core software. After all targets are acquired in this software-based fashion, registration should be completed following the TB approach described in APPENDIX C4. This approach significantly reduces time spent in the field, as it eliminates the need for separate high-resolution scans of each target. However, it

shifts the workload to the office phase, where the accuracy of target recognition depends on the overall scan resolution and the visibility of the targets. If targets are partially obscured or insufficiently detailed, registration precision may be compromised. When scan quality is adequate, this method offers a practical compromise between field efficiency and registration accuracy.

Each method presents trade-offs. High-resolution target acquisition in the field offers the highest accuracy but requires more field time. VA reduces field work, provides flexibility and adaptability but should be applied with careful planning and overlapping strategy to ensure high accuracy, especially in multi-epoch scanning campaigns. The third approach, involving software-based target acquisition, improves field efficiency but depends on scan quality and software performance.

## **Georeferencing**

Regardless of the selected registration method (i, ii, or iii), once all scans have been aligned into a single point cloud model, the next step is to georeference the model to the coordinate system used by the ground control points (GCPs). This requires using the coordinates of the GCPs specifically acquired for this purpose. The GCPs used for georeferencing may be a subset of the total number collected. A minimum of three GCPs is required, though using more is recommended to introduce redundancy, allowing the exclusion of any GCPs that may contribute to higher registration errors.

The georeferencing process itself is relatively straightforward and involves registering 2 point clouds using the previously described TB method. The first point cloud consists solely of the selected GCPs—typically between three and  $m$  points, where  $m$  is the total number of GCPs used. The second point cloud contains all previously registered scans, which exist in an arbitrary reference system. APPENDIX C5 of this report provides a detailed protocol for performing TB georeferencing using Leica’s Cyclone Core software.

## **PART E: OPTIONAL PHOTOGRAMMETRY POSTPROCESSING**

While the creation of 3D models from photographic data is not required for inspections driven by terrestrial LiDAR, it remains a complementary option if further visualization or analysis is desired. The postprocessing of photographic data in Agisoft Metashape offers a practical and flexible approach to enhancing the inspection workflow for MSE/MB retaining walls. This process transforms raw imagery into georeferenced visual products that support documentation, spatial referencing, and optional modeling, depending on the needs of the inspection.

APPENDIX C7 of this report presents a detailed protocol to use Agisoft’s Metashape to model retaining walls.

The workflow begins by importing all photographs into a new Metashape project. Importantly, Metashape fully supports images captured with hand-held cameras, making it especially useful in field conditions where UAV deployment may be limited or impractical. Appendix C7 of this report contains a detailed protocol to use Agisoft’s Metashape. Finally, the processed outputs—

including orthophotos (GeoTIFF) if desired, dense point clouds (LAS/LAZ), and the Metashape project file—should be exported using standardized filenames. These filenames should include the inspection date, wall ID, and camera type to ensure consistency and traceability across datasets. This workflow supports both UAV and hand-held imagery, offering flexibility and adaptability for a wide range of inspection scenarios and structural conditions.

## **PART F: LIDAR COMPARISON AMONG EPOCHS VIA CLOUDCOMPARE**

The purpose of using CloudCompare to compare retaining walls at different epochs is to detect and quantify structural changes or deformations over time. For instance, if a wall has been modeled at three distinct epochs (1, 2, and 3), comparisons can be made between Epoch 2 and Epoch 1, Epoch 3 and Epoch 1, or between successive epochs such as Epoch 3 and Epoch 2. By analyzing point clouds captured at different times, CloudCompare enables precise measurement of surface displacements, supporting the assessment of wall stability, identification of potential failure zones, and informed maintenance or mitigation decisions.

For these comparisons to be accurate, both point clouds must be georeferenced to the same coordinate system. This ensures that any measured differences reflect actual physical changes rather than misalignment or inconsistencies in spatial reference. Preparing the point clouds for analysis in CloudCompare involves a structured workflow. After field data collection, each dataset is postprocessed independently, as explained earlier in this chapter. This includes importing the raw scans into a point cloud processing software—such as Leica’s Cyclone Core—for cleaning. Unwanted elements like pedestrian or vehicular traffic, solar reflections, and



background clutter are removed. Each cleaned scan is then registered into a unified point cloud for its respective epoch and georeferenced using the same set of ground control points (GCPs) to maintain spatial consistency. Once both epochs are processed and georeferenced, the resulting point clouds are exported in a compatible format (e.g., .las, .e57, or .ply) and imported into CloudCompare. A visual inspection is performed to confirm alignment, a step for ensuring the accuracy of comparisons. Before running a comparison, it is often helpful to subsample the denser cloud or both clouds to create a core set of points. This is particularly important for the M3C2 method, which relies on a core cloud and local surface normals to compute distances.

CloudCompare offers two main comparison methods: Cloud-to-Cloud (C2C) and Multiscale Model-to-Model Cloud Comparison (M3C2). C2C is a fast, straightforward method that calculates the absolute distance from each point in one cloud to its nearest neighbor in the other. While useful for quick assessments, it does not account for surface orientation or geometry and may be sensitive to noise or data sparsity. M3C2, on the other hand, is more robust and accurate, especially for complex surfaces. It computes signed distances along local surface normals and accounts for surface roughness, making it appropriate for geometrical monitoring. APPENDIX C8 presents a detailed postprocessing protocol to use the C2C and M3C2 schemes in CloudCompare.

With its flexibility and powerful comparison tools, CloudCompare is an essential component of the postprocessing workflow for temporal analysis of retaining wall structures.

## **PART G: MAINTENANCE AND REHABILITATION DECISIONS**

The final step in this protocol involves interpreting the results of temporal comparisons to support informed decision-making regarding the condition of MSE/MB retaining walls. By systematically analyzing structural changes across multiple epochs, practitioners can identify signs of displacement, deformation, or deterioration that may compromise wall integrity. These findings, grounded in accurate and repeatable spatial data, provide a reliable basis for recommending appropriate maintenance actions, targeted repairs, or full reconstruction when warranted. Incorporating this temporal dimension into inspection protocols enhances long-term asset management and promotes the safety and resilience of transportation infrastructure.

The results derived from temporal comparisons of 3D models—generated through repeated LiDAR and photogrammetry-based inspections—serve as a foundational tool for assessing structural changes in MSE and MB walls over time. Displacements, deformations, surface degradations, or other anomalies identified between successive epochs can indicate early signs of structural distress or instability. These insights must be interpreted in conjunction with field expertise and engineering judgment to determine the appropriate response. In this regard, GDOT’s internal engineering teams—drawing on their technical knowledge, familiarity with site-specific conditions, and institutional experience—play a critical role in contextualizing the data. By evaluating the magnitude, location, and progression of detected changes, GDOT professionals can prioritize walls for maintenance, implement targeted interventions, or, when necessary, initiate reconstruction efforts. The integration of high-resolution temporal data with

GDOT's domain expertise ensures that decisions are not only data-driven but also grounded in practical feasibility, safety standards, and long-term infrastructure performance goals.

## CHAPTER 14. GDOT TECHNOLOGIES, RATING SYSTEM, AND GAM

### CURRENT GDOT RESOURCES, GAPS, AND RECOMMENDATIONS

As part of efforts to establish GDOT's first post-construction protocol for MSE and Modular Block (MB) retaining walls, a critical initial step involves assessing GDOT's current technological capabilities and identifying potential gaps in supporting a long-term data management workflow.

#### Assessment and Potential Leverage of Existing GDOT Equipment and Software

GDOT currently utilizes several key equipment and software assets across inspection and surveying operations that can be highly leveraged to support the new data workflows for MSE and MB wall inspections.

- **Trimble GPS Systems:** Trimble GPS systems are extensively used by GDOT for high-accuracy location data and are compatible with various surveying and inspection applications. These systems can support the georeferencing of inspection imagery, UAV flight paths, and mapped defect locations on wall structures. Specifically, Trimble devices integrated with RTK and PPK correction capabilities allow for centimeter-level accuracy, which is crucial for mapping fine-scale wall deformations, differential settlement, or lateral displacement over time. Trimble's ecosystem includes handheld GNSS receivers and data collectors like the Trimble TSC5 and TDC600, which are field-rugged and compatible with GIS data formats. These devices can be integrated with data collection

software such as Trimble TerraFlex or Esri's Collector for ArcGIS, allowing field personnel to directly log geospatial data, condition ratings, and visual observations tied to exact coordinates. The ability to upload this information to GDOT's GIS platform in near real-time enhances the efficiency and consistency of inspection reporting.

- **Pix4D Photogrammetry Software:** GDOT maintains licenses for Pix4D, a leading photogrammetry software platform used for processing UAV imagery into high-resolution orthomosaics, 3D surfaces models, and point clouds. This existing expertise and infrastructure can be directly leveraged for post-construction inspections of MSE and MB walls. UAVs flown along wall alignments can capture nadir and oblique imagery, which can then be processed through Pix4D to create highly detailed DSM that allow inspectors to detect displacement, settlement, or rotation in wall panels over time. Additionally, Pix4D's ability to overlay thermal imagery from UAVs with visual datasets supports the identification of subsurface moisture intrusion and drainage issues. Pix4D's outputs are compatible with GDOT's existing GIS workflows, allowing seamless integration into ArcGIS databases for long-term monitoring and condition tracking. Pix4Dinspect, a specialized module, allows for automated detection of structural anomalies, measurement of cracks, and tagging of geolocated observations within a 3D model, supporting GDOT's data-driven asset management goals. The cloud-based nature of Pix4Dinspect also allows for remote collaboration.
- **ArcGIS Geographic Information System:** ArcGIS is a widely used platform within GDOT, playing a central role in spatial data visualization and long-term asset management. It is a comprehensive geographic information system developed by Esri that allows users to collect, manage, analyze, and visualize spatial and geographic data. GDOT

uses ArcGIS extensively to support its infrastructure planning, asset management, and maintenance operations, integrating data from roadway and bridge inspections, traffic data, and construction projects. ArcGIS supports field data collection through tools like Survey123 and Collector for ArcGIS, enabling inspectors and engineers to input georeferenced data directly from sites. This real-time data collection streamlines communication, improves inventory accuracy, and facilitates quicker decision-making.

- **Esri Site Scan:** GDOT has access to Esri Site Scan for ArcGIS, a robust cloud-based platform that facilitates end-to-end UAV flight management, image processing, and model generation directly within the Esri ecosystem. Site Scan supports the planning of UAV missions with defined parameters such as overlap, altitude, and flight paths, while also automatically integrating captured imagery into georeferenced point clouds, ortho-mosaics, and 3D mesh. This platform is especially advantageous because of its seamless integration with GDOT's existing ArcGIS workflows and data infrastructure. Site Scan's ability to manage large datasets, maintain version control, and link processed models to asset locations within ArcGIS Online or ArcGIS Enterprise greatly enhances collaboration, repeatability, and accessibility of inspection outputs. Its cloud-hosted architecture enables real-time sharing of datasets between field teams and asset managers, supporting more responsive maintenance planning and spatial analytics
- **AASHTOWare Bridge Management (BrM):** GDOT uses AASHTOWare BrM to manage its bridge inventory and guide resources towards rehabilitation and replacement. BrM is a comprehensive tool for bridge asset management, tracking structural details, condition ratings, and inspection history while ensuring compliance with NBIS. It incorporates deterioration modeling and life-cycle cost analysis to predict bridge

degradation and optimize maintenance strategies. While primarily designed for bridge asset management and not directly used for MSE walls, MSE walls are often adjacent to or integral to bridge abutments, suggesting their inspection and maintenance could be indirectly tracked within BrM if tied to a bridge structure.

- **InspectX Bridge and Asset Inspection Software:** InspectX is a powerful bridge and asset inspection software used by GDOT. GDOT partnered with AssetIntel to implement InspectX, migrating 16 years of historical data from their previous system GAMS. InspectX serves as a centralized platform for planning inspections, collecting field data, conducting electronic reviews, and generating PDF reports. Key features include offline data collection using a tablet app, 3D Inspection capability for documenting defects precisely on a 3D bridge model, and GIS integration for mapping bridge data. It also seamlessly integrates with AASHTO BrM, facilitating smooth data transfer between platforms.
- **Windows Surface Tablets:** Windows Surface tablets are used by GDOT for inspection and surveying operations. These devices support data collection in the field and enhance the paperless workflow, allowing photo capture and speech-to-text functionality directly within apps like InspectX.

## Identified Gaps in Data Workflow

Despite the advantages of these existing assets, identifiable gaps in the data workflow could hinder the development of a seamless post-construction inspection protocol for MSE/MB walls:

- **Lack of Unified Data Integration Platform:** GDOT currently lacks a unified platform for integrating LiDAR, UAV photogrammetry, thermal imagery, and visual inspections into a central database accessible across districts. Currently, some of these datasets are stored in silos or managed locally, which reduces the potential for comprehensive trend analysis and predictive maintenance modeling.
- **Absence of Standardized Digital Forms:** While Windows Surface tablets support data collection, field inspectors may lack standardized digital forms specifically for MSE/MB wall inspections that incorporate all necessary visual, geospatial, and thermal data inputs.
- **Inconsistent UAV Program Standardization:** UAV programs are not yet uniformly standardized across GDOT districts, meaning that training, certification, and flight planning software vary widely in use and sophistication.
- **Workflow Standardization Deficiencies:** There's a need for clear protocols to be established for syncing GPS-collected data with UAV imagery and photogrammetric outputs, particularly for post-processing and integration with ArcGIS-based asset databases.



## Recommended Specifications for a Collection Program at GDOT

To address the identified gaps and establish a robust MSE/MB wall inspection program, the following specifications and actions are recommended for a collection program at GDOT:

- **Unified Data Management System:** Invest in or enhance a central platform capable of integrating and managing diverse data types from LiDAR, UAV photogrammetry, thermal imagery, and visual inspections. Leveraging the integration capabilities of existing platforms like InspectX or ArcGIS is crucial to overcome data silos and enable comprehensive trend analysis.
- **Custom Digital Forms Development:** Develop custom, standardized digital forms within platforms like Survey123 or Collector for ArcGIS. These forms should be specifically tailored for MSE/MB wall inspections to ensure consistent capture of all visual, geospatial, and thermal data inputs in the field.
- **UAV Program Standardization and Expansion:** Implement measures to standardize UAV programs across all GDOT districts. This includes:
  - Developing formal workflows that define flight parameters (e.g., altitude, image overlap, and camera angle), quality control thresholds, and deliverable formats for UAV-derived data.
  - Procuring additional UAV units, especially those with standardized equipment specifications (e.g., dual thermal/visual camera payloads).
  - Expanding and standardizing training and certification programs for UAV operators to ensure consistent data quality and comparability across projects.

- **Enhanced Workflow Protocols:** Establish clear and standardized protocols for data collection and syncing across all devices and technologies (e.g., Trimble GPS, UAVs). This ensures that repeated data collection events can be precisely registered in a spatial context, enabling reliable change detection analyses and cross-time comparisons.
- **Integration with Existing Asset Management Systems:** Fully integrate MSE/MB wall inspection data with existing robust systems like AASHTOWare BrM and InspectX. Although BrM is primarily for bridges, its framework can be adapted, and InspectX's existing capabilities for managing various asset types, including walls, should be leveraged. This integration will support predictive maintenance planning, lifecycle cost analysis, and reinforced infrastructure stewardship.

## CONDITION RATING SYSTEM

Despite the widespread use of MSE and Modular Block Walls (MBWs) across U.S. transportation infrastructure, there is no standardized condition rating protocol tailored specifically to these structures. Unlike bridges, which are federally mandated to undergo inspections every two years under the NBIS, retaining walls are often evaluated only after visible signs of distress are reported. This reactive, inconsistent, and highly subjective approach limits the ability of agencies like GDOT to manage their wall assets proactively and strategically. As part of this study, a comparative review of condition assessment practices from various transportation agencies across the U.S. was conducted. Table 66 summarizes these agency-specific practices, highlighting inspection intervals, the inclusion of bridge walls, and the structure of each rating system. While nearly all agencies include MSE or retaining walls in their bridge asset programs, rating systems differ substantially. Some use simple qualitative labels such as "good–fair–poor," while others adopt numeric scales (e.g., 0–9 or 1–100), risk-based tiers, or hybrid approaches with both element-level and overall condition ratings.

**Table 66. National Overview of Retaining Wall Inspection Frequencies and Condition Rating Systems**

Transportation Agencies	Recommended Inspection Frequency (years)	Include Bridge Walls	Condition Rating System	Relevant References
Alaska DOT-PF	<5 and based on storm events	Yes	Elements: 4-division rating. Overall: good, fair, poor	Beckstrand et al., 2017
Colorado DOT	< 6 for RW and < 4 for BW	Yes	Elements: good, fair, poor, severe. Overall: 0-9	Walters et al., 2016
Indiana DOT	5	Yes	Overall: excellent, good, fair, poor, critical	Khan, 2018
Michigan DOT	4	Yes	Elements and Overall: good, fair, poor, severe	Athanasopoulos-Zekkos et al., 2020
National Park Services (WIP)	<10	Yes	Elements: excellent, good, fair, poor, critical. Overall: 5 - 100	DeMarco et al., 2010b
New York State DOT	< 10 for RW and < 5 for MSE	Yes	Elements and Overall: good, fair, poor, severe	NYSDOT, 2018
North Carolina DOT	Based on the likelihood of failure	Yes	Elements: good, fair, poor, severe. Overall: 1-4	Rasdorf et al., 2015; Butler et al., 2016
Ohio DOT	<10	Yes	Overall: good, fair, poor	Ohio DOT, 2018
Oregon DOT	< 5	Yes	Overall: good, fair, poor	Brutus and Tauber, 2009, p. 11
Tennessee DOT	6	Yes	Overall: good, fair, poor, severe	Wu et al., 2021
Vermont Agency of Transportation		Yes	Risk-based: 5-division rating	VTrans, 2020
Wisconsin DOT	< 6	Yes	Elements and Overall: good, fair, poor, severe	WisDOT, 2017

This Table is extracted from: Macedo, J., Burns, S. E., Torres, J., Jung, Y. S., Liu, C., & Tsai, Y. J. (2023). Towards the Implementation of a Geotechnical Asset Management Program in the State of Georgia (No. FHWA-GA-23-2011). Georgia. Department of Transportation. Office of Performance-Based Management & Research

To enable consistent, objective evaluation of aging MSE and MB retaining walls, this study proposes a condition rating system tailored specifically to the capabilities and accuracy levels of Terrestrial LiDAR technologies in Table 67. Based on extensive validation using controlled displacements at the CW and field deployment at multiple Georgia sites, LiDAR-based models especially those processed using TB and VA registration methods demonstrated reliable performance in capturing structural displacements with millimeter-level precision. Recognizing the practical noise floor of these methods (~12.5 mm), we propose a three-tiered classification

framework to guide GDOT in prioritizing maintenance and inspection schedules based on observed geometric deformation.

**Table 67. Proposed GDOT MSE/MBW Condition Rating Categories (Based on Terrestrial LiDAR – TB & VA Methods)**

Condition Category	Description	Displacement Threshold	Recommended Inspection Interval
<b>Good</b>	No significant deformation; displacement is within expected LiDAR modeling noise.	$\leq 12.5$ mm (0.5 in)	Every 6 years
<b>Fair</b>	Minor surface deformation, bulging, or settlement likely initiated; requires closer monitoring.	$> 12.5$ mm and $\leq 25$ mm (1 in)	Every 2 years
<b>Critical</b>	Evident structural distress: major bowing, sliding, or failure indicators—requires immediate attention.	$> 25$ mm ( $>1$ in)	Immediate inspection and annually

This condition rating system establishes a quantitative, sensor-driven framework to complement visual inspection procedures and support data-informed asset management decisions. By aligning displacement thresholds with validated sensor accuracy and modeling performance, GDOT can implement a scalable inspection program that distinguishes between typical wall behavior, early-stage movement, and critical structural concern. Future enhancements may integrate material-based assessments (e.g., IRT) or automated alerts as sensing technologies continue to mature.

## **GAM APPLICATION AND DATABASE MODEL**

### **Recommendations for GAM Application and Database Model Updates**

As the GDOT advances toward a data-driven approach for the inspection and management of MSE and MB retaining walls, enhancements to the GAM system become imperative. The adoption of nondestructive and noncontact inspection technologies such as Terrestrial LiDAR, Photogrammetry, IRT, and RTS has enabled the collection of high-resolution, multi-epoch spatial data. These include 3D point clouds, thermal image sets, and time-series coordinate data. To transform this wealth of information into actionable insights, the GAM platform must evolve to support the storage, visualization, analysis, and integration of these data types into routine inspection and asset management workflows.

The following recommendations outline a roadmap for updating the GAM application and its underlying database model, ensuring compatibility with advanced inspection outputs and supporting long-term condition monitoring of retaining wall infrastructure

### **Data Model Expansion for New Data Types**

- **3D Point Cloud and Model Data:** The database should be capable of storing or linking to large 3D point cloud datasets and simplified 3D models generated by LiDAR and photogrammetry. This might involve:

- Adding fields to existing asset tables for retaining walls to store file paths or unique identifiers for associated 3D models and point clouds.
- Creating new dedicated tables to manage metadata for these 3D assets, including capture dates, equipment used, processing parameters, and data versions to support multi-temporal analysis.
- **Time-Series Displacement Data:** Implement a structured approach to store precise, georeferenced displacement data obtained from RTS base data. This would require:
  - New tables to record discrete measurement points (e.g., specific target locations on walls).
  - Fields within these tables for timestamped Easting (X), Northing (Y), and Elevation (Z) coordinates, allowing for calculation and tracking of displacement vectors over time.
  - Links to the specific retaining wall asset to which these measurements pertain.

## Application Tools for Data Visualization and Analysis

- **Integrated 3D Visualization:** The GAM application needs enhanced visualization capabilities to render and interact with 3D point clouds and models of retaining walls. This would allow engineers to virtually inspect assets and detect subtle changes.
- **Advanced Data Comparison and Trend Analysis:** Develop tools within the application to perform multi-temporal comparisons of 3D data (e.g., Cloud Compare's C2C and M3C2 comparison schemes) and to visualize displacement trends over time for individual points or sections of a wall.

## **Data-Driven Condition Assessment**

- **Objective Condition Indices:** Update the GAM's condition assessment framework to incorporate quantitative metrics derived from the new technologies (e.g., magnitude of displacement, extent of thermal anomalies) into the overall condition index of retaining walls. This would shift towards a more objective and data-informed assessment, moving beyond subjective visual inspections.
- **Performance Monitoring Dashboards:** Develop dashboards within the GAM application that provide a comprehensive overview of the performance and condition of retaining walls, drawing data from all integrated inspection sources.

These recommendations focus on enabling the GDOT GAM system to effectively store, manage, visualize, and analyze the objective, quantitative data generated by the advanced nondestructive/noncontact inspection protocols developed by this research project.



**APPENDIX A. TRAVERSE CALCULATION DETAILS DATA**  
**TRAVERSE CALCULATION DETAILS: CW, CROSSGATE, OLD RIVER,**  
**SANDERSVILLE, KING GEORGE**

The appendix included in this report presents the detailed traverse calculations conducted as a foundational component of the research. Traverses were established at five distinct locations to develop a reliable geospatial control framework essential for all subsequent surveying and analytical activities. These sites include CW, Crossgate, Old River Road, Sandersville and King George. Where CW comprises of 5 sides, Crossgate, Old River Road and King George are comprised of 6 sides while Sandersville was the most extensive, consisting of 7 sides. At each site, a series of coordinated survey stations were established through precise angular and linear measurements, using standard surveying instruments, RTS. The collected data includes measured internal angles, linear distances between traverse stations, and the application of appropriate traverse adjustment methods such as the Bowditch or Compass rule to correct for measurement errors and misclosures. The primary objective of these traverses was to provide a precise and consistent control network to support all further spatial measurements and geospatial analysis undertaken in the main phase of the research.

This appendix documents all relevant aspects of the traverse process, including raw field observations, computational procedures, error analysis, and the final adjusted coordinates for each station. The inclusion of this material ensures a high level of transparency, reproducibility, and technical reliability in the foundational survey work that underpins the research.

GEORGIA SOUTHERN UNIVERSITY		TRAVERSE CALCULATIONS									
PROJECT:		SIX-VERTEX TRAVERSE via Robotic, 1-sec, Total Station Instrument									
		Undergrad. Students: Photogrammetry Course - Spring 2025									
PARTY:		Graduate Students: Shakil Ahmed									
		Professors: Gus Maldonado, Marcel Maghlar and Soontie Nam									
Date:		Friday, February 14, 2025.									
		Number of Sides =		5		Selected Initial Coordinates		Assum. $X_A =$		50.00	
Approx. azimuth from A to B =				0.000000				Assum. $Y_A =$		30.00	

Measured Horizontal Distances	Traverse Points (Vertices)	Locally ADJUSTED Internal Angles	Globally ADJUSTED Internal Angles			Measured Azimuths (decimal)	Auxiliary Quantities	Traverse Points (Vertices)	Measured Horizontal Distances	Auxiliary Quantities to Calculate Vertex Coordinates				Traverse Points (Vertices)
L (ft)		d	m	s	d	m	s			Latitude L*cos(Az)	Departure L*sin(Az)	Corrections	Balanced	
	A	195	13	14	195	13	18.80	195.221889						A
15.66775	B	179	57	26	179	57	30.80	179.958556	359.95856	0.0000	0.0000	0.0003	15.668	0.001
19.73775	C	45	1	35	45	1	39.80	45.027722	224.98628	0.0004	0.0008	0.0004	19.738	-0.013
64.41075	D	55	24	18	55	24	22.30	55.406194	44.98628	0.0013	0.0026	0.0013	-45.555	-45.532
51.68800	E	64	23	3	64	23	8.30	64.385639	280.39247	0.0010	0.0020	0.0010	-9.323	50.842
20.17925	A				195	13	18.80	195.221889	344.77811	0.0004	-5.2982	0.0004	19.472	-5.297
	Total	538	118	96.00										
Non-Balanced Perimeter	171.584				538	118	120.00	540.00000	171.6835	-0.0034	-0.0068	0.0034	0.0068	Zero
	Decim., °													Zero
	Exact, °													Zero
	Error =	-0.006667	°	=	-24.00	sec								
	Corr/Ang, °													
	Corr/Ang, °													

$$E_c = \sqrt{E_L^2 + E_D^2}$$

$$E_c = \text{Error of Closure}$$

$$E_c = 0.00760 \text{ feet}$$

$$PRECISION = \frac{1}{P} = \frac{1}{|P|E_c}$$

$$PRECISION = 1 \text{ in } 22590$$

Traverse Calculation of CW



TRAVERSE CALCULATIONS									
PROJECT SIX-VERTEX TRAVERSE via Robotic, 1-sec, Total-Station Instrument - Photos's Data									
Undergrad. Students: Aniya Williams, Jakeb Britt, and Garfield Thorpe									
PARTY: Graduate Student: <b>Tanvir Ahmed</b>									
Professors: Marcel Maghlar, Gustavo Maldonado, and <b>Soonkie Nam</b>									
Date: Friday, June 30, 2023									
Number of Sides = <b>6</b>			Selected Initial Coordinates			Assum. $X_1 = 400.00$ Assum. $Y_1 = 200.00$			
Approx. azimuth from 1 to 2 = <b>80.200000</b>									

Traverse Points (Vertices)	Locally ADJUSTED Internal Angles			Globally (Final) ADJUSTED Internal Angles			Measured Azimuths (decimal)	Auxiliary Quantities		Traverse Points (Vertices)	Adopted Horizontal Distances L (ft)	Auxiliary Quantities to Calculate Vertex Coordinates				Traverse Points (Vertices)		
	d	m	s	d	m	s		Back Az. (+/-) 180	Next Angle			Latitude $L' \cdot \cos(Az)$	Departure $L' \cdot \sin(Az)$	Lat.	Dep.		Balanced Lat.	Dep.
A	181	54	44.50	181	54	35.17	181.90377	80.20000	260.20000	432.23060	A	41.99600	7.1481	41.3832	0.0003	7.148	41.384	A
B	172	1	59.50	172	1	50.17	172.03602	72.23060	252.23060	258.79870	B	336.73475	102.7670	320.6700	0.0025	102.770	320.673	B
C	6	34	14.50	6	34	5.17	6.568102	258.79870	78.79870	258.12417	C	349.09325	-67.8136	-342.4433	0.0026	-67.811	-342.440	C
D	179	19	41.00	179	19	31.67	179.325463	258.12417	78.12417	247.54866	D	41.59325	-8.4702	-40.2783	0.0003	-8.470	-40.278	D
E	169	25	37.50	169	25	28.17	169.424491	247.54866	67.54866	78.29023	E	199.23125	-76.0862	-184.1304	0.0015	-76.085	-184.129	E
F	10	44	39.00	10	44	29.67	10.74574	78.29023	258.29023	440.20000	F	209.14100	42.4461	204.7884	0.0016	42.448	204.790	F
A				181	54	35.17	181.903769	80.20000			A		$E_L$	$E_D$	$-E_L$	$-E_D$	Zero	A
Total	717	177	236.00	717	177	180.00	720.000000				Totals:	1177.35550	-0.0089	-0.0103	0.0089	0.0103	Zero	0.000
Decimal	720.01556			720.000000														
Exact																		
Error =	0.0165556			=			56.00 sec											
Corr/Ang.																		
Corr/Ang.	-9.33 sec																	

North (Y)

East (X)

$(X_A, Y_A)$

$(X_B, Y_B)$

Latitude:  $L \times \cos(Az)$

$Az$

Departure  $\times \sin(Az)$

L

$E_c = \sqrt{E_L^2 + E_D^2} \rightarrow$

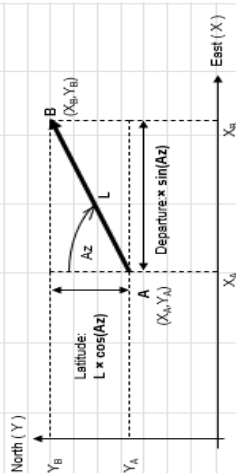
$E_c = \text{Error of Closure}$

PRECISION =  $\frac{1}{P} = \frac{1}{|E_c|}$

$\leftarrow \text{PRECISION} = \frac{1}{P}$

0.01363 feet

1 in 86406



Traverse Calculation of B1- Crossgate

QUANTITIES CALCULATED AFTER CORRECTING THE TRAVERSE MEASUREMENTS																													
CALCULATED COORDINATES				Auxiliary Calculations to Determine Enclosed Area				Traverse Points		Calculated Lengths		Increments		Calculated Bearings (For Counterclockwise Traverse)				Calculated Azimuths		Back Azimuths		Internal Angles		Calculated Int Angles		Traverse Points			
X	Y	Northing	Easting	Enclosed Area		Algebraic Sum		Vertices	Lengths (ft)	Depart. Along X, ft	Latitudes Along Y, ft	(decimal)	d	m	s	(decimal)	d	m	s	(decimal)	d	m	s	(decimal)	d	m	s	Vertices	
►	▲	►	►	+ values	- values			A																					
400.000	200.000	200.000	400.000	88276.7	-82853.4	5417.34		A	41.996	41.384	7.148	1	N 80.19966	E	N 80 11 59 E	80.19966	260.19966	260.19966							181 54	35.10		A	
441.384	207.148	207.148	441.384	157859	-136732.7	21066.12		B	336.738	320.673	102.770	1	N 72.23034	E	N 72 13 49 E	72.23034	252.23034	252.23034							172 00	068	172 1	50.46	B
762.057	309.918	309.918	762.057	130047	-184499.2	-54452.55		C	349.090	-342.440	-67.871	3	S 78.79903	W	S 78 47 57 W	258.79903	78.79903	78.79903							6 58	869	6 34	7.27	C
419.616	242.107	242.107	419.616	91840.4	-98037.9	-6197.45		D	41.159	-40.278	-8.470	3	S 78.12449	W	S 78 7 28 W	258.12449	78.12449	78.12449							179 32	546	179 19	31.64	D
379.338	233.637	233.637	379.338	45608.2	-59765.7	-14157.43		E	199.229	-184.129	-76.085	3	S 67.54886	W	S 67 32 56 W	247.54886	67.54886	67.54886							169 42	438	169 25	27.76	E
195.210	157.552	157.552	195.210	63020.9	-39042.0	23979.00		F	209.143	204.790	42.448	1	N 78.28991	E	N 78 17 24 E	78.28991	258.28991	258.28991							10 74	105	10 44	27.76	F
400.000	200.000	200.000	400.000					A																	181 54	35.10		A	
				Enclosed Area					Perimeter																		720.00000	717 177	180.00
				12172.48 ft²					P (feet)																				
				0.27944 Acres					1177.355																				

Traverse Calculation of B2-Old River Rd



QUANTITIES CALCULATED AFTER CORRECTING THE TRAVERSE MEASUREMENTS																			
Traverse Points (Vertices)	CALCULATED COORDINATES				Auxiliary Calculations to Determine Enclosed Area			Traverse Points (Vertices)	Calculated Lengths (ft)	Increments		Bearing (For Counterclockwise Traverse)	Calculated Azimuths (decimal)	Back Azimuths (decimal)	Internal Angles (decimal)	Calculated Int Angles (d m s)	Traverse Points (Vertices)		
	X (ft)	Y (ft)	Northing (ft)	Easting (ft)	+ values	- values	Algebraic Sum			Depart along X, ft	Latitudes along Y, ft								
A	400.000	250.000	250.000	400.000	90894.79	-111300.8	-20406.03	A	46.0940	-36.421	28.252	4 N 52.19889 W	52 11 56 W	307.80111	127 48 4	179.37607	179 22 33.84	A	
B	363.579	278.252	278.252	363.579	57550.78	-85189.1	-27638.30	B	162.7930	-156.749	-43.945	3 S 74.33899 W	74 20 20 W	254.33899	74 20 20	126.33788	126 32 16.38	B	
C	206.830	234.307	234.307	206.830	74177.55	-30513.1	43664.48	C	139.9158	109.753	-86.779	2 S 51.66742 E	51 40 3 E	128.33258	308 19 57	53.99598	53 59 36.90	C	
D	316.583	147.528	147.528	316.583	52012.01	-37619.8	14392.19	D	46.0185	35.975	-28.697	2 S 51.42120 E	51 25 16 E	128.57080	308 34 44	180.24622	180 14 46.39	D	
E	352.558	118.831	118.831	352.558	60550.88	-57498.5	3052.35	E	163.1165	156.997	44.259	1 N 74.25645 E	74 15 23 E	74.25645	254 15 23	125.67765	125 40 39.55	E	
F	508.555	163.090	163.090	509.555	66295.83	-127368.8	-62152.98	F	139.8420	-103.555	86.910	4 N 51.57496 W	51 34 30 W	128.42504	128 25 30	54.16859	54 10 6.93	F	
A	400.000	250.000	250.000	400.000				A								179.37607	179 22 33.84	A	
Enclosed Area									Perimeter										
24544.14 ft²									P (feet)										
0.56346 Acres									6917.797										
717 177 180.00									720.0000										

GEORGIA SOUTHERN UNIVERSITY		TRAVERSE CALCULATIONS									
PROJECT:		SIX-VERTEX TRAVERSE via Robotic, 1-sec, Total-Station Instrument									
PARTY:		Undergrad. Students: NA									
		Graduate Students: Md. Mehrab Hossain and Shakil Ahmed									
		Professors: Soontie Nam, Gus Maldonado and Marcel Maghlar									
Date:		Friday, July 13, 2024.									
		Number of Sides =		7		Selected Initial Coordinates					
Approx. azimuth from A to B =				105.000000							
		Assum. X <sub>A</sub> =		300.00		Assum. Y <sub>A</sub> =		150.00			

North (Y)

Y<sub>B</sub>

Y<sub>A</sub>

Latitude:  
L × cos(Az)

(X<sub>B</sub>, Y<sub>B</sub>)

(X<sub>A</sub>, Y<sub>A</sub>)

Departure: L × sin(Az)

East (X)

X<sub>B</sub>

X<sub>A</sub>

Measured Horizontal Distances

L (ft)

Traverse Points (Vertices)

A

B

C

X1

D

E

F

A

Locally ADJUSTED Internal Angles

d

m

s

110

0

35.50

180

30

55.75

175

13

11.25

4

22

14.75

181

37

28.25

176

42

52.25

71

32

56.75

Globally ADJUSTED Internal Angles

d

m

s

110

0

33.43

180

30

53.68

175

13

9.18

4

22

12.68

181

37

26.18

176

42

50.18

71

32

54.68

110

0

33.43

Measured Azimuths (decimal)

105.00000

105.51491

100.73413

285.10432

286.72825

283.44219

283.44219

174.99071

105.00000

Auxiliary Quantities

Back Az.

Back Az. + Next Angle

285.00000

465.51491

280.73413

105.10432

106.72825

103.44219

354.99071

465.00000

Traverse Points (Vertices)

A

B

C

X1

D

E

F

A

Measured Horizontal Distances

L (ft)

60.8975

67.3204

507.9496

523.6650

56.9339

68.0436

40.4423

Auxiliary Quantities to Calculate Vertex Coordinates

Latitude L'cos(Az)

Departure L'sin(Az)

-15.7614

58.8225

-18.0075

64.8673

-94.6066

499.0615

136.4552

-505.5739

16.3875

-54.5245

15.8176

-66.1790

-40.2879

3.5313

Traverse Points (Vertices)

A

B

C

X1

D

E

F

A

Balanced Lat.

Balanced Dep.

-15.761

58.822

-18.007

64.867

-94.605

499.060

136.456

-505.576

16.388

-54.525

15.818

-66.179

-40.288

3.531

Traverse Points (Vertices)

A

B

C

X1

D

E

F

A

Latitude L'cos(Az)

Departure L'sin(Az)

-15.7614

58.8225

-18.0075

64.8673

-94.6066

499.0615

136.4552

-505.5739

16.3875

-54.5245

15.8176

-66.1790

-40.2879

3.5313

Traverse Points (Vertices)

A

B

C

X1

D

E

F

A

Balanced Lat.

Balanced Dep.

-15.761

58.822

-18.007

64.867

-94.605

499.060

136.456

-505.576

16.388

-54.525

15.818

-66.179

-40.288

3.531

Traverse Points (Vertices)

A

B

C

X1

D

E

F

A

Latitude L'cos(Az)

Departure L'sin(Az)

-15.7614

58.8225

-18.0075

64.8673

-94.6066

499.0615

136.4552

-505.5739

16.3875

-54.5245

15.8176

-66.1790

-40.2879

3.5313

Traverse Points (Vertices)

A

B

C

X1

D

E

F

A

Balanced Lat.

Balanced Dep.

-15.761

58.822

-18.007

64.867

-94.605

499.060

136.456

-505.576

16.388

-54.525

15.818

-66.179

-40.288

3.531

Traverse Points (Vertices)

A

B

C

X1

D

E

F

A

Latitude L'cos(Az)

Departure L'sin(Az)

-15.7614

58.8225

-18.0075

64.8673

-94.6066

499.0615

136.4552

-505.5739

16.3875

-54.5245

15.8176

-66.1790

-40.2879

3.5313

Traverse Points (Vertices)

A

B

C

X1

D

E

F

A

Balanced Lat.

Balanced Dep.

-15.761

58.822

-18.007

64.867

-94.605

499.060

136.456

-505.576

16.388

-54.525

15.818

-66.179

-40.288

3.531

Traverse Points (Vertices)

A

B

C

X1

D

E

F

A

Latitude L'cos(Az)

Departure L'sin(Az)

-15.7614

58.8225

-18.0075

64.8673

-94.6066

499.0615

136.4552

-505.5739

16.3875

-54.5245

15.8176

-66.1790

-40.2879

3.5313

Traverse Points (Vertices)

A

B

C

X1

D

E

F

A

Balanced Lat.

Balanced Dep.

-15.761

58.822

-18.007

64.867

-94.605

499.060

136.456

-505.576

16.388

-54.525

15.818

-66.179

-40.288

3.531

Traverse Points (Vertices)

A

B

C

X1

D

E

F

A

Latitude L'cos(Az)

Departure L'sin(Az)

-15.7614

58.8225

-18.0075

64.8673

-94.6066

499.0615

136.4552

-505.5739

16.3875

-54.5245

15.8176

-66.1790

-40.2879

3.5313

Traverse Points (Vertices)

A

B

C

X1

D

E

F

A

Balanced Lat.

Balanced Dep.

-15.761

58.822

-18.007

64.867

-94.605

499.060

136.456

-505.576

16.388

-54.525

15.818

-66.179

-40.288

3.531

Traverse Points (Vertices)

A

B

C

X1

D

E

F

A

Latitude L'cos(Az)

Departure L'sin(Az)

-15.7614

58.8225

-18.0075

64.8673

-94.6066

499.0615

136.4552

-505.5739

16.3875

-54.5245

15.8176

-66.1790

-40.2879

3.5313

Traverse Points (Vertices)

A

B

C

X1

D

E

F

A

Balanced Lat.

Balanced Dep.

-15.761

58.822

-18.007

64.867

-94.605

499.060

136.456

-505.576

16.388

-54.525

15.818

-66.179

-40.288

3.531

Traverse Points (Vertices)

A

B

C

X1

D

E

F

A

Latitude L'cos(Az)

Departure L'sin(Az)

-15.7614

58.8225

-18.0075

64.8673

-94.6066

499.0615

136.4552

-505.5739

16.3875

-54.5245

15.8176

-66.1790

-40.2879

3.5313

Traverse Points (Vertices)

A

B

C

X1

D

E

F

A

Balanced Lat.

Balanced Dep.

-15.761

58.822

-18.007

64.867

-94.605

499.060

136.456

-505.576

16.388

-54.525

15.818

-66.179

-40.288

3.531

Traverse Points (Vertices)

A

B

C

X1

D

E

F

A

Latitude L'cos(Az)

Departure L'sin(Az)

-15.7614

58.8225

-18.0075

64.8673

-94.6066

499.0615

136.4552

-505.5739

16.3875

-54.5245

15.8176

-66.1790

-40.2879

3.5313

Traverse Points (Vertices)

A

B

C

X1

D

E

F

A

Balanced Lat.

Balanced Dep.

-15.761

58.822

-18.007

64.867

-94.605

499.060

136.456

-505.576

16.388

-54.525

15.818

-66.179

-40.288

3.531

Traverse Points (Vertices)

A

B

C

X1

D

E

F

A

Latitude L'cos(Az)

Departure L'sin(Az)

-15.7614

58.8225

-18.0075

64.8673

-94.6066

499.0615

136.4552

-505.5739

16.3875

-54.5245

15.8176

-66.1790

-40.2879

3.5313

Traverse Points (Vertices)

A

B

C

X1

D

E

F

A

Balanced Lat.

Balanced Dep.

-15.761

58.822

-18.007

64.867

-94.605

499.060

136.456

-505.576

16.388

-54.525

15.818

-66.179

-40.288

3.531

Traverse Points (Vertices)

A

B

C

X1

D

E

F

A

Latitude L'cos(Az)

Departure L'sin(Az)

-15.7614

58.8225

-18.0075

64.8673

-94.6066

499.0615

136.4552

-505.5739

16.3875

-54.5245

15.8176

-66.1790

-40.2879

3.5313

Traverse Points (Vertices)

A

B

C

X1

D

E

F

A

Balanced Lat.

Balanced Dep.

-15.761

58.822

-18.007

64.867

-94.605

499.060

136.456

-505.576

16.388

-54.525

15.818

-66.179

-40.288

3.531

Traverse Points (Vertices)

A

B

C

X1

D

E

F

A

Latitude L'cos(Az)

Departure L'sin(Az)

-15.7614

58.8225

-18.0075

64.8673

-94.6066

499.0615

136.4552

-505.5739

16.3875

-54.5245

15.8176

-66.1790

-40.2879

3.5313

Traverse Points (Vertices)

A

B

C

X1

D

E

F

A

Balanced Lat.

Balanced Dep.

-15.761

58.822

-18.007

64.867

-94.605

499.060

136.456

-505.576

16.388

-54.525

15.818

-66.179

-40.288

3.531

Traverse Points (Vertices)

A

B

C

X1

D

E

F

A

Latitude L'cos(Az)

Departure L'sin(Az)

-15.7614

58.8225

-18.0075

64.8673

-94.6066

499.0615

136.4552

-505.5739

16.3875

-54.5245

15.8176

-66.1790

-40.2879

3.5313

Traverse Points (Vertices)

A

B

C

X1

D

E

F

A

Balanced Lat.

Balanced Dep.

-15.761

58.822

-18.007

64.867

-94.605

499.060

136.456

-505.576

16.388

-54.525

15.818

-66.179

-40.288

3.531

Traverse Points (Vertices)

A

B

C

X1

D

E

F

A

Latitude L'cos(Az)

Departure L'sin(Az)

-15.7614

58.8225

-18.0075

64.8673

-94.6066

499.0615

136.4552

-505.5739

16.3875

-54.5245

15.8176

-66.1790

-40.2879

3.5313

Traverse Points (Vertices)

A

B

C

X1

D

E

F

A

Balanced Lat.

Balanced Dep.

-15.761

58.822

-18.007

64.867

-94.605

499.060

136.456

-505.576

16.388

-54.525

15.818

-66.179

-40.288

3.531

Traverse Points (Vertices)

A

B

C

X1

D

E

F

A

Latitude L'cos(Az)

Departure L'sin(Az)

-15.7614

58.8225

-18.0075

64.8673

-94.6066

499.0615

136.4552

-505.5739

16.3875

-54.5245

15.8176

-66.1790

-40.2879

3.5313

Traverse Points (Vertices)

A

B

C

X1

D

E

F

A

Balanced Lat.

Balanced Dep.

-15.761

58.822

-18.007

64.867

-94.605

499.060

136.456

-505.576

16.388

-54.525

15.818

-66.179

-40.288

3.531

Traverse Points (Vertices)

A

B

C

X1

D

E

F

A

Latitude L'cos(Az)

Departure L'sin(Az)

-15.7614

58.8225

-18.0075

64.8673

-94.6066

499.0615

136.4552

-505.5739

16.3875

-54.5245

15.8176

-66.1790

-40.2879

3.5313

Traverse Points (Vertices)

A

B

C

X1

D

E

F

A

Balanced Lat.

Balanced Dep.

-15.761

58.822

-18.007

64.867

-94.605

499.060

136.456

-505.576

16.388

-54.525

15.818

-66.179

-40.288

3.531

Traverse Points (Vertices)

A

B

C

X1

D

E

F

A

Latitude L'cos(Az)

Departure L'sin(Az)

-15.7614

58.8225

-18.0075

64.8673

-94.6066

499.0615

136.4552

-505.5739

16.3875

-54.5245

15.8176

-66.1790

-40.2879

3.5313

Traverse Points (Vertices)

A

B

C

X1

D

E

F

A

Balanced Lat.

Balanced Dep.

-15.761

58.822

-18.007

64.867

-94.605

499.060

136.456

-505.576

16.388

-54.525

15.818

-66.179

-40.288

3.531

Traverse Points (Vertices)

A

B

C

X1

D

E

F

A

Latitude L'cos(Az)

Departure L'sin(Az)

-15.7614

58.8225

-18.0075

64.8673

-94.6066

499.0615

136.4552

-505.5739

16.3875

-54.5245

15.8176

-66.1790

-40.2879

3.5313

Traverse Points (Vertices)

A

B

C

X1

D

E

F

A

Balanced Lat.

Balanced Dep.

-15.761

58.822

-18.007

64.867

-94.605

499.060

136.456

-505.576

16.388

-54.525

15.818

-66.179

-40.288

3.531

Traverse Points (Vertices)

A

B

C

X1

D

E

F

A

Latitude L'cos(Az)

Departure L'sin(Az)

-15.7614

58.8225

-18.0075

64.8673

-94.6066

499.0615

136.4552

-505.5739

16.3875

-54.5245

15.8176

-66.1790

-40.2879

3.5313

Traverse Points (Vertices)

A

B

C

X1

D

E

F

A

Balanced Lat.

Balanced Dep.

-15.761

58.822

-18.007

64.867

-94.605

499.060

136.456

-505.576

16.388

-54.525

15.818

-66.179

-40.288

3.531

Traverse Points (Vertices)

A

B

C

X1

D

E

F

A

Latitude L'cos(Az)

Departure L'sin(Az)

-15.7614

58.8225

-18.0075

64.8673

-94.6066

499.0615

136.4552

-505.5739

16.3875

-54.5245

15.8176

-66.1790

-40.2879

3.5313

Traverse Points (Vertices)

A

B

C

X1

D

E

F

A

Balanced Lat.

Balanced Dep.

-15.761

58.822

-18.007

64.867

-94.605

499.060

136.456

-505.576

16.388

-54.525

15.818

-66.179

-40.288

3.531

Traverse Points (Vertices)

A

B

C

X1

D

E

F

A

Latitude L'cos(Az)

Departure L'sin(Az)

-15.7614

58.8225

-18.0075

64.8673

-94.6066

499.0615

136.4552

-505.5739

16.3875

-54.5245

15.8176

-66.1790

-40.2879

3.5313

Traverse Points (Vertices)

A

B

C

X1

D

E

F

A

Balanced Lat.

Balanced Dep.

-15.761

58.822

-18.007

64.867

-94.605

499.060

136.456

-505.576

16.388

-54.525

15.818

-66.179

-40.288

3.531

Traverse Points (Vertices)

A

B

C

X1

D

E

F

A

Latitude L'cos(Az)

Departure L'sin(Az)

-15.7614

58.8225

-18.0075

64.8673

-94.6066

499.0615

136.4552

-505.5739

16.3875

-54.5245

15.8176

-66.1790

-40.2879

3.5313

Traverse Points (Vertices)

A

B

C

X1

D

E

F

A

Balanced Lat.

Balanced Dep.

-15.761

58.822

-18.007

64.867

-94.605

499.060

136.456

-505.576

16.388

-54.525

15.818

-66.179

-40.288

3.531

Traverse Points (Vertices)

A

B

C

X1

D

E

F

A

Latitude L'cos(Az)

Departure L'sin(Az)

-15.7614

58.8225

-18.0075

64.8673

-94.6066

499.0615

136.4552

-505.5739

16.3875

-54.5245

15.8176

-66.1790

-40.2879

3.5313

Traverse Calculation of B3-Sandersville



QUANTITIES CALCULATED AFTER CORRECTING THE TRAVERSE MEASUREMENTS																																
Traverse Points (Vertices)	CALCULATED COORDINATES				Auxiliary Calculations to Determine Enclosed Area			Traverse Points (Vertices)	Calculated Lengths (ft)	Increments		Bearing (For Counterclockwise Traverse)	Calculated Bearings			Calculated Azimuths		Back Azimuths		Internal Angles (decimal)	Calculated Int Angles		Traverse Points (Vertices)									
	X (ft)	Y (ft)	Northing (ft)	Easting (ft)	+ values	- values	Algebraic Sum			Depart along X, ft	Latitudes along Y, ft		(decimal)	d	m	s	(decimal)	d	m		s	(decimal)		d	m	s						
A	300.000	150.000	150.000	300.000	53823.34	-40271.6	13551.72	A	60.8972	58.822	-15.761	2	S	75.00007	E	S	75	0	0	E	104.99993	284	59	60	110.00900	110	0	32.42	A			
B	358.822	134.239	134.239	358.822	56875.5	-41706.4	15169.08	B	67.3201	64.867	-18.007	2	S	74.48516	E	S	74	29	7	E	105.51484	285	30	53	180.51491	180	30	53.69	B			
C	423.689	116.231	116.231	423.689	107252.4	-9162.7	98089.67	C	507.9475	499.060	-94.605	2	S	79.26596	E	S	79	15	57	E	100.73404	280	44	3	175.21920	175	13	9.10	C			
X1	922.749	21.626	21.626	922.749	9021.798	-145870.4	-136848.60	X1	523.6673	-505.576	136.456	4	N	74.89561	W	N	74	53	44	W	285.10439	105	6	16	4.37035	4	22	13.27	X1			
D	417.173	158.082	158.082	417.173	57328.3	-72784.2	-15455.86	D	56.9342	-54.525	16.388	4	N	73.27168	W	N	73	16	18	W	286.72832	106	43	42	181.62393	181	37	26.15	D			
E	362.648	174.470	174.470	362.648	51724.93	-69007.5	-17282.57	E	68.0434	-66.179	15.818	4	N	76.55773	W	N	76	33	28	W	283.44227	103	26	32	176.71395	176	42	50.23	E			
F	296.469	190.288	190.288	296.469	57086.33	-44470.3	12616.00	F	40.4422	3.531	-40.288	2	S	5.00908	E	S	5	0	33	E	174.99892	354	59	27	71.54855	71	32	55.14	F			
A	300.000	150.000	150.000	300.000				A																	110.00900	110	0	32.42	A			
Enclosed Area									Perimeter																							
15080.27 ft²									P (feet)														897		176		240.00					
0.34620 Acres									1325.2518																							

Traverse Calculation of B4-King George

GEORGIA SOUTHERN UNIVERSITY		TRAVERSE CALCULATIONS																		
PROJECT:		SIX-VERTEX TRAVERSE via Robotic, 1-sec, Total Station Instrument - Photos's Data																		
PARTY:		Undergrad. Students: NA																		
		Graduate Students: Md. Meltrab Hossain and Shakil Ahmed																		
		Professors: Soontie Nam, Marcel Maghlar, and Gus Maldonado																		
Date:		Friday, June 21, 2024.																		
		Number of Sides =		6		Selected Initial Coordinates		Assum. $X_A =$		300.00										
Approx. azimuth from A to B =				45.000000				Assum. $Y_A =$		200.00										
Measured Horizontal Distances	Traverse Points (Vertices)	Locally ADJUSTED Internal Angles			Globally ADJUSTED Internal Angles			Measured Azimuths (decimal)	Auxiliary Quantities		Traverse Points (Vertices)	Auxiliary Quantities to Calculate Vertex Coordinates				Traverse Points (Vertices)				
		d	m	s	d	m	s		Back Az. (+/-) 180	Next Angle		Latitude $L' \cos(Az)$	Departure $L' \sin(Az)$	Lat.	Dep.		Balanced			
		L (ft)																		
		A	78	27	30.75	78	27		30.50	225.00000		445.79667	45.00000	78.45847					A	
		B	220	47	48.25	220	47		48.00	265.79667		445.86771	85.79667	220.796667					B	
		C	180	4	16.00	180	4		15.75	265.86771		401.80306	85.86771	180.071042					C	
		D	135	56	7.50	135	56		7.25	221.80306		267.81076	41.80306	135.955347					D	
		E	46	0	28.00	46	0		27.75	87.81076		146.54153	267.81076	46.007708					E	
F	58	43	51.00	58	43	50.75	326.54153	405.00000	146.54153	58.730764				F						
A				78	27	30.50			45.00000	78.458472				A						
Total	717	177	181.50	717	177	180.00			720.00000						Totals:					
Decimal, °	720.00042		720.00000		720.00000		720.00000		720.00000		713.1676		0.0115		-0.0194	-0.0115	0.0194	0.0000	Zero	0.0000
Exact, °	720.00000		720.00000		720.00000		720.00000		720.00000		713.1676		0.0115		-0.0194	-0.0115	0.0194	0.0000	Zero	0.0000
Error =	0.000417 °		=		1.50 sec															
Corr/Ang, °	-0.00007																			
Corr/Ang, °	-0.25 sec																			

North (Y)

East (X)

$(X_A, Y_A)$

$(X_B, Y_B)$

Latitude:  $L \times \cos(Az)$

Departure  $L \times \sin(Az)$

$Az$

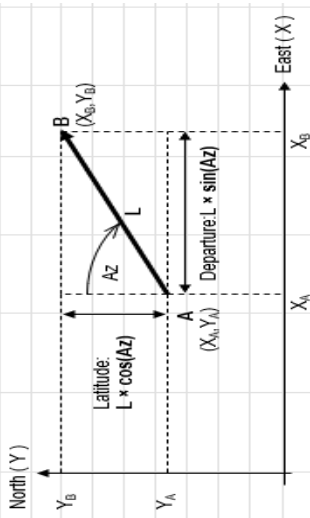
$L$

$E_c = \sqrt{E_L^2 + E_D^2}$

$E_c = \text{Error of Closure}$

$PRECISION = \frac{1}{\frac{E_c}{P}}$

$PRECISION = 1 \text{ in } 31601$



Traverse Calculation of B4-King George

QUANTITIES CALCULATED AFTER CORRECTING THE TRAVERSE MEASUREMENTS																						
Traverse Points (Vertices)	CALCULATED COORDINATES				Auxiliary Calculations to Determine Enclosed Area			Traverse Points (Vertices)	Calculated Lengths (ft)	Increments		Calculated Bearings (For Counterclockwise Traverse)			Calculated Azimuths (decimal)	Back Azimuths (decimal)	Internal Angles (decimal)	Calculated Int Angles		Traverse Points (Vertices)		
	X (ft)	Y (ft)	Northing (ft)	Easting (ft)	+ values	- values	Algebraic Sum			Depart. along X, ft	Latitudes along Y, ft	(decimal)	d	m				s	d		m	s
A	300.000	200.000	200.000	300.000	68418.8	-72627.4	-4208.62	A	59.5280	42.094	42.091	1	N 45.00176 E	N 45 0 6 E	45.00176	225 0 6	78.46102	78 27 39.68	A			
B	342.094	242.091	242.091	342.094	102368	-84847.8	17520.03	B	80.9716	80.754	5.933	1	N 85.79770 E	N 85 47 52 E	85.79770	265 47 52	220.79595	220 47 45.40	B			
C	422.848	248.025	248.025	422.848	122762	-107079.1	15682.69	C	72.2979	72.110	5.208	1	N 85.86874 E	N 85 52 7 E	85.86874	265 52 7	180.07104	180 4 15.74	C			
D	494.958	253.233	253.233	494.958	137957	-152916.8	-14959.85	D	74.7442	49.824	55.716	1	N 41.80483 E	N 41 48 17 E	41.80483	221 48 17	135.98909	135 56 9.93	D			
E	544.782	308.949	308.949	544.782	72852.9	-161872.3	-89019.45	E	308.1991	-308.973	-11.817	3	S 87.80978 W	S 87 48 35 W	87.80978	87 48 35	46.00495	46 0 17.81	E			
F	235.809	297.132	297.132	235.809	89139.7	-47161.8	41977.94	F	116.4268	64.191	-97.132	2	S 33.45927 E	S 33 27 33 E	33.45927	326 32 27	58.73095	58 43 51.43	F			
A	300.000	200.000	200.000	300.000				A									78.46102	78 27 39.68	A			
Enclosed Area									Perimeter													
16503.63 ft <sup>2</sup>									P (feet)								720.00000		717 177		180.00	
0.37887 Acres									713.1676													
									</													

## APPENDIX B. SUPPLIMENTARY DATA OF THERMOGRAPHY ANALYSIS

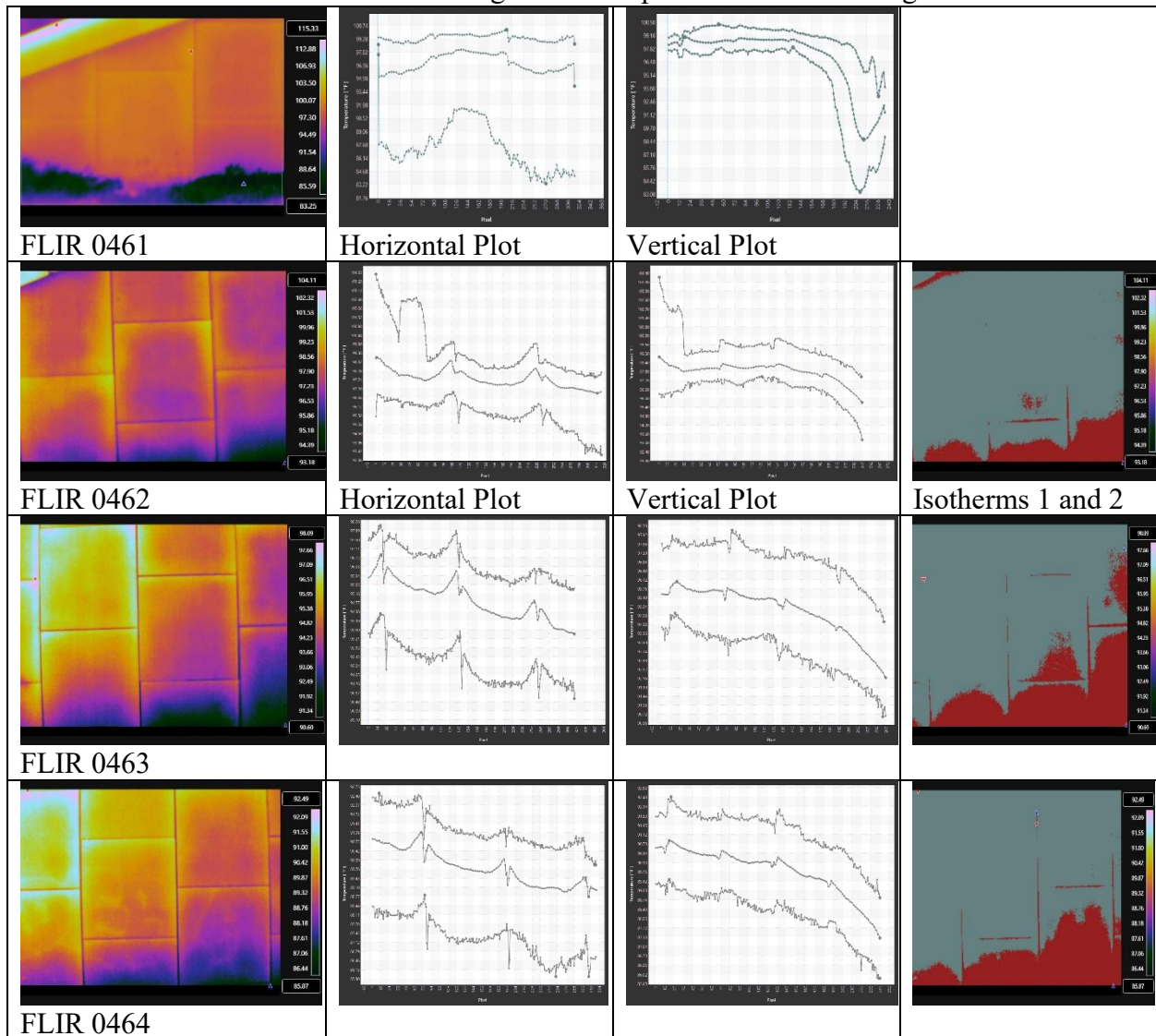
T1-1 West to East Data – Crossgate

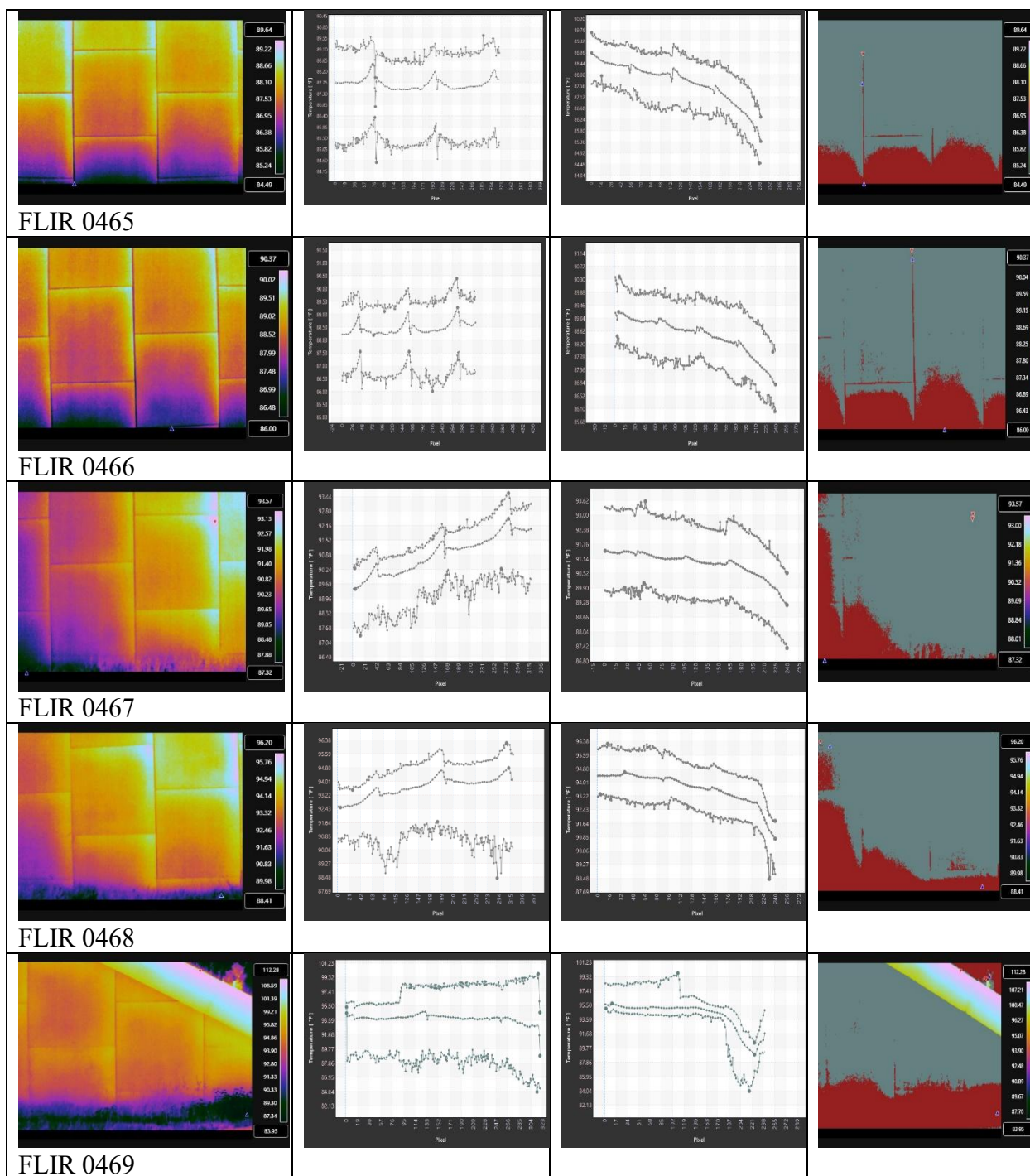
	Image 0461	Polygon 1	
Mean [F]	97.42	96.55	
Std. Dev. [F]	4.59	3.71	
Center [F]	(159.5, 119.5) 98.84	(159.0, 120.5) 98.76	
Maximum [F]	(45, 26) 115.33	(208, 58) 100.23	
Minimum [F]	(272, 212) 83.25	(272, 212) 83.25	
Number of Pixels	76800	64291	
Percentage Area [%]		83.71223958	
	Image 0462	Isotherm 1	Isotherm 2
Mean [F]	97.78	97.99	96.28
Std. Dev. [F]	0.9	0.71	0.65
Center [F]	(159.5, 119.5) 97.61	(159.5, 119.5) 97.61	(159.5, 119.5) 97.61
Maximum [F]	(1, 1) 104.11	(1, 1) 104.11	(90, 3) 97.00
Minimum [F]	(320, 240) 93.18	(90, 3) 97.00	(320, 240) 93.18
Number of Pixels	76800	67206	9727
Percentage Area [%]		87.5078125	12.66536458
	Image 0463	Isotherm 1	Isotherm 2
Mean [F]	94.87	95.43	93.08
Std. Dev. [F]	1.31	0.87	0.73
Center [F]	(159.5, 119.5) 95.15	(159.5, 119.5) 95.15	(159.5, 121.0) 95.10
Maximum [F]	(19, 76) 98.09	(16, 76) 98.07	(313, 7) 93.99
Minimum [F]	(319, 237) 90.60	(316, 37) 94.00	(319, 237) 90.60
Number of Pixels	76800	58581	18218
Percentage Area [%]		91.59505208	8.404947917
	Image 464	Isotherm 1	Isotherm 2
Mean [F]	89.78	90.19	88.17
Std. Dev. [F]	1.06	0.72	0.53
Center [F]	(159.5, 119.5) 89.82	(159.5, 119.0) 89.78	(159.5, 138.0) 89.63
Maximum [F]	(10, 17) 92.49	(10, 17) 92.49	(191, 55) 88.90
Minimum [F]	(309, 239) 85.87	(191, 36) 88.91	(309, 239) 85.87
Number of Pixels	76800	61435	15365
Percentage Area [%]		79.99348958	20.00651042
	Image 0465	Isotherm 1	Isotherm 2
Mean [F]	87.68	88	86.34

Std. Dev. [F]	0.81	0.49	0.46
Center [F]	(159.5, 119.5) 87.64	(159.5, 115.0) 87.67	(159.5, 148.5) 87.36
Maximum [F]	(289, 1) 89.64	(289, 1) 89.64	(79, 65) 86.99
Minimum [F]	(81, 238) 84.49	(78, 100) 87.00	(81, 238) 84.49
Number of Pixels	76800	61907	14893
Percentage Area [%]		80.60807292	19.39192708
	Image 0466	Isotherm 1	Isotherm 2
Mean [F]	87.68	88	86.34
Std. Dev. [F]	0.81	0.49	0.46
Center [F]	(159.5, 119.5) 87.64	(159.5, 115.0) 87.67	(159.5, 148.5) 87.36
Maximum [F]	(289, 1) 89.64	(289, 1) 89.64	(79, 65) 86.99
Minimum [F]	(81, 238) 84.49	(78, 100) 87.00	(81, 238) 84.49
Number of Pixels	76800	61907	14893
Percentage Area [%]		80.60807292	19.39192708
	Image 0467	Isotherm 1	Isotherm 2
Mean [F]	90.9	91.19	89.44
Std. Dev. [F]	1	0.79	0.52
Center [F]	(159.5, 119.5) 91.54	(159.5, 119.5) 91.54	(159.5, 119.5) 91.54
Maximum [F]	(278, 54) 93.57	(279, 48) 93.52	(13, 2) 90.00
Minimum [F]	(13, 240) 87.32	(13, 1) 90.00	(13, 240) 87.32
Number of Pixels	76800	63889	12910
Percentage Area [%]		83.18880208	16.80989583
	Image 0468	Isotherm 1	Isotherm 2
Mean [F]	93.64	94.08	92.07
Std. Dev. [F]	1.06	0.65	0.74
Center [F]	(159.5, 119.5) 93.77	(159.5, 112.5) 93.86	(159.5, 127.5) 93.79
Maximum [F]	(308, 14) 96.20	(309, 16) 96.17	(5, 32) 93.00
Minimum [F]	(291, 232) 88.41	(22, 32) 93.01	(291, 232) 88.41
Number of Pixels	76800	60184	16615
Percentage Area [%]		78.36458333	21.63411458
	Image 0469	Isotherm 1	Isotherm 2
Mean [F]	94.77	94.96	90.74
Std. Dev. [F]	4.18	0.61	2.16
Center [F]	(159.5, 119.5) 94.76	(159.5, 119.5) 94.76	(159.5, 119.5) 94.76
Maximum [F]	(250, 28) 112.28	(115, 12) 98.16	(294, 39) 93.99
Minimum [F]	(314, 217) 83.95	(301, 30) 94.00	(314, 217) 83.95
Number of Pixels	76800	45010	22247
Percentage Area [%]		58.60677083	28.96744792
	Image 0470	Polygon 1	

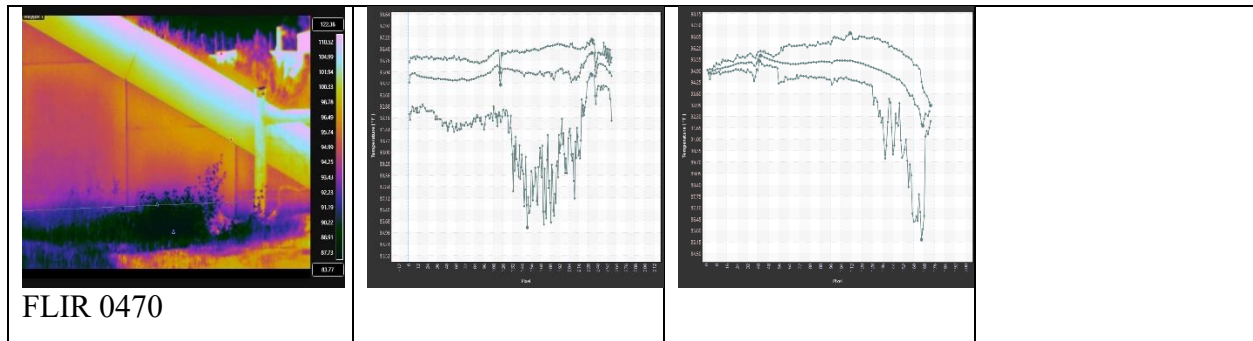
Mean [F]	95.82	94.83	
Std. Dev. [F]	5.41	1.14	
Center [F]	(159.5, 119.5) 96.10	(128.5, 100.0) 96.13	
Maximum [F]	(222, 47) 122.38	(233, 125) 97.03	
Minimum [F]	(169, 205) 83.77	(151, 180) 85.26	
Number of Pixels	76800	27628	
Percentage Area [%]		35.97395833	

TII-1 West to East Images and Temperature Plots – Crossgate









T1-2 East to West Data – Crossgate

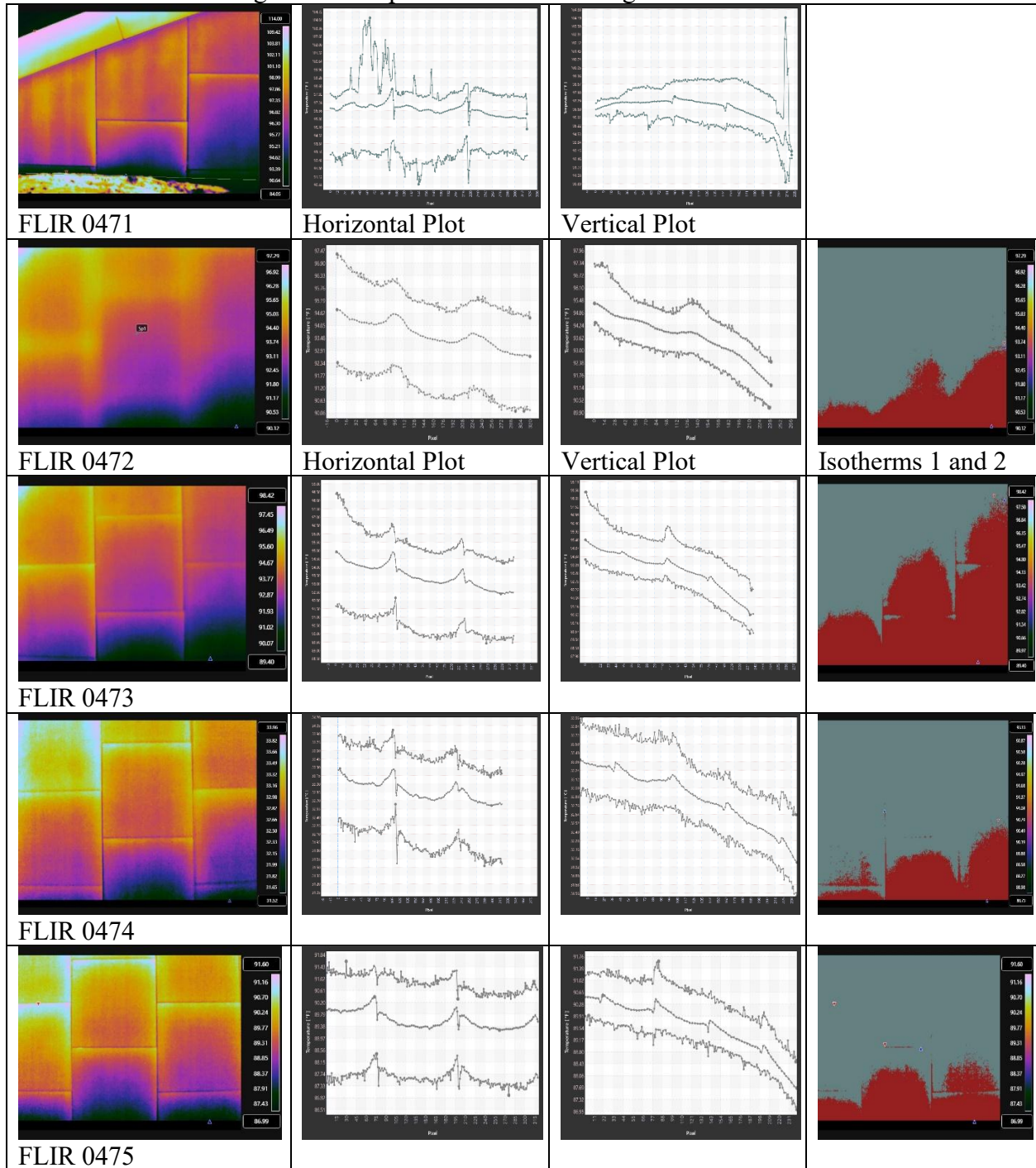
		Image 0471	
Mean [F]	97.56	96.58	
Std. Dev. [F]	3.67	1.17	
Center [F]	(159.5, 119.5) 97.29	(159.5, 111.5) 97.41	
Maximum [F]	(23, 38) 114.00	(65, 216) 104.18	
Minimum [F]	(8, 5) 84.05	(144, 216) 90.48	
Number of Pixels	76800	56616	
Percentage Area [%]		73.71875	
	Image 0472	Isotherm 1	Isotherm 2
Mean [F]	93.64	94.12	91.96
Std. Dev. [F]	1.18	0.8	0.66
Center [F]	(159.5, 119.5) 93.40	(159.5, 112.5) 93.48	(159.5, 166.0) 92.95
Maximum [F]	(1, 11) 97.29	(1, 11) 97.29	(317, 136) 92.80
Minimum [F]	(296, 237) 90.12	(318, 136) 92.81	(296, 237) 90.12
Number of Pixels	76800	59868	16932
Percentage Area [%]		77.953125	22.046875
	Image 0473	Isotherm 1	Isotherm 2
Mean [F]	93.46	94.51	92.28
Std. Dev. [F]	1.4	0.7	1
Center [F]	(159.5, 119.5) 93.24	(159.5, 105.5) 93.55	(159.5, 129.5) 93.08
Maximum [F]	(3, 1) 98.42	(3, 1) 98.42	(298, 29) 93.49
Minimum [F]	(271, 235) 89.40	(315, 30) 93.50	(271, 235) 89.40
Number of Pixels	76800	40582	36218
Percentage Area [%]		52.84114583	47.15885417
	Image 0474	Isotherm 1	Isotherm 2
Mean [F]	91.17	91.44	90.02
Std. Dev. [F]	0.76	0.54	0.36
Center [F]	(159.5, 119.5) 91.01	(159.5, 119.5) 91.01	(159.5, 177.5) 90.65
Maximum [F]	(107, 3) 93.13	(107, 3) 93.13	(304, 141) 90.49
Minimum [F]	(285, 240) 88.73	(113, 125) 90.50	(285, 240) 88.73
Number of Pixels	76800	62129	14671
Percentage Area [%]		80.89713542	19.10286458

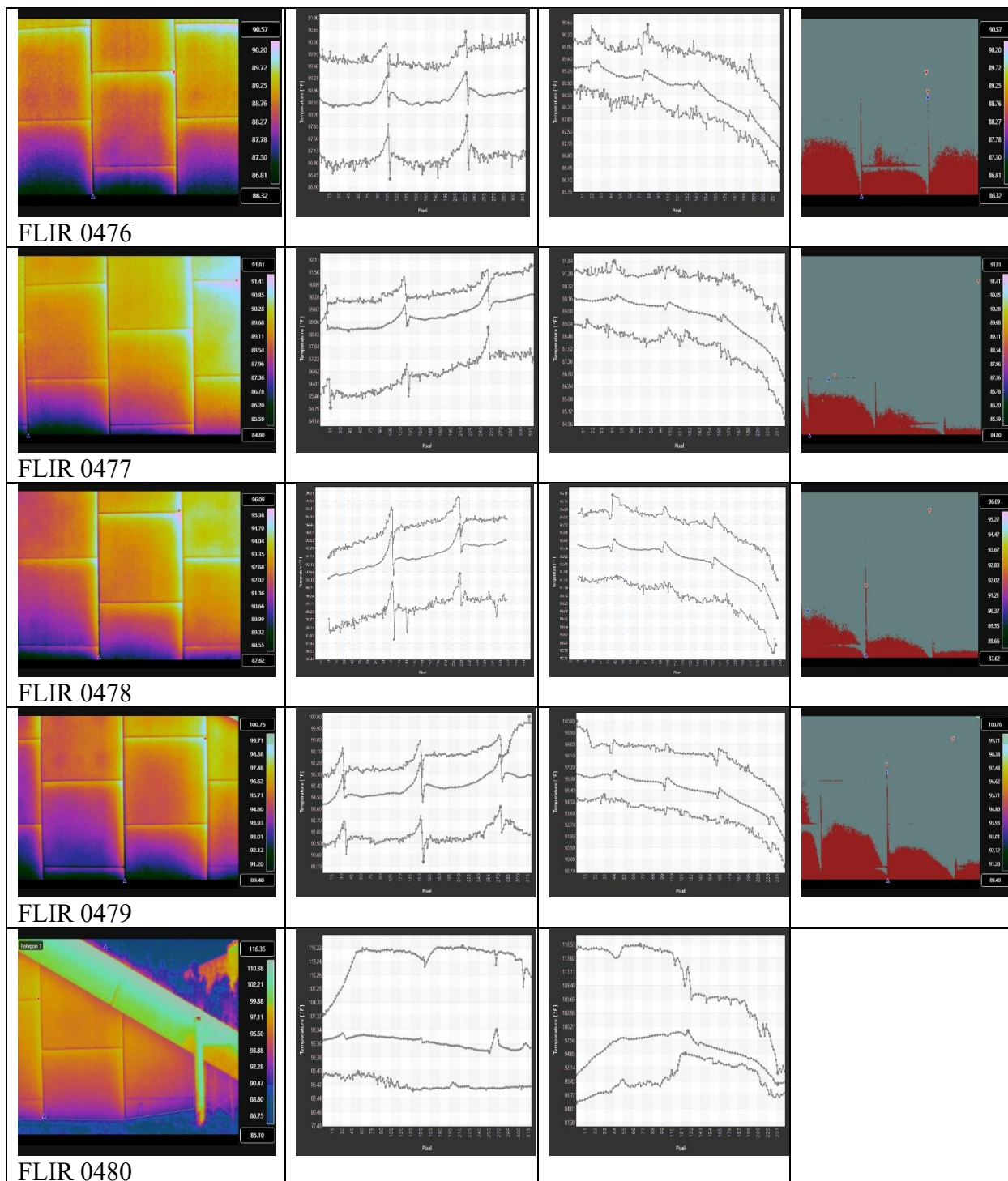


	Image 0475	Isotherm 1	Isotherm 2
Mean [F]	89.58	89.92	88.37
Std. Dev. [F]	0.81	0.51	0.43
Center [F]	(159.5, 119.5) 89.38	(159.5, 114.5) 89.43	(159.5, 181.0) 88.67
Maximum [F]	(30, 84) 91.60	(30, 84) 91.60	(119, 140) 88.95
Minimum [F]	(276, 240) 86.99	(182, 140) 88.96	(276, 240) 86.99
Number of Pixels	76800	60077	16723
Percentage Area [%]		78.22526042	21.77473958
	Image 0476	Isotherm 1	Isotherm 2
Mean [F]	88.67	88.95	87.56
Std. Dev. [F]	0.7	0.43	0.36
Center [F]	(159.5, 119.5) 88.67	(159.5, 119.5) 88.67	(159.5, 141.5) 88.51
Maximum [F]	(227, 87) 90.57	(227, 87) 90.57	(230, 112) 88.10
Minimum [F]	(110, 240) 86.32	(230, 112) 88.10	(110, 240) 86.32
Number of Pixels	76800	61406	15583
Percentage Area [%]		79.95572917	20.29036458
	Image 0477	Isotherm 1	Isotherm 2
Mean [F]	89.36	89.63	87.19
Std. Dev. [F]	1.06	0.74	0.65
Center [F]	(159.5, 119.5) 89.70	(159.5, 119.5) 89.70	(159.5, 160.5) 89.06
Maximum [F]	(316, 47) 91.81	(316, 47) 91.81	(60, 168) 88.00
Minimum [F]	(16, 240) 84.80	(50, 168) 88.01	(16, 240) 84.80
Number of Pixels	76800	68163	8637
Percentage Area [%]		88.75390625	11.24609375
	Image 0478	Isotherm 1	Isotherm 2
Mean [F]	92.58	92.85	90.35
Std. Dev. [F]	1.17	0.91	0.55
Center [F]	(159.5, 119.5) 92.60	(159.5, 119.5) 92.60	(159.5, 158.5) 92.48
Maximum [F]	(233, 42) 96.09	(233, 42) 96.09	(118, 145) 91.00
Minimum [F]	(118, 235) 87.62	(13, 173) 91.01	(118, 235) 87.62
Number of Pixels	76800	68617	8183
Percentage Area [%]		89.34505208	10.65494792
	Image 0479	Isotherm 1	Isotherm 2
Mean [F]	95.31	95.85	93.02
Std. Dev. [F]	1.47	1.01	0.77
Center [F]	(159.5, 119.5) 95.72	(159.5, 118.5) 95.73	(159.5, 152.5) 95.48
Maximum [F]	(273, 48) 99.03	(273, 48) 99.03	(154, 84) 94.00
Minimum [F]	(156, 240) 89.40	(154, 88) 94.01	(156, 240) 89.40
Number of Pixels	76513	61814	14699
Percentage Area [%]		80.78888555	19.21111445
	Image 0480	Polygon 1	
Mean [F]	94.82	95.29	
Std. Dev. [F]	1.99	1.49	
Center [F]	(159.5, 119.5) 96.20	(128.0, 124.5) 96.27	
Maximum [F]	(316, 21) 98.73	(31, 86) 98.72	

Minimum [F]	(128, 20) 90.26	(39, 217) 90.30	
Number of Pixels	46894	33701	
Percentage Area [%]		71.86633684	

### TI1-2 East to West Images and Temperature Plots – Crossgate





## T2-1 West to East Data – Old River Road

	Image 0538	Polygon 1	
Mean [F]	80.17	80.03	
Std. Dev. [F]	3.35	0.92	
Center [F]	(159.5, 119.5) 80.49	(160.0, 104.0) 80.70	
Maximum [F]	(74, 79) 86.46	(212, 133) 81.77	
Minimum [F]	(45, 1) 60.26	(184, 180) 75.52	
Number of Pixels	76800	24329	
Percentage Area [%]		31.67838542	
	Image 0540	Polygon 1	
Mean [F]	80.4	80.25	
Std. Dev. [F]	2.39	0.79	
Center [F]	(159.5, 119.5) 80.42	(159.5, 116.5) 80.24	
Maximum [F]	(5, 47) 86.23	(315, 44) 81.94	
Minimum [F]	(5, 1) 52.49	(163, 227) 75.64	
Number of Pixels	76800	62558	
Percentage Area [%]		81.45572917	
	Image 0544	Isotherm 1	Isotherm 2
Mean [F]	80.18	80.4	78.95
Std. Dev. [F]	0.7	0.48	0.38
Center [F]	(159.5, 119.5) 80.56	(159.5, 119.5) 80.56	(159.5, 119.5) 80.56
Maximum [F]	(214, 9) 81.93	(214, 9) 81.93	(135, 5) 79.40
Minimum [F]	(195, 221) 77.08	(135, 5) 79.40	(195, 221) 77.08
Number of Pixels	76800	65449	11540
Percentage Area [%]		85.22005208	15.02604167
	Image 0546	Isotherm 1	Isotherm 2
Mean [F]	80.02	80.1	78.31
Std. Dev. [F]	0.66	0.55	0.33
Center [F]	(159.5, 119.5) 80.21	(159.5, 119.5) 80.21	(159.5, 118.0) 80.29
Maximum [F]	(27, 41) 81.64	(27, 41) 81.64	(158, 5) 78.70
Minimum [F]	(13, 231) 76.80	(158, 5) 78.70	(13, 231) 76.80
Number of Pixels	76800	73210	3661
Percentage Area [%]		95.32552083	4.766927083
	Image 0548	Isotherm 1	Isotherm 2
Mean [F]	79.82	79.9	78.12
Std. Dev. [F]	0.64	0.53	0.32
Center [F]	(159.5, 119.5) 78.86	(159.5, 119.5) 78.86	(159.5, 118.0) 79.06
Maximum [F]	(47, 4) 81.41	(47, 4) 81.41	(97, 1) 78.49
Minimum [F]	(160, 232) 76.47	(1, 5) 78.50	(160, 232) 76.47
Number of Pixels	76800	73391	3409

Percentage Area [%]		95.56119792	4.438802083
	Image 0550	Isotherm 1	Isotherm 2
Mean [F]	80.09	80.17	78.68
Std. Dev. [F]	0.53	0.43	0.27
Center [F]	(159.5, 119.5) 80.32	(159.5, 119.5) 80.32	(159.5, 115.0) 80.28
Maximum [F]	(305, 240) 81.87	(305, 240) 81.87	(74, 1) 79.00
Minimum [F]	(188, 212) 77.33	(96, 3) 79.01	(188, 212) 77.33
Number of Pixels	76800	72991	3809
Percentage Area [%]		95.04036458	4.959635417
	Image 0552	Isotherm 1	Isotherm 2
Mean [F]	80.04	80.09	78.71
Std. Dev. [F]	0.45	0.37	0.24
Center [F]	(159.5, 119.5) 80.53	(159.5, 119.5) 80.53	(159.5, 121.0) 80.09
Maximum [F]	(28, 117) 81.31	(28, 117) 81.31	(101, 8) 79.00
Minimum [F]	(1, 218) 77.11	(102, 7) 79.01	(1, 218) 77.11
Number of Pixels	76800	74039	2761
Percentage Area [%]		96.40494792	3.595052083
	Image 0554	Isotherm 1	Isotherm 2
Mean [F]	79.85	79.92	78.59
Std. Dev. [F]	0.45	0.34	0.33
Center [F]	(159.5, 119.5) 80.05	(159.5, 119.5) 80.05	(160.5, 134.0) 80.05
Maximum [F]	(1, 240) 81.12	(1, 240) 81.12	(255, 81) 79.00
Minimum [F]	(270, 238) 77.43	(260, 4) 79.01	(270, 238) 77.43
Number of Pixels	76800	72744	4056
Percentage Area [%]		94.71875	5.28125
	Image 0556	Isotherm 1	Isotherm 2
Mean [F]	79.27	79.36	78.02
Std. Dev. [F]	0.49	0.36	0.39
Center [F]	(159.5, 119.5) 79.58	(159.5, 119.5) 79.58	(163.0, 117.0) 79.77
Maximum [F]	(50, 239) 81.07	(50, 239) 81.07	(193, 7) 78.49
Minimum [F]	(196, 233) 76.27	(193, 2) 78.50	(196, 234) 76.30
Number of Pixels	76800	71852	4947
Percentage Area [%]		93.55729167	6.44140625
	Image_0558	Isotherm 1	Isotherm 2
Mean [F]	78.93	79.01	77.53
Std. Dev. [F]	0.51	0.38	0.38
Center [F]	(159.5, 119.5) 79.42	(159.5, 119.5) 79.42	(160.5, 117.5) 79.37
Maximum [F]	(42, 240) 80.50	(42, 240) 80.50	(198, 6) 78.00

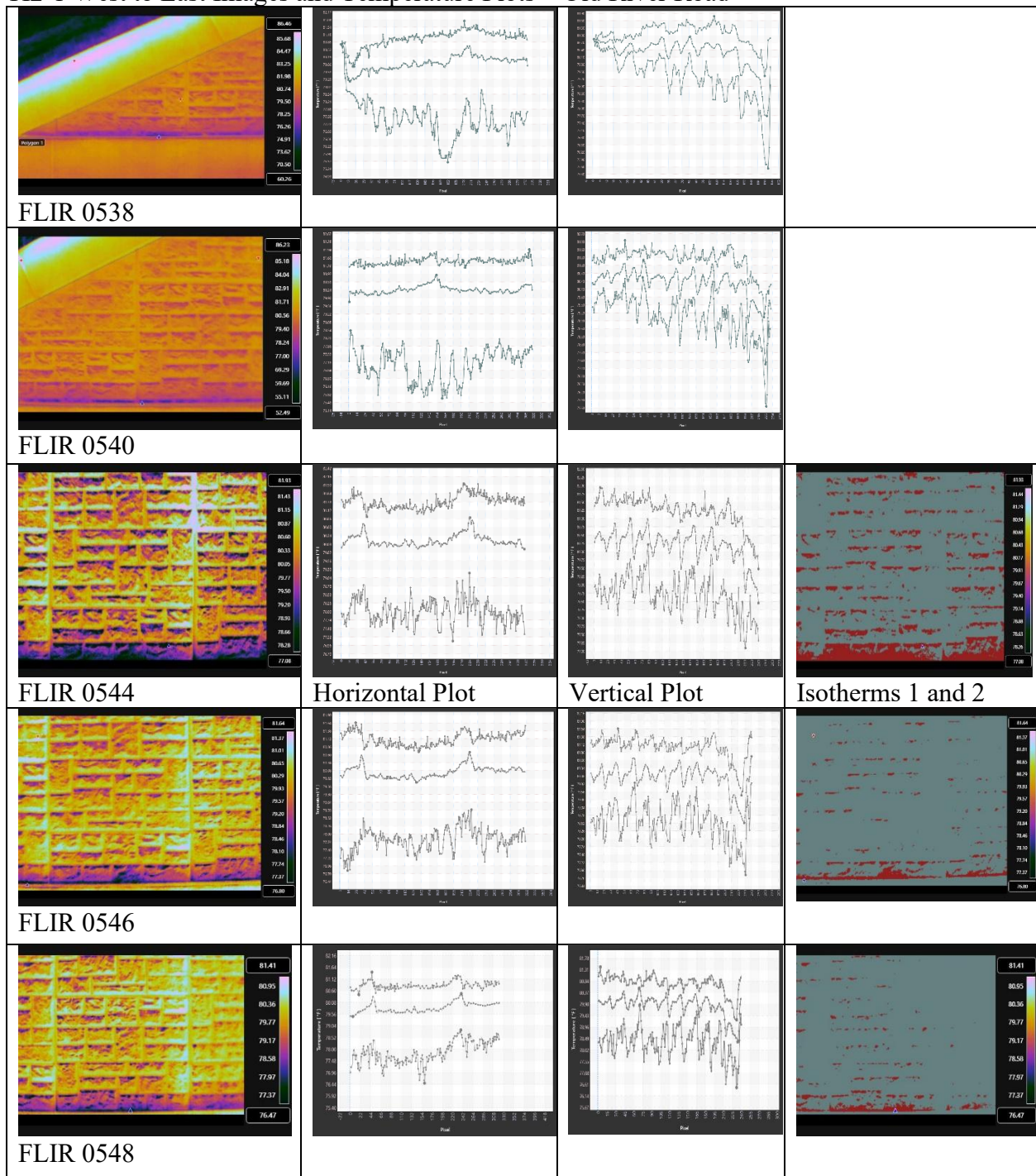
Minimum [F]	(320, 231) 76.08	(199, 25) 78.01	(320, 231) 76.08
Number of Pixels	76800	72582	4218
Percentage Area [%]		94.5078125	5.4921875
	Image 0560	Isotherm 1	Isotherm 2
Mean [F]	78.56	78.63	77.29
Std. Dev. [F]	0.48	0.38	0.35
Center [F]	(159.5, 119.5) 78.85	(159.5, 119.5) 78.85	(166.0, 119.5) 78.71
Maximum [F]	(13, 190) 80.14	(13, 190) 80.14	(17, 31) 77.69
Minimum [F]	(318, 240) 75.70	(140, 5) 77.70	(318, 240) 75.70
Number of Pixels	76800	72898	3902
Percentage Area [%]		94.91927083	5.080729167
	Image 0562	Isotherm 1	Isotherm 2
Mean [F]	78.29	78.41	76.94
Std. Dev. [F]	0.56	0.38	0.46
Center [F]	(159.5, 119.5) 78.53	(159.5, 119.5) 78.53	(159.5, 116.0) 78.58
Maximum [F]	(1, 231) 82.60	(1, 231) 82.60	(191, 9) 77.49
Minimum [F]	(189, 230) 74.81	(85, 32) 77.50	(189, 230) 74.81
Number of Pixels	76800	70447	6353
Percentage Area [%]		91.72786458	8.272135417
	Image 0564	Isotherm 1	Isotherm 2
Mean [F]	78.02	78.23	76.38
Std. Dev. [F]	0.94	0.76	0.5
Center [F]	(159.5, 119.5) 77.53	(159.5, 119.5) 77.53	(159.5, 119.5) 77.53
Maximum [F]	(238, 98) 80.76	(238, 98) 80.76	(254, 1) 77.00
Minimum [F]	(185, 236) 74.01	(180, 10) 77.01	(185, 236) 74.01
Number of Pixels	76800	68021	8779
Percentage Area [%]		88.56901042	11.43098958
	Image 0566	Isotherm 1	Isotherm 2
Mean [F]	77.69	77.83	75.83
Std. Dev. [F]	0.77	0.59	0.52
Center [F]	(159.5, 119.5) 77.69	(159.5, 119.5) 77.69	(165.0, 116.5) 77.77
Maximum [F]	(1, 191) 80.50	(1, 191) 80.50	(96, 2) 76.50
Minimum [F]	(97, 228) 73.28	(96, 7) 76.51	(97, 228) 73.28
Number of Pixels	76800	71551	5249
Percentage Area [%]		93.16536458	6.834635417
	Image 0568	Isotherm 1	Isotherm 2
Mean [F]	78.09	78.21	76.36
Std. Dev. [F]	0.65	0.44	0.53

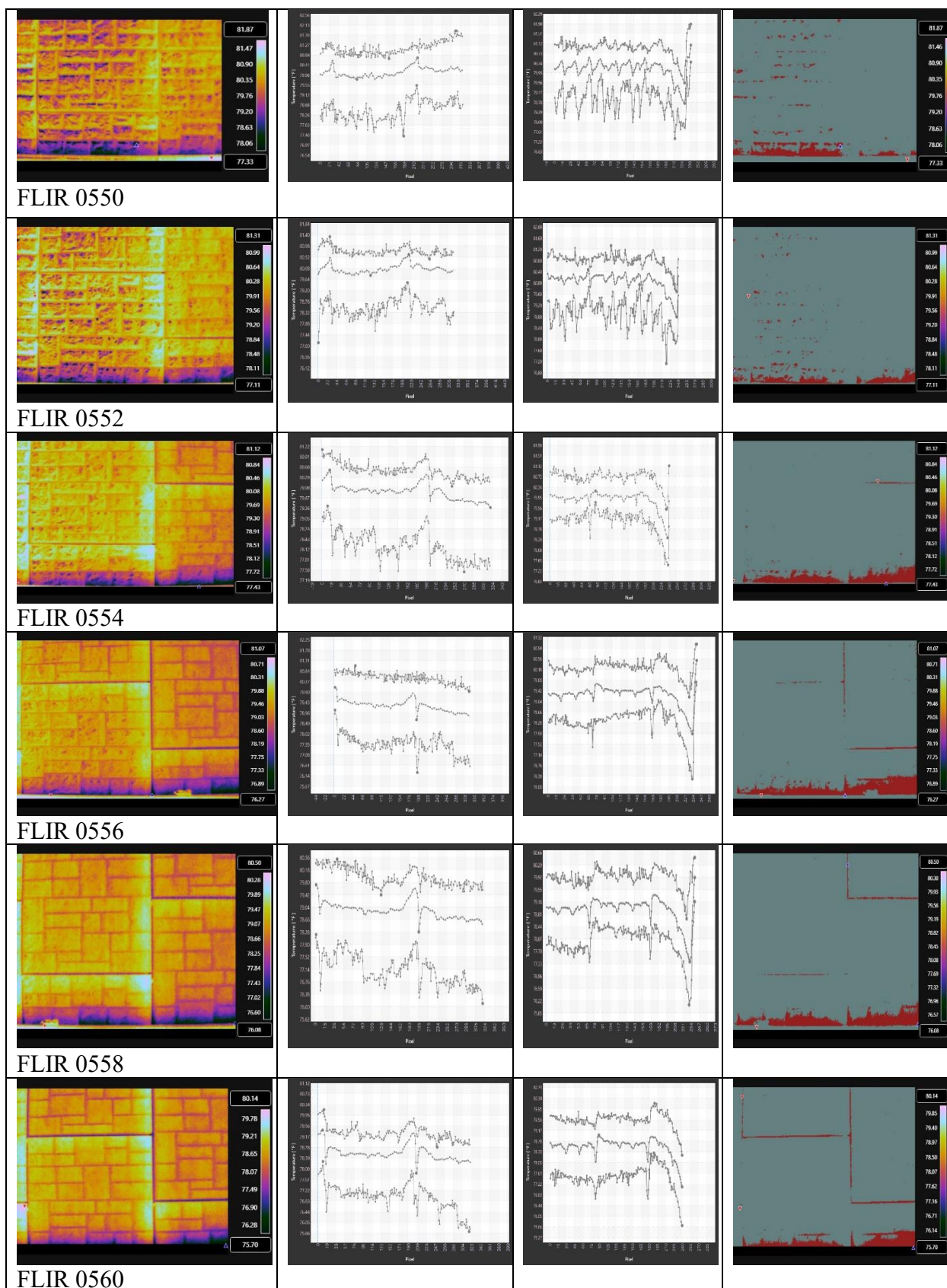
Center [F]	(159.5, 119.5) 78.80	(159.5, 119.5) 78.80	(159.5, 121.5) 78.78
Maximum [F]	(177, 34) 79.72	(177, 34) 79.72	(11, 7) 77.00
Minimum [F]	(6, 231) 73.86	(225, 10) 77.01	(6, 231) 73.86
Number of Pixels	76800	71493	5307
Percentage Area [%]		93.08984375	6.91015625
	Image 0570	Isotherm 1	Isotherm 2
Mean [F]	78.03	78.13	76.07
Std. Dev. [F]	0.67	0.5	0.48
Center [F]	(159.5, 119.5) 78.10	(159.5, 119.5) 78.10	(159.5, 119.5) 78.10
Maximum [F]	(293, 6) 79.85	(293, 6) 79.85	(151, 89) 76.70
Minimum [F]	(124, 240) 73.71	(36, 181) 76.71	(124, 240) 73.71
Number of Pixels	76800	73115	3685
Percentage Area [%]		95.20182292	4.798177083
	Image 0572	Isotherm 1	Isotherm 2
Mean [F]	78.13	78.29	76.21
Std. Dev. [F]	0.74	0.47	0.62
Center [F]	(159.5, 119.5) 78.06	(159.5, 119.5) 78.06	(159.5, 124.0) 78.12
Maximum [F]	(184, 1) 80.17	(184, 1) 80.17	(192, 36) 77.00
Minimum [F]	(193, 238) 73.76	(192, 42) 77.01	(193, 238) 73.76
Number of Pixels	76800	70722	6078
Percentage Area [%]		92.0859375	7.9140625
	Image 0574	Isotherm 1	Isotherm 2
Mean [F]	78.13	78.27	75.69
Std. Dev. [F]	0.79	0.53	0.58
Center [F]	(159.5, 119.5) 78.55	(159.5, 119.5) 78.55	(159.5, 162.5) 78.67
Maximum [F]	(179, 18) 80.05	(179, 18) 80.05	(7, 180) 76.50
Minimum [F]	(186, 238) 73.36	(46, 177) 76.51	(186, 238) 73.36
Number of Pixels	76800	72696	4104
Percentage Area [%]		94.65625	5.34375
	Image 0576	Isotherm 1	Isotherm 2
Mean [F]	78.5	78.61	75.72
Std. Dev. [F]	0.84	0.64	0.63
Center [F]	(159.5, 119.5) 78.80	(159.5, 119.5) 78.80	(159.5, 161.5) 78.68
Maximum [F]	(239, 15) 80.48	(239, 15) 80.48	(30, 220) 76.50
Minimum [F]	(6, 240) 73.56	(29, 202) 76.51	(6, 240) 73.56
Number of Pixels	76800	73952	2848
Percentage Area [%]		96.29166667	3.708333333
	Image 0578	Isotherm 1	Isotherm 2

Mean [F]	78.58	78.73	75.6
Std. Dev. [F]	1	0.74	0.79
Center [F]	(159.5, 119.5) 79.10	(159.5, 119.5) 79.10	(159.5, 125.0) 79.32
Maximum [F]	(184, 90) 80.53	(184, 90) 80.53	(55, 203) 76.59
Minimum [F]	(131, 229) 73.14	(127, 209) 76.51	(131, 229) 73.14
Number of Pixels	76800	73285	3862
Percentage Area [%]		95.42317708	5.028645833
	Image 0580	Isotherm 1	Isotherm 2
Mean [F]	79.04	79.19	75.75
Std. Dev. [F]	1.06	0.8	0.81
Center [F]	(159.5, 119.5) 79.45	(159.5, 119.5) 79.45	(159.5, 164.5) 79.44
Maximum [F]	(316, 7) 81.33	(316, 7) 81.33	(23, 194) 76.80
Minimum [F]	(4, 233) 73.45	(40, 210) 76.80	(4, 233) 73.45
Number of Pixels	76800	73526	3274
Percentage Area [%]		95.73697917	4.263020833
	Image 0582	Polygon 1	
Mean [F]	80.48	80.06	
Std. Dev. [F]	2.97	1.12	
Center [F]	(159.5, 119.5) 80.53	(158.5, 119.0) 80.68	
Maximum [F]	(251, 15) 89.50	(313, 111) 81.99	
Minimum [F]	(295, 1) 55.33	(2, 238) 74.18	
Number of Pixels	76800	61770	
Percentage Area [%]		80.4296875	
	Image 0584	Polygon 1	
Mean [F]	79.84	80.19	
Std. Dev. [F]	5.95	1.18	
Center [F]	(159.5, 119.5) 81.33	(159.5, 128.0) 80.87	
Maximum [F]	(75, 9) 91.09	(96, 83) 82.62	
Minimum [F]	(120, 1) 55.24	(70, 211) 74.55	
Number of Pixels	76800	31840	
Percentage Area [%]		41.45833333	

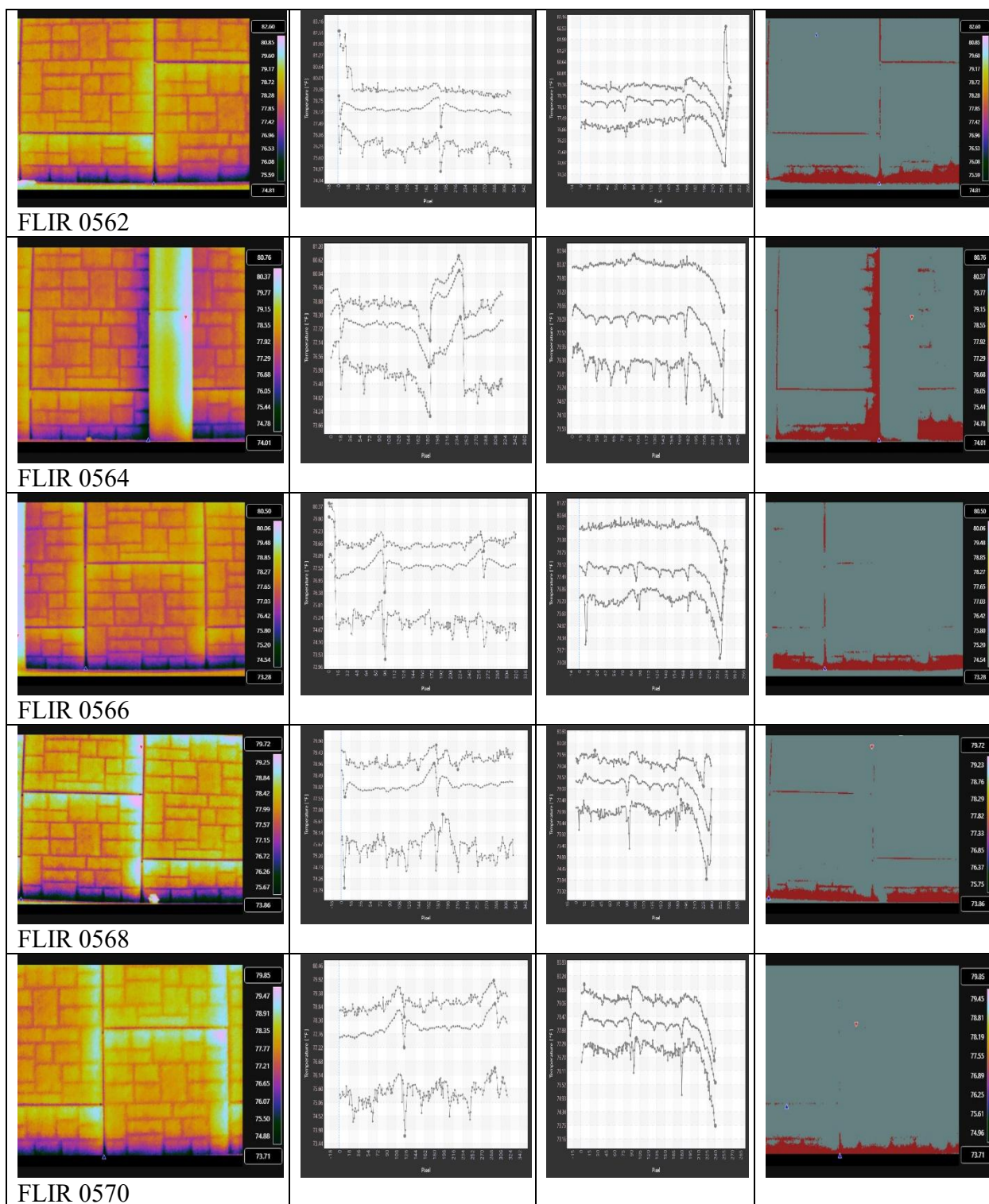


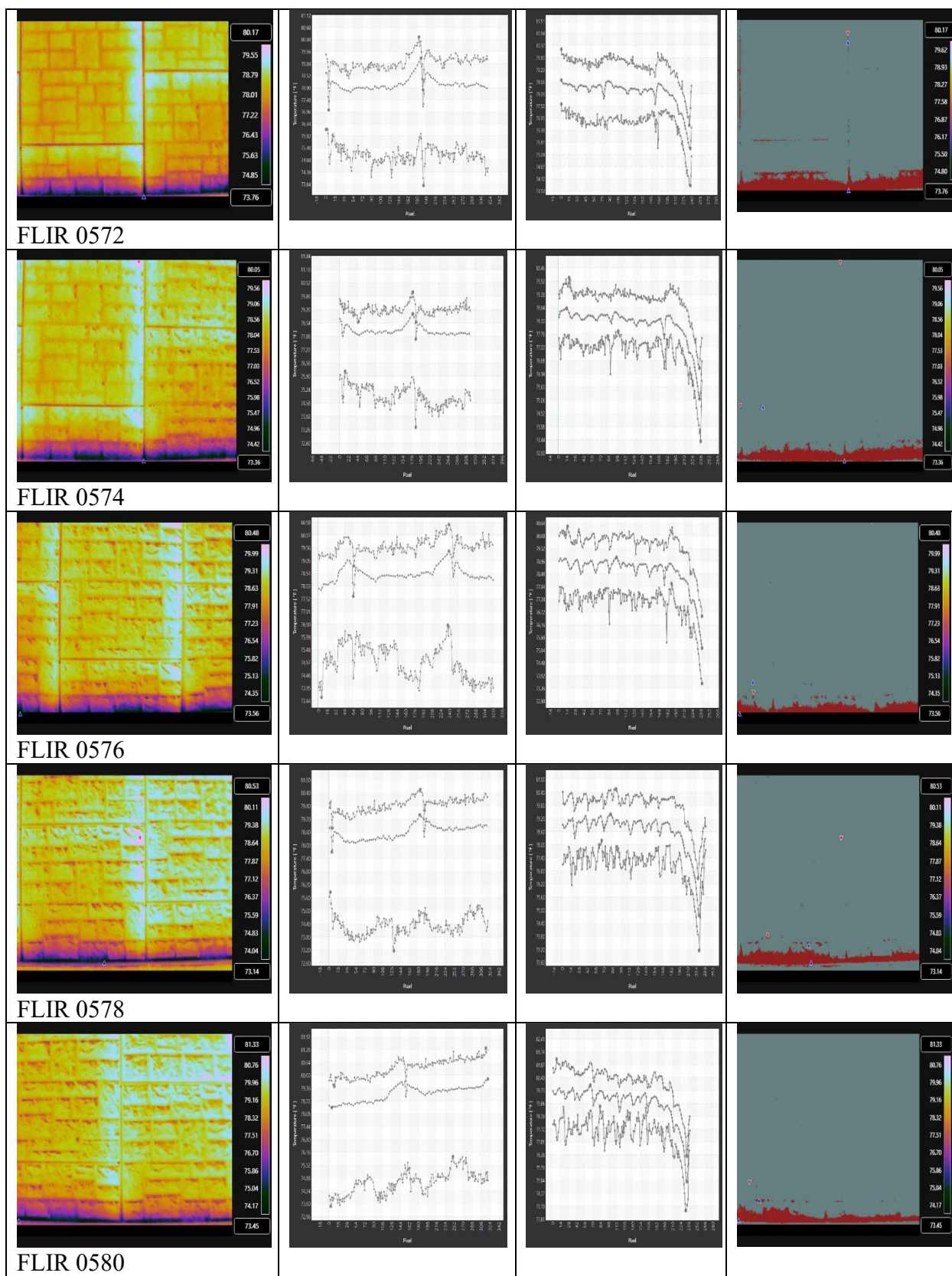
# TI2-1 West to East Images and Temperature Plots – Old River Road

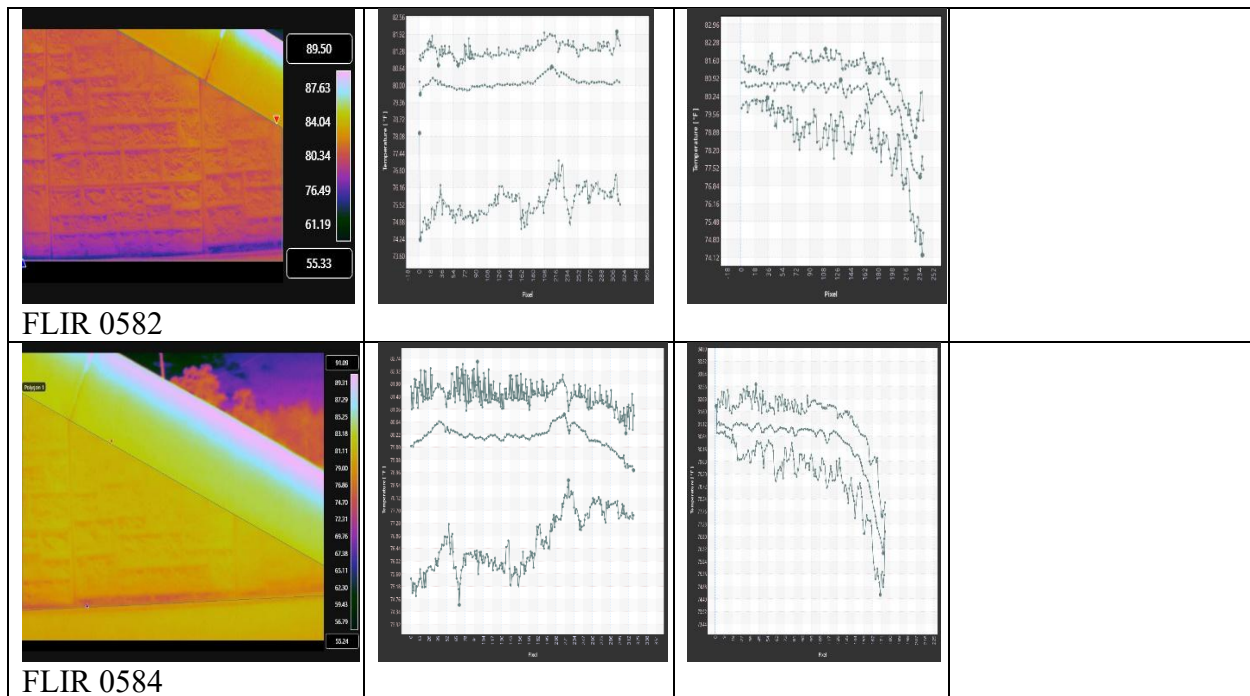












#### T2-2 East to West Data – Old River Road

	Image 0682	Polygon 1	
Mean [F]	71.79	77.87	
Std. Dev. [F]	8.58	0.96	
Center [F]	(159.5, 119.5) 68.83	(225.0, 190.5) 79.35	
Maximum [F]	(1, 230) 83.57	(259, 176) 79.96	
Minimum [F]	(135, 1) 47.83	(230, 235) 75.12	
Number of Pixels	76800	8931	
Percentage Area [%]		11.62890625	
	Image 0684	Polygon 1	
Mean [F]	78.43	78.18	
Std. Dev. [F]	1.83	0.74	
Center [F]	(159.5, 119.5) 78.66	(159.5, 119.5) 78.66	
Maximum [F]	(52, 24) 84.30	(189, 28) 80.07	
Minimum [F]	(5, 1) 50.22	(50, 230) 74.32	
Number of Pixels	76800	61345	
Percentage Area [%]		79.87630208	
	Image 0686	Isotherm 1	Isotherm 2
Mean [F]	77.98	78.1	76.61
Std. Dev. [F]	0.68	0.55	0.36

Center [F]	(159.5, 119.5) 77.94	(159.5, 119.5) 77.94	(159.5, 119.5) 77.94
Maximum [F]	(169, 58) 79.96	(169, 58) 79.96	(225, 10) 76.99
Minimum [F]	(12, 237) 74.28	(164, 7) 77.00	(12, 237) 74.28
Number of Pixels	76800	70345	6455
Percentage Area [%]		91.59505208	8.404947917
	Image 0688	Isotherm 1	Isotherm 2
Mean [F]	77.97	78.09	76.64
Std. Dev. [F]	0.67	0.55	0.32
Center [F]	(159.5, 119.5) 77.99	(159.5, 119.5) 77.99	(159.5, 119.5) 77.99
Maximum [F]	(13, 12) 80.18	(13, 12) 80.18	(254, 4) 76.99
Minimum [F]	(29, 240) 74.91	(258, 1) 77.00	(29, 240) 74.91
Number of Pixels	76800	70522	6278
Percentage Area [%]		91.82552083	8.174479167
	Image 0690	Isotherm 1	Isotherm 2
Mean [F]	78.25	78.33	77.02
Std. Dev. [F]	0.54	0.45	0.26
Center [F]	(159.5, 119.5) 78.20	(159.5, 119.5) 78.20	(161.0, 119.5) 77.87
Maximum [F]	(167, 79) 79.77	(167, 79) 79.77	(24, 1) 77.30
Minimum [F]	(102, 226) 75.54	(117, 2) 77.31	(102, 226) 75.54
Number of Pixels	76800	72176	4624
Percentage Area [%]		93.97916667	6.020833333
	Image 0692	Isotherm 1	Isotherm 2
Mean [F]	78.47	78.57	77.75
Std. Dev. [F]	0.37	0.27	0.21
Center [F]	(159.5, 119.5) 78.26	(159.5, 119.5) 78.26	(159.5, 119.5) 78.26
Maximum [F]	(194, 13) 79.51	(194, 13) 79.51	(184, 2) 78.00
Minimum [F]	(27, 217) 76.53	(6, 2) 78.01	(27, 217) 76.53
Number of Pixels	76800	67236	9564
Percentage Area [%]		87.546875	12.453125
	Image 0694	Isotherm 1	Isotherm 2
Mean [F]	78.49	78.57	77.69
Std. Dev. [F]	0.43	0.35	0.19
Center [F]	(159.5, 119.5) 78.49	(159.5, 119.5) 78.49	(159.5, 118.0) 78.44
Maximum [F]	(173, 237) 80.36	(173, 237) 80.36	(4, 1) 77.89
Minimum [F]	(125, 213) 76.50	(1, 1) 77.90	(125, 213) 76.50
Number of Pixels	76800	69811	6989
Percentage Area [%]		90.89973958	9.100260417
	Image 0696	Isotherm 1	Isotherm 2
Mean [F]	77.95	77.97	76.83

Std. Dev. [F]	0.34	0.3	0.24
Center [F]	(159.5, 119.5) 78.40	(159.5, 119.5) 78.40	(160.0, 120.0) 78.57
Maximum [F]	(164, 88) 78.99	(164, 88) 78.99	(35, 22) 77.10
Minimum [F]	(231, 235) 75.78	(36, 23) 77.11	(231, 235) 75.78
Number of Pixels	76800	75093	1707
Percentage Area [%]		97.77734375	2.22265625
	Image 0698	Isotherm 1	Isotherm 2
Mean [F]	77.62	77.66	76.7
Std. Dev. [F]	0.34	0.28	0.26
Center [F]	(159.5, 119.5) 77.68	(159.5, 119.5) 77.68	(162.0, 120.0) 77.59
Maximum [F]	(1, 172) 78.84	(1, 172) 78.84	(285, 11) 76.99
Minimum [F]	(304, 240) 75.26	(247, 8) 77.00	(304, 240) 75.26
Number of Pixels	76800	73598	3202
Percentage Area [%]		95.83072917	4.169270833
	Image 0700	Isotherm 1	Isotherm 2
Mean [F]	77.19	77.2	76.4
Std. Dev. [F]	0.27	0.25	0.18
Center [F]	(159.5, 119.5) 77.43	(159.5, 119.5) 77.43	(166.0, 119.5) 77.65
Maximum [F]	(184, 202) 78.35	(184, 202) 78.35	(74, 5) 76.60
Minimum [F]	(316, 240) 75.72	(90, 1) 76.61	(316, 240) 75.72
Number of Pixels	76800	75557	1243
Percentage Area [%]		98.38151042	1.618489583
	Image 0702	Isotherm 1	Isotherm 2
Mean [F]	77.07	77.14	75.94
Std. Dev. [F]	0.41	0.31	0.26
Center [F]	(159.5, 119.5) 77.25	(159.5, 119.5) 77.25	(162.0, 124.0) 77.30
Maximum [F]	(16, 235) 78.60	(16, 235) 78.60	(320, 203) 76.29
Minimum [F]	(196, 231) 74.99	(319, 199) 76.30	(196, 231) 74.99
Number of Pixels	76800	72893	3907
Percentage Area [%]		94.91276042	5.087239583
	Image 0704	Isotherm 1	Isotherm 2
Mean [F]	76.86	76.88	75.87
Std. Dev. [F]	0.31	0.28	0.2
Center [F]	(159.5, 119.5) 76.98	(159.5, 119.5) 76.98	(165.5, 121.5) 77.10
Maximum [F]	(183, 95) 77.96	(183, 95) 77.96	(15, 6) 76.10
Minimum [F]	(313, 240) 75.05	(73, 14) 76.11	(313, 240) 75.05
Number of Pixels	76800	75609	1191
Percentage Area [%]		98.44921875	1.55078125
	Image 0706	Isotherm 1	Isotherm 2



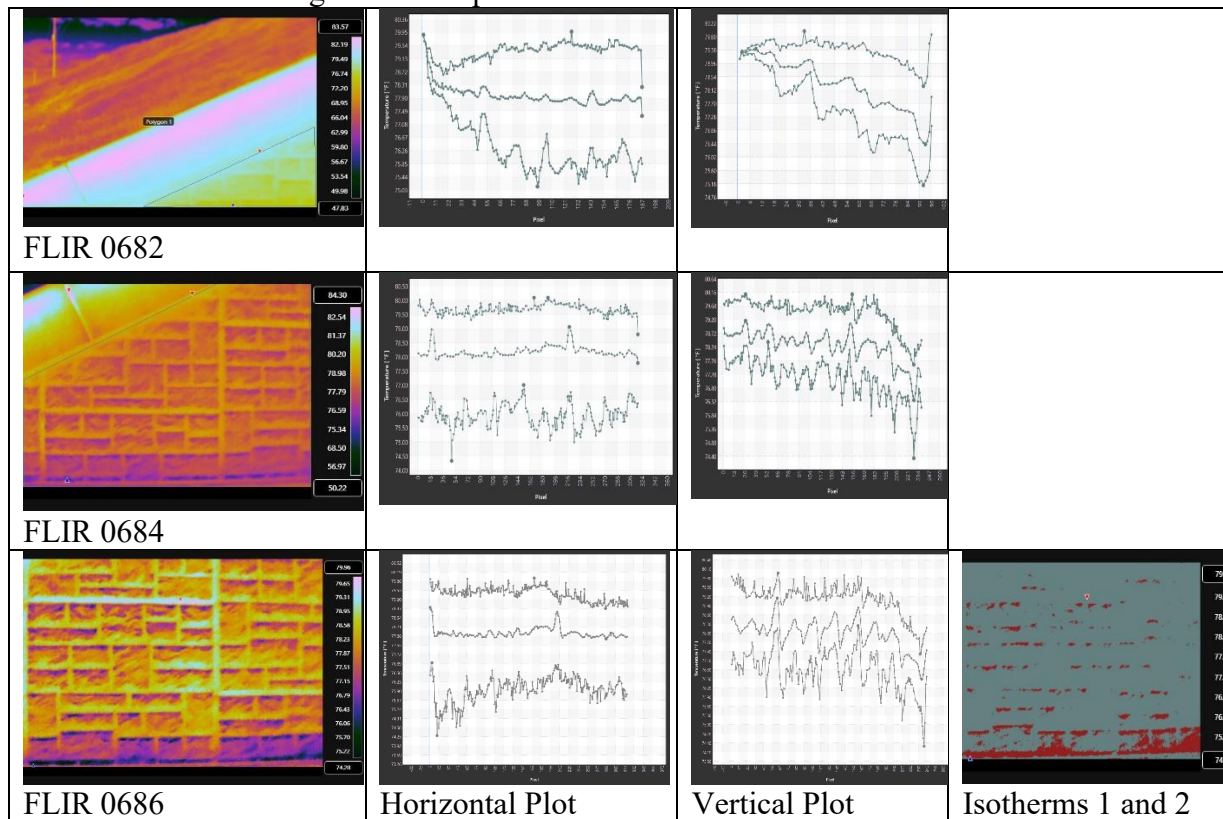
Mean [F]	76.78	76.95	75.61
Std. Dev. [F]	0.8	0.69	0.39
Center [F]	(159.5, 119.5) 76.37	(159.5, 119.5) 76.37	(159.5, 117.5) 76.13
Maximum [F]	(247, 150) 78.99	(247, 150) 78.99	(18, 5) 76.10
Minimum [F]	(192, 233) 73.92	(167, 2) 76.11	(192, 233) 73.92
Number of Pixels	76800	66905	9895
Percentage Area [%]		87.11588542	12.88411458
	Image 0708	Isotherm 1	Isotherm 2
Mean [F]	76.61	76.71	75.35
Std. Dev. [F]	0.48	0.33	0.32
Center [F]	(159.5, 119.5) 76.65	(159.5, 119.5) 76.65	(163.5, 122.0) 76.70
Maximum [F]	(279, 2) 77.80	(279, 2) 77.80	(32, 23) 75.80
Minimum [F]	(298, 236) 74.04	(23, 26) 75.81	(298, 236) 74.04
Number of Pixels	75980	70668	5312
Percentage Area [%]		93.0086865	6.991313504
	Image 0710	Isotherm 1	Isotherm 2
Mean [F]	76.6	76.66	75.13
Std. Dev. [F]	0.46	0.35	0.28
Center [F]	(159.5, 119.5) 76.82	(159.5, 119.5) 76.82	(159.5, 209.0) 76.67
Maximum [F]	(197, 189) 78.03	(197, 189) 78.03	(21, 225) 75.49
Minimum [F]	(16, 240) 73.77	(298, 224) 75.50	(16, 240) 73.77
Number of Pixels	76800	73771	3029
Percentage Area [%]		96.05598958	3.944010417
	Image 0712	Isotherm 1	Isotherm 2
Mean [F]	76.6	76.66	75.11
Std. Dev. [F]	0.47	0.35	0.28
Center [F]	(159.5, 119.5) 76.75	(159.5, 119.5) 76.75	(159.5, 158.5) 76.87
Maximum [F]	(194, 83) 77.90	(194, 83) 77.90	(320, 220) 75.49
Minimum [F]	(15, 236) 73.82	(305, 218) 75.50	(15, 236) 73.82
Number of Pixels	76800	73517	3283
Percentage Area [%]		95.72526042	4.274739583
	Image 0714	Isotherm 1	Isotherm 2
Mean [F]	76.43	76.49	74.91
Std. Dev. [F]	0.49	0.38	0.27
Center [F]	(159.5, 119.5) 76.69	(159.5, 119.5) 76.69	(159.5, 226.0) 75.20
Maximum [F]	(204, 174) 77.67	(202, 173) 77.66	(104, 217) 75.30
Minimum [F]	(150, 235) 73.99	(106, 216) 75.31	(150, 235) 73.99
Number of Pixels	76800	73437	3362
Percentage Area [%]		95.62109375	4.377604167

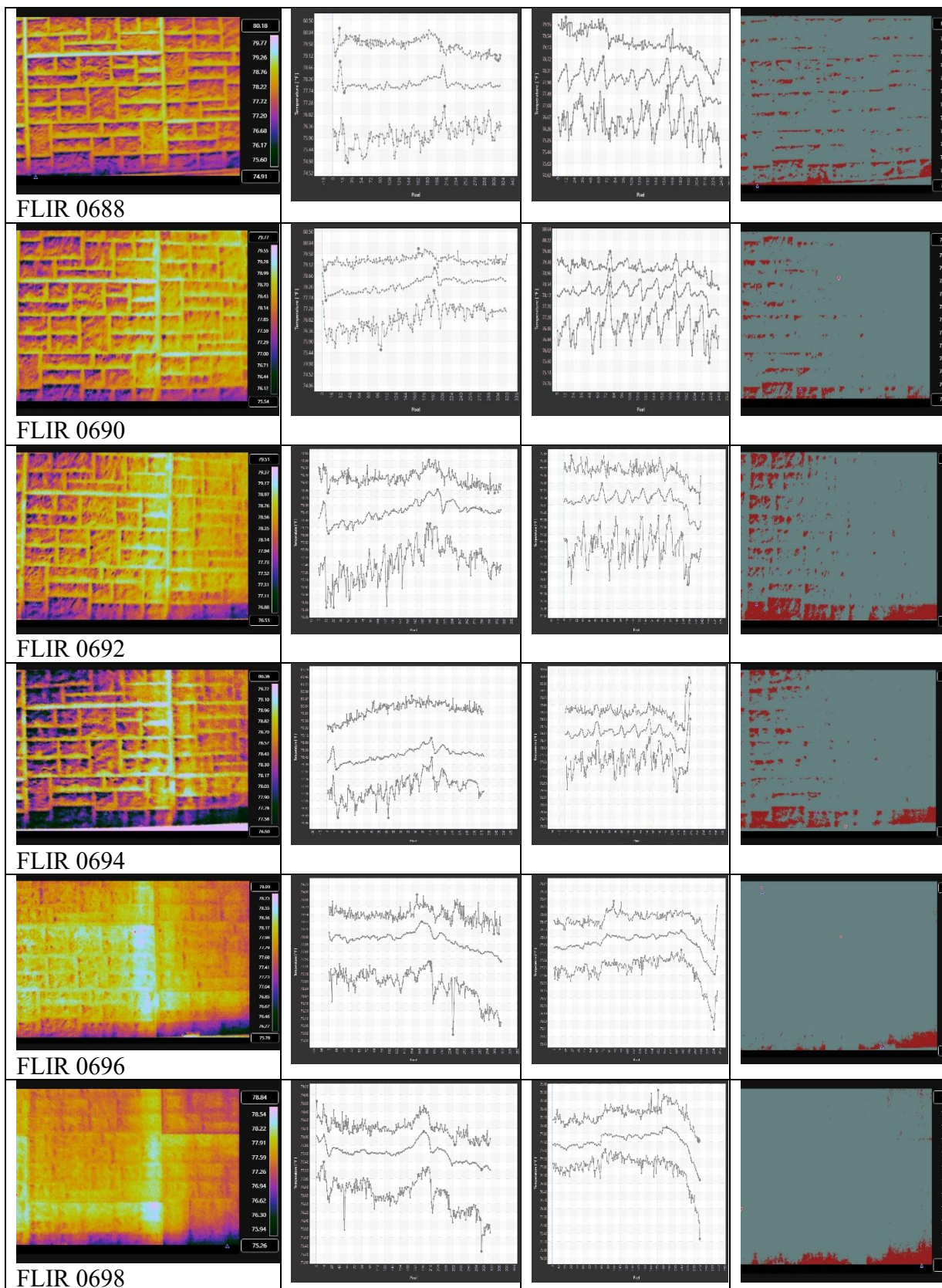


	Image 0716	Isotherm 1	Isotherm 2
Mean [F]	76.33	76.4	74.64
Std. Dev. [F]	0.52	0.41	0.27
Center [F]	(159.5, 119.5) 76.55	(159.5, 119.5) 76.55	(159.5, 220.0) 75.52
Maximum [F]	(195, 68) 77.89	(195, 68) 77.89	(317, 213) 75.00
Minimum [F]	(11, 232) 73.47	(299, 213) 75.01	(11, 232) 73.47
Number of Pixels	76800	74105	2695
Percentage Area [%]		96.49088542	3.509114583
	Image 0718	Isotherm 1	Isotherm 2
Mean [F]	76.07	76.19	74.4
Std. Dev. [F]	0.6	0.39	0.35
Center [F]	(159.5, 119.5) 76.05	(159.5, 119.5) 76.05	(159.5, 215.5) 74.72
Maximum [F]	(13, 16) 77.31	(13, 16) 77.31	(315, 204) 74.90
Minimum [F]	(17, 224) 73.08	(51, 204) 74.91	(17, 224) 73.08
Number of Pixels	76800	71462	5338
Percentage Area [%]		93.04947917	6.950520833
	Image 0720	Isotherm 1	Isotherm 2
Mean [F]	76.09	76.2	74.21
Std. Dev. [F]	0.63	0.43	0.35
Center [F]	(159.5, 119.5) 75.95	(159.5, 119.5) 75.95	(159.5, 221.0) 74.33
Maximum [F]	(15, 4) 77.56	(15, 4) 77.56	(312, 211) 74.70
Minimum [F]	(160, 237) 73.02	(306, 204) 74.71	(160, 237) 73.02
Number of Pixels	76800	72334	4466
Percentage Area [%]		94.18489583	5.815104167
	Image 0722	Isotherm 1	Isotherm 2
Mean [F]	76.1	76.18	74.37
Std. Dev. [F]	0.6	0.47	0.3
Center [F]	(159.5, 119.5) 76.40	(159.5, 119.5) 76.40	(159.5, 139.5) 76.25
Maximum [F]	(268, 3) 77.97	(268, 3) 77.97	(229, 157) 74.79
Minimum [F]	(221, 238) 73.26	(190, 44) 74.80	(221, 238) 73.26
Number of Pixels	76800	73308	3492
Percentage Area [%]		95.453125	4.546875
	Image 0724	Isotherm 1	Isotherm 2
Mean [F]	76.52	76.62	74.81
Std. Dev. [F]	0.72	0.59	0.36
Center [F]	(159.5, 119.5) 75.86	(159.5, 119.5) 75.86	(159.5, 120.5) 75.42
Maximum [F]	(289, 5) 79.17	(289, 5) 79.17	(38, 16) 75.30
Minimum [F]	(60, 239) 73.44	(38, 15) 75.31	(60, 239) 73.44
Number of Pixels	76800	72424	4376

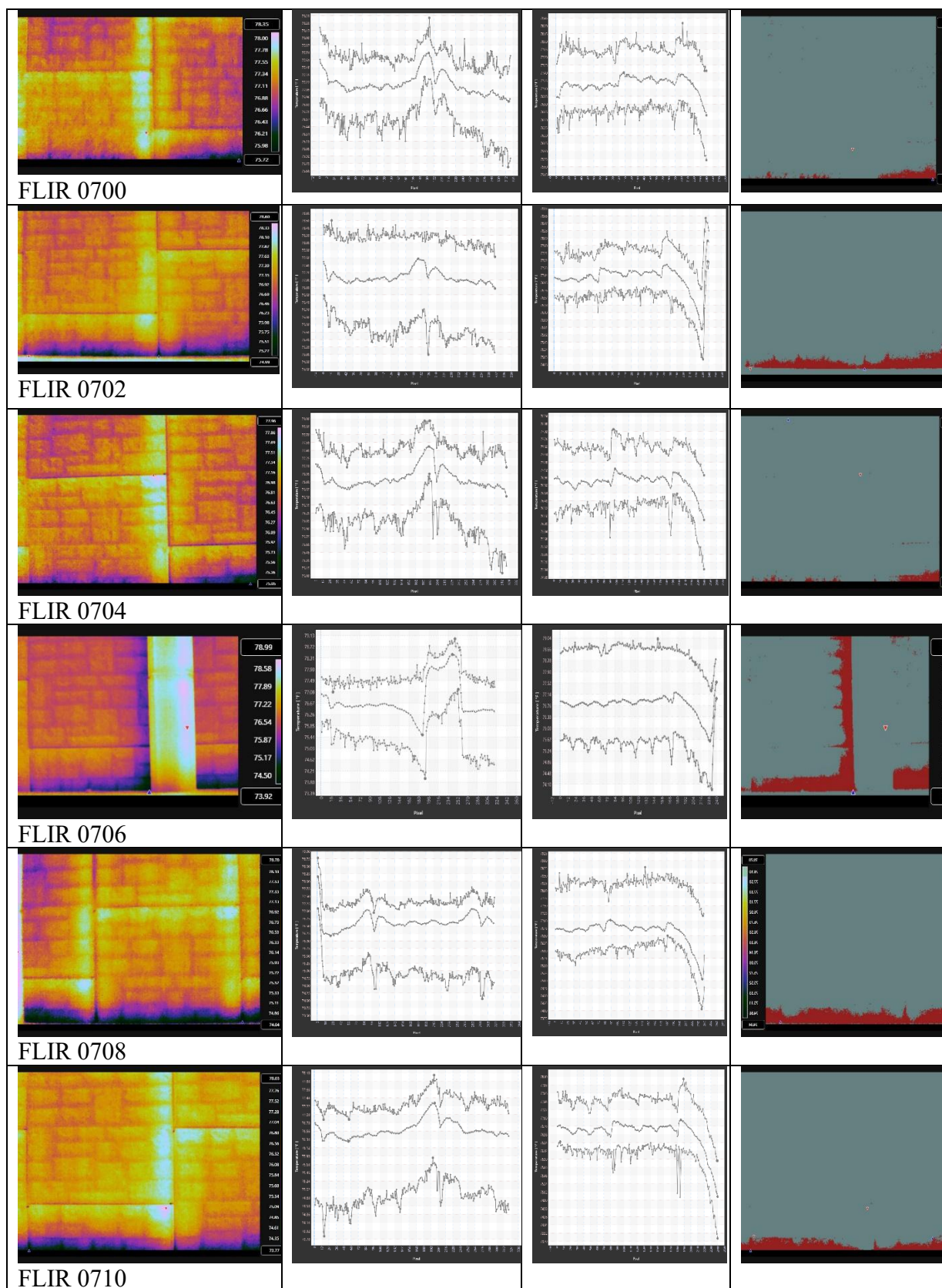
Percentage Area [%]		94.30208333	5.697916667
	Image 0726	Polygon 1	
Mean [F]	77.1	77.44	
Std. Dev. [F]	5.02	0.94	
Center [F]	(159.5, 119.5) 77.71	(158.0, 120.0) 77.64	
Maximum [F]	(276, 53) 86.19	(315, 130) 80.65	
Minimum [F]	(222, 1) 47.16	(262, 233) 73.35	
Number of Pixels	76800	59325	
Percentage Area [%]		77.24609375	
	Image 0728	Polygon 1	
Mean [F]	74.81	77.83	
Std. Dev. [F]	7.83	1.17	
Center [F]	(159.5, 119.5) 82.06	(116.0, 130.5) 79.61	
Maximum [F]	(1, 1) 86.71	(233, 194) 80.95	
Minimum [F]	(246, 1) 53.85	(9, 196) 73.40	
Number of Pixels	76800	16615	
Percentage Area [%]		21.63411458	

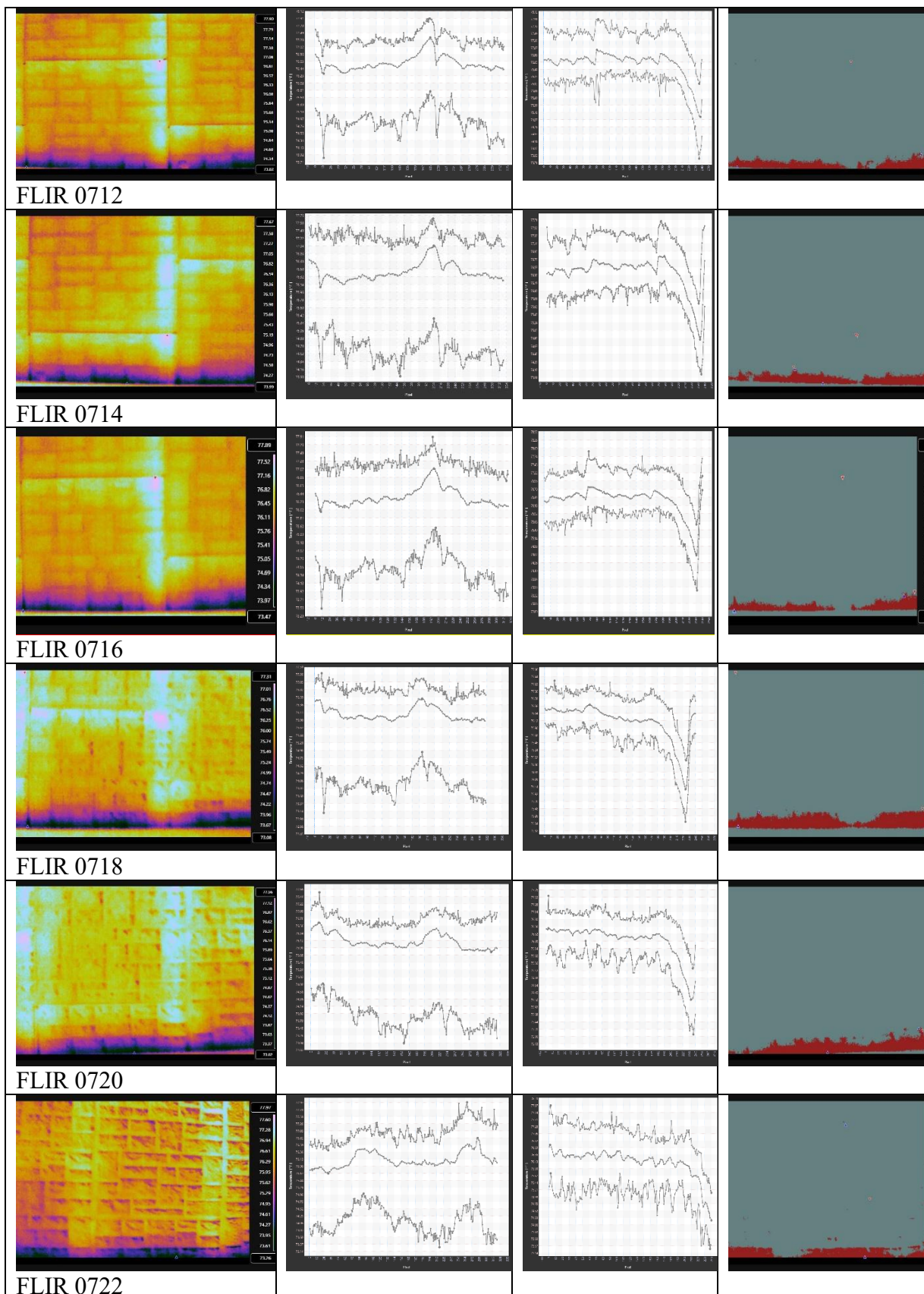
### TI2-2 East to West Images and Temperature Plots – Old River Road

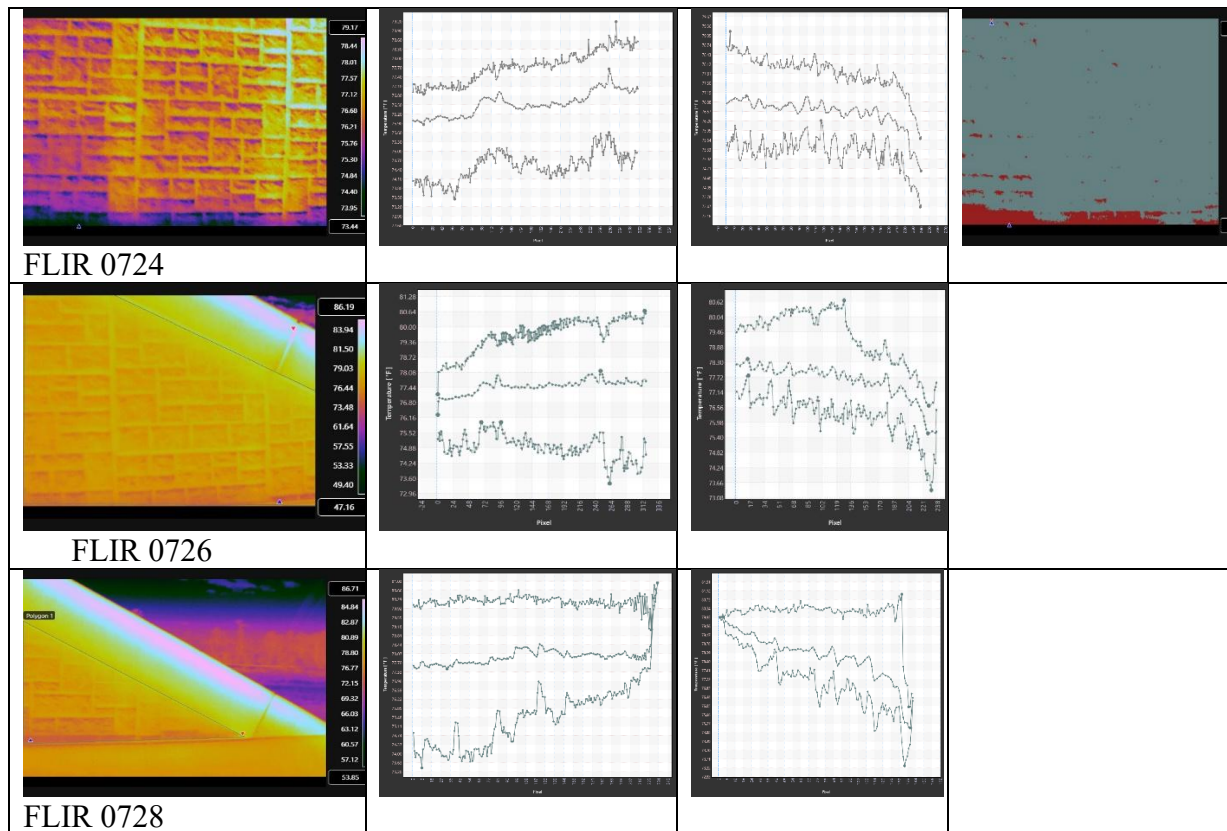












### T3-1West to East Data – King George

	Image 0827	Polygon 1
Mean [F]	67.87	67.88
Std. Dev. [F]	1.33	1.32
Center [F]	(159.5, 119.5) 68.05	(159.5, 120.0) 68.05
Maximum [F]	(261, 137) 74.72	(261, 137) 74.72
Minimum [F]	(229, 235) 64.57	(229, 235) 64.57
Number of Pixels	76800	74931
Percentage Area [%]		97.56640625
	Image 0828	Polygon 1
Mean [F]	66.94	66.93
Std. Dev. [F]	0.75	0.72
Center [F]	(159.5, 119.5) 68.12	(160.0, 116.0) 68.47
Maximum [F]	(314, 38) 69.99	(314, 38) 69.99
Minimum [F]	(41, 3) 64.18	(41, 3) 64.18
Number of Pixels	76800	72982
Percentage Area [%]		95.02864583
	Image 0829	Polygon 1
Mean [F]	65.71	65.71
Std. Dev. [F]	0.7	0.69
Center [F]	(159.5, 119.5) 65.71	(159.0, 118.5) 65.68

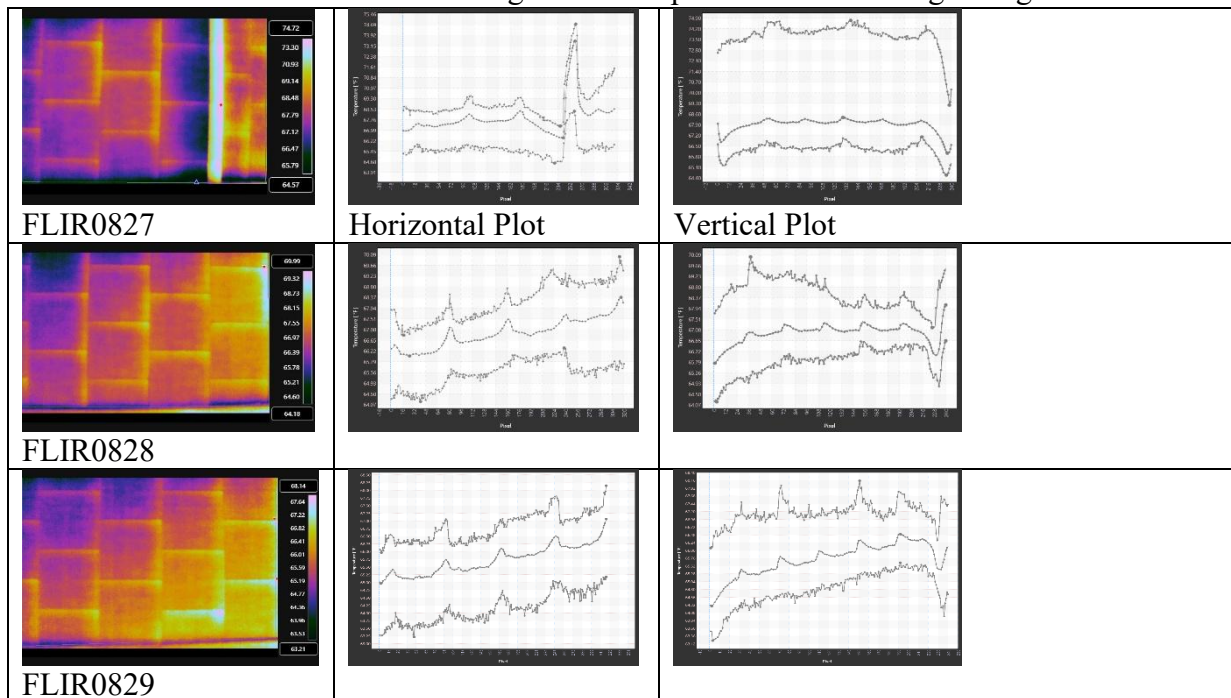
Maximum [F]	(320, 151) 68.14	(317, 71) 67.91
Minimum [F]	(49, 3) 63.21	(49, 3) 63.21
Number of Pixels	76800	73069
Percentage Area [%]		95.14192708
	Image 0830	Polygon 1
Mean [F]	65.27	65.3
Std. Dev. [F]	0.56	0.55
Center [F]	(159.5, 119.5) 65.53	(159.0, 111.5) 65.33
Maximum [F]	(246, 169) 67.09	(246, 169) 67.09
Minimum [F]	(3, 1) 63.55	(2, 3) 63.57
Number of Pixels	76800	67576
Percentage Area [%]		87.98958333
	Image 0831	Polygon 1
Mean [F]	64.57	64.6
Std. Dev. [F]	0.45	0.42
Center [F]	(159.5, 119.5) 64.67	(159.0, 116.5) 64.70
Maximum [F]	(246, 179) 65.96	(246, 179) 65.96
Minimum [F]	(142, 3) 62.60	(122, 5) 62.91
Number of Pixels	76800	71735
Percentage Area [%]		93.40494792
	Image 0832	Polygon 1
Mean [F]	64.23	64.21
Std. Dev. [F]	0.51	0.43
Center [F]	(159.5, 119.5) 64.42	(160.0, 122.0) 64.49
Maximum [F]	(317, 2) 66.43	(319, 102) 66.03
Minimum [F]	(35, 11) 62.22	(35, 11) 62.22
Number of Pixels	76800	72277
Percentage Area [%]		94.11067708
	Image 0833	Polygon 1
Mean [F]	63.78	63.74
Std. Dev. [F]	0.55	0.42
Center [F]	(159.5, 119.5) 64.06	(159.5, 121.5) 64.07
Maximum [F]	(49, 1) 71.31	(315, 138) 65.15
Minimum [F]	(207, 10) 62.17	(207, 10) 62.17
Number of Pixels	76800	71278
Percentage Area [%]		92.80989583
	Image 0834	Polygon 1
Mean [F]	63.38	63.35
Std. Dev. [F]	0.54	0.39
Center [F]	(159.5, 119.5) 63.47	(159.5, 120.0) 63.47
Maximum [F]	(290, 1) 67.33	(250, 131) 64.63
Minimum [F]	(1, 15) 61.14	(14, 17) 61.48
Number of Pixels	76800	71167

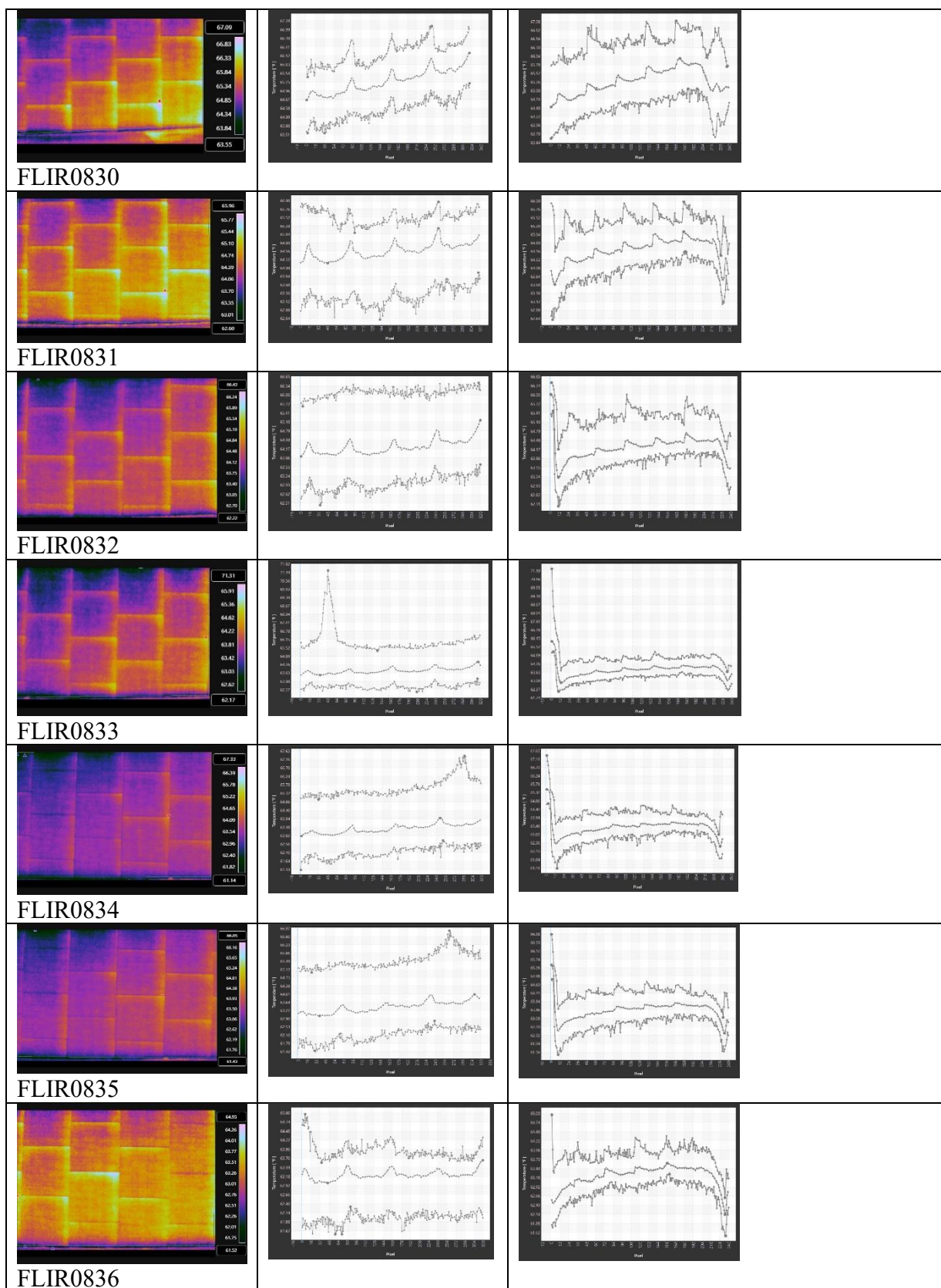
Percentage Area [%]		92.66536458
	Image 0835	Polygon 1
Mean [F]	63.42	63.4
Std. Dev. [F]	0.51	0.42
Center [F]	(159.5, 119.5) 63.55	(159.0, 119.5) 63.44
Maximum [F]	(265, 1) 66.85	(234, 130) 64.72
Minimum [F]	(30, 10) 61.43	(30, 10) 61.43
Number of Pixels	76800	72140
Percentage Area [%]		93.93229167
	Image 0836	Polygon 1
Mean [F]	63.21	63.24
Std. Dev. [F]	0.35	0.31
Center [F]	(159.5, 119.5) 64.09	(159.0, 116.5) 64.14
Maximum [F]	(6, 1) 64.95	(2, 156) 64.35
Minimum [F]	(59, 236) 61.52	(14, 233) 61.69
Number of Pixels	76800	73340
Percentage Area [%]		95.49479167
	Image 0837	Polygon 1
Mean [F]	63.16	63.2
Std. Dev. [F]	0.38	0.34
Center [F]	(159.5, 119.5) 63.69	(159.5, 116.5) 63.70
Maximum [F]	(8, 1) 64.61	(242, 109) 64.42
Minimum [F]	(163, 233) 61.18	(163, 231) 61.31
Number of Pixels	76800	72390
Percentage Area [%]		94.2578125
	Image 0838	Polygon 1
Mean [F]	63.39	63.31
Std. Dev. [F]	0.55	0.32
Center [F]	(159.5, 119.5) 63.96	(159.5, 123.5) 63.86
Maximum [F]	(313, 1) 66.26	(155, 115) 64.55
Minimum [F]	(5, 240) 61.55	(14, 237) 61.84
Number of Pixels	76800	71170
Percentage Area [%]		92.66927083
	Image 0839	Polygon 1
Mean [F]	62.53	62.56
Std. Dev. [F]	0.57	0.49
Center [F]	(159.5, 119.5) 62.55	(159.5, 115.0) 62.49
Maximum [F]	(60, 1) 65.20	(317, 58) 64.04
Minimum [F]	(1, 232) 60.17	(19, 229) 60.30
Number of Pixels	76800	71889
Percentage Area [%]		93.60546875
	Image 0840	Polygon 1
Mean [F]	62.18	62.18

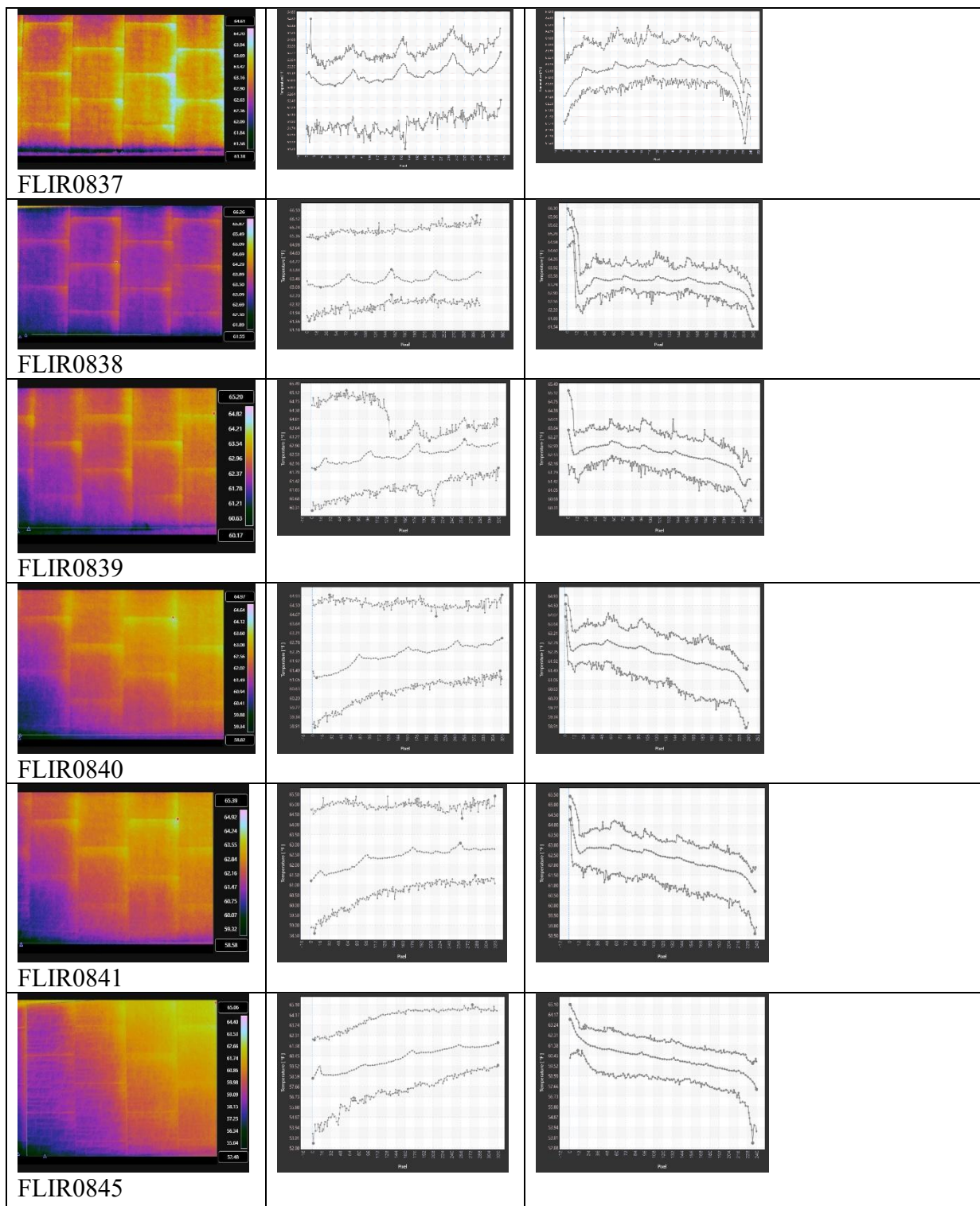


Std. Dev. [F]	0.81	0.72
Center [F]	(159.5, 119.5) 62.69	(159.0, 117.5) 62.67
Maximum [F]	(29, 1) 64.97	(242, 57) 64.12
Minimum [F]	(4, 237) 58.82	(5, 232) 59.27
Number of Pixels	76800	72667
Percentage Area [%]		94.61848958
	Image 0841	Polygon 1
Mean [F]	62.34	62.3
Std. Dev. [F]	0.83	0.74
Center [F]	(159.5, 119.5) 62.58	(160.0, 119.5) 62.59
Maximum [F]	(320, 1) 65.39	(263, 58) 64.23
Minimum [F]	(7, 238) 58.58	(7, 238) 58.58
Number of Pixels	76800	73436
Percentage Area [%]		95.61979167
	Image 0845	Polygon 1
Mean [F]	60.19	60.14
Std. Dev. [F]	1.49	1.34
Center [F]	(159.5, 119.5) 60.45	(166.5, 121.5) 60.66
Maximum [F]	(276, 1) 65.06	(319, 20) 63.23
Minimum [F]	(2, 235) 52.48	(45, 238) 54.15
Number of Pixels	76800	69591
Percentage Area [%]		90.61328125

### TI3-1 West to East Images and Temperature Plots – King George







### T3-1 East to West Data –King George

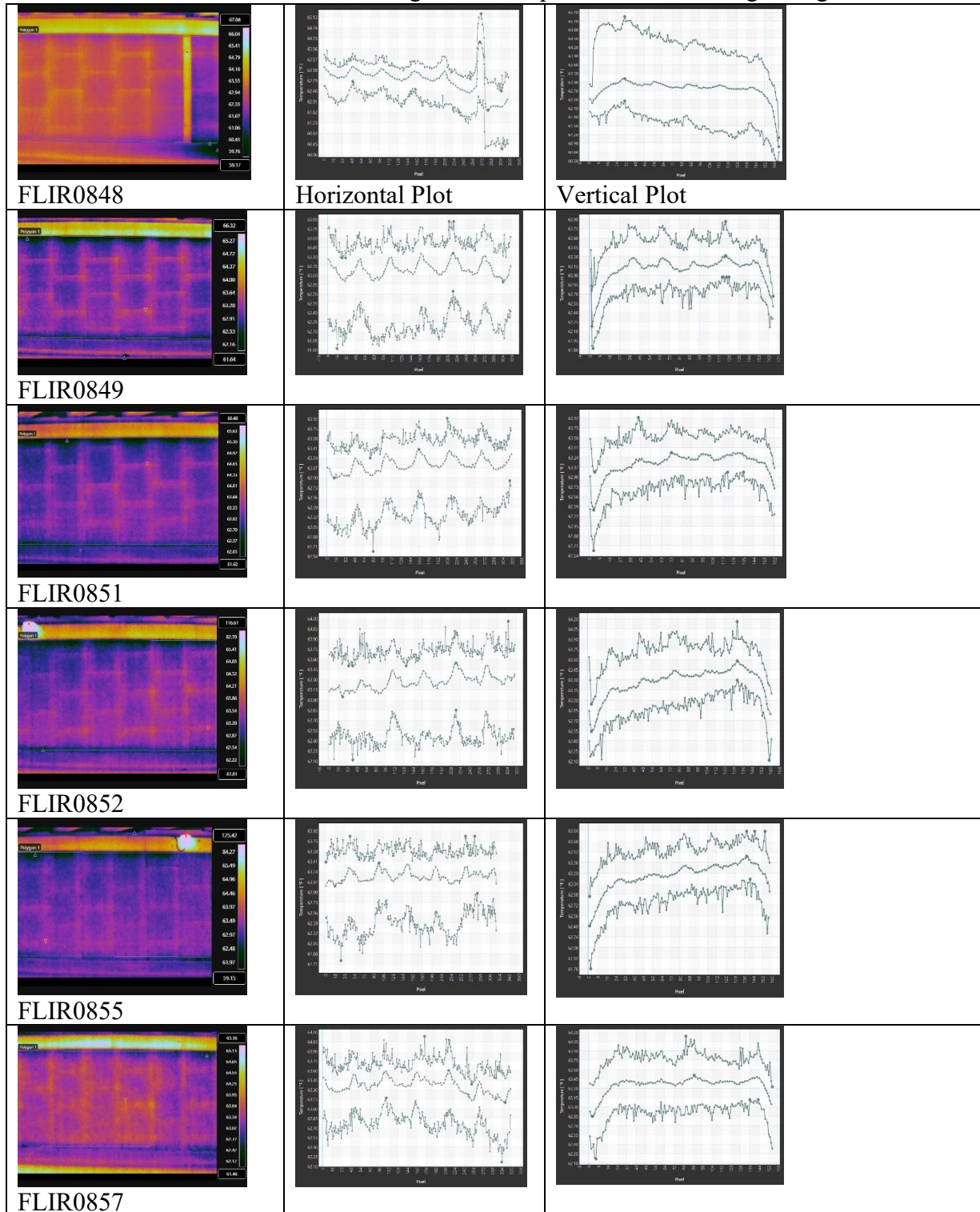
	Image 0848	Polygon 1
Mean [F]	62.95	62.79
Std. Dev. [F]	0.86	0.55

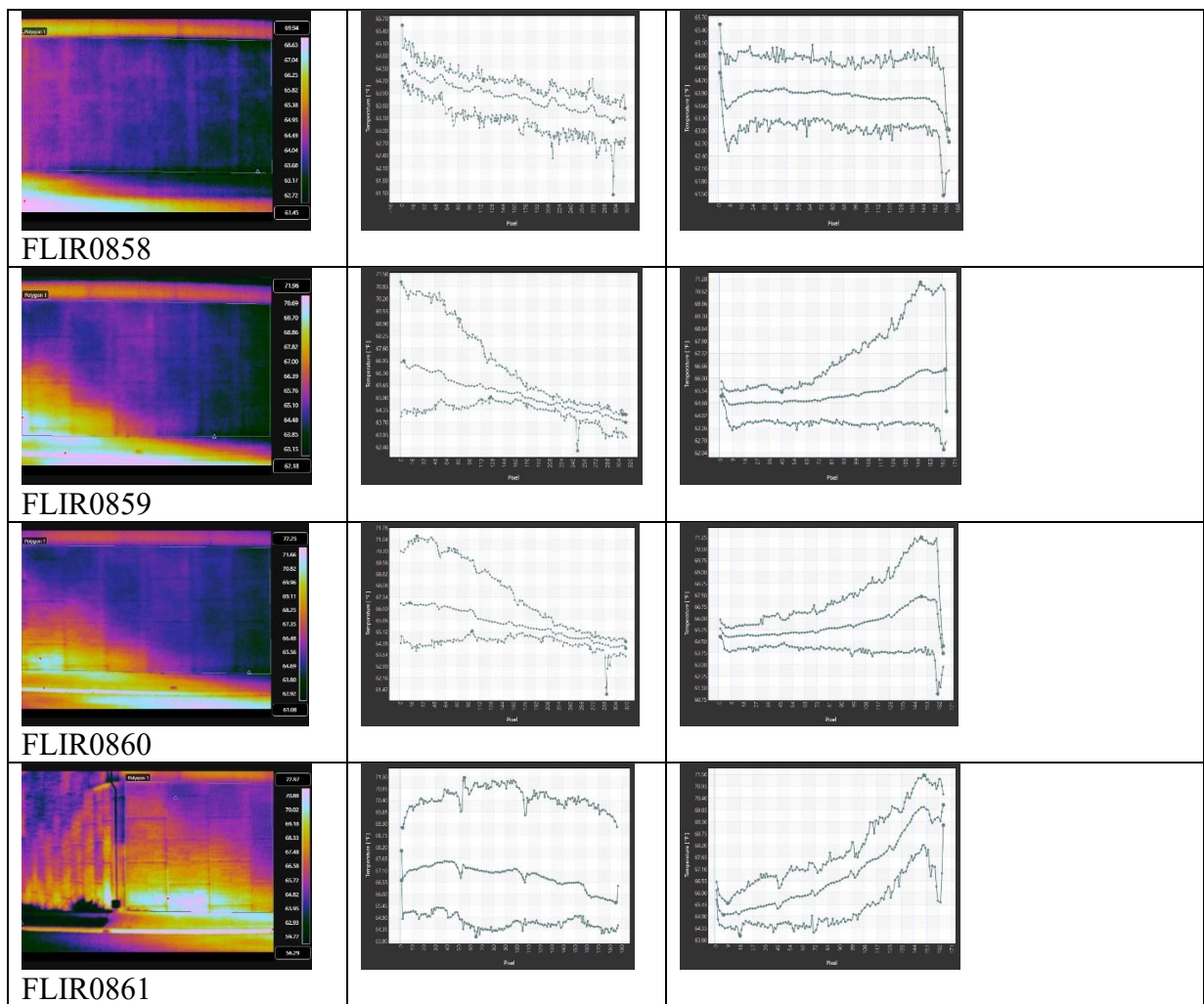
Center [F]	(159.5, 119.5) 63.13	(158.5, 125.5) 63.16
Maximum [F]	(320, 2) 67.08	(271, 75) 65.24
Minimum [F]	(319, 217) 59.17	(307, 207) 60.25
Number of Pixels	76800	50322
Percentage Area [%]		65.5234375
	Image 0849	Polygon 1
Mean [F]	63.24	63.09
Std. Dev. [F]	0.53	0.25
Center [F]	(159.5, 119.5) 63.30	(159.5, 124.5) 63.28
Maximum [F]	(316, 1) 66.32	(212, 165) 63.86
Minimum [F]	(177, 237) 61.64	(17, 45) 61.82
Number of Pixels	76800	51834
Percentage Area [%]		67.4921875
	Image 0851	Polygon 1
Mean [F]	63.24	63.12
Std. Dev. [F]	0.5	0.26
Center [F]	(159.5, 119.5) 63.63	(159.0, 129.5) 63.55
Maximum [F]	(84, 7) 66.48	(208, 92) 63.93
Minimum [F]	(80, 53) 61.62	(80, 53) 61.62
Number of Pixels	76800	51359
Percentage Area [%]		66.87369792
	Image 0852	Polygon 1
Mean [F]	63.46	63.26
Std. Dev. [F]	1.76	0.27
Center [F]	(159.5, 119.5) 63.48	(159.0, 126.0) 63.46
Maximum [F]	(19, 27) 116.61	(307, 177) 64.15
Minimum [F]	(35, 11) 61.81	(42, 205) 62.11
Number of Pixels	76800	50721
Percentage Area [%]		66.04296875
	Image 0855	Polygon 1
Mean [F]	63.38	63.16
Std. Dev. [F]	1.95	0.24
Center [F]	(159.5, 119.5) 63.10	(159.5, 129.5) 63.27
Maximum [F]	(279, 31) 125.42	(47, 189) 63.83
Minimum [F]	(194, 20) 59.15	(30, 53) 61.76
Number of Pixels	76800	49768
Percentage Area [%]		64.80208333
	Image 0857	Polygon 1
Mean [F]	63.44	63.35
Std. Dev. [F]	0.47	0.2
Center [F]	(159.5, 119.5) 63.54	(160.0, 119.0) 63.67
Maximum [F]	(260, 31) 65.36	(174, 124) 64.13
Minimum [F]	(285, 198) 61.46	(305, 48) 62.16

Number of Pixels	76800	49049
Percentage Area [%]		63.86588542
	Image 0858	Polygon 1
Mean [F]	64.16	63.81
Std. Dev. [F]	1.06	0.38
Center [F]	(159.5, 119.5) 63.97	(159.5, 112.5) 64.01
Maximum [F]	(5, 231) 69.94	(2, 33) 65.52
Minimum [F]	(302, 190) 61.45	(302, 190) 61.45
Number of Pixels	76800	49924
Percentage Area [%]		65.00520833
	Image 0859	Polygon 1
Mean [F]	65.67	65.18
Std. Dev. [F]	1.91	1.31
Center [F]	(159.5, 119.5) 65.05	(159.0, 122.0) 65.03
Maximum [F]	(57, 229) 71.96	(2, 186) 71.06
Minimum [F]	(248, 203) 62.18	(248, 203) 62.18
Number of Pixels	76800	51355
Percentage Area [%]		66.86848958
	Image 0860	Polygon 1
Mean [F]	66.35	65.59
Std. Dev. [F]	2.09	1.47
Center [F]	(159.5, 119.5) 65.09	(160.0, 112.0) 65.20
Maximum [F]	(30, 217) 72.25	(25, 179) 71.23
Minimum [F]	(293, 191) 61.08	(293, 191) 61.08
Number of Pixels	76800	51036
Percentage Area [%]		66.453125
	Image 0861	Polygon 1
Mean [F]	66.38	66.81
Std. Dev. [F]	2.15	1.72
Center [F]	(159.5, 119.5) 67.17	(225.0, 107.0) 66.73
Maximum [F]	(320, 215) 72.97	(187, 176) 71.44
Minimum [F]	(1, 201) 56.29	(197, 43) 63.98
Number of Pixels	76800	30319
Percentage Area [%]		39.47786458



## TI3-2 East to West Images and Temperature Plots – King George





## APPENDIX C1. LEICA SCANSTATION OPERATING PROTOCOL

### Leica Geosystems Scanner P50



## 1. USER INTERFACE

### 1.1 Face Plate

The below figure shows the *face plate* of the P50 scanner. Please, consider Figure 1 and become familiar with its different parts.



Overview of face plate

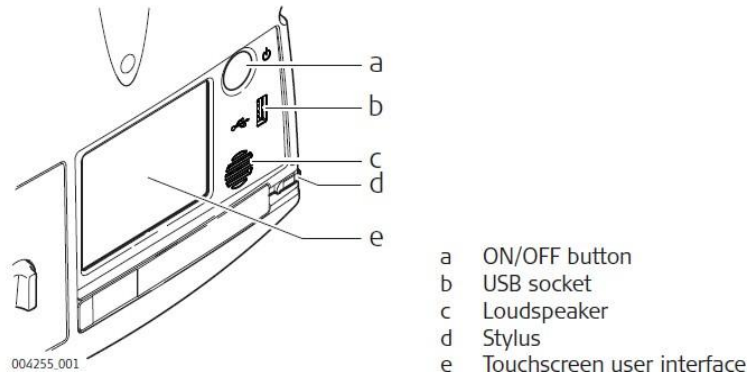


**Figure 1**

## 1.2 Battery Setup

Please, follow the following instructions for battery setting up and details in Figures 2 and 3, respectively.

1. Unlock and open the battery compartment.
2. Remove the battery holder.
3. Remove the battery from the battery holder. Insert the new battery into the battery holder, ensuring that the contacts are facing outward and that the tip on the holder fits into the slot of the battery. The battery should click into position.
4. Insert the battery holder back into the battery compartment.
5. Turn the knob to lock the battery holder in place.
6. Switch on the instrument to start the boot process.

**Figure 2**

Insert and remove the  
internal battery  
step-by-step

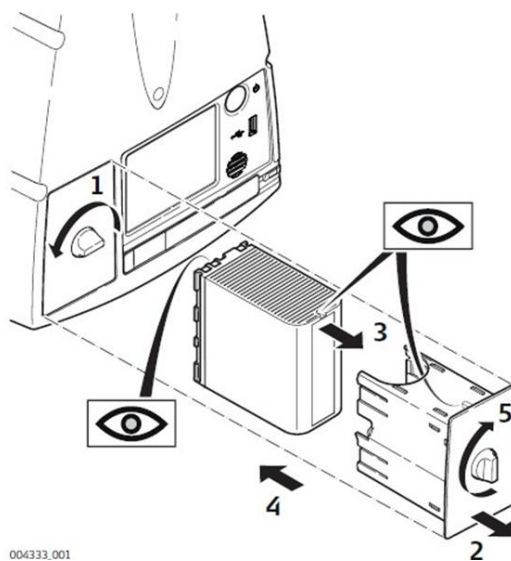
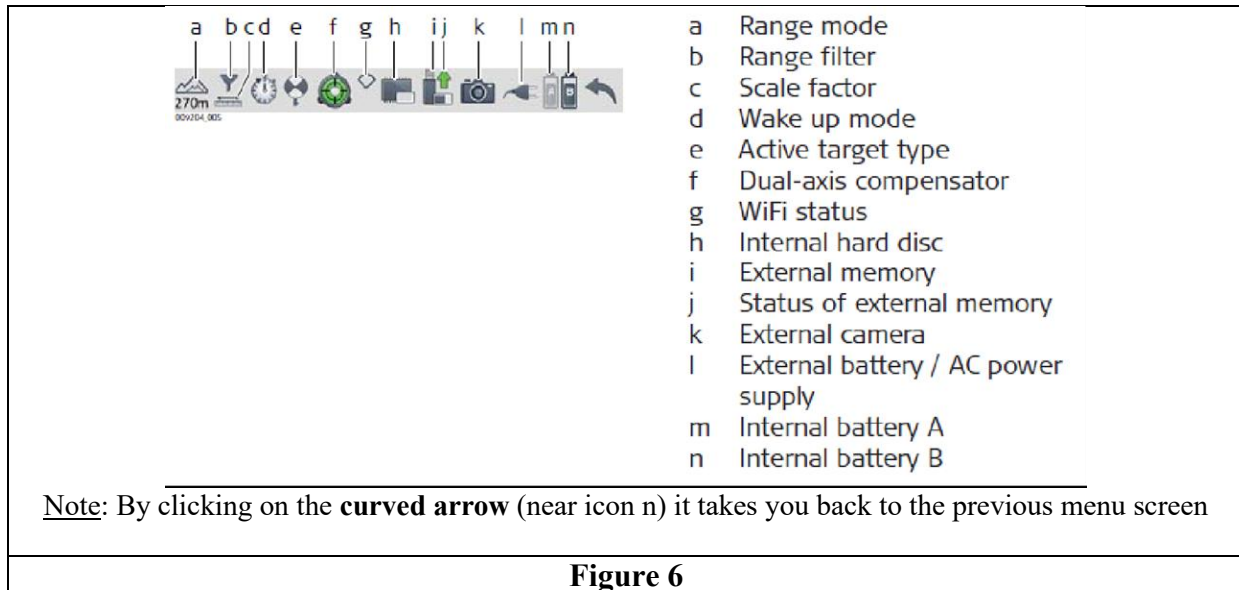


**Figure 3**



## 1.5 Overview of Status Bar Icons

As seen in Figure 6, become familiar with the different icons presented in the top bar of the P50 scanner.



## 2. INSTRUMENT SETUP

### 2.1 Scanner Setup (on the Tripod) and Verticalization

- Place the tripod at your selected scanning location. Always set up the instrument on its tripod. Do not place it directly on the ground for scanning operations.
- Properly tight the scanner on top of the tripod with the screw.
- Usually, you will not need to set the scanner exactly above a nail marking a ground control point. However, if that were the case, you would prefer to be assisted by the laser plummet. For that purpose, click on the Dual Axis Compensator icon (which is icon f in above Figure 3) to invoke the Level & Laser Plummet screen. Then, click on the Plummet tab and make sure the Laser Plummet is ON. Preferably its intensity should be 100%. Then, you will be able to use it to assist in this process. If you do not need the laser plummet, keep it OFF. Also, while on this screen, click on the Compensator tab, and make sure the Compensator is ON. Also, choose what the scanner should do in case the compensator becomes out of range. In this case you have two options: Cancel Scan & Image or Flag Data & Cont. Your choice. However,

to be safer, it is preferable to choose the canceling option.

- After setting the scanner up, adjust the legs of the tripod (change their lengths) to approximately level the instrument by observing the physical spherical level vial (on the back of the instrument). Try to place the bubble in the center of the marked circle by adjusting the tripod legs.
- Finally, use the electronic level vial to refine your leveling. For this you should be on the Level & Laser Plummet screen. If you are not there, click on the f icon (indicated in above Figure 3) to invoke the Dual Axis Compensator icon. Then, select the Level tab to see the electronic level vial. Use the leveling screws to adjust the bubble exactly in the center of the electronic circle. Try that the *Tilt L* and *Tilt T* sensors are less than |10| seconds each. If you cannot attain that, try less than |15| seconds.

### 3. INSTRUCTIONS FOR PARAMETERS SETUP

#### 3.1 Main Menu

The Main Menu screen shows 6 icons: Scanning, Traverse, Manage, Status, Configuration, and Tools.

#### 3.2 Setting Projects and Targets in the Management Menu

- In the Main Menu, click on Manage to access the Management Menu screen. There, you will see 3 icons: Projects, Targets and Control Points. Then, click on the Projects icon (see Figure 7).



Figure 7

- Then, while on the Projects screen, click on New (see Figure 8) and input a job name for your new project. In this example, our new job was named Trial A. That name was typed within the corresponding box.

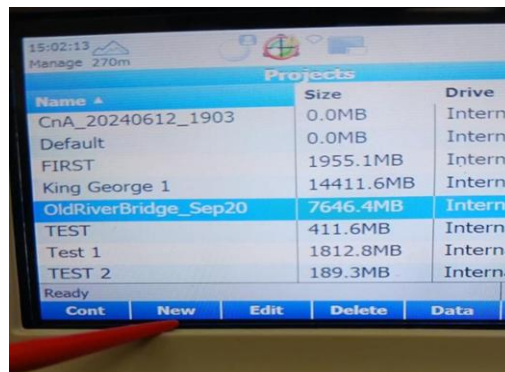


**Figure 8**

- Then, click on Cont (see Figure 9). Starting on page 13 of this protocol, we present another example, providing additional details in this regard.

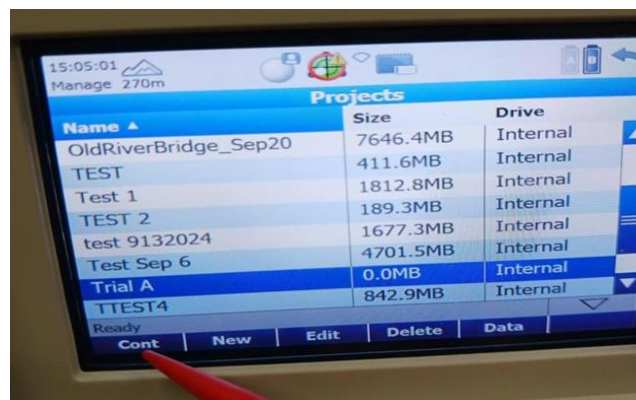


**Figure 9**

- After the new project has been created, go back to the Management Menu screen and click on Targets (see Figure 10). This is to define the targets we will be using for the new project. However, in this scanner, we have already defined several different types of targets and may select from the already defined ones. Alternatively, if necessary, we can edit their characteristics or create new ones.

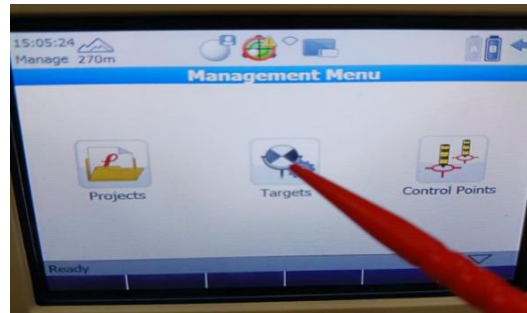


**Figure 10**

- For example, you may select an existing target type from the list, e.g., 6-inch Sphere (see Figure 11) and then press Cont. Alternatively, you may create a new target by selecting New.



**Figure 11**

### 3.3 Setting Parameters in the Scanning Menu

- Go back to the Main Menu and click the Scanning icon (see Figure 12). At that point you will reach the Scan Begin screen. Make sure the project name remains as the one you already set. That is, Trial A in this example (see Figure 13).



**Figure 12**



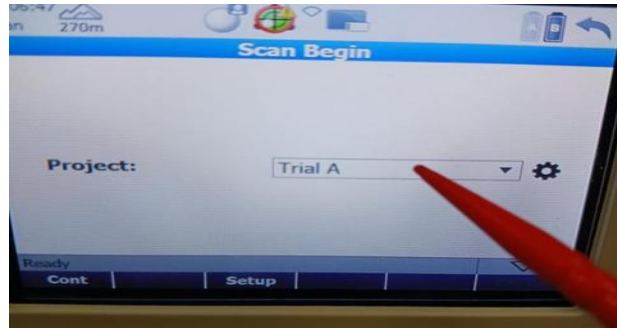


**Figure 13**

- Then, while at the Scan Begin screen, click on Setup (see Figure 13). That will take you to the Station Setup screen (see Figure 14). There, select Quick Orientation as the Setup Method, and keep the correct job name in the Ctrl Pnt Project (Trial A, in this case). Also, you will need to define a new station ID for your current scanning position. That is, you will need to select the New option (see bottom of Figure 14). That will open the New Control Point screen where you need to input 4 items: (1) your station ID in the Point ID field (in this case, we chose the station to be called ST1), (2) input 0.000 for Northing, (3) input 0.000 for Easting, and (4) 0.000 for Height. Then, at the bottom of the New Control Point screen, press Store. That will take you back to the Station Setup screen (see Figure 14). There, input 0.000 for the Instrument Ht and the Azimuth fields.

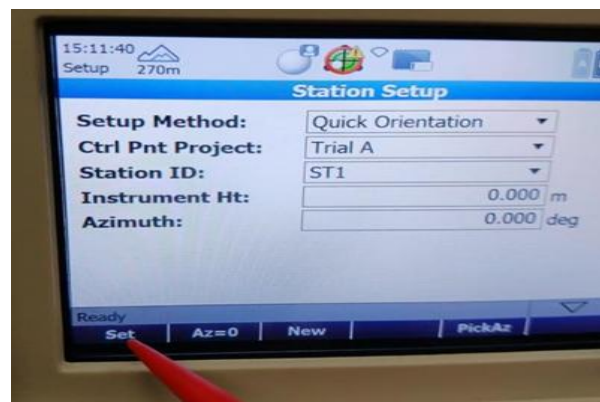


**Figure 14**

- **IMPORTANT:** After completing the information on the Station Setup screen, click on Set (see bottom left corner of Figure 14). That will take you to your current Scanning Station screen (in this case, that screen is entitled Trial A: ST1). In that screen, visit the Field of View tab and select all the parameters as shown in Figure 15. Please note that the Task field should be Scan & Image.





**Figure 15**

- While still at your Scanning Station screen (in this example, it is the Trial A: ST1 screen), visit the Resolution tab and select the same parameters as indicated in Figure 16.

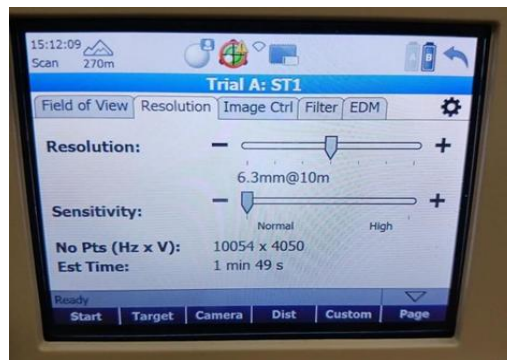


**Figure 16**

- Then, visit the Image Ctrl tab and select the same parameters as indicated in Figure 17.

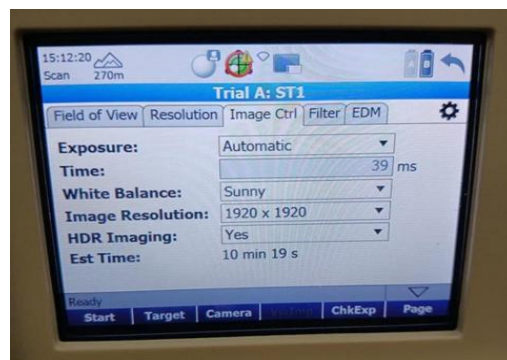


**Figure 17**

- Then, visit the Filter tab and leave the Min and Max ranges at 0.000 (see Figure 18).



**Figure 18**

- Finally, visit the EDM tab and select 120m for the Max Range, but it could be selected larger, if preferred. The Scan Rate will show as 1,000,000 points per second (see Figure 19).



**Figure 19**

- **IMPORTANT**: DO NOT START THE SCANNING YET!!! YOU NEED TO PICK ALL TARGETS AND STORE THEM BEFORE SCANNING.

### **3.4 Setting the Parameters and Picking the Targets for Your Scanning Station**

- Click on Field of View and then again click on Target as shown in Figure 20. That will take you to the Target Definition screen (see Figure 21).

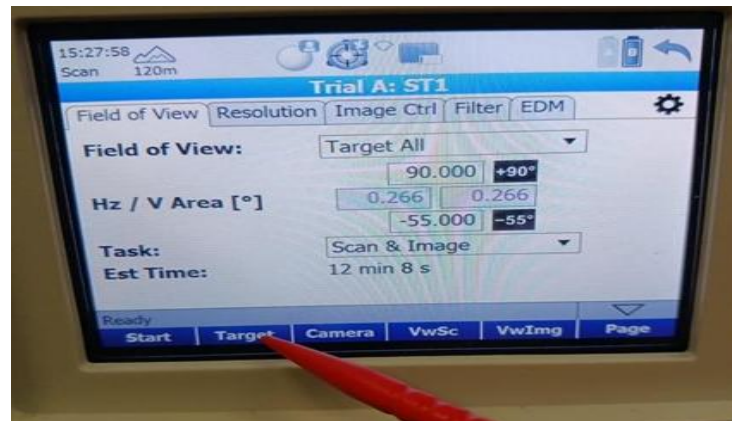


**Figure 20**

- Once you reach the Target Definition screen (see Figure 21), in the Target ID field, provide an ID (name) to your first target (in this case, we named it as TA). Select the Target Type (in this example, we used 6-inch Sphere target). The field corresponding to the target height will automatically adopt the height used when that type of target was first defined. Often, that first definition occurred in a previous project or all types of targets were defined for this project, before reaching this point (see explanations corresponding to previous Figures 10 and 11). Select the Pick Method as Video Image. Leave the target height as provided, unless you need to change it. Then click on PickT (see Figure 21).



**Figure 21**

- After clicking PickT, the screen will change to show an image of the current live view observed by the scanning telescope. At this point, you will need to manually rotate the scanner and point its telescope to the actual physical target you want to acquire. After those manual aiming motions, you will see an image of the needed target on the screen. Then, you will pick that target. This requires you to click on cross-hair icon, as shown in Figure 22 and, after that, use the stylus to pick at the approximate center of that target. To facilitate this task, you may use the magnifying lens and other options shown on Figure 22. After you have approximately picked on the center of the target, click on the check-mark icon (as seen in Figure 23) to confirm your pick.

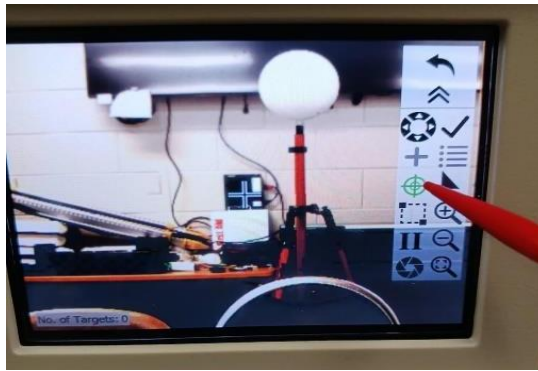


**Figure 22**

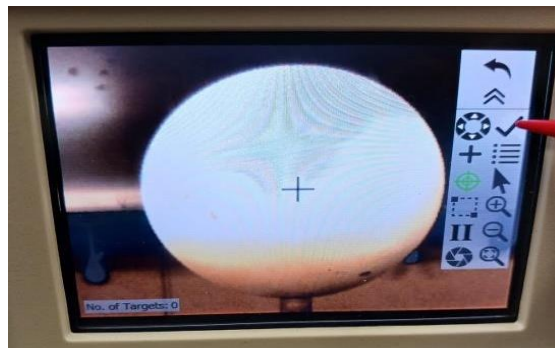


**Figure 23**

- After clicking on the check-mark icon, you will go back to the Target Definition screen. There, click on Meas (see bottom left corner of Figure 21) to start the actual target acquisition process at high resolution. The scanner will take a few minutes to complete this target scanning process.
- After completing the target acquisition, check if the target was properly (OK) or inadequately (Bad) captured. If OK, then store the captured target by clicking Store in the screen. This is very important step. Do not forget to store the captured targets.
- If the resulting scanning state is Bad, delete the acquired target and reacquire it.
- You will need to repeat this target acquisition process until you acquire all targets assigned to that particular scanning station.

#### **4. SCANNING**

After finishing the picking of all targets at your current station, go back to the Scanning Station screen (in this case, Trial A: ST1), select the Field of View tab, check that Scan & Image is selected in the Task field, and click on the Start button, at the bottom left corner of the screen (see Figure 24). This will run and complete the full scan at that station. It may take several minutes to complete it.

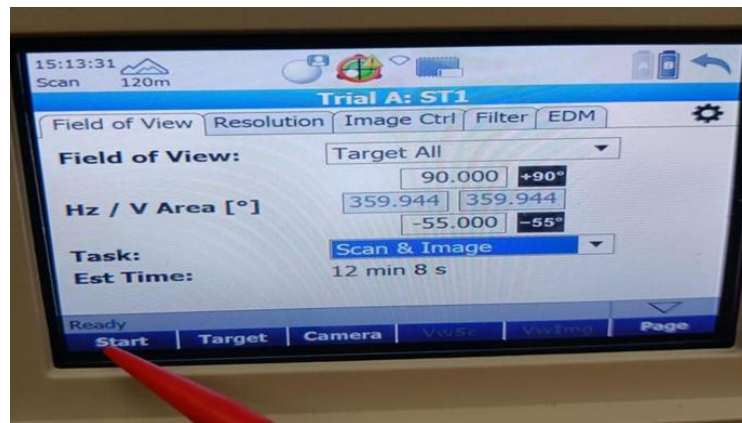


**Figure 24**

After finishing the scanning of the first station (in this example, ST1), move the scanner to the next station, verticalize it, and start the process again at that new location. That is, go back to the Scan Begin screen (see Figures 12 and 13) and select the Setup option to set the new Station Name (say ST2). Repeat this whole process, station after station, until the final station is completed.

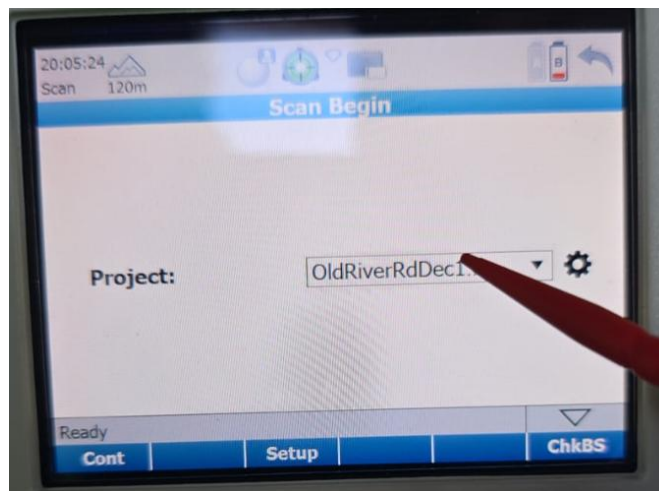
Note: The next pages present a step-by-step example for better understanding of the above process.

### **REAL SCANNING EXAMPLE USING LEICA'S P50 SCANNER**

Project: **OldRiverRdDec192024**

Station: **ST5**

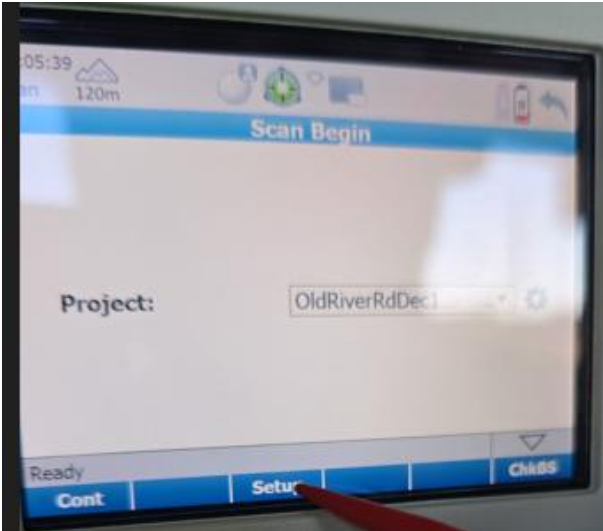
**Step 1:** In this example, the name of the project is OldRiverRdDec192024, as shown in the below picture [a].



**[a]**

**Step 2:** Then, we clicked on Setup (see pic [b]). Then, in the Station Setup screen, we opened the

options in the Station ID field and clicked on New (see pic [c]).



[b]



[c]



Step 3: In this example, we have already completed stations ST1, ST2, ST3, and ST4. Therefore, we will be working on the 5<sup>th</sup> station. Its name is ST5 (see pic [d]). For ST5, we input the Northing, Easting, Height as 0.000 (see pic [d]) and then selected Store (see pic [e]).

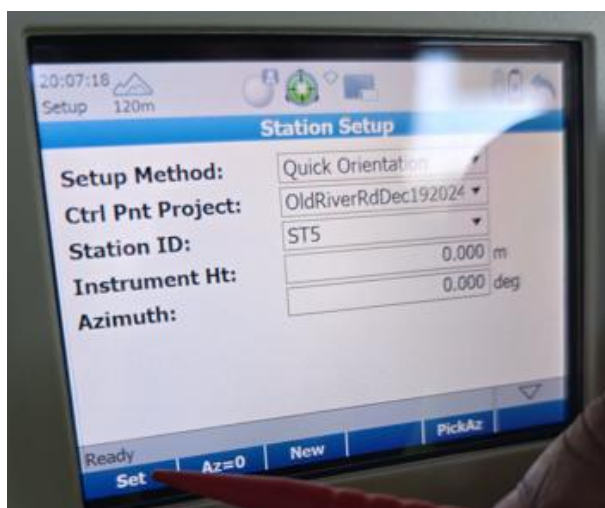


[d]



[e]

**Step 4:** Then, we went back to the Station Setup screen and selected the parameters as seen in the left pic. They include 0.000 values for **Instrument Ht** and for **Azimuth** (see pic [f]). Then, we clicked on **Set** (see pic [f]). Then, at the Scanning Station screen (see pic [g]) we clicked on **Target** (see pic [g]).



[f]



[g]

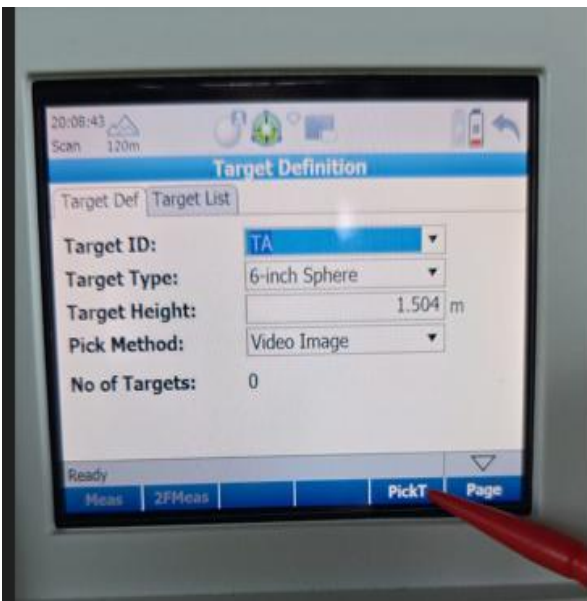
Step 5: At the Target Definition screen, we selected the Target ID as TA (see pic [h]). Since we defined the targets before starting the scanning process, the other information on the targets was automatically filled. We accepted all the parameters as they were automatically presented (see pic [i]) and clicked the PickT command (see pic [j]). Then, we selected the cross-hair icon to approximately pick on the center of the target (see pic [k]).



[h]



[i]



[j]



[k]



Step 6: After that, we clicked on the target (see pic [l]). Then, we clicked on the check mark (see pic [m]). Then, we clicked on Meas to scan the target (see pic [n]). When the scanning of the target finished, its status showed as OK (see pic [o]). Recall that, sometimes, the result will not be OK, it may show Bad. This means the target was not properly scanned and we should not proceed with the next step. If this happens, we need to delete that wrongly scanned target and reacquire it by repeating the process until an OK status is received.



[l]



[m]



[n]

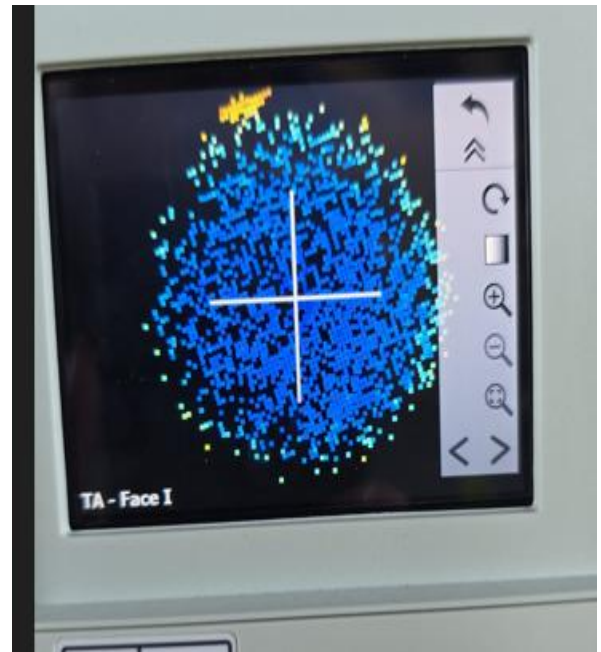


[o]

**Step 7:** In our example, the scanning target was OK, and we clicked on **View** (see pic [p]) to confirm that the scanning was good (see pic [q]). Then we went back and stored the acquired target (see pic [r]). **IMPORTANT: Do not forget to store the properly acquired target.**



[p]



[q]

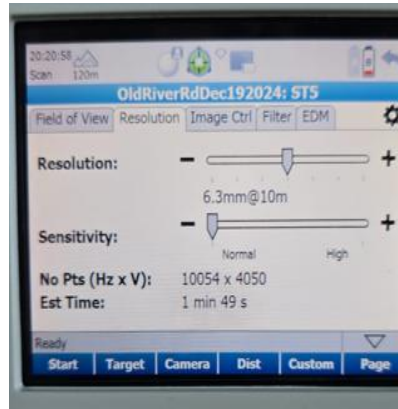


[r]

**Step 8:** Our final parameters, for Scanning Station ST5, were as presented in the below pictures. After that, we started the full scan. When the scan was finished, we moved the scanner to the next station and repeated the same process mentioned above.



Field of View



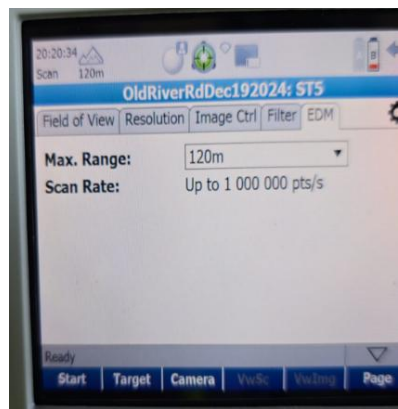
Resolution



Image Control



Filter



EDM



Start the Scan

Cheers and Good Luck  
Team



## **APPENDIX C2. NOISE REMOVAL PROTOCOLS IN CYCLONE CORE**

### **PERMANENTLY CLEANING SCANS IN CYCLONE 9 CORE**

The correct procedure for cleaning scans before registration in Cyclone is not as straightforward as one might imagine. This is mostly due to the complicated structure of Cyclone databases; one needs to understand the hierarchy and relationships among ControlSpace, ModelSpace, ScanWorld and Scans. After much experimentation and communication with Leica support, it has been determined that in the latest version of Cyclone (9.1.3), the cloud alignment algorithm works with the point cloud inside the ScanWorld's ControlSpace, not with ModelSpace or Default Clouds. However, in the registered ScanWorld, it is the Default Clouds that appear for each individual ScanWorld. Which can be useful in some cases but also confusing. Do you clean in ModelSpace or ControlSpace? And if in the ControlSpace, which ControlSpace? Cyclone creates a "child" ControlSpace for every time the ScanWorld appears in a registration within the database.

As it stands at the moment, the process for cleaning scans is as follows:

1. In the tree view, go to each ScanWorld's ModelSpace and clean unwanted objects. The cleaning procedures are explained in corresponding BEaM Lab protocol(s).
2. While in the ModelSpace, you may want to verify that all targets are at their right location, have their right types, names and heights. All these items could be changed at this stage. If you need to move a target, select it, grab the blue insertion handle and move it to your desired location. To edit a target (change type, name, and height), select it, right click and select Add/Edit Annotations. Complete your desired edits.
3. While still at the ModelSpace, select all points, targets, etc., of the cleaned point cloud

(Selection|All) and make it the ScanWorld's Default Cloud (Tools|Scanner|Set Scans' Default Clouds).

4. Now, in the ModelSpace, select all points, targets, etc. of the cleaned cloud (Selection|All) and copy it (Edit|Copy).
5. Then, go to the ControlSpace and delete all points, targets, etc., from that space (Selection|All and then Edit/Delete).
6. While still at the ControlSpace, paste there the cleaned cloud (with targets) copied from the ModelSpace (Edit|Paste).

This process will ensure that:

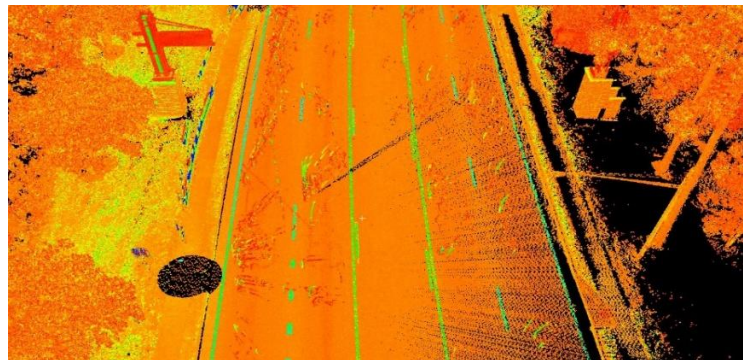
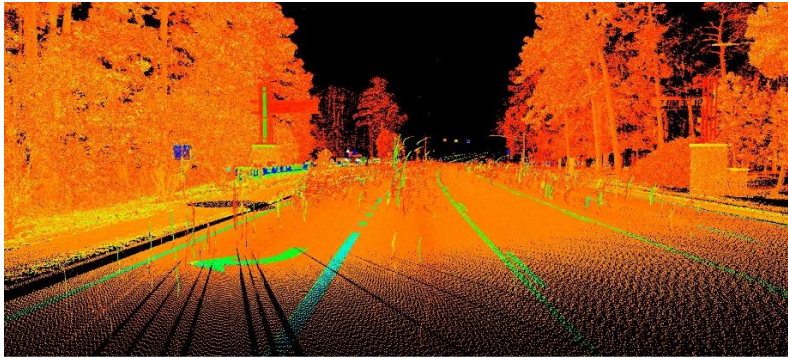
- (a) The cloud alignment algorithm will use the clean clouds (from ControlSpace), therefore improving registration results.
- (b) Any new ModelSpaces created, as well as the registered ScanWorld ModelSpace, will contain only the clean clouds (Default Clouds).



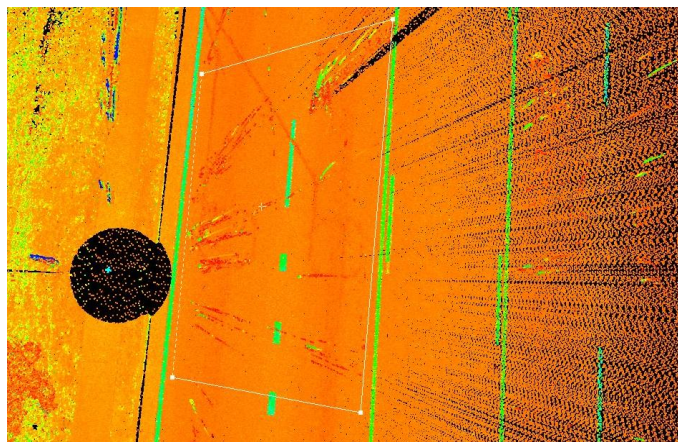
## REMOVING NOISE ABOVE A SURFACE (Traffic, Pedestrians, Vehicles, etc.)

(Updated by By Mariah Peart, 9/25/2018)

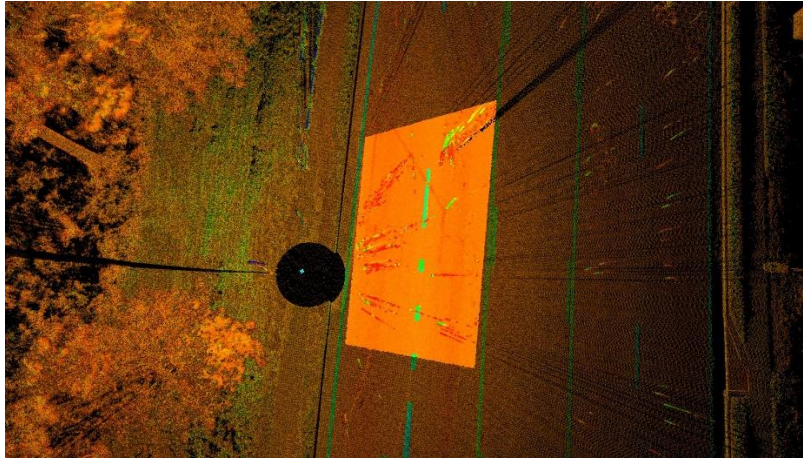
In View Mode, orient the model to a top view for a proper sight of the noise (*Recommended*).



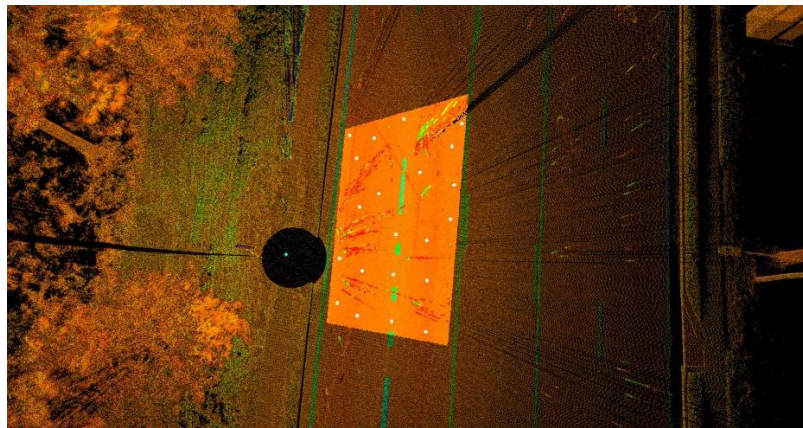
Select the Polygonal Fence Mode and create a fence around the noise.



Right-click and select Point Cloud Sub-Selection, then select Add Inside Fence.

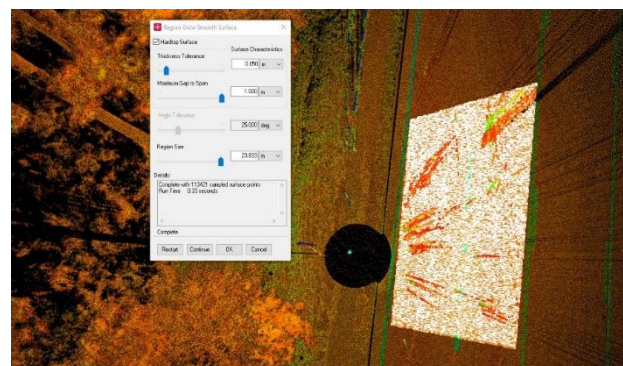


To define the surface from the noise, select Multi-Pick Mode and carefully place multiple points on the surface. Be sure the points do not interfere with the noise.



Right-click and select Region Grow, then Smooth Surface.

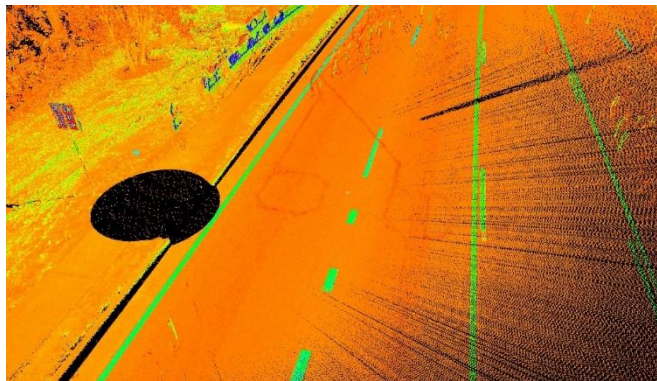
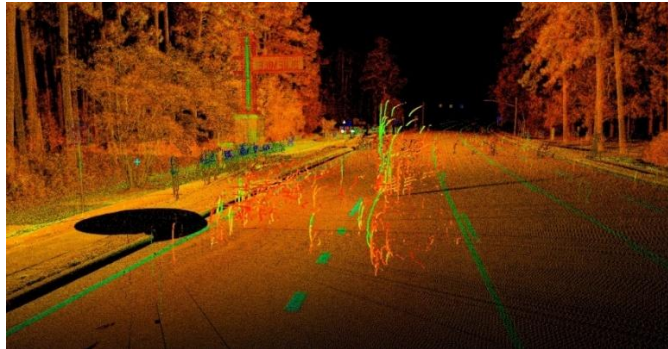
The Region Grow Smooth Surface window will appear. When the Region Grow Run Time is complete, click OK. If the region does not have enough points, then click Continue or recreate the region. Orient the view to observe the highlighted noise, by



using the View Mode. If the noise is properly selected, then press the Delete button. If some surface points are highlighted, click on Selection at the top of the task bar, then select **Invert Selection**.



Wait for all points to load, then select Invert Selection, again. This step will re-establish the distinction between the surface and the noise.

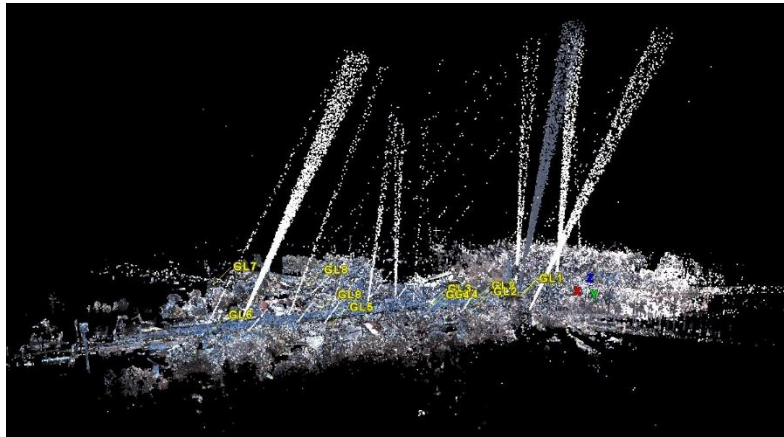




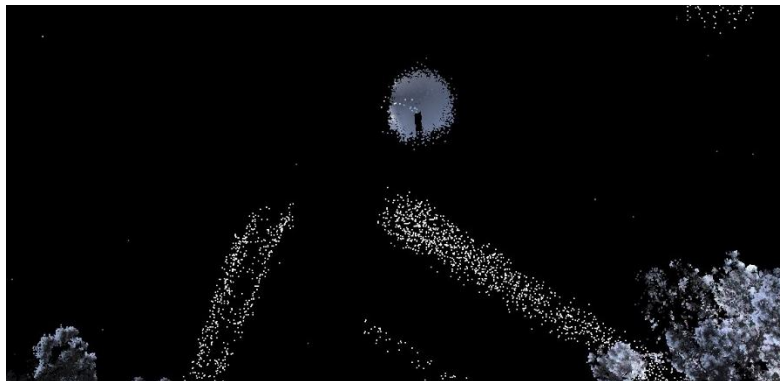
## REMOVING SUN BEAMS FROM THE SCAN ORIGIN

(Updated by By Mariah Peart, 9/25/2018)

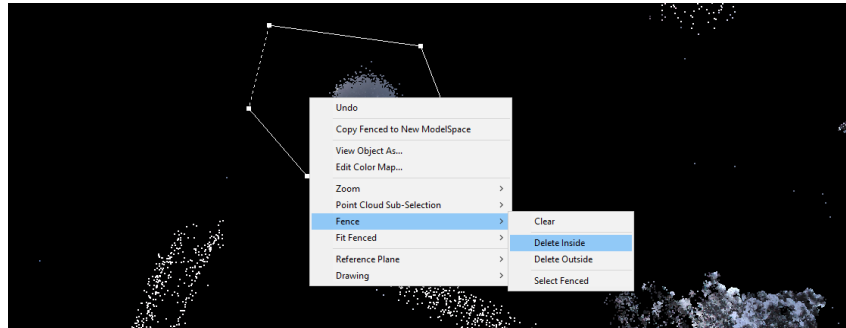
Select the SEEK cursor (alternatively, press the “s” key on the keyboard to turn on the “SEEK” mode.



Then, hold the shift key and left-click a point on the Sun beam. That will bring your point of view positioned at the scan origin (center of the scanner) and looking towards the point you clicked in the Sun beam.



Now, use the Polygonal Fence mode to surround the cloud containing the sun beam (that cloud should look somehow rounded), right-click, select Fence and then Delete Inside.



### **Cyclone Cleaning Data inside a 3D box**

For a detailed explanation, watch the following YouTube video:

[https://www.youtube.com/watch?v=0wu0yW3mAiI&ab\\_channel=ScanToBIM](https://www.youtube.com/watch?v=0wu0yW3mAiI&ab_channel=ScanToBIM)

It explains the following:

1. It is recommended that you view your model from the top. For that click on the TOP VIEW icon (it is an eye on top of a little cube with solid green top).
2. Select the PERSPECTIVE icon (it is a small transparent cube in perspective).
3. Pull down the View tab and select “Set Limit Box by Cursor”. Click and drag near the noise you wish to remove. Then, that noise will be seen inside the cube you just generated. You will only see points inside that cube. The other points are no longer on your screen.
4. Resize the cube as you need. For that use the PICK MODE icon (it is a small white arrow pointing to 10 O’clock). Click on any side of the cube and drag the cube handles.
5. You can also rotate the cube by using the VIEW MODE icon (it is the little right hand with the index finger pointing to 10 O’clock).
6. Press the SPACE BAR to deselect the box.

7. Click the POLYGONAL FENCE MODE icon (it is the one looking like a polygonal star) and enclose the noise you want to remove making sure you only enclose what is to be deleted. For this, you may need to rotate the cube to a proper position, as indicated in point 5 above.
8. While still in the POLYGONAL FENCE MODE, right click and select “Point Cloud Sub-Selection”, and “Add Inside Fence”.
9. Use the VIEW MODE to check your selection.
10. Press the DELETE key to erase the selected noise.
11. Turn off the limit box. For this, click the PERSPECTIVE icon, select the View tab and uncheck the “Set Limit Box by Cursor”. Your noise should be gone.

## **CLEANING DATA INSIDE A 3D BOX**

It explains the following:

1. It is recommended that you view your model from the top. For that click on the TOP VIEW icon (it is an eye on top of a little cube with solid green top).
2. Select the PERSPECTIVE icon (it is a small transparent cube in perspective).
3. Pull down the View tab and select “Set Limit Box by Cursor”. Click and drag near the noise you wish to remove. Then, that noise will be seen inside the cube you just generated. You will only see points inside that cube. The other points are no longer on your screen.
4. Resize the cube as you need. For that use the PICK MODE icon (it is a small white arrow pointing to 10 O’clock). Click on any side of the cube and drag the cube handles.
5. You can also rotate the cube by using the VIEW MODE icon (it is the little right hand with the index finger pointing to 10 O’clock).
6. Press the SPACE BAR to deselect the box.
7. Click the POLYGONAL FENCE MODE icon (it is the one looking like a polygonal star) and enclose the noise you want to remove making sure you only enclose what is to be deleted. For this, you may need to rotate the cube to a proper position, as indicated in point 5 above.
8. While still in the POLYGONAL FENCE MODE, right click and select “Point Cloud Sub-Selection”, and “Add Inside Fence”.
9. Use the VIEW MODE to check your selection.
10. Press the DELETE key to erase the selected noise.
11. Turn off the limit box. For this, click the PERSPECTIVE icon, select the View tab and uncheck the “Set Limit Box by Cursor”. Your noise should be gone.

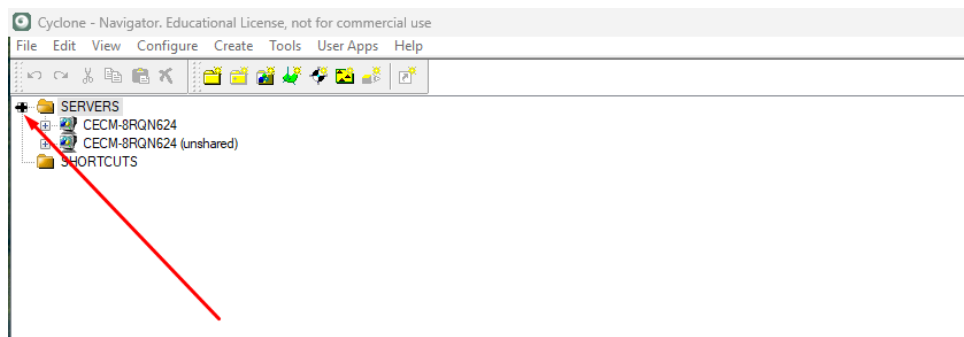
## APPENDIX C3. VISUAL-ALIGNMENT REGISTRATION ON CYCLONE CORE

### VISUAL-ALIGNMENT REGISTRATION ON CYCLONE CORE

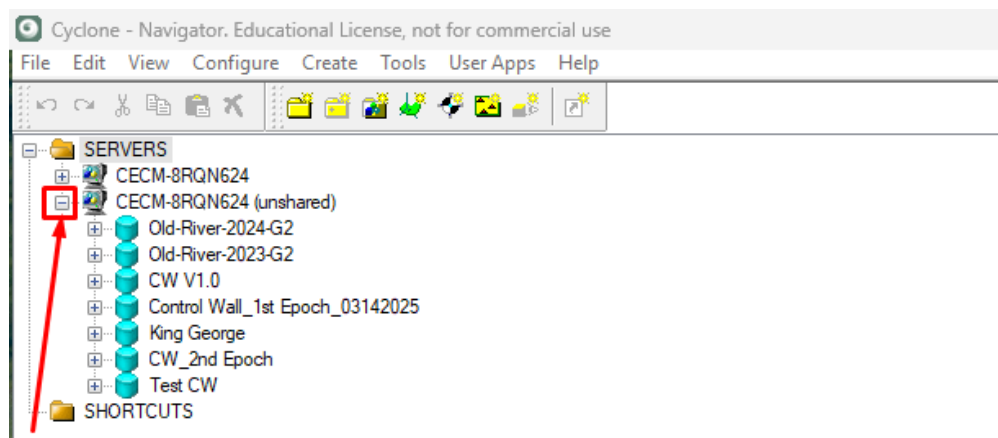
(By Shakil Ahmed, July 2025)

#### Creating a New Visual Based Registration

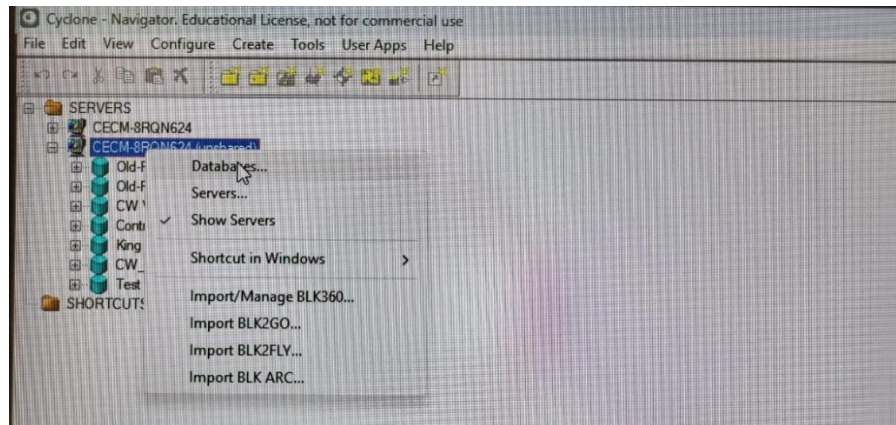
1. Launch Cyclone Core and expand the “Servers” tab by clicking the “+” sign. Figure shown below.



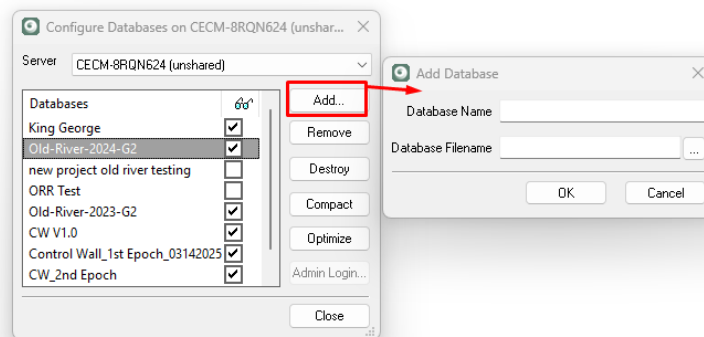
2. Expand the “(Unshared)” or your preferred folder to begin setting up your new database/project.  
See figure below.



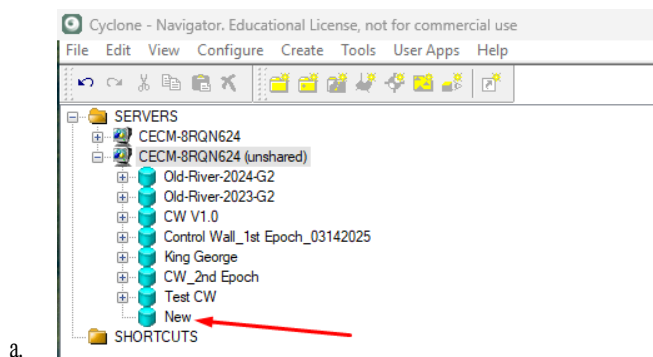
3. Left-click on “Unshared”, then right-click to bring up options and select “Database”. Figure shown below.



4. In the database window, click the “Add” button. Give the project a name and select a save location. See figure below.

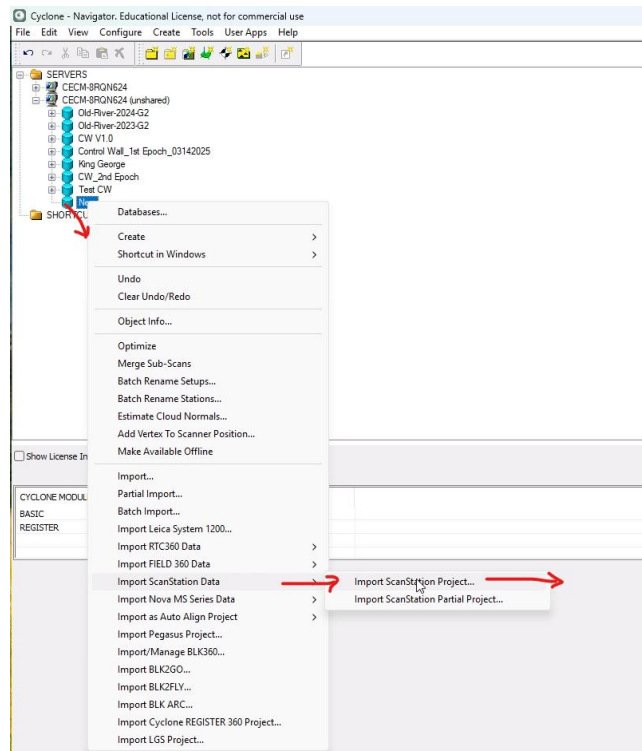


5. Your New project should now appear under the “Unshared” section. Figure shown below.

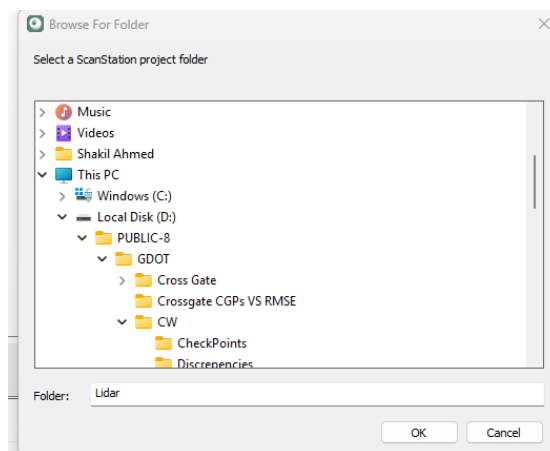


b.

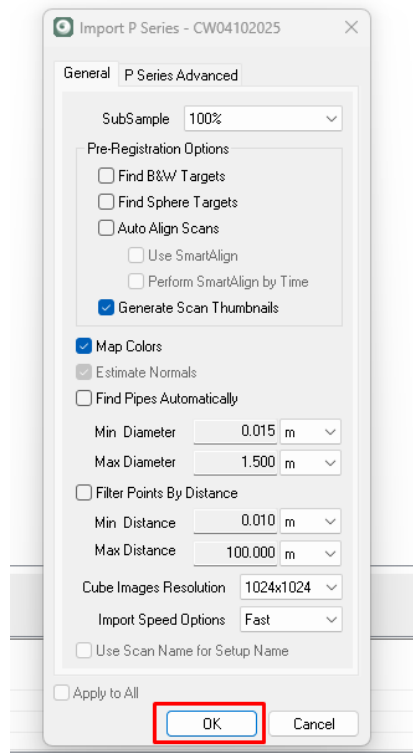
6. Right-click the new project name and choose Import ScanStation Data → Import ScanStation Project. See figure below



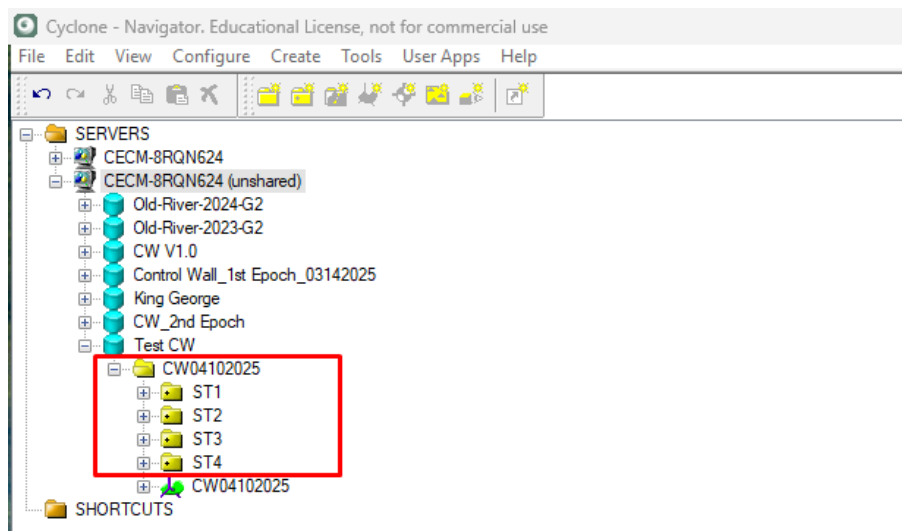
7. Browse the raw scan folder on your PC, select the files, and click **OK** to begin import. Figure shown below.



8. Adjust the import parameters to match the reference settings, then click **OK** to proceed. See figure below.



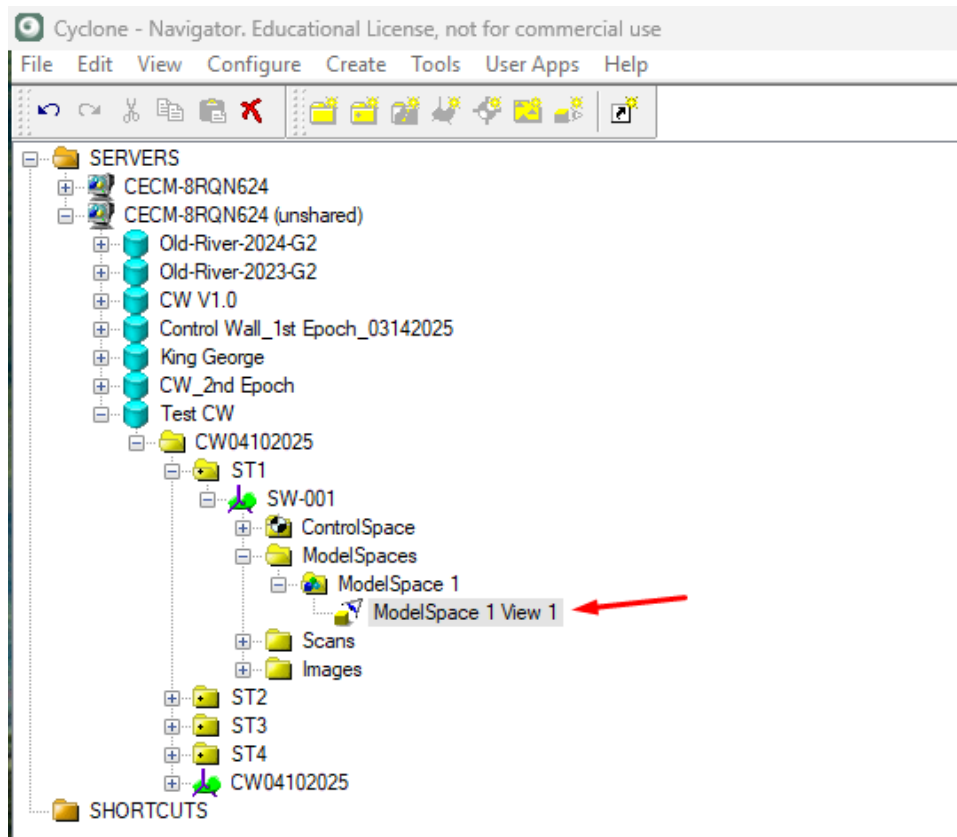
9. A progress bar will indicate the status. After completion, all scans appear under the new project. See figure below.



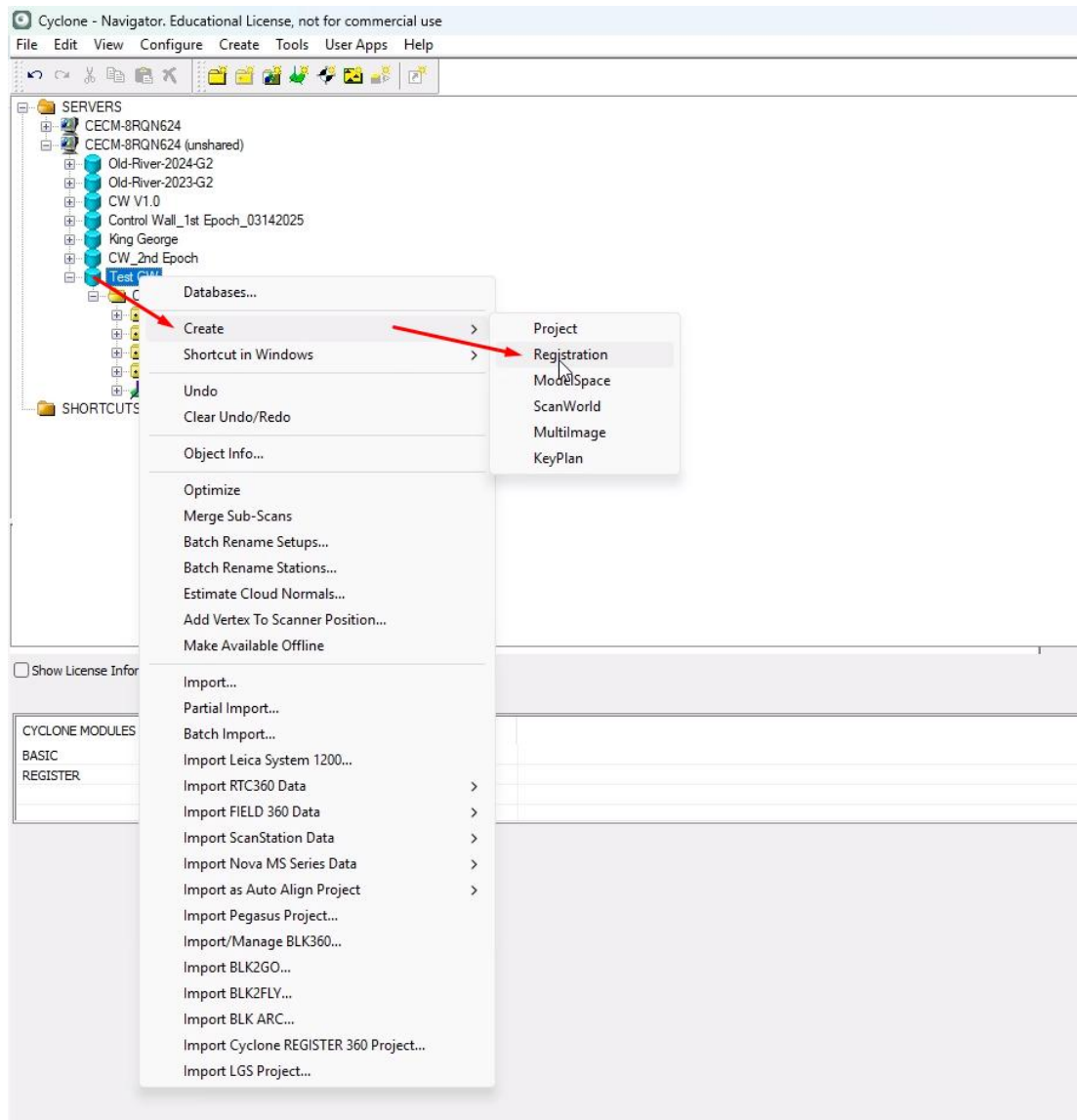


10. Expand each scan folder and double-click “ModelSpace 1 View 1” to review the scan quality.

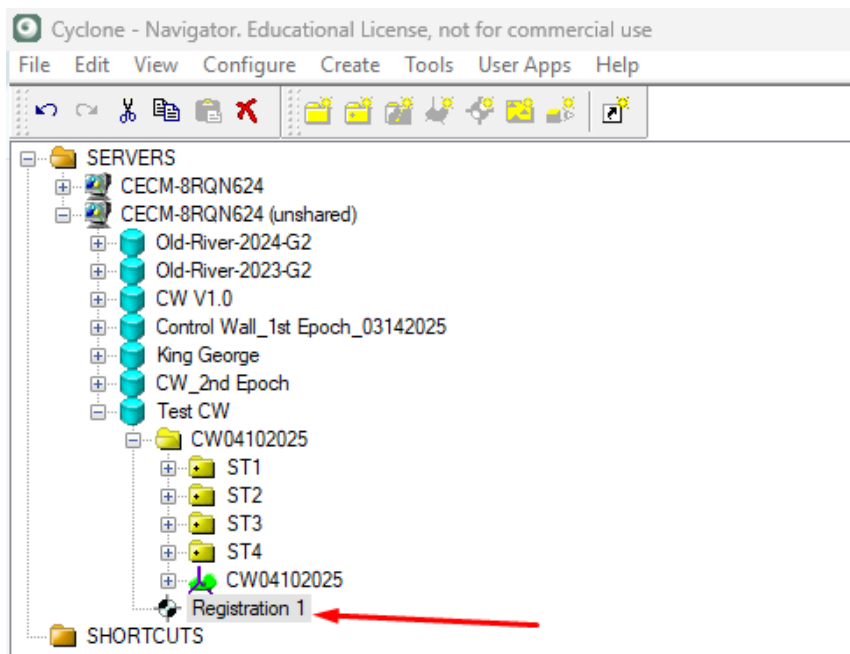
Figure shown below.



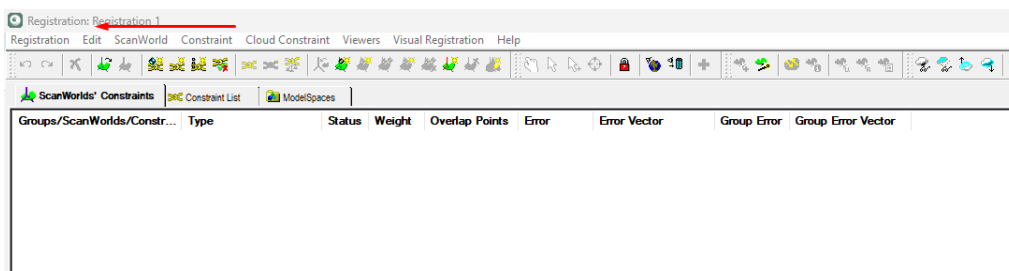
11. If all the scans are good to start the registration, select the project and right-click the project folder, choose Create → Registration to begin registration. See figure below



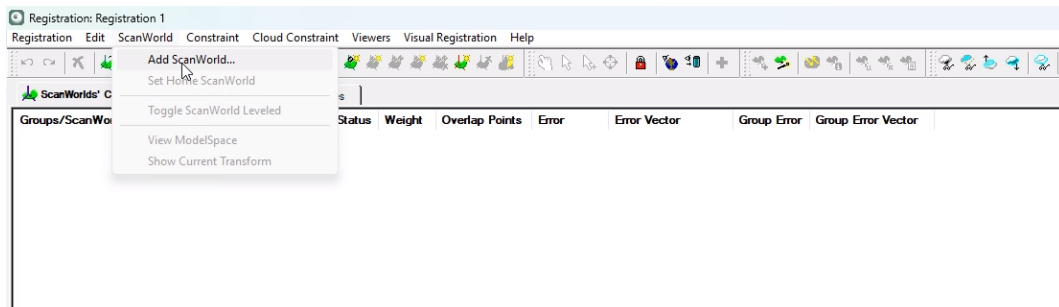
12. The new Registration 1 will be listed under the project folder. Figure shown below.



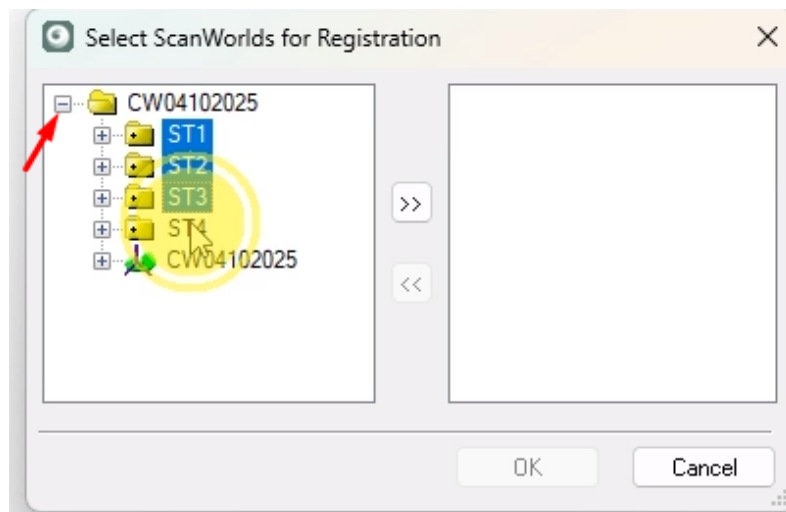
13. Double-click on the Registration 1 to open the workspace window called “Registration”. Figure shown below



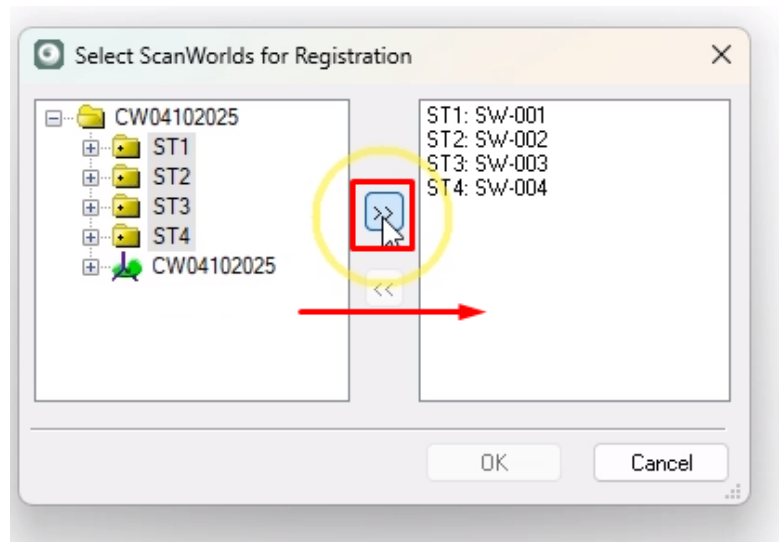
14. In the registration window, click ScanWorld → ADD ScanWorld to start adding scans. See figure below”



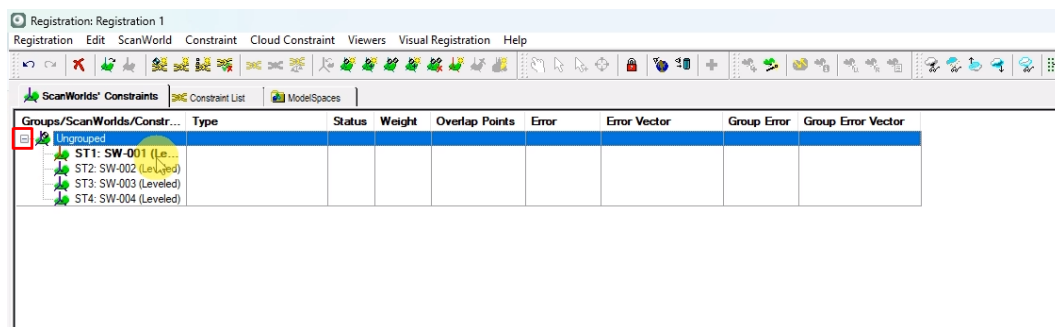
15. In the popup titled “Select ScanWorld for Registration” and expand the file “+” at left side of the window. Figure shown below



16. Select all the Scans and click on the right direction arrow to send these scans to the right side of the window. Then click ‘OK’. Figure shown below

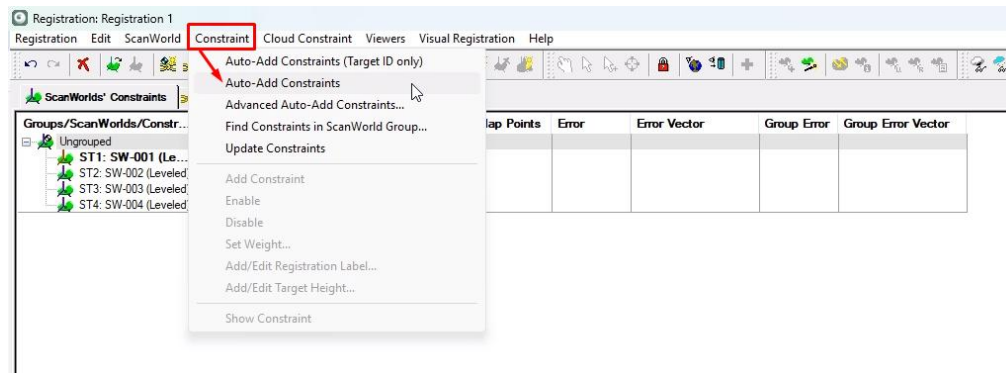


17. Now all these scans are visible in the Registration windows. Expand the “+” sign marked in red in the below figure.

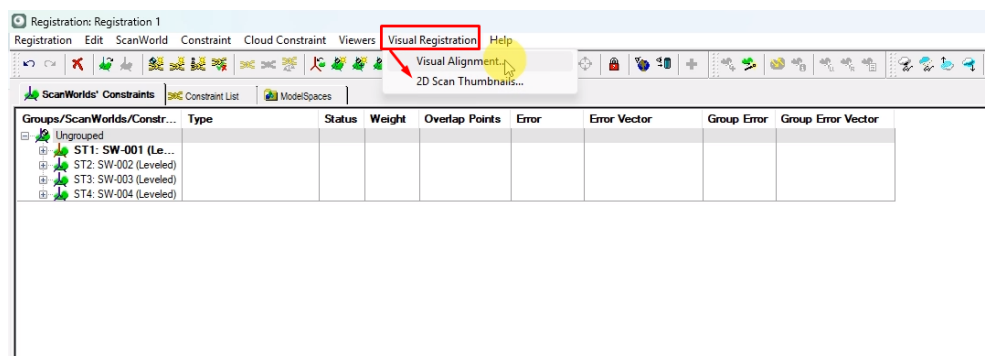


18. Click the Constraint tab and choose Auto-Add Constraints to initialize constraint relationships.

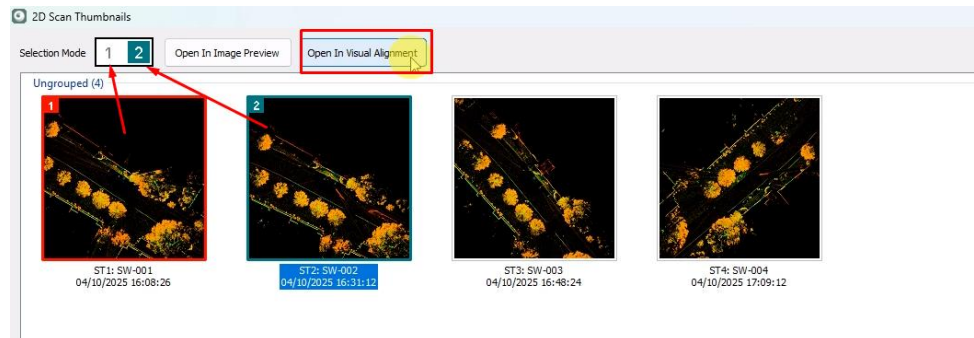
Figure shown below



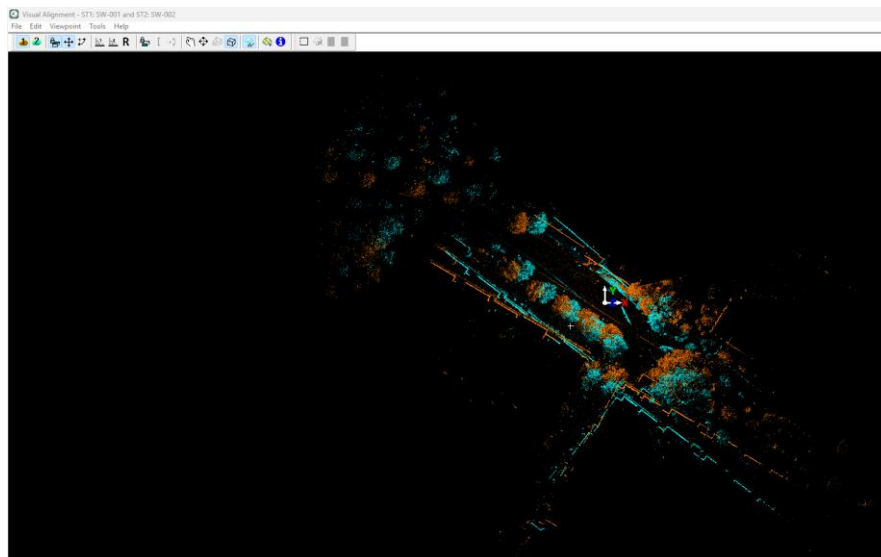
19. Now click on the “Visual Registration” option and click on the ‘2D Scan Thumbnails’. Figure shown below



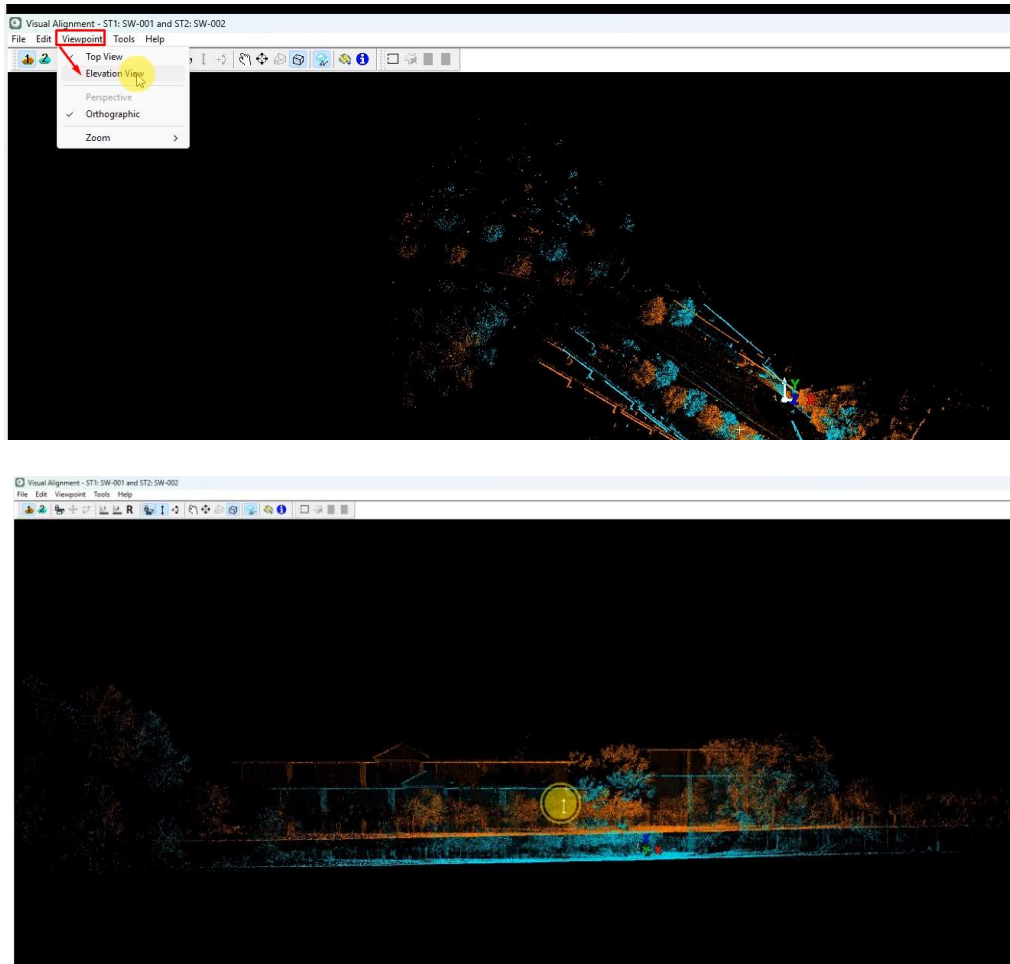
20. Now another window will open, Choose Scan 1 (red) and Scan 2 (green), maintaining a sequential loop (1–2, 2–3, etc.), and click Open in VA. See figure below”



21. The alignment window opens. Use pan and rotate tools to align Scan 1 and Scan 2 in top view.  
Figure shown below.

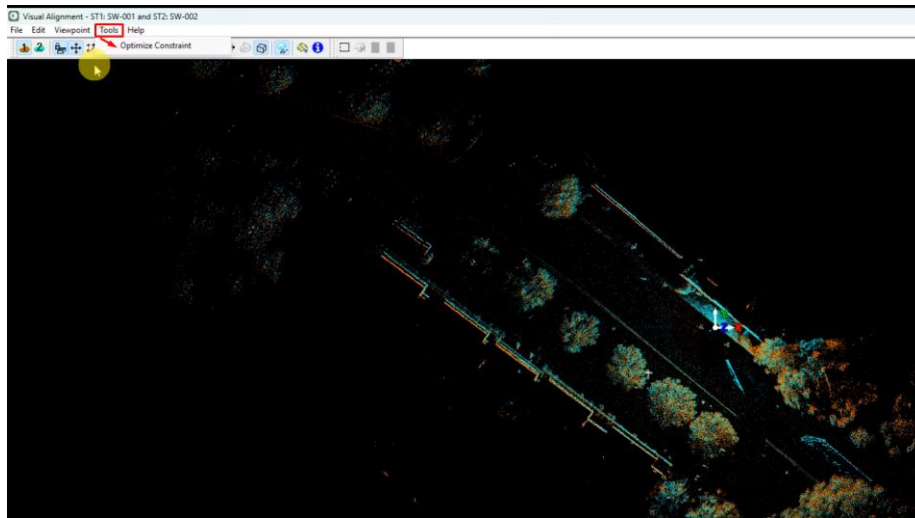


22. Navigate to the Viewpoint tab and select Elevation View to match elevation height levels. If needed, switch to Viewpoint >Top View again to refine horizontal alignment. Figures shown below.



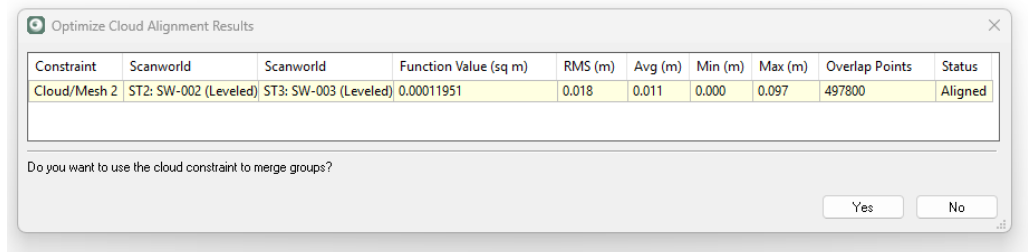


23. Click on Optimize Constraints to process and refine the visual match. Figure shown below



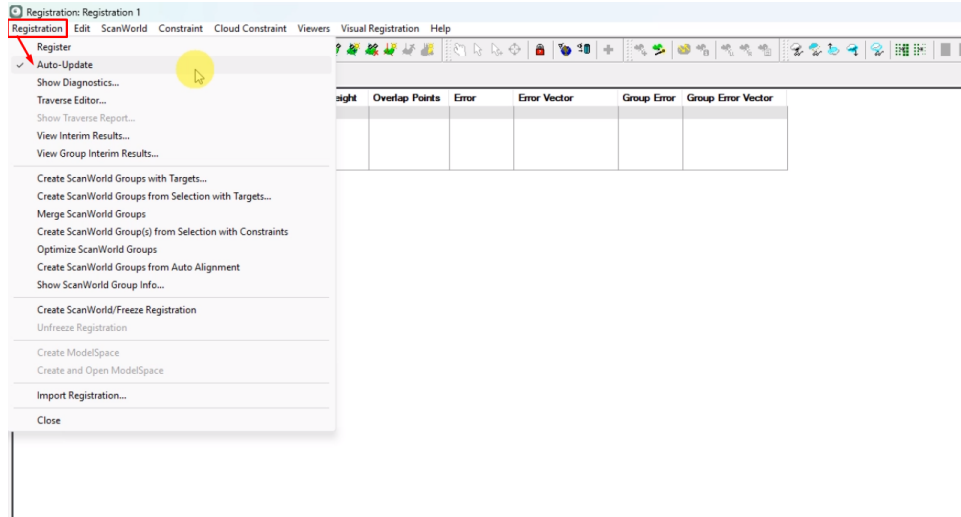
24. You will now see a result bar titled "Optimize Cloud Alignment Result" for the two recently merged scans. Aim to minimize the RMS and Avg values as much as possible. Click "Yes" to confirm and close the dialog box. Then, close the VA tab to proceed with merging and overlapping the next two scans. Refer to the figure below for guidance

c.



25. Return to the Registration window, click on "Registration" in the tab, and then select the "Auto-Update" option. Refer to the figure below for guidance

d.



26. Now, click on the "Constraints List" option. A new window will appear, as shown in the reference figure below.

The screenshot shows the 'Constraints List' window. It displays a table with the following columns: Constraint ID, ScanWorld, ScanWorld, Type, Status, Weight, Overlap Points, Error, Error Vector, Group Error, Group Error Vector, and Group. The table lists various constraints, including 'TD', 'TC', 'TE', 'TA', 'Cloud Mes', and 'Cloud Mes', with their respective details.

Constraint ID	ScanWorld	ScanWorld	Type	Status	Weight	Overlap Points	Error	Error Vector	Group Error	Group Error Vector	Group
TD	S11 SW-001	S12 SW-002	Consistent: Sphere - Sphere	On	1.0000	n/a	0.015 m	(0.014, 0.006, 0.004) m	0.207 m	(0.145, 0.016, 0.212) m	Group 1
TD	S11 SW-001	S14 SW-004	Consistent: Sphere - Sphere	On	1.0000	n/a	0.015 m	(0.024, 0.012, 0.007) m	0.484 m	(0.378, 0.213, 0.213) m	Group 1
TC	S11 SW-001	S12 SW-002	Consistent: Sphere - Sphere	On	1.0000	n/a	0.015 m	(0.014, 0.007, 0.002) m	0.427 m	(0.371, 0.024, 0.210) m	Group 1
TC	S11 SW-001	S14 SW-004	Consistent: Sphere - Sphere	On	1.0000	n/a	0.019 m	(0.016, 0.008, 0.004) m	0.779 m	(0.705, 0.222, 0.218) m	Group 1
TE	S11 SW-001	S12 SW-002	Consistent: Sphere - Sphere	On	1.0000	n/a	0.018 m	(0.000, -0.015, 0.008) m	0.351 m	(0.251, -0.127, 0.200) m	Group 1
TE	S11 SW-001	S14 SW-004	Consistent: Sphere - Sphere	On	1.0000	n/a	0.012 m	(0.002, -0.011, 0.005) m	0.362 m	(0.254, -0.127, 0.210) m	Group 1
TA	S11 SW-001	S12 SW-002	Consistent: Sphere - Sphere	On	1.0000	n/a	0.011 m	(0.001, -0.009, 0.005) m	0.576 m	(0.533, 0.002, 0.219) m	Group 1
TA	S11 SW-001	S14 SW-004	Consistent: Sphere - Sphere	On	1.0000	n/a	0.012 m	(0.005, -0.003, 0.005) m	0.362 m	(0.288, 0.064, 0.208) m	Group 1
Cloud Mes	S11 SW-001	S12 SW-002	Consistent: Sphere - Sphere	On	1.0000	n/a	0.006 m	(0.004, -0.003, 0.004) m	0.362 m	(0.288, 0.064, 0.208) m	Group 1
Cloud Mes	S11 SW-001	S14 SW-004	Consistent: Sphere - Sphere	On	1.0000	n/a	0.008 m	(0.007, -0.001, 0.005) m	0.629 m	(0.583, 0.093, 0.218) m	Group 1
Cloud Mes	S12 SW-002	S14 SW-004	Consistent: Sphere - Sphere	On	1.0000	n/a	0.009 m	(0.007, -0.003, 0.005) m	0.303 m	(0.286, 0.196, 0.000) m	Group 1
Cloud Mes	S12 SW-002	S12 SW-002	Consistent: Sphere - Sphere	On	1.0000	n/a	0.012 m	(0.009, -0.006, -0.005) m	0.002 m	(0.001, -0.001, 0.000) m	Group 1
Cloud Mes	S12 SW-002	S12 SW-002	Consistent: Sphere - Sphere	On	1.0000	n/a	0.006 m	(0.007, -0.004, -0.003) m	0.002 m	(0.001, -0.001, 0.001) m	Group 1
Cloud Mes	S12 SW-002	S12 SW-002	Consistent: Sphere - Sphere	On	1.0000	n/a	0.005 m	(0.005, 0.000, -0.004) m	0.001 m	(0.001, -0.001, 0.001) m	Group 1
Cloud Mes	S12 SW-002	S14 SW-004	Consistent: Sphere - Sphere	On	1.0000	n/a	0.004 m	(0.002, 0.002, 0.002) m	0.334 m	(0.295, 0.157, 0.010) m	Group 1
Cloud Mes	S12 SW-002	S12 SW-002	Consistent: Sphere - Sphere	On	1.0000	n/a	0.008 m	(0.005, -0.005, -0.004) m	0.001 m	(0.001, -0.001, 0.000) m	Group 1
Cloud Mes	S12 SW-002	S12 SW-002	Consistent: Sphere - Sphere	On	1.0000	n/a	0.007 m	(0.001, 0.006, -0.003) m	0.308 m	(0.280, 0.126, 0.010) m	Group 1
Cloud Mes	S12 SW-002	S12 SW-002	Consistent: Sphere - Sphere	On	1.0000	487000	0.022 m	aligned [0.018 m]	0.000 m	aligned [0.018 m]	Group 1
Cloud Mes	S12 SW-002	S12 SW-002	Consistent: Sphere - Sphere	On	1.0000	n/a	0.008 m	(0.005, -0.005, -0.004) m	0.001 m	(0.001, -0.001, 0.000) m	Group 1
Cloud Mes	S12 SW-002	S14 SW-004	Consistent: Sphere - Sphere	On	1.0000	n/a	0.004 m	(0.003, 0.002, 0.001) m	0.334 m	(0.294, 0.158, 0.009) m	Group 1
Cloud Mes	S12 SW-002	S12 SW-002	Consistent: Sphere - Sphere	On	1.0000	n/a	0.003 m	(0.003, 0.002, 0.000) m	0.307 m	(0.278, 0.136, 0.009) m	Group 1
Cloud Mes	S12 SW-002	S14 SW-004	Consistent: Sphere - Sphere	On	1.0000	n/a	0.003 m	(0.002, 0.002, 0.002) m	0.307 m	(0.332, 0.199, 0.000) m	Group 1
Cloud Mes	S12 SW-002	S14 SW-004	Consistent: Sphere - Sphere	On	1.0000	n/a	0.004 m	(0.002, 0.003, -0.002) m	0.302 m	(0.229, 0.197, 0.000) m	Group 1
Cloud Mes	S14 SW-004	S12 SW-002	Consistent: Sphere - Sphere	On	1.0000	195233	0.121 m	aligned [0.027 m]	n/a	aligned [0.027 m]	Group 1

27. In the "Error" column, identify the higher error values. Sort the values from lowest to highest.

Then, disable the entries with larger errors by right-clicking on the specific row and selecting

"Disable" under the "Status" column. Refer to the figures below for guidance.

Registration: Registration 1

Registration Edit ScanWorld Constraint Cloud Constraint Viewers Visual Registration Help

ScanWorlds Constraints Constraint List ModelSpaces

Constraint ID	ScanWorld	ScanWorld	Type	Status	Weight	Overlap Points	Error	Error Vector	Group Error	Group Error Vector	Group
TC	ST3 SW-003	ST4 SW-004	Coincident: Sphere - Sphere	On	1.0000	n/a	0.003 m	(0.002, 0.002, 0.002) m	0.387 m	(0.332, 0.199, 0.008) m	Group 1
TE	ST3 SW-003	ST4 SW-004	Coincident: Sphere - Sphere	On	1.0000	n/a	0.003 m	(0.003, 0.002, 0.000) m	0.307 m	(0.278, 0.130, 0.009) m	Group 1
TA	ST3 SW-003	ST4 SW-004	Coincident: Sphere - Sphere	On	1.0000	n/a	0.004 m	(0.003, 0.002, 0.001) m	0.334 m	(0.294, 0.158, 0.009) m	Group 1
TD	ST3 SW-003	ST4 SW-004	Coincident: Sphere - Sphere	On	1.0000	n/a	0.004 m	(0.002, 0.003, -0.002) m	0.302 m	(0.229, 0.197, 0.000) m	Group 1
TA	ST2 SW-002	ST4 SW-004	Coincident: Sphere - Sphere	On	1.0000	n/a	0.004 m	(-0.002, 0.002, -0.002) m	0.334 m	(0.295, 0.157, 0.010) m	Group 1
TE	ST2 SW-002	ST3 SW-003	Coincident: Sphere - Sphere	On	1.0000	n/a	0.006 m	(-0.002, 0.004, -0.003) m	0.002 m	(0.001, -0.001, 0.001) m	Group 1
TA	ST2 SW-002	ST3 SW-003	Coincident: Sphere - Sphere	On	1.0000	n/a	0.006 m	(-0.005, 0.000, -0.004) m	0.001 m	(0.001, -0.001, 0.001) m	Group 1
TE	ST2 SW-002	ST4 SW-004	Coincident: Sphere - Sphere	On	1.0000	n/a	0.007 m	(0.001, 0.006, -0.003) m	0.308 m	(0.280, 0.129, 0.010) m	Group 1
TD	ST2 SW-002	ST3 SW-003	Coincident: Sphere - Sphere	On	1.0000	n/a	0.008 m	(0.006, -0.005, -0.004) m	0.001 m	(0.001, -0.001, 0.000) m	Group 1
TA	ST1 SW-001	ST4 SW-004	Coincident: Sphere - Sphere	On	1.0000	n/a	0.008 m	(0.007, -0.001, 0.005) m	0.629 m	(0.583, 0.093, 0.218) m	Group 1
TC	ST2 SW-002	ST4 SW-004	Coincident: Sphere - Sphere	On	1.0000	n/a	0.009 m	(-0.007, -0.004, -0.003) m	0.388 m	(0.334, 0.198, 0.008) m	Group 1
TD	ST2 SW-002	ST4 SW-004	Coincident: Sphere - Sphere	On	1.0000	n/a	0.009 m	(0.007, -0.003, -0.005) m	0.303 m	(0.230, 0.196, 0.000) m	Group 1
TE	ST1 SW-001	ST4 SW-004	Coincident: Sphere - Sphere	On	1.0000	n/a	0.011 m	(0.001, -0.009, 0.005) m	0.576 m	(0.533, 0.002, 0.219) m	Group 1
TA	ST1 SW-001	ST2 SW-002	Coincident: Sphere - Sphere	On	1.0000	n/a	0.012 m	(0.009, -0.003, 0.007) m	0.362 m	(0.288, -0.064, 0.208) m	Group 1
TC	ST2 SW-002	ST3 SW-003	Coincident: Sphere - Sphere	On	1.0000	n/a	0.012 m	(-0.009, -0.006, -0.005) m	0.002 m	(0.001, -0.001, 0.000) m	Group 1
TE	ST1 SW-001	ST3 SW-003	Coincident: Sphere - Sphere	On	1.0000	n/a	0.012 m	(-0.002, -0.011, 0.005) m	0.353 m	(0.254, -0.127, 0.210) m	Group 1
TD	ST1 SW-001	ST4 SW-004	Coincident: Sphere - Sphere	On	1.0000	n/a	0.015 m	(0.012, 0.006, 0.002) m	0.484 m	(0.378, 0.213, 0.218) m	Group 1
TC	ST1 SW-001	ST3 SW-003	Coincident: Sphere - Sphere	On	1.0000	n/a	0.016 m	(-0.014, 0.005, 0.004) m	0.260 m	(0.149, 0.016, 0.212) m	Group 1
TC	ST1 SW-001	ST3 SW-003	Coincident: Sphere - Sphere	On	1.0000	n/a	0.016 m	(0.014, -0.007, 0.002) m	0.428 m	(0.372, 0.023, 0.210) m	Group 1
TE	ST1 SW-001	ST2 SW-002	Coincident: Sphere - Sphere	On	1.0000	n/a	0.018 m	(0.000, -0.015, 0.008) m	0.351 m	(0.253, -0.127, 0.208) m	Group 1
TC	ST1 SW-001	ST4 SW-004	Coincident: Sphere - Sphere	On	1.0000	n/a	0.019 m	(0.016, 0.009, 0.004) m	0.770 m	(0.705, 0.222, 0.218) m	Group 1
Cloud/Mes...	ST2 SW-002	ST3 SW-003	Cloud: Cloud/Mesh - Cloud...	On	1.0000	437300	0.022 m	aligned [0.018 m]	0.000 m	aligned [0.018 m]	Group 1
TD	ST1 SW-001	ST2 SW-002	Coincident: Sphere - Sphere	On	1.0000	n/a	0.023 m	(-0.019, 0.012, 0.008) m	0.259 m	(0.148, 0.017, 0.212) m	Group 1
TC	ST1 SW-001	ST2 SW-002	Coincident: Sphere - Sphere	On	1.0000	n/a	0.028 m	(0.024, 0.012, 0.007) m	0.427 m	(0.371, 0.024, 0.210) m	Group 1
Cloud/Mes...	ST4 SW-004	ST3 SW-003	Cloud: Cloud/Mesh - Cloud...	On	1.0000	189233	0.121 m	aligned [0.027 m]	n/a	aligned [0.027 m]	Group 1
Cloud/Mes...	ST1 SW-001	ST2 SW-002	Cloud: Cloud/Mesh - Cloud...	On	1.0000	84466	0.250 m	aligned [0.041 m]	0.000 m	aligned [0.041 m]	Group 1

Registration: Registration 1

Registration Edit ScanWorld Constraint Cloud Constraint Viewers Visual Registration Help

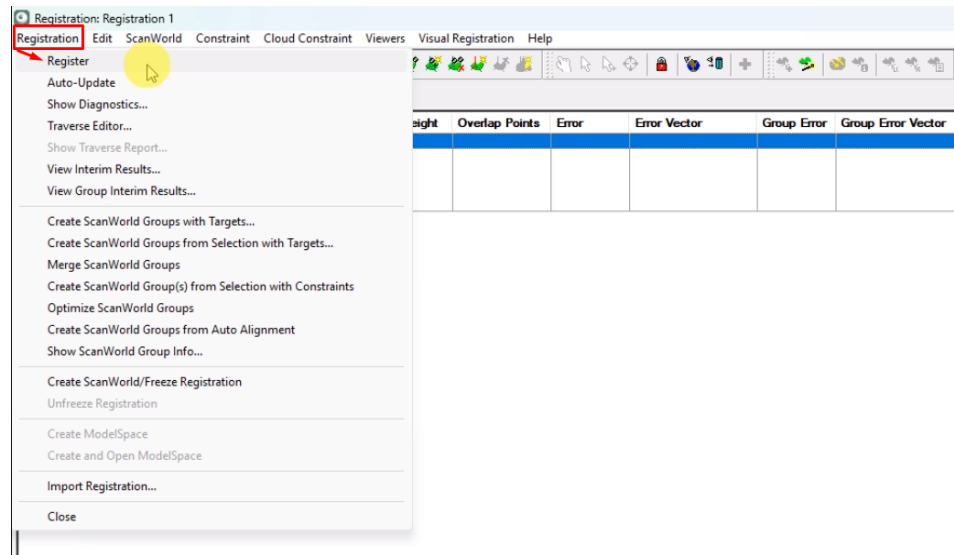
ScanWorlds Constraints Constraint List ModelSpaces

Constraint ID	ScanWorld	ScanWorld	Type	Status	Weight	Overlap Points	Error	Error Vector	Group Error	Group Error Vector	Group
TC	ST3 SW-003	ST4 SW-004	Coincident: Sphere - Sphere	On	1.0000	n/a	0.003 m	(0.002, 0.002, 0.002) m	0.387 m	(0.332, 0.199, 0.008) m	Group 1
TE	ST3 SW-003	ST4 SW-004	Coincident: Sphere - Sphere	On	1.0000	n/a	0.003 m	(0.003, 0.002, 0.000) m	0.307 m	(0.278, 0.130, 0.009) m	Group 1
TA	ST3 SW-003	ST4 SW-004	Coincident: Sphere - Sphere	On	1.0000	n/a	0.004 m	(0.003, 0.002, 0.001) m	0.334 m	(0.294, 0.158, 0.009) m	Group 1
TD	ST3 SW-003	ST4 SW-004	Coincident: Sphere - Sphere	On	1.0000	n/a	0.004 m	(0.002, 0.003, -0.002) m	0.302 m	(0.229, 0.197, 0.000) m	Group 1
TA	ST2 SW-002	ST4 SW-004	Coincident: Sphere - Sphere	On	1.0000	n/a	0.004 m	(-0.002, 0.002, -0.002) m	0.334 m	(0.295, 0.157, 0.010) m	Group 1
TE	ST2 SW-002	ST3 SW-003	Coincident: Sphere - Sphere	On	1.0000	n/a	0.006 m	(-0.002, 0.004, -0.003) m	0.002 m	(0.001, -0.001, 0.001) m	Group 1
TA	ST2 SW-002	ST3 SW-003	Coincident: Sphere - Sphere	On	1.0000	n/a	0.006 m	(-0.005, 0.000, -0.004) m	0.001 m	(0.001, -0.001, 0.001) m	Group 1
TA	ST1 SW-001	ST3 SW-003	Coincident: Sphere - Sphere	On	1.0000	n/a	0.006 m	(0.004, -0.003, 0.004) m	0.363 m	(0.289, -0.065, 0.209) m	Group 1
TE	ST2 SW-002	ST4 SW-004	Coincident: Sphere - Sphere	On	1.0000	n/a	0.007 m	(0.001, 0.006, -0.003) m	0.308 m	(0.280, 0.129, 0.010) m	Group 1
TD	ST2 SW-002	ST3 SW-003	Coincident: Sphere - Sphere	On	1.0000	n/a	0.008 m	(0.005, -0.005, -0.004) m	0.001 m	(0.001, -0.001, 0.000) m	Group 1
TA	ST1 SW-001	ST4 SW-004	Coincident: Sphere - Sphere	On	1.0000	n/a	0.009 m	(-0.007, -0.004, -0.003) m	0.388 m	(0.334, 0.198, 0.008) m	Group 1
TC	ST2 SW-002	ST4 SW-004	Coincident: Sphere - Sphere	On	1.0000	n/a	0.009 m	(0.007, -0.003, -0.005) m	0.303 m	(0.230, 0.196, 0.000) m	Group 1
TE	ST1 SW-001	ST4 SW-004	Coincident: Sphere - Sphere	On	1.0000	n/a	0.011 m	(0.001, -0.009, 0.005) m	0.576 m	(0.533, 0.002, 0.219) m	Group 1
TC	ST2 SW-002	ST3 SW-003	Coincident: Sphere - Sphere	On	1.0000	n/a	0.012 m	(0.009, -0.003, 0.007) m	0.362 m	(0.288, -0.064, 0.208) m	Group 1
TE	ST1 SW-001	ST3 SW-003	Coincident: Sphere - Sphere	On	1.0000	n/a	0.012 m	(-0.009, -0.006, -0.005) m	0.002 m	(0.001, -0.001, 0.000) m	Group 1
TD	ST1 SW-001	ST4 SW-004	Coincident: Sphere - Sphere	On	1.0000	n/a	0.015 m	(0.012, 0.006, 0.002) m	0.484 m	(0.378, 0.213, 0.218) m	Group 1
TC	ST1 SW-001	ST3 SW-003	Coincident: Sphere - Sphere	On	1.0000	n/a	0.016 m	(-0.002, -0.011, 0.005) m	0.353 m	(0.254, -0.127, 0.210) m	Group 1
TE	ST1 SW-001	ST2 SW-002	Coincident: Sphere - Sphere	On	1.0000	n/a	0.018 m	(0.000, -0.015, 0.008) m	0.351 m	(0.253, -0.127, 0.208) m	Group 1
TC	ST1 SW-001	ST4 SW-004	Coincident: Sphere - Sphere	On	1.0000	n/a	0.019 m	(0.016, 0.009, 0.004) m	0.770 m	(0.705, 0.222, 0.218) m	Group 1
Cloud/Mes...	ST2 SW-002	ST3 SW-003	Cloud: Cloud/Mesh - Cloud...	On	1.0000	437300	0.022 m	aligned [0.018 m]	0.000 m	aligned [0.018 m]	Group 1
TD	ST1 SW-001	ST2 SW-002	Coincident: Sphere - Sphere	On	1.0000	n/a	0.023 m	(-0.019, 0.012, 0.008) m	0.259 m	(0.148, 0.017, 0.212) m	Group 1
TC	ST1 SW-001	ST2 SW-002	Coincident: Sphere - Sphere	On	1.0000	n/a	0.028 m	(0.024, 0.012, 0.007) m	0.427 m	(0.371, 0.024, 0.210) m	Group 1
Cloud/Mes...	ST4 SW-004	ST3 SW-003	Cloud: Cloud/Mesh - Cloud...	On	1.0000	189233	0.121 m	aligned [0.027 m]	n/a	aligned [0.027 m]	Group 1
Cloud/Mes...	ST1 SW-001	ST2 SW-002	Cloud: Cloud/Mesh - Cloud...	On	1.0000	84466	0.250 m	aligned [0.041 m]	0.000 m	aligned [0.041 m]	Group 1

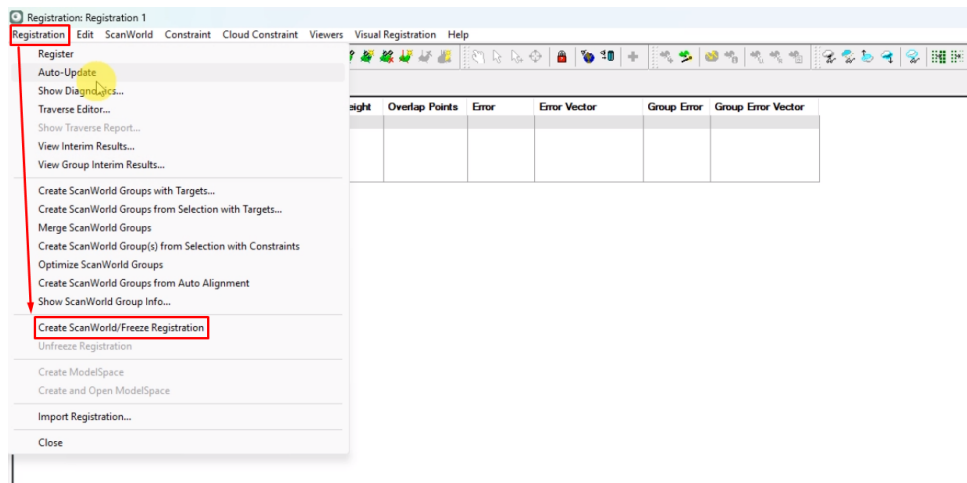
Right-click context menu:

- Register
- Show Diagnostics...
- View Interim Results...
- Create ScanWorld Groups with Targets...
- Merge ScanWorld Groups
- Create ScanWorld Groups from Auto Alignment
- Undo
- Clear Undo/Redo
- Cloud Constraint >
- Enable
- Disable**
- Set Weight...
- Add/Edit Registration Label...
- Add/Edit Target Height...
- Show Constraint
- Auto-Add Constraints (Target ID only)
- Auto-Add Constraints
- Advanced Auto-Add Constraints...
- Update Constraints
- Add ScanWorld...

28. Once you have disabled the points with larger errors, return to the Registration tab and click on the "Register" option from the list. Refer to the figure below for guidance.

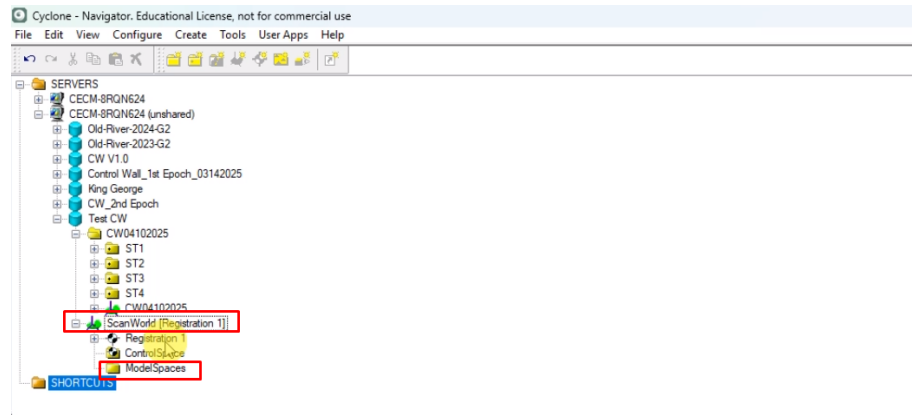


29. Now, go to the Registration tab again and click on "Create ScanWorld / Freeze Registration" to lock in the current alignment. Refer to the figure below for guidance

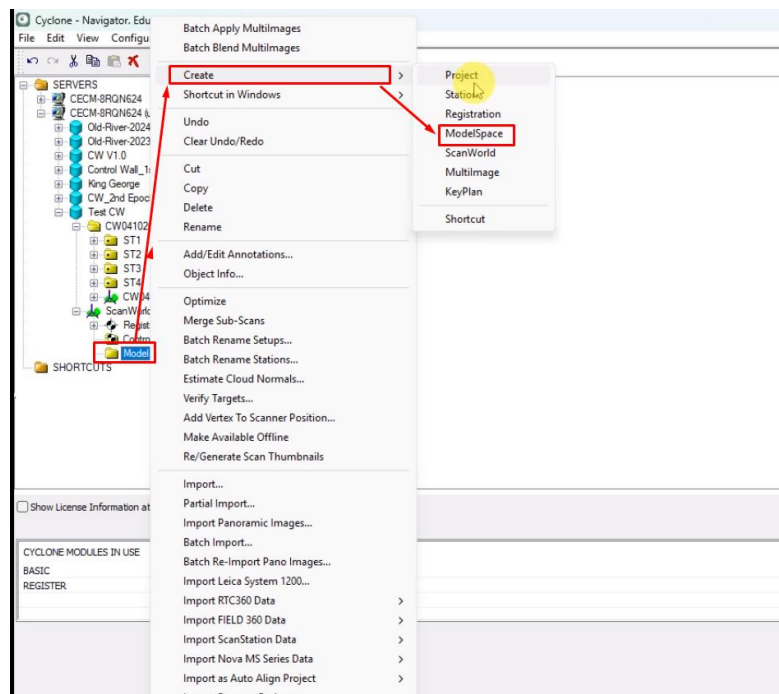


30. Close the Registration window. Navigate to the Cyclone Navigator, where your project is saved.

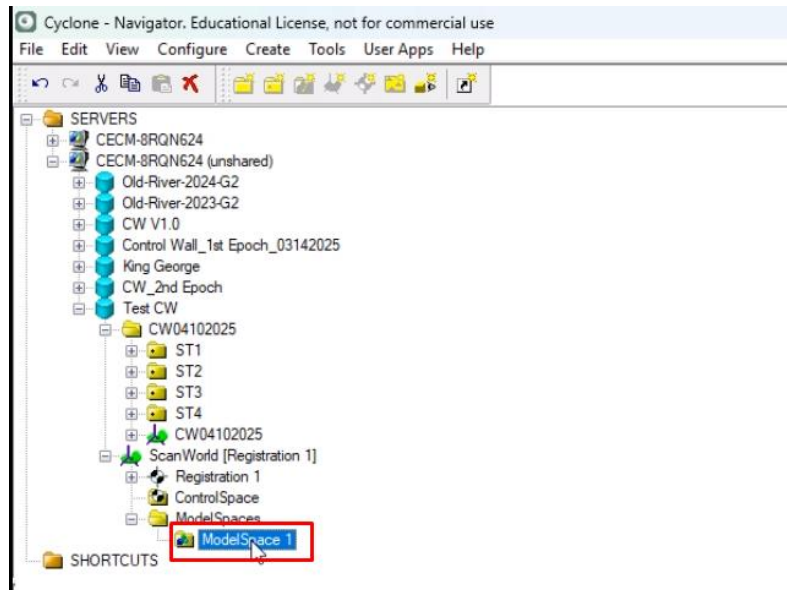
Click the “+” icon next to ScanWorld [Registration 1] to expand its contents. Then, right-click on the ModelSpaces option. Refer to the figure below for visual guidance.



31. After right-clicking on ModelSpaces, a pop-up menu will appear. Select "Create", then click on "ModelSpace" to generate a new ModelSpace.

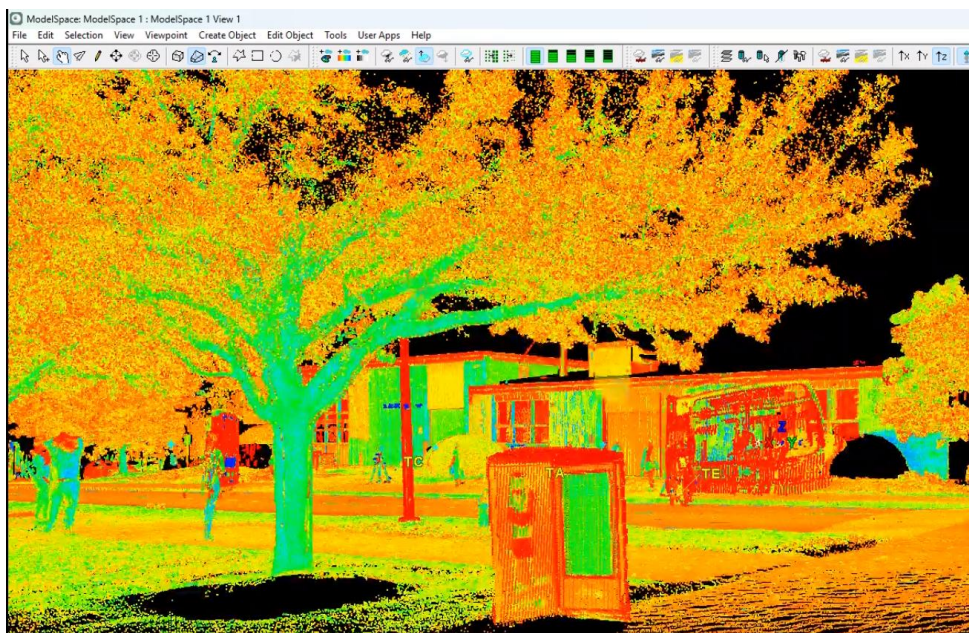
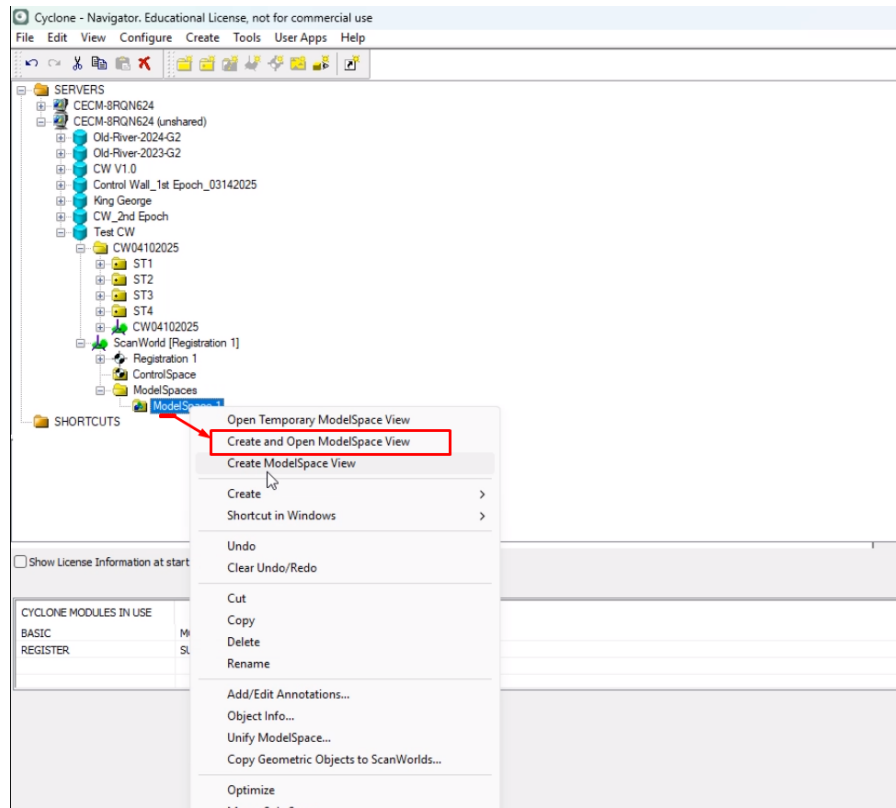


32. The ModelSpace 1 will now appear under the ModelSpaces section. Refer to the figure below for reference





33. Right-click on ModelSpace 1 and select "Create and Open ModelSpace View." This will open the fully registered LiDAR model in a new window. Refer to the figure below for reference.



To georeference the already registered full point-cloud model, use the procedure indicated in the Appendix entitled “PROTOCOL FOR GEOREFERENCING AN ALREADY COMPLETED FULL MODEL”



## **APPENDIX C4. TARGET-BASED REGISTRATION IN CYCLONE CORE**

### **TARGET-BASED REGISTRATION PROCESS IN CYCLONE 9 and CORE**

(by Sam Newsome, 2015)

- Open cyclone
- If it is the first time running under your username it will ask to run the configuration setup o
  1. This allows you to change where you save your databases etc.
  2. No changes are necessary, but you may want to make note of where the database saves
  3. Hit okay, and it will bring up the license server configuration
  4. Make sure the license server is set to the proper name. For example, in our lab that server is named: GSP1V-LICAPP001, if not change it!!!!

#### **Data importing**

- In the main cyclone screen, click the plus sign next to servers [+]
- Right click on the unshared server (the actual name will be the name of the computer you are using, in this case, our computer is CMCE2321118XR02)
- Select databases
- Select Add
  1. If you are adding a new database, simple enter the name you would like in the “Database Name” field and hit [OK]
  2. If you are importing a database, select the [...] button next to the “Database Filename” field. Select the database .imp file you need and hit [Open]

- Select the [+] next to “CMCE2321118XR02(unshared)” (your computer name will be different), and right click on the newly created database
- Under “Import ScanStation C10/P50 Data” select “Import ScanStation P50/C10 Project”
- Select the location of the RAW scanner data and select the main project folder to import all the scans
- Another window will open. Make sure that only “generate scan thumbnails,” “map colors,” and “estimate normal” is checked and hit [OK] button
- Cyclones will import raw data

### **Creating registration**

- Open your database
- Right click on the main file folder → “create” → “registration”
- Open the new registration
- Add the scanworlds to the registration by clicking “Scanworld” at top of screen → “Add ScanWorld”
- Select all the scanworlds and hit the [ >> ] button to add them. Hit [OK] when finished
- Open the “Constraint” at top of screen → “Auto-Add Constraints (Target ID only)”
- Open the “Constraint list” tab
- At the top select “Registration” → “Show Diagnostics”
- At the top select “Registration” → “Auto-Update”
- In the Constraints List tab, sort by highest error
- Start disabling targets until the desired error is achieved in the Diagnostics window

e.

1. To disable a target in the list right click on it and hit disable, the program will update the registration, and a new error will be generated in the diagnostics window
- When the registration is finished, at the top select “Registration” → “Create Scanworld/ Freeze Registration”
  - Close the registration
  - To view the registration, double click on it and select “ModelSpaces” → “Create” → “ModelSpace”
  - Double click on the newly created modelspace (usually is ModelSpace 1, but could differ if more than one has been created), select “Create and Open ModelSpace View”
  -

To georeference the already registered full point-cloud model, use the procedure indicated in the Appendix entitled “PROTOCOL FOR GEOREFERENCING AN ALREADY COMPLETED FULL MODEL”

## **APPENDIX C5. GEOREFERENCING IN CYCLONE CORE**

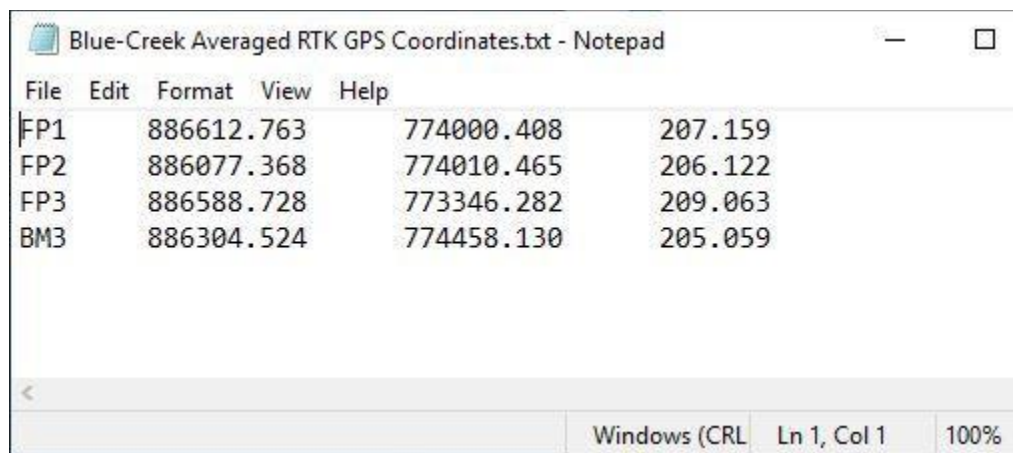
### **PROTOCOL FOR GEOREFERENCING AN ALREADY COMPLETED FULL MODEL**

#### **Georeferencing a 3D Point-Cloud Model**

(By Dr. Gustavo Maldonado, October 14, 2022)

#### **Creating a Text Document containing GPS Coordinates**

1. Open the Notepad application and create a new text document.
2. Enter the GPS coordinates of the control points, as shown in the following figure.
  - a. Enter the point identifier and its coordinates (Northing, Easting and Elevation), separating all of them in columns by using the tab button.
  - b. Column headers are NOT necessary.

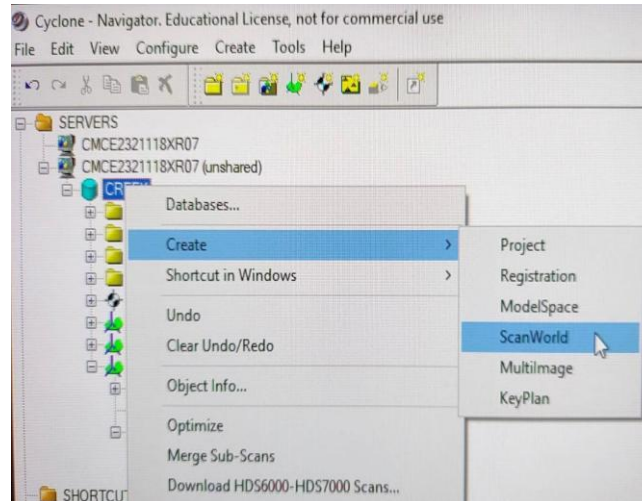


FP1	886612.763	774000.408	207.159
FP2	886077.368	774010.465	206.122
FP3	886588.728	773346.282	209.063
BM3	886304.524	774458.130	205.059

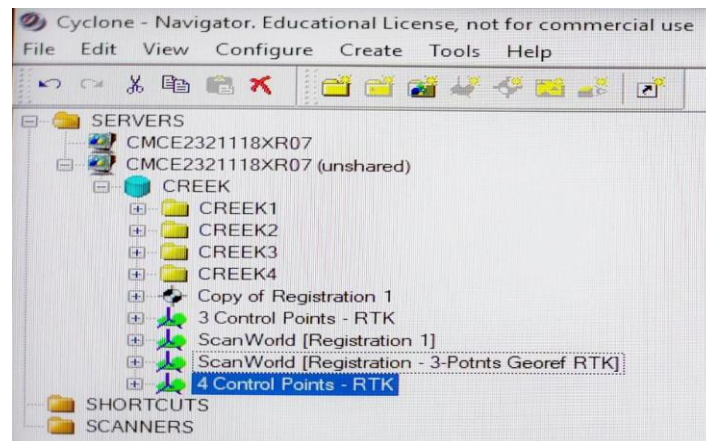
#### **Importing Control Points for Georeferencing**

1. Open the Cyclone Software.
2. Double-click on your project database, light-blue cylinder icon.

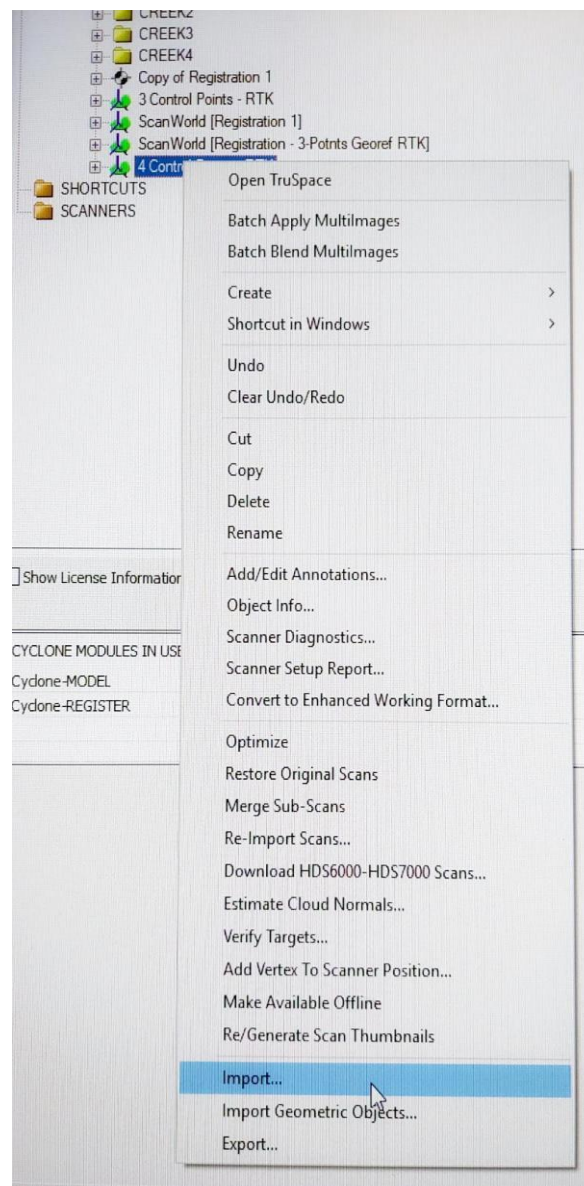
3. Right-click on your project database icon or on your main project folder, then go to “Create” and select “ScanWorld”, as shown in the following figure.



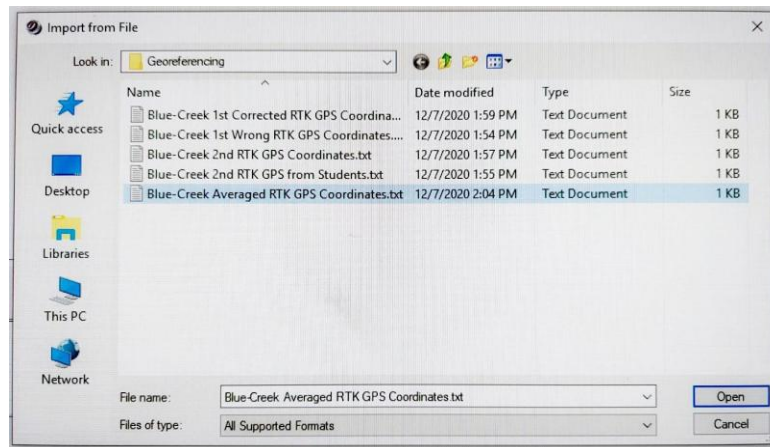
4. Rename the ScanWorld as you prefer, i.e., “4 Control Points - RTK”



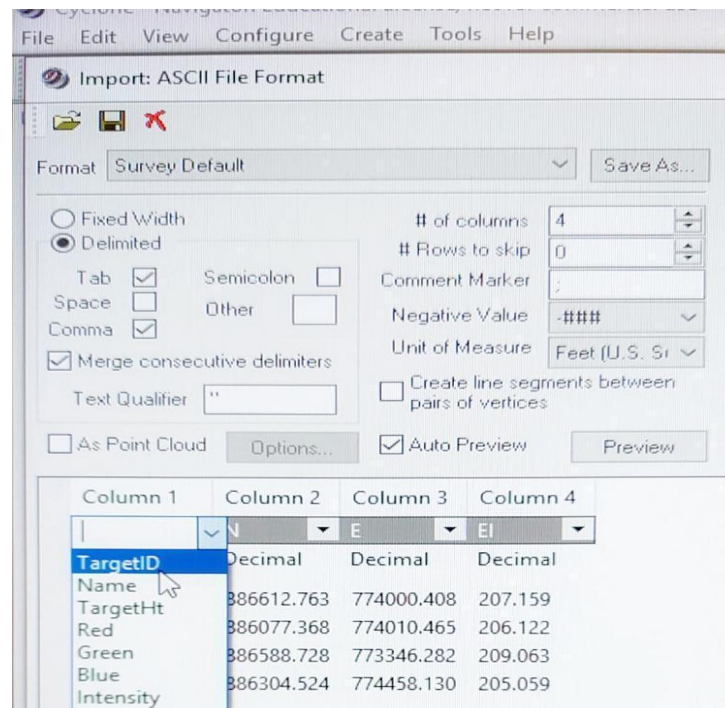
5. **IMPORTANT:** This step has changed from the previous version of Cyclone. Before, we needed to right-click on the new ScanWorld to import. However, now in Cyclone Core, we need to click on the ControlSpace of the just created ScanWorld (i.e. on ControlSpace of 4 Control Points -RTK) and select “Import”.



6. Search in your folders (fixed or portable hard disk or USB drive, etc.) and locate the created text document, containing the GPS coordinates and click on “Open”, as shown in the following figure.

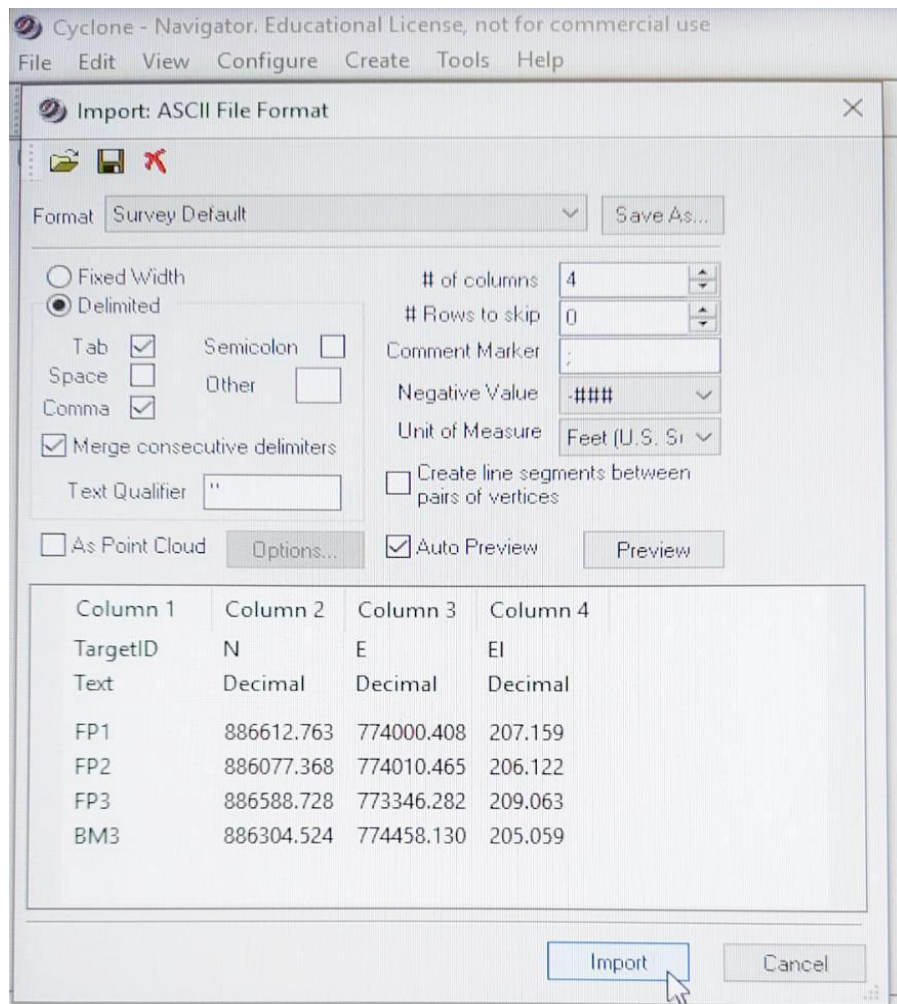


7. The “Import: ASCII File Format” window will open, as shown in the following figure

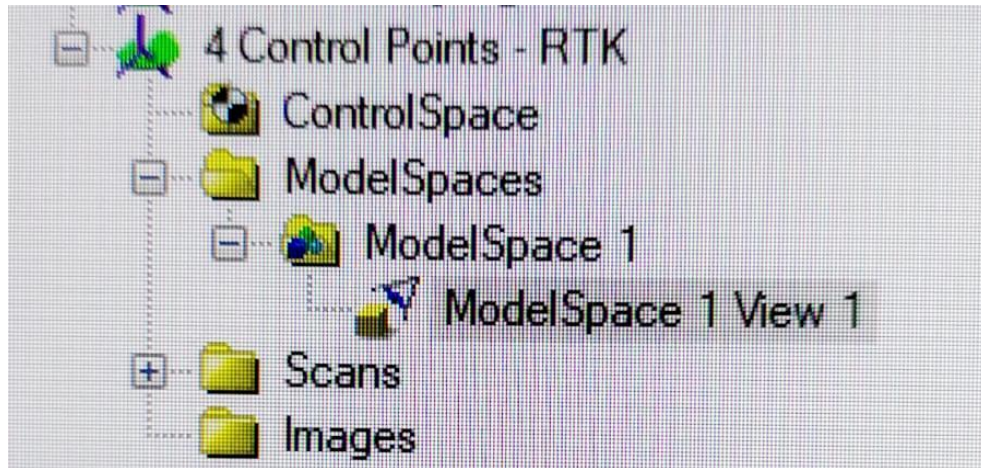


8. See the previous figure. Under the “Delimited” section, select “Tab” (and may unselect “Comma”).
9. See previous figures. Adjust the “Number of Columns” to 4 and adjust the “Unit of Measure” to US Survey Feet. If you have one header row in your text document, set the “# Rows to skip” to “1”.
10. See previous figure. Select the first row under the title of Column 1 and adjust the “Point Number” to “TargetID”. Also, check to make sure that Northing, Easting, and Elevation are set correctly under Columns 2, 3 and 4.
11. Select “Import,” when finished, as indicated in the below figure...





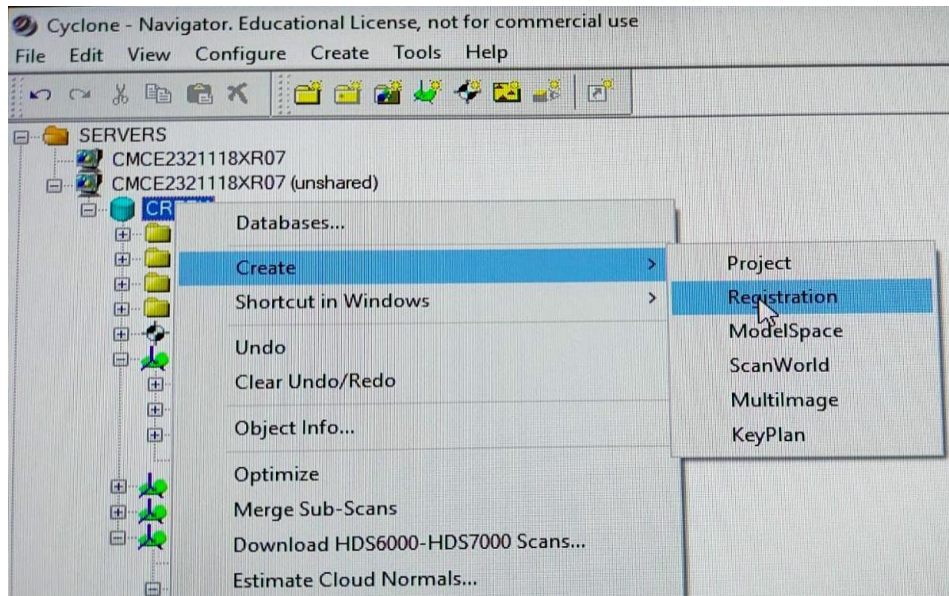
At this point, you may want to locate and click on the ModelSpace 1 View 1. There, you should be able to see the control points contained in your text file, as indicated in the following two figures:



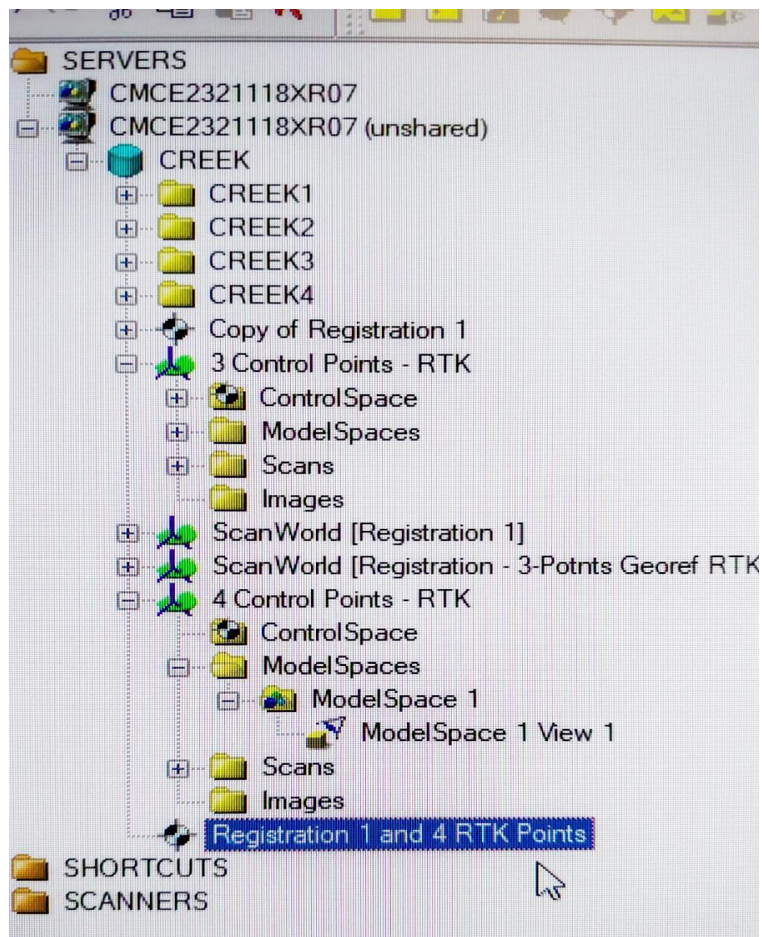
## Creating a New Registration

1. Open your database (press the + sign on the light-blue cylinder for your project).

2. Right-click on your project main database (i.e., CREEK) and go to “Create,” then select “Registration”, as seen in the following figure.

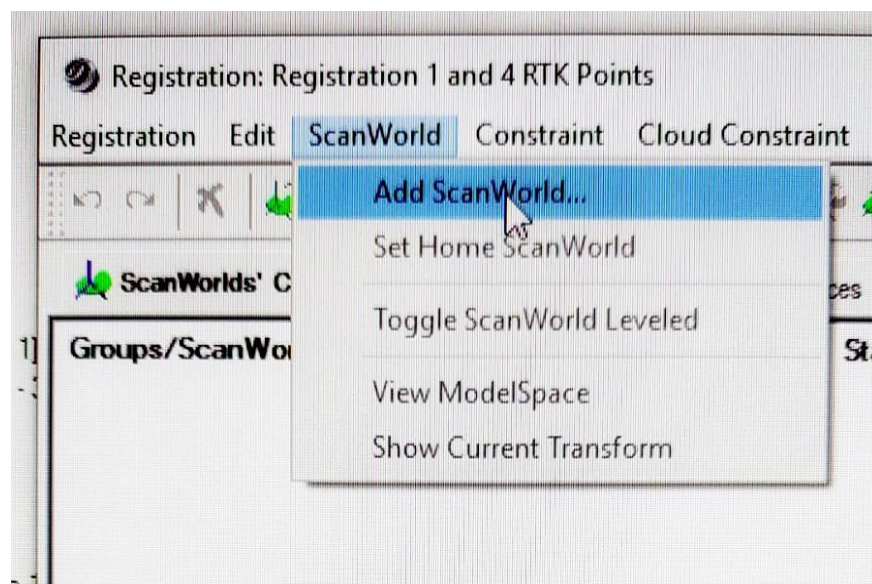


At this point, a new registration folder will be generated (should appear as Registration #). You may rename it as you prefer. In this example, it is renamed to “Registration 1 and 4 RTK Points”, as indicated in the figure on the next page.





3. Now, we need to add two ScanWorlds to this registration. For this, double-click on this new registration folder to open the corresponding registration window. This window will contain the name of the registration on top of it (in this case that name is Registration 1 and 4 RTK Points). In this window, click on the ScanWorld tab, and select Add ScanWorld, as shown in the following figure.

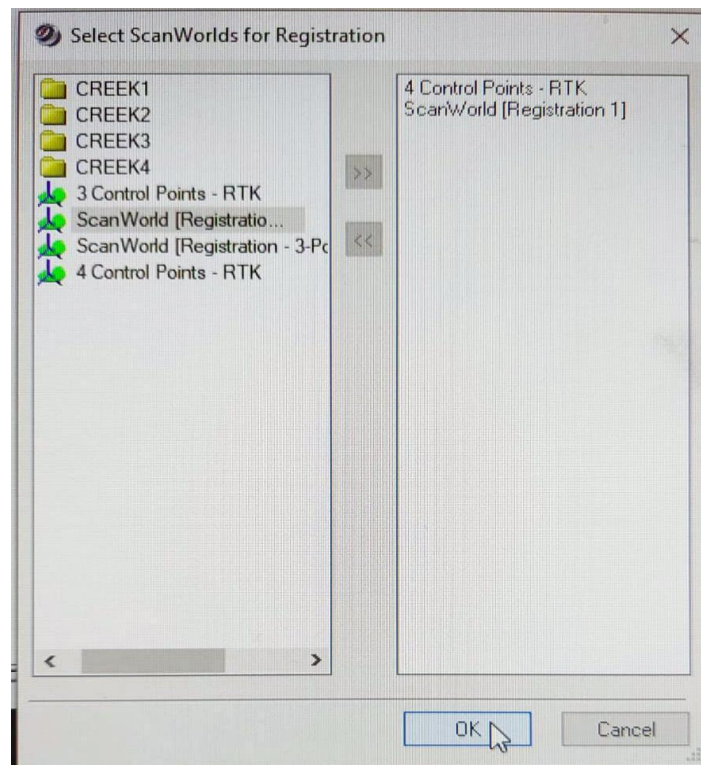


This action will open a new window (see next page) where we will indicate the two scan worlds that are to be added to this registration.

It is important that the first one to be added to the one containing the control points. In this example, that first one is the 4 Points - RTK ScanWorld. To add it, select it and then press the [ $>>$ ] button to copy it into the right-hand side panel.

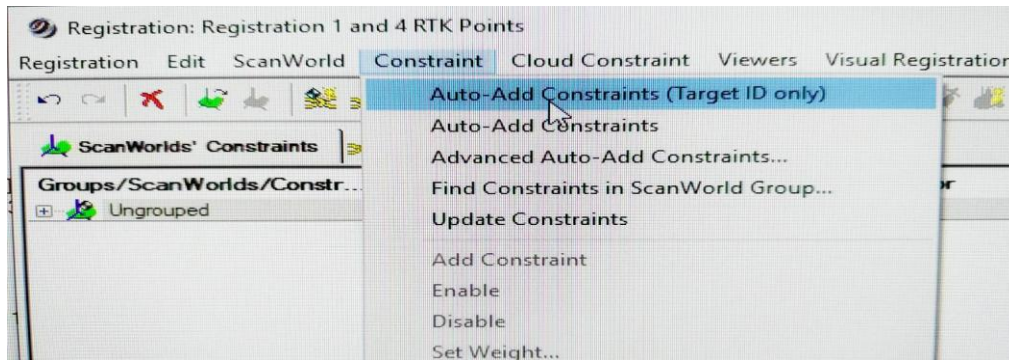
The second ScanWorld to be added is the one containing the actual full model, the one that has not been georeferenced yet. In this example, this ScanWorld is named ScanWorld [Registration 1]. Select and send it to the right-hand side panel using the [>>] button.

After these operations, the Select ScanWorlds for Registration window should look as indicated in the following figure.

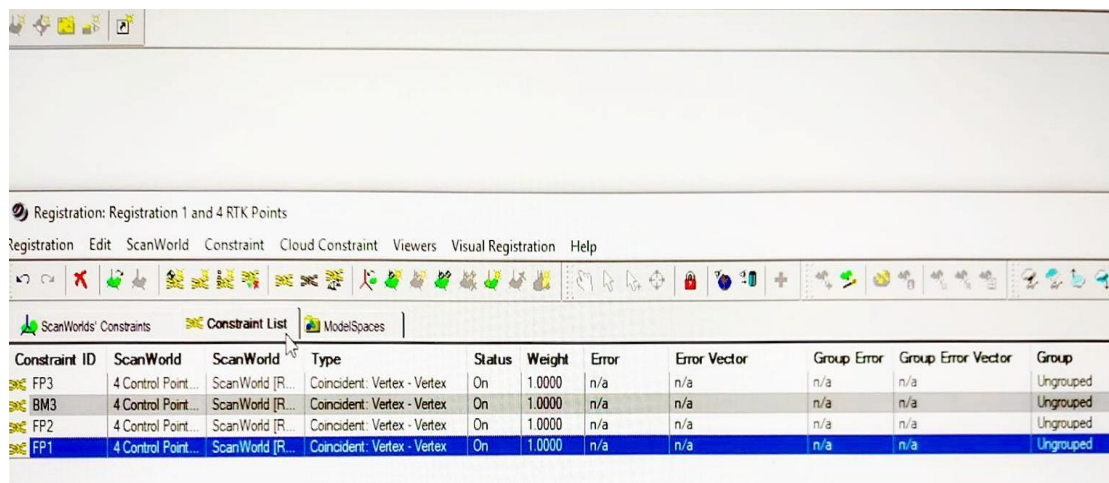


At this point, click the OK button. This will close the above window and you will see your registration window. In this example, that registration window is called Registration 1 and 4 RTK Points.

4. Open the “Constraint” tab at the top of the screen, then select “Auto-Add Constraints (Target ID only)”, as indicated in the following window.

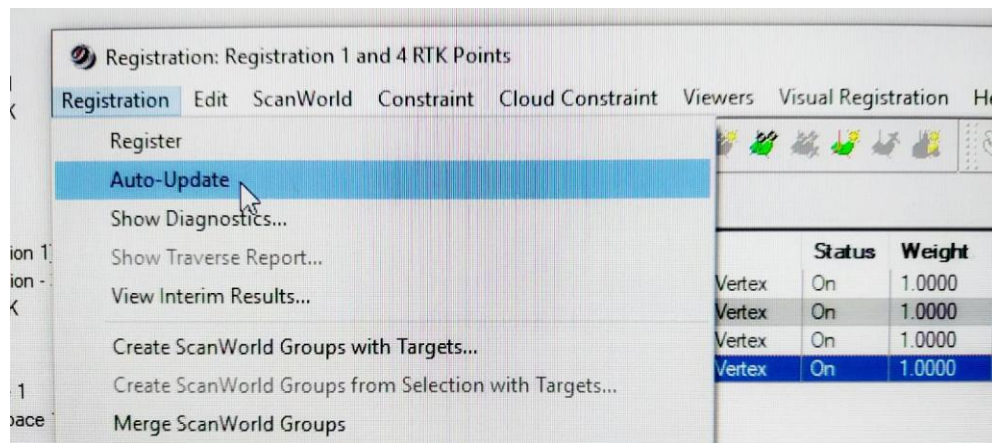


5. Open the “Constraint List” tab. This tab is indicated with the cursor in the following figure.



Most likely, at this point, you will notice that all the error columns show not applicable (n/a) entries. This is because the registration has not been completed yet. That is, the errors have not been calculated yet.

6. Open the “Registration” tab at the upper-right corner of the registration window and select “Auto-Update” (Auto-Update should be checked after any changes in the registration). See this on the following figure. After that, the error columns should be populated.



7. In the Constraints List tab, click on “Error” (see location of cursor in below figure) until the constraint list is sorted from lowest to highest error or from highest to lowest error (your preference). This is to facilitate the location of the control point producing the largest error. At this point, if you have enough control points, you may disable the ones that produce the largest error.

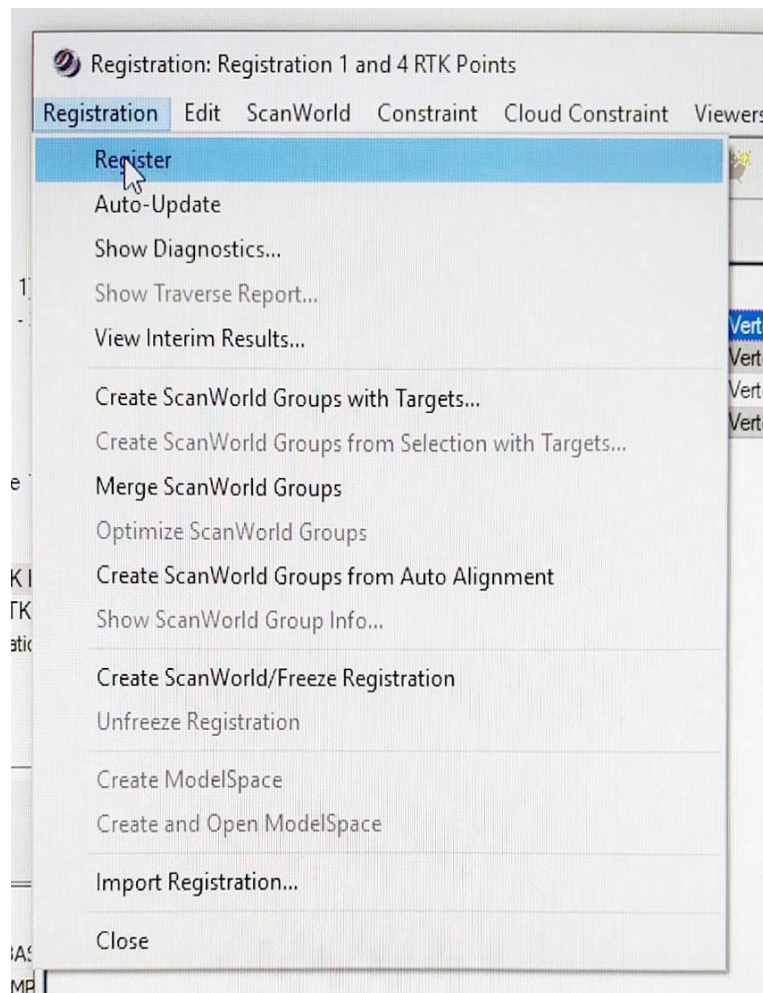
Constraint ID	ScanWorld	ScanWorld	Type	Status	Weight	Error	Error Vector	Group E
FP1	4 Control Point...	ScanWorld [R...	Coincident: Vertex - Vertex	On	1.0000	0.076 m	(0.063, 0.031, 0.028) m	n/a
BM3	4 Control Point...	ScanWorld [R...	Coincident: Vertex - Vertex	On	1.0000	0.095 m	(0.002, -0.095, 0.009) m	n/a
FP2	4 Control Point...	ScanWorld [R...	Coincident: Vertex - Vertex	On	1.0000	0.103 m	(0.053, 0.089, 0.007) m	n/a
FP3	4 Control Point...	ScanWorld [R...	Coincident: Vertex - Vertex	On	1.0000	0.128 m	(-0.118, -0.025, -0.044) m	n/a



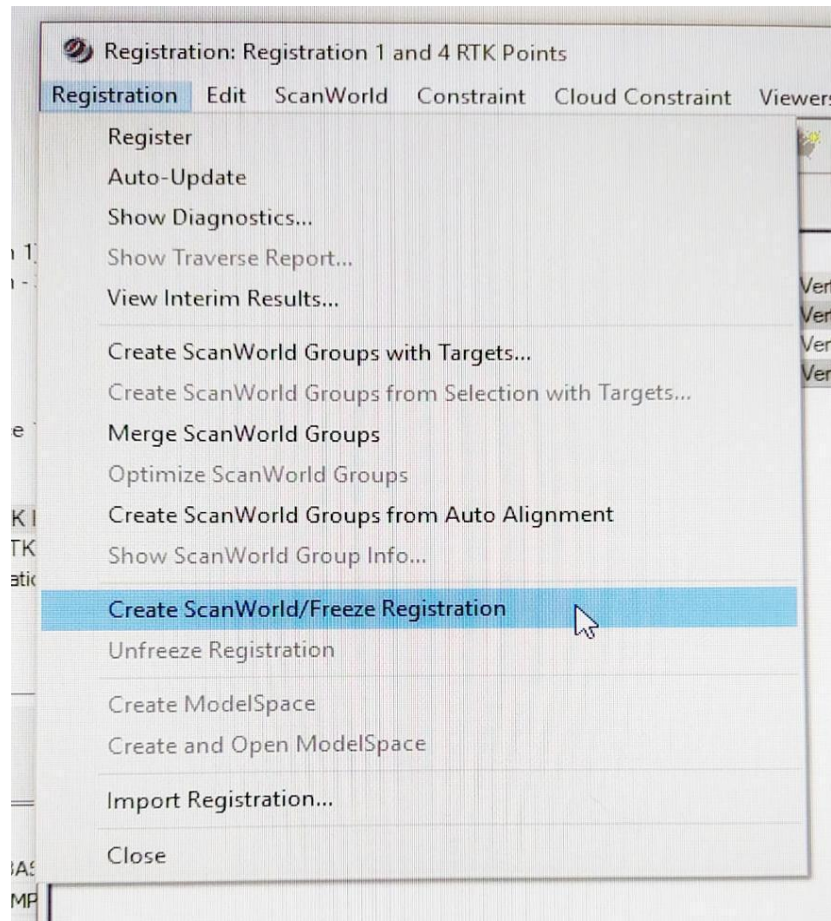
8. To disable control points (targets) containing high errors, right click on the corresponding row and select “Disable”. The program will update automatically and generate new errors for each control point (see the following figure). Do this, if you have enough targets, until you have reached the desired maximum error limit (usually 0.010 meters, which is not the case in our current example).

## Completing the Registration

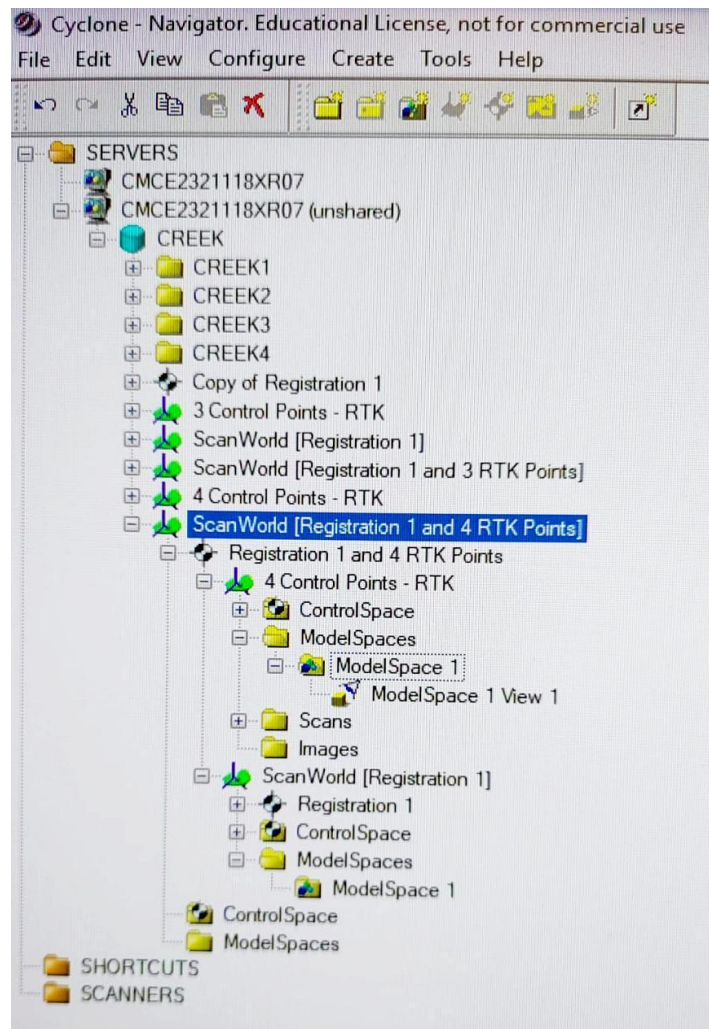
Click on the registration tab (upper right corner of the registration window) and select “Register”, as indicated in the following figure.



Then, open the same pull-down menu and select “Create ScanWorld/Freeze Registration”, as indicated in the below figure.

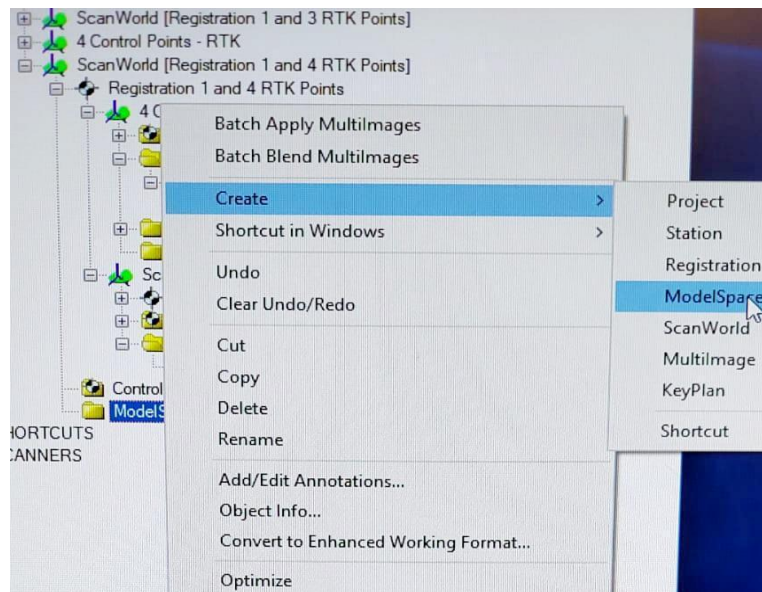


At this point, the registration should be completed. Close the registration window. You should notice that a new ScanWorld folder has been generated for this new registration. In this example it is named “ScanWorld [Registration 1 and 4 RTK Points]”. If you open all the subfolders in that ScanWorld, you should see the branches shown in the below figure.



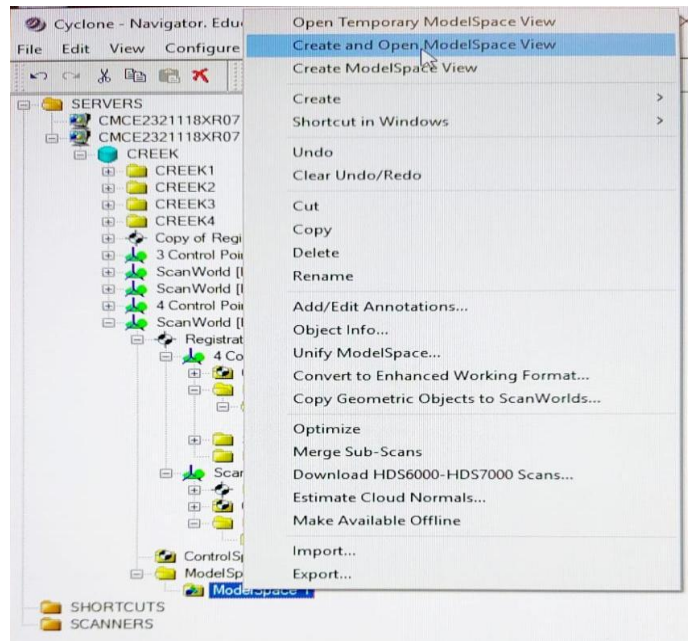
## Creating a ModelSpace for the New Registration

1. In the main screen, after opening the new ScanWorld folder (in this case, ScanWorld [Registration 1 and 4 RTK Points], right-click on “ModelSpaces” folder (at bottom) and select “Create,” then select “ModelSpace”, as shown in the following figure.

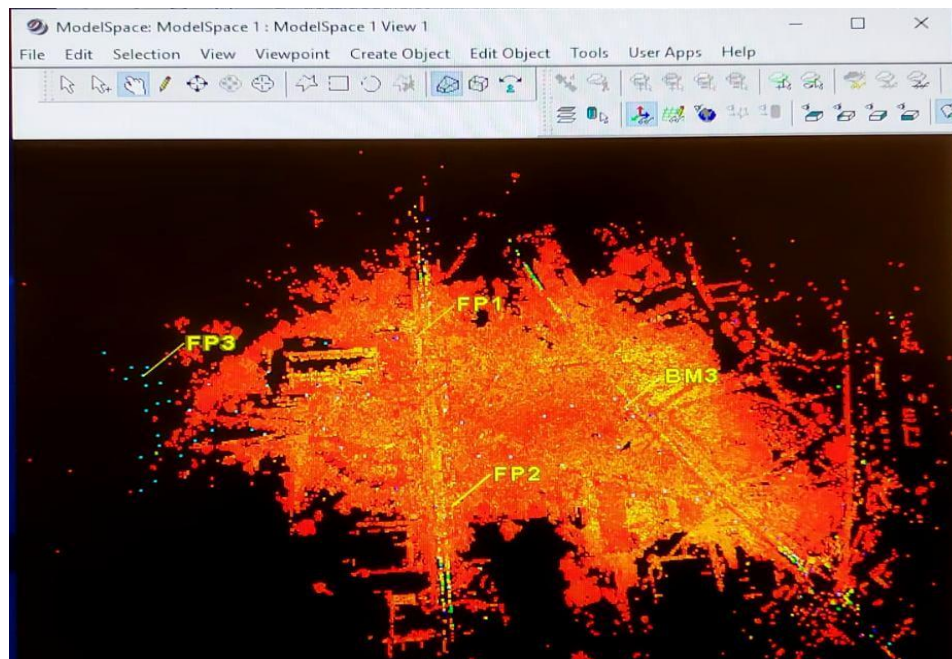


2. Double-click on the newly created modelspace (in this case, ModelSpace 1), then select “Create and Open ModelSpace View”, as seen in the following figure.





This will open a View window of the registered ModelSpace. In this example, the name of this window is ModelSpace1 View1, as seen in the below figure.

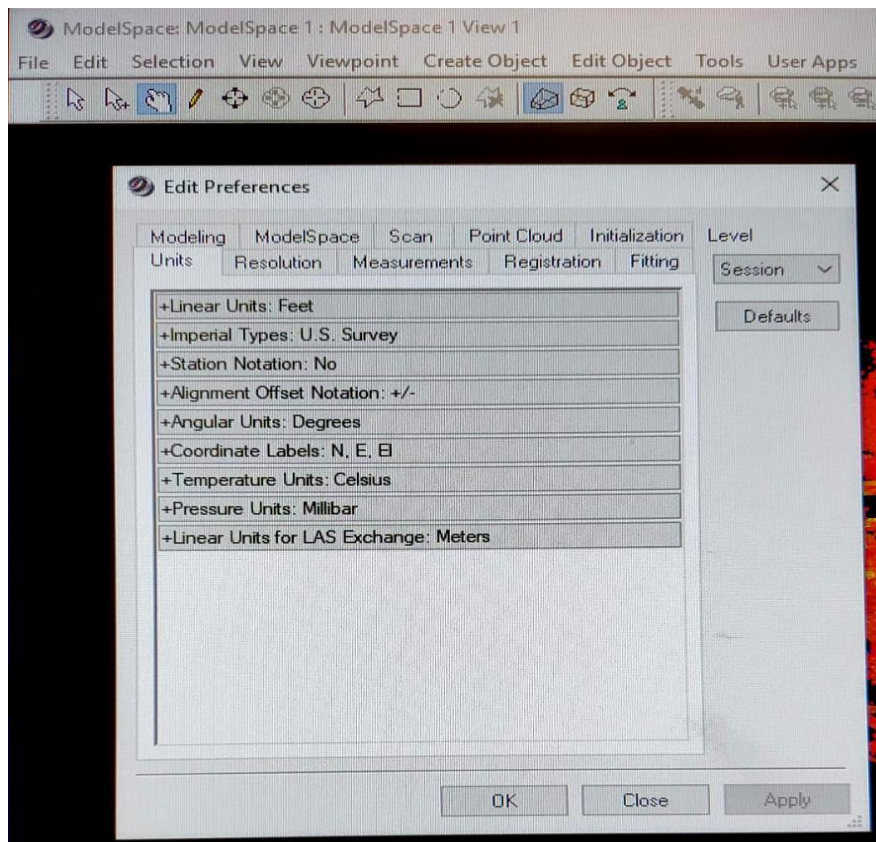


The above window shows the final registered model.

The following page indicates how to select some useful parameters, such as the length unit and the preferred names for the coordinates.

## Selecting Units of Length and COORDINATES

In the main View screen, select the “Edit” tab and then, in the pull-down menu select “Preferences”. This will open the window shown in the below figure. In that window select the “Units” tab and select your “Linear Units” (Feet), “Imperial Types” (U.S. Survey), and “Coordinate Labels” (N, E, El), as shown in the below figure (or other preferences).





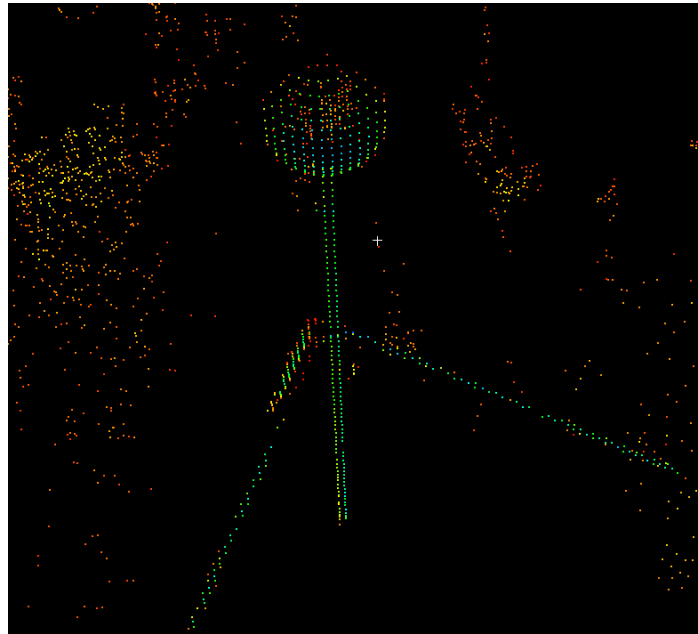


## APPENDIX C6. ACQUIRE TARGETS FROM SOFTWARE (CYCLONE CORE)

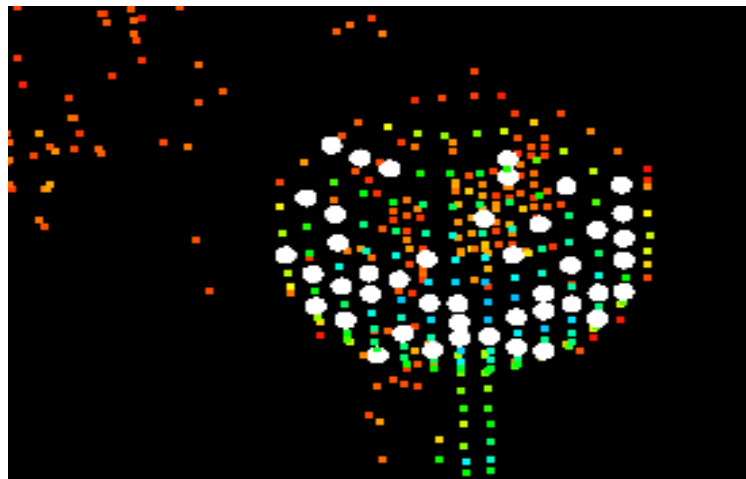
### HOW TO ACQUIRE TARGETS FROM SOFTWARE (CYCLONE CORE)

(By Md. Mehrab Hossain, 2024)

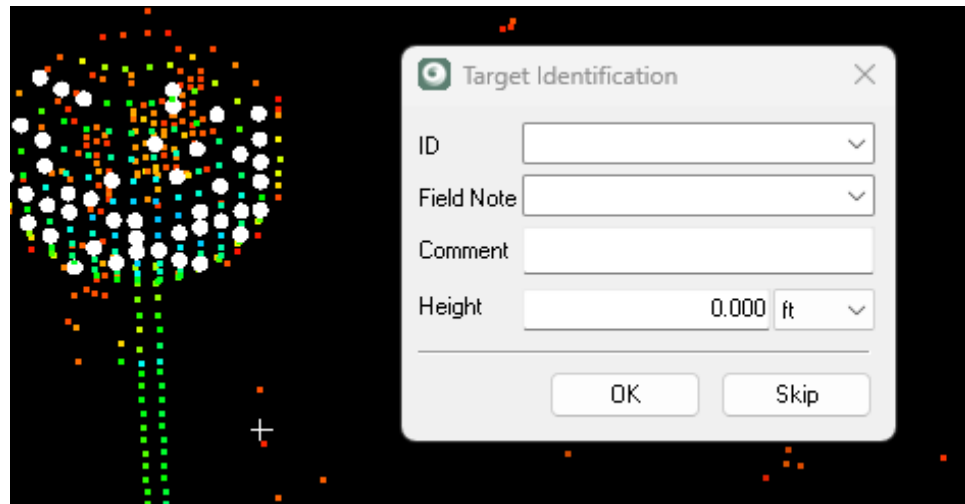
- When you open your cyclone core with the view of the individual scan in model space, you will see the target as like as below figure. Remember, you must scan the targets in the fields otherwise you cannot see them.



- Then, select “***Multi-pick Mode***” and then click points inside the circular portion of targets that were scanned by scanner during the scanning. Click as many points as possible to cover the area of the circle as shown below.



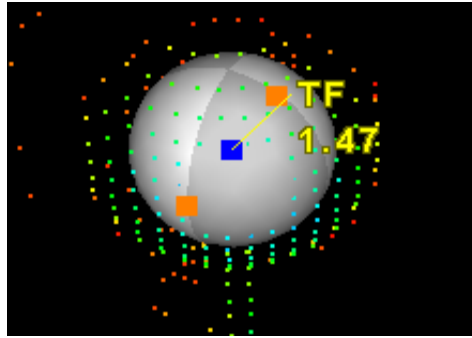
- Then, right click inside the circle and select *“Fit to Cloud”* and then select *“Sphere Targets”* if you used sphere targets in the fields. You may choose any other targets, but you must make sure the targets you are choosing here must be applied in the field too. When you click the sphere targets (in this case), you will see the following window. You can set all the information such as *Target ID*, any notes and comments and importantly the *Height* of the targets. In our case the Height was 1.470 m and Target ID name was TF. Then click *OK*.



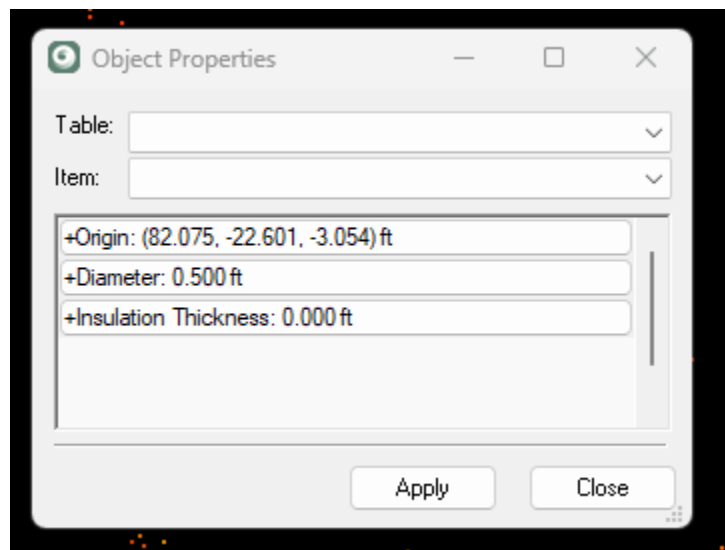
- When you click the *OK*, you will see the following window. In this window, you need to check mark the *“Apply to all related ControlSpaces”*. And then click on *Add*.



- Then you will see that the target is automatically generated in the software as shown below.



- The diameter of the sphere is defined by the software automatically. You need to adjust the diameter according to your requirements.
- If you need to adjust the properties of the sphere especially to change the diameter of the sphere, you can right click, and you will see “*Edit Properties*” option. Click on this option and you will see the following window.



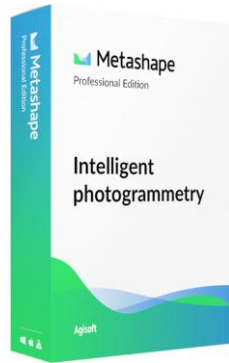
- Now, adjust the diameters according to the specification. And then click on “*Apply*”. You may change other properties too by clicking the right button and choose your desired options.

## APPENDIX C7. METASHAPE PROTOCOL

### METASHAPE PROTOCOL

#### Agisoft Metashape Professional (2.1.0 Build)

(By Md. Mehrab Hossain, and Dr. Gustavo Maldonado, 2024)



#### Example

This protocol was developed following a real-world example. It consisted of 265 pictures (ranging from 5.7 MB to 10.6 MB) of a roundabout at the South Statesboro Campus of GSU. The employed computer is a Lenovo ThinkStation P500 with an Intel Xeon CPU ES-1650 v3 @ 3.5GHz, 6 cores, 12 logical, and with 32 GB of Random Access Memory (RAM). Note that the Metashape Manual will be herein referred to as MM.

#### Generate a Close-Range Photogrammetric Model

##### 1. Save the file

- a. Open Agisoft Metashape Professional (64 bit)
- b. Go to File and select Save. This is to name and save the project as soon as we start, even before loading pics.
- c. Enter the filename and save the project.

## **2. Add Photos**

- a. Go to the Workflow tab in the toolbar and select Add Photos
- b. Select the pictures and click Open.
- c. All the selected photos will be grouped under one chunk. If more than one chunk is created, this process must be repeated for each chunk individually. Generally, to avoid stitching issues, one chunk is preferred. However, in large projects, it is advised to use several chunks.
- d. The chunk will be displayed in the workspace as seen in Figure 1. To see the info on Cameras and Aligned cameras click on Chunk 1 (265 images). In this case we are considering 265 pictures.

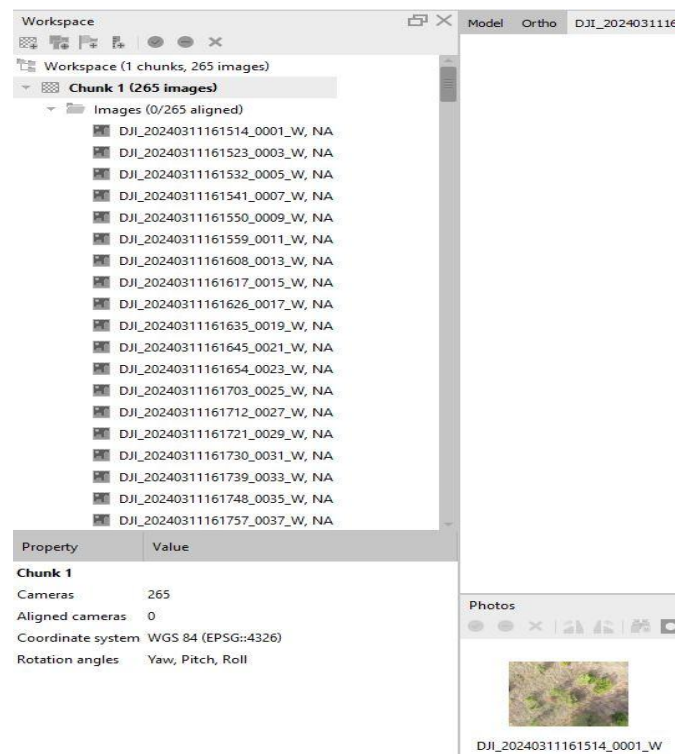


Figure 1: Workspace view

When processing drone-captured images (GPS/RTK enabled in camera images), GPS/RTK metadata may incorrectly assign identical camera positions, causing the model to appear improperly scaled or projected. Since Metashape does not require geotags for accurate alignment, the solution involves removing or disabling the geographic coordinates from the images.

Before going to the steps “Align Photos”, the following instructions must be followed:

To exclude the use of the image geotags for model referencing, perform the following:

- Uncheck all cameras in the Reference pane (or just clear them).
- Switch to local coordinates (or proper coordinate system that you will be using for the marker coordinates) option in the *Reference pane setting dialog*.
- Right-click on the *chunk's label* in the *Workspace plane* and choose the “Reset Transform” option from the context menu.

Now these images are without geo tags and ready to proceed to the next step accordingly.

### **3. Align Photos**

This procedure may be fast, or it may take a relatively long time. This depends on the number of images and on the data regarding the accuracy of the estimated location of the camera at the instant it took each picture.

- a. Go to Workflow and Select Align Photos. At that point the window shown in Figure 2 will pop up. Then, in that window, select appropriate parameters for this task. A brief explanation of those parameters is included in the below points.

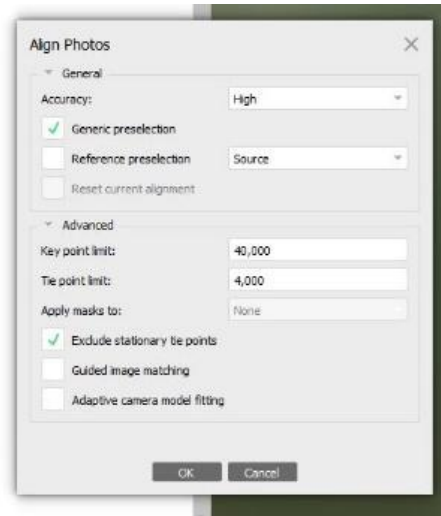


Figure 2: Parameter Selection in the Aling Photos window

- b. **Accuracy:** Select it from Highest/High/Medium/Low/Lowest. This setting affects the alignment time. The higher the accuracy setting, the more processing time. According to the MM, the Highest setting upscales are the original photos by a factor of 4 (2 times per side). This setting is good to accurately localize the tie points (points used to stitch the pictures). However, the Highest setting is only recommended for very sharp images and mostly for research purposes. This is because its processing requires considerable time. The High setting uses images with their original size. The Medium option uses downscaled images by a factor of 4 (2 times per side). The Low option downscales the pictures by a factor of 16 (4 times per side). The Lowest option further downscales the images by 4 times more. In our example, we selected High accuracy which uses the full resolution of the pictures.
- c. **Generic preselection:** In this example, we checked this option. The MM indicates this option will make the alignment process start by preselecting overlapping pairs of photos (by considering matching pictures). This is done by using lower accuracy first. This scheme may speed up the alignment process.

- d. **Reference preselection:** In this example we unchecked this option. The MM mentions that checking this option and unchecking the previous one (Generic preselection), it is good when a few tie points are expected to be detected, for example when modeling forested areas or crop fields. We also selected the Source mode (out of the Source/Estimated/Sequential options). According to the MM, the Source mode preselects overlapping pairs of pictures based on the measured camera locations (if present). However, for oblique imagery, it is necessary to specify the Capture Distance value in the Settings dialog of the Reference pane to make the preselection procedure work effectively. The MM indicates that the Estimated preselection mode considers the calculated exterior orientation parameters for the aligned cameras. That is, if the alignment operation has been already completed for the project, the estimated camera locations will be considered when the Align Photos procedure is run again with the Estimated preselection selected. When using the Sequential preselection mode, the correspondence between the images is determined according to the sequence of photos (the sequence number of the image). It is worth noting that with this adjustment, the first and the last images in the sequence will also be compared.
- e. **Reset current alignment:** When this option is checked, all previous tie, key, and matching points will be discarded, and the alignment procedure will start from the very beginning. When you align pics for the first time, this option will be unchecked by default. However, if you are realigning pics for a second or third time, this option could be checked by default.
- f. Open Advanced and input a value for Key point limit (upper limit of feature points in an image) and a value for Tie point limit (upper limit of matching points for every image). In this example, we used their default values, Key point limit: 40,000, Tie point limit: 4,000.



These default values have been suggested in the online Agisoft Forum. A member of that Forum suggested estimating the Key point limit by multiplying the megapixels of a picture by 6,400. In our example, that would be  $\sim 7.5 \text{ MP} \times 6,400 = 48,000$ . Using zero value for the Key point limit allows Metashape to find as many key points as possible, but this may result in many less reliable points. Also, several users select 1,000 for the Tie point limit. The option Apply mask to exclude points from the feature detection procedure. Those excluded points are in previously masked areas in photos.

- g. **Exclude stationary tie points.** As per the MM, if this option is checked, the process will exclude tie points that remain stationary across multiple different images. This option enables alignment without masks for datasets with a static background, e.g. in the case of a turntable with a fixed camera scenario. Also enabling this option will help to eliminate false tie points related to the camera sensor or lens artefacts.
- h. **Guided image matching.** As per the MM, this option allows to effectively boost the number of key points per image as if the value of Key point limit was straightforwardly increased, but without significant growth of processing time. Using this parameter can improve results for images with vegetation (wooded terrain, grass, cornfields and so on), spherical cameras and high-resolution images (captured by professional grade cameras, satellites or acquired by high-resolution scanning of archival aerial images). To enable Guided image matching, check the corresponding option in Align Photos dialog and adjust Key point limit per Mpx if needed. The number of detected points per image is calculated as  $(\text{Keypoint limit per Mpx}) \times (\text{image size in Mpx})$ . Small fractions will be extensively matched and used as guidance for matching the remaining points.

- i. **Adaptive camera model fitting.** As per the MM, this option enables automatic selection of camera parameters to be included into adjustment based on their reliability estimates. For data sets with strong camera geometry, like images of a building taken from all the sides around, including different levels, it helps to adjust more parameters during initial camera alignment. For data sets with weak camera geometry, like a typical aerial data set, it helps to prevent divergence of some parameters. For example, estimation of radial distortion parameters for data sets with only small central parts covered by the object is very unreliable. When the option is unchecked, Metashape will refine only the fixed set of parameters: focal length, principal point position, three radial distortion coefficients (K1, K2, K3) and two tangential distortion coefficients (P1, P2).
- j. Select **OK** to start the alignment process. In this example, it took a total of 5' 35". (3' 0" for matching time and 2' 35" for alignment time). After completion, we see a window as indicated Figure 2.1.

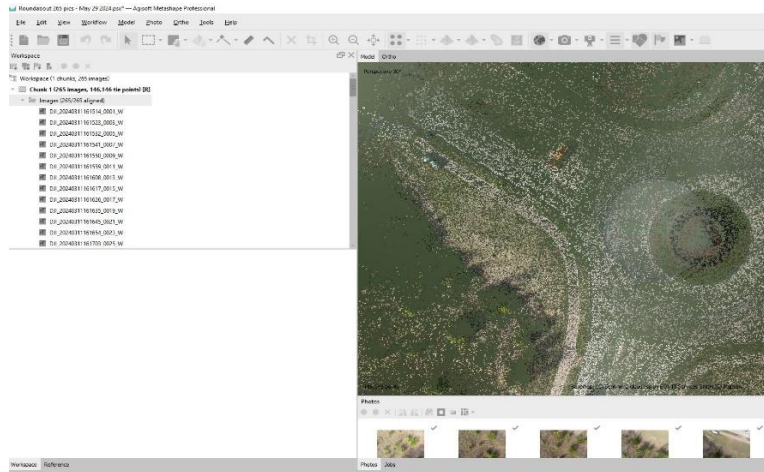


Figure 2.1: Window showing the end of the alignment process.

In the above screen, by clicking on the arrow on the left of the word Images (265/265 aligned), you will close the list of pictures. Then, click on the Tie Points (146,146 points) line to

obtain the window shown in Figure 2.2, where you can read information related to employed tie points and alignment parameters.

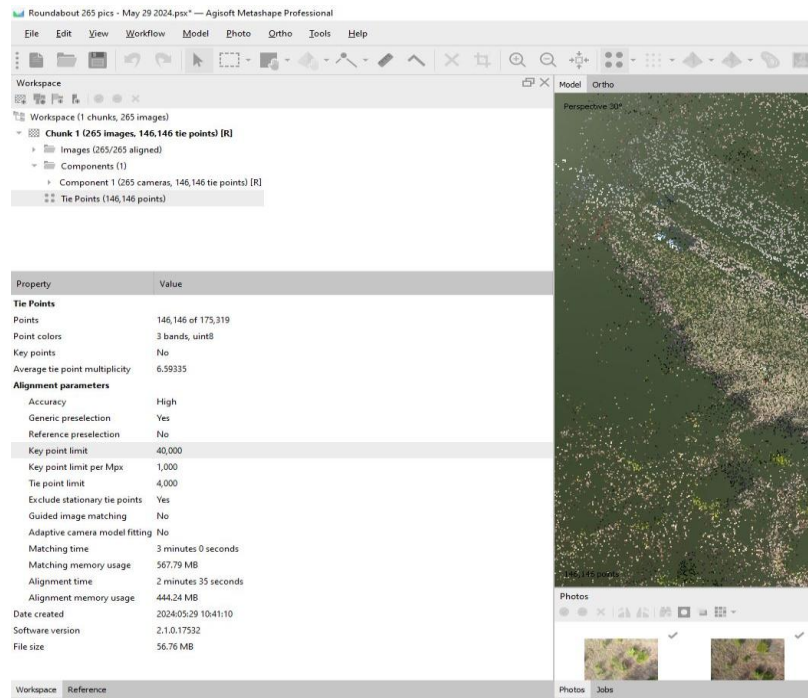


Figure 2.2: Window showing the Tie Points and Alignment Parameters.

Note: In one instance, we unchecked Generic Preselection and checked Reference Preselection.

In that case, the following window (see Fig. 2.3) showed up. At that point, we selected Yes to start the aligning process. It was still successful, but it took approximately 12 minutes.

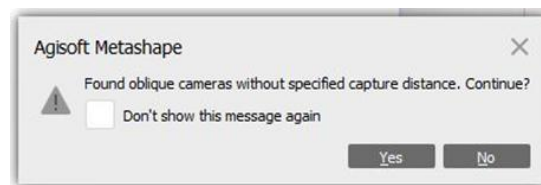


Figure 2.3: Start the aligning process.

#### **4. Build Point Cloud**

- a. This procedure may take considerable time. However, the time indication will fluctuate often. So, do not get confused with the amount of time it shows on screen. The total time depends on the processing power of the computer and also on the processing capability of the software.
- b. Go to Workflow and Select Build Point Cloud and make the following adjustments, as seen in Figure 3.
- c. Adjust Quality to Ultra High/ High/ Medium/ Low/Lowest (based on available time and resources).
- d. Adjust Depth filtering to Disable/Mild/Moderate/Aggressive. In this example, we selected Moderate. However, if you are interested in more details (say, better modeled trees), select Aggressive.
- e. Check Calculate point colors. If you wish, you may also check Calculate Point Confidence.
- f. Select OK. In our example this took a bit more than 12 minutes.

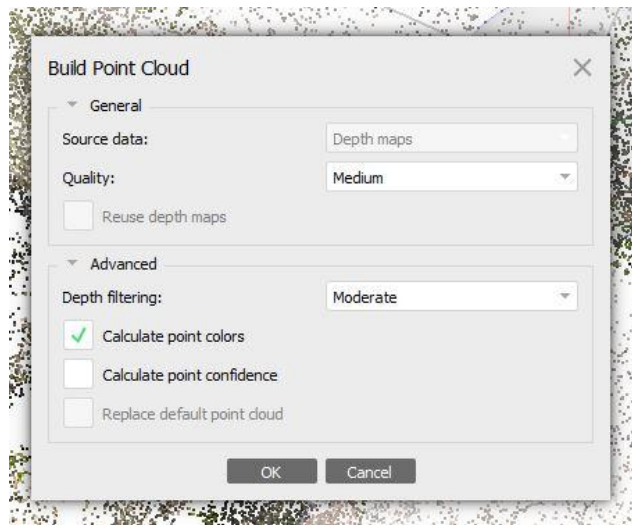


Figure 3: Build point cloud model.

## **5. Build Model**

- a. Go to Workflow and Select Build Model.
- b. Select Source data from Tie Points/Depth Maps/Point Cloud. In this example, we selected Point Cloud.
- c. Select Surface type as Arbitrary (3D).
- d. The option “Quality” is blank in by default. Leave this option like the figure below.
- e. Select Face count from High/Medium/Low/Custom. In this example, we selected High (2,900.000).
- f. In Blocks, uncheck the “Split in blocks” option. In here, the coordinate system is “WGS 84” as default. We can change this coordinate system later for georeferencing purposes but right now it will be the same as shown in the figure below. Block size, Grid origin and other parameters in “Blocks” section will remain same as the following figure below.
- g. In “Advanced” option, set the Interpolation as “Enabled (default)” and leave the Depth filtering as blank.
- h. Only check the “Calculate vertex colors” in point classes section. Leave all other options in this section are unchecked.
- i. Select OK.
- j. At this point, the window shown as Figure 5 may pop up. If so, respond Yes. In our example, this took 4 minutes.

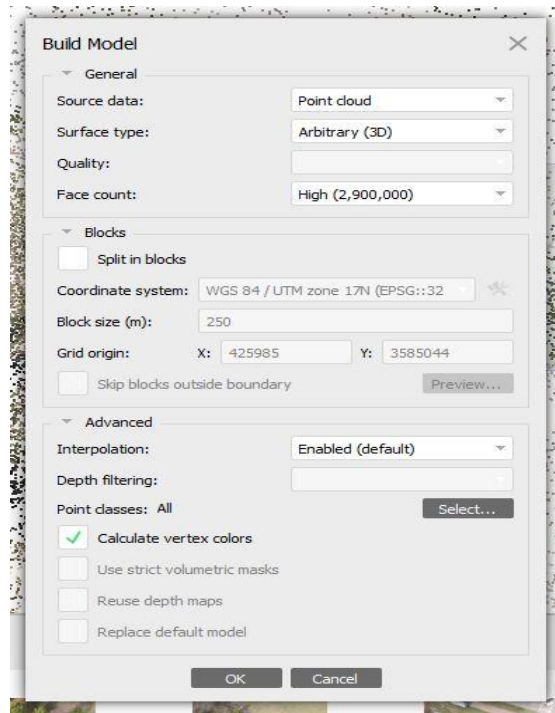


Figure 4: Build Model

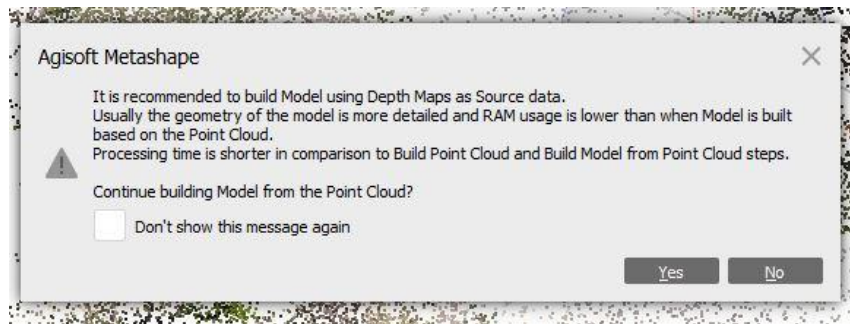


Figure 5: Warning from Metashape.

## **6. Build Texture**

- Go to Workflow and Select Build Texture
- The default values are the ones shown in Figure 6.
- Select OK. This took 5 minutes, for example.
- At this point the model will show as shown in Figure 7.

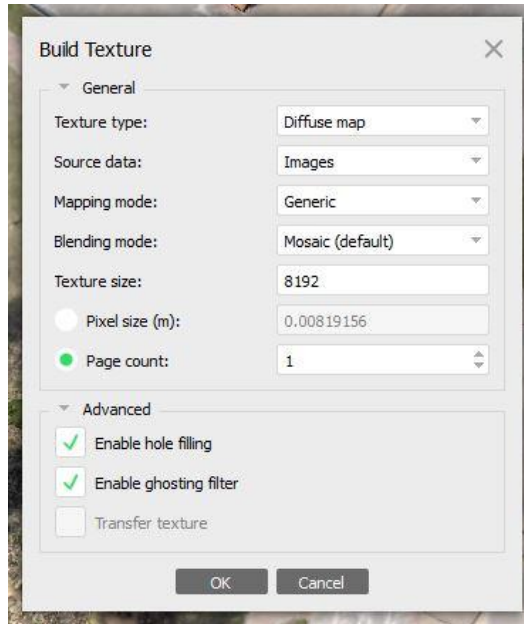


Figure 6: Build Texture

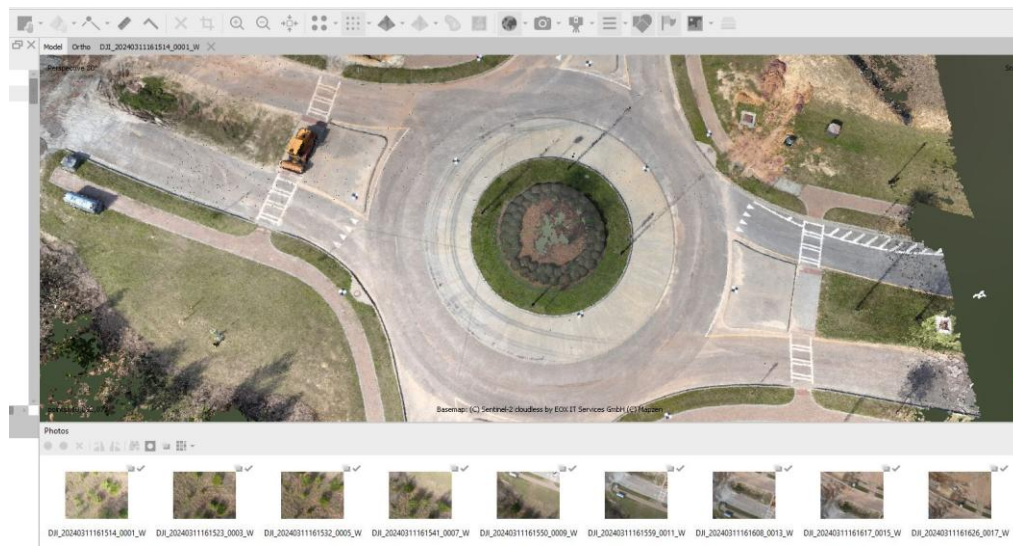


Figure 7: Model

- Use the Navigation tool in Toolbar to move the model around.
- You can turn on or off the camera positions by selecting the camera icon at the toolbar. See Figure 8.
- Go to File and Select Save.





Figure 8: Model showing the location of the camera for each picture.



## SCALING AND EXTRACTING POINT COORDINATES





### **8. Add Marker**

1. To measure from within a model, we need to place markers. Zoom in to a selected location to place a marker. Right click and select Add Marker. A flag will appear at that location. You can rename the markers by right clicking and then selecting rename. In this example, we created four markers at the locations of the previously established GCPs. Then, they were renamed GCP1, GCP2, GCP3, and GCP4.



Figure 9.1: Markers on Model

Note that, at this point, the coordinates of those 4 GCPs will remain in the default coordinate system (In here the WGS 84 coordinate system was set as default from the system). That is, their coordinates will be in World Geodetic System 84 (WGS 84). You will see this as shown in Figure 9.2.

Markers	▲	Longitude	Latitude	Altitude (m)	Accuracy (m)	Error (m)	Projections	Error (pix)	
<input type="checkbox"/>		GCP1	-81.785690	32.400779	29.019258	0.005000	0.000000	36	0.000
<input type="checkbox"/>		GCP2	-81.785545	32.401042	29.216710	0.005000	0.000000	31	0.000
<input type="checkbox"/>		GCP3	-81.786009	32.400964	28.841771	0.005000	0.000000	34	0.000
<input type="checkbox"/>		GCP4	-81.785798	32.401174	29.038201	0.005000	0.000000	38	0.000
Total Error									
Control points									
Check points						0.000000		0.000	

Scale Bars	▲	Distance (m)	Accuracy (m)	Error (m)
Total Error				
Control scale ...				
Check scale b...				

Figure 9.2: Default Coordinates of Markers

## 9. Create Scale Bar

1. To create a Scale bar between two markers, first select the two markers on the left side of the screen and then right click and select Create Scale Bar. Every time, you need to select two markers on the left side of the screen as shown in figure 9.2 to create a scale bar. In this example, we generated 4 scale bars. They are the orange lines seen in Figure 11, GCP1-GCP2, GCP2-GCP4, GCP4-GCP3, and GCP3-GCP1.

IMPORTANT: you need to create at least THREE scale bars. In our example. we used four scale bars according to the needs of this example.

2. Before inputting the distance of those scale bars, the default coordinate system (WGS 84) is to be changed to our desired system. In this example, we will use NAD 83 (North American Datum 1983) Georgia East (ESPG 6445). To do that, we need to select the Convert icon in Reference. Then select Projected Coordinate System, then select NAD 83 (National Spatial Reference System 2011) following NAD 83 Georgia East (ESPG 6445).

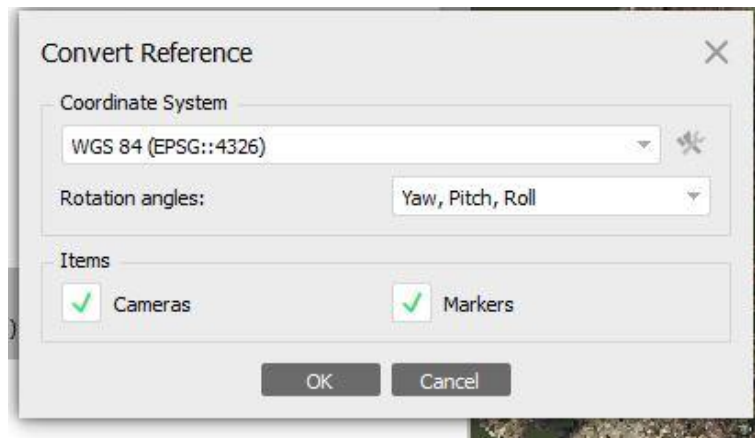


Figure 10.1: Converting the default coordinate to state plane coordinate.

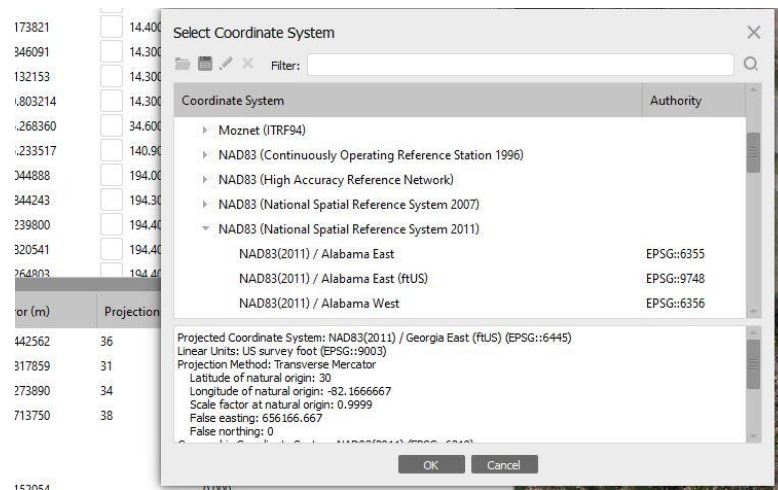


Figure 10.2: Converting the default coordinates to North American Datum 1983 (NAD83) Georgia East (EPSG 6445)

3. Using the Distance formula calculates the distance between two points.

4. 
$$\text{Distance} = \sqrt{(x_2 - x_1)^2 + (y_2 - y_1)^2 + (z_2 - z_1)^2}$$

5. Input the distance in feet.



Figure 11.1: Scaling Bars

✓	DJI_20...	773635.182194	873561.809227	164.714336	10.000000	0.096063	194.400	-0.100	0.000	10.000
✓	DJI_20...	773628.223036	873533.732516	164.615911	10.000000	0.097574	194.400	-0.100	0.000	10.000
✓	DJI_20	773620.878843	873504.485196	164.487959	10.000000	0.102391	194.400	-0.100	0.000	10.000

Markers		Easting (ft)	Northing (ft)	Altitude (ft)	Accuracy (m)	Error (m)	Projections	Error (pix)
✓	GCP1	773747.458811	873419.337949	95.207448	0.005000	0.000000	36	0.000
✓	GCP2	773791.911096	873515.101751	95.855254	0.005000	0.000000	31	0.000
✓	GCP3	773648.989902	873486.477877	94.625143	0.005000	0.000000	34	0.000
✓	GCP4	773713.902477	873562.888319	95.269596	0.005000	0.000000	38	0.000

**Total Error**

Control points

Check points

Scale Bars		Distance (ft)	Accuracy (m)	Error (m)
✓	GCP2_GCP4	91.564000	0.001000	-0.022041
✓	GCP3_GCP4	100.356000	0.001000	-0.025719
✓	GCP1_GCP2	105.501000	0.001000	0.026927
✓	GCP1_GCP3	119.348000	0.001000	-0.047520

**Total Error**

Control scale bars

Check scale bars

Figure 11.2: Distance among the GCPs in scale bars

## GEOREFERENCING

- a. Uncheck all the camera images. See in the following figure 12.

Cameras		Easting (ft)	Northing (ft)	Altitude (ft)
<input type="checkbox"/>	DJI_20...	773561.066794	873386.944917	164.442027
<input type="checkbox"/>	DJI_20...	773567.808344	873414.618479	164.599507
<input type="checkbox"/>	DJI_20...	773574.822994	873442.994777	164.494520
<input type="checkbox"/>	DJI_20...	773581.616605	873470.776211	164.491239
<input type="checkbox"/>	DJI_20...	773588.988129	873500.160769	164.438746
<input type="checkbox"/>	DJI_20...	773596.305741	873530.034079	164.530609
<input type="checkbox"/>	DJI_20...	773603.251128	873558.258799	164.576541
<input type="checkbox"/>	DJI_20...	773610.367936	873586.964342	164.665124
<input type="checkbox"/>	DJI_20...	773617.295319	873615.384724	164.547014
<input type="checkbox"/>	DJI_20...	773626.106427	873644.285111	164.412499
<input type="checkbox"/>	DJI_20...	773652.212673	873639.567571	164.471554
<input type="checkbox"/>	DJI_20...	773648.173750	873614.985324	164.514205
<input type="checkbox"/>	DJI_20...	773641.840920	873589.138725	164.701213
<input type="checkbox"/>	DJI_20...	773635.182194	873561.809227	164.714336
<input type="checkbox"/>	DJI_20...	773628.223036	873533.732516	164.615911
<input type="checkbox"/>	DJI_20...	773620.878843	873504.485196	164.487959

Figure 12: Unchecked camera images

- b. Go to “Settings”
- c. First, adjust the coordinate system to Local coordinates (meter). We selected the Local coordinates in meter at first and then we selected local coordinate in feet US as sometimes, “Local coordinates (ftUS)” does not show in the system. If the Local coordinate (ftUS) is shown, select this option directly. In our example, it did not show and that’s why we followed this rule which we are describing below. Please remain in the same as figure 13.1 below.

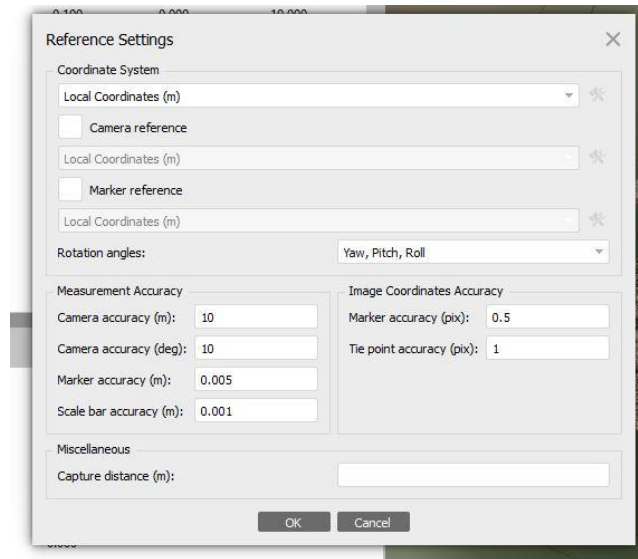


Figure 13.1: Local coordinates (meter)

- d. Then click on “Local coordinates (m)” again and click “More” also. After that select “Local Coordinates (ftUS). Select “OK”. Please see figure 13.2 below for better understanding.

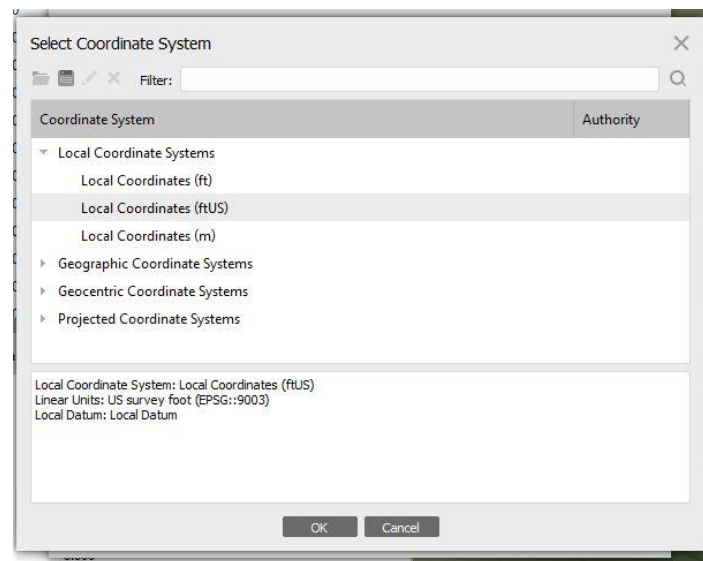


Figure 13.2: Local coordinates (ftUS)



- e. Place the cursor on the Markers in scale bar and click the right button. Then select Easting, Northing, Altitude one by one and input the customized local coordinates of each parameter in feetUS as we used our model and GCP in feetUS. See figure 14 below.

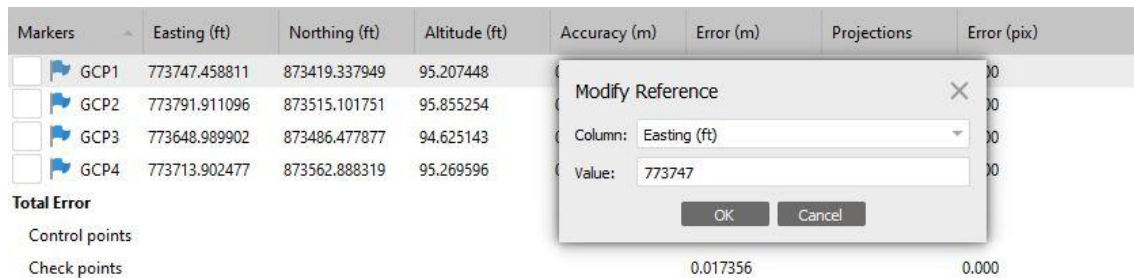


Figure 14: Inputting customized local coordinates.

- f. Check all the Markers. The system considers the unchecked markers as a Check Point.
- g. Then click on the “Update Transform”. I repeat, don’t forget to click “Update Transform” otherwise the model will not be georeferenced. In this time, the model will be transformed into the customized local coordinate system.

### Note:

After georeferencing, the model may not appear, display duplicate instances, or show incorrect scaling. To resolve this, click the "Reset Now" option in the panel bar which will restore the correct georeferenced model in its proper position and scale.

## OPTIMIZE CAMERA

Go to “Optimize camera alignment” in toolbar.

The Optimize Camera Alignment window will open as shown in figure 15.

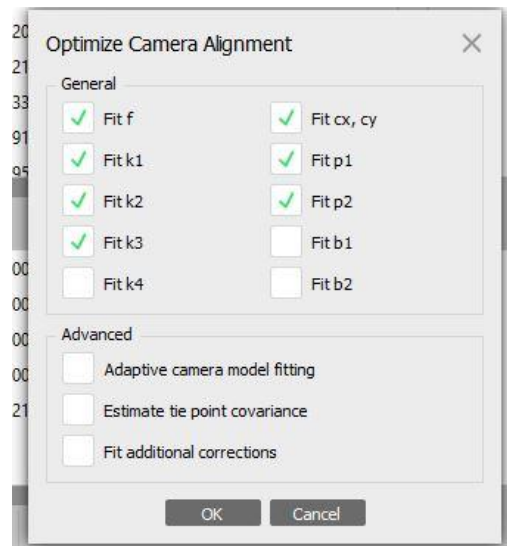


Figure 15: Parameters in camera alignment.

- a. Select according to the above figure. We may uncheck all the parameters in “Advanced” section unless we change the default camera settings.
- b. Select OK.

#### **FINAL MODEL (AS EXAMPLE)**

- a. Add Markers on the specific point as per your requirements. You will see the coordinate in customized local coordinates. See figures 16 and 17 below.





Figure 16: Point cloud model in local coordinates.
















Markers		X (ft)	Y (ft)	Z (ft)	Accuracy (m)	Error (m)	Projections	Error (pix)	
<input type="checkbox"/>		CP1	163.940217	177.944270	100.637280	0.005000	0.000000	36	0.000
<input type="checkbox"/>		CP2	77.876711	203.230168	99.691627	0.005000	0.000000	37	0.000
<input type="checkbox"/>		CP3	109.554296	223.748733	100.183747	0.005000	0.000000	33	0.000
<input type="checkbox"/>		CP4	150.047859	273.336530	100.809909	0.005000	0.000000	34	0.000
<input type="checkbox"/>		CP5	178.617313	236.340553	100.390514	0.005000	0.000000	33	0.000
<input type="checkbox"/>		CP6	217.337979	197.858066	100.974263	0.005000	0.000000	30	0.000
<input type="checkbox"/>		CP7	144.873727	124.412082	98.662221	0.005000	0.000000	35	0.000
<input checked="" type="checkbox"/>		GCP1	200.000000	150.000000	100.000000	0.005000	0.029330	36	0.075
<input checked="" type="checkbox"/>		GCP2	200.005000	255.498000	100.763000	0.005000	0.021295	31	0.066
<input checked="" type="checkbox"/>		GCP3	82.230000	169.334000	99.433000	0.005000	0.026676	34	0.075
<input checked="" type="checkbox"/>		GCP4	109.052000	266.037000	100.091000	0.005000	0.011741	38	0.036
Total Error									
Control points						0.023255	0.064		
Check points						0.000000	0.000		
Scale Bars		Distance (ft)	Accuracy (m)	Error (m)					
<input checked="" type="checkbox"/>		GCP2_GCP4	91.564000	0.001000	-0.006802				
<input checked="" type="checkbox"/>		GCP3_GCP4	100.356000	0.001000	-0.008956				
<input checked="" type="checkbox"/>		GCP1_GCP2	105.501000	0.001000	0.043348				
<input checked="" type="checkbox"/>		GCP1_GCP3	119.348000	0.001000	-0.027198				
Total Error									
Control scale bars				0.026198					
Check scale bars									

Figure 16: Local coordinates of check points.

## APPENDIX C8. CLOUDCOMPARE PROTOCOL

### POST PROCESSING PROTOCOL OF CC CC v2.13.2

(by Md. Mehrab Hossain, 2024)



## 1. User Interface of CC

The following figure 1 shows the user interface of CC.

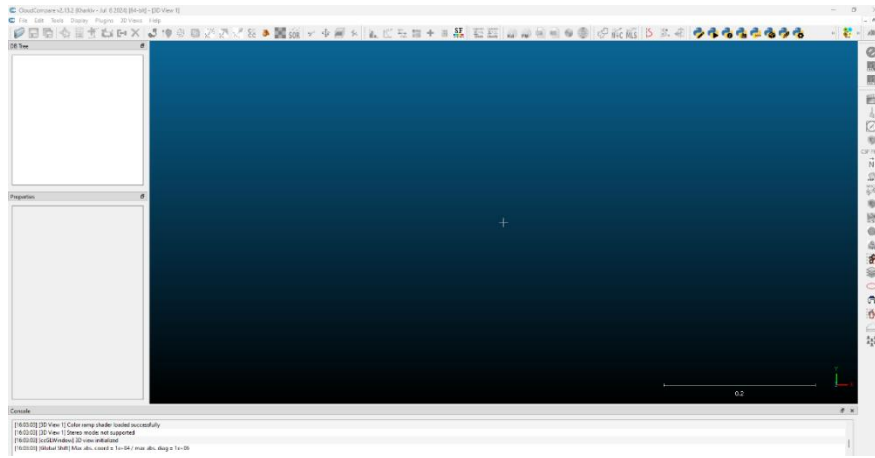


Figure 1

## 2. Process of Uploading Files

- Then click on “File” tab and open the “las” file (in here we open a “las” file – Sandersville) as shown in figure 2. Then leave all the parameters as like as figure 3 and click on “Apply All”.

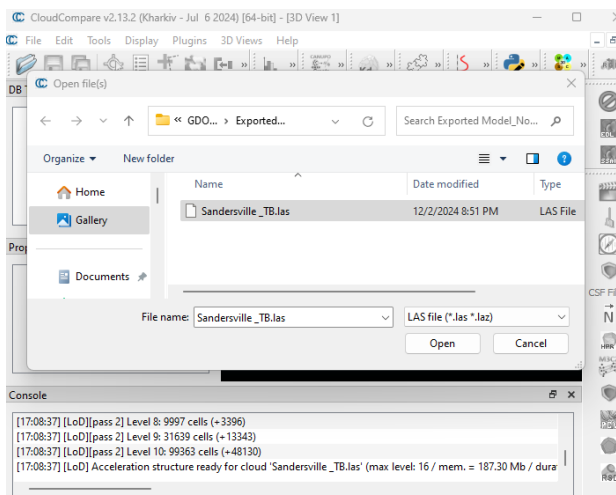
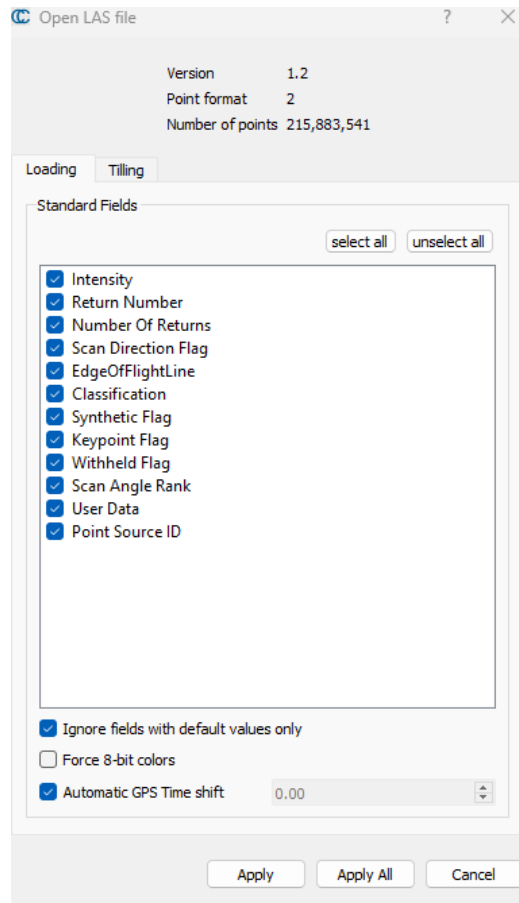


Figure 2



**Figure 3**

- Then set “Automatic” and click “Yes to All” as shown in figure 4.

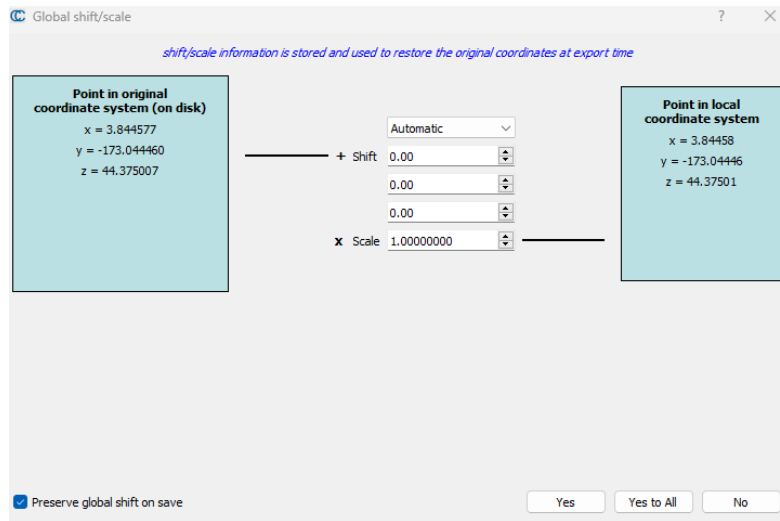


Figure 4

- After uploading the file, the model shows as like as figure 5.

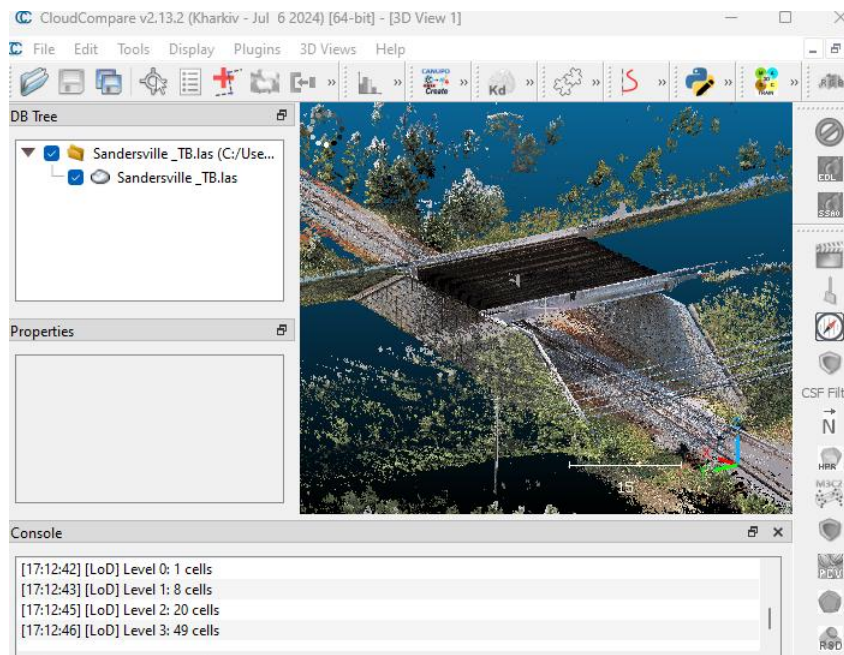
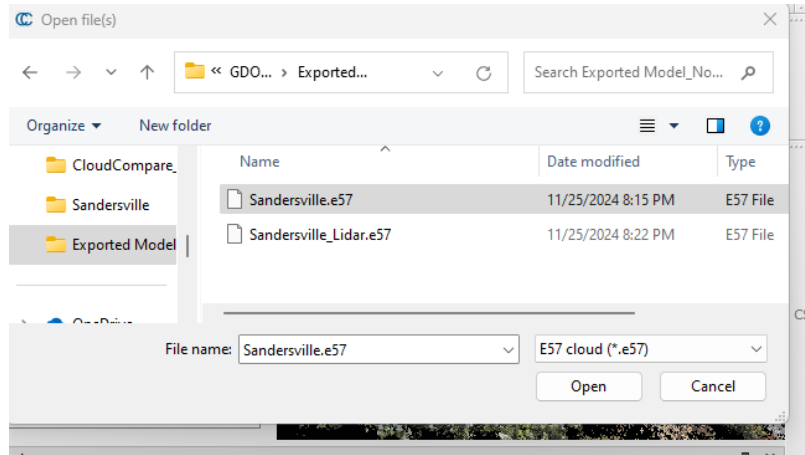


Figure 5

- After that upload the another “las file” that you want to compare (In our case, we used e57 file format as this format is also allowed). This file came from Metashape point cloud. Please see figure 6.



**Figure 6**

- The process of uploading is shown in figure 7 and after uploading the model looks like figure 8.

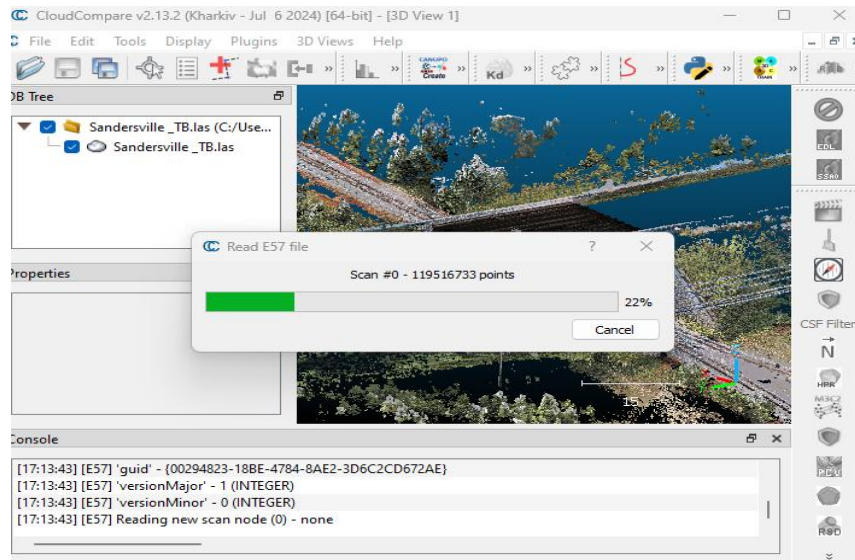


**Figure 7**

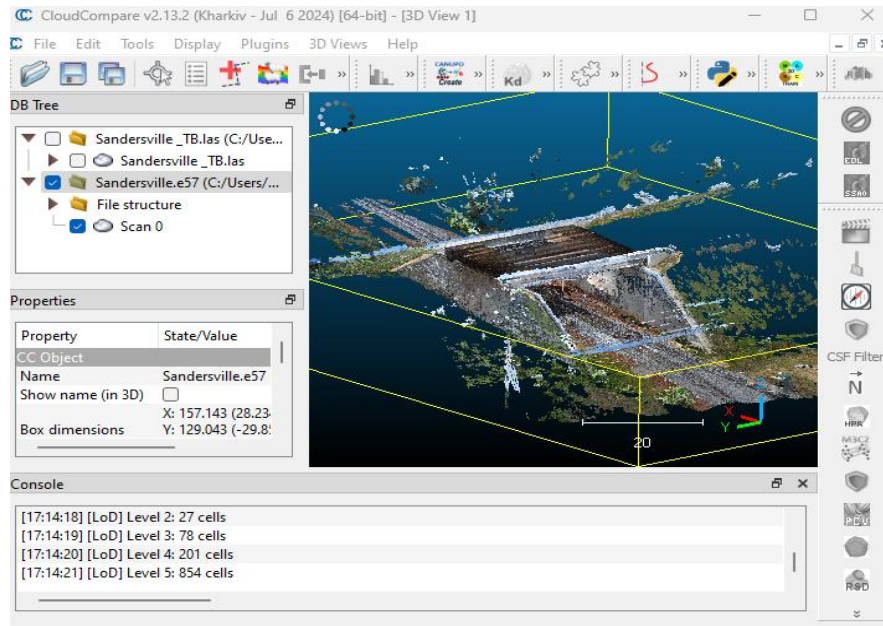


Figure 8

### 3. C2C Comparison Process

- Select the two files in Database(DB) Tree (left side) and click on C2C distance tools which is marked in circular red in the figure 9 below.

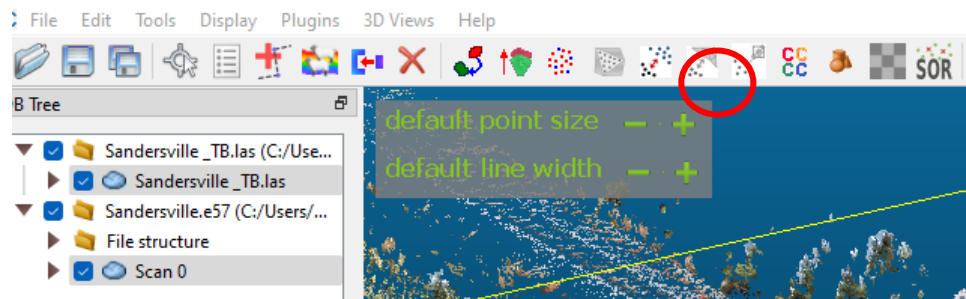


Figure 9

- After clicking C2C distance tool, the following window displays where red is compared model and yellow is reference model. We may swap the model by clicking “Swap” and then click on “OK”. In our case we didn’t swap as it was okay for us. Please see figure 10.



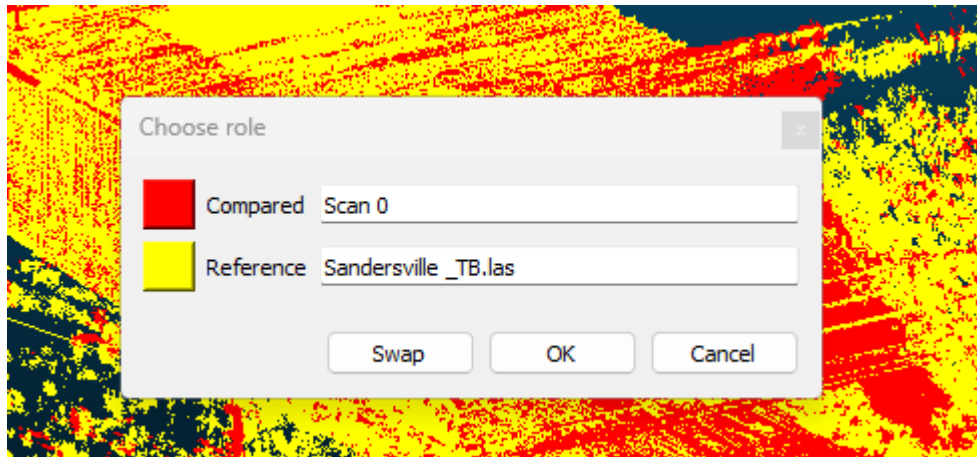


Figure 10

- Then the following window is shown in figure 11. In “General parameters” section, you will see “max distance”. It means that you may add how much maximum C2C distance you want to see. In our case, we put 1 m max distance.

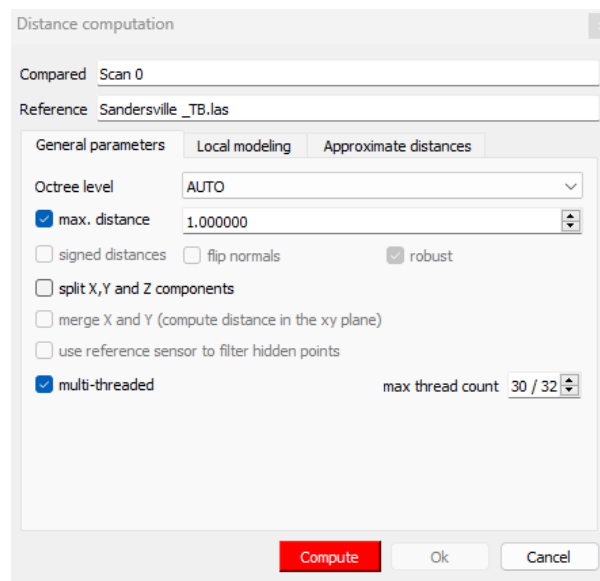
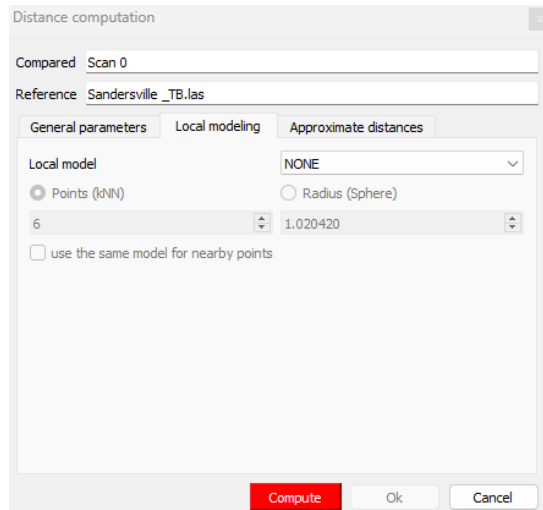


Figure 11

- In “Local modeling” section, leave all the parameters as like as in figure 12.





**Figure 12**

- In “Approximate distance”, leave all the parameters like as in figure 13. Don’t worry if the max distance 10.0188 m in here as it is by default and it has not impact on C2C distance computation as we already set max distance 1 m in previous “General Parameters”.

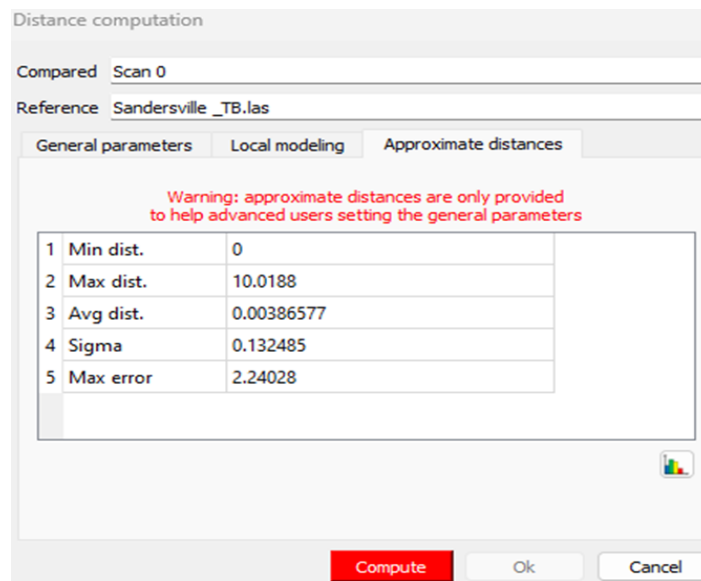


**Figure 13**

- Then click in “Compute”. After clicking, the C2C distance computation will be started as shown in figure 14 and model looks like as shown in figure 15.

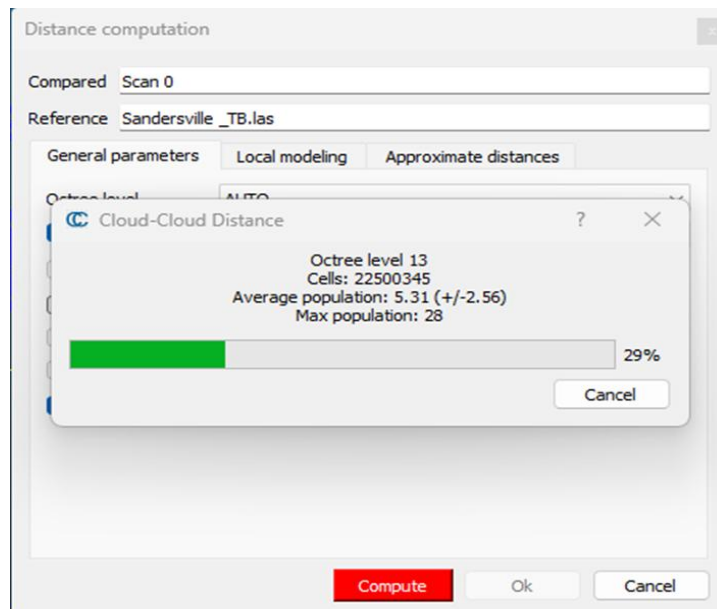


Figure 14

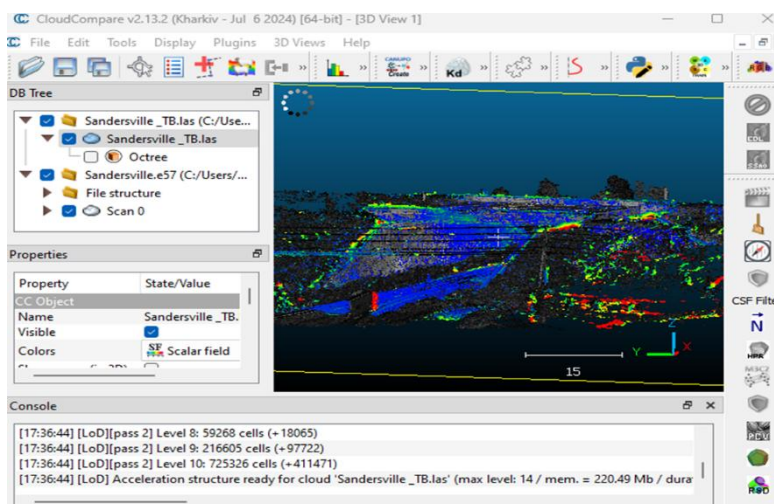


Figure 15

#### 4. Display the Analysis Results

- To show the scale bar in the screen, go to the “Display” and click on “Active scalar field” and then select “Toggle color scale”. Then the scalar field bar will be displayed as shown in figure 16.

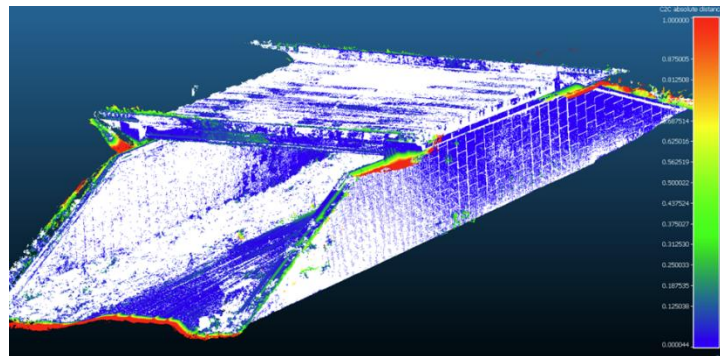
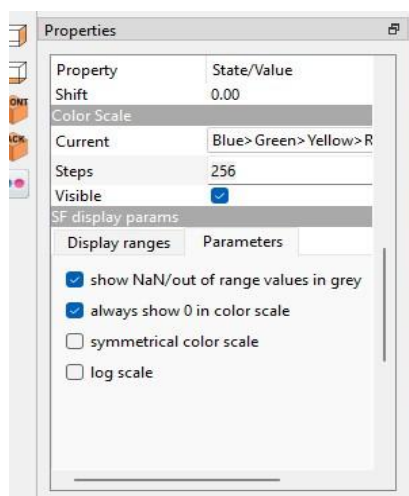


Figure 16

- To adjust the scale type and boundary of the scale, adjust the parameters as shown below:  
1) Check mark the “show NaN/out of range values in grey”. 2) Check mark the “always show 0 in color scale” for better understanding from zero to boundary value. 3) Other “symmetrical color scale” and “log scale”, you may check mark these if you want to show this scale.



**Figure 17**

- To adjust the concentration of the color aligned with scale, click on “Display ranges” and adjust the saturation limit by moving the triangular red area in left and right.

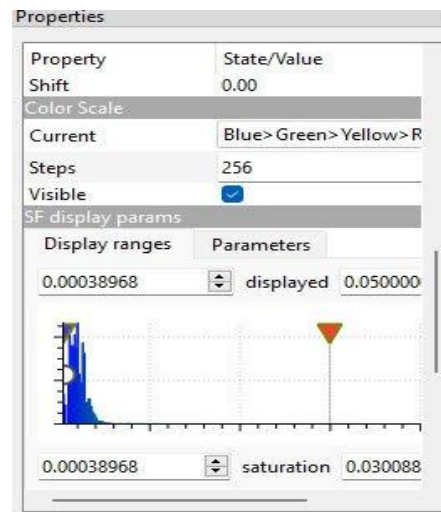


**Figure 18**

- To see the color scale make sure you click on “Scalar field” as shown in below figure.



**Figure 19**

- If you want to see the graphical representation of C2C distance computation, go to tools bar and select “Show histogram”.



**Figure 20**

- Then the graph will be shown as shown in figure 21.

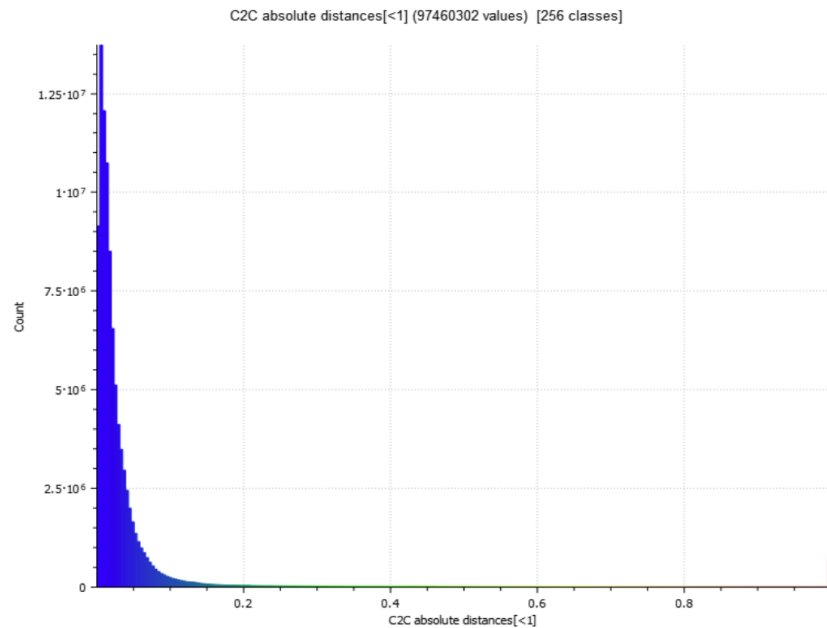


**Figure 21**

- If you need to see the distribution fitting, click on “Distribution fitting” and you may see the “Gauss”. You may change the fitting by clicking the pop-up menu and you can see the other option “Weibull” as shown in below figure 22.

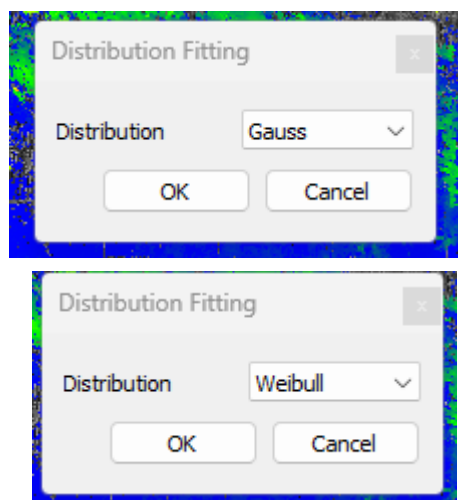


**Figure 22**

- Click on “OK”. You can see the Gauss curve as shown below:

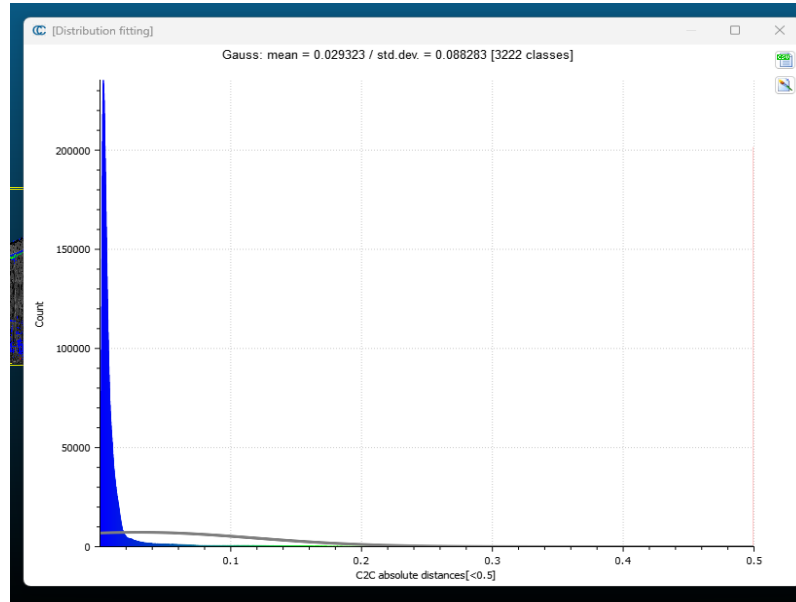


**Figure 23**

- To export this curve or C2C absolute distance curve in “CSV” file, click on “csv” icon in the top right of the above curve or histogram.

## 5. M3C2 Comparison Process

- To compare the two-point clouds in M3C2 analysis, you need to select the two-point clouds from the “DB Tree” as shown in figure 24 below. Then select the “Plugins” tab and you will see the option “M3C2 Distance”. Click on this option.

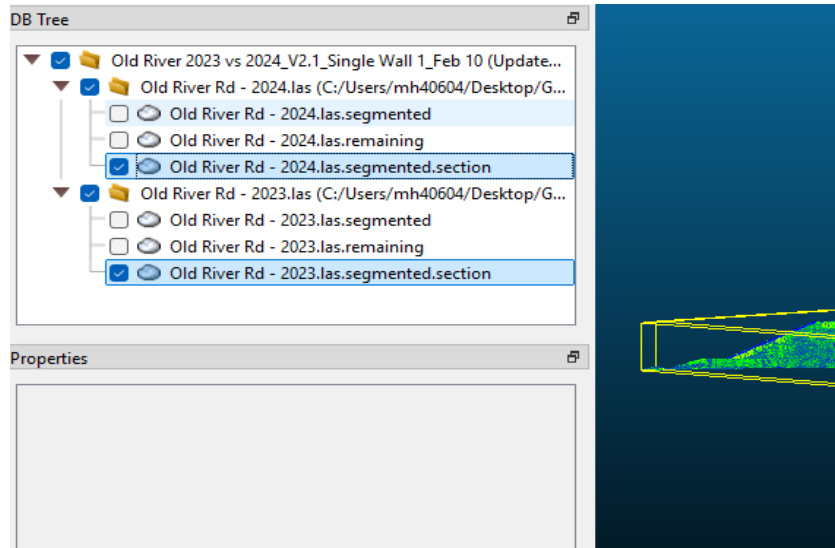


**Figure 24**

- After clicking the M3C2 Distance plugin, the following message will appear in the front and click “OK”.

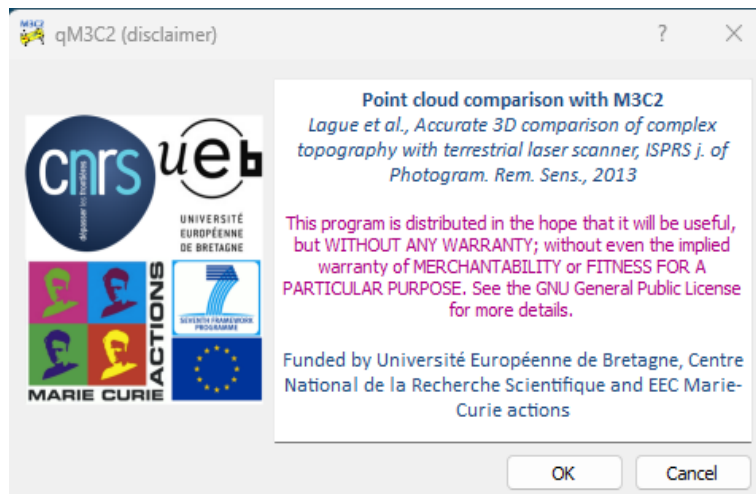


**Figure 25**

- After that the following window (Figure 26) will appear. In here, you will see cloud 1 and cloud 2. You need to check which cloud you want to make as reference which one is comparable. The location of the Cloud 1 in this case is always fixed but you can change

the reference cloud to comparable and vice versa by clicking the curved arrow at the top right of this window.

- In the “Main Parameters” section, check mark the “use cloud # 1” under “Core points”. All other parameters are unchanged.

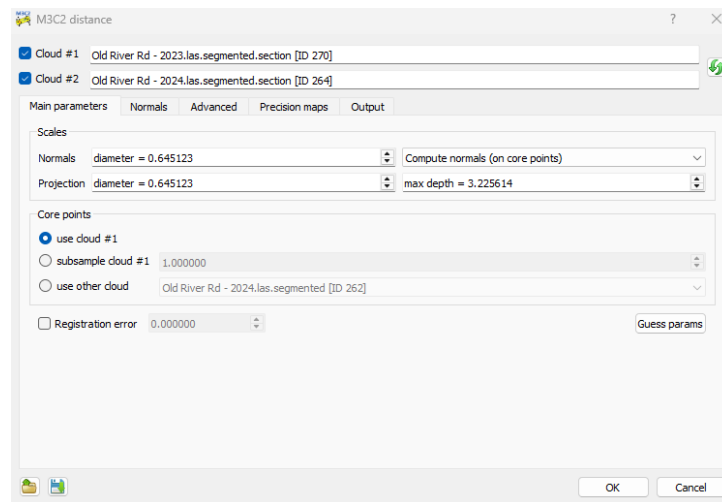


**Figure 26**

- For the next section is “Normals”. In this section, make the “Calculation mode” default and “Preferred orientation” is “+Z” under the orientation as shown in the figure 27 below.

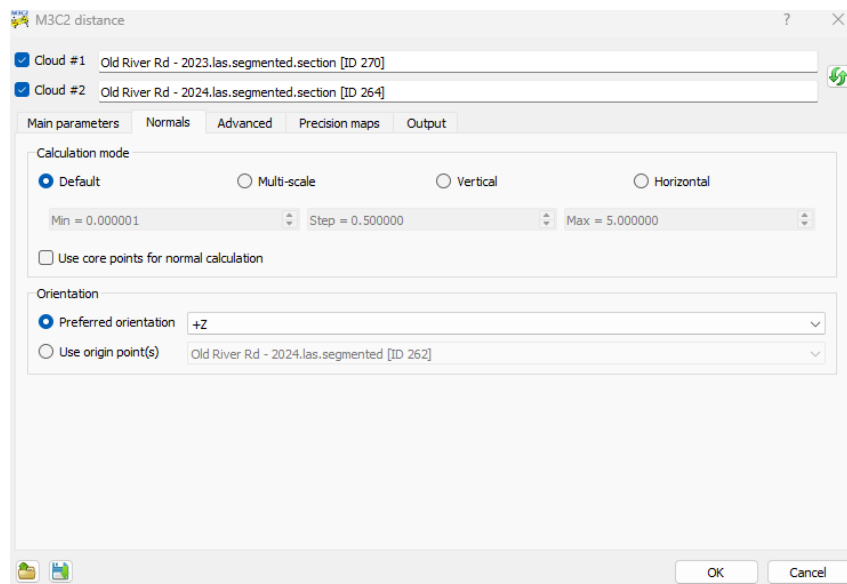


**Figure 27**



- In the “Advanced” section maximum thread will be (a/a), where  $a = 32$  for both sides in this case as shown in figure 28 below. The author has written it as (a/a) because the number may be changed but it should be the same on both sides. All other parameters remain unchanged.

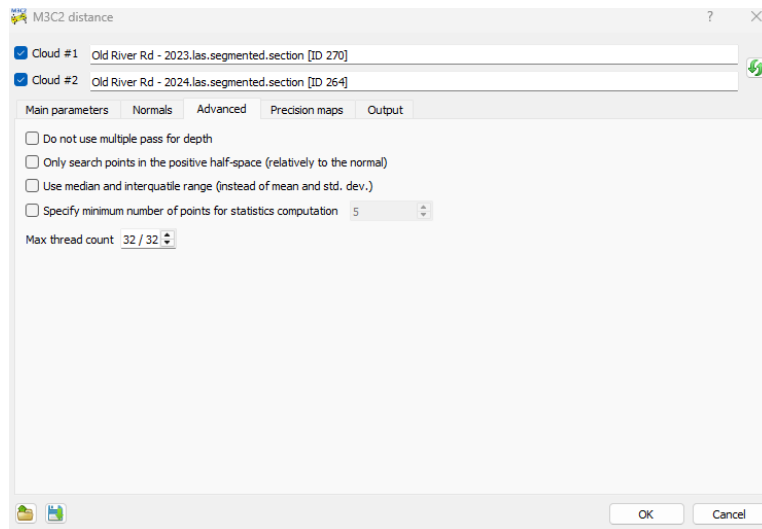
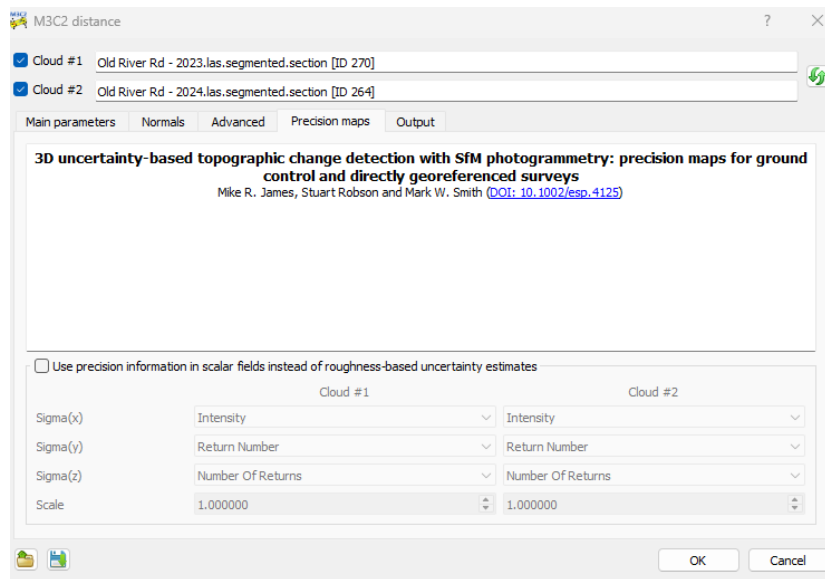


Figure 28

- In the “Precision maps”, keep “Use precision information in scalar fields instead of roughness-based uncertainty estimates” unchecked as shown figure 29 in below.



**Figure 29**

- In “Output” section, keep all parameters unchanged and finally click on “OK” as shown in figure 30 below.

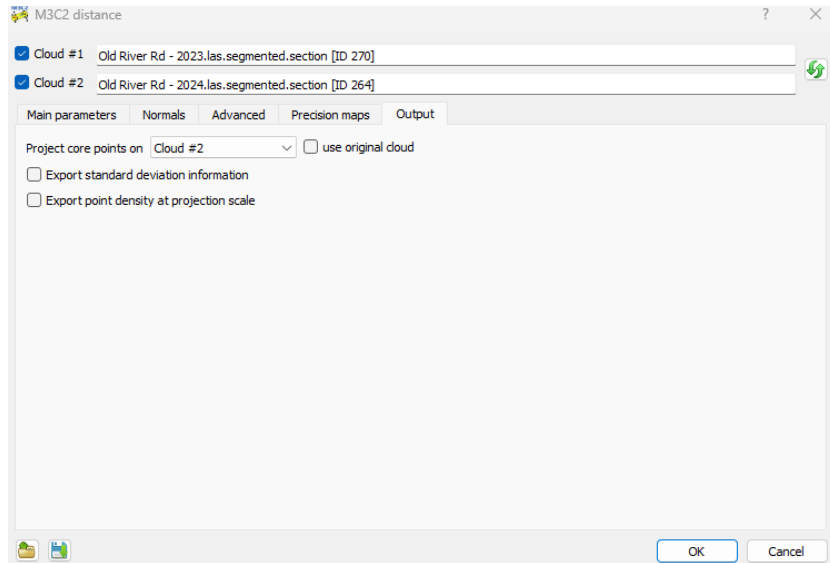


**Figure 30**

- Then the software first computes the normal and then calculates the signed distance. The process of both these mentioned dins the following figure 31 and 32.

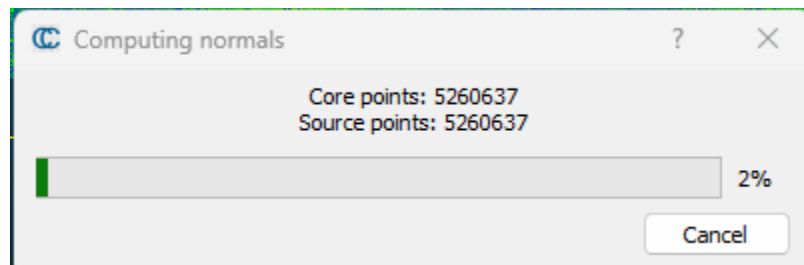


**Figure 31**

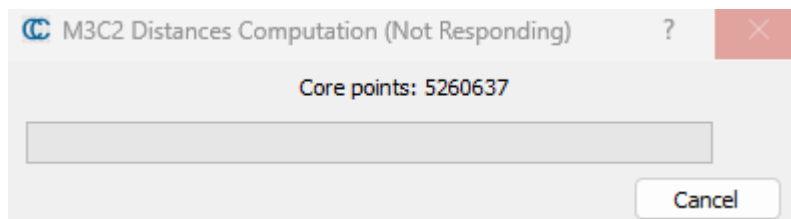


**Figure 32**

- After completing the calculation, you will see the following figure 33 where you will notice that M3C2 output scale will be produced in “DB tree” as shown below. To see the M3C2 distance colored scale, follow the similar way as like as to see the C2C. Go to display tab and select “Active Scalar Field” and then click on “Toggle color scale”.

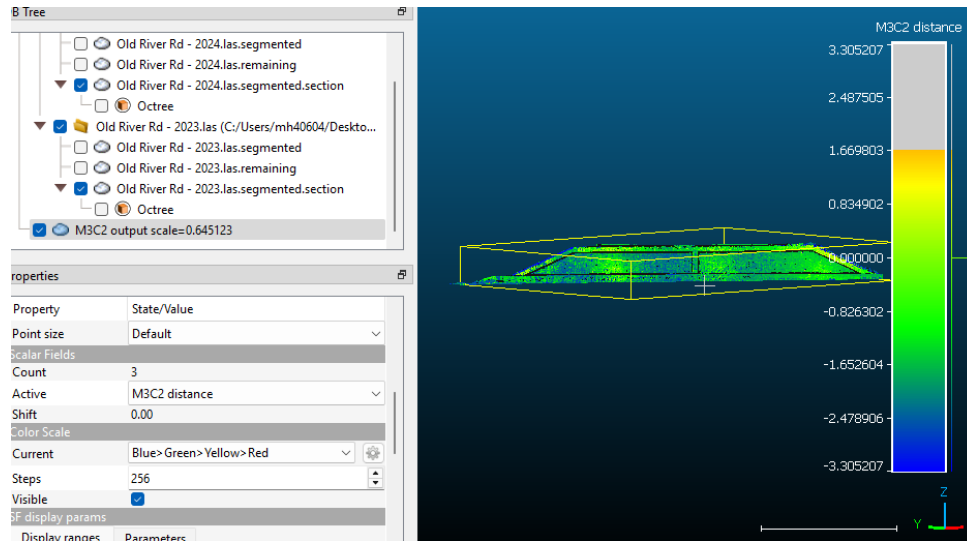


**Figure 33**

- To fit the color scale, click the “min max” icon and you will see the ranges shown the figure 34 below. Fit your scale according to your requirements and click on “Split”.

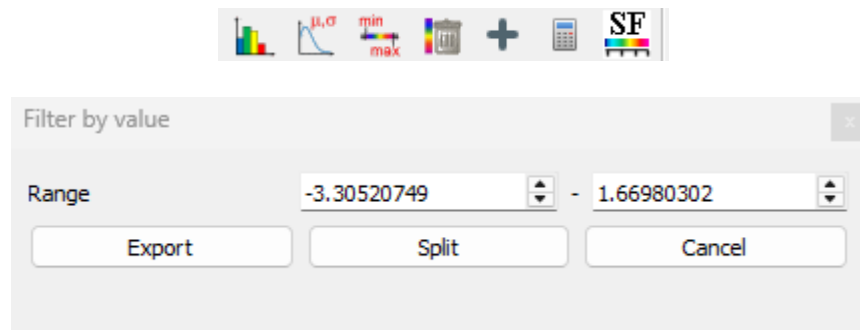


**Figure 34**

- To see the statistics, you can click on show histogram icon shown in above figure 34 and you will see the following histogram. Also, you may export the data in “**csv**” file by clicking the icon in just top right of the following figure.

## **APPENDIX C9. PIX4D MAPPER PROTOCOL**

Pix4D Mapper PROTOCOL

(By Shakil Ahmed, 2025)



Date of Version V.10 - **May 2025**

## 1 – Pix4D Mapper Home Interface

After launching and logging into the Pix4D Mapper software on the computer, the home interface is displayed.

- Under the Project tab, you have the option to create a New Project or open an Existing Project stored on your device.
- Additionally, the interface provides Quick Access to recently opened projects—for example, "CW\_01312025.p4d" is shown in the recent project list.

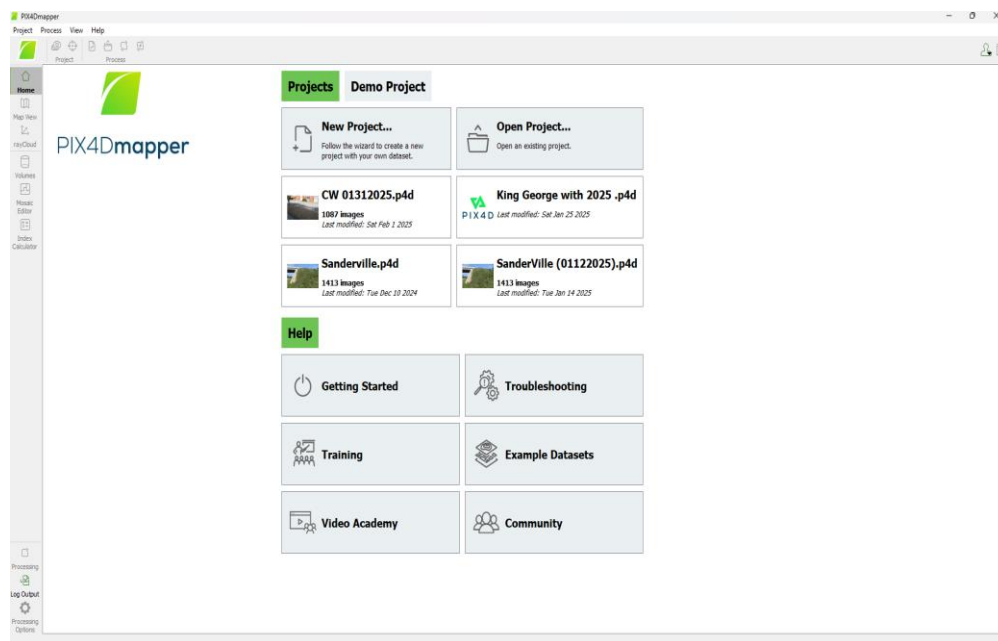


**Figure 1 – Pix4D Mapper Home Interface**

## 2 – Creating a New Project in Pix4D Mapper

This window appears after selecting New Project. At this stage, users must provide the following project details:

- Name: Enter a unique name for your new project in the text box labeled “Name” (highlighted as box 1).
- Create In: Specify the folder path where the project files will be saved (highlighted as box 2). You can use the Browse button to choose a directory.
- Project Type: Select either New Project or Project Merged from Existing Projects, depending on your workflow.

In this screenshot, the Next button is inactive because the project name field is empty. Once all required fields are completed, the Next button becomes clickable, allowing you to proceed to the next step.

**Figure 2 – Creating a New Project in Pix4D Mapper**

### **3 – Project Details Completed and Ready to Proceed**

In this window, all required project details have been filled out:

- Name: The project name has been entered as “Test.”
- Create In: A specific directory path has been selected – in this case, “C:/Users/sa16502/Desktop/CC test.”
- Project Type: The option for New Project is selected.

Now that the mandatory fields are completed, the Next button becomes active (highlighted with a check mark), allowing the user to move forward with the project setup.

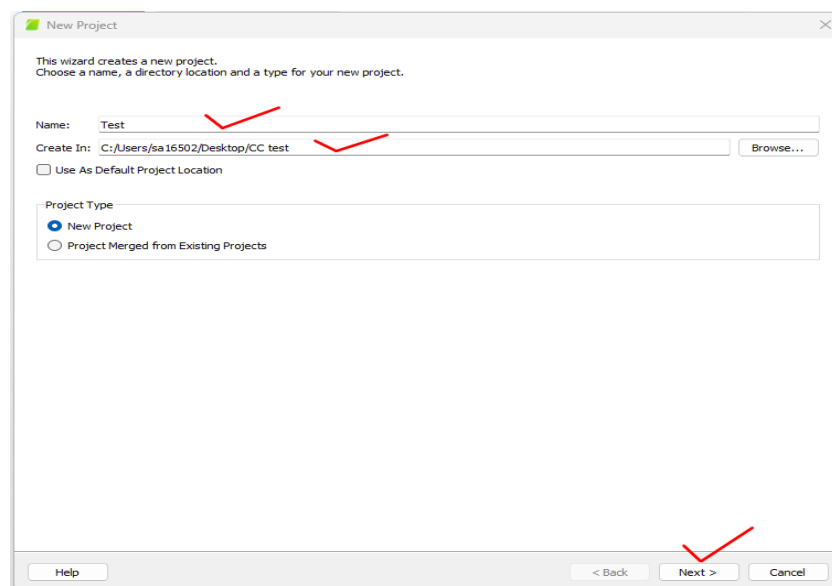


**Figure 3 – Project Details Completed and Ready to Proceed**

#### **4 – Selecting Images for the Project**

In this step, the user is prompted to import at least three images in Joint Photographic Experts Group (JPG) or Tagged Image File Format (TIFF) format to proceed with the project. The interface provides three options for importing:

1. Add Images... – Allows the user to manually select individual images from the computer.



2. Add Directory... – Lets the user select an entire folder containing images, which are then automatically added.
3. Add Video... – Offers the option to import frames from a video file (useful for some mapping workflows).

At this point, no images have been selected yet, so the Next button remains inactive. Once the required number of images is added, the button will be enabled to move forward

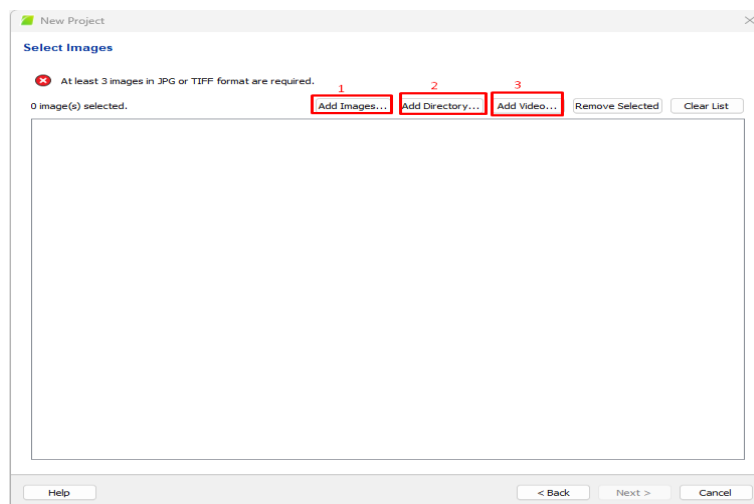


**Figure 4 – Selecting Images for the Project**

## **5 – Images Successfully Imported and Ready for Processing**

In this step, a total of 7 images have been successfully added to the project. As shown in the file list, these images are in the folder:

C:/Users/sa16502/Desktop/CW Photos 01312025/.

Once the minimum requirement of 3 images is met, Pix4D Mapper confirms this with a green check message: *“Enough images are selected: press Next to proceed.”*

Key interface buttons:

- Remove Selected (4): Deletes only the highlighted images from the list.
- Clear List (5): Removes all imported images from the list.

With valid image input, the Next button (6) at the bottom becomes active, allowing the user to move forward to the next stage of the project setup.

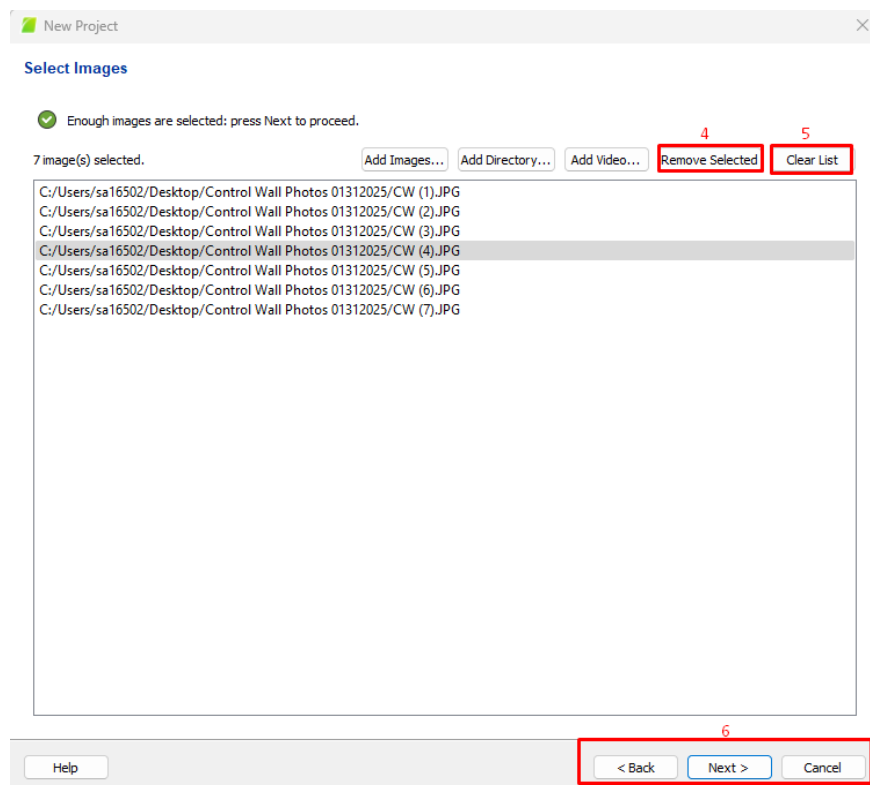


Figure 5 – Images Successfully Imported and Ready for Processing

## 6 – Notification: Geotags Discarded Due to Redundant Coordinates

After clicking the Next button, Pix4D Mapper displays a warning message:

*"More than 80% of the image coordinates of the camera model were the same and therefore the corresponding geotags have been discarded."*

This notification typically appears when:

- The imported images lack proper geotags, or
- The geotags are identical or invalid—commonly the case with images captured using a non-GPS-enabled camera such as a DSLR.

In this instance, DSLR images without geotags were used, which triggered this message.

Action Required:

Click OK to acknowledge the warning. This does not affect the ability to continue the project;

Pix4D will simply proceed without using image geolocation metadata.

After confirming, the user should click Next to move forward to the camera model setup or image calibration stage.

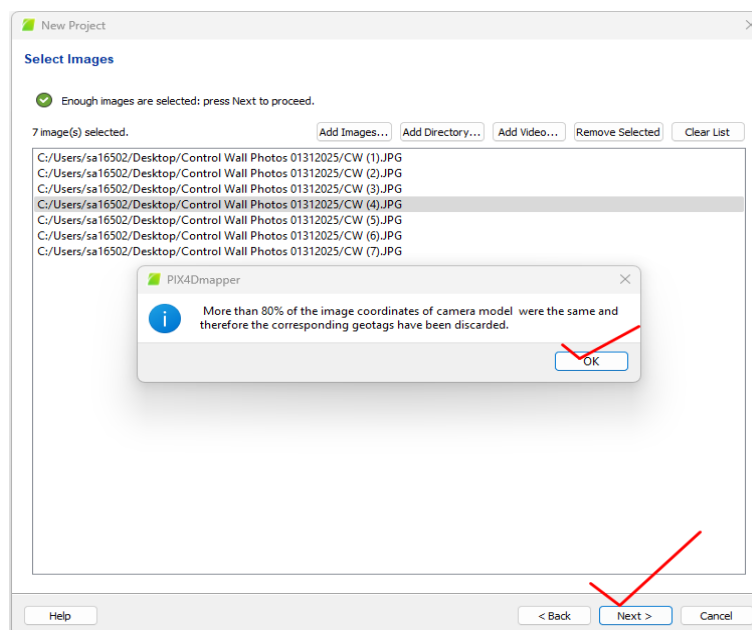


**Figure 6 – Notification: Geotags Discarded Due to Redundant Coordinates**

## Figure 7 – Image Properties and Geolocation Setup

This window allows the user to review and modify image geolocation details and camera model settings:

1. Coordinate System (Box 1): Clicking the Edit button opens a window to define or change the coordinate system used for the images.
2. Geolocation and Orientation (Box 2):
  - Since DSLR images without geotags are used, the system shows: Geolocated Images: 0 out of 7.
  - You can manage coordinates via:
    - Clear – Remove geolocation data.
    - From EXIF – Extract from image metadata.
    - From File... – Import geolocation data (e.g., from a CSV).
    - To File... – Export current data.
3. Selected Camera Model (Box 3): Pix4D automatically detects the camera model (e.g., NIKOND5300\_18.0\_6000x4000). You can click Edit to modify this if needed.

All images currently show zero values for latitude, longitude, and altitude, confirming the absence of geotags.

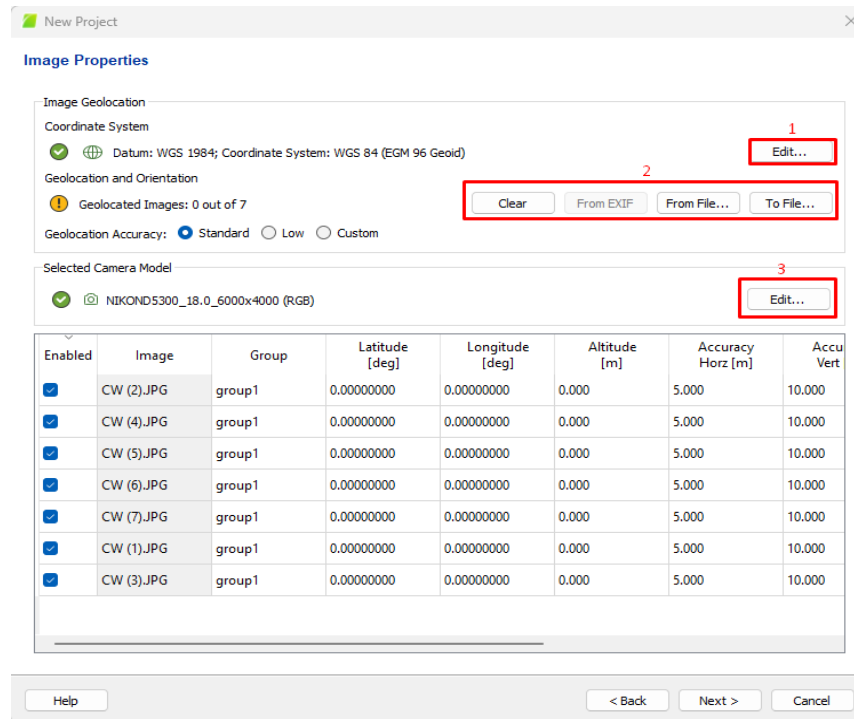


**Figure 7 – Image Properties and Geolocation Setup**

## 8 – Editing the Image Coordinate System

When the Edit button next to Coordinate System is clicked (from Figure 7), this dialog appears.

Here, the coordinate system for the image geolocation can be configured:

- Unit Selection: You can choose between feet (ft) or meters.
- Coordinate System Definition:
  - Arbitrary Coordinate System: For local reference systems.
  - Known Coordinate System (Selected): Choose from standard geospatial systems.
- In this case, the coordinate system is set to:

NAD83(2011) / Georgia East (ftUS) (EGM 96 Geoid)

This coordinate system matches local surveying standards and ensures compatibility with GCPs and field measurements.

Click **OK** to confirm and apply the new coordinate system to the image geolocation settings.

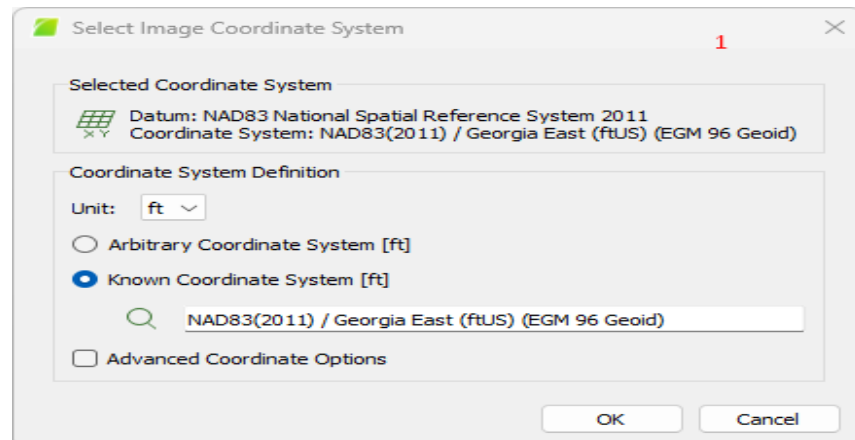


**Figure 8 – Editing the Image Coordinate System**

## 9 – Setting the Vertical Coordinate System

This window allows the user to define the Vertical Coordinate System as part of the geolocation settings for the images.

- The selected coordinate system is:  
NAD83(2011) / Georgia East (ftUS) with EGM 96 Geoid.
- Unit: Set to feet (ft).
- Under the Vertical Coordinate System section:
  - MSL (Mean Sea Level) is unchecked, meaning the project will not reference a standard vertical datum like Earth Gravitational Model EGM 96.
  - Instead, the setting shows a Geoid Height Above Geodetic Reference System (GRS) 1980 Ellipsoid of 0.00 ft, likely used for local or arbitrary elevation reference.
  - Arbitrary is also unchecked, indicating that no vertical transformation is being applied.

This configuration implies that vertical positioning is either not relevant or will be handled manually using ground control or CPs.

Click OK to confirm and apply the coordinate system settings.

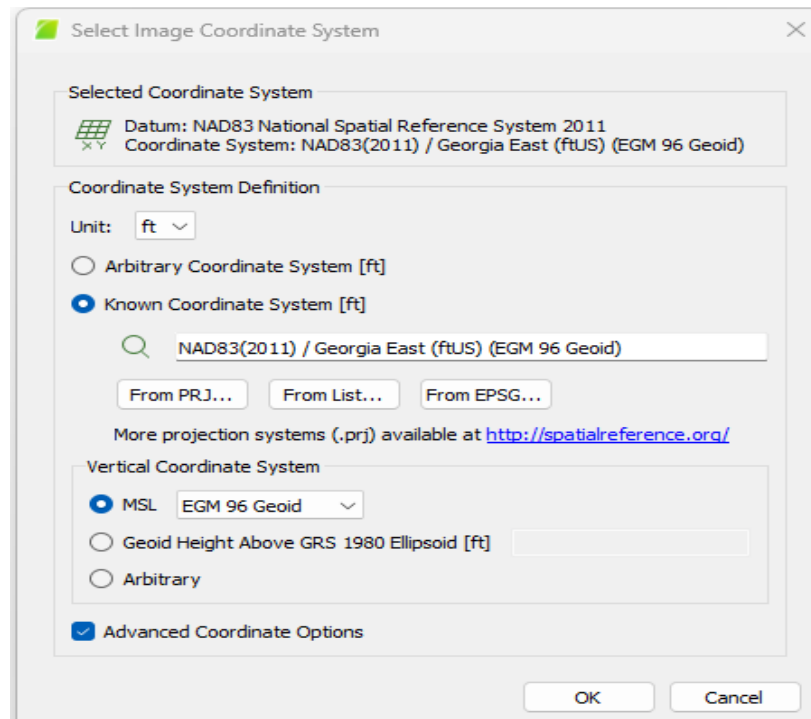


**Figure 9 – Setting the Vertical Coordinate System**

## **10 – Geotag Warning After Returning from Coordinate System Setup**

After completing the vertical coordinate system setup in Step 9, the software returns to the Image Properties window.

At this point, Pix4D Mapper shows a warning message:

*"More than 80% of the image coordinates of camera model NIKOND5300\_18.0\_6000x4000 (RGB) were the same and therefore the corresponding geotags have been discarded."*

This is expected behavior when working with DSLR images that lack embedded GPS data.

### Action Steps:

- Click OK to dismiss the warning.
- Review the coordinate system and camera model settings.
- If everything appears correct in this window, click Next to proceed to the processing options.

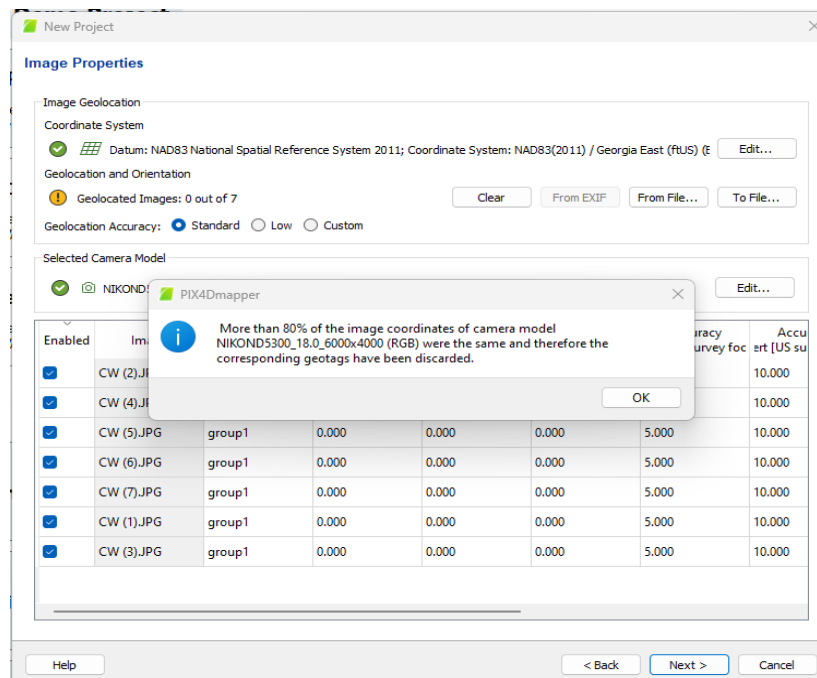


**Figure 10 – Geotag Warning After Returning from Coordinate System Setup**



## 11 – Selecting a Processing Options Template

This step appears after completing the initial project setup in Pix4D Mapper. Users must select a Processing Options Template based on the objectives and type of data collected.

Template Categories:

- Standard – Recommended for general mapping and modeling tasks: *3D Maps*, *3D Models*, *Ag Multispectral*
- Rapid – Optimized for faster results at lower resolution; ideal for previews or quick assessments: *3D Maps - Rapid/Low Res*, *Ag RGB - Rapid/Low Res*, etc.
- Advanced – Designed for use with specialized sensors or modified cameras: *Ag Modified Camera*, *Ag RGB*, *Thermal Camera*, *ThermoMAP Camera*

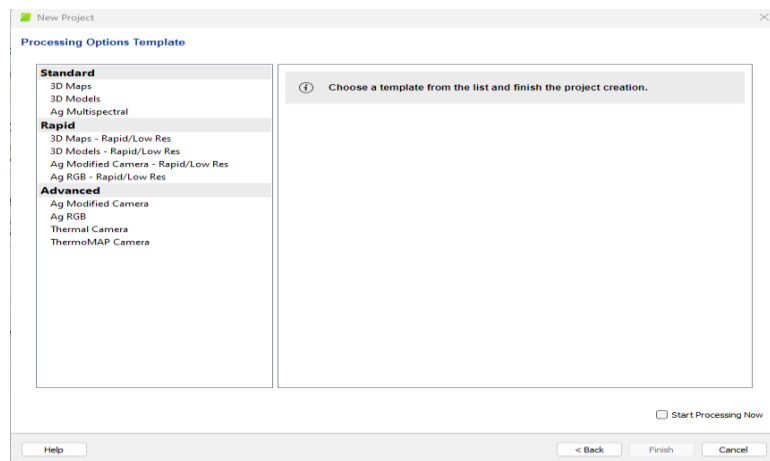


**Figure 11 – Selecting a Processing Options Template**

## 12 – Template Details: 3D Models Selected

In this step, the 3D Models template has been selected from the Standard category. The right panel displays detailed information about this template to help users understand its suitability for their project.

### Key Template Details:

- Purpose: To generate a 3D model from any set of overlapping images.
- Image Acquisition Types:
  - Suitable for oblique flight and terrestrial images (e.g., photos taken from the ground or at an angle).
- Outputs Quality/Reliability: *Rated High for this template.*
- Processing Speed: *Medium to slow, due to high-detail reconstruction.*

### Image Recommendations:

- Use images with a high amount of overlap, especially those taken from ground level or using oblique angles.
- Ideal for DSLR image sets with consistent coverage of a scene.

### Outputs Generated:

- 3D Mesh
- Point Cloud

### Final Step:

- ☐ The Start Processing Now option is intentionally left unchecked. This allows users to complete project setup without triggering immediate processing—useful when further settings need to be reviewed or processing is scheduled for later.
- ☐ Click Finish to finalize and save the project setup

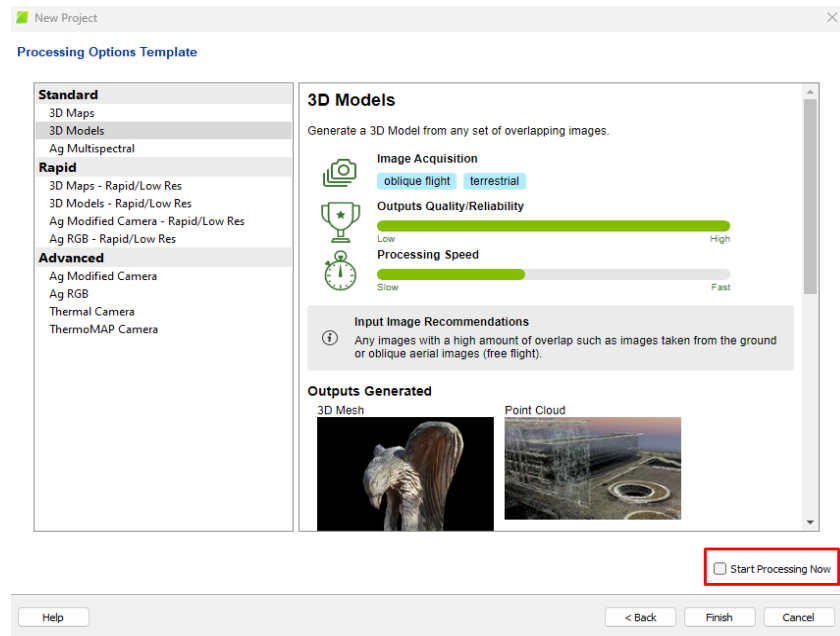


**Figure 12 – Template Details: 3D Models Selected**

### 13 – Project Successfully Created and Ready for Processing

After completing all setup steps and selecting the appropriate template, the Pix4D Mapper interface opens to the main workspace. The background displays a satellite basemap by default, and the project name (“Test”) appears in the window title.

Key Interface Elements:

- Map View: The central display shows a world map where image positions and outputs will appear once processing begins.
- Processing Bar (Bottom Left):
  - Displays the three main processing steps:
    1. Initial Processing

2. Point Cloud and Mesh
  3. DSM, Orthomosaic, and Index
    - Each step has its own status indicator.
- Start Button: Since the “Start Processing Now” option was left unchecked in the previous step, processing has not started automatically.
    - To begin processing manually, click the Start button in this panel.
  - Coordinate Information (Bottom Right):
    - Shows current projection settings, including:
      - WGS84 (World Geodetic System 1984)
      - and NAD83(2011) / Georgia East (ftUS)
      - Coordinates in both degrees and US survey feet

At this point, the user can choose to review project settings, add GCPs, or begin processing by selecting specific steps.

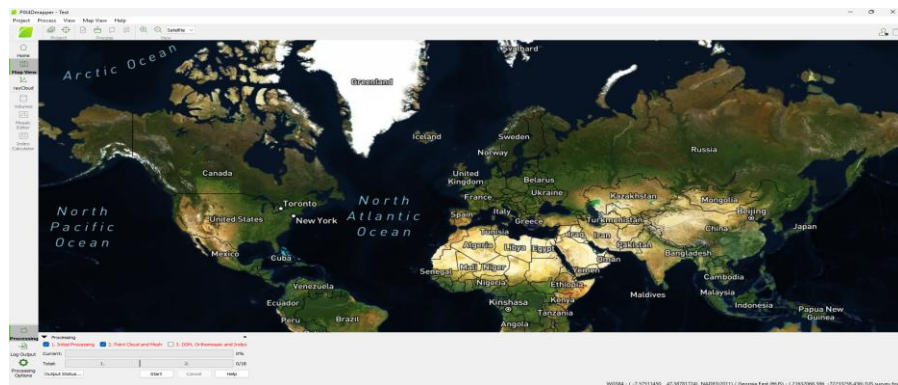


**Figure 13 – Project Successfully Created and Ready for Processing**

## 14 – Adjusting Initial Processing Options (Advanced Settings Enabled)

Before initiating processing, users can fine-tune their workflow using the Processing Options panel. In this figure, the Initial Processing tab is selected, and the Matching settings are being configured.

Advanced Options Enabled: The Advanced checkbox in the bottom left corner is checked, unlocking additional configuration options for more precise control over processing behavior.  
Matching Image Pairs Settings:

- Selected Option: Free Flight or Terrestrial

This is the appropriate choice for *DSLR or non-grid UAV image captures*, where image overlap is achieved through manual or irregular camera paths.

- Matching Strategy:
  - Use Geometrically Verified Matching is checked, which improves accuracy by ensuring that only geometrically consistent tie points are used for model generation.

Navigation: The left panel displays the full workflow: (keep these other options default)

Action: After configuring the settings, click OK to apply them and return to the main interface.

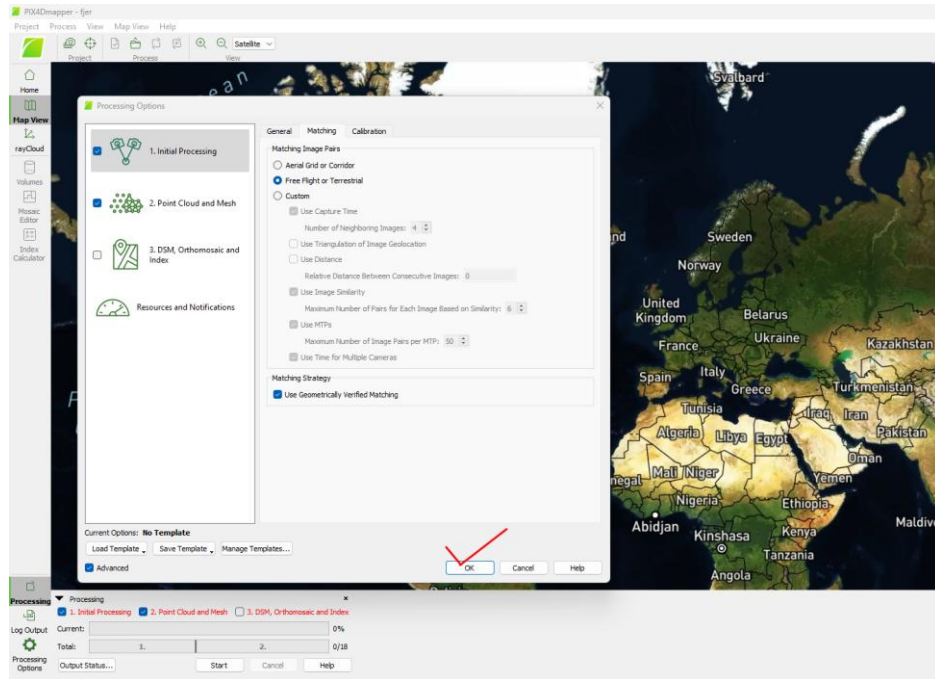


Figure 14 – Adjusting Initial Processing Options

## 15 – Starting the Processing Workflow

After configuring all project settings and verifying the processing options, the user is now ready to begin the photogrammetry workflow.

Processing Panel (Bottom Left):

- All three processing steps are currently selected:
  1. Initial Processing
  2. Point Cloud and Mesh
  3. DSM, Orthomosaic and Index

These steps represent the full processing pipeline in Pix4D Mapper, from image alignment to the generation of dense 3D data and 2D map outputs.

### Status Panel:

- Progress bars for each step are currently at 0%, indicating that processing has not started.
- Total Tasks: 25, as shown at the bottom right.

### Important Note:

👉 If DSM, Orthomosaic and Index outputs are not needed for the project, *uncheck Step 3* before clicking *Start* to save time and computational resources.

### Action:

- To begin processing, click the bolded *Start* button at the bottom center of the panel.

Reminder: Since the “Start Processing Now” checkbox was left unchecked during template setup, you must manually start processing from this screen.

Once started, Pix4D will run the selected steps sequentially and display progress in real time.

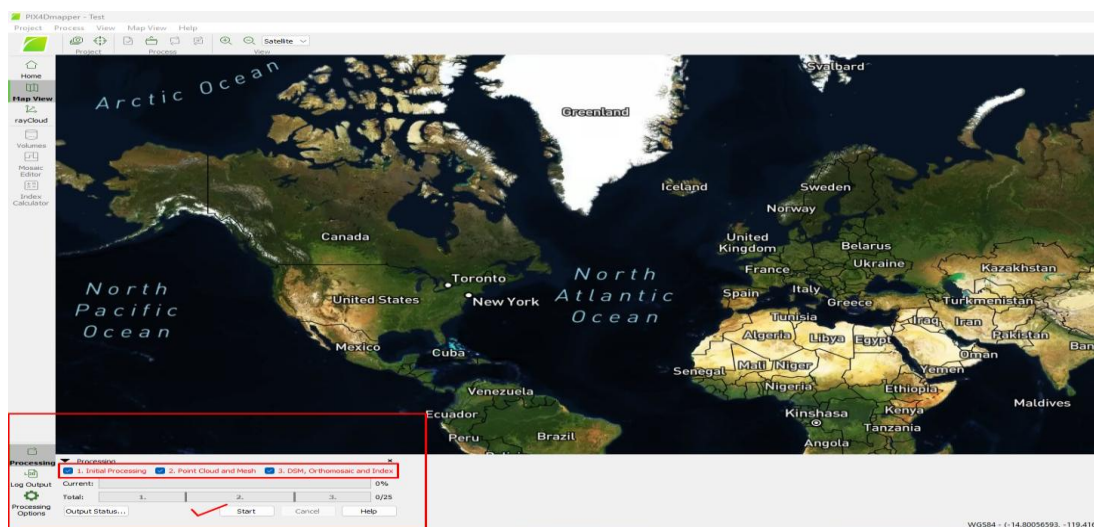


Figure 15 – Starting the Processing Workflow

## 16 – Initial Processing: Computing Keypoints

After clicking Start, Pix4D begins Initial Processing.

The software is currently computing keypoints—distinct features used for aligning overlapping images.

- Progress: 86% complete
- Active Step: 1. Initial Processing
- Steps 2 and 3: Pending
- Start button: Disabled
- Cancel and Output Status: Available for control and monitoring

Keypoints are essential for accurate image alignment and overall model quality.

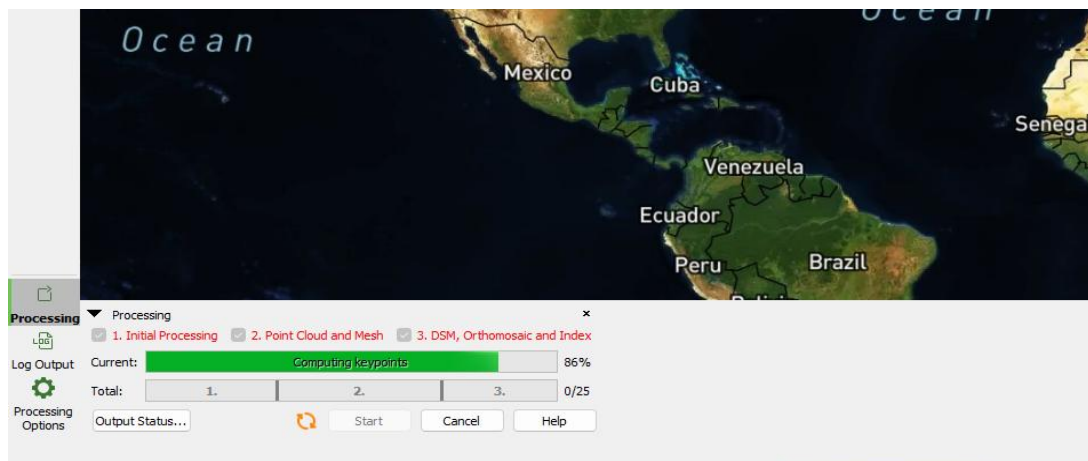


Figure 16 – Initial Processing: Computing Keypoints

## 17 – Quality Report: Key Metrics

After Initial Processing, the Quality Report provides key quality indicators.

The most important section is the Quality Check table (shown above), which uses icons to indicate result status:



## Highlighted Results:

✅ Images: Median of 74,908 keypoints per image

✅ *This sign shows everything is okay and meets recommended standards.*

⚠️ Dataset: 5 out of 7 images calibrated (71%)

⚠️ *This indicates some images were not successfully calibrated. Need to aligned images.*

✅ Camera Optimization: 3.4% difference

✅ *Acceptable difference between initial and optimized internal camera parameters.*

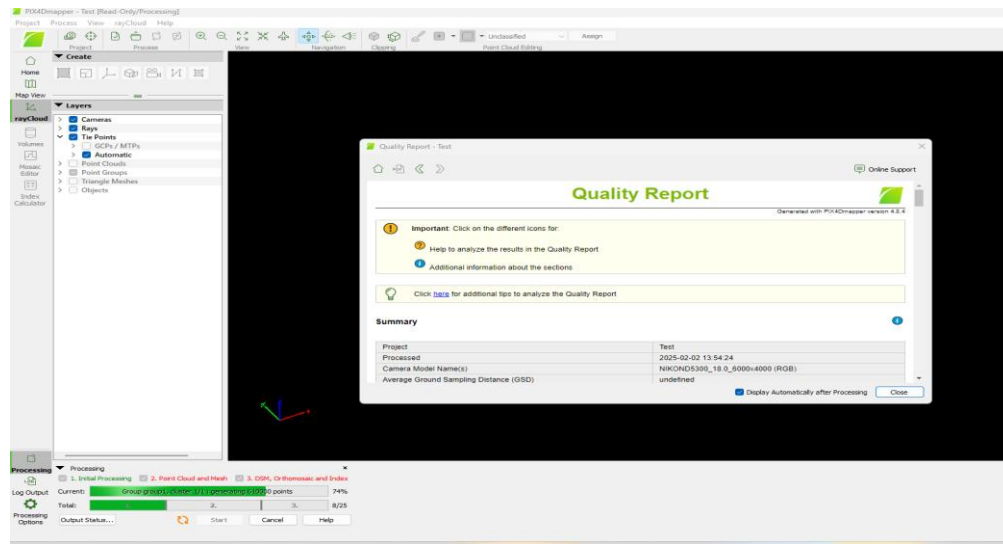
✅ Matching: 14,804 matches per image

✅ *Indicates good tie point matching performance.*

⚠️ Georeferencing: No 3D GCPs used

⚠️ *Model is not georeferenced; consider adding GCPs.*

⚠️ Warnings suggest reviewing image quality or adding GCPs for improved accuracy.



Quality Check		
Images	median of 74908 keypoints per image	✓
Dataset	5 out of 7 images calibrated (71%), all images enabled	⚠
Camera Optimization	3.4% relative difference between initial and optimized internal camera parameters	✓
Matching	median of 14804 matches per calibrated image	✓
Georeferencing	no, no 3D GCP	⚠

Figure 17 – Quality Report


## 18 – Completed Processing and rayCloud Visualization

After all selected processing steps are complete (100%), Pix4D displays the reconstructed scene in the rayCloud view.

Visible Elements:

- Green camera icons: Indicate camera positions and orientations.
- Point cloud: Shows the reconstructed 3D structure of the scene.
- Model output: Visible surface from aligned images and generated tie points.

Status Bar:

-  All processing steps completed
- Total Tasks: 25/25

- Current Step: Finished (populated with 100% progress)

Users can now inspect, edit, or export the point cloud and 3D outputs for further analysis.

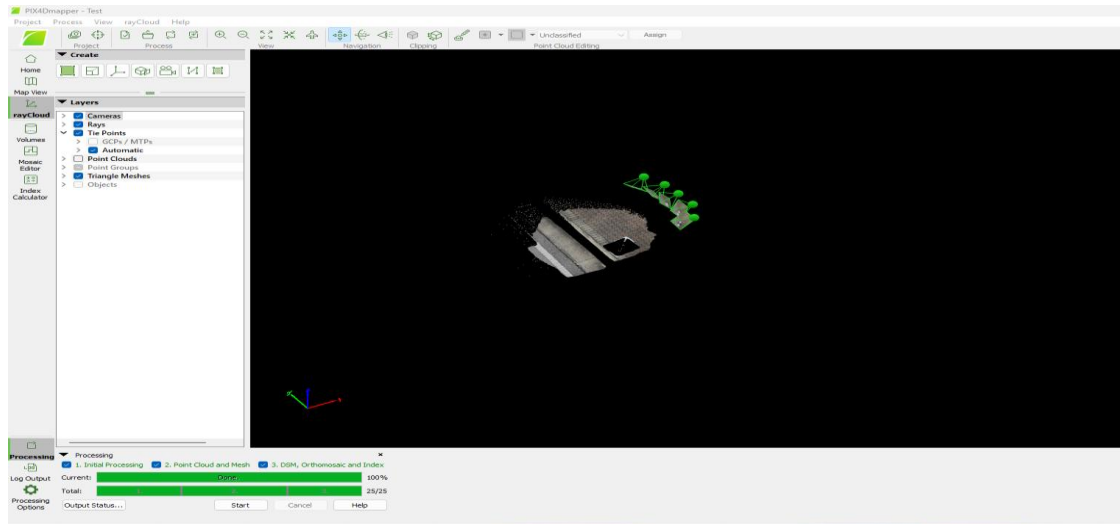


**Figure 18 – Completed Processing**

## 19 – rayCloud View with Camera Layer Hidden

After completing processing, the user can customize the rayCloud display.

What Changed:

- Cameras layer in the Layers panel is unchecked, which hides the green camera positions from the 3D view.

Visible Elements:

- The dense point cloud of the scene remains visible.
- All processing steps (1, 2, 3) show 100% completion in the status bar.

*Hiding the Cameras layer helps focus on the point cloud and surface model for analysis or presentation.*

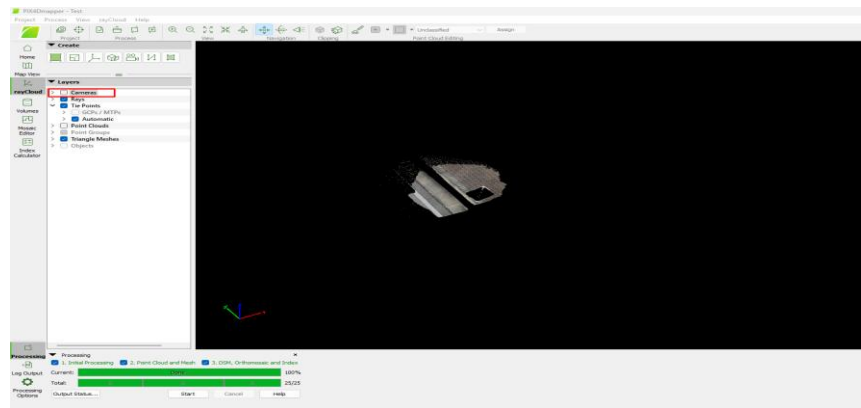


**Figure 19 – rayCloud View with Camera Layer Hidden**

## **20 – Point Cloud View with Triangle Meshes Hidden**

To focus only on the dense point cloud, the user can hide the mesh overlay.

What's Changed:

- Triangle Meshes layer is unchecked in the rayCloud Layers panel, removing the surface mesh from view.

Visible Output:

- Only the dense 3D point cloud is displayed.
- The scene appears clearer for feature analysis or inspection without mesh surfaces.

This helps in reviewing raw 3D data before exporting or performing further modeling.

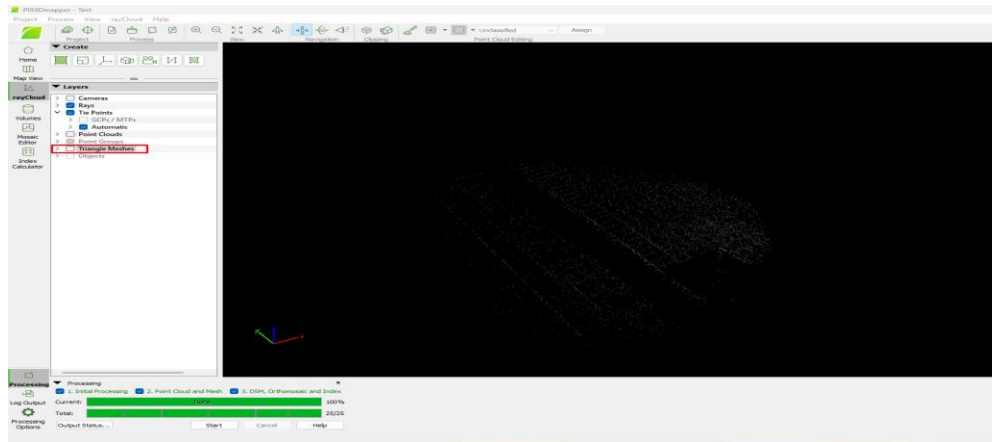


**Figure 20 – Point Cloud View with Triangle Meshes Hidden**

## **21 – No GCPs/Manual Tie Point (MTPs) Shown Under Tie Points**

In the rayCloud Layers panel, the GCPs/MTPs checkbox is empty because no GCPs were added to this project.

Reason:

- The model is not georeferenced, as confirmed in the Quality Report.
- Therefore, no GCPs or MTPs are available to display under the Tie Points section.

Adding GCPs improves model accuracy and geolocation. This step is recommended for georeferenced outputs or survey-grade results.

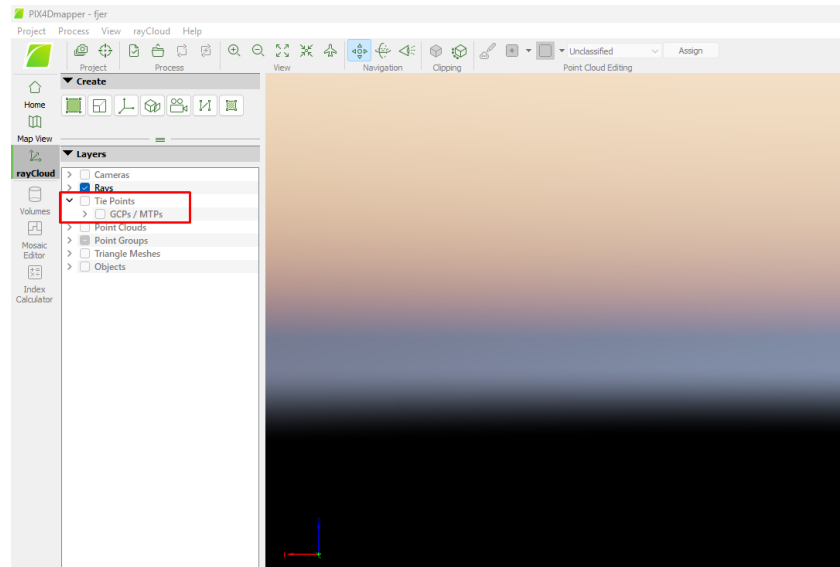


Figure 21 – No GCPs/MTPs Shown Under Tie Points

## 22 – Opening the GCP/ Manual Tie Point (MTP Manager for Georeferencing

To georeference the model in Pix4D Mapper, users must open the GCP/MTP Manager.

Steps:

1. Go to the Project menu on the top-left.
2. Select GCP/MTP Manager... from the dropdown list.

This tool allows you to import, mark, and manage GCPs or MTPs to accurately geolocate your 3D model.

Georeferencing is essential for aligning the model to real-world coordinates.

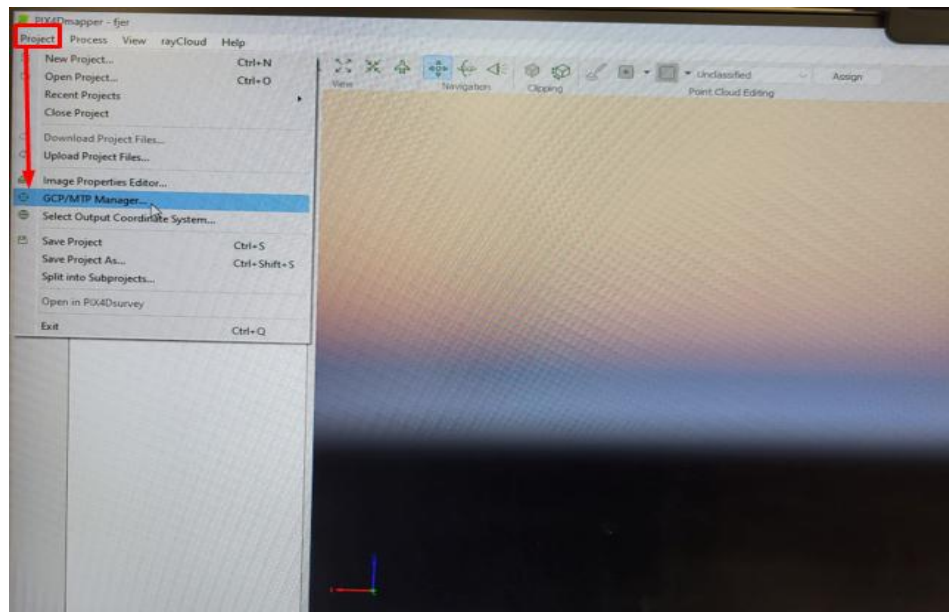


Figure 22 – Opening the GCP/MTP Manager for Georeferencing

## 23 – GCP/MTP Manager Interface for Adding Control Points

This window is used to import or manually add GCPs or MTPs to georeference the model.

### Key Options:

- Edit: Click to set or change the coordinate system for GCPs.
- Import GCPs...: Import a GCP file with known coordinates (CSV or TXT).
- Add Point: Manually add a new GCP/MTP entry.
- Import Marks...: Load previously marked image positions of GCPs.

To activate georeferencing, at least three GCPs must be added and marked on a minimum of two images each.

Tip: Use the rayCloud Editor (after initial processing) for precise marking and accuracy verification

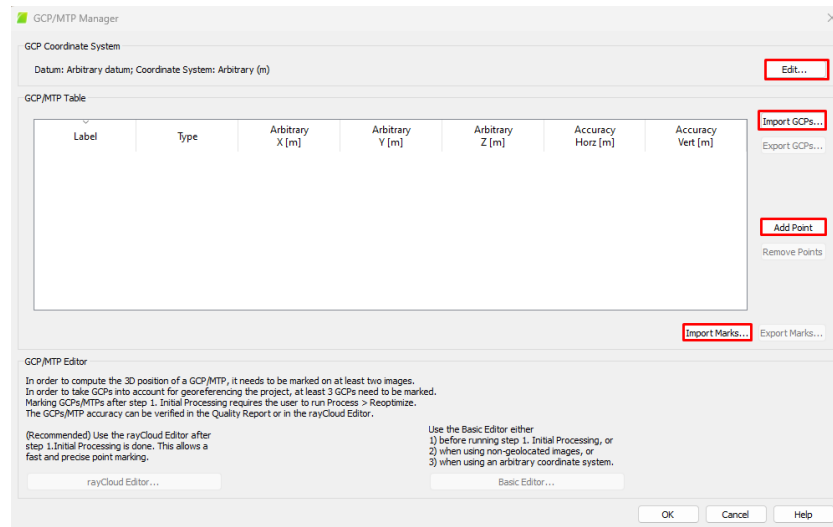


**Figure 23 – GCP/MTP Manager Interface**

## 24 – Defining GCP Coordinate System

To georeference the model correctly, click the "Edit..." button at the top-right of the GCP/MTP Manager.

Steps:

- Choose Known Coordinate System
- Unit: ft or m — *select based on your project requirement*
- From the list, select:

NAD83(2011) / Georgia East (ftUS)

— *or choose the relevant coordinate system depending on your project needs*  
*(as shown in the highlighted (Blue) selection box)*



This step ensures the GCPs are placed within the correct spatial reference system for accurate model alignment.

Click **OK** to confirm.

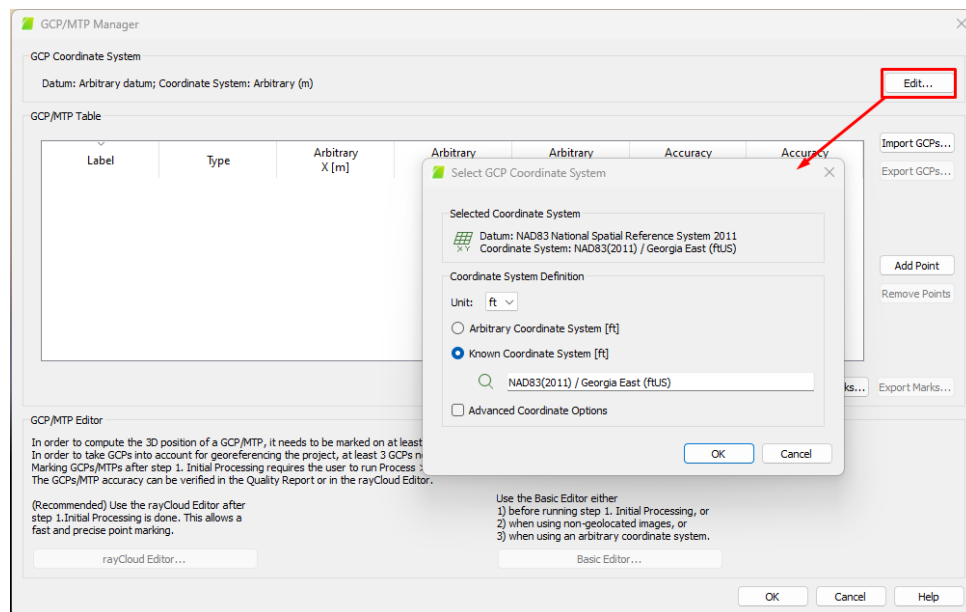


**Figure 24 – Defining GCP Coordinate System**

## 25 – Importing GCP Coordinates from File

To import GCPs for georeferencing, follow these steps:

1. In the GCP/MTP Manager, click Import GCPs... on the right.
2. The Import GCPs window will pop up.
  - Set the Coordinates Order to X, Y, Z (or as appropriate for your file).
  - Click the Browse... button to locate your GCP file.
3. In the file browser, navigate to your GCP text file (.txt or .csv format).
  - Make sure **\*\*\*txt files (.txt; .csv)** is selected in the file type dropdown.
4. Select the correct GCP file and click Open.

Note: Ensure the file is properly formatted with X, Y, Z coordinates separated by commas or tabs and that it matches the selected coordinate system.

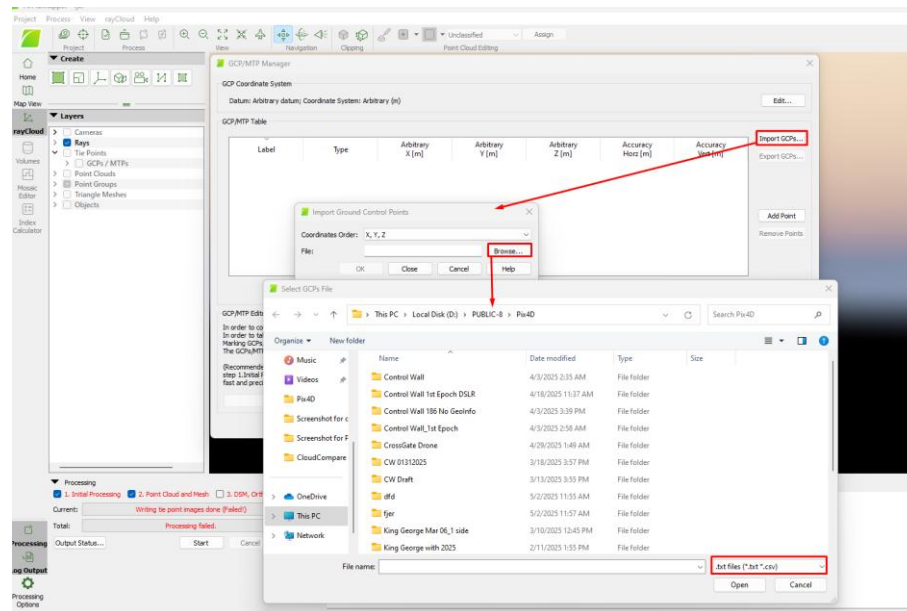


**Figure 25 – Importing GCP Coordinates from File**

## 26 – Adding GCP/MTP/Checkpoint

If you don't have a file to import GCPs, you can manually add points for georeferencing:

1. Click the Add Point button on the right.
2. A new row will appear in the GCP/MTP Table labeled as mtp1 with the type Manual Tie Point.
3. You can enter the coordinates manually in the columns for X, Y, Z, and specify the Horizontal and Vertical Accuracy if known.

Tip: You need at least three GCPs or MTPs with known positions to properly georeference a model. Use this method if your data is limited or if you're marking points from a known map or drawing.

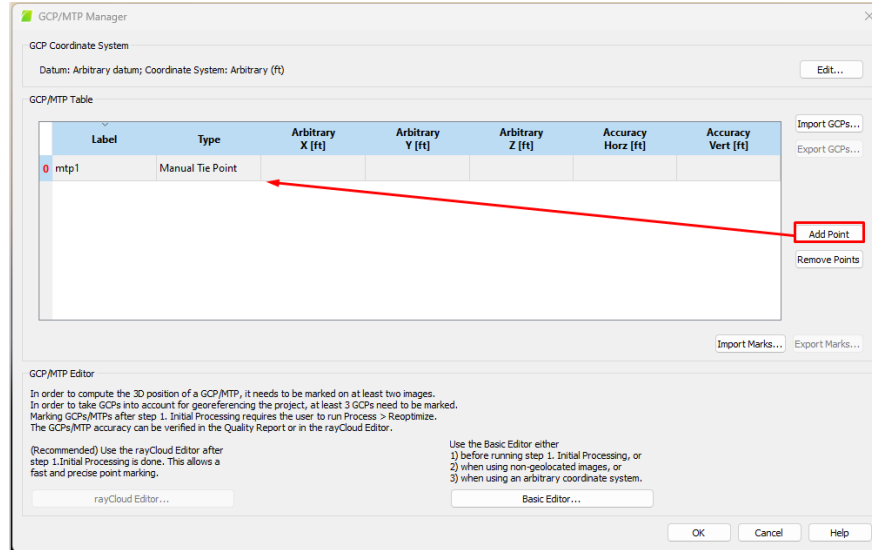


**Figure 26 – Adding GCPs/MTPs**

## 27 – Renaming and Assigning GCP/MTP Types

To customize GCPs , Manual Tie Points (MTPs), or CPs:

- Double-click the “Label” cell to rename the point (e.g., GCP A, Check 1, MTP3).
- Double-click the “Type” cell to open the drop-down list and select from the available types:
  - 2D GCP – for control in X and Y only
  - 3D GCP – for full control in X, Y, and Z
  - Check Point – for accuracy validation
  - Manual Tie Point – for internal model referencing only

Ensure that at least three 3D GCPs are defined and marked on two or more images for successful georeferencing.

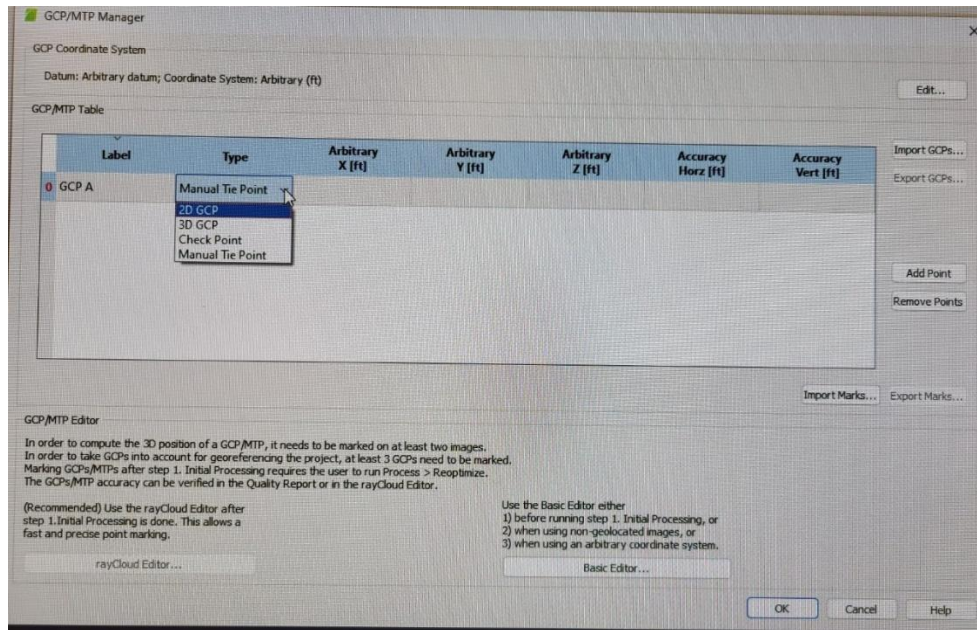


**Figure 27 – Renaming and Assigning GCP/MTP Types**

## 28 – GCP/MTP Table with Entered Coordinates

This table displays manually added 3D GCPs and a Checkpoint with their respective coordinates and accuracy values.

This is just an example to demonstrate how labels, types, coordinates (X, Y, Z), and accuracy fields are filled in:

- GCP A and GCP B are labeled as 3D GCPs with full XYZ coordinates and associated horizontal/vertical accuracies.
- CP 1 is labeled as a Checkpoint, used to verify the model's positional accuracy.
- Coordinates are listed in arbitrary units (ft), based on the current coordinate system.
- The note "0/2 GCPs with enough image marks" indicates that GCPs still need to be manually marked on at least two images each using the rayCloud Editor for georeferencing to take effect.

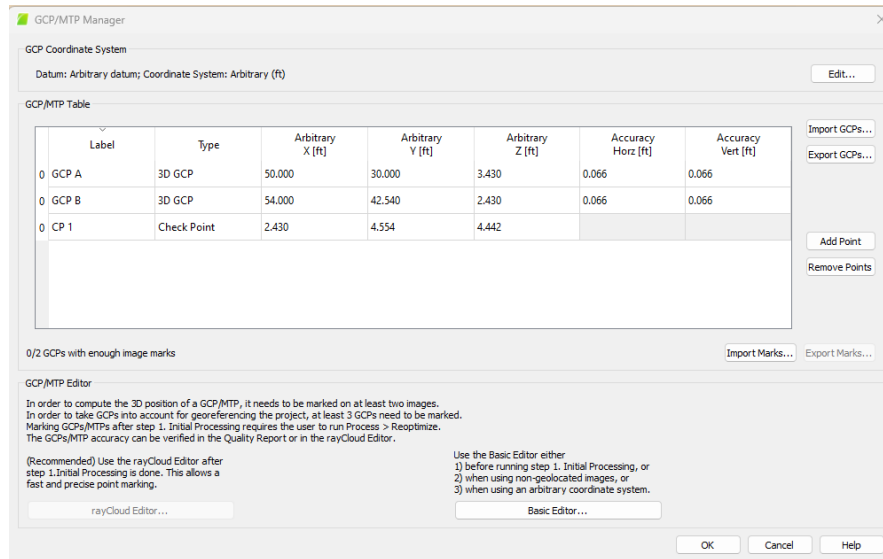


**Figure 28 – GCP/MTP Table with Entered Coordinates**

## 29 – GCP/MTP Visibility in rayCloud

This window shows the GCPs/MTPs listed in the Layer panel under Tie Points after importing or manually adding them.

Each point (e.g., GCP A, GCP B, CP 1) has a “(0)” beside it, meaning:

- They have not yet been marked on any images.
- For georeferencing to work, each GCP must be marked on at least two images.

Action Required: Open rayCloud Editor, locate each GCP/checkpoint, and manually mark them on corresponding images to complete the georeferencing process.

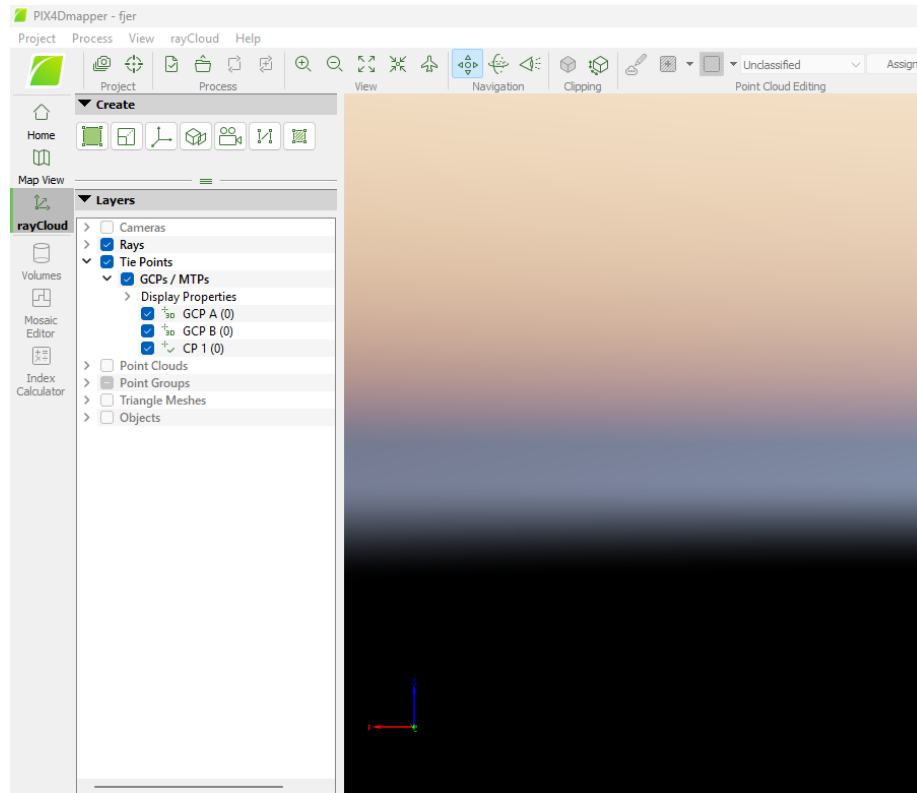



**Figure 29 – GCP/MTP Visibility in rayCloud**

### 30 – Manual GCP Marking in rayCloud Editor

This figure shows the manual GCP marking process using the rayCloud Editor in Pix4Dmapper:

- The red circle highlights the selected GCP (e.g., GCP A) on the 3D point cloud model.
- On the bottom-right panel, multiple images are displayed where this GCP appears.
- Users manually place the green crosshair on the exact GCP location in each image to improve georeferencing accuracy.

 Here, it is shown that for GCP A, 76 images were marked manually by placing the green crosshair at the exact center of the 2 ft × 2 ft GCP marker to enhance positional accuracy.

- ✓ *Tip:* A GCP should be marked on at least 10-15 images, but more images (as in this case) further improve the reliability and precision of the computed position.

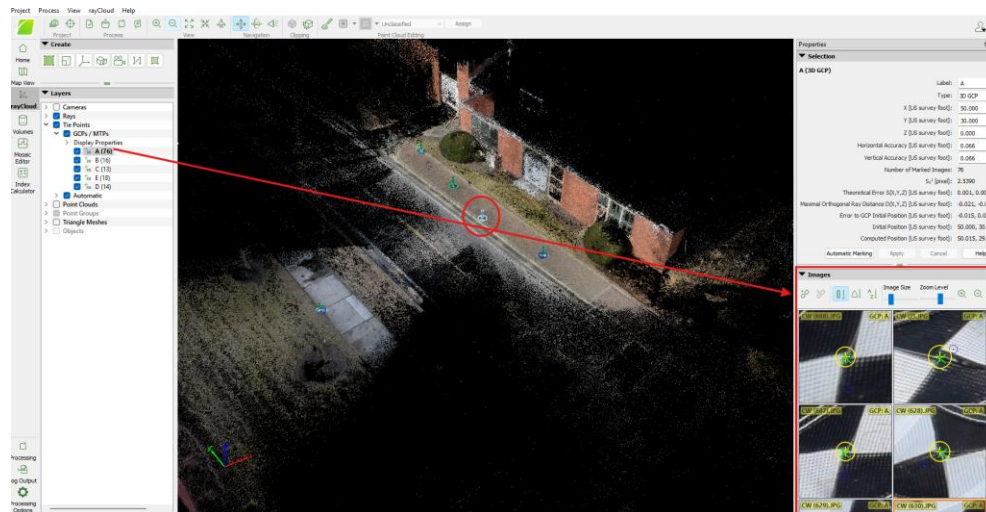


**Figure 30 – Manual GCP Marking**

### 31 – Finalizing GCP Position After Manual Marking

Once you have manually marked the exact location of the GCP (e.g., GCP A) using the green crosshairs in all relevant images:

- ✓ Click the "Apply" button in the right-side panel.
- This updates the GCP with improved accuracy and recalculates its 3D position.
- The "Computed Position" field will now show the final coordinate for that GCP after all manual inputs are considered.

- ✦ *Tip:* This step ensures that the GCP coordinates reflect true alignment in both the point cloud and the source images, enhancing overall model georeferencing precision.

➡ Now repeat the same process for all other GCPs (e.g., GCP B, GCP C, etc.) to complete the georeferencing process.

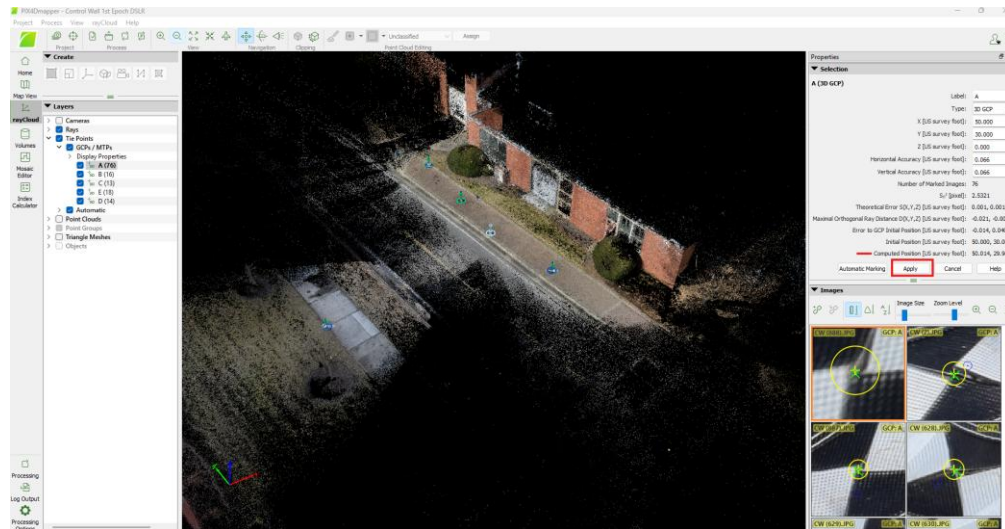


**Figure 31 – Finalizing GCP Position After Manual Marking**

## 32 – Reoptimizing the Model After GCP Updates

Once you have manually marked all GCPs/MTPs (e.g., GCP A–E) and finalized their positions:

✅ Click the "Reoptimize" button (highlighted in the toolbar).

This command recalculates the camera positions and model coordinates based on the newly added or updated GCPs.

✦ Tip: You must reoptimize the model every time you:

- Edit any GCP coordinate values
- Add or remove GCPs
- Change the GCP type or labels
- Re-mark GCPs manually in images

⚠ Skipping this step will result in misaligned models and inaccurate georeferencing.



- ➔ Once re-optimization is complete, the updates will reflect across the 3D model, Ortho mosaics, and point clouds—ensuring improved spatial accuracy.

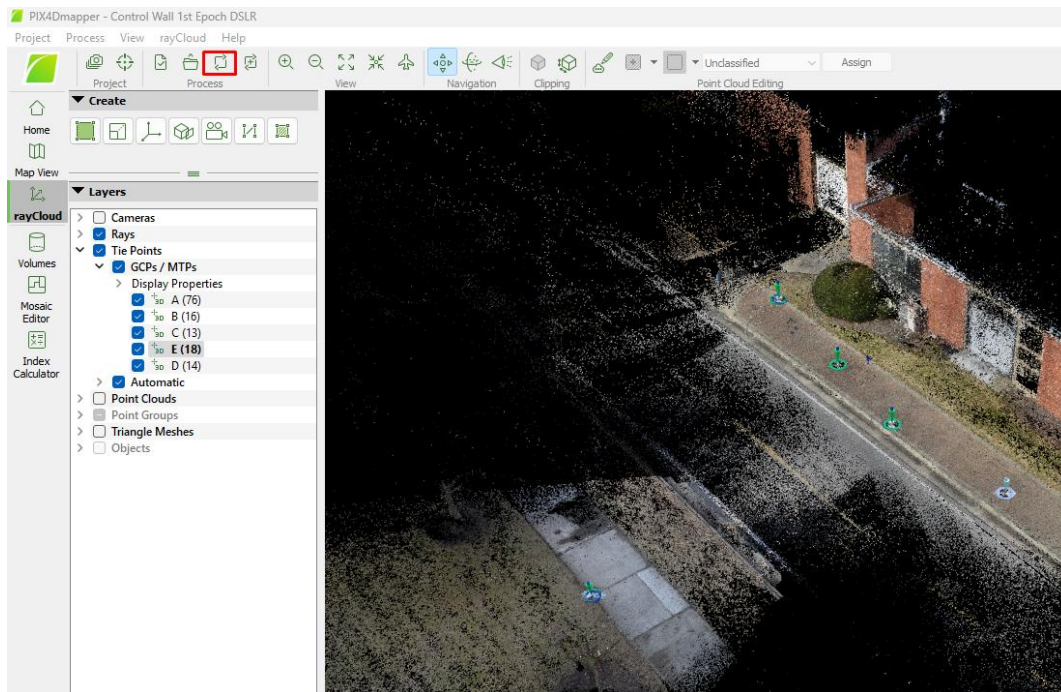


**Figure 32 – Reoptimizing the Model After GCP Updates**

## **APPENDIX C10. DRONEDEPLOY PROTOCOL**

### **DRONEDEPLOY PROTOCOL**

#### **Drone Deploy Enterprise (2025)**

(By Shakil Ahmed, 2025)



Date of Version V.10 - Feb 2025

# GENERATE A CLOSE-RANGE PHOTOGRAMMETRIC MODEL

## 1. Open the DroneDeploy Platform

- a. DroneDeploy is a cloud-based platform, you need to open a web browser.
- b. Click here, [DroneDeploy](https://www.dronedeploy.com/app2/auth/signin), to navigate the sign-in/login page, or just go to this web address <https://www.dronedeploy.com/app2/auth/signin>. You will see a webpage like Figure 1.

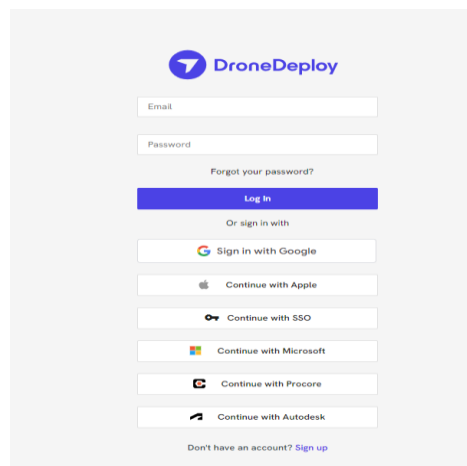


Figure 1: Log in/Sign up page of Drone Deploy

- c. Log in with your credentials to navigate your projects in Drone Deploy.
- d. After successful login, you will reach the Projects tab of Drone Deploy on your account, as shown in Figure 2.

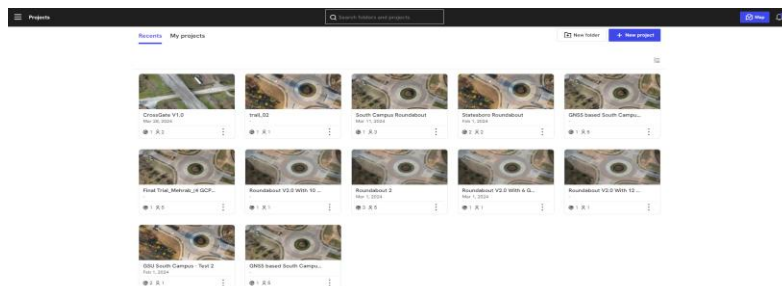


Figure 2: The Project tab of Drone Deploy in the cloud.

## 2. Create New Project

- a. Click the New Projects (this button appears in the top right corner in Figure 2)
- b. After clicking on New Projects, the figure 3 below, like tab will appear
- c. Find your site by searching by name, zip, or place coordinates. (Figure 3)



Figure 3: After clicking on the New Project, the above tab will appear.

- d. Preferably search your site by Zip and then navigate to a specific site or have surveys/pictures. Follow the 2 figures below to follow the process.



Figure 4a: Select the suggested address after you put the zip code in the search bar.



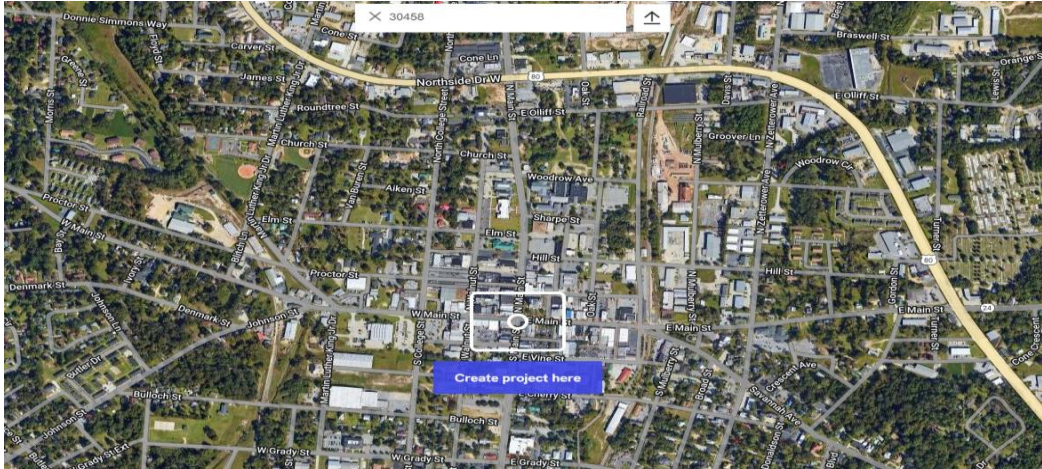


Figure 4b: Now you can see the satellite map of the zip code.

- e. Now, click on the Create project here button to create a new project. (See figure 4b)
- f. Then you must give a suitable name in Project Name for your project (see Figure 5)

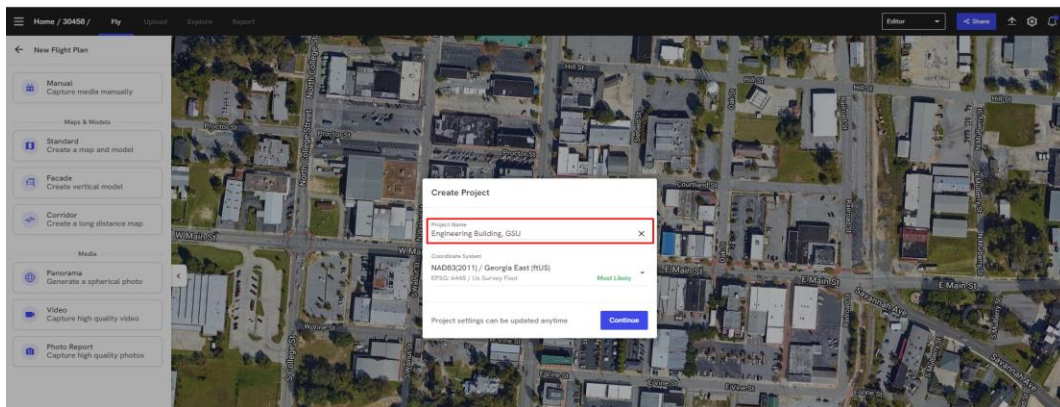


Figure 5: Naming the project step in creating a new project process.

- g. Now select the Coordinate System from the dropdown menu that best fits your project. For Georgia, and this Lab, we prefer Georgia East U.S. Survey Foot (USft) (NAD83(2011)). See figure 6 for reference.

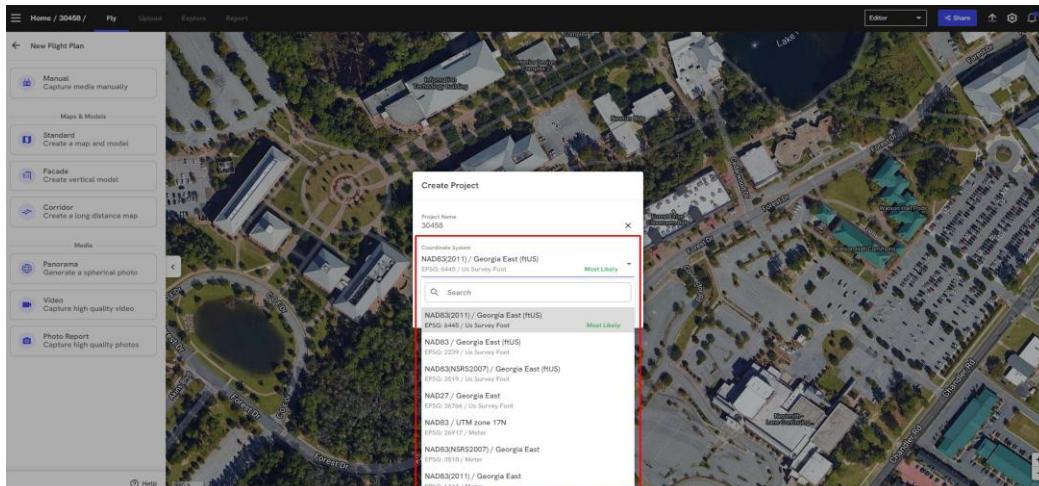


Figure 6: Selecting the coordinate system step in creating a new project process.

- h. You can also search any coordinate system by Name or EPSG code. (See figure 7)

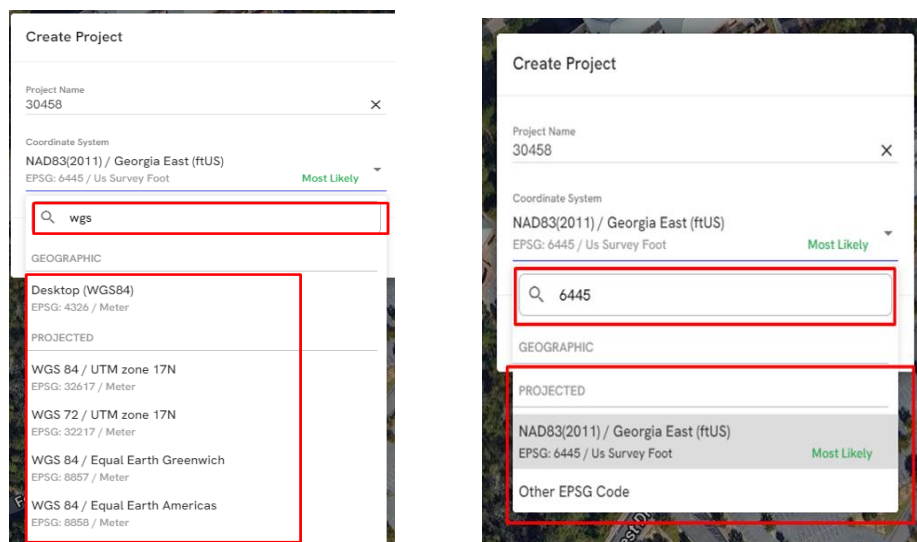


Figure 7: The Left one is a search by Name & right one is a search by EPSG code

- i. Then click on the Continue button for the next step.
- j. A new project is created in the Drone Deploy account, and you will see a tab like Figure 8 in front of you on the screen.



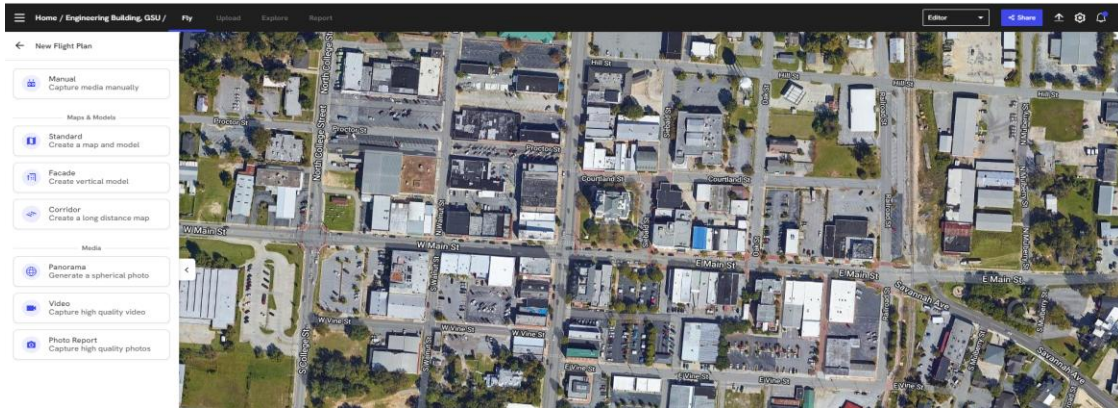


Figure 8: A new project, “Engineering Building, GSU,” is created.

### **3. Add photos**

- a. Go to the Upload tab in your newly created project (see figure 9)

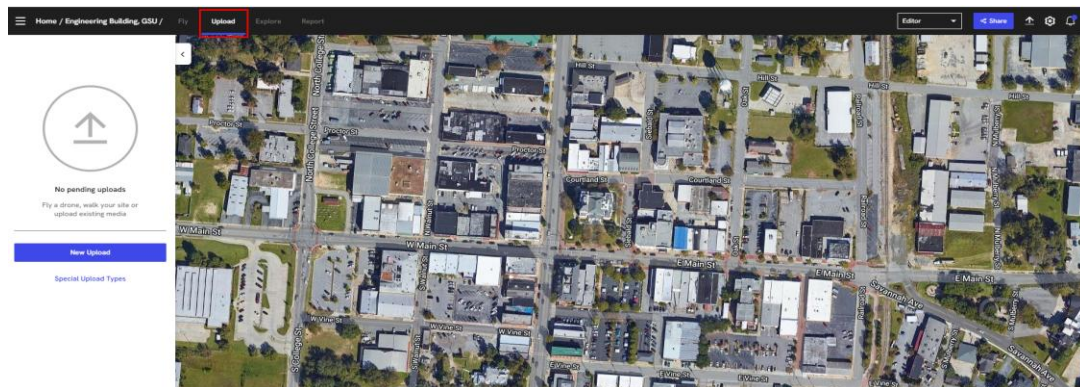


Figure 9: Upload tab of a new project in Drone Deploy

- b. Now, click on New Upload (see figure 9)
- c. Then Choose Files from your computer (navigate the location). Drone Deploy only supports .jpeg, .jpg, .mp4, .insv, .mrk, .obs & .mov type files.
- d. Then you will find a page like Figure 10. You can see a map named ‘Map #1’ that you can rename the map by clicking on the name. In Medi, you can see the number of files you have uploaded, you can see a projected area of the survey area on the left side of the window. If you want to add more files, you can still have the option to Choose Files here.

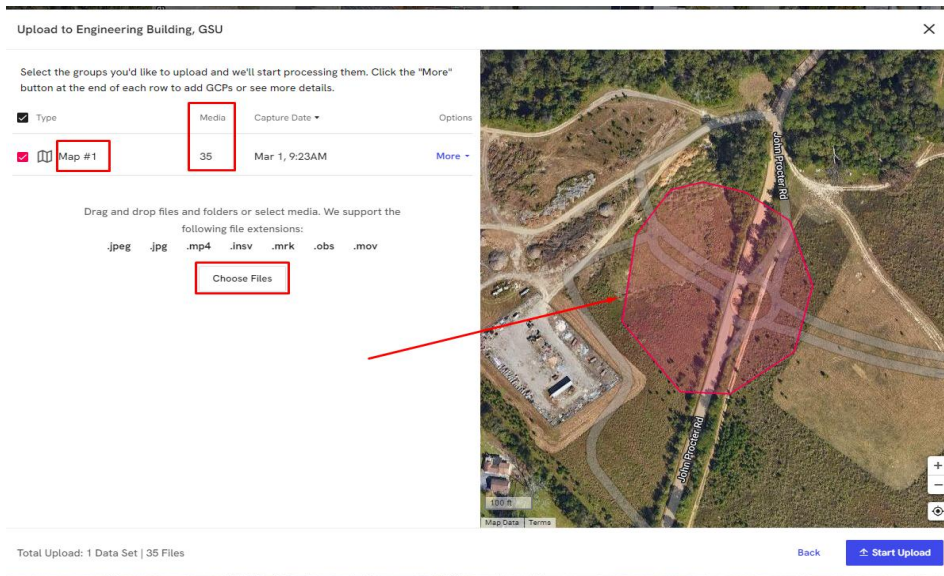


Figure 10: Choose Files window of the Drone Deploy system.

- e. When you click on the More dropdown menu in Figure 10, you will get Figure 11.

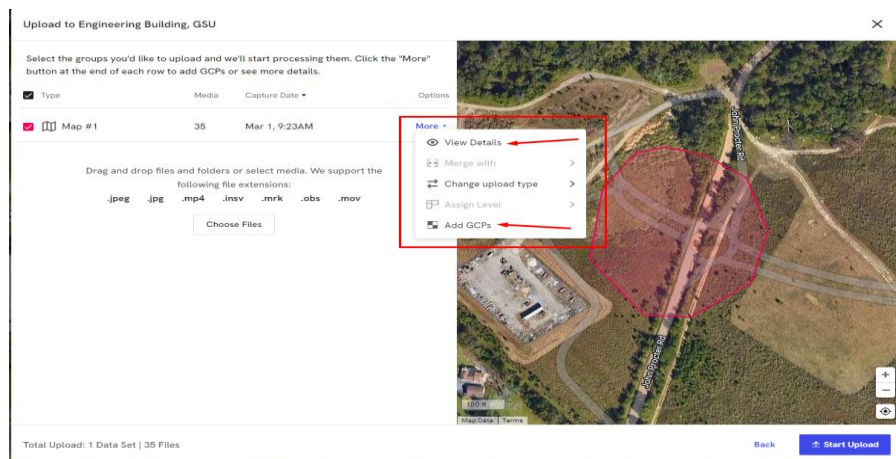


Figure 11: Add GCPs and View Details tab.

- f. If you click on "View Details", you will see a new window like Figure 12, where you can see each image's location on the map. You can unselect any of them if you want by clicking on the photo.





Figure 12: View Details tab

g. If you don't want to upload GCPs, then click on the **Start Upload Button**. If you want, follow chapter 4.

#### 4. Add GCPs and CPs

- a. In Figure 11 and Figure 12, both tabs have an option to upload CGPs and CPs. You can add a .csv file to upload the GCPs and CPs. There is a prescribed format for the CSV file (see Figure 13a).

	A	B	C	D	E
1	GCP Label	Northing	Easting	Elevation (ft)	
2	1	873428.2	773740.6	128.32	
3	2	873523.9	773785	129.54	
4	3	873495.2	773642.2	126.62	
5	4	873571.7	773707.1	128.06	
6	5	873427.9	773679.9	126.32	
7	6	873560.9	773747.3	129.2	
8	7	873527.8	773652.2	127.1	
9	8	873464.3	773776.5	129.67	
10	9	873533.2	773689.8	127.97	
11	10	873468.6	773719.8	128.76	
12	11	873515.4	773757.6	128.9	
13	12	873432.9	773697.3	126.51	
14					
15					
16					
17					

Figure 13a: GCPs format in csv file.

- b. It is available on the Drone Deploy website. When you are uploading GCPs and CPs, make sure you select the same coordinate system as the project. See figures 13b & 13c.

Figure 13b: Add GCPs and CPs tab.

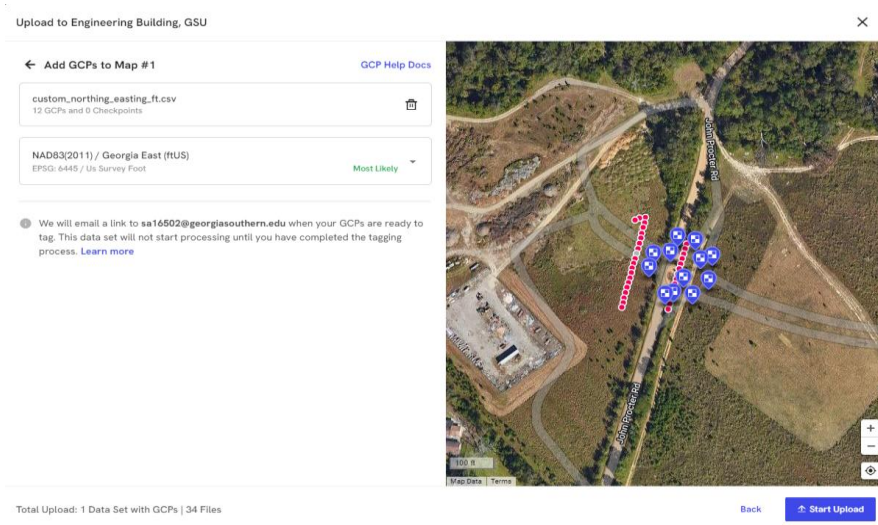


Figure 13c: Uploading a .csv file and selecting the coordinates of GCPs.

- c. After uploading the .csv file, click on Start Upload.

#### 4.1. Elevated GCP/Auxiliary GCP

- **Leverage Elevated GCPs for Higher Accuracy**

Field experiments show that incorporating elevated GCPs—markers placed above ground level—reduces the root mean square error (RMSE) and enhances the overall geospatial accuracy of DroneDeploy 3D models.

##### ☐ Recommended Placement

- Use at least two GCPs positioned at heights that differ from the ground plane.
- For buildings, place Additional GCPs high on the façade or roof—e.g., one on each of the four walls—to provide robust vertical control.

## □ Simple Integration in the Workflow

- No extra processing steps are required beyond your standard GCP workflow described in Section 4.
- In the same CSV file used for ground GCPs (see the sample in Section 4 (a)), add the elevated GCPs as new rows and enter their corresponding **X, Y, Z** coordinates.
- Ensure the “Number/Name” column clearly distinguishes these elevated points from groundlevel GCPs.

## 5. Processing

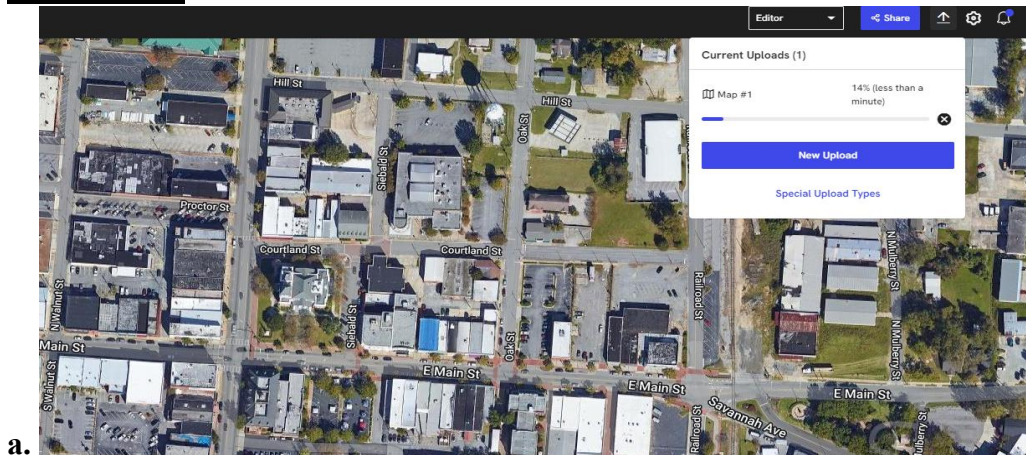


Figure 14: Uploading the photos with/without GCPs.



- b. When completing the uploading process, we will see the window like figure 15 with a message ‘Once processing is complete, you will receive an email.’

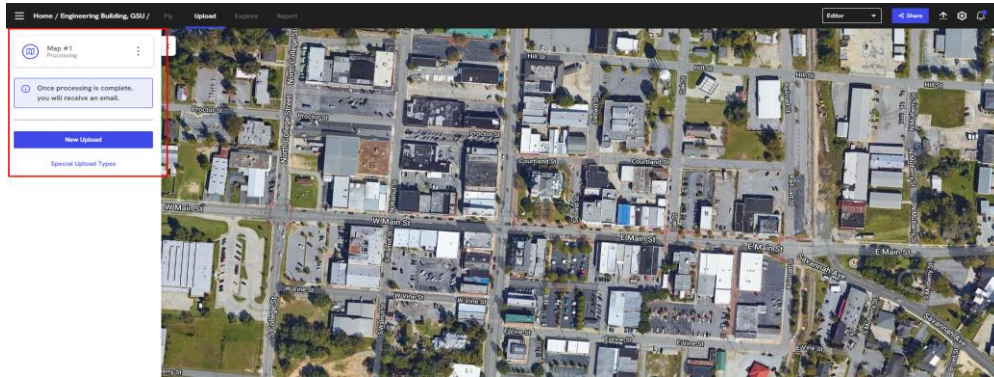


Figure 15: Drone Deploy processing the map and model in the back end.

- c. After completing the processing, Drone Deploy sends you an email that your model is ready to view. See figure 16a for reference. You can view the model by clicking on View Map, or go to your Drone Deploy account “My Projects” tab and navigate the map/model.

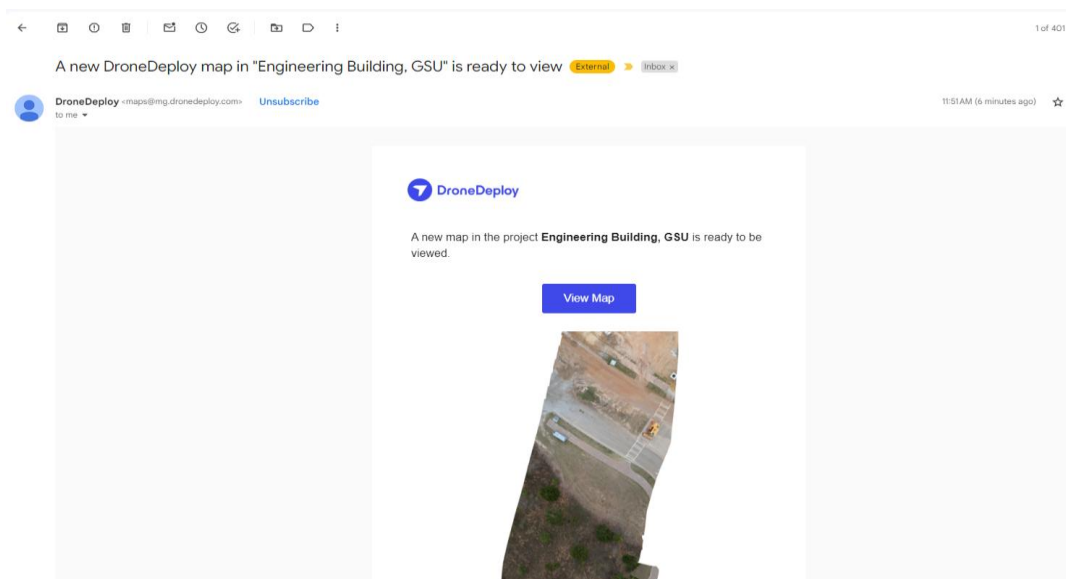


Figure 16: Confirmation mail of Map/Model is ready to view.

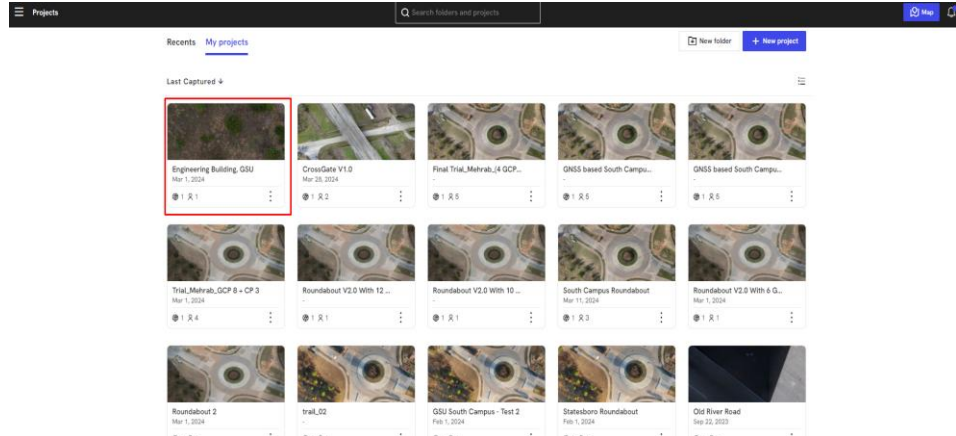


Figure 16a: Navigate the newly processed project from the My Projects tab.

## **5.1. Processing; review GCPs**

- a. If you uploaded GCPs in chapter 4, then you have to review the GCPs. Otherwise, skip this sub-chapter 5.1.
- b. For review GCPs, we will get an email from Drone Deploy saying “GCP map is ready for review”. Just click on the review GCPs button in the mail. See figure 17 for reference.

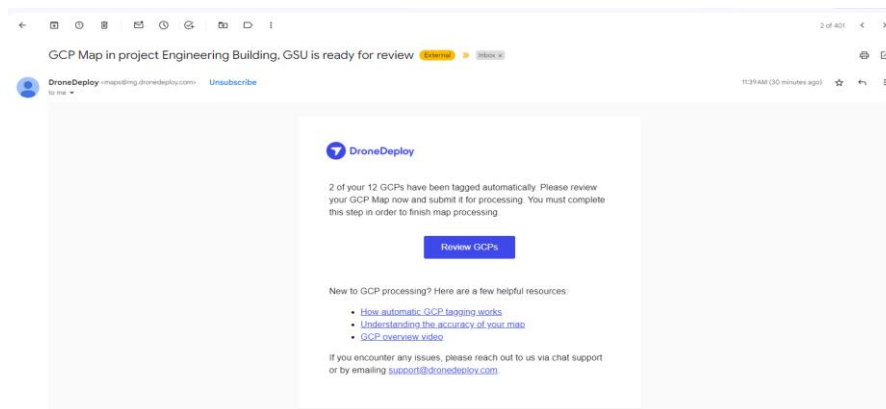


Figure 17: Confirmation mail of GCPs in Map/Model is ready to review.

## **6. Converting the Model to Local Coordinate System**

- a. To convert the model with local coordinates, go to the Explore tab of the Map/Model. Then click on the Settings icon at the top right corner of the window.

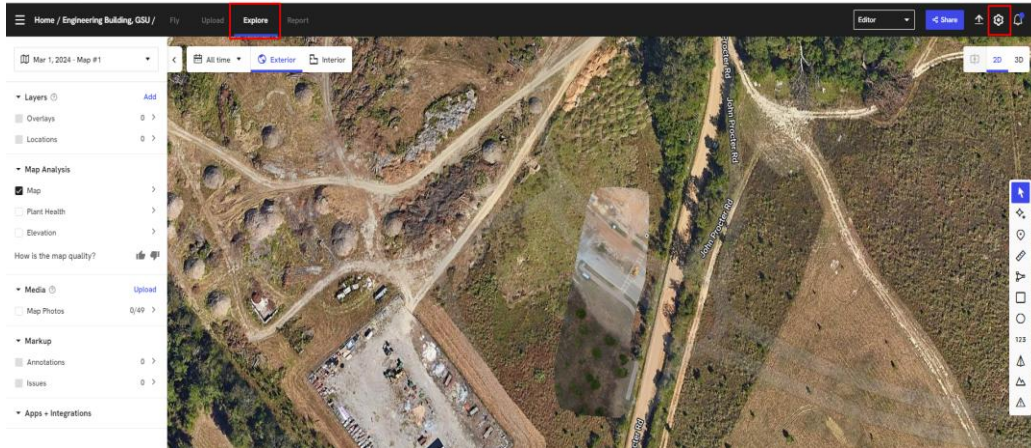


Figure 21: Explore Tab of Drone Deploy map/model.

b. You will get a new tab ‘Project Setting’ with many options on the left side of the window.

Here, click on the dropdown menu of ‘Coordinate System’. See Figure 22 for reference.



Figure 22: Project Setting tab.

c. From the bottom/last option from the dropdown menu, select the ‘Upload Custom Grid’ option (See figure 23 for reference), and you will see a new pop-up window.





Figure 23: Upload Custom Grid option.

- d. In the “Import Custom Coordinate System” tab, choose the CSV file to convert the coordinate to local. If you need a template (this is available in ft & m), click on the download option. See figure 24 for reference.

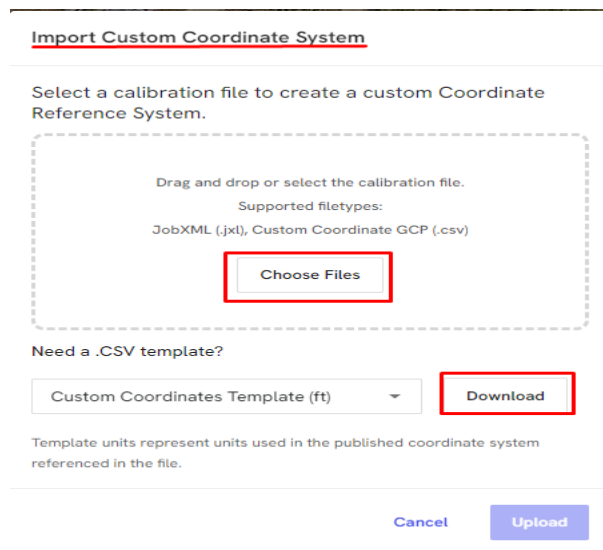


Figure 24: Import Custom Coordinate System tab.

- e. The .csv format is like Figure 25 below. “A” column is the GCP's number. “B to C” is the original/global reference system. And “E to G” is for those local coordinate values that will replace the global value.

A	B	C	D	E	F	G	H
GCP Label	Northing	Easting	Elevation (ft)	Custom Northing	Custom Easting	Custom Elevation (ft)	
1	782348.2	963636	22.51	242.107	419.616	99.655	
2	782357.8	963676.1	22.56	233.637	379.338	99.655	
3	782390.8	963654.3	22.83	200	400	100	
4	782382.3	963613.2	22.87	207.148	441.384	100.043	
5	782395.9	963568.5	35.48	192.094	485.603	112.648	
6	782344.6	963720	34.71	248.242	335.734	112.005	

Figure 25: Local coordinate value of the GCPs (CSV format)

- f. Select the CSV file by clicking on Choose File in Figure 24, then you will see a tab like Figure 26. There, you have to select a suitable coordinate system.

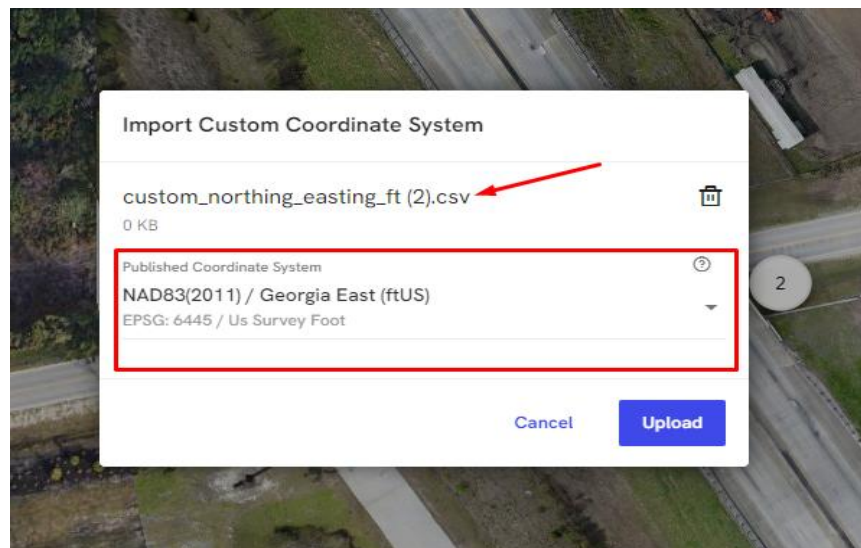


Figure 26: Uploading the CSV file for the local coordinate system.

g. Click on the Upload button. You will see that the coordinates of the points have changed. See the images below, 26a is before the upload of local coordinates, and 26b is after the upload.

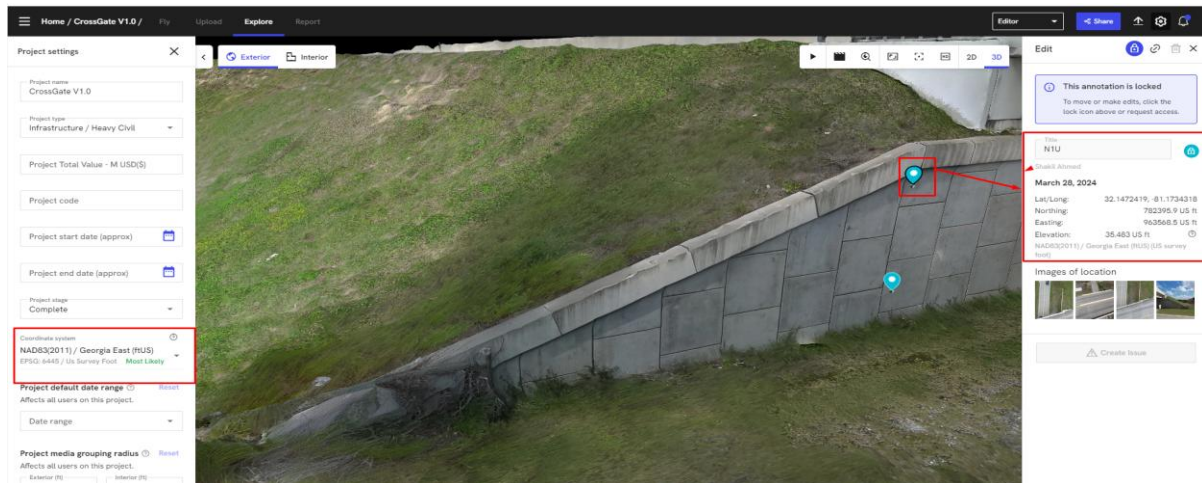


Figure 26a: N1U points coordinate value before the upload of the local coordinate system.

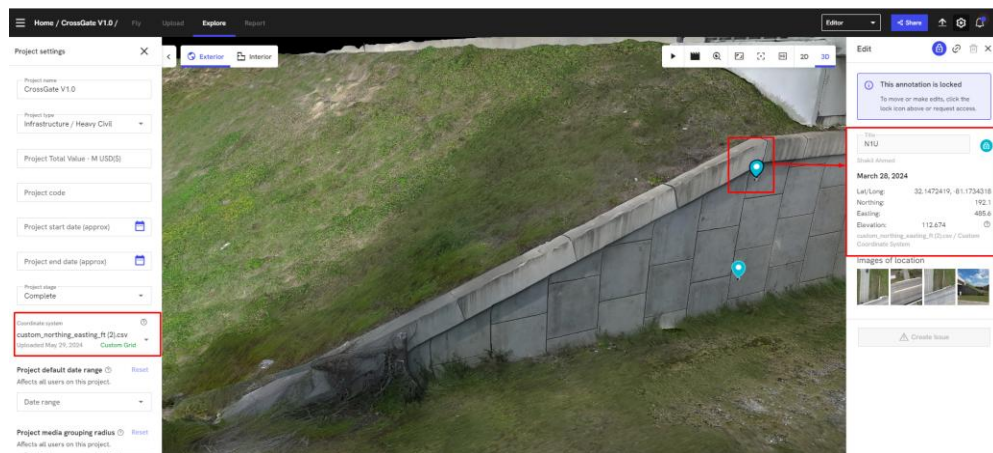


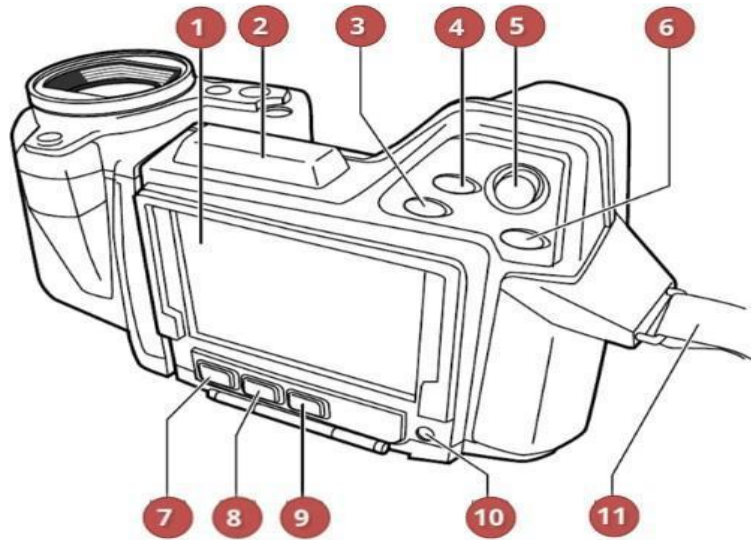
Figure 26b: N1U points coordinate value after the upload of the local coordinate system.



## APPENDIX C10. FLIR T420BX THERMAL CAMERA PROTOCOL

### Protocol On How to Operate (FLIR) T420bx Thermal Camera

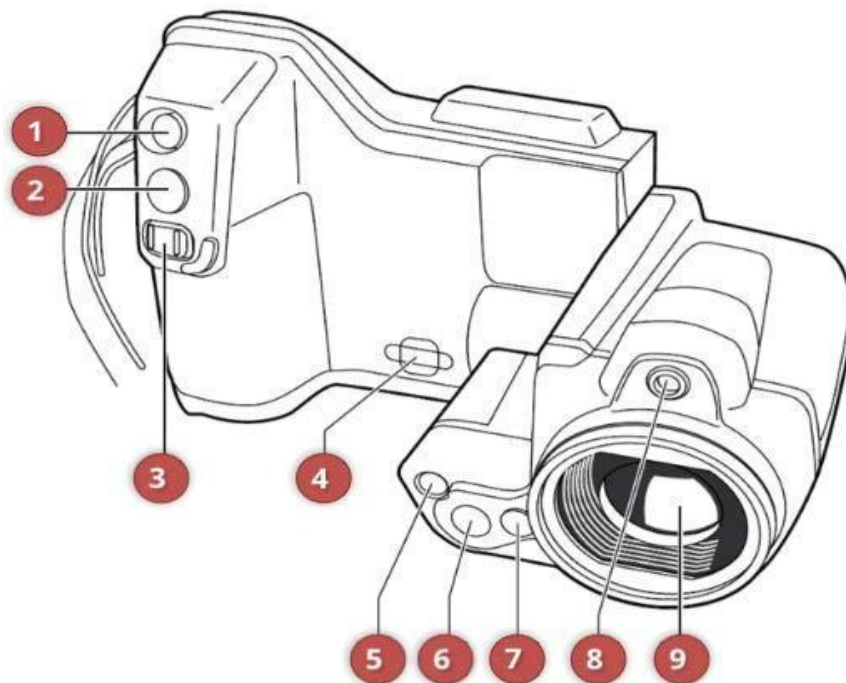
#### Components of the Thermal Camera



View from the Rear

1. Touch Screen LCD
2. Antenna
3. Digital zoom button
4. Programmable button
5. Joystick and push button
6. Back button

- 7. Camera lamp
- 8. Button to switch from automatic to manual pictures
- 9. Picture gallery
- 10. On/off button
- 11. Hand Strap



View from the Front

- 1. Laser pointer button

2. Auto focus and save button

3. Focus button

4. Neck strap attachment

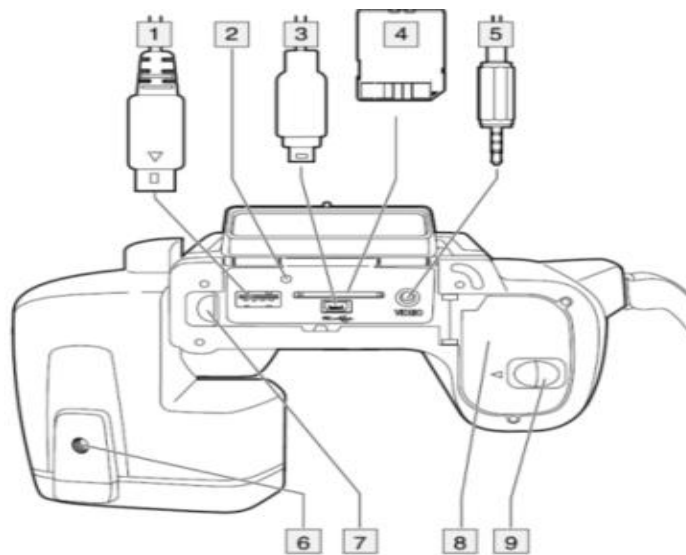
5. Camera lamp

6. Digital camera

7. Release button

8. Laser pointer

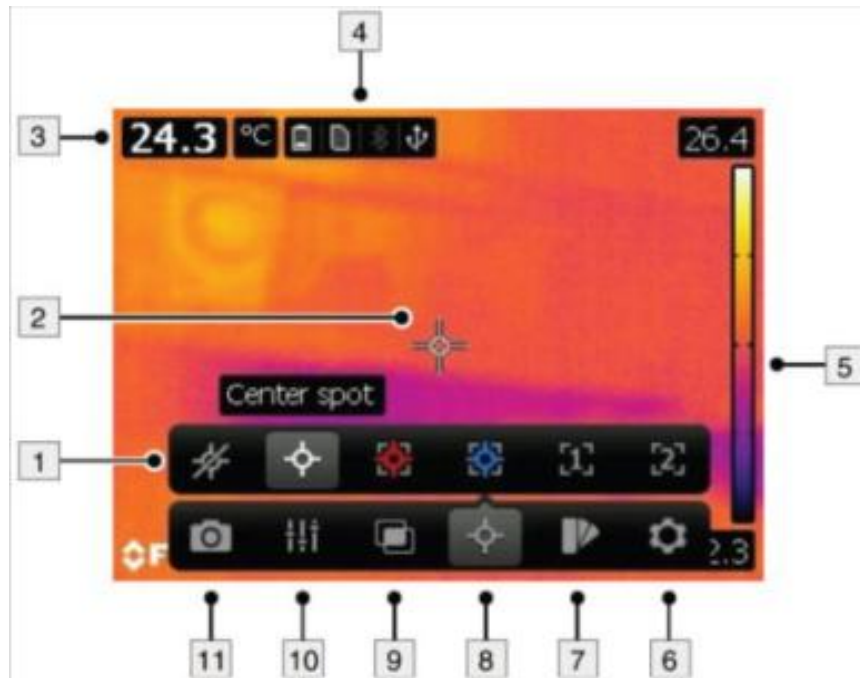
9. Infrared lens



## View from the Bottom

1. USB-A cable (to connect an external USB device to the camera)
2. Indicator showing the memory card is busy
3. USB Mini-B cable (to connect camera to a computer)
4. Memory card
5. Video cable
6. Tripod mount
7. Latch for the cover to the connector bay
8. Battery compartment cover
9. Latch for the battery compartment cover





Screen Element of the Thermal Camera Interface

1. Measurement toolbar
2. Measurement tool (e.g., spotmeter)
3. Result table
4. Status icon
5. Temperature scale
6. Settings toolbar button
7. Color toolbar button

8. Measurement toolbar button
9. Image mode toolbar button
10. Measurement parameters toolbar button
11. Recording mode toolbar button

#### Other Equipment Needed to Capture Thermal Image

1. Tape Measure to measure the distance between the body or object of interest and the camera
2. Hand-held thermometer to capture the natural temperature of the body at the time

#### Steps to Capture a Thermal Image

1. Insert the battery into the battery compartment
2. Insert the memory card into the card slot
3. Push the on/off button to turn on the camera

4. Enter the data acquisition parameter into the camera with a stylus or hand touch (This includes Emissivity of the body, Reflected Temperature, Atmospheric Temperature, Relative Humidity, Wind Speed and the Distance)

Note: The reflected temperature can be obtained with the Hand-held Thermometer

The Distance from the object to the camera can be obtained with the Tape Measure

5. Select the image mode using the image mode toolbar button whether:

Thermal Only (Infrared Image)

Picture in Picture (Infrared Image and Visual overlay)

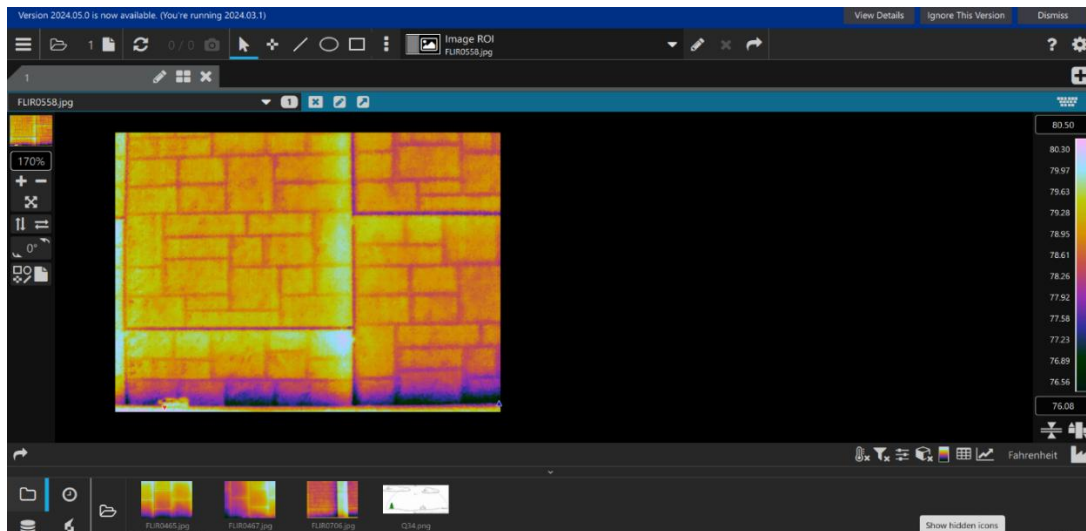
MSX (Enhanced Infrared Image with Visual Edges)

6. Focus the camera on the body and allow the camera to self-calibrate for some seconds (You will hear a silent click sound in this process)
7. Push the Yellow Focus button to adjust left or right for the clarity of the Image.
8. Push the Laser Pointer button to ensure the camera is pointing at the body
9. Push the Auto-Focus button for more than 1 second to capture and save the image (you can delete the image and retake it if it is not good enough).

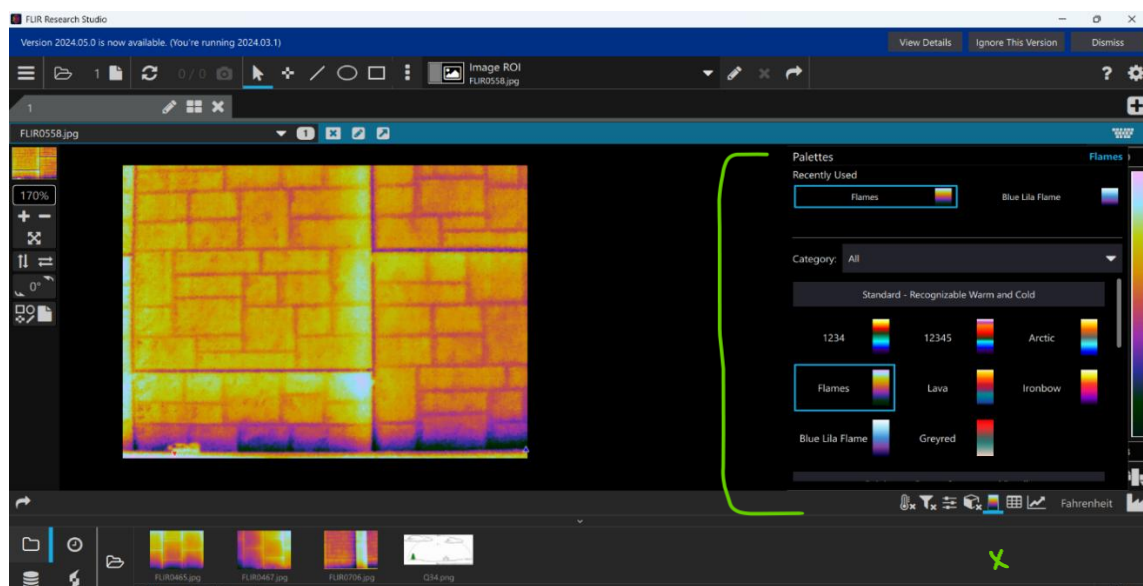
10. After capturing the images, remove the Memory Card from the slot and transfer the captured images to your computer.

## APPENDIX C11. FLIR RESEARCH STUDIO SOFTWARE PROTOCOL

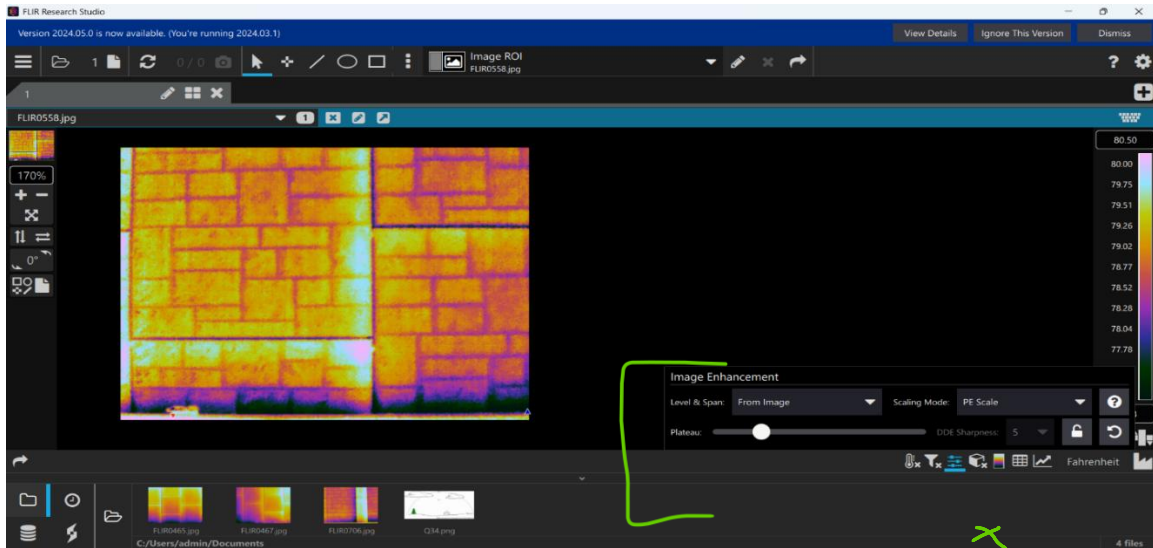
### PROTOCOL ON HOW TO USE FLIR RESEARCH STUDIO SOFTWARE



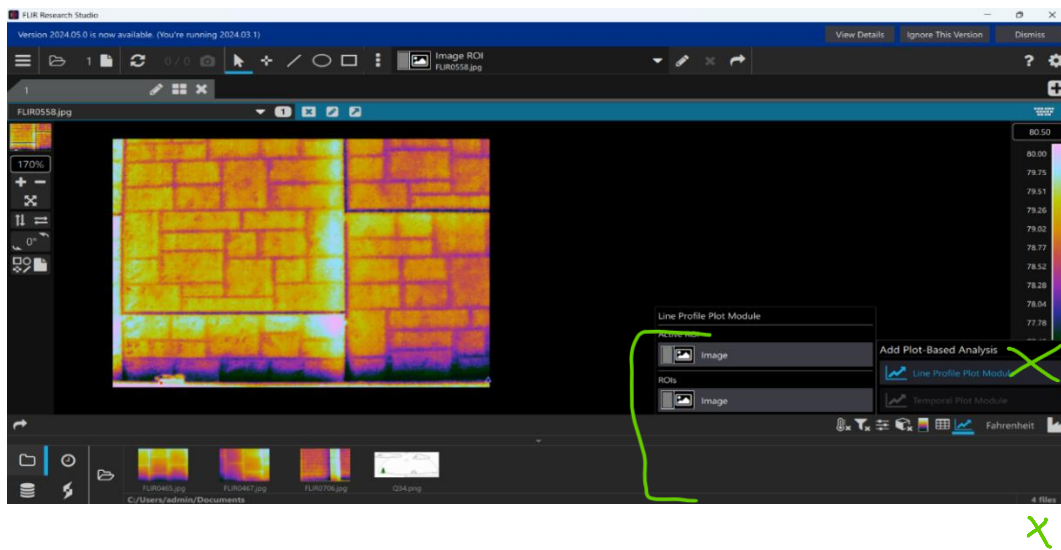
1. Upload the image from the folder in your computer to the FLIR Research Studio software



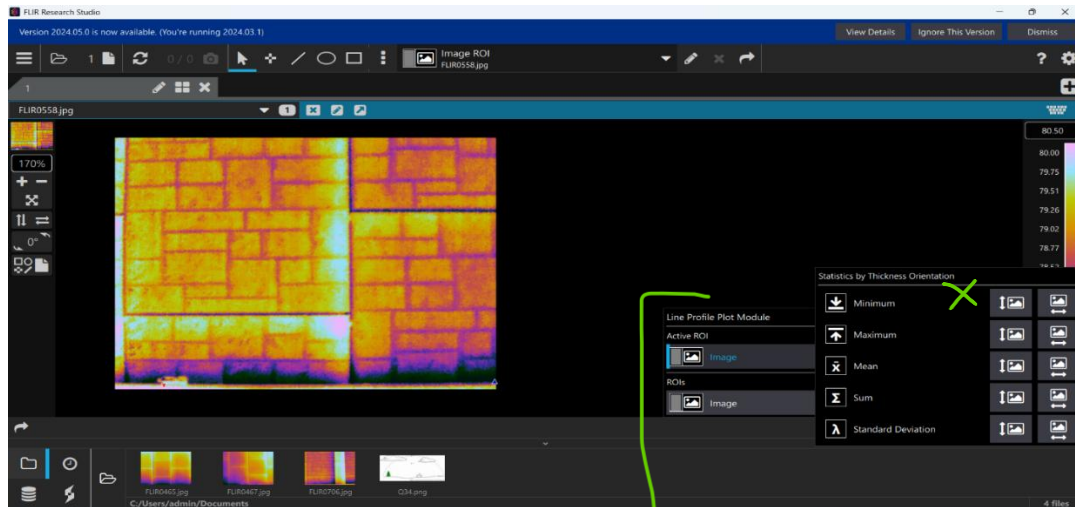
2. Select your desired Color Palettes for the image



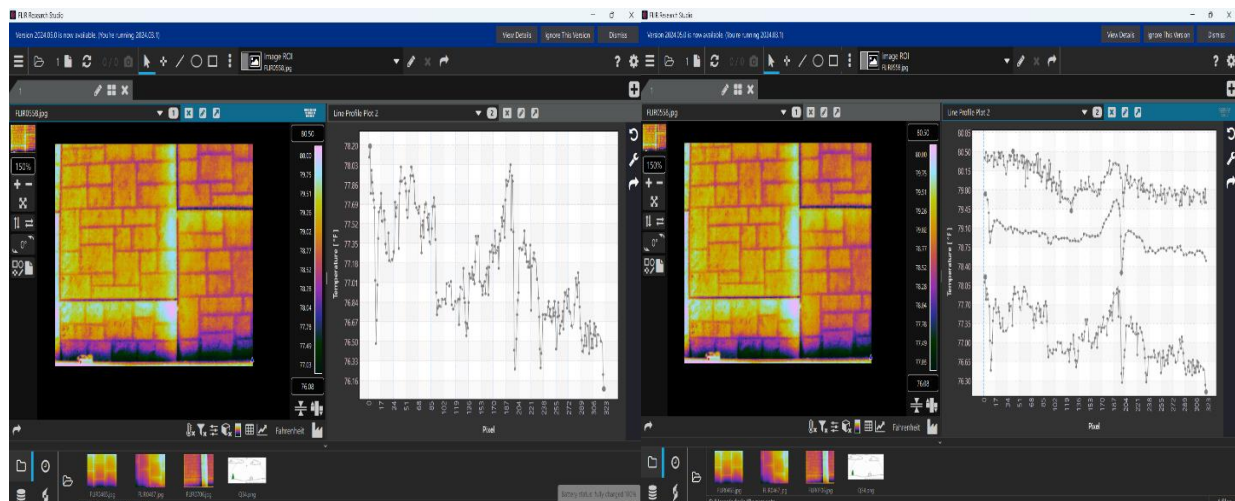
3. Enhance the image color palette by adjusting the Plateau left or right



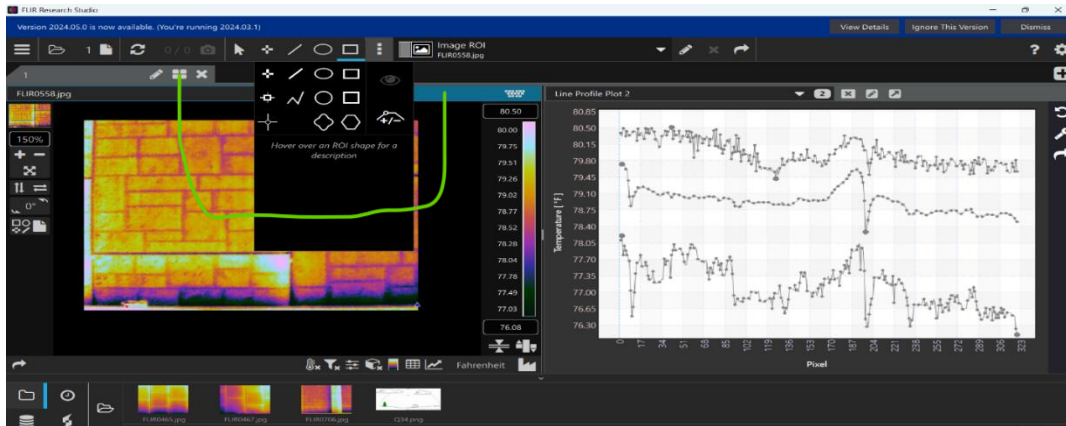
4. Click on the Plot tool, Select the Line Plot Based Module, Select the Image



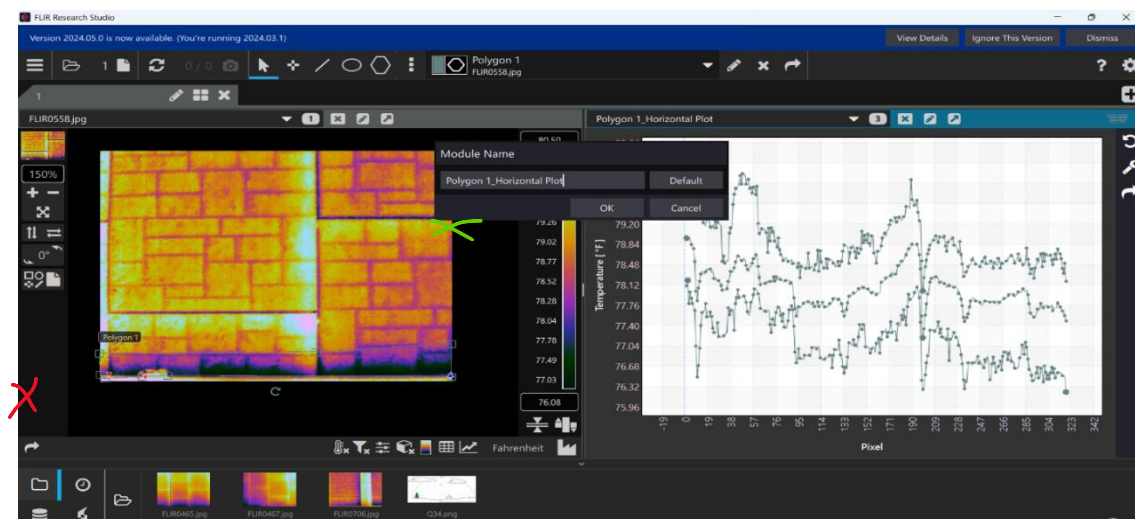
5. After selecting Image, Select either Vertical or Horizontal Plot, then Select the Minimum, Maximum or Mean temperatures



6. The Plots come out this way on the page, you can have all related plots on the same page. This is for Horizontal plot for Minimum, Mean and Maximum Temperatures on the Image

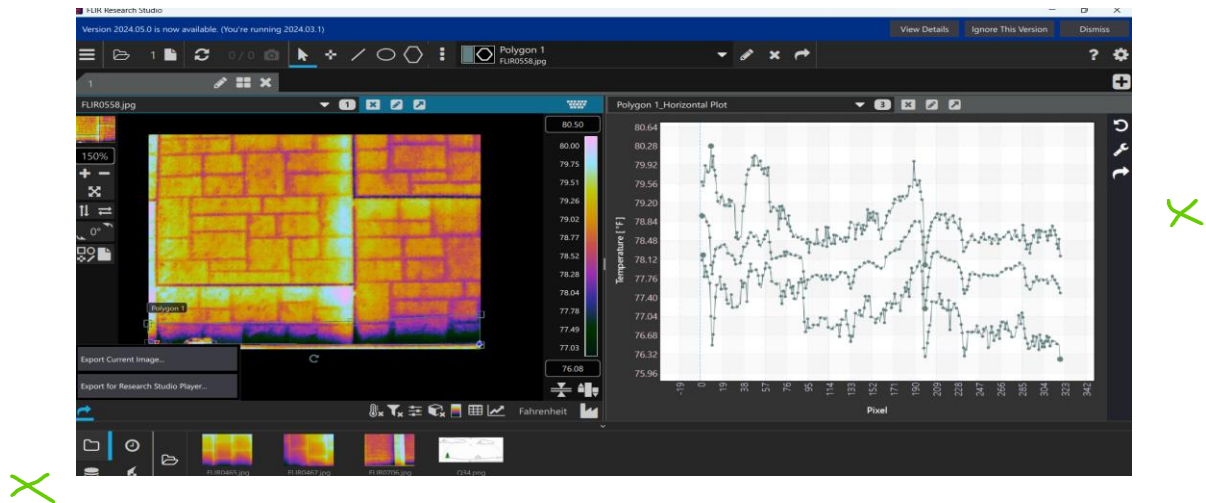


7. If you have a region of interest, use any of the tools in the top bar, like the Square, Rectangle, Polygon, Spot, Line, etc., to mask or identify the area for further assessment.



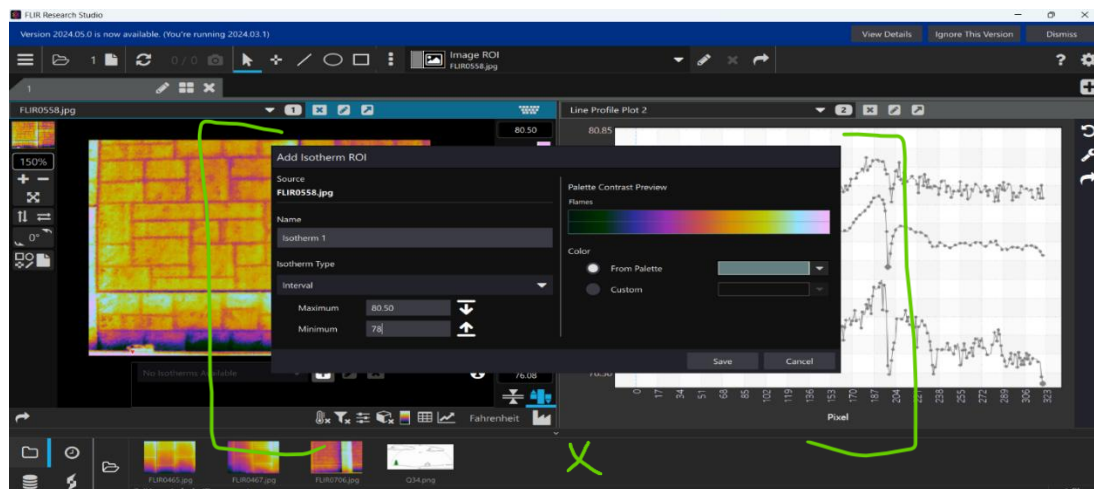
8. The polygon is drawn at the bottom of the Image for further assessment, and the Horizontal Plots for the Minimum, Maximum and Mean temperatures are provided.



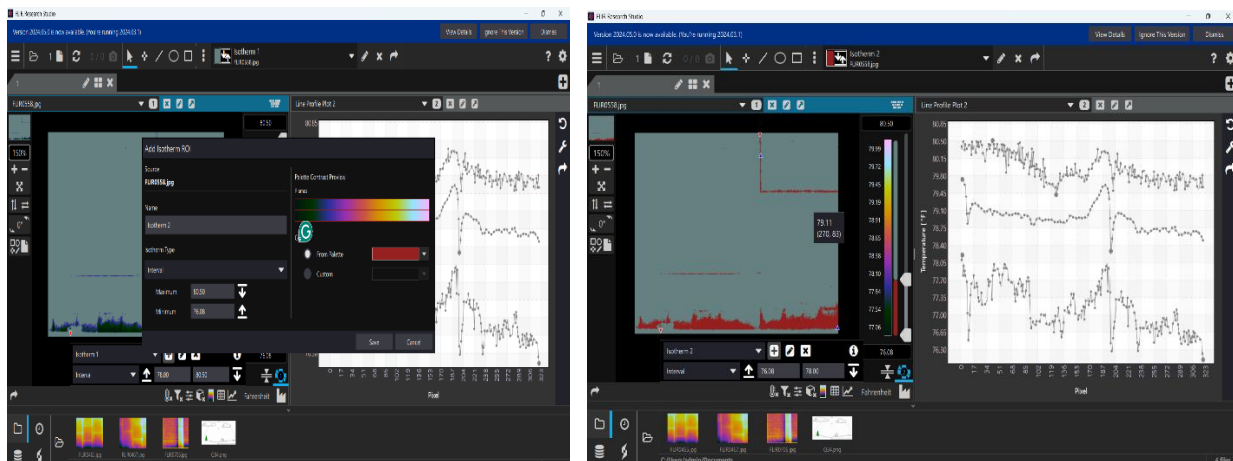


9. Export the Image to save it to a folder on your computer with the Export arrow tool at the bottom left marked in green. You can export the plots with the Export arrow on the right marked in green.

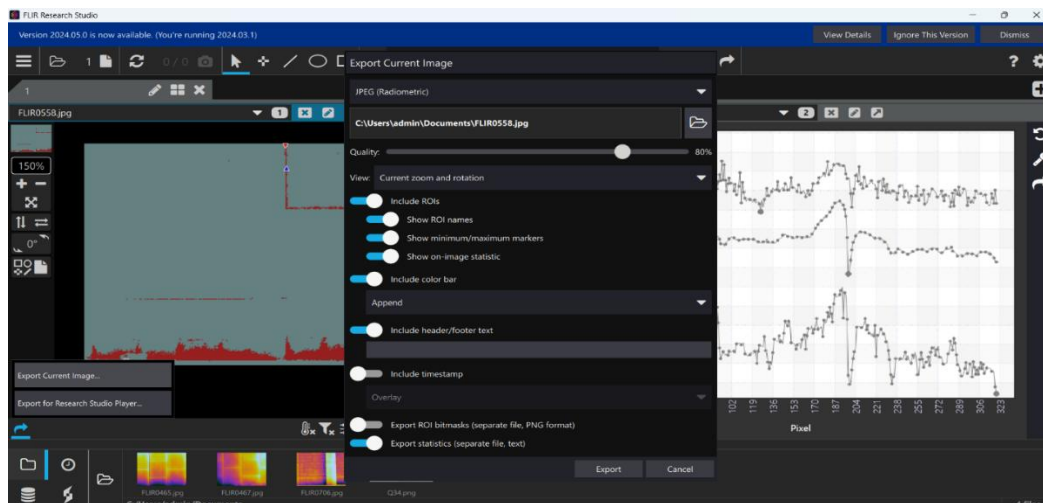
Note: The export process saves the Image(s) with a Text file that has the temperature data and can be converted into an Excel file for further analysis.



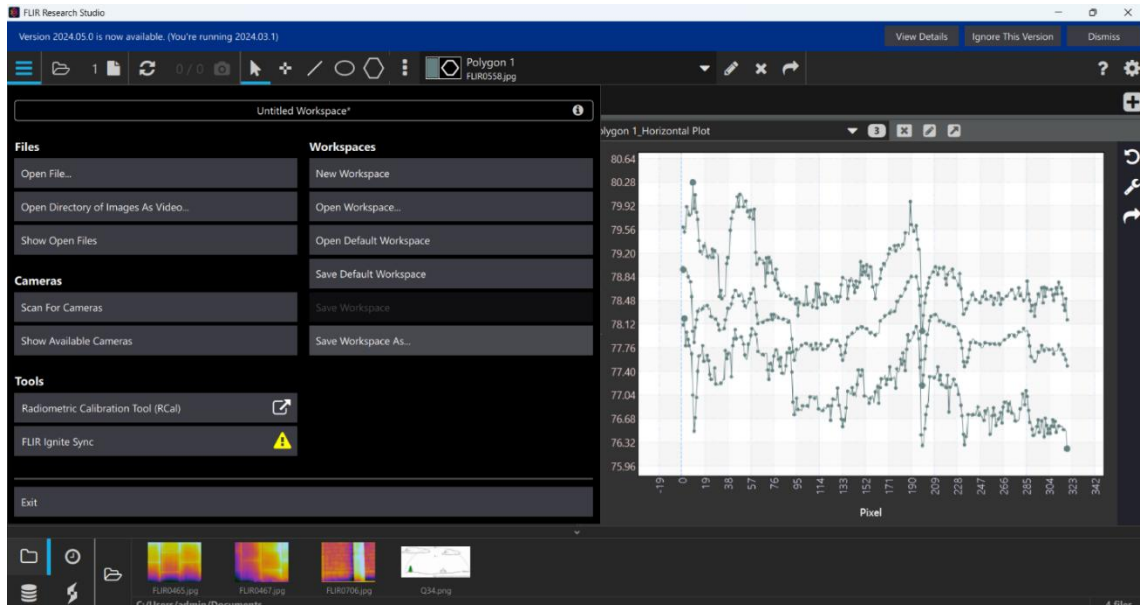
10. Perform Isotherm operation to segment the Image, input the temperature ranges you desire, and save; the software names it Isotherm 1



11. Repeat the same for Isotherm 2



12. Export the Isotherms analysis too



12. Save the entire workspace as a \*.frswsp file to your computer.



STATE OF OHIO DEPARTMENT OF TRANSPORTATION  
**MSE WALL INSPECTION CHECKLIST**

District	<input style="width: 90%;" type="text"/>	Date Inspected	<input style="width: 95%;" type="text"/>				Name of Inspector	<input style="width: 95%;" type="text"/>		
Is MSE wall at a bridge? (Y/N)	<input style="width: 30px;" type="text"/>	County	Route	Section	L/R	RA/FA	End Sec.	Instructions are on the 2nd page.		
Comments										

Instructions

1. Enter the District, date inspected, and the name of the inspector.
  
2. Identify the MSE wall location.  
 For MSE walls at bridges, use the section for the bridge in the C/R/S. For twin bridges with separate MSE walls, identify if the MSE wall is on the left or right. Identify if the MSE wall is at the rear or forward abutment.  
 For MSE walls away from bridges, use the section at the beginning of the wall in the C/R/S. Identify if the wall is on the left or right of the roadway. Fill in the section for the end of the MSE wall.
  
3. Inspect the wall and answer the 20 questions. Refer to the example photos to identify the parts of an MSE wall and for guidance as to what to look for. A "Yes" answer to any of the questions may indicate a potential problem with the wall. When required, take an approximate measurement and record it in the box to the right of the question.
  
4. Take photos showing the entire height of the wall. For long walls, take multiple photos to show the entire length of the wall. For walls at bridges, take one photo of each section of wall.
  
5. For each "Yes" answer to a question, take a photo that shows the relevant item in sufficient detail to understand the reason for the "Yes" answer.

Necessary equipment

Digital camera, ruler, and flashlight.

STATE OF UTAH MSE WALL INSPECTION FORM				
Compiled As Part of Research By The Utah Department of Transportation				
<b>Instructions:</b>				
1-Fill out required sections for MSE Wall Inspector and Wall Characteristics.				
2-Inspect the wall using the attached form. Questions that require a 'Yes' answer should be documented by noting the extent of the problem in the right most column and photo documentation. Photo documentation should consist of wall or bridge number, nature of problem, date, photo number for wall, and a size reference, which should be indicated in the photo (white board/paper). Photos taken should be placed on the Top View layout and indicated with the appropriate number. Note should be taken by the inspector that often anomalies are due to construction and should be distinguished from those that are a result of post-construction. If it is observable that they existed at the time of construction note should be taken in the space provided for drawings.				
3- Shoot digital photos of the entire wall. This may require the use of a variety of shots and angles on each wall to cover the wall in its entirety.				
4- Indicate Layout of MSE Wall in respect to major intersections, roadways, potential hazards, irrigation, vegetation, locations of conditions for which 'Yes' was marked, etc. in space provided below. Also Indicate approximate GPS Coordinates of Site of Interest in space provided below				
Inspector Information				
<b>Inspection Date</b>		<b>Names Of Inspectors</b>		
<b>Region</b>		<b>Identifying Road/Intersection</b>		
MSE WALL CHARACTERISTICS				
MSE Wall at Bridge	Y    N	Bridge Number if applicable:	Wall Number	
Surrounding Structures			Maximum Height of Wall (ft)	
Distance to Each Structure			One Stage, Two Stages or Block Wall	
State Route Number			Estimated Max Length of Wall Abutment	
Approximate Mile Marker			Max Slope of Ground in front of wall:	
GPS Datum	WGS/84,   NAD/83,   or   NAD/27		Max Height of wall burial line above surrounding level ground:	
MSE Wall GPS Coordinates (Location of Measurement shown on plan view)		Please draw rough layout of panel with approximate dimensions in space provided below:		
If known, Panel or System Manufacturer				
Are there coupons available for this wall? If so, how many?				
<b>Summary of Key Observations:</b>				

**Plan/Drainage View:**

<u>Cross Sections:</u>	
<u>Cross Sections:</u>	



# SPECIFIC WALL CHARACTERISTICS

## DRAINAGE

Required Tests:				N/A or Make- Water Bottle-Cannae-Tape Measure		Measurement/Explanation (regional)		Percentage of wall affected/Extent of Problem/Photo Number			
Yes	No	N/A	UKN	Drainage							
Y	N	N/A	UKN	Is there an active water source near the toe of the wall (as the wall meet a body of water with some potential)? (Percentage of wall affected)				0/N0 1% 5% 10% 25% 50% 75% 90% 95% 100%			
Y	N	N/A	UKN	If applicable, are the water sources at the base of the wall blocked? (Percentage of wall affected)				0/N0 1% 5% 10% 25% 50% 75% 90% 95% 100%			
Y	N	N/A	UKN	Are there elements protruding through the wall? (Percentage of wall affected)				0/N0 1% 5% 10% 25% 50% 75% 90% 95% 100%			
Y	N	N/A	UKN	Are there vertical drains that extend through the backfill? (Percentage of wall affected)				0/N0 1% 5% 10% 25% 50% 75% 90% 95% 100%			
Y	N	N/A	UKN	Is there evidence in the base of the wall or footing pad? (Percentage of wall affected)				0/N0 1% 5% 10% 25% 50% 75% 90% 95% 100%			
Y	N	N/A	UKN	Is there evidence along the side wall? (Percentage of wall affected)				0/N0 1% 5% 10% 25% 50% 75% 90% 95% 100%			
Y	N	N/A	UKN	Are there any signs of water flow along the base of the wall? (Percentage of wall affected)				0/N0 1% 5% 10% 25% 50% 75% 90% 95% 100%			
Y	N	N/A	UKN	Is there less than 1 ft between irrigation sprinklers and wall? (Percentage of wall affected)				0/N0 1% 5% 10% 25% 50% 75% 90% 95% 100%			
Y	N	N/A	UKN	Does the backfill or joint there appear to be saturated? (Percentage of wall affected)				0/N0 1% 5% 10% 25% 50% 75% 90% 95% 100%			
Y	N	N/A	UKN	Are there plants growing in joint/joint? (Percentage of wall affected)				0/N0 1% 5% 10% 25% 50% 75% 90% 95% 100%			
Y	N	N/A	UKN	Are the deck drains and outlets at the top of the wall blocked? (Percentage of wall affected)				0/N0 1% 5% 10% 25% 50% 75% 90% 95% 100%			
Y	N	N/A	UKN	Can water enter the wall between coping and deck (if a. Drains appropriately)? (Percentage of wall affected)				0/N0 1% 5% 10% 25% 50% 75% 90% 95% 100%			
Y	N	N/A	UKN	Is there evidence of discharge point of fill washing through debris panel? (Percentage of wall affected)				0/N0 1% 5% 10% 25% 50% 75% 90% 95% 100%			

## MSE Wall Joints

Required Tests:				Long Level-String-Camera-Tape Measure		Measurement/Explanation (regional)		Percentage of wall affected/Extent of Problem/Photo Number			
Yes	No	N/A	UKN	Joints							
Y	N	N/A	UKN	Is backfill coming out of joints or are there piles of backfill at the base of the wall? (Percentage of wall affected)				0/N0 1% 5% 10% 25% 50% 75% 90% 95% 100%			
Y	N	N/A	UKN	Are the joints wide enough to see (this is backfill behind panels when looking into joint)? (Percentage of wall affected) If yes, record the approximate maximum joint width in inches.				0/N0 1% 5% 10% 25% 50% 75% 90% 95% 100%			
Y	N	N/A	UKN	Is exposed backfill visible in the horizontal joints? (Percentage of wall affected)				0/N0 1% 5% 10% 25% 50% 75% 90% 95% 100%			
Y	N	N/A	UKN	Are there visible tears in the fabric? (Percentage of wall affected)				0/N0 1% 5% 10% 25% 50% 75% 90% 95% 100%			
Y	N	N/A	UKN	Is there evidence of backfill or water leaking through tears in fabric behind panels? (Do not include additional damage to fabric) (Percentage of wall affected)				0/N0 1% 5% 10% 25% 50% 75% 90% 95% 100%			
Y	N	N/A	UKN	Do the joints have a non-uniform horizontal spacing? (If a. Are some horizontal joints larger/smaller than others?) (Percentage of wall affected)				0/N0 1% 5% 10% 25% 50% 75% 90% 95% 100%			
Y	N	N/A	UKN	Do the joints have a non-uniform vertical spacing? (If a. Are some horizontal joints larger/smaller than others?) (Percentage of wall affected)				0/N0 1% 5% 10% 25% 50% 75% 90% 95% 100%			
Y	N	N/A	UKN	Are the panels offset at the joints either in or out of the wall? (Percentage of wall affected) If yes, record the approximate maximum offset.				0/N0 1% 5% 10% 25% 50% 75% 90% 95% 100%			
Y	N	N/A	UKN	Does the fabric appear brittle or appear as if it has undergone excessive UV exposure? (Percentage of wall affected)				0/N0 1% 5% 10% 25% 50% 75% 90% 95% 100%			

## WALL FACING

Required Tests:				Long Level-String-Camera-Tape Measure		Measurement/Explanation (regional)		Percentage of wall affected/Extent of Problem/Photo Number			
Yes	No	N/A	UKN	Wall Facing							
Y	N	N/A	UKN	Were the panels built using "Tilt-Up" construction? (Percentage of wall affected) Is there excessive cracking in the panels?				0/N0 1% 5% 10% 25% 50% 75% 90% 95% 100%			
Y	N	N/A	UKN	Is there excessive cracking in panels? (Percentage of wall affected)				0/N0 1% 5% 10% 25% 50% 75% 90% 95% 100%			
Y	N	N/A	UKN	Are there cracks that continue vertically through adjacent panels? (Percentage of wall affected)				0/N0 1% 5% 10% 25% 50% 75% 90% 95% 100%			
Y	N	N/A	UKN	Are there cracks that continue horizontally through adjacent panels? (Percentage of wall affected)				0/N0 1% 5% 10% 25% 50% 75% 90% 95% 100%			
Y	N	N/A	UKN	Are the panels making contact with each other? (Percentage of wall affected)				0/N0 1% 5% 10% 25% 50% 75% 90% 95% 100%			
Y	N	N/A	UKN	Are the panels "bumped-off" or clipped from contact with adjacent panels? (Percentage of wall affected)				0/N0 1% 5% 10% 25% 50% 75% 90% 95% 100%			
Y	N	N/A	UKN	Does crack spacing suggest differential settlement? (Percentage of wall affected)				0/N0 1% 5% 10% 25% 50% 75% 90% 95% 100%			

Y	N	N/A	UKN	Does the existing coping exhibit vertical offset? (Percentage of wall affected)		0/0g	1%	5%	10%	25%	50%	75%	90%	95%	100%
Y	N	N/A	UKN	Are the coping and parapet base or detailing? (Percentage of wall affected)		0/0g	1%	5%	10%	25%	50%	75%	90%	95%	100%
Y	N	N/A	UKN	Are the parapets in danger of falling off? (Percentage of wall affected)		0/0g	1%	5%	10%	25%	50%	75%	90%	95%	100%
Y	N	N/A	UKN	Do the parapets exhibit bulging? (Percentage of wall affected) If so, record maximum deformation from acceptable copings to leveling pad.		0/0g	1%	5%	10%	25%	50%	75%	90%	95%	100%
Y	N	N/A	UKN	Is there flapping at the top or bottom of the wall? (Percentage of wall affected) If so, record maximum degree of flapping from airside using wet/dry level and standard survey.		0/0g	1%	5%	10%	25%	50%	75%	90%	95%	100%
Y	N	N/A	UKN	Is there excessive degradation of wall parapet? (Percentage of wall affected)		0/0g	1%	5%	10%	25%	50%	75%	90%	95%	100%

MSE TOP OF WALL

Required Tools:		Long Level-Cradle Gauge-Camera-Tape Measure		Top Of Wall		Measurement/Explanation of quantity		Percentage of wall affected/Extent of Problem/Photo Number							
Yes	No	N/A	UKN												
Y	N	N/A	UKN	Is there evidence of settlement at the top of the wall? (movement cracking, etc?) (Percentage of wall affected?)				0/0g							
Y	N	N/A	UKN	Are there any non loadline cracks in the concrete coping? (Percentage of wall affected) If yes, record the approximate maximum crack width.				0/0g							
Y	N	N/A	UKN	How do the construction joints in the concrete coping appear? (Percentage of wall affected) If yes, record the maximum joint width.				0/0g							
Y	N	N/A	UKN	Is there a large gap between the approach slab and pavement? (Percentage of wall affected) Other: this produces a bumping sensation as the car passes is crossed. Record the approximate maximum gap size.				0/0g							
Y	N	N/A	UKN	At the abutment, how the joint between the wall coping and abutment opened up significantly? (Percentage of wall affected) If so record maximum distance.				0/0g							
Y	N	N/A	UKN	Is the coping wall pulling away from pavement and roadway section? (Percentage of wall affected) Please record maximum displacement for wall.				0/0g							

FOUNDATION CONDITIONS AND EXTERNAL STABILITY

Required Tools:		Shovel, GEO-Probe-Tape Measure		Foundation Condition & External Stability		Measurement/Explanation of quantity		Percentage of wall affected/Extent of Problem/Photo Number							
Yes	No	N/A	UKN												
Y	N	N/A	UKN	What is the location depth of leveling wall? (Percentage of wall affected) Ground Geo-Probe into soil located 2 inches from wall to a maximum depth of 24 inches (24 inches is the minimum depth for MSE Wall)				0/0g							
Y	N	N/A	UKN	Is the leveling pad exposed?				0/0g							
Y	N	N/A	UKN	Is there cracking in the leveling pad? (Percentage of wall affected) If so, record maximum crack size with gauge.				0/0g							
Y	N	N/A	UKN	Is there a four foot bench (level slope) along the base of the wall before the slope changes? (Percentage of wall affected) If not record width of bench?				0/0g							
Y	N	N/A	UKN	Is there a slope steeper than 3:1.5 to V1 behind the wall? (Percentage of wall affected) Please record slope.				0/0g							
Y	N	N/A	UKN	Is there a slope greater than V: 1.5 to H:1 behind front of the wall? (Percentage of wall affected) Please record slope.				0/0g							

CORROSION

Required Tools:		Nylon Marker-Camera-Zip Lock Bag-Trowel-Tape Measure		Corrosion		Measurement/Explanation of quantity		Percentage of wall affected/Extent of Problem/Photo Number							
Yes	No	N/A	UKN												
Y	N	N/A	UKN	Is there excessive corrosion on fasteners or other exposed metal that might indicate serious conditions? (Percentage of wall affected)				0/0g							
Y	N	N/A	UKN	Are there significant rust stains on face of the wall? Along joints? (Percentage of wall affected)				0/0g							
Y	N	N/A	UKN	Are there any internal rust exposed? (Percentage of wall affected)				0/0g							
Y	N	N/A	UKN	If exposed, does there appear to be corrosion or rust? (Percentage of wall affected)				0/0g							
Y	N	N/A	UKN	Was a reactivity sample taken of soil? If so, please indicate depth taken in inches				0/0g							
Y	N	N/A	UKN	Is there indication of water corrosion (i.e. swelling bars, rust, exposed metal inside epoxy coating)? (Percentage of wall affected)				0/0g							
Y	N	N/A	UKN	Is there evidence of Test Wire or Coupons installed in the wall? If so, please indicate the possible number of Test wires available?				0/0g							

IMPACT AND COLLISION

Required Tools:		Camera													
Yes	No	N/A	UKN												

Yes		No	N/A	UKN	Impact and Collision	Measurement/Explanation <i>(if applicable)</i>	Percentage of wall affected/Extent of Problem/Photo Number									
Y	N	N/A	UKN	UKN	Are guardrails/wall protections in place at the base of the wall (to protect it from potential traffic hazards)? (Percentage of wall affected?)		0/No	1%	5%	10%	25%	50%	75%	90%	95%	100%
Y	N	N/A	UKN	UKN	Does it appear that the wall has been involved in an accident (replaced panel, recent dings in the wall)? (Percentage of wall affected?)		0/No	1%	5%	10%	25%	50%	75%	90%	95%	100%
Y	N	N/A	UKN	UKN	Does it appear the wall's functionality and integrity has been compromised by a collision or accident? (Percentage of wall affected?)		0/No	1%	5%	10%	25%	50%	75%	90%	95%	100%
MISCELLANEOUS																
Required Tools:					Available Drawings-Camera-Tape Measure		Percentage of wall affected/Extent of Problem/Photo Number									
Yes		No	N/A	UKN	Miscellaneous	Measurement/Explanation <i>(if applicable)</i>										
Y	N	N/A	UKN	UKN	Are there acute wall angles (<90)? (Percentage of wall affected?)		0/No	1%	5%	10%	25%	50%	75%	90%	95%	100%
Y	N	N/A	UKN	UKN	Are there available drawings for the wall? Please indicate type (Situation and Layout, Design, As Built, etc.) (Percentage of wall affected?)		0/No	1%	5%	10%	25%	50%	75%	90%	95%	100%
Y	N	N/A	UKN	UKN	Is the layout in general accordance with drawings? (Percentage of wall affected?)		0/No	1%	5%	10%	25%	50%	75%	90%	95%	100%
Y	N	N/A	UKN	UKN	Are the panels CIP (Cast in Place)? (Percentage of wall affected?)		0/No	1%	5%	10%	25%	50%	75%	90%	95%	100%
Y	N	N/A	UKN	UKN	Was Goodform used in the construction of the wall? (Percentage of wall affected?)		0/No	1%	5%	10%	25%	50%	75%	90%	95%	100%
Y	N	N/A	UKN	UKN	Are there any structures on or near wall that were not included in initial drawings? (Percentage of wall affected?)		0/No	1%	5%	10%	25%	50%	75%	90%	95%	100%
Y	N	N/A	UKN	UKN	Are there any irrigation, utilities, or intrusions that are not part of the initial drawings? (Percentage of wall affected?)		0/No	1%	5%	10%	25%	50%	75%	90%	95%	100%
Y	N	N/A	UKN	UKN	Have there been any excavations or evidence of excavations near the wall? (Percentage of wall affected?)		0/No	1%	5%	10%	25%	50%	75%	90%	95%	100%
Y	N	N/A	UKN	UKN	Have local property owners changed the dynamics of the wall (additional structures, irrigation, vegetation, etc.)? (Percentage of wall affected?)		0/No	1%	5%	10%	25%	50%	75%	90%	95%	100%
Y	N	N/A	UKN	UKN	Are there piles or other bridge support systems located in the wall (bridge abutment)? (Percentage of wall affected?)		0/No	1%	5%	10%	25%	50%	75%	90%	95%	100%

Nebraska Department of Transportation MSE wall Inspection Form (Modified from Jensen, 2009 and Sharma et al., 2019)

#	Items	Attribute	Value
1.	Wall Tilting (Panel Walls)	ection of the entire wall has failed due to tilting.	0
		ection of or entire wall is inclined such that separation is beginning in the wall face.	1
		ection of or the entire wall is inclined outward at 10° (1H:6V) to 15° (1H:4V).	3
		ection of or the entire wall is inclined outward at 5° (1H:12V) to 10° (1H:6V).	5
		ection of or the entire wall is inclined outward at 0° - 5° (1H:12V).	7
		ere is no change in wall inclination from construction specifications.	9
	Wall Tilting (Block Walls)	ock wall has positive inclination.	0
		ock wall is vertical (it has no tilt).	5
		ock wall has negative inclination.	9
2.	Structural Cracking	ore than 50% of wall area shows structural cracking.	0
		etween 33 - 50% of wall area shows structural cracking.	1
		etween 20 - 33% of wall area shows structural cracking.	3
		etween 10 - 20% of wall area shows structural cracking.	5
		ss than 10% of wall area shows structural cracking.	7
		ne or only an insignificantly small area shows structural cracking.	9
3.	Facial Deteriorati on	ore than 50% of wall area shows facial deterioration.	0
		etween 50% and 25% of the wall area shows deterioration.	3
		ss than 25% of the wall area shows deterioration.	6
		ne or only an insignificantly small area shows facial deterioration.	9
4.	Bowing of the Wall	all panels have bowed outward to the point where backfill loss is evident.	0
		all panels have bowed outward to the point where filter fabric is visible at the joints; connectors between panels have broken.	3
		all panels have bowed outward to where connectors between panels are visible and deforming.	5
		all panels have bowed outward to the point where bowing is visible standing directly in front of the wall.	7
		signs of bowing on the wall face.	9
5.	Panel Staining	ore than 50% of the wall surface is stained.	0
		ss than 25% of the wall surface is stained.	5
		ne or only an insignificantly small area of the wall surface is stained.	9
6.	Exposure of Fabric at Joints	reater than 10% of the joints allow fabric exposed to sunlight.	0
		ver than 5% of joints allow fabric exposed to sunlight.	3
		abric is currently exposed at joints, but some joints appear to be increasing in width, which may allow fabric behind to become visible.	6
		nts appear to be stable; no fabric is currently exposed.	9

#	Items	Attribute	Value
7.	Loss of Backfill	Backfill loss has resulted in significant settlement of the v-ditch or roadway or has affected wall inclination or alignment.	0
		Significant areas/quantities of backfill loss are visible.	3
		Backfill loss is occurring, but only minor areas/quantities of backfill loss are visible.	6
		Visual evidence of backfill loss.	9
8.	Erosion: Front of Wall	Area in front of the wall is paved.	N/A
		Erosion has exposed more than 50% of the wall base.	0
		Erosion has exposed more than 25% of the wall base.	3
		Erosion has exposed less than 25% of the wall base.	5
		Erosion is occurring but the wall base remains covered.	7
		Visual evidence of erosion in front of the wall.	9
9.	Erosion: Back of Wall	All reinforcement is visible in several locations.	0
		All reinforcement is being exposed at two or more locations.	3
		Effects of erosion are visible, but no wall reinforcement has been exposed.	5
		Minor effects of erosion are visible; plant roots may be exposed or higher original soil levels on concrete structures may be indicative of erosion.	7
		There is no visual evidence that erosion is occurring behind the wall.	9
10.	Joint Spacing	Wall is not a panel wall; wall has no joints.	N/A
		Joint width appears almost totally irregular and random.	0
		Joint width varies widely across the wall face.	3
		Joint width appears marginally regular, but considerable variation exists in different areas or at different heights along the wall.	5
		Joint width appears generally uniform with the exception of some discrepancies in localized areas.	7
		Joint width appears generally uniform across the entire wall.	9
11.	Condition of V-Ditch	The wall has no V-Ditch.	N/A
		The V-Ditch is nonfunctional due to backfill movement, cracking, etc.	0
		The V-Ditch has separated from the wall face; extensive cracking or breakup of the V-Ditch has rendered it almost nonfunctional.	3
		The V-Ditch is still attached to wall, but large cracks are developing in the V-Ditch at several locations. The V-Ditch can transport less water than intended.	5
		The V-Ditch is still attached to the wall, but minor cracks are developing; the ability of the V-ditch to transport water has not been affected.	7
		Cracks in the V-Ditch; no separation of the V-Ditch from the wall. The V-Ditch is functioning as intended.	9
12.	Coping Deterioration	The wall has no coping.	N/A
		More than 25% of the coping shows signs of severe cracking, has become detached, or is spalling.	0
		Less than 25% of the coping shows signs of severe cracking, has become detached or is spalling.	5
		There are no signs of coping deterioration.	9

#	Items	Attribute	Value
13.	Drainage Runoff	structure above wall to cause drainage runoff.	N/A
		erosion runoff is actively moving significant quantities of backfill material from its original location.	0
		indications of erosion runoff are present; quantity of backfill material being moved appears significant.	3
		indications of erosion runoff are present but there is no indication that the quantity of backfill material being moved is significant.	6
		signs of erosion due to drainage runoff.	9
14.	Drainage: Front of Wall	signs of water ponding consistently in front of the wall (Cattails growing, stain lines left from standing water on the wall, etc.).	0
		water ponds in front of the wall infrequently or only during periods of intense precipitation.	5
		front of the wall is well drained; no ponding occurs.	9
	Comments		

## State DOT Documents - Inspection Guidelines for MSE and Retaining Walls

State	Name of Document	Rating System/Checklist	Inspection Frequency/ Inspection Requirements	Inspection Techniques/ Inspection Types	Published Date and Link
Alabama	Geotechnical Manual (2021)	<ul style="list-style-type: none"> <li>Pre-construction checklist with “yes” or “no” questions based on FHWA ED-88-053 (2003)</li> </ul>		<ul style="list-style-type: none"> <li>Instrumentation and monitoring for pre-construction. Additional information can be found in FHWA-HI-98-034 Geotechnical Instrumentation Reference Manual (1998).</li> </ul>	<a href="https://www.dot.state.al.us/publications/Materials/pdf/ALDOTGeotechManual.pdf">https://www.dot.state.al.us/publications/Materials/pdf/ALDOTGeotechManual.pdf</a>
Alaska	Alaska Bridges and Structures Manual (2017)			<ul style="list-style-type: none"> <li>Visual Inspection for substructures and foundation for Bridge Inspection</li> <li>In-depth Bridge Inspections</li> </ul>	<a href="https://dot.alaska.gov/stwdes/desbridge/assets/grant/southcoast/ak_Bridge_Manual_Sept_2017%20-%20ref%20on%20p%2011%20but%20not%20sure%20you%20need%20this%20mike.pdf">https://dot.alaska.gov/stwdes/desbridge/assets/grant/southcoast/ak_Bridge_Manual_Sept_2017%20-%20ref%20on%20p%2011%20but%20not%20sure%20you%20need%20this%20mike.pdf</a>
	Geotechnical Asset Management Plan (2017)	<ul style="list-style-type: none"> <li>Retaining walls in Good, Fair, and Poor</li> </ul>			<a href="https://rosap.nrl.bts.gov/view/dot/36139">https://rosap.nrl.bts.gov/view/dot/36139</a>
Arizona	Mechanically Stabilized Earth (MSE) Walls Design Support Document Section 929: MSE Walls (2020)	<ul style="list-style-type: none"> <li>MSE wall design requirements</li> </ul>			<a href="https://azdot.gov/sites/default/files/media/2020/09/929MSEW.pdf">https://azdot.gov/sites/default/files/media/2020/09/929MSEW.pdf</a>
	Bridge Inspection Guidelines (2018)	<ul style="list-style-type: none"> <li>NBI Substructure Condition Rating (Item #60): 0 (Fail) to 9 (Excellent)</li> <li>No specific comments for MSE walls</li> </ul>			<a href="https://azdot.gov/sites/default/files/2019/09/1803BridgeInspectionGuidelines.pdf">https://azdot.gov/sites/default/files/2019/09/1803BridgeInspectionGuidelines.pdf</a>
Arkansas	Bridge Inspection Manual (2022)	<ul style="list-style-type: none"> <li>NBI Substructure Condition Rating (Item #60): 0 (Fail) to 9 (Excellent)</li> <li>Wingwalls or retaining walls</li> </ul>			<a href="https://www.ardot.gov/wp-content/uploads/2022/05/ARDOT_BIM_20220507.pdf">https://www.ardot.gov/wp-content/uploads/2022/05/ARDOT_BIM_20220507.pdf</a>
California	Bridge Construction Records and Procedures Manual Volume II Section 47-2 Mechanically Stabilized Embankment Construction Checklist (2018)	<ul style="list-style-type: none"> <li>Includes Mechanically Stabilized Embankment Construction Checklist</li> </ul>			<a href="https://dot.ca.gov/-/media/dot-media/programs/engineering/documents/structureconstruction/bcrp-vol2/bcm-47-2att1-a11y.pdf">https://dot.ca.gov/-/media/dot-media/programs/engineering/documents/structureconstruction/bcrp-vol2/bcm-47-2att1-a11y.pdf</a>
Colorado	Retaining Noise Wall Inspections and Asset Management Manual (2016)	<ul style="list-style-type: none"> <li>Condition States: <ul style="list-style-type: none"> <li>h. 1 - Good</li> <li>i. 2 - Fair</li> <li>j. 3 - Poor</li> <li>k. 4 - Severe</li> </ul> </li> </ul>	<ul style="list-style-type: none"> <li>Routine inspections: every 6 years or less for retaining and noise walls, and every 4 years or less for bridge walls</li> </ul>	<ul style="list-style-type: none"> <li>When the risk grade is below C or D, a special inspection is conducted and LIDAR and Non-Destructive Testing, etc. can be used as needed</li> </ul>	<a href="https://www.codot.gov/programs/bridge/bridgemanuals/retaining_and_noise_wall_inspection_and_asset_management_manual_20160413.pdf">https://www.codot.gov/programs/bridge/bridgemanuals/retaining_and_noise_wall_inspection_and_asset_management_manual_20160413.pdf</a>

State	Name of Document	Rating System/Checklist	Inspection Frequency/ Inspection Requirements	Inspection Techniques/ Inspection Types	Published Date and Link
Connecticut	Bridge Inspection Manual (2017)	<ul style="list-style-type: none"> <li>No specific guidelines for MSE and retaining walls</li> </ul>			<a href="https://portal.ct.gov/dot/-/media/dot/publications/inspection_manual_2019-11-15rev.pdf?rev=45191d05169945e6a34c5f5fb5bdad7f&amp;hash=FE86BA57E2596F9EAC085A459E109C2D">https://portal.ct.gov/dot/-/media/dot/publications/inspection_manual_2019-11-15rev.pdf?rev=45191d05169945e6a34c5f5fb5bdad7f&amp;hash=FE86BA57E2596F9EAC085A459E109C2D</a>
	Retaining Wall Inventory and Assessment Guidelines (2023)	<ul style="list-style-type: none"> <li>Document cannot be found.</li> </ul>			
Delaware	Inspection Guidelines for Construction and Post-Construction of MSE Wall (Research Report 2002)	<ul style="list-style-type: none"> <li>Checklist 1 <ul style="list-style-type: none"> <li>Field Inspection Checklist for Construction: 12 items</li> <li>Field Inspection Checklist for Post Construction: 6 items</li> </ul> </li> <li>Checklist 2: Yes or No Questions for Construction</li> </ul>		<ul style="list-style-type: none"> <li>ble instruments for different types of issues (e.g. movement of facing) but should be installed during the construction.</li> <li>aying methods <ul style="list-style-type: none"> <li>Inclinometer</li> <li>Multipoint extensometers</li> <li>Strain gauges</li> <li>Load cells</li> <li>Induction coil gauges</li> <li>Telltals</li> <li>Thermocouples</li> </ul> </li> </ul>	<a href="https://cpb-us-w2.wpmucdn.com/sites.udel.edu/dist/1/1139/files/2013/10/Rpt.-143-Mechanically-Stabilized-Earth-Wall-Final-Leshchinsky-xyyg38.pdf">https://cpb-us-w2.wpmucdn.com/sites.udel.edu/dist/1/1139/files/2013/10/Rpt.-143-Mechanically-Stabilized-Earth-Wall-Final-Leshchinsky-xyyg38.pdf</a>
	Bridge Element Inspection Manual (2021)	MSE wall Bridge Substructure Elements 4 condition states (Good (1), Fair (2), Poor (3), and Severe (4)) for 11 items			<a href="https://deldot.gov/Publications/manuals/bridge_inspection/pdfs/bridge_element_inspection_manual.pdf">https://deldot.gov/Publications/manuals/bridge_inspection/pdfs/bridge_element_inspection_manual.pdf</a>
Florida	MSE Wall Inspector's Handbook (2012)	<ul style="list-style-type: none"> <li>Checklists for construction of MSE Retaining Wall in a "Yes" or "No" format.</li> </ul>			<a href="https://www.fdot.gov/docs/default-source/construction/CONSTADM/guidelist/InspectGuidelist/FY1213/MSE-Wall-Inspectors-Handbook.pdf">https://www.fdot.gov/docs/default-source/construction/CONSTADM/guidelist/InspectGuidelist/FY1213/MSE-Wall-Inspectors-Handbook.pdf</a>
Georgia	Bridge structure Maintenance and Rehabilitation Repair Manual (2012)	<ul style="list-style-type: none"> <li>MSE walls are not mentioned in the manual.</li> <li>Abutment as part of substructure</li> </ul>	<ul style="list-style-type: none"> <li>Bridge substructure preventative maintenance: as needed</li> </ul>		<a href="https://www.dot.ga.gov/GDOT/pages/RoutineMaintenance.aspx">https://www.dot.ga.gov/GDOT/pages/RoutineMaintenance.aspx</a>
	Bridge, Culvert, and Retaining Wall Construction Manual (2024)	Appendix F. MSE wall Basic components of an MSE wall and the potential effects resulting from poor materials and construction.			<a href="https://www.dot.ga.gov/PartnerSmart/Business/Source/bridges/Bridge_Manual.pdf#search=What%20can%20we%20help%20you%20find%3FBridge%2C%20Culvert%2C%20and%20Retaining%20Wall%20Construction%20Manual">https://www.dot.ga.gov/PartnerSmart/Business/Source/bridges/Bridge_Manual.pdf#search=What%20can%20we%20help%20you%20find%3FBridge%2C%20Culvert%2C%20and%20Retaining%20Wall%20Construction%20Manual</a>
Hawaii	Bridge Inspection Manual (2024)	<ul style="list-style-type: none"> <li>No specific guidelines for MSE and retaining walls</li> </ul>			<a href="https://hidot.hawaii.gov/highways/files/2024/10/BIP-Manual-20241001.pdf">https://hidot.hawaii.gov/highways/files/2024/10/BIP-Manual-20241001.pdf</a>



State	Name of Document	Rating System/Checklist	Inspection Frequency/ Inspection Requirements	Inspection Techniques/ Inspection Types	Published Date and Link
Idaho	Development of an Inventory and Inspection Database Framework for Asset Management of MSE Walls (Research Report)	<ul style="list-style-type: none"> <li>Summarizes retaining wall inspection guidelines for multiple agencies (e.g. NPS, OH, NC, NE DOTs, City of Cincinnati, State of Victoria, Australia)</li> </ul>		<ul style="list-style-type: none"> <li>Thermal Imaging</li> <li>Ultrasonic testing</li> <li>UAVS (drones) Video/picture recording, can be used to measure crack/panel joint opening, settlement, wall bulge and tilt. → coordinate and elevation control must be established.</li> </ul>	<a href="https://apps.itd.idaho.gov/apps/research/Completed/RP270.pdf">https://apps.itd.idaho.gov/apps/research/Completed/RP270.pdf</a>
Illinois	Bridge condition report procedures and practices 2023	<ul style="list-style-type: none"> <li>They use Bridge Condition Report</li> <li>Requires Retaining walls with a retained height greater than 7'</li> <li>No specific check or rating list</li> </ul>			<a href="https://public.powerdms.com/IDOT/documents/2083224/Bridge%20Condition%20Report%20Procedures%20and%20Practices">https://public.powerdms.com/IDOT/documents/2083224/Bridge%20Condition%20Report%20Procedures%20and%20Practices</a>
	Bridge Element Inspection Manual (2015)	<ul style="list-style-type: none"> <li>Check as one of precast and precast prestressed concrete elements</li> </ul>			<a href="https://public.powerdms.com/IDOT/documents/2083248/Bridge%20Element%20Inspection%20Manual">https://public.powerdms.com/IDOT/documents/2083248/Bridge%20Element%20Inspection%20Manual</a>
Indiana	Checklist for MSE Wall Construction	<ul style="list-style-type: none"> <li>Yes/No (35 questions)</li> </ul>			<a href="https://www.in.gov/indot/engineering/files/MSE-wall-construction-checklist.pdf">https://www.in.gov/indot/engineering/files/MSE-wall-construction-checklist.pdf</a>
	MSE Wall Design Review Checklist (2021)	<ul style="list-style-type: none"> <li>Yes/No</li> </ul>			<a href="https://view.officeapps.live.com/op/view.aspx?src=https%3A%2F%2Fwww.in.gov%2Fdot%2Fdiv%2Fcontracts%2Fdesign%2Fdmforms%2FMSE%2520Wall%2520Design%2520Review%2520Checklist.docx&amp;wdOrigin=BROWSELINK">https://view.officeapps.live.com/op/view.aspx?src=https%3A%2F%2Fwww.in.gov%2Fdot%2Fdiv%2Fcontracts%2Fdesign%2Fdmforms%2FMSE%2520Wall%2520Design%2520Review%2520Checklist.docx&amp;wdOrigin=BROWSELINK</a>
	MSE Wall Shop Drawing Review Checklist	<ul style="list-style-type: none"> <li>Yes/No</li> </ul>			<a href="https://view.officeapps.live.com/op/view.aspx?src=https%3A%2F%2Fwww.in.gov%2Fdot%2Fdiv%2Fcontracts%2Fdesign%2Fdmforms%2Fmse%2520shop%2520draw%2520rev%2520check.docx&amp;wdOrigin=BROWSELINK">https://view.officeapps.live.com/op/view.aspx?src=https%3A%2F%2Fwww.in.gov%2Fdot%2Fdiv%2Fcontracts%2Fdesign%2Fdmforms%2Fmse%2520shop%2520draw%2520rev%2520check.docx&amp;wdOrigin=BROWSELINK</a>
	MSE Wall Maintenance Manual (2025)	<ul style="list-style-type: none"> <li>9 maintenance items</li> </ul>	<ul style="list-style-type: none"> <li>Panel joint: an interval of 6 months</li> <li>Expansion joints (MSE wall top): an interval of a maximum of 3 years,</li> <li>Drainage inlets and pipes : an interval of a maximum of 3 years</li> <li>Grubbing, cleaning, and correction of the overall drainage system: an interval of a maximum of 3 years</li> </ul>		<a href="https://www.in.gov/indot/engineering/files/MSEW_Maintenance_Manual.pdf">https://www.in.gov/indot/engineering/files/MSEW_Maintenance_Manual.pdf</a>
Iowa	MSE Wall Evaluations (2014)	<ul style="list-style-type: none"> <li>MSE wall design requirements</li> </ul>			<a href="https://iowadot.gov/design/dmanual/200F-03.pdf">https://iowadot.gov/design/dmanual/200F-03.pdf</a>
	Manual- Chapter 6 Retaining Walls Bridge Design Manual	<ul style="list-style-type: none"> <li>Checklist for preliminary design for Noise Walls</li> </ul>			<a href="https://iowadot.gov/bridge/policy/CONNECT_Preliminary%20Design%20Checklist%20-%20NoiseWall.pdf">https://iowadot.gov/bridge/policy/CONNECT_Preliminary%20Design%20Checklist%20-%20NoiseWall.pdf</a>

State	Name of Document	Rating System/Checklist	Inspection Frequency/ Inspection Requirements	Inspection Techniques/ Inspection Types	Published Date and Link
	(2024)				
Kansas	Bridge Construction Manual 4.1 Mechanically Stabilized Earth (MSE) Walls (2008)	<ul style="list-style-type: none"> <li>Construction Checklist: "Yes or No Format"</li> <li>MSE Wall Construction Do's and Don'ts</li> </ul>			<a href="https://www.ksdot.gov/Assets/wwwksdot.org/bureaus/burStructGeotech/ConstructionManual/mse_walls.pdf">https://www.ksdot.gov/Assets/wwwksdot.org/bureaus/burStructGeotech/ConstructionManual/mse_walls.pdf</a>  A username and password are required to access the Bridge design manual.
Kentucky	Evaluation of Mechanically Stabilized Earth (MSE) Walls for Bridge Ends in Kentucky, What Next? (Research, 2013)	<ul style="list-style-type: none"> <li>Rating systems 4 (Excellent, Good, Fair and, Poor) or 9 (Similar to NBI)</li> </ul>			<a href="https://uknowledge.uky.edu/cgi/viewcontent.cgi?article=1316&amp;context=ktr_researchreports">https://uknowledge.uky.edu/cgi/viewcontent.cgi?article=1316&amp;context=ktr_researchreports</a>
	Special Note for Mechanically Stabilized Earth Retaining Walls (2025)	<ul style="list-style-type: none"> <li>Design and Construction guidelines (e.g. QC, materials, etc.</li> </ul>			<a href="https://transportation.ky.gov/StructuralDesign/Current%20Special%20Notes/Special%20Note%20for%20MSE%20Retaining%20Walls%20(rev%204-7-2025).docx">https://transportation.ky.gov/StructuralDesign/Current%20Special%20Notes/Special%20Note%20for%20MSE%20Retaining%20Walls%20(rev%204-7-2025).docx</a>
Louisiana	Geotechnical Asset Management (GAM) Manual (2023)	<ul style="list-style-type: none"> <li>For retaining walls including MSE walls</li> <li>1-5 Scale</li> <li>Drawing Review Checklists</li> <li>Specification Compliance Checklist</li> <li>Construction Inspection Checklist</li> <li>Post- Construction Inspection Checklist</li> <li>GAM planner model and risk analysis</li> </ul>	<ul style="list-style-type: none"> <li>Inspection Frequency for Wall Assets</li> <li>1 year, 5 years, 3 years, 6 months + Stage2,</li> </ul>	<ul style="list-style-type: none"> <li>No information is provided.</li> </ul>	<a href="https://www.ltrc.lsu.edu/pdf/2023/DOTD_%20GAM_Guide.pdf">https://www.ltrc.lsu.edu/pdf/2023/DOTD_%20GAM_Guide.pdf</a>
Maine	Construction Manual (2003)	<ul style="list-style-type: none"> <li>Guidelines for the proper Design Requirement of MSE Wall</li> <li>Division 500 of the Manual provides inspection guidelines during construction.</li> </ul>			<a href="https://www.maine.gov/dot/sites/maine.gov.dot/files/2023-08/ConstructionManual-complete.pdf">https://www.maine.gov/dot/sites/maine.gov.dot/files/2023-08/ConstructionManual-complete.pdf</a>
	Standard Specification Special Provision, Section 636: Mechanically Stabilized Earth Retaining Wall (2009)	<ul style="list-style-type: none"> <li>For design</li> </ul>		<ul style="list-style-type: none"> <li>Visual Inspection for acceptance of materials</li> </ul>	<a href="https://digitalmaine.com/mdot_docs/2388/">https://digitalmaine.com/mdot_docs/2388/</a>
Massachusetts	Building Code 780 CMR 18.00 Foundations and Retaining Walls (2017)	<ul style="list-style-type: none"> <li>Design requirements</li> </ul>	<ul style="list-style-type: none"> <li>Types of Inspections mentioned in their Bridge Inspection Manual: (Routine Inspection, Fracture Critical (should not exceed 24 months, Underwater Inspection, Special Member Inspection,</li> </ul>		<a href="https://www.mass.gov/doc/7th-edition-780-cmr-massachusetts-building-code-780-cmr-1800-foundations-and-retaining-walls/download">https://www.mass.gov/doc/7th-edition-780-cmr-massachusetts-building-code-780-cmr-1800-foundations-and-retaining-walls/download</a>

State	Name of Document	Rating System/Checklist	Inspection Frequency/ Inspection Requirements	Inspection Techniques/ Inspection Types	Published Date and Link
	<b>Bridge Inspection Handbook (2015)</b>	<ul style="list-style-type: none"> <li>• General Bridge Inspection: condition ratings (Good, Fair, Poor, and Severe)</li> <li>• No mention of Retaining wall or MSE wall</li> </ul>			<a href="https://www.mass.gov/files/documents/2018/05/14/bih-chapter3.pdf">https://www.mass.gov/files/documents/2018/05/14/bih-chapter3.pdf</a> <a href="https://www.mass.gov/files/documents/2018/05/14/bih-chapter4.pdf">https://www.mass.gov/files/documents/2018/05/14/bih-chapter4.pdf</a>
Maryland	<b>Office of Structures – Guidelines and Procedures Memorandum</b>	<ul style="list-style-type: none"> <li>• Proprietary Retaining Wall Approval Process (D-82-25(4))</li> </ul>			<a href="https://www.roads.maryland.gov/OBD/GP-M-OOS-01-Design.pdf">https://www.roads.maryland.gov/OBD/GP-M-OOS-01-Design.pdf</a>
	<b>Design Section</b> <b>Office of Structures – Guidelines and Procedures Memorandum</b> <b>Structure Inspection Section</b>	<ul style="list-style-type: none"> <li>• Generic inspection guidelines for small structures including retaining wall.</li> </ul>			<a href="https://www.roads.maryland.gov/OBD/GP-M-OOS-03-Inspection.pdf">https://www.roads.maryland.gov/OBD/GP-M-OOS-03-Inspection.pdf</a>
Michigan	<b>Asset Management for Retaining Walls (Research Report, 2020)</b>	<ul style="list-style-type: none"> <li>• Summarizes retaining wall inspection guidelines for multiple agencies (e.g. PA, NE, KY, OH, NC, NE DOTs, City of Cincinnati, City of Seattle, British Columbia-Canada, Victoria-Australia)</li> </ul>	<ul style="list-style-type: none"> <li>• Routine wall inspections range from two to ten years, with the most common being a 5-year interval</li> </ul>	<ul style="list-style-type: none"> <li>• Two common remote sensing techniques tested: optical photogrammetry and 3D laser scanning.</li> <li>• Provide others' techniques such as LiDAR, GPR, digital protractor, down-hole camera, and fiber optics.</li> </ul>	2020 <a href="https://www.michigan.gov/mdot/-/media/Project/Websites/MDOT/Programs/Research-Administration/Final-Reports/SPR-1676-Report.pdf">https://www.michigan.gov/mdot/-/media/Project/Websites/MDOT/Programs/Research-Administration/Final-Reports/SPR-1676-Report.pdf</a>
Minnesota	<b>Bridge Inspection Field Manual (2025)</b>	<ul style="list-style-type: none"> <li>• Substructure Condition Rating (SNBI Item B.C.03)</li> <li>• Structural Element Condition Rating (B.3.11.3 Non-Integral Retaining Wall)</li> </ul>			<a href="https://edocs-public.dot.state.mn.us/edocs_public/DMResultSet/download?docId=32020342">https://edocs-public.dot.state.mn.us/edocs_public/DMResultSet/download?docId=32020342</a>
Mississippi	<b>Bridge Safety Inspection Policy and Procedure Manual</b>	<ul style="list-style-type: none"> <li>• NBI Substructure Condition Rating: 0 (Fail) to 9 (Excellent)</li> <li>• No info. specifically for MSE walls</li> </ul>			<a href="https://mdot.ms.gov/documents/Bridge%20Design/Manuals/Bridge%20Safety%20Inspection%20Policy%20and%20Procedures.pdf">https://mdot.ms.gov/documents/Bridge%20Design/Manuals/Bridge%20Safety%20Inspection%20Policy%20and%20Procedures.pdf</a>
Missouri	<b>Development of a Geotechnical Asset Management Collection and Rating Program for the Missouri Department of Transportation (Research, 2023)</b>	<ul style="list-style-type: none"> <li>• Condition State Score               <ul style="list-style-type: none"> <li>- Good</li> <li>- Fair</li> <li>- Poor</li> </ul> </li> <li>• 1-100 points</li> </ul>			<a href="https://rosap.nrl.bts.gov/view/dot/66994/dot_66994_DS1.pdf">https://rosap.nrl.bts.gov/view/dot/66994/dot_66994_DS1.pdf</a>
Montana	<b>Bridge Inspection and Rating Manual (2018)</b>	<ul style="list-style-type: none"> <li>• Bridge abutment – retaining wall</li> <li>• Condition State Score               <ul style="list-style-type: none"> <li>1 - Good</li> <li>2 - Fair</li> <li>3 - Poor</li> <li>4 - Severe</li> </ul> </li> </ul>			<a href="https://www.mdt.mt.gov/other/webdata/external/bridge/Bridge-inspection-manual.pdf">https://www.mdt.mt.gov/other/webdata/external/bridge/Bridge-inspection-manual.pdf</a>

State	Name of Document	Rating System/Checklist	Inspection Frequency/ Inspection Requirements	Inspection Techniques/ Inspection Types	Published Date and Link
Nebraska	<b>Inspector's Manual for Mechanically Stabilized Earth Walls (2009)</b>	<ul style="list-style-type: none"> <li>• 14 items with 0-9 scale.</li> </ul>			<a href="https://digitalcommons.unl.edu/cgi/viewcontent.cgi?article=1013&amp;context=matcreports">https://digitalcommons.unl.edu/cgi/viewcontent.cgi?article=1013&amp;context=matcreports</a>
Nevada	<b>Field Inspection Guide (2017)</b>	<ul style="list-style-type: none"> <li>• Includes a retaining wall subchapter</li> <li>• Check items before and during the construction</li> </ul>			<a href="https://www.dot.nv.gov/home/showpublisheddocument/9280/636451512302730000">https://www.dot.nv.gov/home/showpublisheddocument/9280/636451512302730000</a>
New Hampshire	<b>Bridge Inspection Manual (2017)</b>	<ul style="list-style-type: none"> <li>• Inspections for bridge substructures</li> <li>• Not specifically for MSE or retaining walls</li> </ul>			<a href="https://www.dot.nh.gov/sites/g/files/ehbemt811/files/remote-docs/nhdotbridgeinspectionmanual.pdf">https://www.dot.nh.gov/sites/g/files/ehbemt811/files/remote-docs/nhdotbridgeinspectionmanual.pdf</a>
New Jersey	<b>Bridge Element Inspection Manual (2015)</b>	<ul style="list-style-type: none"> <li>• Bridge abutment – retaining wall</li> <li>• Condition State Score               <ul style="list-style-type: none"> <li>1 - Good</li> <li>2 - Fair</li> <li>3 - Poor</li> <li>4 - Severe</li> </ul> </li> </ul>			<a href="https://www.nj.gov/transportation/eng/structureval/pdf/BridgeElInsManual.pdf">https://www.nj.gov/transportation/eng/structureval/pdf/BridgeElInsManual.pdf</a>
New Mexico	<b>Proprietary Earth Retaining Systems Evaluation and Approval Process 2017</b>	<ul style="list-style-type: none"> <li>• Manual only provides system evaluation and approval process for the Proprietary Earth Retaining Systems (PER Systems) Evaluation and Approval Process</li> <li>• Not for any inspection/maintenance</li> </ul>			<a href="https://api.realfile.rtsclients.com/PublicFiles/f260a66b364d453e91ff9b3fedd494dc/782eecbf-04b6-4bf6-82b6-764f735e2d50/Proprietary%20Earth%20Retaining%20(PER)%20Systems%20Evaluation%20and%20Approval%20Process">https://api.realfile.rtsclients.com/PublicFiles/f260a66b364d453e91ff9b3fedd494dc/782eecbf-04b6-4bf6-82b6-764f735e2d50/Proprietary%20Earth%20Retaining%20(PER)%20Systems%20Evaluation%20and%20Approval%20Process</a>
	<b>Bridge Procedures and Design Guide 2018</b>	<ul style="list-style-type: none"> <li>• Only for design</li> </ul>			
New York	<b>Mechanically Stabilized Earth System Inspection Manual (2020)</b>	<ul style="list-style-type: none"> <li>• Checklists for design and each phase of construction of MSE Walls with yes or no format</li> </ul>		<ul style="list-style-type: none"> <li>• Ground Penetrating (GPR) surveys, Borescope Inspection, Laser Scanning (LiDAR), Tilt meters.</li> </ul>	<a href="https://www.dot.ny.gov/divisions/engineering/technical-services/technical-services-repository/GEM-16.pdf">https://www.dot.ny.gov/divisions/engineering/technical-services/technical-services-repository/GEM-16.pdf</a>
North Dakota	<b>Bridge Inventory – Structure Inventory and Appraisal Sheet (2020)</b>	<ul style="list-style-type: none"> <li>• Chapter 4 (Page 59) mentions the parameters that need to be considered for retaining wall design.</li> <li>• Moreover, Chapter 4 (appendix IV-04 F) includes a checklist for Bridge Plans.</li> <li>• No inspection procedure is available in this report.</li> </ul>			<a href="https://www.dot.nd.gov/divisions/ets/RFPs/docs/1373/2020%20Structures%20SIA.pdf">https://www.dot.nd.gov/divisions/ets/RFPs/docs/1373/2020%20Structures%20SIA.pdf</a>
	<b>Bridge Inspection Procedures (2013)</b>	<ul style="list-style-type: none"> <li>• NBI (Culvert and Retaining walls)</li> </ul>			<a href="https://www.ndltap.org/resources/downloads/bridge-manual-nbi-pontis.pdf">https://www.ndltap.org/resources/downloads/bridge-manual-nbi-pontis.pdf</a>
	<b>Bridge Inspection Manual 2025</b>	<ul style="list-style-type: none"> <li>• NBI (Culvert and Retaining walls)</li> <li>• No specific guidelines for MSE walls.</li> </ul>			<a href="https://www.dot.nd.gov/sites/www/files/documents/construction-and-planning/Bridge-Inspection-Manual.pdf">https://www.dot.nd.gov/sites/www/files/documents/construction-and-planning/Bridge-Inspection-Manual.pdf</a>

State	Name of Document	Rating System/Checklist	Inspection Frequency/ Inspection Requirements	Inspection Techniques/ Inspection Types	Published Date and Link
North Carolina	Retaining Wall Inventory and Assessment System (Research, 2015)	<ul style="list-style-type: none"> <li>• 1 – Good (Low Severity Distress)</li> <li>• 2 – Fair (Low-to-Medium Extent of Medium Severity Distress)</li> <li>• 3 – Poor (Medium- to- High Extent of Medium Severity Distress)</li> <li>• 4 – Severe (High Severity Distress).</li> </ul>		<ul style="list-style-type: none"> <li>• Aerial Photographs to locate walls.</li> <li>• For critical walls, always conduct a LiDAR survey</li> <li>• For noncritical walls, do not initially conduct a LiDAR survey. Conduct a LiDAR only when the answer to any of the first 3 questions on the Filed Condition Assessment Data Collection Form is “YES”.</li> </ul>	<a href="https://connect.ncdot.gov/projects/research/RNAProjDocs/2014-10FinalReport.pdf">https://connect.ncdot.gov/projects/research/RNAProjDocs/2014-10FinalReport.pdf</a>
Ohio	ODOT Retaining Wall Inventory Manual (2021)	<ul style="list-style-type: none"> <li>• The DOT website mentions the overall conditions for Retaining Wall Systems.</li> <li>• Good (No deformation or damage to the wall)</li> <li>• Fair – (Little or no deformation)</li> <li>• Poor (Deformation or damage to the wall)</li> </ul>		<ul style="list-style-type: none"> <li>• Each District should have a complete retaining wall inventory, including inventory and inspection of all constructed walls, within three years of launching the retaining wall inventory application. Subsequently, each inventoried wall should be re-inspected on a maximum 10-year cycle. Walls showing distress should be re-inspected on a shorter cycle, determined by the district.</li> </ul>	<a href="https://dam.assets.ohio.gov/image/upload/transportation.ohio.gov/geotechnical/asset-management/Retaining-Wall-Inventory-Manual.pdf">https://dam.assets.ohio.gov/image/upload/transportation.ohio.gov/geotechnical/asset-management/Retaining-Wall-Inventory-Manual.pdf</a>
Oklahoma	BrM Bridge Inspection Office Manual For Oklahoma Bridges (2022)	<ul style="list-style-type: none"> <li>• Bridge substructure</li> <li>• No specific guidelines for MSE and retaining walls</li> </ul>			<a href="https://www.odot.org/pontis_files/2022%20BrM%20Bridge%20Insp%20Office%20Manual.pdf">https://www.odot.org/pontis_files/2022%20BrM%20Bridge%20Insp%20Office%20Manual.pdf</a>
Oregon	Oregon Standard Specifications for Construction (2024)	<ul style="list-style-type: none"> <li>• Design and construction requirements for MSE walls</li> </ul>			<a href="https://www.oregon.gov/odot/Business/Specs/2024_STANDARD_SPECIFICATIONS.pdf">https://www.oregon.gov/odot/Business/Specs/2024_STANDARD_SPECIFICATIONS.pdf</a>
Pennsylvania	Bridge Safety Inspection Manual 2024	<ul style="list-style-type: none"> <li>• The Bridge Safety Inspection Manual provides MSE Wall Inspection Procedures</li> <li>• It also provides an Inspection Report Quality Control Verification Checklist.</li> </ul>		<ul style="list-style-type: none"> <li>• * The three-dimensional survey should be completed in accordance with the guidelines in the Surveying and Mapping Manual, Publication 122M, Part A Chapter 3 and Chapter 6.7. The Photogrammetry and Survey Section and Multiple Districts have LiDAR scanners with three-dimensional survey capability available for use in the Engineering Districts” (Page IP 02-67)</li> <li>• Neither reinforcement nor backfill will be able to be inspected; therefore, a close visual inspection of the facing panels and drainage facilities is required to provide information on all three of the major components. This includes visual inspection of the roadway surface (i.e., pavement) above the MSE wall for tension cracking.</li> <li>• Inspection of the leveling pads, if visible, can provide information on scour, erosion or settlement. Inspection of the barriers can also provide important information regarding movement of the MSE wall’</li> </ul>	<a href="https://www.pa.gov/content/dam/copapwp-pagov/en/pennndot/documents/public/pubsforms/publications/pub%2038.pdf">https://www.pa.gov/content/dam/copapwp-pagov/en/pennndot/documents/public/pubsforms/publications/pub%2038.pdf</a>

State	Name of Document	Rating System/Checklist	Inspection Frequency/ Inspection Requirements	Inspection Techniques/ Inspection Types	Published Date and Link
Rhode Island	Bridge Inspection Manual (2016)	<ul style="list-style-type: none"> <li>Retaining wall as a part of bridge system</li> <li>No specific guidelines for MSE and retaining walls</li> </ul>			<a href="https://www.dot.ri.gov/documents/doingbusiness/RIDOT_Bridge_Inspection_Manual.pdf">https://www.dot.ri.gov/documents/doingbusiness/RIDOT_Bridge_Inspection_Manual.pdf</a>
South Carolina	MSE Wall Appendix C (2022)	<ul style="list-style-type: none"> <li>This manual doesn't provide any checklist or condition rating system for MSE Wall Maintenance.</li> <li>However, it provides specific design requirements and provides steps for the proper Construction procedures.</li> </ul>			<a href="https://www.scdot.org/content/dam/scdot-legacy/business/pdf/geotech/2022-by-chapter/Z-Appendix-C-MSEWalls-02092022.pdf">https://www.scdot.org/content/dam/scdot-legacy/business/pdf/geotech/2022-by-chapter/Z-Appendix-C-MSEWalls-02092022.pdf</a>
	Supplemental Technical Specification for Mechanically Stabilized Earth (MSE) Walls (2024)	<ul style="list-style-type: none"> <li>Design, materials, and construction of MSE walls</li> </ul>			<a href="https://www.scdot.org/business/technicalPDFs/supTechSpecs/SC-M-713-1-MSE-Walls-(01-24)-FHWA-Approval.pdf">https://www.scdot.org/business/technicalPDFs/supTechSpecs/SC-M-713-1-MSE-Walls-(01-24)-FHWA-Approval.pdf</a>
South Dakota	Structures Construction Manual Chapter 17- Mechanically Stabilized Earth (MSE) Retaining Walls (2022)	<ul style="list-style-type: none"> <li>Checklist for pre-construction preparation, materials inspection, and inspection during construction.</li> </ul>			<a href="https://dot.sd.gov/media/4f9lfdsn/structuremanual.pdf">https://dot.sd.gov/media/4f9lfdsn/structuremanual.pdf</a>
	Bridge Inspection Field Manual (2023)	<ul style="list-style-type: none"> <li>Substructure Condition Rating System for NBI Item 60</li> </ul>	•	<ul style="list-style-type: none"> <li>Allows UAS use for aerial photography, photogrammetry, bridge inspection, planning, geotechnical field investigations, Light Detection and Ranging (LiDAR) applications, public outreach, mapping construction sites, asset management, asset inspections, traffic monitoring, incident management, disaster response, and training exercise.</li> </ul>	<a href="https://dot.sd.gov/media/e318511a/South%20Dakota%20Bridge%20Inspection%20Field%20Manual%20-%20April%202023.pdf">https://dot.sd.gov/media/e318511a/South%20Dakota%20Bridge%20Inspection%20Field%20Manual%20-%20April%202023.pdf</a>
Tennessee	Rating and Inventory of TDOT Retaining Walls (Research, 2021)	<ul style="list-style-type: none"> <li>Elements conditions ratings (1 to 9 or Critical, Good, Fair, Poor, Excellent)</li> <li>Conditions ratings scheme (1 to 4 or Severe, Poor, Fair, Good)</li> <li>Introduce others' scales (NPS, NY, PA, NE, and OR)</li> </ul>		<ul style="list-style-type: none"> <li>UAVs, digital cameras, infrared cameras, LiDAR.</li> <li>Automatic Road Analyzer (ARAN) surveys.</li> <li>Systematic AHP &amp; Markov Model Based Retaining Wall Assessment Procedure</li> </ul>	<a href="https://rosap.nrl.bts.gov/view/dot/60915/dot_60915_DS1.pdf">https://rosap.nrl.bts.gov/view/dot/60915/dot_60915_DS1.pdf</a>
Texas	Retaining Walls- Geotechnical Manual – Texas Department of Transportation	<ul style="list-style-type: none"> <li>Website</li> <li>Provides retaining wall selection, layouts, design, excavation supports of retaining and MSE wall.</li> <li>The DOT website provides General information of retaining wall and design procedure</li> </ul>			<a href="https://www.txdot.gov/business/resources/highway/bridge/geotechnical/retaining-walls.html">https://www.txdot.gov/business/resources/highway/bridge/geotechnical/retaining-walls.html</a>

State	Name of Document	Rating System/Checklist	Inspection Frequency/ Inspection Requirements	Inspection Techniques/ Inspection Types	Published Date and Link
Utah	<b>Structures Design and Detailing Manual (2022)</b>	<ul style="list-style-type: none"> <li>Includes information regarding proper inspection during construction.</li> </ul>			<a href="https://drive.google.com/file/d/1YSUKgvnoGIQ1xKzcVnNgBvMUckoGiYnI/view">https://drive.google.com/file/d/1YSUKgvnoGIQ1xKzcVnNgBvMUckoGiYnI/view</a>
	<b>Development of MSE wall inspection plan and procedure for failure mode analysis and risk assessment (Thesis, 2009)</b>	<ul style="list-style-type: none"> <li>Detail inspection recommendations for MSE walls</li> </ul>			
Vermont	<b>Geotechnical Engineering Instruction on Soil Slope Stability Investigation and Evaluation (2014)</b>	<ul style="list-style-type: none"> <li>Steps for Construction and Post Construction Monitoring Inspection for slopes</li> </ul>		<ul style="list-style-type: none"> <li>(Slope) Site geometry is reviewed from acquired field surveys, including but not limited to LiDAR, topographic surveys as well as current and historic aerial photographs.</li> </ul>	<a href="https://outside.vermont.gov/agency/vtrans/external/docs/construction/03GeotechEng/Engineering/GEI%2014-01SoilSlopeStabilityInvestigationandEvaluationOctober2014Approved%20Engineering.pdf">https://outside.vermont.gov/agency/vtrans/external/docs/construction/03GeotechEng/Engineering/GEI%2014-01SoilSlopeStabilityInvestigationandEvaluationOctober2014Approved%20Engineering.pdf</a>
Virginia	<b>Manual of the structure and bridge division Part 2 Design Guidelines</b>  <b>Chapter 10 – Earth Retaining Structures</b> <b>Chapter 18 - Earth Retaining Walls (2022)</b>	<ul style="list-style-type: none"> <li>No checklist</li> <li>Guidelines for the design/construction</li> <li>No inspection/maintenance</li> </ul>			<a href="https://www.vdot.virginia.gov/media/vdotvirginiagov/doing-business/technical-guidance-and-support/technical-guidance-documents/structure-and-bridge/manuals-of-structure-and-bridge-acc/part11/Chapter10.pdf">https://www.vdot.virginia.gov/media/vdotvirginiagov/doing-business/technical-guidance-and-support/technical-guidance-documents/structure-and-bridge/manuals-of-structure-and-bridge-acc/part11/Chapter10.pdf</a>  <a href="https://www.virginiadot.org/business/resources/bridge/Manuals/Part2/chapter18.pdf">https://www.virginiadot.org/business/resources/bridge/Manuals/Part2/chapter18.pdf</a>
	<b>Inspection Manual (2018)</b>	<ul style="list-style-type: none"> <li>Inspection manual for all items</li> <li>Check guidelines for Retaining walls during construction</li> <li>No grading system</li> </ul>			<a href="https://www.vdot.virginia.gov/media/vdotvirginiagov/doing-business/technical-guidance-and-support/technical-guidance-documents/construction/InspectionManual_acc091322.pdf">https://www.vdot.virginia.gov/media/vdotvirginiagov/doing-business/technical-guidance-and-support/technical-guidance-documents/construction/InspectionManual_acc091322.pdf</a>
Washington	<b>Chapter 8 – Walls and Buried Structures</b>	<ul style="list-style-type: none"> <li>Design requirements for retaining walls.</li> </ul>			<a href="https://wsdot.wa.gov/publications/manuals/fulltext/m23-50/chapter8.pdf">https://wsdot.wa.gov/publications/manuals/fulltext/m23-50/chapter8.pdf</a>
	<b>Geotechnical Design Manual (2020)</b>	<ul style="list-style-type: none"> <li>Geotechnical Design Manual provides Preapproved Proprietary Wall/Reinforced Slope Design and Construction Review Checklist (Appendix 15-B)</li> </ul>			<a href="https://www.wsdot.wa.gov/publications/manuals/fulltext/M46-03/Geotech.pdf">https://www.wsdot.wa.gov/publications/manuals/fulltext/M46-03/Geotech.pdf</a>
	<b>Bridge Inspection Manual (2025)</b>	<ul style="list-style-type: none"> <li>Not specifically for MSE walls.</li> <li>Following general FHWA inspection guidelines (Bridge)</li> </ul>			<a href="https://wsdot.wa.gov/engineering-standards/all-manuals-and-standards/manuals/bridge-inspection-manual">https://wsdot.wa.gov/engineering-standards/all-manuals-and-standards/manuals/bridge-inspection-manual</a>

State	Name of Document	Rating System/Checklist	Inspection Frequency/ Inspection Requirements	Inspection Techniques/ Inspection Types	Published Date and Link
West Virginia	Bridge Design Manual (2006)	<ul style="list-style-type: none"> <li>The Bridge Design Manual provides sections with tasks regarding Retaining Walls for Planning, Development and Engineering Phase, Project Design Phase and Construction Phase</li> </ul>			<a href="https://transportation.wv.gov/highways/engineering/files/WVBDML%202006.pdf">https://transportation.wv.gov/highways/engineering/files/WVBDML%202006.pdf</a>
Wisconsin	WisDOT Structure Inspection Manual- Chapter 4- Retaining Walls (2017)	<ul style="list-style-type: none"> <li>- Condition Rating (4 scales)</li> </ul>		<ul style="list-style-type: none"> <li>For Retaining wall inspections</li> <li>Routine Inspections (24 months + 12 months for high risk (NBI value 4 or less))</li> <li>In-Depth (as needed) <ul style="list-style-type: none"> <li>For large MSE structures (more than 20' in exposed height) where movements are suspected, three dimensional (LiDAR) surveys may be requested at 10-year intervals to ascertain movements by the WISDOT survey crew.</li> </ul> </li> <li>Damage or Interim (as necessary)</li> <li>Non-destructive Evaluation equipment and/or other materials tests may need to be performed.</li> </ul>	<a href="https://wisconsindot.gov/dtsdManuals/structure/inspection/insp-fm-pt4ch4.pdf">https://wisconsindot.gov/dtsdManuals/structure/inspection/insp-fm-pt4ch4.pdf</a>
Wyoming	Bridge Applications Manual (2020)	<ul style="list-style-type: none"> <li>MSE Wall Drawing Checklists</li> </ul>			<a href="https://www.dot.state.wy.us/home/engineering_technical_programs/bridge/bridge_applications_manual.html">https://www.dot.state.wy.us/home/engineering_technical_programs/bridge/bridge_applications_manual.html</a>  <a href="https://www.dot.state.wy.us/files/live/sites/wydot/files/shared/Bridge/Bridge%20Applications%20Manual/Section%204.21%20-%20Earth%20Retaining%20Structures%20with%20Checklist.pdf">https://www.dot.state.wy.us/files/live/sites/wydot/files/shared/Bridge/Bridge%20Applications%20Manual/Section%204.21%20-%20Earth%20Retaining%20Structures%20with%20Checklist.pdf</a>
	Bridge Inspection Program	<ul style="list-style-type: none"> <li>Website</li> <li>Bridge ratings including substructure</li> <li>Inspections with the National Bridge Inspection Standards (NBIS).</li> <li>No specific comments for MSE and retaining walls.</li> </ul>			<a href="https://www.dot.state.wy.us/home/engineering_technical_programs/bridge/bridge_inspection_program.html">https://www.dot.state.wy.us/home/engineering_technical_programs/bridge/bridge_inspection_program.html</a>



## ACKNOWLEDGMENT

This research was sponsored by the Georgia Department of Transportation (GDOT) under Research Project RP 22-17, titled “*Nondestructive/Noncontact Inspection Protocols and Technologies for Aging Mechanically Stabilized Earth (MSE) and Modular Block Retaining Walls.*” The authors gratefully acknowledge the support and guidance of GDOT’s Office of Performance-Based Management and Research.

Special thanks are extended to the GDOT Office of Bridge Design and Maintenance and the Office of Materials and Testing for their collaboration and for facilitating access to necessary documents related to the considered walls and sites. We also appreciate the logistical coordination and safety support provided by GDOT Districts 2 and 5 during site surveys.

We thank the faculty, staff, and student researchers at Georgia Southern University (GSU) for their contributions to data collection, analysis, and modeling. In particular, undergraduate and graduate students enrolled in the Department of Civil Engineering and Construction courses—*Senior Project, Introduction to Terrestrial LiDAR, and Introduction to Close-Range Photogrammetry*—during Summer 2023 through Spring 2025, played a vital role in fieldwork and data processing. Their enthusiastic participation significantly advanced the project’s objectives.

We also acknowledge the Built Environment and Modeling (BEaM) Lab at GSU for providing access to facilities, field equipment, and licensed software platforms essential to the research.

The following students contributed directly to the project or participated through coursework:

Jonas Adams, Tanvir Ahmed, Oluwatunmise Akanmu, Jose Cruz Ramirez, David Anderson, David Arteaga, Oliver Arteaga, Jakeb Britt, Mason Bruning, John Busler, Turvon Casey, Zachary Dean, Olivia Duffy, Blake Forbes, Ralph Franks, Jabari Greene, Evan Hall, Noah Hallman, Iffat Haq, Reece Hart, Chase Hovis, S. Tahmid Hussain, William Immel, Azharul Islam, Kobe Keise, Garyn King, Cooper Korn, Ana Lanza Hernandez, Amber Lawrence, W. Rhett Loyed, Andrew Musmanno, Laila O'claire, Anu Pradeep, Jacob Reaves, Riyadhul Riyad, M. Garrett Roberson, Joshua Rogers, Peya Sharif, Ariful Shuvo, Chase Simington, Michael Snipes, Zachary Swindell, Jerry Thomas, Garfield Thorpe, Aniya Williams, Jared Worthy, Chandler Yarbrough, and Mashfiq Zihad.

Equally important, we extend our appreciation to Shawn Jackson, Laboratory Coordinator in the department, for his valuable support throughout the project, and to Anna M. McDonald for her dedicated editing efforts.

## REFERENCES

- Aggelis, D. G., Kordatos, E. Z., & Matikas, T. E. (2011). "Acoustic emission for fatigue damage characterization in metal plates". *Mechanics Research Communications*, 38(2), 106-110.
- Aljagoub, D., Na, R., & Cheng, C. (2025). "Delamination detection in concrete decks using numerical simulation and UAV-based infrared thermography with deep learning". *Automation in Construction*, 170, 105940.
- Debees, M., & Catbas, F. N. (2025). "Rapid Evaluation and Decision-Making for Concrete Bridges". *Transportation Research Record*, 03611981251330892.
- Garrido, I., Lagüela, S., & Arias, P. (2018). "Infrared thermography's application to infrastructure inspections". *Infrastructures*, 3(3), 35.
- Hiasa, S. (2016). "Investigation of infrared thermography for subsurface damage detection of concrete structures". Doctoral Dissertation, University Central Florida.
- Huang, Y., Chiang, C. H., & Hsu, K. T. (2018, March). "Combining the 3D model generated from point clouds and thermography to identify the defects presented on the facades of a building". In *Nondestructive Characterization and Monitoring of Advanced Materials, Aerospace, Civil Infrastructure, and Transportation XII* (Vol. 10599, pp. 61-69). SPIE.
- Ibrahim, A., Faris, N., Zayed, T., Qureshi, A. H., Abdelkhalek, S., & Abdelkader, E. M. (2024). "Application of infrared thermography in concrete bridge deck inspection: current practices, challenges and future needs". *Nondestructive Testing and Evaluation*, 1-44.
- Jin, H., & Zou, L. L. (2021). "Detection of hidden disease of concrete bridge based on infrared thermal imaging". In *Journal of Physics: Conference Series* (Vol. 1748, No. 4, p. 042041). IOP Publishing.
- Macedo, J., Burns, S. E., Torres, J., Jung, Y. S., Liu, C., & Tsai, Y. J. (2023). Towards the Implementation of a Geotechnical Asset Management Program in the State of Georgia (No. FHWA-GA-23-2011). Georgia. Department of Transportation. Office of Performance-Based Management & Research
- Maldague, X. (2001). "NDT Techniques: Thermographic". *Encyclopedia of Materials: Science and Technology*, 6036-6039.
- Shrestha, P., Avci, O., Rifai, S., Abla, F., Seek, M., Barth, K., & Halabe, U. (2025). "A Review of Infrared Thermography Applications for Civil Infrastructure". *Structural Durability and Health Monitoring*, 19(2).
- Sirca Jr, G. F., & Adeli, H. (2018). "Infrared thermography for detecting defects in concrete structures". *Journal of Civil Engineering and Management*, 24(7), 508-515.

Titman, D. J. (2001). "Applications of thermography in non-destructive testing of structures". *NDT & e International*, 34(2), 149-154.

Zhao, G., & Chen, J. G. (2013). "Infrared thermo-graphic inspection technique for concrete retaining wall". *Electronic Journal of Geotechnical Engineering*, 18(1), 1521-1528.